frontiers | Research Topics

Tuberculosis diagnosis, drug resistance, and drug target discovery

Edited by
Robert Jansen, Xueqiong Wu, Lin Fan and Ranjan Nanda

Coordinated by
Raquel Villar-Hernández

Published in
Frontiers in Microbiology
Frontiers in Medicine
Frontiers in Public Health
Frontiers in Tuberculosis

ISSN 1664-8714
ISBN 978-2-8325-6386-1
DOI 10.3389/978-2-8325-6386-1

About Frontiers

Frontiers is more than just an open access publisher of scholarly articles: it is a pioneering approach to the world of academia, radically improving the way scholarly research is managed. The grand vision of Frontiers is a world where all people have an equal opportunity to seek, share and generate knowledge. Frontiers provides immediate and permanent online open access to all its publications, but this alone is not enough to realize our grand goals.

Frontiers journal series

The Frontiers journal series is a multi-tier and interdisciplinary set of open-access, online journals, promising a paradigm shift from the current review, selection and dissemination processes in academic publishing. All Frontiers journals are driven by researchers for researchers; therefore, they constitute a service to the scholarly community. At the same time, the *Frontiers journal series* operates on a revolutionary invention, the tiered publishing system, initially addressing specific communities of scholars, and gradually climbing up to broader public understanding, thus serving the interests of the lay society, too.

Dedication to quality

Each Frontiers article is a landmark of the highest quality, thanks to genuinely collaborative interactions between authors and review editors, who include some of the world's best academicians. Research must be certified by peers before entering a stream of knowledge that may eventually reach the public - and shape society; therefore, Frontiers only applies the most rigorous and unbiased reviews. Frontiers revolutionizes research publishing by freely delivering the most outstanding research, evaluated with no bias from both the academic and social point of view. By applying the most advanced information technologies, Frontiers is catapulting scholarly publishing into a new generation.

What are Frontiers Research Topics?

Frontiers Research Topics are very popular trademarks of the *Frontiers journals series*: they are collections of at least ten articles, all centered on a particular subject. With their unique mix of varied contributions from Original Research to Review Articles, Frontiers Research Topics unify the most influential researchers, the latest key findings and historical advances in a hot research area.

Find out more on how to host your own Frontiers Research Topic or contribute to one as an author by contacting the Frontiers editorial office: frontiersin.org/about/contact

Tuberculosis diagnosis, drug resistance, and drug target discovery

Topic editors

Robert Jansen — Radboud University, Netherlands

Xueqiong Wu — Institute for Tuberculosis Research, the 8th Medical Center of Chinese PLA General Hospital, China

Lin Fan — Tongji University, China

Ranjan Nanda — International Centre for Genetic Engineering and Biotechnology, India

Topic coordinator

Raquel Villar-Hernández — Genome Identification Diagnostisch GmbH (GenID), Germany

Citation

Jansen, R., Wu, X., Fan, L., Nanda, R., Villar-Hernández, R., eds. (2025). *Tuberculosis diagnosis, drug resistance, and drug target discovery*. Lausanne: Frontiers Media SA. doi: 10.3389/978-2-8325-6386-1

Table of contents

frontiers | Frontiers in Microbiology

TYPE Original Research
PUBLISHED 25 August 2023
DOI 10.3389/fmicb.2023.1236599

OPEN ACCESS

EDITED BY
Lin Fan,
Tongji University, China

REVIEWED BY
Julio César Flores Gonzalez,
National Institute of Respiratory Diseases-Mexico (INER), Mexico
John S. Spencer,
Colorado State University, United States
Leslie Chavez-Galan,
National Institute of Respiratory Diseases-Mexico (INER), Mexico

*CORRESPONDENCE
Xiao-Yong Fan
✉ xyfan008@fudan.edu.cn
Guodong Sui
✉ gsui@fudan.edu.cn

†These authors have contributed equally to this work

RECEIVED 08 June 2023
ACCEPTED 07 August 2023
PUBLISHED 25 August 2023

CITATION
Huang H, Qu R, Wu K, Xu J, Li J, Lu S, Sui G and Fan X-Y (2023) Proteinase K-pretreated ConA-based ELISA assay: a novel urine LAM detection strategy for TB diagnosis. *Front. Microbiol.* 14:1236599. doi: 10.3389/fmicb.2023.1236599

Proteinase K-pretreated ConA-based ELISA assay: a novel urine LAM detection strategy for TB diagnosis

Huan Huang[1,2†], Rong Qu[2,3†], Kang Wu[2], Jinchuan Xu[2], Jianhui Li[2], Shuihua Lu[2,4], Guodong Sui[1,5*] and Xiao-Yong Fan[2,3,5*]

[1]Shanghai Key Laboratory of Atmospheric Particle Pollution Prevention (LAP3), Department of Environmental Science and Engineering, Fudan University, Shanghai, China, [2]Shanghai Public Health Clinical Center, Fudan University, Shanghai, China, [3]School of Laboratory Medicine and Life Science, Wenzhou Medical University, Wenzhou, China, [4]National Clinical Research Center for Infectious Disease, Shenzhen Third People's Hospital, Shenzhen, China, [5]Shanghai Institute of Infectious Disease and Biosecurity, Fudan University, Shanghai, China

Objectives: Lipoarabinomannan (LAM), an abundant cell wall glycolipid of mycobacteria including *Mycobacterium tuberculosis* (*Mtb*), is a promising TB diagnostic marker. The current commercially available urine LAM assays are not sufficiently sensitive, and more novel detection strategies are urgently needed to fill the current diagnostic gap.

Methods: A proteinase K-pretreated Concanavalin A (ConA)-based ELISA assay was developed. Diagnostic performance was assessed by several bacterial strains and clinical urine samples.

Results: The limit of detection (LoD) of the assay against ManLAM was 6 ng/ml. The assay reacted strongly to *Mtb* H37Rv and *M. bovis* BCG, intermediately to *M. smegmatis* mc^{2}155, and weakly to four non-mycobacteria pathogens. This method could distinguish TB patients from healthy controls (HCs) and close contacts (CCs) in 71 urine samples treated with proteinase K, which increases urine LAM antibody reactiveness. In TB^+HIV^+ and TB^+HIV^- patients, the sensitivity was 43.8 and 37.5%, respectively, while the specificity was 100.0%. The areas under ROC curves (AUCs) were 0.74 and 0.82, respectively.

Conclusion: This study implies that ConA can be paired with antibodies to detect LAM. Proteinase K treatment could effectively enhance the sensitivity by restoring the reactiveness of antibodies to LAM.

KEYWORDS

***Mycobacterium tuberculosis*, LAM, ConA, ELISA, urine, proteinase K**

Introduction

Tuberculosis (TB), a lung disease caused by *Mycobacterium tuberculosis (Mtb)*, is a leading cause of illness and death worldwide (WHO, 2022). *Mtb* infects 25% of the world's population, and 5–10% may develop TB (WHO, 2022). The COVID-19 pandemic continues to hinder TB diagnosis, resulting in a global decline in new TB diagnoses from 7.1 million in 2019 to 6.4 million in 2021 (WHO, 2022). It is estimated that approximately 40% of new infections go undiagnosed (WHO, 2022), making it more challenging to eradicate TB.

Currently, there are many limitations to TB diagnosis as follows: (1) Bacteriological detection by acid-fast staining and sputum culture is widely used. However, these tests are low-sensitivity or lengthy, respectively (Acharya, 2020). (2) Antigen-specific immunological-mediated detection using tuberculin skin testing (TST) or interferon-gamma release assay (IGRA) is the main method to diagnose *Mtb* infection, but both are unable to differentiate latent TB infection (LTBI) from TB (Acharya, 2020). (3) Nucleic acid amplification tests (NAATs), e.g., Xpert MTB/RIF, are fast and sensitive, but they are not widely available in low- and middle-income countries due to cost (Nadjib, 2022). More innovative diagnostic strategies are needed to overcome these limitations and reduce TB underdiagnosis.

Urine lipoarabinomannan (LAM) could be a promising TB diagnostic biomarker (Flores and Cancino, 2021). LAM, an abundant (approximately 15% of bacterial dry weight) glycolipid located on the mycobacterial cell wall, is a critical virulence component in the *Mtb* infection pathway (Fukuda, 2013). Different LAM derivatives are identified in various groups of mycobacteria, of which ManLAM is a type of LAM with non-reducing mannose caps and is found only in slow-growing mycobacteria (e.g., *Mtb*) (Chatterjee et al., 1992). ManLAM is a glycolipid made up of a mannosyl-phosphatidyl-myo-inositol anchor (MPI), a polysaccharide backbone composed of D-mannan and D-arabinan, and various mannose-capping motifs (Flores and Cancino, 2021). LAM is actively secreted by infected phagocytes or membrane vesicles and may be present in blood, as well as in urine via glomeruli (Prados-Rosales et al., 2011; De, 2015). The amounts of LAM are approximately 1–1,000 ng/ml in sputum (Kawasaki et al., 2019), 2.3–132 pg/ml in serum (Brock et al., 2020), and tens of fg/ml (Chen et al., 2023) to hundreds of ng/ml in urine (Flores and Cancino, 2021). The amounts of LAM in clinical samples collectively reflect the bacterial load, metabolic activity, and degradation ratio of the bacteria in the host body, which mirror the infection status and the responsiveness of anti-TB treatment (Hamasur et al., 2015; Bjerrum et al., 2019; Wood et al., 2019).

There are currently two commercial assays available for LAM-based TB diagnosis: Clearview TB ELISA and Alere DetermineTM TB LAM Ag test (AlereLAM). Clearview TB ELISA is the first one utilizing polyclonal rabbit antibodies (Hamasur et al., 2001), resulting in limited sensitivity and specificity in TB^+HIV^+ patients (51 and 94%, respectively), especially in TB^+HIV^- patients (14 and 97%, respectively) (Correia-Neves et al., 2019). AlereLAM is the second one based on colloidal gold immunochromatography assay (ICA) and uses the same polyclonal rabbit antibodies as used in Clearview TB ELISA (Correia-Neves et al., 2019). The result of AlereLAM can be obtained within 25 min using only a 60 μl urine sample, but the sensitivity is also low (42% under 95% specificity in TB^+HIV^+ patients). AlereLAM is not suitable for TB^+HIV^- patients due to its low sensitivity (Shah et al., 2016; Bjerrum et al., 2019). Fujifilm SILVAMP TB LAM (FujiLAM) (Fujifilm, Japan), being tested clinically, is an improved LAM-based ICA (70.4% sensitivity and 90.8% specificity in TB^+HIV^+ patients) utilizing a pair of high-affinity LAM-specific monoclonal antibodies and a silver amplification step (Mitamura et al., 2013; Broger et al., 2019). However, relatively complex methodology and subjective naked-eye reading induce high error rates and substantial variability (Mitamura et al., 2013; Székely et al., 2022), which hinders its clinical transformation.

Concanavalin A (ConA), a lectin originally extracted from *Canavalia ensiformis* (jack bean), could recognize specifically some internal and non-reducing terminal α-mannosyl and α-glucosyl groups of various sugars or sugar moieties (e.g., LAM, which contains various α-mannosyl groups) (Ij, 1986). Pathogens or their antigens are readily enriched by ConA by binding to their sugar moieties and subsequently detected using a specific antibody. This ConA-antibody strategy can be used for the detection of norovirus (Hong et al., 2015), breast cancer (Choi et al., 2018), and invasive aspergillosis (Raval et al., 2019). CS35 (BEI Resources, USA) is a LAM-specific monoclonal antibody that recognizes the arabinose group, which is different from that recognized by ConA (α-mannosyl group) (Sigal et al., 2018). In theory, the pairing between them could form a stable sandwich structure with LAM. In this study, we first investigated whether ConA and CS35 could be paired to detect LAM in urine. We then developed a simple ELISA assay with proteinase K pretreatment and tested its performance in lysates of several bacterial strains and clinical urine samples for TB diagnosis.

Materials and methods

Materials and reagents

CS35 and HRP-goat anti-mouse IgG antibodies were purchased from BEI Resources (USA) and Biodragon (China), respectively. ConA and BSA were obtained from Sigma–Aldrich (USA). Middlebrook 7H9 broth and oleic acid-albumin-dextrose-catalase enrichment (OADC) were purchased from BD Difco (USA). The vacuum freeze dryer was purchased from Labconco (USA). HiPrep 16/60 Sephacryl S-100 HR column was obtained from Cytiva (USA). Moreover, the 96-well plates were purchased from Greiner (Germany). 3,3',5,5'-Tetramethylbenzidine (TMB) substrate was obtained from Millipore (USA) substrate. Alexa Fluor® 594-conjugated ConA was obtained from Invitrogen (USA). All other chemicals were of analytical purity. *Mycobacterium tuberculosis* H37Rv (ATCC 27294), *Mycolicibacterium smegmatis* (ATCC 700084), and *Mycobacterium bovis* BCG (ATCC 35734) were preserved in our laboratory. *Klebsiella pneumoniae* (ATCC 10031), *Pseudomonas aeruginosa* (ATCC 27853), and *Acinetobacter Baumannii* (ATCC 19606) were provided by Jianhui Li (Shanghai Public Health Clinical Center). *E. coli* Top10 was purchased from Sangon Biotech (China).

Urine sample collection

The Ethics Committee of Shanghai Public Health Clinical Center (SPHCC) approved this study (No. 2022-S044-03), and all patients enrolled in this study signed a written informed consent form. From November 2018 to April 2019, 71 urine samples were collected from 13 healthy controls (HCs), 7 close contacts (CCs) of TB patients, 48 bacteriologically confirmed tuberculosis, and 3 non-tuberculosis mycobacteria (NTM)-infected patients (Table 1).

Each patient was required to provide mid-stream urine samples, which were kept at 4°C within 2 h and then immediately moved to −80°C until analysis. All CCs were without TB symptoms, or abnormal CXR, but shared the same enclosed living space for at least 1 night/week or extended periods during the day with the active tuberculosis (ATB) patient for 3 months before the diagnosis of TB. All HCs were without TB symptoms, abnormal CXR, and any contact with a pulmonary tuberculosis patient. All TB patients enrolled in this study had at least one TB-specific positive assay of culture, smear, and Xpert MTB/RIF. Of them, 32 were HIV-negative (10 for extrapulmonary TB and 22 for pulmonary TB), and 16 were HIV-positive. All participants were negative for hepatitis B virus (HBV) and HCV.

Bacterial strains used and their culture conditions

Mycobacteria strains were grown at 37°C in liquid Middlebrook 7H9 broth supplemented with 10% (v/v) OADC, 0.5% glycerol, and 0.05% Tween-80. *Klebsiella pneumonia*, *Pseudomonas aeruginosa*, *Acinetobacter Baumannii*, and *E. coli* Top10 were grown in a liquid LB medium. The cultures in the exponential stage were frozen at −80°C as stock after adding glycerol (final concentration 10%).

Purification, identification, and quantification of ManLAM

ManLAM was purified from a clinical isolate of *Mtb* following the procedures described previously (Torrelles et al., 2006; Grzegorzewicz and Jackson, 2013; Pan et al., 2014). In brief, the *Mtb* pellet was inactivated at 80°C for 30 min. The bacteria were resuspended in chloroform/methanol (2:1, v/v) and then placed in a shaking incubator at 37°C for 12 h. Then, the collected pellet was resuspended in chloroform/methanol/water (10:10:3, v/v/v) solution and placed in a shaking incubator at 37°C for 12 h. The collected pellet was freeze-dried overnight using a vacuum freeze dryer. The dried pellet was resuspended in PBS (containing DNase, RNase, lysozyme, and PMSF) and lysed via ultrasonication. The lysed sample was placed at 37°C for 2 h. Then, Triton X-114 was added (final concentration 8%) and incubated overnight at 4°C. The solution was centrifuged at 27,000 *g* for 1 h, and the supernatant was collected and placed at 37°C until obvious stratification. The lower organic phase was collected, added with anhydrous ethanol, and incubated overnight at −20°C. The pellet was collected via centrifugation and freeze-dried. The pellet was resuspended in PBS containing proteinase K (final concentration: 2 mg/ml), incubated in a water bath at 37°C for 2 h, and then dialyzed against PBS at 4°C. The dialyzed solution was freeze-dried. The crude LAM powder was resuspended in PBS and applied to a HiPrep 16/60 Sephacryl S-100 HR column. Fractions of effluent were collected.

Fractions of effluent containing ManLAM were identified via glycogen staining (Tang et al., 2016). In brief, after separating the fractions of effluent in sodium dodecyl sulfate-polyacrylamide gel electrophoresis (SDS-PAGE) gel, ManLAM contained in the gel was oxidized with periodate to form an aldehyde group, followed by staining with Schiff reagent. The Schiff reagent was prepared from basic fuchsin and sodium sulfite, which reacts with aldehyde groups to form an amaranth substance. ManLAM-positive fractions of effluent were pooled, dialyzed against PBS, and quantified via the orcinol sulfuric acid method as described previously (Yin et al., 2013). The residual protein content in the dialyzed/pooled ManLAM sample was also routinely quantified via the BCA method. The dialyzed/pooled ManLAM sample was re-validated via glycogen staining and Western blotting using biotin-labeled ConA/HRP-Streptavidin.

ConA/CS35-based ELISA for ManLAM detection

"ConA/CS35" in this study means that ConA was tested as a capture protein and CS35 was tested as the detection antibody. ConA was diluted with PBS containing 0.1 mM $CaCl_2$ (PBSCa). ELISA plate wells coated with (serially diluted) ConA (100 μl/well) were incubated at 4°C overnight. The next morning, the plate wells were blocked with 1% BSA, and then the samples to be tested were added (ManLAM in PBS or urine, bacterial strain lysis, and clinical samples) and incubated for 1 h at room temperature. Negative wells were incubated with PBS. After washing with PBS containing 0.05% tween-20 (PBST) five times, the plate wells were added with CS35 (100 μl/well, final concentration: 2 μg/ml, dissolved in PBS) and incubated for 1 h at room temperature. After washing with PBST five times, the plate wells were added with 100 μl HRP-goat anti-mouse IgG (100 μl/well, diluted 1:5000 in PBS) and incubated for 30 min at room temperature. The plate wells were rinsed six times with PBST, then added with TMB substrate (100 μl/well), and incubated at room temperature for 10 min. The reaction was terminated by adding 2 M H_2SO_4 (50 μl/well), and OD_{450} was measured. CS35 was also tested as a capture antibody, and accordingly, ConA was tested as a detection protein (i.e., CS35/ConA-based ELISA). Alexa Fluor® 594-conjugated Con was also diluted with PBS and used to visualize the dose-dependent coating pattern in ELISA plate wells under a fluorescent microscope.

The limit of detection (LoD) of ConA/CS35-based ELISA to ManLAM and the reactiveness of ConA/CS35-based ELISA to bacterial strains

ELISA plate wells were coated with ConA (200 μg/ml) (100 μl/well). For LoD analysis, serial diluted ManLAM samples were used. For analyzing the reactiveness of ConA/CS35-based ELISA to other strains, several different strains were used including two *Mtb* complex (MTBC) strains (i.e., *Mtb* H37Rv and *M. bovis* BCG Pasteur), one non-tuberculous mycobacterium (NTM) (i.e.,

TABLE 1 Demographic and clinical characteristics.

	HCs ($n = 13$)	CCs ($n = 7$)	EPTB ($n = 10$)	PTB ($n = 22$)	TB^+HIV^+ ($n = 16$)	NTM ($n = 3$)	*p*
Age, years	26 (25–32)	41 (32–50)	27 (17–47)	51.5 (27–65)	35.5 (31–63)	61 (11–64)	>0.05
Sex							>0.05
Women	6 (46%)	3 (43%)	3 (30%)	7 (32%)	3 (19%)	0	
Men	7 (54%)	4 (57%)	7 (70%)	15 (68%)	13 (81%)	3 (100%)	
Bacterial test							<0.05
Culture+ and/or Smear+			10 (100%)	16 (73%)	7 (44%)	3 (100%)	
Culture– and Smear–			0	6 (27%)	9 (56%)	0	
T-SPOT.*TB*							<0.05
+		0	9 (90%)	21 (95%)	7 (44%)	2 (67%)	
-		7 (100%)	0	1 (5%)	9 (56%)	1 (33%)	
Xpert MTB/RIF							<0.05
+			9 (90%)	14 (64%)	4 (25%)	0	
–			1 (10%)	8 (36%)	2 (13%)	3 (100%)	
CD4 count, cells/μl					65 (24–112)		NA
Data are median (IQR) or *n* (%)							

M. smegmatis mc^2155), and four non-mycobacteria strains (i.e., *Klebsiella pneumoniae*, *Pseudomonas aeruginosa*, *Acinetobacter baumannii*, and *E. coli* Top10). The fresh cultures of the strains were adjusted to $OD_{600} = 1$ and inactivated at 80°C for 30 min. The pellets from 1 ml liquid were washed twice with PBS, resuspended with 1 ml PBS, and lysed via ultrasonication. The diluted lysed liquids (1:100 with PBS) were added into plate wells (100 μl/well) for comparative analysis.

The treatment of urine samples with proteinase K

The urine sample (300 μl) was treated with proteinase K (final concentration 200 μg/ml) at 37°C for 30 min and then inactivated at 100 °C for 3 min (Shah et al., 2016). The supernatants were collected via centrifugation (12,000 × *g*, 10 min) for ConA/CS35-based ELISA.

Statistical analysis

Statistical analysis was performed using SPSS (version 27), and the data were visualized using GraphPad Prism software (version 8.0.1). The Shapiro–Wilk test was used to determine the normality of the data. Unpaired, two-tailed Student's *t*-test was used to access the statistical significance between the two groups. One-way ANOVA with Tukey's tests or Games–Howell's multiple comparisons tests were used to access the statistical significance among multiple experimental groups. The 95% confidence interval (CI) of the ROC curve was calculated using the method of Wilson/Brown.

Results

ConA/CS35-based ELISA could detect ManLAM

As shown in Figure 1, the molecular weight of ManLAM purified from a clinical isolate of *Mtb* is between 35 and 45 kDa, which is consistent with ManLAM extracted from other *Mtb* strains (Torrelles et al., 2006; Choudhary et al., 2018). The purified ManLAM was used for subsequent analysis.

Figure 2A shows that the epitopes of ManLAM that ConA and CS35 recognize are different. ConA recognizes the α-mannosyl groups of ManLAM, whereas CS35 binds to the arabinosyl groups of LAM (Sigal et al., 2018). Moreover, we tested whether ConA could be paired with CS35 to detect ManLAM in the ELISA platform. We observed that ConA could be coated to ELISA plate wells in a dose-dependent manner (Figure 2B), which resulted in the dose-dependent capturing of ManLAM, and the signals plateaued at 200 μg/ml (i.e., 20 μg in 100 μl) when using CS35 as detection antibody (Figure 2C). In contrast to ConA/CS35-based ELISA, CS35/ConA-based ELISA (i.e., CS35 being used as a capture antibody and ConA being used as detection protein) could not detect ManLAM (Figure 2D). In conclusion, ConA/CS35-based ELISA could successfully detect ManLAM.

The LoD of ConA/CS35-based ELISA to ManLAM

As shown in Figure 3A, the LoD of ConA/CS35-based ELISA to ManLAM was 6 ng/ml when coating ConA at 200 μg/ml (i.e., 20 μg in 100 μl).

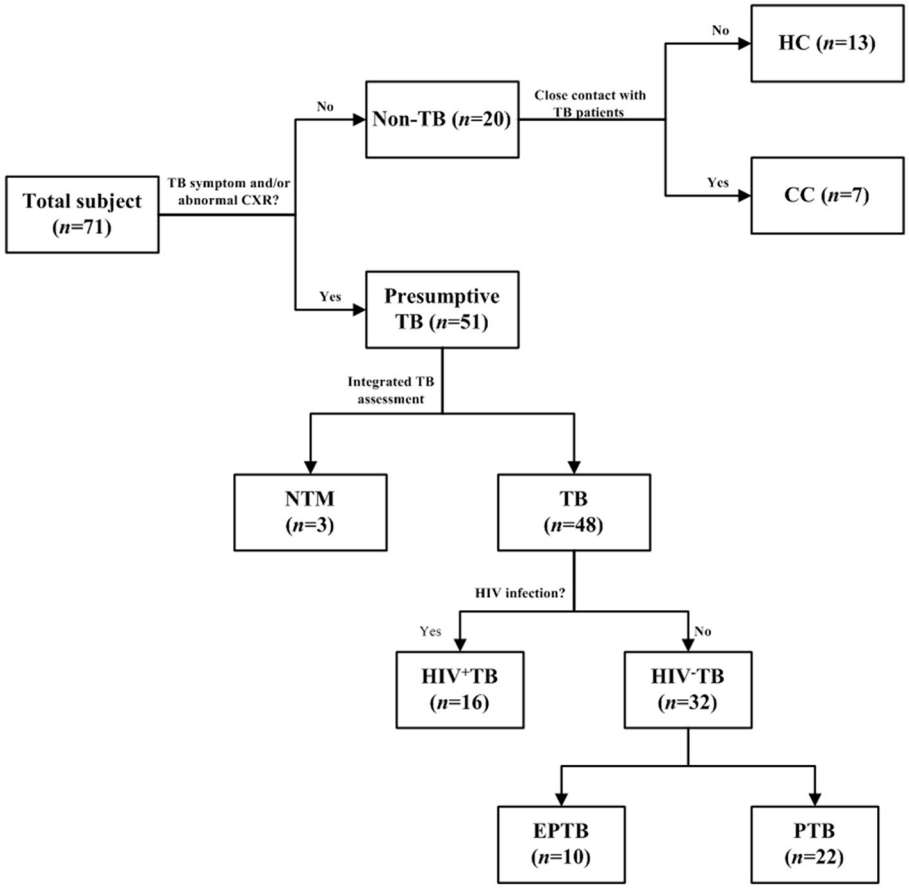

FIGURE 1
Selection flow of recruited patients. The ConA/CS35 was evaluated with cryopreserved urine samples from individuals with tuberculosis, NTM infection, and non-tuberculosis. CC, close contact: no TB symptom and abnormal CXR and close contact with TB patient 2 weeks before recruitment. HC, health control: no TB symptom and abnormal CXR and no history of exposure to TB. TB, tuberculosis: the diagnosis of a TB patient was confirmed by one or a combination of smear, culture, and GeneXpert. NTM, non-tuberculous mycobacteria; EPTB, extrapulmonary tuberculosis; PTB, pulmonary tuberculosis.

The reactiveness of ConA/CS35-based ELISA to several other strains

As shown in Figure 3B, the assay displayed the highest signals to two *Mtb* complex strains (i.e., *Mtb* H37Rv and *M. bovis* BCG Pasteur), intermediate signals to one non-tuberculous mycobacteria (i.e., *M. smegmatis* mc^{2}155), and the lowest signals (S/B ratio < 2) to four non-mycobacteria pathogens (i.e., *Klebsiella pneumoniae*, *Pseudomonas aeruginosa*, *Acinetobacter baumannii*, and *E. coli* Top10).

The signals in urine samples using ConA/CS35-based ELISA

The signals in urine samples of TB patients (either TB^+HIV^- or TB^+HIV^+) were higher than the signals in HC, CC, and NTM; there was neither any difference in signals between the HC and CC groups nor between the TB^+HIV^+ and TB^+HIV^- groups (Figure 4A). The sensitivities of the assay for TB^+HIV^+ patients and TB^+HIV^- patients were 43.8% (95% CI: 23.1–66.8%) and 37.5% (95% CI: 22.9–54.8%), respectively, under the specificity of 100% (95% CI: 83.9–100.0%); the AUC was 0.8234 for TB^+HIV^+ patients and 0.7438 for TB^+HIV^- patients (Figures 4B, C). When TB^+HIV^- patients were further divided into PTB and EPTB, the signals were higher in PTB patients than in HCs, but there was no statistical difference between EPTB patients and HCs (Figure 4D). The sensitivities of the assay for PTB^+HIV^- and $EPTB^+HIV^-$ patients were 45.5% (95% CI: 26.9–65.3%) and 20% (95% CI: 3.5–51.0%), respectively, under the specificity of 100.0% (95% CI: 83.9–100.0%); the AUC was 0.8193 for PTB^+HIV^- patients and 0.5775 for $EPTB^+HIV^-$ patients (Figures 4E, F).

Discussion

The only urine LAM assay approved by the World Health Organization is AlereLAM, but its clinical application may be limited for its low sensitivity, especially in those without HIV. Thus, the detection of urinary LAM requires additional innovative assays to fill the current diagnostic gap, such as new signal amplification techniques (e.g., FujiLAM), high-affinity and specific antibody screening, and non-antibody-based assays (e.g., aptamer and ConA). In this study, we developed a simple ConA/CS35-based

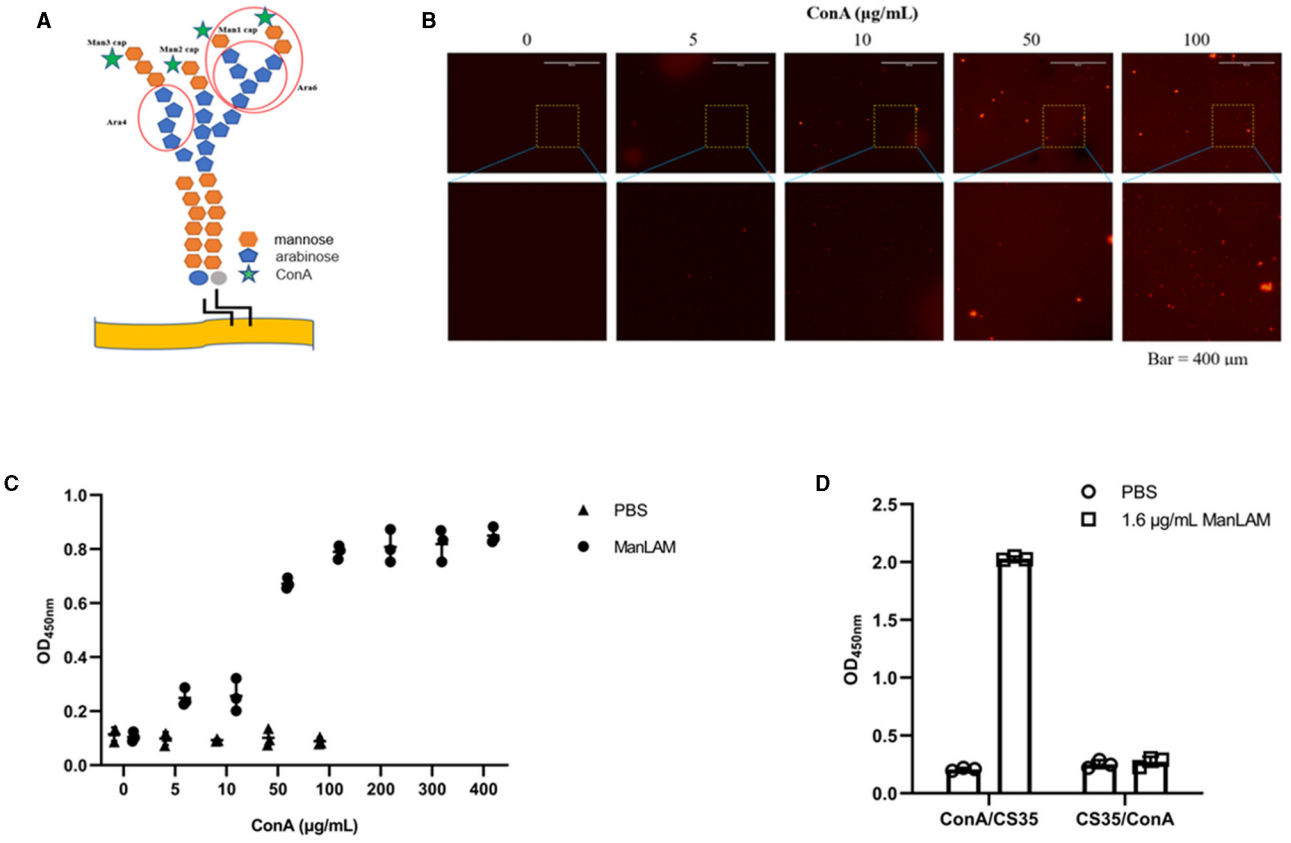

FIGURE 2
ConA/CS35-based ELISA could detect ManLAM. **(A)** The illustration of epitopes recognized by ConA and CS35. The red circles present the recognized epitopes of CS35, which mainly recognize tetra-arabinoside and branched hexa-arabinoside (Mitamura et al., 2013). Green star: ConA, which recognizes some mannosyl groups (Correia-Neves et al., 2019). **(B)** The dose-dependent coating of Alexa Fluor 594-conjugated ConA on ELISA plate. **(C)** The ELISA detection of ManLAM (10 μg/ml of ManLAM was used, and the LAM solution and ConA coated were reacted at room temperature for 1.5 h.), of which the ELISA plate wells were coated with serial diluted ConA. CS35 was used as the detection antibody. **(D)** The comparative detection of ManLAM between ConA/CS35-based ELISA and CS35/ConA-based ELISA. "ConA/CS35" means that the capture protein was ConA and the detection antibody was CS35, whereas "CS35/ConA" means that the capture antibody was CS35 and the detection protein was ConA. Data are means ± SD of three or four biological repeats. $^{****}P < 0.0001$ (unpaired, two-tailed Student's *t*-test).

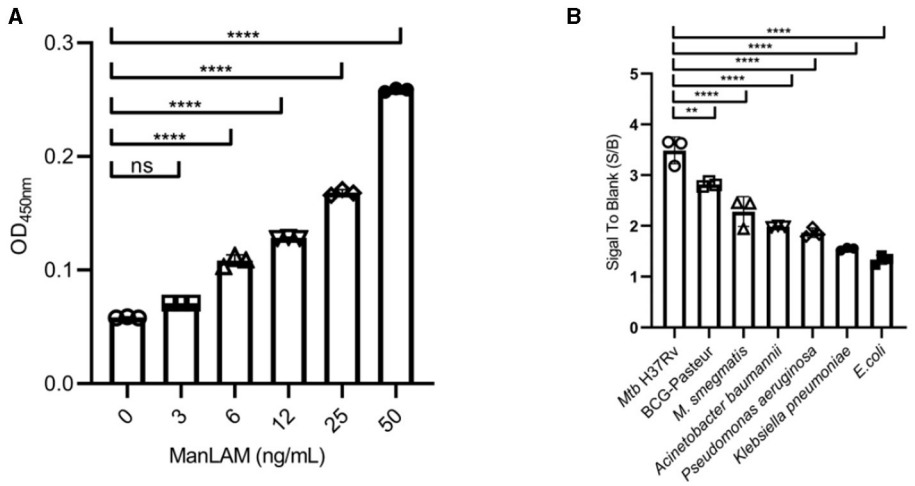

FIGURE 3
Diagnostic performance of the ConA/CS35-based ELISA to **(A)** ManLAM standards and **(B)** several strains of bacteria. ManLAM standards and bacterial lysates were diluted through PBS buffer and did not pretreat via proteinase K. Data are means ± SD of three or four biological repeats. $^{ns}P > 0.05$, $^{**}P < 0.01$, $^{****}P < 0.0001$ (one-way ANOVA with Tukey's multiple comparison tests).

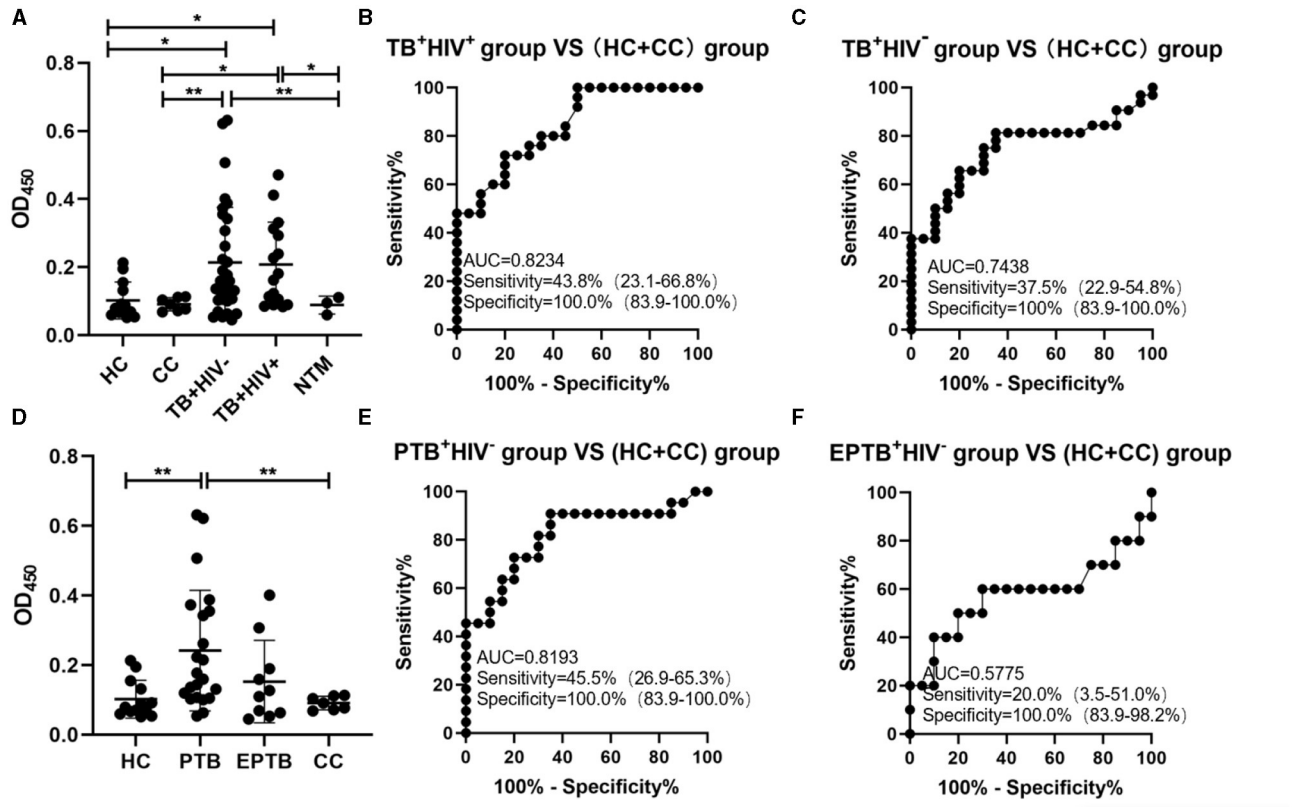

FIGURE 4
ConA/CS35-based ELISA using urine samples. **(A** and **D)** The signals detected using ConA/CS35-based ELISA were subtracted by the signals of negative wells (i.e., PBS). **(B**, **C**, **E**, and **F)** ROC analysis. $^{*}P < 0.05$, $^{**}P < 0.01$ (one-way ANOVA with Games–Howell's multiple comparison tests).

ELISA assay for urine LAM detection, based on the principle that ConA and the monoclonal antibody CS35 can recognize different LAM epitopes (Choudhary et al., 2018; WHO, 2022). To the best of our knowledge, this is the first research endeavor to utilize non-antibody protein for the detection of LAM. ConA is much cheaper than antibodies (approximately 50 times) (Hong et al., 2015); therefore, the ConA-antibody paired assays have the potential to lower the cost of TB testing, especially with the development of ConA-based point-of-care test, which will be beneficial for TB diagnosis in resource-limited areas.

The sensitivity of urine LAM analysis seems to be positively correlated with the LoD of the method. In a study addressing $TB^{+}HIV^{-}$ patients, AlereLAM, FujiLAM, and EclLAM had sensitivities of 10.8, 53.2, and 66.7%, respectively, and EclLAM and FujiLAM had LoDs of 5 and 10–20 pg/ml, respectively, which were at least 10 times lower than AlereLAM (Broger et al., 2020). In our study, the LoDs of ConA/CS35 ELISA were only 6 ng/ml; however, the sensitivity in HIV-negative patients was 37.5% (higher than Alere) when the specificity was 100%. This seems to be explained by the formation of complexes between LAM and proteins in the urine sample. These complexes may spatially affect the correct binding/reactivity of the antibody to LAM and can be largely restored by proteinase K treatment in our ConA/CS35 ELISA assays and capture ELISA (Amin et al., 2018). It is suggested that proteinase K treatment is a successful sensitivity booster for urine LAM detections.

The specificity of urine LAM analysis depends on the reactivity of the ligands used (e.g., antibodies) between different bacterial strains. The LAM-specific polyclonal antibodies utilized in Clearview TB ELISA and AlereLAM could react to mycobacteria stains from both MTBC and NTM strains and could not react to the tested non-mycobacteria pathogens (Amin et al., 2018). The monoclonal antibody, being used as a gold particle-conjugated antibody in FujiLAM or a capture antibody in EclLAM, reacts strongly to MTBC strains and reacts weakly or could not react to the tested NTM strains and non-mycobacteria pathogens (Sigal et al., 2018). ConA could react to some mannosyl group-containing sugars (Ij, 1986), which are non-specifically present in various bacteria or viruses. However, CS35, a relatively specific monoclonal antibody that recognizes mostly MTBC and few NTM strains (Boehme et al., 2005), can compensate for the lack of ConA's specificity. As a result, ConA/CS35-based ELISA could react strongly to *Mtb* H37Rv and *M. bovis* BCG but react weakly to other non-mycobacteria pathogens (Figure 3B).

However, this study has the following limitations. First, even with proteinase K pretreatment, the sensitivities of ConA/CS35 ELISA in urine from HIV TB patients were 37.5% and 43.8%, which is similar to AlereLAM [almost 42% in HIV-positive adults (Bjerrum et al., 2019)] but lower than Fuji LAM [75% in HIV-positive (Li et al., 2021)]. However, it should be noted that this is only a preliminary study demonstrating the availability of ConA paired with monoclonal antibodies, and the enhanced

effect of Proteinase K treatment on sensitivity was achieved. Further improvements in this method, such as the replacement of higher affinity antibodies or stronger signal probes (e.g., electrochemiluminescence and quantum dots), are very likely to improve the current diagnostic performance. Second, as a method of testing non-sputum samples, our test duration is still too long (~4 h), which is longer than AlerelAM (25 min) and FujiLAM (60 min) (Bulterys et al., 2019). However, we are certain that this assay may readily be converted to a POCT version (e.g., test strips) with appropriate improvements. Simultaneous improvements in the sensitivity and test time of ConA-based LAM assays could further enhance the attractiveness of this method as a cost-effective and easy-to-use TB screening tool, especially in low-resource communities with a higher TB burden. Third, we did not evaluate the effect of the use or no use of proteinase K on the improvement of sensitivity in this study. However, the enhancement of LAM analysis by proteinase K has been confirmed by several studies (Amin et al., 2021; Clarke et al., 2023; Panraksa et al., 2021), based on a different LAM analysis than ours. The role of proteinase K in the ConA/CS35 ELISA will be further elucidated in our further studies.

In conclusion, we established a simple ELISA assay for urine LAM detection for TB diagnosis. Our assay demonstrates that ConA can be paired with antibodies to detect LAM in urine, broadening the idea of non-antibody-based methods. In addition, our results show that proteinase K treatment could effectively enhance sensitivity by restoring the reactiveness of antibodies to LAM.

Data availability statement

The original contributions presented in the study are included in the article/Supplementary material, further inquiries can be directed to the corresponding authors.

Ethics statement

The studies involving humans were approved by the Shanghai Public Health Clinical Center (SPHCC) Ethics Committee. The studies were conducted in accordance with the local legislation and institutional requirements. The participants provided their written informed consent to participate in this study.

Author contributions

HH, RQ, KW, and X-YF conceived and designed the experiments and wrote the manuscript. HH, RQ, and KW acquired, analyzed, and interpreted the data. GS, KW, and X-YF contributed to overall supervision, critical comments, and the manuscript review. GS, JL, JX, and SL gave critical comments on the manuscript. All authors read and approved the final manuscript.

Funding

This study was supported by grants from the National Key Research and Development Program of China (2022YFC2302900 and 2021YFC2301503), the National Natural and Science Foundation of China (82171815 and 82171739), the Shanghai Hygiene and Health Outstanding Leader Project (2022XD060), and the Shanghai Science and Technology Commission (20Y11903400).

Acknowledgments

The authors would like to thank Dr. Douglas B. Lowrie for his critical comments and suggestions to improve the manuscript.

Conflict of interest

The authors declare that the research was conducted in the absence of any commercial or financial relationships that could be construed as a potential conflict of interest.

Publisher's note

Supplementary material

The Supplementary Material for this article can be found online at: https://www.frontiersin.org/articles/10.3389/fmicb.2023.1236599/full#supplementary-material

FIGURE S1
The identification of purified ManLAM. 2 μg of ManLAM was added to each lane for electrophoresis, and ManLAM on SDS gel was oxidized by periodate followed by Schiff reagent staining **(left)** or biotin-labeled ConA recognition followed by visualized reaction of HRP-Streptavidin **(right)**. M, protein marker. kD, kiloDalton.

References

Acharya, B, Acharya, A, Gautam, S, Ghimire, S. P, Mishra, G, Parajuli, N, et al. (2020). Advances in diagnosis of tuberculosis: an update into molecular diagnosis of mycobacterium tuberculosis. *Mol. Biol. Rep.* 47, 4065–75. doi: 10.1007/s11033-020-05413-7

Amin, A. G., De, P., Graham, B., Calderon, R. I., Franke, M. F., and Chatterjee, D. (2021). Urine lipoarabinomannan in HIV uninfected, smear negative, symptomatic TB patients: effective sample pretreatment for a sensitive immunoassay and mass spectrometry. *Sci. Rep.* 11, 2922. doi: 10.1038/s41598-021-82445-4

Amin, A. G., De, P., Spencer, J. S., et al. (2018). Detection of lipoarabinomannan in urine and serum of HIV-positive and HIV-negative TB suspects using an improved capture-enzyme linked immuno absorbent assay and gas chromatography/mass spectrometry. *Tuberculosis.* 111, 178–87. doi: 10.1016/j.tube.2018.06.004

Bjerrum, S., Schiller, I., Dendukuri, N., et al. (2019). Lateral flow urine lipoarabinomannan assay for detecting active tuberculosis in people living with HIV. *Cochrane Datab. Syst. Rev.* 10, D11420. doi: 10.1002/14651858.CD011420.pub3

Boehme, C., Molokova, E., Minja, F., et al. (2005). Detection of mycobacterial lipoarabinomannan with an antigen-capture ELISA in unprocessed urine of Tanzanian patients with suspected tuberculosis. *Trans. R Soc. Trop. Med. Hyg.* 99, 893–900. doi: 10.1016/j.trstmh.2005.04.014

Brock, M., Hanlon, D., Zhao, M., et al. (2020). Detection of mycobacterial lipoarabinomannan in serum for diagnosis of active tuberculosis. *Diagn. Microbiol. Infect. Dis.* 96, 114937. doi: 10.1016/j.diagmicrobio.2019.114937

Broger, T., Nicol, M. P., Sigal, G. B., et al. (2020). Diagnostic accuracy of 3 urine lipoarabinomannan tuberculosis assays in HIV-negative outpatients. *J. Clin. Invest.* 130, 5756–64. doi: 10.1172/JCI140461

Broger, T., Sossen, B., Du Toit, E., et al. (2019). Novel lipoarabinomannan point-of-care tuberculosis test for people with HIV: a diagnostic accuracy study. *Lancet Infect Dis.* 19, 852–61. doi: 10.1016/S1473-3099(19)30001-5

Bulterys, M. A., Wagner, B., Redard-Jacot, M., et al. (2019). Point-of-care urine LAM tests for tuberculosis diagnosis: a status update. *J. Clin. Med.* 9, 111. doi: 10.3390/jcm9010111

Chatterjee, D., Lowell, K., Rivoire, B., et al. (1992). Lipoarabinomannan of Mycobacterium tuberculosis. Capping with mannosyl residues in some strains. *J. Biol. Chem.*. 267, 6234–9. doi: 10.1016/S0021-9258(18)42686-5

Chen, P., Meng, Y., Liu, T., et al. (2023). Sensitive urine immunoassay for visualization of lipoarabinomannan for noninvasive tuberculosis diagnosis. *ACS Nano.* 17, 6998–7006. doi: 10.1021/acsnano.3c01374

Choi, J. W., Moon, B. I., Lee, J. W., et al. (2018). Use of CA15-3 for screening breast cancer: an antibody-lectin sandwich assay for detecting glycosylation of CA15-3 in sera. *Oncol. Rep.* 40, 145–54. doi: 10.3892/or.2018.6433

Choudhary, A., Patel, D., Honnen, W., et al. (2018). Characterization of the antigenic heterogeneity of lipoarabinomannan, the major surface glycolipid of mycobacterium tuberculosis, and complexity of antibody specificities toward this antigen. *J. Immunol.* 200, 3053–66. doi: 10.4049/jimmunol.1701673

Clarke, E., Robinson, R., Laurentius, L. B., et al. (2023). Proteinase K pretreatment for the quantitative recovery and sensitive detection of the tuberculosis biomarker mannose-capped lipoarabinomannan spiked into human serum. *Anal. Chem.* 95, 9191–8. doi: 10.1021/acs.analchem.3c00214

Correia-Neves, M., Fröberg, G., Korshun, L., et al. (2019). Biomarkers for tuberculosis: the case for lipoarabinomannan. *ERJ Open Res.* 5, 1–5. doi: 10.1183/23120541.00115-2018

De, P, Amin, A. G, Valli, E, Perkins, M. D, McNeil, M, Chatterjee, D. (2015). Estimation of D-arabinose by gas chromatography/mass spectrometry as surrogate for mycobacterial lipoarabinomannan in human urine. *PLoS ONE.* 10, e144088. doi: 10.1371/journal.pone.0144088

Flores, J., and Cancino, J. C. (2021). Lipoarabinomannan as a point-of-care assay for diagnosis of tuberculosis: how far are we to use it? *Front. Microbiol.* 12, 638047. doi: 10.3389/fmicb.2021.638047

Fukuda, T, Matsumura, T, Ato, M, Hamasaki, M, Nishiuchi, Y, Murakami, Y, et al. (2013). Critical roles for lipomannan and lipoarabinomannan in cell wall integrity of mycobacteria and pathogenesis of tuberculosis. *MBio.* 4, e412–72. doi: 10.1128/mBio.00472-12

Grzegorzewicz, A. E., and Jackson, M. (2013). Subfractionation and analysis of the cell envelope (lipo)polysaccharides of Mycobacterium tuberculosis. *Methods Mol. Biol.* 966, 309–24. doi: 10.1007/978-1-62703-245-2_19

Hamasur, B., Bruchfeld, J., Haile, M., et al. (2001). Rapid diagnosis of tuberculosis by detection of mycobacterial lipoarabinomannan in urine. *J. Microbiol. Methods.* 45, 41–52. doi: 10.1016/S0167-7012(01)00239-1

Hamasur, B., Bruchfeld, J., Van Helden, P., et al. (2015). A sensitive urinary lipoarabinomannan test for tuberculosis. *PLoS ONE.* 10, e123457. doi: 10.1371/journal.pone.0123457

Hong, S. A., Kwon, J., Kim, D., et al. (2015). A rapid, sensitive and selective electrochemical biosensor with concanavalin A for the preemptive detection of norovirus. *Biosens. Bioelectr.* 64, 338–44. doi: 10.1016/j.bios.2014.09.025

Ij, G. (1986). Isolation, physicochemical characterization, and carbohydrate-binding specificity of lectins. *The Lectins* 2, 233–47.

Kawasaki, M., Echiverri, C., Raymond, L., et al. (2019). Lipoarabinomannan in sputum to detect bacterial load and treatment response in patients with pulmonary tuberculosis: analytic validation and evaluation in two cohorts. *PLoS Med.* 16, e1002780. doi: 10.1371/journal.pmed.1002780

Li, Z., Tong, X., Liu, S., et al. (2021). The value of fujilam in the diagnosis of tuberculosis: a systematic review and meta-analysis. *Front. Pub. Health.* 9, 757133. doi: 10.3389/fpubh.2021.757133

Mitamura, K., Shimizu, H., Yamazaki, M., et al. (2013). Clinical evaluation of highly sensitive silver amplification immunochromatography systems for rapid diagnosis of influenza. *J Virol. Methods.* 194, 123–8. doi: 10.1016/j.jviromet.2013.08.018

Nadjib, M, Dewi, R. K, Setiawan, E, Miko, T. Y, Putri, S, Hadisoemarto, P. F, et al. (2022). Cost and affordability of scaling up tuberculosis diagnosis using Xpert MTB/RIF testing in West Java, Indonesia. *PLoS ONE.* 17, e0264912. doi: 10.1371/journal.pone.0264912

Pan, Q., Wang, Q., Sun, X., et al. (2014). Aptamer against mannose-capped lipoarabinomannan inhibits virulent Mycobacterium tuberculosis infection in mice and rhesus monkeys. *Mol. Ther.* 22, 940–51. doi: 10.1038/mt.2014.31

Panraksa, Y., Amin, A. G., Graham, B., et al. (2021). Immobilization of proteinase K for urine pretreatment to improve diagnostic accuracy of active tuberculosis. *PLoS ONE.* 16, e257615. doi: 10.1371/journal.pone.0257615

Prados-Rosales, R., Baena, A., Martinez, L. R., et al. (2011). Mycobacteria release active membrane vesicles that modulate immune responses in a TLR2-dependent manner in mice. *J. Clin. Invest.* 121, 1471–83. doi: 10.1172/JCI44261

Raval, K. M., Ghormade, V., Rajamohanan, P. R., et al. (2019). Development of a nano-gold immunodiagnostic assay for rapid on-site detection of invasive aspergillosis. *J. Med. Microbiol.* 68, 1341–52. doi: 10.1099/jmm.0.001040

Shah, M., Hanrahan, C., Wang, Z. Y., et al. (2016). Lateral flow urine lipoarabinomannan assay for detecting active tuberculosis in HIV-positive adults. *Cochrane Datab. Syst. Rev.* 2016, D11420. doi: 10.1002/14651858.CD011420.pub2

Sigal, G. B., Pinter, A., Lowary, T. L., et al. (2018). A novel sensitive immunoassay targeting the 5-methylthio-d-xylofuranose-lipoarabinomannan epitope meets the WHO's performance target for tuberculosis diagnosis. *J. Clin. Microbiol.* 56, 12. doi: 10.1128/JCM.01338-18

Székely, R., Sossen, B., Mukoka, M., et al. (2022). Multicentre accuracy trial of FUJIFILM SILVAMP TB LAM test in people with HIV reveals lot variability. *medRxiv [Preprint].* doi: 10.1101/2022.09.07.22278961

Tang, X. L., Wu, S. M., Xie, Y., et al. (2016). Generation and application of ssDNA aptamers against glycolipid antigen ManLAM of Mycobacterium tuberculosis for TB diagnosis. *J. Infect.* 72, 573–86. doi: 10.1016/j.jinf.2016.01.014

Torrelles, J. B., Azad, A. K., and Schlesinger, L. S. (2006). Fine discrimination in the recognition of individual species of phosphatidyl-myo-inositol mannosides from Mycobacterium tuberculosis by C-type lectin pattern recognition receptors. *J. Immunol.* 177, 1805–16. doi: 10.4049/jimmunol.177.3.1805

WHO (2022). *Global, WHO Tuberculosis Report 2022*. Geneva: World Health Organization.

Wood, A., Barizuddin, S., Darr, C. M., et al. (2019). Ultrasensitive detection of lipoarabinomannan with plasmonic grating biosensors in clinical samples of HIV negative patients with tuberculosis. *PLoS ONE.* 14, e214161. doi: 10.1371/journal.pone.0214161

Yin, A. B., Hawke, D., and Zhou, D. (2013). Mass spectrometric analysis of glycosphingolipid antigens. *J. Vis. Exp.* 74, 1–4. doi: 10.3791/4224

frontiers | Frontiers in Microbiology

TYPE Review
PUBLISHED 04 October 2023
DOI 10.3389/fmicb.2023.1225438

OPEN ACCESS

EDITED BY
Robert Jansen,
Radboud University, Netherlands

REVIEWED BY
Stefan Panaiotov,
National Center of Infectious and Parasitic Diseases (NCIPD), Bulgaria
Wondwossen Amogne Degu,
Addis Ababa University, Ethiopia

*CORRESPONDENCE
Matúš Dohál
matus.dohal@uniba.sk

RECEIVED 19 May 2023
ACCEPTED 22 September 2023
PUBLISHED 04 October 2023

CITATION
Dohál M, Porvazník I, Solovič I and Mokrý J (2023) Advancing tuberculosis management: the role of predictive, preventive, and personalized medicine.
Front. Microbiol. 14:1225438.
doi: 10.3389/fmicb.2023.1225438

Advancing tuberculosis management: the role of predictive, preventive, and personalized medicine

Matúš Dohál[1]*, Igor Porvazník[2,3], Ivan Solovič[2,3] and Juraj Mokrý[4]

[1]Biomedical Centre Martin, Jessenius Faculty of Medicine in Martin, Comenius University in Bratislava, Martin, Slovakia, [2]National Institute of Tuberculosis, Lung Diseases and Thoracic Surgery, Vyšné Hágy, Slovakia, [3]Faculty of Health, Catholic University in Ružomberok, Ružomberok, Slovakia, [4]Department of Pharmacology, Jessenius Faculty of Medicine in Martin, Comenius University in Bratislava, Martin, Slovakia

Tuberculosis is a major global health issue, with approximately 10 million people falling ill and 1.4 million dying yearly. One of the most significant challenges to public health is the emergence of drug-resistant tuberculosis. For the last half-century, treating tuberculosis has adhered to a uniform management strategy in most patients. However, treatment ineffectiveness in some individuals with pulmonary tuberculosis presents a major challenge to the global tuberculosis control initiative. Unfavorable outcomes of tuberculosis treatment (including mortality, treatment failure, loss of follow-up, and unevaluated cases) may result in increased transmission of tuberculosis and the emergence of drug-resistant strains. Treatment failure may occur due to drug-resistant strains, non-adherence to medication, inadequate absorption of drugs, or low-quality healthcare. Identifying the underlying cause and adjusting the treatment accordingly to address treatment failure is important. This is where approaches such as artificial intelligence, genetic screening, and whole genome sequencing can play a critical role. In this review, we suggest a set of particular clinical applications of these approaches, which might have the potential to influence decisions regarding the clinical management of tuberculosis patients.

KEYWORDS

tuberculosis, PPPM, artificial intelligence, whole genome sequencing, treatment failure

1. Introduction

Tuberculosis (TB) is an infectious disease caused by the bacterium *Mycobacterium tuberculosis* (*Mtb*). The World Health Organization (WHO) formulated the End TB Strategy to achieve the ultimate eradication of TB. The strategy gained approval in 2014 from the 67th World Health Assembly and aims to terminate the global TB epidemic by 2035 (WHO, 2021). Initially, the strategy has aimed to diminish the number of individuals afflicted with TB by 90%, along with lowering the mortality rate by 95% and safeguarding families from the adverse outcomes of TB. Predictive, preventive, and personalized medicine (PPPM) can significantly contribute to achieving this goal (Sadkovsky et al., 2014; Khan and Das, 2022). This approach emphasizes the use of advanced technologies and data analysis to predict an individual's susceptibility to a disease, prevent its onset, and personalize treatment to optimize expected outcomes (Huang et al., 2022). In the case of TB, PPPM plays an important role in several ways:

1. Predictive medicine in the context of TB refers to the application of data analysis and advanced screening techniques to identify individuals with a high probability of contracting TB. This strategy can also predict the risk of treatment failure and improve TB management strategies. Predictive models are developed using various data sources, such as clinical, genetic, and environmental data (MacNeil et al., 2019; Martinez et al., 2020).
2. Preventive medicine involves strategies to prevent the onset of a disease. Various prophylactic measures can be implemented in the management of TB and prevention of the development of active TB. The most common is the use of the Bacillus Calmette-Guérin (BCG) vaccine. Other preventive measures include identifying and treating latent TB infection (LTBI) in individuals who have been exposed to *Mtb* but have not yet developed active TB (Pooransingh and Sakhamuri, 2020; Berrocal-Almanza et al., 2022; Migliori et al., 2022).
3. Personalized (precision) medicine refers to the approach of tailoring medical treatment to individual patients by considering their unique traits and requirements. In TB, personalized medicine is mostly used to optimize treatment regimens for patients based on *Mtb* resistance and individual genetic variations in TB patients in responding to drugs (such as drug metabolism efficacy; Joshi, 2011). Many studies have shown an association between the genotype of *Mtb* and a higher risk of developing resistance. For example, the Beijing lineage is currently considered the most prevalent among multidrug-resistant (MDR) strains (Zhou et al., 2017; Karmakar et al., 2019; Bakuła et al., 2023). Also, *Mtb* strains of this lineage are predominantly linked to active TB and carry an elevated risk of treatment failure (Keikha and Majidzadeh, 2021). Genetic testing can identify patients with a higher risk of acquiring drug-resistant TB or experiencing adverse effects, and the treatment regimen can be customized accordingly (Richardson et al., 2018). The treatment regimens can be tailored based on a patient's clinical characteristics, such as age, alcoholism, anaemia, and HIV co-infection, as well as sodium, iron, and albumin deficiency (Resende and dos Santos-Neto, 2015). In addition, measurement of plasma concentrations of anti-tuberculosis can be implemented in adjusting the doses of respective drugs in case of various interactions or individual discrepancies despite using their recommended doses (Pršo et al., 2023).

This literature review includes the findings of the latest studies aimed at PPPM strategies, including artificial intelligence (AI), genetic screening, microRNA (miRNA) and whole genome sequencing (WGS). Importantly, we explore the possibility of applying these approaches in enhancing TB diagnosis, treatment, and prevention by identifying individuals at high risk, preventing the spread of the disease, and personalizing treatment regimens to individual patients.

2. Transforming tuberculosis care with artificial intelligence-powered PPPM

Identifying and treating individuals at high risk of TB infection or disease progression are currently considered the most cost-effective measures for TB control and prevention (Kielmann et al., 2020). Among the tools available for these purposes, the latest analytical tools are currently demonstrating the greatest efficacy. Out of all the available analytical instruments, artificial intelligence (AI) is considered the most potent and encouraging for humanity. AI employs mathematical techniques such as 'machine learning' to learn patterns in training data and then applies this knowledge to make decisions when similar patterns are detected in new data (Silver et al., 2017; Fitzpatrick et al., 2020). Simultaneous advancements in information technology (IT) infrastructure and the processing power of mobile computing have created optimism that AI could offer possibilities to tackle health issues also in low- and middle-income countries (LMICs; Wahl et al., 2018).

In TB screening, chest radiography is recommended and the most preferred method globally (WHO, 2021; Moodley et al., 2022). Despite its usefulness, the main constraint of using chest X-ray (CXR) for screening TB patients in low-resource, high-burden areas is the shortage of radiologists, which has led to its limited implementation (Pande et al., 2015). In 2021, the WHO revised its TB screening guidelines, suggesting computer-aided detection software to evaluate digital CXR for predicting the likelihood of TB-related signs. This leads to better diagnostic decision-making, screening, and triaging TB in individuals aged 15 years and above (WHO, 2022). Over the past decade, AI-assisted diagnostic systems have progressed and advanced rapidly. Various medical-image-analyzing AI algorithms based on deep learning and deep convolutional neural networks (DCNNs), have been utilized for interpreting radiographs (Lakhani and Sundaram, 2017). A recent study highlighted the potential of a deep learning web-based diagnostic assistant in the prediction of TB in HIV-positive patients without the need for advanced radiological expertise (Rajpurkar et al., 2020). Acharya and colleagues created a normalization-free deep learning network model that enables the diagnosis and classification of TB with a sensitivity and specificity of 91.81 and 98.42%, respectively, on a dataset containing multiple classes. In addition, the model achieves an accuracy of 96% for binary classification (Acharya et al., 2022). The most extensive study using five commercial AI algorithms (AD4TB, InferRead DR, Lunit INSIGHT CXR, JF CXR-1, qXR) was performed in Bangladesh. Furthermore, aside from the fact that all the algorithms demonstrated a sensitivity of over 90%, the findings of the investigation revealed that utilizing these tools can potentially diminish the need for costly molecular diagnostic tests (e.g., Xpert MTB/RIF, Cepheid, United States) by up to 50% (Qin et al., 2021). The DCNN algorithm ResNet exhibited exceptional performance in the timely detection of active TB, a critical factor in managing the alarming increase in TB incidence (Nijiati et al., 2022). The deep learning method was utilized to distinguish between TB, COVID-19, and lung adenocarcinoma in patients with abnormal CXRs. The findings demonstrated a significant level of sensitivity and highlighted the potential utilization of AI methodologies to diagnose emerging respiratory infections (Feng et al., 2021; Yoo et al., 2021). Numerous research studies have been conducted to create AI predictive models that can differentiate between susceptible TB and multidrug-resistant TB using CXRs. The results indicate variable performance, with the area under the curve (AUC) values ranging from 0.74 to 0.85 (Jaeger et al., 2018; Karki et al., 2021). In addition, portable X-rays (MINE 2 HDT, Gwangju, Republic of Korea; Xair FDR XD2000, Fujifilm Corporation, Tokyo, Japan; Delft Ultra, Delft Imaging Systems, Netherlands) are currently

available on the market, which have been confirmed to be useful in the search for active cases of TB in high-burden and rural areas (Vo et al., 2021; Odume et al., 2022). The Delft Ultra and Xair systems can integrate with software platforms that support AI-driven interpretation. Hence, the utilization of this tool can effectively contribute to the early detection of TB and facilitate the swift initiation of treatment. The potential hazard for medical personnel lies in their exposure to radiation, albeit in the case of portable X-rays, the risk is significantly diminished compared to that posed by a traditional apparatus (Kamal et al., 2023).

Coughing is another common symptom of pulmonary TB (Farina et al., 2022). AI algorithms can undergo training to analyze audio recordings of cough sounds and recognize patterns that are suggestive of TB infection. This method, referred to as "acoustic cough analysis," possesses immense potential as a non-invasive and cost-efficient technique for TB screening. The accuracy of cough monitoring achieved high accuracy, however, and AI methods for diagnosing TB depend on various factors such as the quality and diversity of the training data, the specific AI algorithms used, and the stage of development and validation of the methods (Botha et al., 2018; Pahar et al., 2021; Zimmer et al., 2022). Additionally, AI can assist in epidemiological monitoring by examining cough data obtained from diverse sources, including wearable devices or mobile applications. Through the analysis of cough patterns in particular regions or communities, health authorities can obtain valuable information regarding the prevalence of TB, identify areas at high risk, and allocate resources more efficiently (Huddart et al., 2023). Despite its potential, the utilization of acoustic cough analysis and artificial intelligence (AI) in diagnosing and managing TB is currently in the research and development stage. Continuous studies and collaborations involving medicine, machine learning, and public health experts are essential to enhance and validate these methodologies. Addressing challenges such as personal data, standardization of cough recording protocols, and equitable access to AI technologies are crucial for their widespread implementation.

AI can predict the onset of TB and assess the efficacy of treatment by analyzing patient data such as demographics, medical history, and biomarkers. Asad et al. (2020) employed a machine learning model to predict the likelihood of treatment failure by analyzing various factors, such as social and health-related attributes. Similarly, Samson Balogun et al. (2021) tested 5 different machine learning models that performed well in classifying the TB treatment outcome (ranging between 67.5 and 73.4%). The latest research by Liao and colleagues has emphasized the potential of AI in anticipating side effects associated with the treatment of TB. The findings show that AI can identify acute hepatitis at an early stage in TB patients (based on levels of serum alanine aminotransferase, aspartate aminotransferase and total bilirubin), and also predict acute respiratory failure or death and may assist in clinical decision-making before these adverse effects occur (Liao et al., 2023). Moreover, Larkins-Ford et al. developed a mathematical model including a series of criteria to determine what drug combinations must be met for effective treatments when administered as three- or four-drug cocktails. This method can be used in the development of novel regimens, including twelve commonly used anti-TB drugs, to narrow down the potential combinations for subsequent pharmacokinetic/pharmacodynamic and preclinical studies (Larkins-Ford et al., 2022). To enhance medication adherence monitoring in TB patients, Sekandi et al. developed an AI model using video images of TB medication intake from Uganda and the rest of Africa. Their results can significantly contribute to determining whether the individuals have taken the pill or not, particularly in developing countries (Sekandi et al., 2023). It's important to note that while AI can be a valuable tool in predicting TB onset and assessing treatment efficacy, it should always be used in conjunction with clinical expertise and human decision-making. AI models should be continuously validated and updated with new data to ensure their accuracy and reliability in real-world scenarios.

AI can also play an important role in TB prevention by helping to identify and track TB cases and predict outbreaks. Mandal et al. used AI algorithms to predict TB risk among TB patients' household contacts in India. They found that the algorithm was able to accurately predict the risk of TB based on demographic and clinical data, including age, sex, body mass index, and history of exposure to TB (Mandal et al., 2020). During the COVID-19 pandemic, there was a significant increase in the development and deployment of AI models for digital contact tracing (Haneya et al., 2021; Almotairi et al., 2023). These models were used to track the spread of the virus and identify individuals who may have been exposed to the virus, allowing faster and more effective tracing. The success of these models has highlighted the potential of AI for tracking other infectious diseases, including TB (Shahroz et al., 2021).

In summary, AI-driven methodologies, encompassing deep learning and other conventional machine learning techniques employed in the context of TB, offer a self-directed, convenient, and time-efficient approach to enhance diagnostic efficacy and precision, surpassing the performance of radiologists and other medical personnel (Figure 1). Nevertheless, the clinical applicability of these approaches requires further clarification, while challenges such as model reproducibility and data standardization need to be effectively tackled.

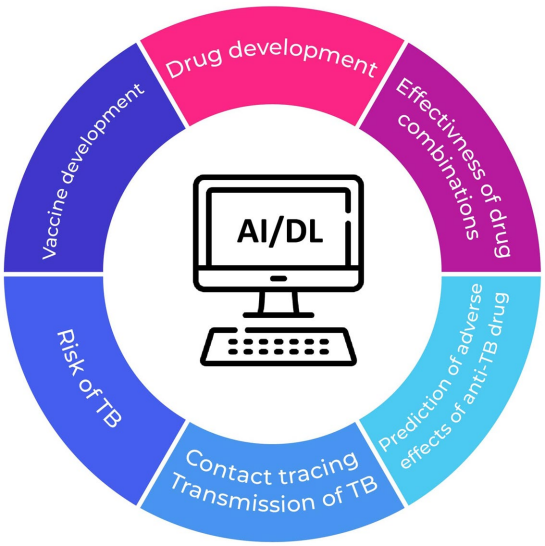

FIGURE 1
Potential applications of AI in preventing TB and mitigating the risk of treatment failure.

3. Utility of genetic screening and miRNA in PPPM for TB

3.1. Detecting particular mutations and miRNAs to predict and prevent active TB

Genetic screening can play a significant role in the management of TB. This approach can help identify individuals who are at higher risk of developing TB and personalize treatment regimens for individuals who have already been diagnosed with TB (Yan et al., 2022). The susceptibility of the host to TB has been linked to numerous genetic polymorphisms (Aravindan, 2019). Despite prior research linking several genetic polymorphisms to TB susceptibility, recent studies have identified numerous gene variations and microRNA (miRNA) biomarkers strongly associated with the risk of TB as well as the efficacy of treatment.

To enable more precise intervention in TB, it is crucial to identify biomarkers and genetic variants that can accurately predict the risk of developing active disease from latent TB infection (LTBI), as well as the progression of the infection. It is well-established that genetic factors in the host play a crucial role in the development of active TB. The majority of studies investigating the genes associated with immunity, including DC-SIGN, TLR1/2, vitamin D receptor, tumour necrosis factor, interleukin 1β, interferon γ, and HLA II molecules (Azad et al., 2012; Tervi et al., 2023). Moreover, Zhang et al. investigated the association between individual single nucleotide polymorphisms (SNPs) located within the rs1135216 and rs1057141 in the transporter-associated antigen processing gene (*TAP*)*1*, as well as rs2228396 in *TAP2*, and the likelihood of developing of pulmonary TB. According to their findings, rs1057141 may serve as a genetic indicator of decreased risk for TB in individuals aged 60 or older, whereas rs1135216 may be a potential genetic indicator for those under the age of 60 (Zhang et al., 2015). Xing et al. (2021) found a relationship between polymorphisms in cytochrome P450 (CYP450) and TB susceptibility. *CYP2C8* and *CYP2E1* variants were linked to a higher susceptibility to TB, implying the identification of these variants could be critical in defining new therapeutic strategies for chemoprevention. Recently, genetic variants in the cytokine genes (*IFGN*, *IL-12*, *IL14*, *TNFB,* and *IL1RA*) and transporter associated with *TAP* were associated with the susceptibility to pulmonary TB and genetic variants in *LIA4H*, *P2RX7*, *DCSIGN,* and *SP110* associated with susceptibility to LTBI (Abhimanyu et al., 2023; Lu et al., 2023). While these studies make valuable contributions to expanding the understanding of the genetic basis of PTB and EPTB manifestations, further research is warranted with larger sample sizes and diverse populations. Moreover, the identification of a whole-blood-based host genetic signature comprising four transcripts that predict progression to TB is promising and represents a big step forward in the personalization of TB treatment. This simple PCR test may also help predict TB transmission (Suliman et al., 2018).

The results of Xin et al. (2022) showed a possible correlation in the prediction of the development of active TB from LTBI with circulating miRNA hsa-miR-451a levels. The function of certain additional miRNAs (e.g., 146a, 149) in the risk of active TB progression has been elucidated; however, these studies were conducted with restricted sample sizes (Li et al., 2011; Zhang et al., 2015; Sinigaglia et al., 2020). Similarly, (Angria et al., 2022) discovered that assessing the expression of miRNA-29a-3p could serve as a screening method for individuals with LTBI.A recent study revealed the potential of miRNAs in predicting extrapulmonary forms of TB. The hsa-mir-425-5p miRNA expression levels in patients with lymph node TB were significantly higher compared to the other groups (including patients with LTBI and pulmonary TB; Massi et al., 2023). Research focusing on specific miRNA profiles for distinguishing latent LTBI, extrapulmonary- and pulmonary TB remains relatively limited but holds significant importance. This is because diagnosing extrapulmonary TB can be challenging in clinical settings, as conventional methods like AFB smear and culture are not always effective. Moreover, paucibacillary samples such as cerebrospinal fluid and aspirates are commonly encountered, contributing to milder forms of infection. Further exploration of miRNA in this context is expected to yield substantial benefits, particularly in the development of miRNA-based vaccines, biomarkers, and host-directed therapeutic approaches.

In the PPPM context, preventing excessive inflammation and death in TB patients is necessary. miRNA-27b-3p, miRNA-223-3p, and miR-99b-5p may play an important role in achieving these goals (Sinigaglia et al., 2020). By inhibiting the production of pro-inflammatory agents and nuclear factor kappa B activity, miR-27b-3p helps to decrease bacterial load and prevent excessive inflammation during *Mtb* infection (Liang et al., 2018). Lower miR-99b-5p expression results in decreased bacterial proliferation in dendritic cells and the enhancement of several pro-inflammatory cytokines, including IL-6, IL-12, and IL-1β (Singh and Goyal, 2013). We believe that identifying relevant miRNAs whose expression consistently correlates with the onset of active TB or divergent response to treatments could hold considerable clinical significance. Their collective efficacy lies in establishing routine diagnostic screening tests that exhibit substantial predictive capability, thereby enhancing the accuracy of existing tests predominantly reliant on the tuberculin skin test or interferon-gamma release assay (IGRA) which do not have a high accuracy for predicting active TB based on WHO recommendations (Gualano et al., 2019).

Integrating genetic screening and miRNA analysis can provide a more comprehensive understanding of TB pathogenesis and individualized patient management. By identifying genetic variants associated with TB susceptibility and miRNAs related to disease progression or treatment response, researchers can develop predictive models to guide personalized treatment decisions. This approach may also help identify novel therapeutic targets for drug development.

3.2. Advantages of genetic analysis in the individualized treatment of TB

In personalized medicine, pharmacogenetics and pharmacogenomics are two emerging fields that play a critical role in predicting individual responses to medication. Research has shown that differences in pharmacokinetic (PK) vulnerability to drugs among individuals contributed to some unfavorable outcomes, even in patients who followed the prescribed dosage regimen. This finding challenges the traditional idea that treatment failure, relapse, and the development of antimicrobial resistance are mostly attributed to non-adherence, thereby highlighting the need for genetic screening in TB patients (Sloan et al., 2017; Khan et al., 2022).

Several studies have also indicated a link between different genetic mutations and alterations in the plasma concentrations and adverse

effects of first- and second-line anti-tuberculosis drugs in TB patients. Adverse reactions to the anti-tuberculosis drugs frequently include hepatotoxicity, severe cutaneous reactions (e.g., Stevens-Johnson syndrome, toxic epidermal necrolysis, acute generalized exanthematous pustulosis, maculopapular exanthema), queasiness, vomiting, purpura, lethargy, dizziness, abdominal discomfort, rare cases of osteomalacia, hyperuricaemia, rare incidents of acute kidney failure, rare instances of anemia, gastrointestinal or neurological disorders (Gholami et al., 2006; Tostmann et al., 2008; World Health Organization, 2010; Yu et al., 2017; Minardi et al., 2021). Hepatotoxicity is the most critical (Huai et al., 2019). Genetic factors have been recently widely studied to predict the risk of developing a drug-induced liver injury. At present, liver toxicity has been predominantly linked with variations in drug metabolism genes such as N-Acetyltransferase 2 (*NAT2*), *CYP2E1*, pregnane X receptor (*PXR*), and glutathione S-transferase (*GST*; Roy et al., 2001; Leiro et al., 2008). A better understanding of these mutations could facilitate in designing and developing a more effective personalized treatment for TB (Meitei et al., 2022). Lyu et al. (2019) described a significant correlation between single nucleotide polymorphisms (SNPs) in calcium signaling-related genes, specifically bradykinin receptor B2 (*BDKRB2*) and transforming growth factor beta 2 (*TGFB2*), and the onset of liver injury induced by anti-tuberculosis drugs. Moreover, performing genotyping on the *ABCB11* gene, which encodes the bile salt export pump (BSEP), could offer advantages for personalizing anti-tuberculosis treatment regimens (Cavaco et al., 2022). Regarding rifampicin, alterations in the solute carrier organic anion transporter family member 1B1 gene (*SLCO1B1*) have been extensively studied (Khan et al., 2022). Previous research showed that a genetic variant known as rs4149056 might decrease the expression of *SLCO1B1*, resulting in reduced uptake/transport activity of organic anion-transporting polypeptide 1B1 (*OATP1B1*) and higher levels of rifampicin in the bloodstream. Genetic screening of this variant may help to predict the increased rifampicin concentration (Niemi et al., 2011; Allegra et al., 2017). In contrast, patients carrying the rs11045819 or rs2306283 variant in *SLCO1B1* reached notably lower plasma levels of rifampicin compared to those with the wild-type genotype (Weiner et al., 2010; Dompreh et al., 2018). Similarly, Weiner et al. examined the impact of the –11187G > A mutation in the *SLCO1B1* gene on the pharmacokinetics of the second-line anti-tuberculosis drug moxifloxacin. The authors observed that patients carrying the variant exhibited significantly elevated Cmax values. This increase in the drug's plasmatic concentration may contribute to the adverse effects of moxifloxacin, especially the prolongation of QT interval (Weiner et al., 2018). Song et al. (2013) found the c.-22263A > G mutation in the carboxylesterase (*CES2*) gene and described its correlation with elevated concentrations of rifampicin in the plasma of TB patients. Concerning isoniazid, the first step in the metabolism of this drug involves the non-inducible hepatic and intestinal enzyme NAT type 2, which is encoded by a highly polymorphic gene called the *NAT2* gene (Khan et al., 2013). Previous studies on genotyping the *NAT2* as a pharmacogenetic biomarker for the personalization of isoniazid therapeutic dosage revealed a direct correlation between the plasmatic concentration and the *NAT2* allele (Kinzig-Schippers et al., 2005; Fukino et al., 2008). In addition, the gene polymorphisms in *NAT2* have consistently demonstrated an association with an elevated risk of isoniazid-induced hepatotoxicity in various studies (Jaramillo-Valverde et al., 2022; Masiphephethu et al., 2022; Mohamed Noor et al., 2022). On the contrary, the study conducted by Kim et al. yielded results indicating that severe cutaneous adverse reactions associated with first-line anti-tuberculosis drugs are not linked to polymorphisms in *NAT2* or *CYP2E1* genes. However, these reactions are indeed associated with mutations in the *CYP2C9* and *CYP2C19* genes (Kim et al., 2011).

Among patients receiving drug-resistant TB therapy that includes aminoglycoside antibiotics, the most severe potential adverse effect is ototoxicity (Selimoglu, 2007). Previous studies have indicated that variations in mitochondrial DNA, particularly in the 12S rRNA genes, may be linked to increased susceptibility and toxicity to these antibiotics (Stocco et al., 2020). The m1555A > G and m.1494C > T variants in the 12 s rRNA gene have been extensively investigated and were conclusively associated with an increased risk of developing hearing loss after exposure to aminoglycosides (Guan, 2011; Zhang et al., 2013). It is hypothesized that several additional mitochondrial variations may eventually be identified as key contributors to the development of hearing loss. However, the complete biochemical mechanisms underlying this phenomenon have yet to be fully understood. These findings suggest that personalized antibiotic prescribing based on the patient's 12 s rRNA genotype has the potential to lower the incidence of aminoglycoside-induced hearing loss in patients with drug-resistant TB (McDermott et al., 2022).

We recommend screening the established and well-defined genetic polymorphisms in the *CYP2E1* and *NAT2* genes, as their effects have been confirmed through robust association studies involving large population cohorts. As demonstrated in this review, ongoing research is investigating the association between polymorphisms in numerous candidate genes and adverse effects of anti-TB drugs. However, it is important to note that these associations are supported by limited studies with smaller sample sizes, often conducted in highly specific patient populations. Implementing genotyping tests as a part of a personalized medicine approach for TB treatment in high-endemic regions could be a crucial step toward achieving the "End-TB" goal by 2025 (Khan and Das, 2022). However, it's important to emphasize that the inclusion of genetic screening for these factors may depend on several factors, including the availability of tests, cost-effectiveness, and the specific adverse effects of concern in the local population. Additionally, individual patient characteristics, such as liver function and comorbidities, should also be taken into consideration when assessing the risk of adverse effects and determining personalized treatment plans. Further investigation and consultation with experts in pharmacogenetics and personalized medicine are recommended to obtain the most relevant and up-to-date information for a particular clinical context (Sharma et al., 2022).

4. Unlocking the potential of next-generation sequencing in the context of PPPM in TB

Next,-generation sequencing (NGS) has emerged as a powerful tool for understanding the genetic background of various infectious diseases, including TB (Gordon et al., 2021). In the context of PPPM, NGS can transform and accelerate the delivery of personalized treatment to patients affected by TB, thus revolutionizing the way TB is diagnosed and treated.

A more comprehensive drug susceptibility profile is needed to design an effective treatment plan for patients with drug-resistant TB (WHO, 2022). WGS has been identified as a highly promising tool for this particular purpose (Figure 2; Gröschel et al., 2018; Wu et al., 2020; Dohál et al., 2022). Cox et al. recently employed WGS to assess the accuracy of treatment regimens (derived from standard drug susceptibility testing and clinical information) in individuals with drug-resistant TB. Overall, 305 (24%) patients had MDR/rifampicin resistant (RR)-TB with second-line TB drug resistance, where the availability of WGS-derived drug susceptibility testing (DST) would have enabled more effective treatment personalization for these patients, such as reducing drug dosages or removing ineffective drugs (Cox et al., 2022; Xiao et al., 2023). Similarly, the results of Korhonen demonstrated that WGS could aid in the selection of optimal treatment regimens in the future, primarily for patients with resistance to ethambutol (Korhonen et al., 2022). The application of WGS in routine clinical practice also enables rapid identification of isoniazid monoresistance, reducing delays in treatment decisions and initiating WHO-recommended treatment for isoniazid-resistant TB (Park et al., 2022). In settings with a low incidence of TB, WGS reduced the time required for appropriate treatment modification, thus decreasing the expenses associated with hospitalization and treatment (Mugwagwa et al., 2021).

Bedaquiline and pretomanid, novel oral anti-tuberculosis drugs, have demosntrated excellent efficacy against both drug-susceptible and drug-resistant strains of *Mtb* and have been recommended by WHO (2022) as "reserved drug" for the treatment of MDR. As primary resistance to bedaquiline has been reported for several years, determining the sensitivity is essential for every patient being considered for a treatment regimen that includes this drug (Villellas et al., 2017). According to Hu et al. (2023) a combination of phenotypic drug sensitivity testing (pDST) and WGS was beneficial for the timely diagnosis and personalized treatment of bedaquiline-resistant TB. Similarly, as there is a lack of defined cutoffs and critical concentrations for conducting pDST of pretomanid, it is crucial to integrate conventional methods with WGS in determining its resistance (Bateson et al., 2022). In the past, the major limitation in using the WGS approach was the reliance on limited available mutation knowledge only. To overcome this limitation, WHO has developed a catalog of *Mtb* mutations and their association with phenotypic drug resistance to support personalized medicine in TB treatment. The catalog provides a reference standard for the interpretation of mutations conferring resistance to all first-line and a variety of second-line drugs (Walker et al., 2022b). Due to the complex bioinformatics analysis involved in processing WGS data, various non-commercial, freely available, and user-friendly software tools have been developed (such as TB Profiler, Mykrobe Predictor, TGS-TB, PhyResSE, and KvarQ). These software solutions enable medical personnel to rapidly diagnose TB, and interpret comprehensive drug resistance profiles directly from raw sequencing data (FASTQ files; Steiner et al., 2014; Feuerriegel et al., 2015; Sekizuka et al., 2015; Phelan et al., 2019).

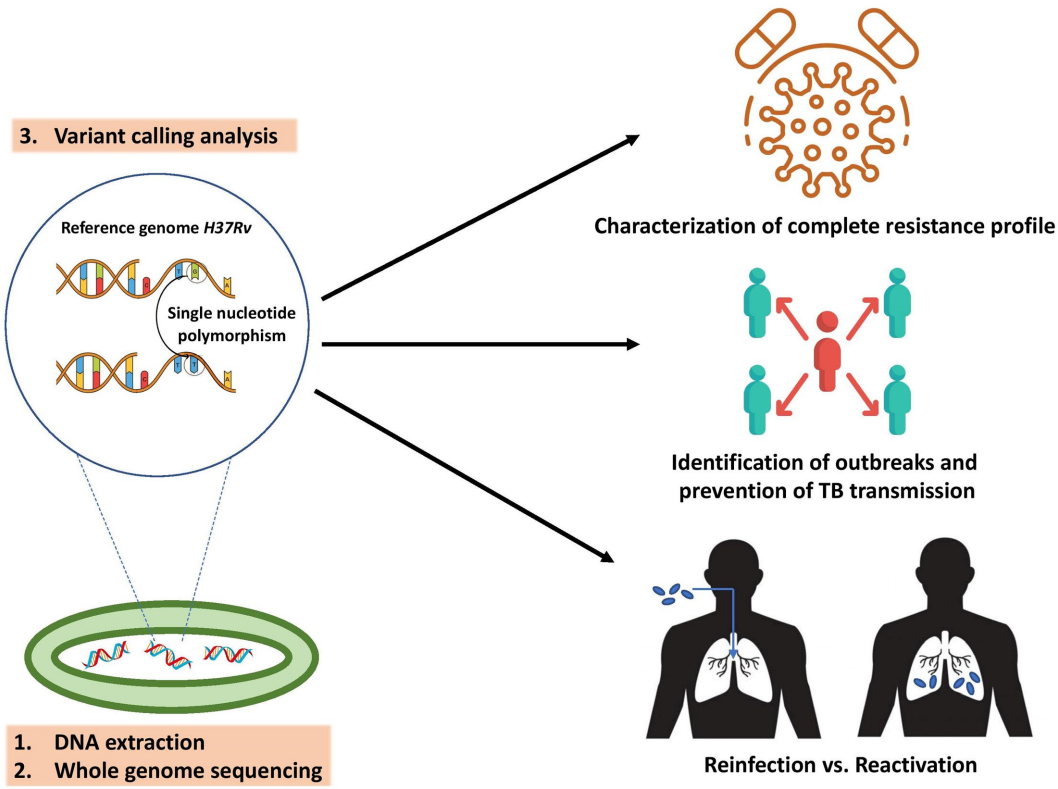

FIGURE 2
Key applications of *M. tuberculosis* WGS in PPPM include characterization of complete resistance profile to reach the highest treatment efficacy, determination of transmission chains and outbreaks to prevent the spread of TB, and distinguishing the cause of TB recurrence to guide TB control and treatment.

The recurrence of TB is another factor that can complicate treatment individualization in TB patients (Dooley et al., 2011). Distinguishing the cause of TB recurrence is crucial to guide TB control and treatment. The potential of WGS lies in its ability to differentiate between relapse and reinfection, the two distinct mechanisms underlying TB recurrence (Nikolenka et al., 2021). WGS demonstrated its capability to differentiate between treatment failure (with the necessity to use a new drug regimen) and reinfection with a new strain in clinical trials evaluating novel anti-tuberculosis drugs (Gillespie et al., 2014). Another study utilizing WGS demonstrated a relatively high incidence of fluoroquinolone resistance during the second episode of TB relapse. These findings lead to caution when using fluoroquinolones for treating patients with recurrent TB and suggest the use of DST results for any treatment decisions (He et al., 2023).

To personalize TB treatment, it is crucial to consider if a mutation accurately identifies a strain with a higher minimum inhibitory concentration as well as if this mutation is linked to treatment failure (Chen et al., 2020). Recently, Domínguez et al. (2023) reviewed studies linking the treatment outcome with the presence of a specific mutation encoding resistance to first- and second-line anti-tuberculosis drugs. We consider these data to be very important, as they could prompt the clinician to consider a change in the treatment regimen in patients showing these mutations associated with resistance.

The utilization of WGS can also facilitate the identification and prediction of TB transmission. Recent research has demonstrated that the application of this technology enables the identification of transmission hotspots, both in countries with a low and high incidence of TB (Alaridah et al., 2019; Asare et al., 2020; Gordon et al., 2021; Dale et al., 2022). To prevent the spread of TB, it is crucial to describe the transmission chains in particular communities. Prisons are widely acknowledged to have an exceptionally high burden of TB (28 times greater) compared to the general population, serving as a reservoir for persistent MDR TB (Witbooi and Vyambwera, 2017; Anselmo et al., 2023). The recent findings demonstrated that 43 and 45.4% of TB cases among prisoners were due to direct transmission (Anselmo et al., 2023; Sanabria et al., 2023). WGS-based screening for TB before and after the transfer of prisoners could contribute to preventing TB transmission and reducing the number of TB cases. Migrants are another at-risk demographic group, accounting for up to 40–60% of TB cases in many high-income countries (Iñigo et al., 2013; Ospina et al., 2016). WGS-based cross-border surveillance is essential to present TB epidemiological monitoring to differentiate between imported and recent transmission cases (Abascal et al., 2019). Overall, TB tracing with WGS may be an effective strategy in the treatment and/or chemoprophylaxis of close contacts.

One of the limitations of WGS is its reliance on obtaining high-quality genomic DNA from cultured *Mtb* isolates. The cultivation process can take several weeks, presenting an additional disadvantage of this technology from a clinical perspective (Dookie et al., 2022; Walker et al., 2022a). Increasing interest is focused on culture-free target-based NGS (Cabibbe et al., 2020). The use of direct sputum samples for analysis makes targeted NGS an attractive method, primarily because of its capability to provide results more rapidly (Mansoor et al., 2023). Recently, several studies have demonstrated the efficacy of culture-free targeted NGS for the detection of drug-resistant *Mtb* using Deeplex Myc-TB (Genoscreen, Lille, France). This assay achieved excellent sensitivity and specificity in the detection of resistance to 13 anti-tuberculosis drugs compared to pDST and could be a breakthrough in the rapid diagnosis of MDR TB in routine practice (Bonnet et al., 2021; Feuerriegel et al., 2021; Jouet et al., 2021). Another benefit of this assay is its ability to be utilized in conjunction with nanopore-based DNA sequencing instruments, such as the MinION (Oxford Nanopore Technologies (ONT), Oxford, UK). This characteristic makes it especially advantageous in settings with limited resources (Cabibbe et al., 2020). These sequencing instruments exhibit portability, resilience, and cost-effectiveness, which renders them suitable for potential use in point-of-care settings to perform targeted NGS (Dippenaar et al., 2022; Hall et al., 2023). This capability has the potential to revolutionize TB DST and personalize the treatment process. Moreover, Sibandze et al. conducted focused NGS to detect drug resistance directly from stool samples provided by individuals with TB. This offers a valuable opportunity to gather essential diagnostic information for TB patients who encounter challenges in providing respiratory specimens (Sibandze et al., 2022).

The choice of method depends on the specific research or diagnostic goals, as well as the available resources and expertise. The field of NGS is continually evolving, and new methods and technologies are being developed to improve our understanding and management of TB.

5. Conclusion

PPPM can help improve TB prevention, diagnosis, and treatment by considering individual differences in risk and response to interventions. Adopting this approach can also help engage patients and communities in managing TB, leading to better health outcomes and reduced disease burden. Currently, the most promising strategies in PPPM for TB include the use of AI, genetic screening, and NGS.

More specifically, AI has the potential to assist in the prediction and diagnosis of TB in developing countries where advanced radiological expertise is lacking. Additionally, this technology may be useful in predicting the effectiveness of treatment regimens and acute adverse effects during therapy and tracking TB cases. Genetic screening can also have a crucial function in anticipating active TB and ensuring the efficacy of therapy.

Recently, a variety of mutations in genes related to immune function, CYP450, and certain miRNAs linked to LTBI reactivation have been identified. Furthermore, identifying mutations in certain genes can predict the likelihood of adverse reactions and the efficacy of treatment. Based on these assumptions, it may be worth considering the clinical relevance of genetic screening and its potential application in routine diagnostics.

The development of novel molecular diagnostic methods has also made a huge contribution to the personalization of therapy and the prevention of TB transmission. Utilizing the full potential of NGS, comprehensive insights into the phylogenetic lineage of infecting strains can provide clinicians with valuable information regarding the likelihood of the strain developing additional drug resistance. These innovative approaches in TB treatment signify a new era in the management of MDR-TB that will aid in mitigating treatment failure and ongoing transmission.

In contrast to the aforementioned advantages, there are several potential knowledge gaps and areas for future research regarding

the management of TB and the roles of AI, genetic screening, and WGS. The successful integration of AI into clinical practice for TB management requires a holistic approach that addresses technical, regulatory, educational, and usability aspects. Research in these areas can pave the way for more effective and widespread use of AI to combat TB and improve patient outcomes. In the realm of genetic screening for TB management, research should focus on understanding population-specific variations, and assessing the cost-effectiveness of these screening methods. It's essential to determine the accuracy of genetic markers, integrate them effectively into clinical decision-making, and provide ethical patient counseling. Additionally, research should explore the impact on healthcare systems and potential contributions to drug development. Global collaboration and data sharing are also vital for advancing this field. In summary, addressing these knowledge gaps and conducting research in these areas can contribute to more effective TB control and management strategies, ultimately reducing the global burden of this disease.

Author contributions

MD wrote the manuscript. IS and IP edited the manuscript. JM supervised and finalized the manuscript. All authors contributed to the study's conception and design, read, and approved the final manuscript.

Funding

This research was funded by grant APVV-18-0084, grant APVV-22-0342, and grant VEGA-1/0093/22.

Acknowledgments

We thank Peter Buran for contributing to the preparation of figure illustrations and all the reviewers who participate in the review.

Conflict of interest

The authors declare that the research was conducted in the absence of any commercial or financial relationships that could be construed as a potential conflict of interest.

Publisher's note

References

Abascal, E., Pérez-Lago, L., Martínez-Lirola, M., Chiner-Oms, Á., Herranz, M., Chaoui, I., et al. (2019). Whole genome sequencing-based analysis of tuberculosis (TB) in migrants: rapid tools for crossborder surveillance and to distinguish between recent transmission in the host country and new importations. *Eur. Secur.* 24:1800005. doi: 10.2807/1560-7917.ES.2019.24.4.1800005/CITE/PLAINTEXT

Abhimanyu, B. M., Giri, A., and Varma-Basil, M. (2023). Comparative genetic association analysis of human genetic susceptibility to pulmonary and lymph node tuberculosis. *Genes* 14:207. doi: 10.3390/GENES14010207

Acharya, V., Dhiman, G., Prakasha, K., Bahadur, P., Choraria, A., Sushobhitha, M., et al. (2022). AI-assisted tuberculosis detection and classification from chest X-rays using a deep learning normalization-free network model. *Comput. Intell. Neurosci.* 2022:2399428. doi: 10.1155/2022/2399428

Alaridah, N., Hallbäck, E. T., Tångrot, J., Winqvist, N., Sturegård, E., Florén-Johansson, K., et al. (2019). Transmission dynamics study of tuberculosis isolates with whole genome sequencing in southern Sweden. *Sci. Rep.* 9:4931. doi: 10.1038/s41598-019-39971-z

Allegra, S., Fatiguso, G., Calcagno, A., Baietto, L., Motta, I., Favata, F., et al. (2017). Role of vitamin D pathway gene polymorphisms on rifampicin plasma and intracellular pharmacokinetics. *Pharmacogenomics* 18, 875–890. doi: 10.2217/PGS-2017-0176

Almotairi, K. H., Hussein, A. M., Abualigah, L., Abujayyab, S. K. M., Mahmoud, E. H., Ghanem, B. O., et al. (2023). Impact of artificial intelligence on COVID-19 pandemic: a survey of image processing, tracking of disease, prediction of outcomes, and computational medicine. *Big Data Cogn. Comput.* 7:11. doi: 10.3390/BDCC7010011

Angria, N., Massi, M. N., Bukhari, A., Djaharuddin, I., Jumadi, O., Ahmad, A., et al. (2022). Expression of miRNA-29a-3p and IFN-γ as biomarkers in active and latent pulmonary tuberculosis. *Ann. Med. Surg.* 83:104786. doi: 10.1016/J.AMSU.2022.104786

Anselmo, L. M. P., Gallo, J. F., Pinhata, J. M. W., Peronni, K. C., da Silva Junior, W. A., Ruy, P. C., et al. (2023). New insights on tuberculosis transmission dynamics and drug susceptibility profiles among the prison population in southern Brazil based on whole-genome sequencing. *Rev. Soc. Bras. Med. Trop.* 56:2023. doi: 10.1590/0037-8682-0181-2022

Aravindan, P. (2019). Host genetics and tuberculosis: theory of genetic polymorphism and tuberculosis. *Lung India* 36:244. doi: 10.4103/LUNGINDIA.LUNGINDIA_146_15

Asad, M., Mahmood, A., and Usman, M. (2020). A machine learning-based framework for predicting treatment failure in tuberculosis: a case study of six countries. *Tuberculosis (Edinb.)* 123:101944. doi: 10.1016/J.TUBE.2020.101944

Asare, P., Otchere, I. D., Bedeley, E., Brites, D., Loiseau, C., Baddoo, N. A., et al. (2020). Whole genome sequencing and spatial analysis identifies recent tuberculosis transmission hotspots in Ghana. *Front. Med.* 7:161. doi: 10.3389/FMED.2020.00161/FULL

Azad, A. K., Sadee, W., and Schlesinger, L. S. (2012). Innate immune gene polymorphisms in tuberculosis. *Infect. Immun.* 80, 3343–3359. doi: 10.1128/IAI.00443-12

Bakuła, Z., Marczak, M., Bluszcz, A., Proboszcz, M., Kościuch, J., Krenke, R., et al. (2023). Phylogenetic relationships of *Mycobacterium tuberculosis* isolates in Poland: the emergence of Beijing genotype among multidrug-resistant cases. *Front. Cell. Infect. Microbiol.* 13:1161905. doi: 10.3389/FCIMB.2023.1161905/BIBTEX

Bateson, A., Ortiz Canseco, J., Mchugh, T. D., Witney, A. A., Feuerriegel, S., Merker, M., et al. (2022). Ancient and recent differences in the intrinsic susceptibility of *Mycobacterium tuberculosis* complex to pretomanid. *J. Antimicrob. Chemother.* 77, 1685–1693. doi: 10.1093/JAC/DKAC070

Berrocal-Almanza, L. C., Harris, R. J., Collin, S. M., Muzyamba, M. C., Conroy, O. D., Mirza, A., et al. (2022). Effectiveness of nationwide programmatic testing and treatment for latent tuberculosis infection in migrants in England: a retrospective, population-based cohort study. *Lancet Public Health* 7, e305–e315. doi: 10.1016/S2468-2667(22)00031-7

Bonnet, I., Enouf, V., Morel, F., Ok, V., Jaffré, J., Jarlier, V., et al. (2021). A comprehensive evaluation of GeneLEAD VIII DNA platform combined to Deeplex Myc-TB® assay to detect in 8 days drug resistance to 13 antituberculous drugs and transmission of *Mycobacterium tuberculosis* complex directly from clinical samples. *Front. Cell. Infect. Microbiol.* 11:707244. doi: 10.3389/FCIMB.2021.707244

Botha, G. H. R., Theron, G., Warren, R. M., Klopper, M., Dheda, K., Van Helden, P. D., et al. (2018). Detection of tuberculosis by automatic cough sound analysis. *Physiol. Meas.* 39:045005. doi: 10.1088/1361-6579/AAB6D0

Cabibbe, A. M., Spitaleri, A., Battaglia, S., Colman, R. E., Suresh, A., Uplekar, S., et al. (2020). Application of targeted next-generation sequencing assay on a portable sequencing platform for culture-free detection of drug-resistant tuberculosis from clinical samples. *J. Clin. Microbiol.* 58, e00632–e00620. doi: 10.1128/JCM.00632-20

Cavaco, M. J., Alcobia, C., Oliveiros, B., Mesquita, L. A., Carvalho, A., Matos, F., et al. (2022). Clinical and genetic risk factors for drug-induced liver injury associated with anti-tuberculosis treatment—a study from patients of Portuguese health centers. *J. Pers. Med.* 12:790. doi: 10.3390/JPM12050790/S1

Chen, X., He, G., Lin, S., Wang, S., Sun, F., Chen, J., et al. (2020). Analysis of serial multidrug-resistant tuberculosis strains causing treatment failure and within-host evolution by whole-genome sequencing. *mSphere* 5, e00884–e00820. doi: 10.1128/MSPHERE.00884-20

Cox, H., Goig, G. A., Salaam-Dreyer, Z., Dippenaar, A., Reuter, A., Mohr-Holland, E., et al. (2022). Whole-genome sequencing has the potential to improve treatment for rifampicin-resistant tuberculosis in high-burden settings: a retrospective cohort study. *J. Clin. Microbiol.* 60:e0236221. doi: 10.1128/JCM.02362-21

Dale, K., Globan, M., Horan, K., Sherry, N., Ballard, S., Tay, E. L., et al. (2022). Whole genome sequencing for tuberculosis in Victoria, Australia: a genomic implementation study from 2017 to 2020. *Lancet Reg. Health West Pac.* 28:100556. doi: 10.1016/j.lanwpc.2022.100556

Dippenaar, A., Goossens, S. N., Grobbelaar, M., Oostvogels, S., Cuypers, B., Laukens, K., et al. (2022). Nanopore sequencing for *Mycobacterium tuberculosis*: a critical review of the literature, new developments, and future opportunities. *J. Clin. Microbiol.* 60:e0064621. doi: 10.1128/JCM.00646-21

Dohál, M., Dvořáková, V., Šperková, M., Pinková, M., Spitaleri, A., Norman, A., et al. (2022). Whole genome sequencing of multidrug-resistant *Mycobacterium tuberculosis* isolates collected in the Czech Republic, 2005-2020. *Sci. Rep.* 12:7149. doi: 10.1038/S41598-022-11287-5

Domínguez, J., Boeree, M. J., Cambau, E., Chesov, D., Conradie, F., Cox, V., et al. (2023). Clinical implications of molecular drug resistance testing for *Mycobacterium tuberculosis*: a 2023 TBnet/RESIST-TB consensus statement. *Lancet Infect. Dis.* 23, e122–e137. doi: 10.1016/S1473-3099(22)00875-1

Dompreh, A., Tang, X., Zhou, J., Yang, H., Topletz, A., Ahwireng, E. A., et al. (2018). Effect of genetic variation of NAT2 on isoniazid and SLCO1B1 and CES2 on rifampin pharmacokinetics in Ghanaian children with tuberculosis. *Antimicrob. Agents Chemother.* 62, e02099–e02017. doi: 10.1128/AAC.02099-17

Dookie, N., Khan, A., Padayatchi, N., and Naidoo, K. (2022). Application of next generation sequencing for diagnosis and clinical management of drug-resistant tuberculosis: updates on recent developments in the field. *Front. Microbiol.* 13:775030. doi: 10.3389/FMICB.2022.775030/BIBTEX

Dooley, K. E., Lahlou, O., Ghali, I., Knudsen, J., Elmessaoudi, M. D., Cherkaoui, I., et al. (2011). Risk factors for tuberculosis treatment failure, default, or relapse and outcomes of retreatment in Morocco. *BMC Public Health* 11, 1–7. doi: 10.1186/1471-2458-11-140/TABLES/2

Farina, E., D'Amore, C., Lancella, L., Boccuzzi, E., Ciofi degli Atti, M. L., Reale, A., et al. (2022). Alert sign and symptoms for the early diagnosis of pulmonary tuberculosis: analysis of patients followed by a tertiary pediatric hospital. *Ital. J. Pediatr.* 48, 90–98. doi: 10.1186/S13052-022-01288-5

Feng, Y., Wang, Y., Zeng, C., and Mao, H. (2021). Artificial intelligence and machine learning in chronic airway diseases: focus on asthma and chronic obstructive pulmonary disease. *Int. J. Med. Sci.* 18:2871. doi: 10.7150/IJMS.58191

Feuerriegel, S., Kohl, T. A., Utpatel, C., Andres, S., Maurer, F. P., Heyckendorf, J., et al. (2021). Rapid genomic first- and second-line drug resistance prediction from clinical *Mycobacterium tuberculosis* specimens using Deeplex-MycTB. *Eur. Respir. J.* 57:2001796. doi: 10.1183/13993003.01796-2020

Feuerriegel, S., Schleusener, V., Beckert, P., Kohl, T. A., Miotto, P., Cirillo, D. M., et al. (2015). PhyResSE: a web tool delineating *Mycobacterium tuberculosis* antibiotic resistance and lineage from whole-genome sequencing data. *J. Clin. Microbiol.* 53, 1908–1914. doi: 10.1128/JCM.00025-15

Fitzpatrick, F., Doherty, A., and Lacey, G. (2020). Using artificial intelligence in infection prevention. *Curr. Treat. Options Infect. Dis.* 12:135. doi: 10.1007/S40506-020-00216-7

Fukino, K., Sasaki, Y., Hirai, S., Nakamura, T., Hashimoto, M., Yamagishi, F., et al. (2008). Effects of N-acetyltransferase 2 (NAT2), CYP2E1 and glutathione-S- transferase (GST) genotypes on the serum concentrations of isoniazid and metabolites in tuberculosis patients. *J. Toxicol. Sci.* 33, 187–195. doi: 10.2131/jts.33.187

Gholami, K., Kamali, E., Hajiabdolbaghi, M., and Shalviri, G. (2006). Evaluation of anti-tuberculosis induced adverse reactions in hospitalized patients. *Pharm Pract (Granada)* 4, 134–138.

Gillespie, S. H., Crook, A. M., McHugh, T. D., Mendel, C. M., Meredith, S. K., Murray, S. R., et al. (2014). Four-month moxifloxacin-based regimens for drug-sensitive tuberculosis. *N. Engl. J. Med.* 371, 1577–1587. doi: 10.1056/NEJMOA1407426

Gordon, A. K., Marais, B., Walker, T. M., and Sintchenko, V. (2021). Clinical and public health utility of whole genome sequencing. *Int J Infect Dis* 113 Suppl, S40–S42. doi: 10.1016/j.ijid.2021.02.114

Gröschel, M. I., Walker, T. M., van der Werf, T. S., Lange, C., Niemann, S., and Merker, M. (2018). Pathogen-based precision medicine for drug-resistant tuberculosis. *PLoS Pathog.* 14:e1007297. doi: 10.1371/JOURNAL.PPAT.1007297

Gualano, G., Mencarini, P., Lauria, F. N., Palmieri, F., Mfinanga, S., Mwaba, P., et al. (2019). Tuberculin skin test – outdated or still useful for latent TB infection screening? *Int. J. Infect. Dis.* 80, S20–S22. doi: 10.1016/j.ijid.2019.01.048

Guan, M. X. (2011). Mitochondrial 12S rRNA mutations associated with aminoglycoside ototoxicity. *Mitochondrion* 11, 237–245. doi: 10.1016/J.MITO.2010.10.006

Hall, M. B., Rabodoarivelo, M. S., Koch, A., Dippenaar, A., George, S., Grobbelaar, M., et al. (2023). Evaluation of nanopore sequencing for *Mycobacterium tuberculosis* drug susceptibility testing and outbreak investigation: a genomic analysis. *Lancet Microbe* 4, e84–e92. doi: 10.1016/S2666-5247(22)00301-9

Haneya, H., Alkaf, D., Bajammal, F., and Brahimi, T. (2021). A meta-analysis of artificial intelligence applications for tracking COVID-19: the case of the U.A.E. *Procedia. Comput. Sci.* 194:180. doi: 10.1016/J.PROCS.2021.10.072

He, W., Tan, Y., Song, Z., Liu, B., Wang, Y., He, P., et al. (2023). Endogenous relapse and exogenous reinfection in recurrent pulmonary tuberculosis: a retrospective study revealed by whole genome sequencing. *Front. Microbiol.* 14:423. doi: 10.3389/FMICB.2023.1115295/BIBTEX

Hu, Y., Fan, J., Zhu, D., Liu, W., Li, F., Li, T., et al. (2023). Investigation of bedaquiline resistance and genetic mutations in multi-drug resistant *Mycobacterium tuberculosis* clinical isolates in Chongqing, China. *Ann. Clin. Microbiol. Antimicrob.* 22, 1–8. doi: 10.1186/S12941-023-00568-0

Huai, C., Wei, Y., Li, M., Zhang, X., Wu, H., Qiu, X., et al. (2019). Genome-wide analysis of DNA methylation and Antituberculosis drug-induced liver injury in the Han Chinese population. *Clin. Pharmacol. Ther.* 106, 1389–1397. doi: 10.1002/CPT.1563

Huang, H. L., Lee, J. Y., Lo, Y. S., Liu, I. H., Huang, S. H., Huang, Y. W., et al. (2022). Whole-blood 3-gene signature as a decision aid for Rifapentine-based tuberculosis preventive therapy. *Clin. Infect. Dis.* 75, 743–752. doi: 10.1093/CID/CIAC003

Huddart, S., Asege, L., Jaganath, D., Golla, M., Dang, H., Lovelina, L., et al. (2023). Continuous cough monitoring: a novel digital biomarker for TB diagnosis and treatment response monitoring. *Int. J. Tuberc. Lung Dis.* 27:221. doi: 10.5588/IJTLD.22.0511

Iñigo, J., García de Viedma, D., Arce, A., Palenque, E., Herranz, M., Rodríguez, E., et al. (2013). Differential findings regarding molecular epidemiology of tuberculosis between two consecutive periods in the context of steady increase of immigration. *Clin. Microbiol. Infect.* 19, 292–297. doi: 10.1111/J.1469-0691.2012.03794.X

Jaeger, S., Juarez-Espinosa, O. H., Candemir, S., Poostchi, M., Yang, F., Kim, L., et al. (2018). Detecting drug-resistant tuberculosis in chest radiographs. *Int. J. Comput. Assist. Radiol. Surg.* 13, 1915–1925. doi: 10.1007/S11548-018-1857-9

Jaramillo-Valverde, L., Levano, K. S., Tarazona, D. D., Capristano, S., Zegarra-Chapoñan, R., Sanchez, C., et al. (2022). NAT2 and CYP2E1 polymorphisms and antituberculosis drug-induced hepatotoxicity in Peruvian patients. *Mol. Genet. Genomic. Med.* 10:e1987. doi: 10.1002/MGG3.1987

Joshi, J. M. (2011). Tuberculosis chemotherapy in the 21 century: back to the basics. *Lung India* 28, 193–200. doi: 10.4103/0970-2113.83977

Jouet, A., Gaudin, C., Badalato, N., Allix-Béguec, C., Duthoy, S., Ferré, A., et al. (2021). Deep amplicon sequencing for culture-free prediction of susceptibility or resistance to 13 anti-tuberculous drugs. *Eur. Respir. J.* 57:2002338. doi: 10.1183/13993003.02338-2020ï

Kamal, R., Singh, M., Roy, S., Adhikari, T., Gupta, A. K., Singh, H., et al. (2023). A comparison of the quality of images of chest X-ray between handheld portable digital X-ray & routinely used digital X-ray machine. *Indian J. Med. Res.* 157, 204–210. doi: 10.4103/IJMR.IJMR_845_22

Karki, M., Kantipudi, K., Yu, H., Yang, F., Kassim, Y. M., Yaniv, Z., et al. (2021). Identifying drug-resistant tuberculosis in chest radiographs: evaluation of CNN architectures and training strategies. *Annu. Int. Conf. IEEE Eng. Med. Biol. Soc.* 2021, 2964–2967. doi: 10.1109/EMBC46164.2021.9630189

Karmakar, M., Trauer, J. M., Ascher, D. B., and Denholm, J. T. (2019). Hyper transmission of Beijing lineage *Mycobacterium tuberculosis*: systematic review and meta-analysis. *J. Infect.* 79, 572–581. doi: 10.1016/J.JINF.2019.09.016

Keikha, M., and Majidzadeh, M. (2021). Beijing genotype of *Mycobacterium tuberculosis* is associated with extensively drug-resistant tuberculosis: a global analysis. *New Microbes New Infect* 43:100921. doi: 10.1016/J.NMNI.2021.100921

Khan, A., Abbas, M., Verma, S., Verma, S., Rizvi, A. A., Haider, F., et al. (2022). Genetic variants and drug efficacy in tuberculosis: a step toward personalized therapy. *Glob. Med. Genet.* 9, 090–096. doi: 10.1055/S-0042-1743567

Khan, N., and Das, A. (2022). Time for isoniazid pharmacogenomic-guided therapy of tuberculosis based on NAT2 acetylation profiles in India. *Eur. J. Drug Metab. Pharmacokinet.* 47, 443–447. doi: 10.1007/S13318-022-00764-X

Khan, N., Pande, V., and Das, A. (2013). NAT2 sequence polymorphisms and acetylation profiles in Indians. *Pharmacogenomics* 14, 289–303. doi: 10.2217/PGS.13.2

Kielmann, K., Karat, A. S., Zwama, G., Colvin, C., Swartz, A., Voce, A. S., et al. (2020). Tuberculosis infection prevention and control: why we need a whole systems approach. *Infect. Dis. Poverty* 9, 1–4. doi: 10.1186/S40249-020-00667-6

Kim, S. H., Kim, S. H., Yoon, H. J., Shin, D. H., Park, S. S., Kim, Y. S., et al. (2011). NAT2, CYP2C9, CYP2C19, and CYP2E1 genetic polymorphisms in anti-TB drug-induced maculopapular eruption. *Eur. J. Clin. Pharmacol.* 67, 121–127. doi: 10.1007/S00228-010-0912-4

Kinzig-Schippers, M., Tomalik-Scharte, D., Jetter, A., Scheidel, B., Jakob, V., Rodamer, M., et al. (2005). Should we use N-acetyltransferase type 2 genotyping to personalize isoniazid doses? *Antimicrob. Agents Chemother.* 49, 1733–1738. doi: 10.1128/AAC.49.5.1733-1738.2005

Korhonen, V., Kivelä, P., Haanperä, M., Soini, H., and Vasankari, T. (2022). Multidrug-resistant tuberculosis in Finland: treatment outcome and the role of whole-genome sequencing. *ERJ Open Res.* 8, 00214–02022. doi: 10.1183/23120541.00214-2022

Lakhani, P., and Sundaram, B. (2017). Deep learning at chest radiography: automated classification of pulmonary tuberculosis by using convolutional neural networks. *Radiology* 284, 574–582. doi: 10.1148/RADIOL.2017162326

Larkins-Ford, J., Degefu, Y. N., Van, N., Sokolov, A., and Aldridge, B. B. (2022). Design principles to assemble drug combinations for effective tuberculosis therapy using interpretable pairwise drug response measurements. *Cell Rep. Med.* 3:100737. doi: 10.1016/J.XCRM.2022.100737

Leiro, V., Fernández-Villar, A., Valverde, D., Constenla, L., Vázquez, R., Piñeiro, L., et al. (2008). Influence of glutathione S-transferase M1 and T1 homozygous null mutations on the risk of antituberculosis drug-induced hepatotoxicity in a Caucasian population. *Liver Int.* 28, 835–839. doi: 10.1111/J.1478-3231.2008.01700.X

Li, D., Wang, T., Song, X., Qucuo, M. L., Yang, B., Zhang, J., et al. (2011). Genetic study of two single nucleotide polymorphisms within corresponding microRNAs and susceptibility to tuberculosis in a Chinese Tibetan and Han population. *Hum. Immunol.* 72, 598–602. doi: 10.1016/J.HUMIMM.2011.03.004

Liang, S., Song, Z., Wu, Y., Gao, Y., Gao, M., Liu, F., et al. (2018). MicroRNA-27b modulates inflammatory response and apoptosis during *Mycobacterium tuberculosis* infection. *J. Immunol.* 200, 3506–3518. doi: 10.4049/JIMMUNOL.1701448

Liao, K.-M., Liu, C.-F., Chen, C.-J., Feng, J.-Y., Shu, C.-C., and Ma, Y.-S. (2023). Using an artificial intelligence approach to predict the adverse effects and prognosis of tuberculosis. *Diagnostics* 13:1075. doi: 10.3390/DIAGNOSTICS13061075

Lu, T., Wang, M., Liu, N., Zhang, S., Shi, L., Bao, L., et al. (2023). Transporter associated with antigen processing 1 gene polymorphisms increase the susceptibility to tuberculosis. *Pharmgenomics Pers. Med.* 16, 325–336. doi: 10.2147/PGPM.S404339

Lyu, M., Zhou, J., Chen, H., Bai, H., Song, J., Liu, T., et al. (2019). The genetic variants in calcium signaling related genes influence anti-tuberculosis drug induced liver injury: a prospective study. *Medicine* 98:e17821. doi: 10.1097/MD.0000000000017821

MacNeil, A., Glaziou, P., Sismanidis, C., Maloney, S., and Floyd, K. (2019). Global epidemiology of tuberculosis and Progress toward achieving global targets — 2017. *Morb. Mortal. Wkly Rep.* 68:263. doi: 10.15585/MMWR.MM6811A3

Mandal, S., Bhatia, V., Sharma, M., Mandal, P. P., and Arinaminpathy, N. (2020). The potential impact of preventive therapy against tuberculosis in the WHO south-east Asian region: a modelling approach. *BMC Med.* 18, 1–10. doi: 10.1186/S12916-020-01651-5/FIGURES/3

Mansoor, H., Hirani, N., Chavan, V., Das, M., Sharma, J., Bharati, M., et al. (2023). Clinical utility of target-based next-generation sequencing for drug-resistant TB. *Int. J. Tuberc. Lung Dis.* 27:41. doi: 10.5588/IJTLD.22.0138

Martinez, L., Cords, O., Horsburgh, C. R., Andrews, J. R., Acuna-Villaorduna, C., Desai Ahuja, S., et al. (2020). The risk of tuberculosis in children after close exposure: a systematic review and individual-participant meta-analysis. *Lancet* 395, 973–984. doi: 10.1016/S0140-6736(20)30166-5

Masiphephethu, M. V., Sariko, M., Walongo, T., Maro, A., Mduma, D., Gratz, J., et al. (2022). Pharmacogenetic testing for NAT2 genotypes in a Tanzanian population across the lifespan to guide future personalized isoniazid dosing. *Tuberculosis* 136:102246. doi: 10.1016/J.TUBE.2022.102246

Massi, M. N., Hidayah, N., Handayani, I., Iskandar, I. W., Djannah, F., Angria, N., et al. (2023). MicroRNA Hsa-miR-425-5p and Hsa-miR-4523 expressions as biomarkers of active pulmonary tuberculosis, Latent Tuberculosis Infection, And Lymph Node Tuberculosis. *Noncoding RNA Res.* 8, 527–533. doi: 10.2139/SSRN.4398252

McDermott, J. H., Wolf, J., Hoshitsuki, K., Huddart, R., Caudle, K. E., Whirl-Carrillo, M., et al. (2022). Clinical pharmacogenetics implementation consortium guideline for the use of aminoglycosides based on MT-RNR1 genotype. *Clin. Pharmacol. Ther.* 111, 366–372. doi: 10.1002/CPT.2309

Meitei, H. N., Pandey, A., and Haobam, R. (2022). Polymorphisms in drug metabolism genes as a risk factor for first-line anti-tuberculosis drug-induced liver injury. *Mol. Biol. Rep.* 50, 2893–2900. doi: 10.1007/S11033-022-08158-7/TABLES/1

Migliori, G. B., Wu, S. J., Matteelli, A., Zenner, D., Goletti, D., Ahmedov, S., et al. (2022). Clinical standards for the diagnosis, treatment and prevention of TB infection. *Int. J. Tuberc. Lung Dis.* 26, 190–205. doi: 10.5588/IJTLD.21.0753

Minardi, M. L., Fato, I., Di Gennaro, F., Mosti, S., Mastrobattista, A., Cerva, C., et al. (2021). Common and rare hematological manifestations and adverse drug events during treatment of active TB: a state of art. *Microorganisms* 9:1477. doi: 10.3390/MICROORGANISMS9071477

Mohamed Noor, N. F., Salleh, M. Z., Mohd Zim, M. A., Bakar, Z. A., Fakhruzzaman Noorizhab, M. N., Zakaria, N. I., et al. (2022). NAT2 polymorphism and clinical factors that increase antituberculosis drug-induced hepatotoxicity. 531–541. *Pharmacogenomics* 23, 531–541. doi: 10.2217/PGS-2022-0022

Moodley, N., Velen, K., Saimen, A., Zakhura, N., Churchyard, G., and Charalambous, S. (2022). Digital chest radiography enhances screening efficiency for pulmonary tuberculosis in primary health clinics in South Africa. *Clin. Infect. Dis.* 74, 1650–1658. doi: 10.1093/CID/CIAB644

Mugwagwa, T., Abubakar, I., and White, P. J. (2021). Using molecular testing and whole-genome sequencing for tuberculosis diagnosis in a low-burden setting: a cost-effectiveness analysis using transmission-dynamic modelling. *Thorax* 76, 281–291. doi: 10.1136/THORAXJNL-2019-214004

Niemi, M., Pasanen, M. K., and Neuvonen, P. J. (2011). Organic anion transporting polypeptide 1B1: a genetically polymorphic transporter of major importance for hepatic drug uptake. *Pharmacol. Rev.* 63, 157–181. doi: 10.1124/PR.110.002857

Nijiati, M., Zhou, R., Damaola, M., Hu, C., Li, L., Qian, B., et al. (2022). Deep learning based CT images automatic analysis model for active/non-active pulmonary tuberculosis differential diagnosis. *Front. Mol. Biosci.* 9:1086047. doi: 10.3389/FMOLB.2022.1086047/FULL

Nikolenka, A., Mansjo, M., Skrahina, A., Hurevich, H., Grankov, V., Nikisins, S., et al. (2021). Whole-genome sequencing differentiates relapse from re-infection in TB. *Int. J. Tuberc. Lung Dis.* 25, 995–1000. doi: 10.5588/IJTLD.21.0274

Odume, B., Chukwu, E., Fawole, T., Nwokoye, N., Ogbudebe, C., Chukwuogo, O., et al. (2022). Portable digital X-ray for TB pre-diagnosis screening in rural communities in Nigeria. *Public Health Action* 12:85. doi: 10.5588/PHA.21.0079

Ospina, J. E., Orcau, Á., Millet, J. P., Ros, M., Gil, S., and Caylà, J. A. (2016). Epidemiology of tuberculosis in immigrants in a large city with large-scale immigration (1991-2013). *PLoS One* 11:e0164736. doi: 10.1371/JOURNAL.PONE.0164736

Pahar, M., Klopper, M., Reeve, B., Theron, G., Warren, R., and Niesler, T. (2021). Automatic cough classification for tuberculosis screening in a real-world environment. *Physiol. Meas.* 42:10.1088/1361-6579/ac2fb8. doi: 10.1088/1361-6579/ac2fb8

Pande, T., Pai, M., Khan, F. A., and Denkinger, C. M. (2015). Use of chest radiography in the 22 highest tuberculosis burden countries. *Eur. Respir. J.* 46, 1816–1819. doi: 10.1183/13993003.01064-2015

Park, M., Lalvani, A., Satta, G., and Kon, O. M. (2022). Evaluating the clinical impact of routine whole genome sequencing in tuberculosis treatment decisions and the issue of isoniazid mono-resistance. *BMC Infect. Dis.* 22:349. doi: 10.1186/S12879-022-07329-Y

Phelan, J. E., O'Sullivan, D. M., Machado, D., Ramos, J., Oppong, Y. E. A., Campino, S., et al. (2019). Integrating informatics tools and portable sequencing technology for rapid detection of resistance to anti-tuberculous drugs. *Genome Med.* 11, 1–7. doi: 10.1186/S13073-019-0650-X/TABLES/3

Pooransingh, S., and Sakhamuri, S. (2020). Need for BCG vaccination to prevent TB in high-incidence countries and populations. *Emerg. Infect. Dis.* 26:624. doi: 10.3201/EID2603.191232

Pršo, K., Žideková, N., Porvazník, I., Solovič, I., Mokrý, J., and Kertys, M. (2023). A high-throughput LC–MS/MS method for simultaneous determination of isoniazid, ethambutol and pyrazinamide in human plasma. *Rapid Commun. Mass Spectrom.* 37:e9425. doi: 10.1002/RCM.9425

Qin, Z. Z., Ahmed, S., Sarker, M. S., Paul, K., Adel, A. S. S., Naheyan, T., et al. (2021). Tuberculosis detection from chest x-rays for triaging in a high tuberculosis-burden setting: an evaluation of five artificial intelligence algorithms. *Lancet Digit. Health* 3, e543–e554. doi: 10.1016/S2589-7500(21)00116-3

Rajpurkar, P., O'Connell, C., Schechter, A., Asnani, N., Li, J., Kiani, A., et al. (2020). Cheaid: deep learning assistance for physician diagnosis of tuberculosis using chest x-rays in patients with HIV. *NPJ Digit. Med.* 3, 1–8. doi: 10.1038/s41746-020-00322-2

Resende, L. S. O., and dos Santos-Neto, E. T. (2015). Risk factors associated with adverse reactions to antituberculosis drugs. *J. Bras. Pneumol.* 41:77. doi: 10.1590/S1806-37132015000100010

Richardson, M., Kirkham, J., Dwan, K., Sloan, D. J., Davies, G., and Jorgensen, A. L. (2018). CYP genetic variants and toxicity related to anti-tubercular agents: a systematic review and meta-analysis. *Syst. Rev.* 7, 1–15. doi: 10.1186/S13643-018-0861-Z/TABLES/1

Roy, B., Chowdhury, A., Kundu, S., Santra, A., Dey, B., Chakraborty, M., et al. (2001). Increased risk of antituberculosis drug-induced hepatotoxicity in individuals with glutathione S-transferase M1 "null" mutation. *J. Gastroenterol. Hepatol.* 16, 1033–1037. doi: 10.1046/J.1440-1746.2001.02585.X

Sadkovsky, I. A., Golubnitschaja, O., Mandrik, M. A., Studneva, M. A., Abe, H., Schroeder, H., et al. (2014). PPPM (predictive, preventive and personalized medicine) as a new model of the national and international healthcare services and thus a promising strategy to prevent a disease: from basics to practice. *Int J Clin Med* 2014, 855–870. doi: 10.4236/IJCM.2014.514115

Samson Balogun, O., Olaleye, S. A., Mohsin, M., and Toivanen, P. (2021). "Investigating machine learning methods for tuberculosis risk factors prediction – a comparative analysis and evaluation," *Proceedings of the 37th International Business Information Management Association (IBIMA)*, Cordoba: Spain.

Sanabria, G. E., Sequera, G., Aguirre, S., Méndez, J., dos Santos, P. C. P., Gustafson, N. W., et al. (2023). Phylogeography and transmission of *Mycobacterium tuberculosis* spanning prisons and surrounding communities in Paraguay. *Nat. Commun.* 14, 1–10. doi: 10.1038/s41467-023-35813-9

Sekandi, J. N., Shi, W., Zhu, R., Kaggwa, P., Mwebaze, E., and Li, S. (2023). Application of artificial intelligence to the monitoring of medication adherence for tuberculosis treatment in Africa: algorithm development and validation. *JMIR AI* 2:e40167. doi: 10.2196/40167

Sekizuka, T., Yamashita, A., Murase, Y., Iwamoto, T., Mitarai, S., Kato, S., et al. (2015). TGS-TB: Total genotyping solution for *Mycobacterium tuberculosis* using short-read whole-genome sequencing. *PLoS One* 10:e0142951. doi: 10.1371/JOURNAL.PONE.0142951

Selimoglu, E. (2007). Aminoglycoside-induced ototoxicity. *Curr. Pharm. Des.* 13, 119–126. doi: 10.2174/138161207779313731

Shahroz, M., Ahmad, F., Younis, M. S., Ahmad, N., Kamel Boulos, M. N., Vinuesa, R., et al. (2021). COVID-19 digital contact tracing applications and techniques: a review post initial deployments. *Transp. Eng.* 5:100072. doi: 10.1016/J.TRENG.2021.100072

Sharma, P., Ghildiyal, S., Rodrigues, R., Kumar Arora, M., and Professor, A. (2022). A review on the role of pharmacogenomics and pharmacotherapy for the treatment of tuberculosis to optimize patient care strategies. *JPSP* 6, 4688–4693.

Sibandze, D. B., Kay, A., Dreyer, V., Sikhondze, W., Dlamini, Q., DiNardo, A., et al. (2022). Rapid molecular diagnostics of tuberculosis resistance by targeted stool sequencing. *Genome Med.* 14, 1–11. doi: 10.1186/S13073-022-01054-6/FIGURES/2

Silver, D., Schrittwieser, J., Simonyan, K., Antonoglou, I., Huang, A., Guez, A., et al. (2017). Mastering the game of go without human knowledge. *Nature* 550, 354–359. doi: 10.1038/NATURE24270

Singh, P. P., and Goyal, A. (2013). Interleukin-6: a potent biomarker of mycobacterial infection. *Springerplus* 2:686. doi: 10.1186/2193-1801-2-686

Sinigaglia, A., Peta, E., Riccetti, S., Venkateswaran, S., Manganelli, R., and Barzon, L. (2020). Tuberculosis-associated MicroRNAs: from pathogenesis to disease biomarkers. *Cells* 9:2160. doi: 10.3390/CELLS9102160

Sloan, D. J., McCallum, A. D., Schipani, A., Egan, D., Mwandumba, H. C., Ward, S. A., et al. (2017). Genetic determinants of the pharmacokinetic variability of rifampin in Malawian adults with pulmonary tuberculosis. *Antimicrob. Agents Chemother.* 61, 7, e00210–e00217. doi: 10.1128/AAC.00210-17

Song, S. H., Chang, H. E., Jun, S. H., Park, K. U., Lee, J. H., Lee, E. M., et al. (2013). Relationship between CES2 genetic variations and rifampicin metabolism. *J. Antimicrob. Chemother.* 68, 1281–1284. doi: 10.1093/JAC/DKT036

Steiner, A., Stucki, D., Coscolla, M., Borrell, S., and Gagneux, S. (2014). KvarQ: targeted and direct variant calling from fastq reads of bacterial genomes. *BMC Genomics* 15:881. doi: 10.1186/1471-2164-15-881

Stocco, G., Lucafò, M., and Decorti, G. (2020). Pharmacogenomics of antibiotics. *Int. J. Mol. Sci.* 21, 1–20. doi: 10.3390/IJMS21175975

Suliman, S., Thompson, E. G., Sutherland, J., Weiner, J., Ota, M. O. C., Shankar, S., et al. (2018). Four-gene Pan-African blood signature predicts progression to tuberculosis. *Am. J. Respir. Crit. Care Med.* 197, 1198–1208. doi: 10.1164/RCCM.201711-2340OC

Tervi, A., Junna, N., Broberg, M., Jones, S. E., Partinen, M., Pirinen, M., et al. (2023). Large registry-based analysis of genetic predisposition to tuberculosis identifies genetic risk factors at HLA. *Hum. Mol. Genet.* 32, 161–171. doi: 10.1093/HMG/DDAC212

Tostmann, A., Boeree, M. J., Aarnoutse, R. E., De Lange, W. C. M., Van Der Ven, A. J. A. M., and Dekhuijzen, R. (2008). Antituberculosis drug-induced hepatotoxicity: concise up-to-date review. *J. Gastroenterol. Hepatol.* 23, 192–202. doi: 10.1111/J.1440-1746.2007.05207.X

Villellas, C., Coeck, N., Meehan, C. J., Lounis, N., De Jong, B., Rigouts, L., et al. (2017). Unexpected high prevalence of resistance-associated Rv0678 variants in MDR-TB patients without documented prior use of clofazimine or bedaquiline. *J. Antimicrob. Chemother.* 72, 684–690. doi: 10.1093/JAC/DKW502

Vo, L. N. Q., Codlin, A., Ngo, T. D., Dao, T. P., Dong, T. T. T., Mo, H. T. L., et al. (2021). Early evaluation of an ultra-portable x-ray system for tuberculosis active case finding. *Trop. Med. Infect Dis.* 6:163. doi: 10.3390/TROPICALMED6030163/S1

Wahl, B., Cossy-Gantner, A., Germann, S., and Schwalbe, N. R. (2018). Artificial intelligence (AI) and global health: how can AI contribute to health in resource-poor settings? Handling editor Seye Abimbola. *BMJ Glob. Health* 3:798. doi: 10.1136/bmjgh-2018-000798

Walker, T. M., Crook, D. W., Walker, T. M., and Crook, D. W. (2022a). Realising the potential of genomics for *M. tuberculosis*: a silver lining to the pandemic? *China CDC Wkly* 4, 437–439. doi: 10.46234/CCDCW2022.063

Walker, T. M., Fowler, P. W., Knaggs, J., Hunt, M., Peto, T. E., Walker, A. S., et al. (2022b). The 2021 WHO catalogue of *Mycobacterium tuberculosis* complex mutations associated with drug resistance: a genotypic analysis. *Lancet Microbe* 3, e265–e273. doi: 10.1016/S2666-5247(21)00301-3

Weiner, M., Gelfond, J., Johnson-Pais, T. L., Engle, M., Peloquin, C. A., Johnson, J. L., et al. (2018). Elevated plasma moxifloxacin concentrations and SLCO1B1 g.-11187G>a polymorphism in adults with pulmonary tuberculosis. *Antimicrob. Agents Chemother.* 62, e01802–e01817. doi: 10.1128/AAC.01802-17

Weiner, M., Peloquin, C., Burman, W., Luo, C. C., Engle, M., Prihoda, T. J., et al. (2010). Effects of tuberculosis, race, and human gene SLCO1B1 polymorphisms on rifampin concentrations. *Antimicrob. Agents Chemother.* 54, 4192–4200. doi: 10.1128/AAC.00353-10

WHO. WHO consolidated guidelines on tuberculosis: module 2: screening: systematic screening for tuberculosis disease (2021). Available at: https://www.who.int/publications/i/item/9789240022676. Accessed May 2, 2023.

WHO. WHO consolidated guidelines on tuberculosis. Module 4: treatment - drug - World Health Organization (2022). Available at: https://books.google.sk/books?hl=en&lr=&id=w-aiEAAAQBAJ&oi=fnd&pg=PR5&ots=OE67rW3HuJ&sig=BZ1bWfM0g1dXkHKukGB4mxkH8T8&redir_esc=y#v=onepage&q&f=false. Accessed May 2, 2023

Witbooi, P., and Vyambwera, S. M. (2017). A model of population dynamics of TB in a prison system and application to South Africa. *BMC. Res. Notes* 10:643. doi: 10.1186/S13104-017-2968-Z

World Health Organization. Treatment of tuberculosis: guidelines. (2010). Available at: https://apps.who.int/iris/handle/10665/44165. Accessed June 22, 2023.

Wu, X., Gao, R., Shen, X., Guo, Y., Yang, J., Wu, Z., et al. (2020). Use of whole-genome sequencing to predict *Mycobacterium tuberculosis* drug resistance in Shanghai, China. *Int. J. Infect. Dis.* 96, 48–53. doi: 10.1016/J.IJID.2020.04.039

Xiao, Y. X., Liu, K. H., Lin, W. H., Chan, T. H., and Jou, R. (2023). Whole-genome sequencing-based analyses of drug-resistant *Mycobacterium tuberculosis* from Taiwan. *Sci. Rep.* 13, 1–11. doi: 10.1038/s41598-023-29652-3

Xin, H., Cao, X., Du, Y., Yan, J., He, R., Liu, Z., et al. (2022). The association between circulating microRNAs and the risk of active disease development from latent tuberculosis infection: a nested case-control study. *Microbiol. Spectr.* 10, e02625–e02621. doi: 10.1128/SPECTRUM.02625-21

Xing, S., Wang, Y., He, X., Yang, W., Hu, Q., He, Y., et al. (2021). CYP2C8 and CYP2E1 genetic variants increase risk of tuberculosis in northwest Chinese Han population. *Infect. Genet. Evol.* 95:105022. doi: 10.1016/J.MEEGID.2021.105022

Yan, M. Y., Zheng, D., Li, S. S., Ding, X. Y., Wang, C. L., Guo, X. P., et al. (2022). Application of combined CRISPR screening for genetic and chemical-genetic interaction profiling in *Mycobacterium tuberculosis*. *Sci. Adv.* 8:5907. doi: 10.1126/SCIADV.ADD5907/SUPPL_FILE/SCIADV.ADD5907_TABLES_S1_TO_S7.ZIP

Yoo, H., Lee, S. H., Arru, C. D., Doda Khera, R., Singh, R., Siebert, S., et al. (2021). AI-based improvement in lung cancer detection on chest radiographs: results of a multi-reader study in NLST dataset. *Eur. Radiol.* 31, 9664–9674. doi: 10.1007/S00330-021-08074-7

Yu, M., Guo, D., Hu, Y., and Wu, X. (2017). Severe skin rash and liver toxic effects caused by first-line anti-tuberculosis drugs: a case report. *Int. J. Complement. Altern. Med.* 5:00160. doi: 10.15406/IJCAM.2017.05.00160

Zhang, X., Li, Y., Li, X., Zhang, W., Pan, Z., Wu, F., et al. (2015). Association of the miR-146a, miR-149, miR-196a2 and miR-499 polymorphisms with susceptibility to pulmonary tuberculosis in the Chinese Uygur, Kazak and southern Han populations. *BMC Infect. Dis.* 15, 1–11. doi: 10.1186/S12879-015-0771-9

Zhang, J., Wang, P., Han, B., Ding, Y., Pan, L., Zou, J., et al. (2013). Newborn hearing concurrent genetic screening for hearing impairment-a clinical practice in 58,397 neonates in Tianjin, China. *Int. J. Pediatr. Otorhinolaryngol.* 77, 1929–1935. doi: 10.1016/J.IJPORL.2013.08.038

Zhou, Y., Van Den Hof, S., Wang, S., Pang, Y., Zhao, B., Xia, H., et al. (2017). Association between genotype and drug resistance profiles of *Mycobacterium tuberculosis* strains circulating in China in a national drug resistance survey. *PLoS One* 12:e0174197. doi: 10.1371/JOURNAL.PONE.0174197

Zimmer, A. J., Ugarte-Gil, C., Pathri, R., Dewan, P., Jaganath, D., Cattamanchi, A., et al. (2022). Making cough count in tuberculosis care. *Commun. Med.* 2, 1–8. doi: 10.1038/s43856-022-00149-w

frontiers | Frontiers in Public Health

TYPE Original Research
PUBLISHED 27 October 2023
DOI 10.3389/fpubh.2023.1254658

OPEN ACCESS

EDITED BY
Ranjan Nanda,
International Centre for Genetic Engineering and Biotechnology, India

REVIEWED BY
Mihaela-Simona Subtirelu,
University of Medicine and Pharmacy of Craiova, Romania
Debasis Dash,
Institute of Life Sciences (ILS), India
Anjali Agrawal,
Teleradiology Solutions, India

*CORRESPONDENCE
Samer Abuzerr
✉ samer_516@hotmail.com

RECEIVED 07 July 2023
ACCEPTED 09 October 2023
PUBLISHED 27 October 2023

CITATION
Abuzerr S and Zinszer K (2023) Computer-aided diagnostic accuracy of pulmonary tuberculosis on chest radiography among lower respiratory tract symptoms patients.
Front. Public Health 11:1254658.
doi: 10.3389/fpubh.2023.1254658

Computer-aided diagnostic accuracy of pulmonary tuberculosis on chest radiography among lower respiratory tract symptoms patients

Samer Abuzerr[1]* and Kate Zinszer[2]

[1]Department of Medical Sciences, University College of Science and Technology, Gaza, Palestine, [2]School of Public Health, Department of Social and Preventive Medicine, University of Montreal, Montréal, QC, Canada

Even though the Gaza Strip is a low pulmonary tuberculosis (TB) burden region, it is well-known that TB is primarily a socioeconomic problem associated with overcrowding, poor hygiene, a lack of fresh water, and limited access to healthcare, which is the typical case in the Gaza Strip. Therefore, this study aimed at assessing the accuracy of the automatic software computer-aided detection for tuberculosis (CAD4TB) in diagnosing pulmonary TB on chest radiography and compare the CAD4TB software reading with the results of geneXpert. Using a census sampling method, the study was conducted in radiology departments in the Gaza Strip hospitals between 1 December 2022 and 31 March 2023. A digital X-ray, printer, and online X-ray system backed by CAD4TBv6 software were used to screen patients with lower respiratory tract symptoms. GeneXpert analysis was performed for all patients having a score $>$ 40. A total of 1,237 patients presenting with lower respiratory tract symptoms participated in this current study. Chest X-ray readings showed that 7.8% ($n = 96$) were presumptive for TB. The CAD4TBv6 scores showed that 11.8% ($n = 146$) of recruited patients were presumptive for TB. GeneXpert testing on sputum samples showed that 6.2% ($n = 77$) of those with a score $>$ 40 on CAD4TB were positive for pulmonary TB. Significant differences were found in chest X-ray readings, CAD4TBv6 scores, and GeneXpert results among sociodemographic and health status variables (P-value < 0.05). The study showed that the incidence rate of TB in the Gaza Strip is 3.5 per 100,000 population in the Gaza strip. The sensitivity of the CAD4TBv6 score and the symptomatic review for tuberculosis with a threshold score of $>$40 is 80.2%, and the specificity is 94.0%. The positive Likelihood Ratio is 13.3%, Negative Likelihood Ratio is 0.2 with 7.8% prevalence. Positive Predictive Value is 52.7%, Negative Predictive Value is 98.3%, and accuracy is 92.9%. In a resource-limited country with a high burden of neglected disease, combining chest X-ray readings by CAD4TB and symptomatology is extremely valuable for screening a population at risk. CAD4TB is noticeably more efficient than other methods for TB screening and early diagnosis in people who would otherwise go undetected.

KEYWORDS

computer-aided detection, chest radiography, diagnostic accuracy, GeneXpert, Gaza Strip, pulmonary tuberculosis

Introduction

Tuberculosis (TB) stands out as the most widespread illness attributed to a single infectious agent, holding a place among the top 10 leading causes of death worldwide. Although TB can be prevented and treated, it impacts individuals of all age groups. In the year 2019 alone, nearly 10 million people across the globe contracted TB. Among them were 5.6 million males, 3.2 million females, and 1.2 million children (1).

Plain chest radiography remains a crucial tool in identifying early-stage pulmonary tuberculosis (TB) and monitoring the progress of treatments (2). Even when TB patients exhibit no symptoms, chest X-rays (CXRs) exhibit a high degree of sensitivity in detecting abnormalities related to pulmonary TB, particularly when interpreted by proficient radiologists. However, despite this capability, only 7.1 million out of an estimated 10 million TB cases worldwide were actually detected and reported in 2019 (3). Despite a decline in the global incidence rates of TB, these rates still fall short of the targets established by the World Health Organization's (WHO) End TB Strategy (3).

While improvements in digital radiography technology have improved the CXR image quality (4), lack of access to these facilities and skilled radiologists continues to be a problem, especially in underdeveloped regions with a high TB prevalence (5). However, the role of artificial intelligence (AI) in enhancing the accuracy of computer-aided diagnosis for pulmonary tuberculosis (TB) on chest radiography has become increasingly pivotal. AI technologies, such as deep learning algorithms, offer a unique capacity to analyze vast amounts of medical imagery with remarkable precision and speed. In the context of TB diagnosis, AI systems can swiftly and accurately detect subtle abnormalities and patterns on chest X-rays that may elude even skilled human radiologists. By providing reliable and consistent assessments, AI-driven computer-aided diagnosis has the potential to significantly expedite the identification of TB cases, especially in asymptomatic patients, ultimately leading to more timely interventions and improved treatment outcomes. This symbiotic integration of AI with medical diagnostics not only augments the overall diagnostic accuracy but also holds promise for more efficient resource utilization within healthcare systems, thus reinforcing its significance in combating pulmonary tuberculosis on a global scale (6–9). If they perform accurately, these CAD systems may facilitate CXR reading for TB screening and advance the WHO's End TB agenda (3, 10). There are only a few studies in this field, and the majority have methodological flaws, focus on a single CAD program, have scant screening data, or are industry-funded (11, 12).

Furthermore, most studies compared performance against a suboptimal reference standard of a single sputum specimen tested with Xpert MTB/RIF evaluated an online CAD processing system or shared images with the CAD vendors (13, 14). This highlights the need for independent and thorough studies. Offline and multiple AI systems have been the focus of more recent research (15–17), but there are still very few. An international meeting by WHO in 2016 concluded that more data on the effectiveness and application of CAD systems for TB screening were needed (18).

Although the Gaza Strip is a low TB burden region, it is well-known that tuberculosis is primarily a socioeconomic problem associated with overcrowding, poor hygiene, a lack of fresh water, and limited access to health care, which is typical in the Gaza Strip (19, 20). There is a lack of well-organized healthcare infrastructure, which affects the finding and treatment of TB cases, complicated disease control in the Gaza Strip, and a lack of statistics on TB after 2016.

Accordingly, this study aims to evaluate the performance of the automatic software computer-aided detection for tuberculosis (CAD4TBv6) in diagnosing pulmonary TB on chest radiography and compare the CAD4TB software reading with the results of radiologists' reports in the Gaza Strip, Palestine.

Methods

Study setting and period

The current study was conducted in radiology departments in the Gaza Strip hospitals between 1 December 2022 and 31 March 2023.

Study design and study participants

We conducted a cross-sectional study to recruit patients with lower respiratory tract symptoms. Data were collected from respiratory patients referred from the chest department who underwent digital CXRs during the study period using a census sampling method. A digital X-ray, printer, and online X-ray system backed by CAD4TBv6 software were used to screen patients. Patients of both sexes ranging in age from 15 to 80 years were included in this study.

Sociodemographic and clinical information tool

The acquisition of sociodemographic and clinical information including signs and symptoms of tuberculosis and a history of respiratory diseases was facilitated through the utilization of a meticulously crafted and rigorously validated questionnaire. The questionnaire's design was rooted in a thorough review of pertinent literature and established health assessment frameworks (21–25). This instrument was developed through a systematic process that involved collaboration with domain experts, iterative refinement, and comprehensive pilot testing.

Assessment of body mass index

Using a measuring rod attached to the balanced beam scale, participants' heights (measured in cm) were recorded to the nearest 0.5 cm while standing barefoot and with their heads up. A common digital weighing scale (SECA, Germany) was used to measure weight (kg). Participants were asked to remove their bulky outerwear before being weighed, and the results were recorded to the nearest 0.1 kg (26).

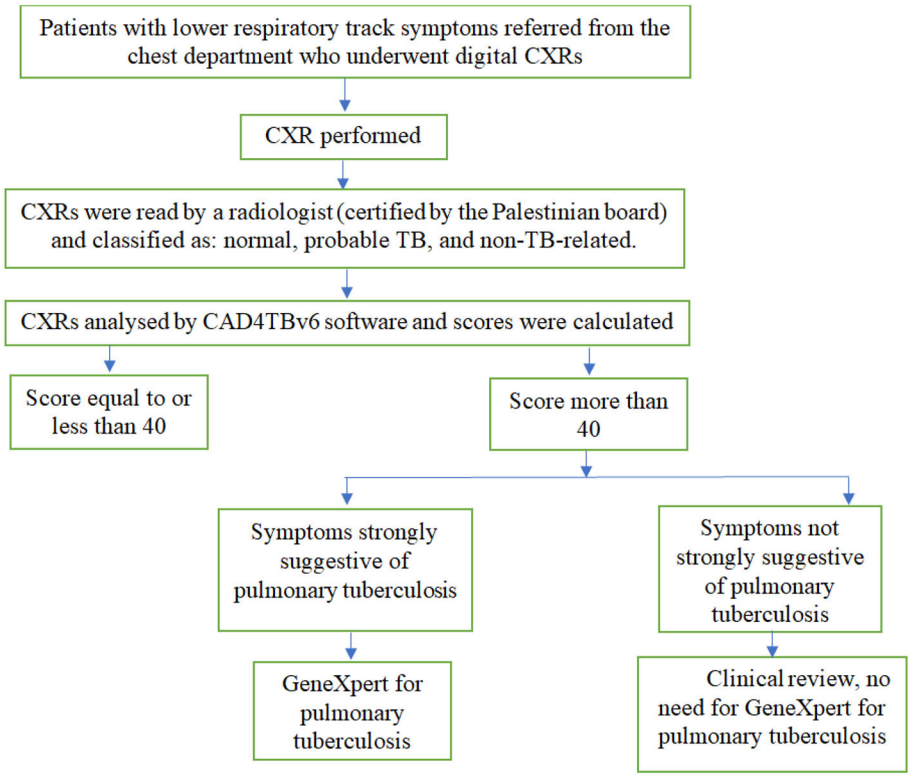

FIGURE 1
Tuberculosis screening flowchart for patients presenting with lower respiratory tract symptoms.

CXRs scoring procedures

The obtained CXRs were read within 48 h by a radiologist (certified by the Palestinian board) and classified as normal, probable TB, and non-TB-related. Digital CXRs were scored using CAD4TBv6 (Delft Imaging Systems, Veenendaal, The Netherlands), with scores from 0 to 100 (0 being completely normal and 100 very suggestive of TB) (27).

The analysis was based on identifying aberrant lung field shapes and textures using automatically segmented lung fields. The cutoff point of 40 was chosen (28). Patients who had CXRs images with a score equal to or <40 underwent clinical examination. Whereas, patients who had CXRs with a score higher than 40 were assumed to have tuberculosis. Sputum samples for GeneXpert analysis were obtained only from those with a score > 40 and with symptoms strongly suggestive of pulmonary TB such as hemoptysis, night sweat, weight loss, breathlessness, and fever (Figure 1).

Statistical analysis

IBM SPSS Statistics for Windows, version 26.0 (IBM Corp., Armonk, NY, USA), was used for statistical analysis. We calculated the frequency and percentage for categorical variables. Continuous variables were analyzed using mean and SD. The chi-square test was used to determine the significant differences between categorical variables. With GeneXpert serving as the reference standard, the following metrics were used for CAD4TB: sensitivity (True Positives x 100/Total Diseased), specificity (True Negatives × 100/Total Non-Diseased), negative predictive value (True Negatives/True Negatives + False Negatives), and positive predictive value (True Positives/True Positives + False Positives).

Results

Sociodemographic and health status characteristics, CAD4TBv6 score, and GeneXpert result

A total of 1,237 patients presenting with lower respiratory tract symptoms participated in this current study. More than half of the study participants (56.4%) were males. 45.1% (n = 558) of study participants were 41–60 years old, with a mean age ± standard deviation of 47.4 ± 14.2 years. Only 22.1% of study participants (n = 273) had a typical BMI of 18.5–24.9, with a mean BMI±std of 30.1 ± 6. 2. 44.9% of the study participants were active tobacco smokers. 75.4% of study participants had a cough of any duration; only 20.0% of them were diabetic patients; 17.5% had hemoptysis; 36.6% had a night sweat; 43.2% experienced weight loss; 79.9% suffered from breathlessness; and 39.7% had a fever. Only 10% of study participants had a past history of TB. Chest X-ray readings showed that 64.8% (n = 801) were normal, 27.5% (n = 340) were abnormal but not TB and only 7.8% (n = 96) were presumptive

TABLE 1 Sociodemographic and health status characteristics of patients with presumptive TB by chest x-ray reading, CAD4TB scores, and GeneXpert testing.

	Chest X-ray reading					CAD4TBv6 score							GeneXpert testing on sputum samples			
	All *n* (%)	Normal *n* (%)	Abnormal, not TB *n* (%)	Suggestive of TB *n* (%)	*P*-value*	All *n* (%)	≤20 *n* (%)	21–40 *n* (%)	41–60 *n* (%)	61–80 *n* (%)	>81 *n* (%)	*P*-value*	All *n* (%)	Positive	Negative	*P*-value*
Gender																
Male	698 (56.4)	446 (57.1)	190 (55.9)	62 (64.6)	0.244	698 (56.4)	429 (55.3)	180 (57.1)	20 (55.6)	12 (54.5)	57 (54.5)	0.555	62 (64.6)	48 (62.3)	14 (73.7)	0.164
Female	539 (43.6)	335 (42.9)	150 (44.1)	34 (35.4)		539 (43.6)	347 (44.7)	135 (42.9)	16 (44.4)	10 (45.5)	31 (35.2)		34 (35.4)	29 (37.7)	5 (26.3)	
Age (mean ± std = 47.4 ± 14.2)																
<25	83 (6.7)	65 (8.1)	18 (5.3)	0 (0.0)	0.001	83 (6.7)	64 (8.2)	18 (5.7)	1 (2.8)	0.0 (0.0)	0.0 (0.0)	0.001	0 (0.0)	0 (0.0)	0 (0.0)	0.001
25–40	330 (26.7)	236 (29.5)	78 (22.9)	16 (16.7)		330 (26.7)	225 (29.0)	78 (24.8)	6 (16.7)	5 (22.7)	16 (18.2)		16 (16.7)	13 (16.9)	3 (15.8)	
41–60	558 (45.1)	355 (44.3)	139 (40.9)	64 (66.7)		558 (45.1)	345 (44.5)	126 (40.0)	16 (44.4)	14 (63.6)	57 (64.8)		64 (66.7)	52 (67.5)	12 (63.2)	
>60	266 (21.5)	145 (18.1)	105 (30.9)	16 (16.7)		266 (21.5)	142 (18.3)	93 (29.5)	13 (36.1)	3 (13.6)	15 (17.0)		16 (16.7)	12 (15.6)	4 (21.1)	
BMI (mean ± std = 30.1 ± 6.2)																
<18.5	7 (0.6)	4 (0.5)	3 (0.9)	0 (0.0)	0.949	7 (0.6)	4 (0.5)	3 (0.1)	0.0 (0.0)	0.0 (0.0)	0.0 (0.0)	0.999	0 (0.0)	0 (0.0)	0 (0.0)	0.481
18.5–24.9	273 (22.1)	177 (22.1)	71 (20.9)	25 (26.0)		273 (22.1)	173 (22.3)	65 (20.6)	7 (19.4)	5 (22.7)	23 (26.1)		25 (26.0)	22 (28.6)	3 (15.8)	
25–29.9	383 (31.1)	249 (31.1)	103 (30.3)	31 (32.3)		383 (31.0)	243 (31.3)	94 (29.8)	12 (33.3)	7 (31.8)	27 (30.7)		31 (32.3)	23 (29.9)	8 (42.1)	
30–34.9	317 (25.6)	203 (35.3)	90 (26.5)	24 (25.0)		317 (25.6)	197 (25.4)	82 (26.0)	9 (25.0)	7 (31.8)	22 (25.0)		24 (25.0)	21 (27.3)	3 (15.8)	
35–40	165 (13.3)	106 (13.2)	47 (13.8)	12 (12.5)		165 (13.3)	99 (12.8)	47 (14.9)	5 (13.9)	2 (9.1)	12 (13.6)		12 (12.5)	7 (9.1)	5 (26.3)	
>40	92 (7.4)	62 (7.7)	26 (7.6)	4 (4.2)		92 (7.4)	60 (7.7)	24 (7.6)	3 (8.3)	1 (4.5)	4 (4.5)		4 (4.2)	4 (5.2)	0 (0.0)	
Active tobacco smoker																
Yes	556 (44.9)	346 (43.2)	160 (47.1)	50 (52.1)	0.167	556 (44.9)	334 (43.0)	149 (47.3)	16 (44.4)	12 (54.5)	45 (51.1)	0.402	50 (52.1)	37 (48.1)	13 (68.4)	0.096

(Continued)

10.3389/fpubh.2023.1254658

TABLE 1 (Continued)

	Chest X-ray reading					CAD4TBv6 score							GeneXpert testing on sputum samples			
	All *n* (%)	Normal *n* (%)	Abnormal, not TB *n* (%)	Suggestive of TB *n* (%)	*P*-value*	All *n* (%)	≤20 *n* (%)	21–40 *n* (%)	41–60 *n* (%)	61–80 *n* (%)	>81 *n* (%)	*P*-value*	All *n* (%)	Positive	Negative	*P*-value*
No	681 (55.1)	455 (56.8)	180 (52.9)	46 (47.9)		681 (55.1)	442 (57.0)	166 (52.7)	20 (55.6)	10 (45.5)	43 (48.9)		46 (47.9)	40 (51.9)	6 (31.6)	
Cough of any duration																
Yes	933 (75.4)	594 (74.2)	260 (76.5)	79 (82.3)	0.189	933 (75.4)	575 (74.1)	244 (77.5)	24 (66.7)	19 (86.4)	71 (80.7)	0.226	79 (82.3)	62 (80.5)	17 (89.5)	0.191
No	304 (24.6)	207 (25.8)	80 (23.5)	17 (17.7)		304 (24.6)	201 (25.9)	71 (22.5)	12 (33.3)	3 (13.6)	17 (19.3)		17 (17.7)	15 (19.5)	2 (10.5)	
Diabetes																
Yes	248 (20.0)	133 (16.6)	92 (27.1)	23 (24.0)	0.001	248 (20.0)	131 (16.9)	81 (25.7)	12 (33.3)	5 (22.7)	19 (21.6)	0.004	23 (24.0)	16 (20.8)	7 (36.8)	0.179
No	989 (80.0)	668 (83.4)	248 (72.9)	73 (76.0)		989 (80.0)	645 (83.1)	234 (74.3)	24 (66.7)	17 (77.3)	69 (78.4)		73 (76.0)	61 (79.2)	12 (63.2)	
Hemoptysis																
Yes	216 (17.5)	2 (0.2)	119 (35.0)	95 (99.0)	0.001	216 (17.5)	2 (0.3)	101 (32.1)	13 (36.1)	13 (59.1)	87 (98.9)	0.001	95 (99.0)	76 (98.7)	19 (100.0)	0.001
No	1,021 (82.5)	799 (99.8)	221 (65.0)	1 (1.0)		1,021 (82.5)	774 (99.7)	214 (67.9)	23 (63.9)	9 (40.9)	1 (1.1)		1 (0.1)	1 (1.3)	0 (0.0)	
Night sweat																
Yes	453 (36.6)	175 (21.8)	185 (54.1)	95 (99.0)	0.001	453 (36.6)	169 (21.8)	163 (51.7)	18 (50.0)	16 (72.7)	87 (98.9)	0.001	95 (99.0)	76 (98.7)	19 (100.0)	0.001
No	784 (63.4)	626 (78.2)	157 (45.9)	1 (1.0)		784 (63.4)	607 (78.2)	152 (48.3)	18 (50.0)	6 (27.3)	1 (1.1)		1 (0.1)	1 (1.3)	0 (0.0)	
Weight loss																
Yes	535 (43.2)	240 (30.0)	200 (58.8)	95 (99.0)	0.001	535 (43.2)	233 (30.0)	176 (55.9)	23 (63.9)	16 (72.7)	87 (98.9)	0.001	95 (99.0)	76 (98.7)	19 (100.0)	0.001
No	702 (56.8)	561 (70.0)	140 (41.2)	1 (1.0)		702 (56.8)	543 (70.0)	139 (44.1)	13 (36.1)	6 (27.3)	1 (1.1)		1 (0.1)	1 (1.3)	0 (0.0)	
Breathlessness																
Yes	988 (79.9)	625 (87.0)	280 (82.4)	83 (86.5)	0.061	988 (79.9)	604 (77.8)	263 (83.5)	27 (75.0)	19 (86.4)	75 (85.2)	0.123	83 (86.5)	66 (85.7)	17 (89.5)	0.230

(Continued)

10.3389/fpubh.2023.1254658

TABLE 1 (Continued)

		Chest X-ray reading				CAD4TBv6 score						GeneXpert testing on sputum samples			
	All *n* (%)	Normal *n* (%)	Abnormal, not TB *n* (%)	Suggestive of TB *n* (%)	*P*-value*	All *n* (%)	≤20 *n* (%)	21–40 *n* (%)	41–60 *n* (%)	61–80 *n* (%)	>81 *n* (%)	*P*-value*	All *n* (%)	Positive	Negative	*P*-value*
No	249 (20.1)	176 (22.9)	60 (17.6)	13 (13.5)		249 (20.1)	172 (22.2)	52 (16.5)	9 (25.0)	3 (13.6)	13 (14.8)		13 (13.5)	11 (14.3)	2 (10.5)	
Fever																
Yes	491 (39.7)	202 (25.2)	193 (56.8)	96 (1000)	0.001	491 (39.7)	193 (24.9)	176 (55.9)	18 (50.0)	16 (72.7)	88 (100.0)	0.001	96 (100.0)	77 (100.0)	19 (100.0)	0.001
No	746 (60.3)	599 (74.8)	147 (43.2)	0 (0.0)		746 (60.3)	583 (75.1)	139 (44.1)	18 (50.0)	6 (27.3)	0 (0.0)		0 (0.0)	0 (0.0)	0 (0.0)	
Past history of TB																
Yes	124 (10.0)	0 (0.0)	74 (21.8)	50 (52.1)	0.001	124 (10.0)	0 (0.0)	62 (19.7)	8 (22.2)	5 (22.7)	49 (62.8)	0.001	50 (52.1)	41 (53.2)	9 (47.4)	0.001
No	1,113 (90.0)	801 (100.0)	266 (78.2)	46 (47.9)		1,113 (90.0)	776 (100.0)	253 (80.3)	28 (77.8)	17 (77.3)	29 (37.2)		46 (47.9)	36 (46.8)	10 (52.6)	

*P-value was calculated using the chi-squared test.

for TB. There were statistically significant differences in chest X-ray readings between age groups, diabetes status, hemoptysis, night sweats, weight loss, fever, and TB history (*P*-value 0.05).

The CAD4TBv6 scores showed that 11.8% (n = 146) of recruited patients were presumptive for TB. Significant differences in CAD4TBv6 scores were discovered across age groups, diabetes status, hemoptysis, night sweats, weight loss, fever, and TB history (P-value < 0.05).

GeneXpert testing on sputum samples showed that 6.2% (n = 77) of those with a score > 40 on CAD4TB were positive for pulmonary TB. Significant differences were found in GeneXpert results among age groups, hemoptysis, night sweats, weight loss, fever, and history of TB (P-value < 0.05).

The study showed that the incidence rate of TB in the Gaza Strip is 3.5 per 100,000 population in the Gaza strip (Table 1).

The sensitivity of the CAD4TBv6 score and the symptomatic review for tuberculosis with a threshold score of >40 is 80.2%, and the specificity is 94.0%. The positive likelihood ratio is 13.3%, negative likelihood ratio is 0.2, with a 7.8% prevalence. The positive predictive value is 52.7%, the negative predictive value is 98.3%, and the accuracy is 92.9% (Table 2).

CAD4TB analysis

Machine learning methods are used by the commercial software package CAD4TB to automatically identify TB from CXR pictures. Using separate annotated datasets, the software has been trained to recognize recognizable TB features in CXR pictures. It generates a number (0–100) that can be interpreted as the likelihood that the person has active TB that can be seen on CXR. Figure 2 shows an anomaly heatmap showing areas the software deems suspicious.

Figure 3 shows a few instances in which the radiograph's appearance conflicts with the outcome of the geneXpert test. The first case shows a radiograph that appears consistent with tuberculosis. Still, the geneXpert test was negative, and the second case shows a normal radiograph, but the subject had a positive geneXpert test result. Both times, CAD4TB functions as anticipated and under-qualified observers. The causes of the discrepancy between these specific cases' geneXpert results and radiograph appearance are unknown.

In contrast, Figure 4 illustrates two simple situations where the results of the geneXpert and the radiograph (as evaluated by CAD4TB and radiologists) agreed.

Discussion

To the best of our knowledge, this is the first study to evaluate the performance of the automatic software computer-aided detection for tuberculosis (CAD4TBv6) in diagnosing pulmonary TB on chest radiography and compare the CAD4TB software reading with the results of radiologists' reports in the Gaza strip, Palestine. Sputum samples were obtained from those with a score > 40 for GeneXpert analysis and those with symptoms strongly suggestive of pulmonary TB. A certified radiologist read the obtained CXRs.

TABLE 2 Estimated diagnostic accuracy of CAD4TBv6 software in diagnosing pulmonary TB on chest radiography with a threshold score of >40.

Test	Pulmonary TB				
	Present	*n*	Absent	*n*	Total
Positive	True positive	77	False positive	69	146
Negative	True negative	19	True negative	1,072	1,091
Total		96		1,141	
Statistics	**Value**	**95% CI**			
		Upper		Lower	
Sensitivity	80.2%	70.8%		89.6%	
Specificity	94.0%	92.4%		95.3%	
Positive likelihood ratio	13.3	10.3%		17.0%	
Negative likelihood ratio	0.2	0.1%		0.3%	
TB prevalence*	7.8%	6.3%		9.4%	
Positive predictive value*	52.7%	46.5%		58.9%	
Negative predictive value*	98.3%	97.4%		98.8%	
Accuracy*	92.9%	91.3		94.3%	

*These values are dependent on disease prevalence. CI, confidence interval.

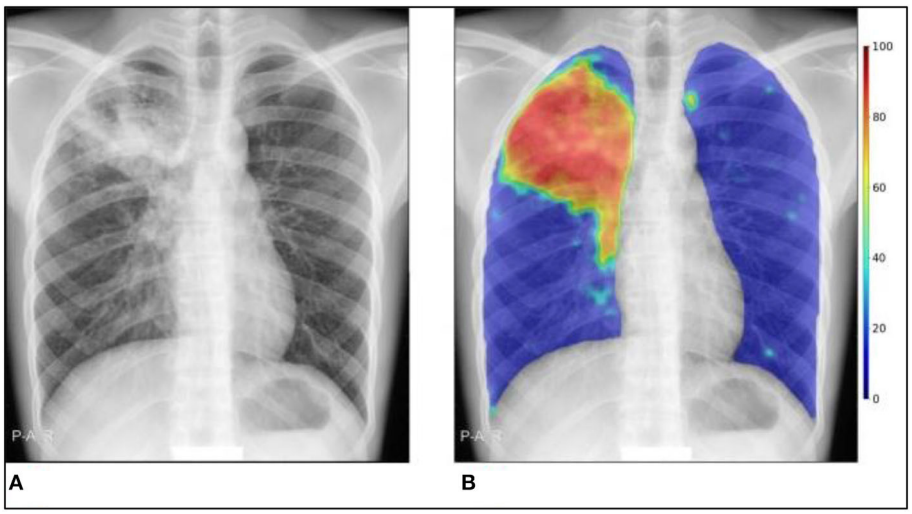

FIGURE 2
CAD4TB v6 output example. **(A)** Original CXR, **(B)** CXR with abnormality heatmap overlay. The Xpert test was positive, and the final composite CAD4TB score for this person was 91.7 (0 = normal, 100 = most abnormal).

Although the utilization of Xpert in programmed applications has increased recently, the WHO has also advocated using screening instruments like CXR that employ more affordable diagnostic algorithms (17, 29–32). Using an automated system to analyze a chest radiograph for the presence of active pulmonary TB produces objective, repeatable results and a consistent format for reporting. Creating software that provides automated CXR interpretation is a significant step toward connecting technology advancements to mass-screening initiatives for TB (23). In addition to increasing case identification in screening programs, using CAD4TB as a triage tool to pre-screen people for Xpert may help lower program expenses (33). Those with low CAD4TB scores had a low likelihood of testing positive for TB, so they might not be prioritized for Xpert testing using this method. Employing a triage tool such as CAD4TB might encourage more judicious use of Xpert by reducing the number of cartridges used in resource-constrained environments where there is not enough money to cover testing for all individuals with presumptive TB. This also applies to settings where onsite radiologists might not always be present to review CXRs. It is important to bear in mind that the costs associated with acquiring and operating digital X-ray devices must be balanced against the potential savings resulting from a reduced need for Xpert exams. This underscores the need for a comprehensive

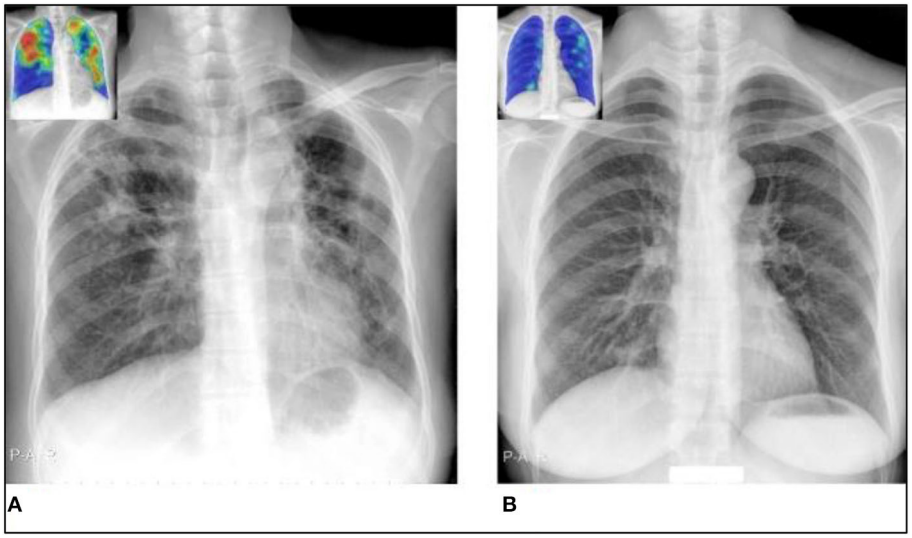

FIGURE 3
Situations in which the radiograph presentation does not match the geneXpert result, making radiograph-only prediction challenging for both observers and CAD4TB. The CAD4TB heatmaps are displayed in the inset photos, with blue denoting the majority of normal texture and red denoting the majority of abnormal texture. **(A)** A geneXpert-negative case identified by all five observers as TB positive (score 3) and by CAD4TB v6 (score = 100). **(B)** A geneXpert-positive case that received a score of 1 (no-TB) from four experts and a score of 2 from the final expert. When a sensitivity of 99% is reached, the 18.7 CAD4TB score for this case indicates that TB has not yet been detected.

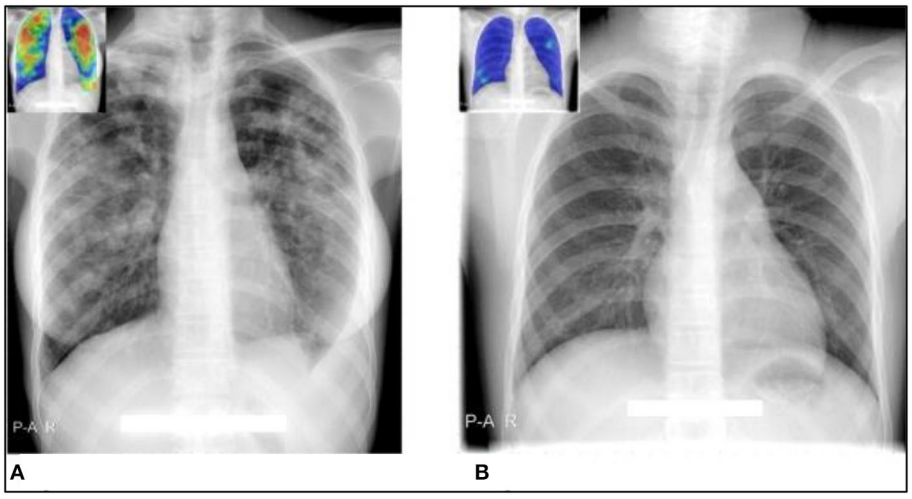

FIGURE 4
Cases where CAD4TB and observers' interpretations of radiographs agree well with geneXpert results. The CAD4TB heatmaps are displayed in the inset photos, with blue denoting the majority of normal texture and red denoting the majority of abnormal texture. **(A)** A case that tested positive for TB using geneXpert was rated as such by all five observers and CAD4TB v6 (score = 91.7). **(B)** A case that received a score of one (no-TB) from all five experts was geneXpert-negative. The case's CAD4TB score is 7.1.

analysis that examines both the financial implications and consequences of widespread mass-screening through chest X-rays (CXR) (25).

According to research by Gautam et al. diabetes has been proven to increase both the likelihood of contracting TB and the severity of the illness (34). Additionally, research has demonstrated that smoking contributes significantly to the development of TB and raises the severity and fatality rates (35). However, our findings were in line with Tavaziva et al. as smoking and diabetes do not seem to make TB more likely to strike or to progress more severely (22).

According to 12 single-center assessment studies, the WHO estimates that Xpert's pooled sensitivity and specificity values for the detection of TB are 92.5 and 98%, respectively (36). However, the accessibility of digital radiography is a need for CAD utilization, which is not yet available in most resource-constrained low-burden settings. Nevertheless, it has been determined to be viable. It produces chest radiography significantly superior to traditional

X-ray equipment in regions with low resources, such as Gaza Strip (37).

The findings of the current study of high specificity, high negative predictive value, high sensitivity, high diagnostic accuracy, and relatively low positive predictive value were consistent with findings from other studies in different settings testing CAD4TB (24, 25, 27, 38, 39). Compared to a confirmatory test like the Xpert, triage tests should have a sensitivity of 90% and a specificity of 70%, according to a 2014 WHO consensus meeting to define targets for new TB diagnostic technologies (40).

The findings of this study point to a feasible, effective, and even cost-effective strategy for TB screening in a symptomatic group that combines CAD4TB and symptomatology. Earlier research from different contexts are consistent with our findings (41–43).

The direct comparison between computerized and radiologist reading on the same set of pictures is one of the study's strengths. The extent to which this comparison may be generalized is severely constrained by the inter-reader variance in the reading of chest X-rays and the possibility of involving only one board-certified radiologist. The fact that our short-term study was only done in a single low-burden region presents a second limit that Data gathered from patients who presented with lower respiratory tract symptoms may not accurately reflect the prevalence of illness in the general community.

It is imperative that forthcoming research endeavors direct their attention toward comprehensively examining the multifaceted ramifications encompassing the adoption of Computer-Aided Diagnosis (CAD) within diverse low-burden nations. In particular, a rigorous investigation is warranted to elucidate the intricate interplay of financial, practical, and ethical considerations inherent in the deployment of CAD within these unique contexts. Subsequent investigative trajectories should encompass an exploration of the potential synergies arising from amalgamating CAD-generated outcomes with an array of clinical parameters, encompassing symptomatic manifestations and risk profiling. Furthermore, a profound research agenda should be undertaken to systematically assess the efficacy of CAD not only within the spectrum of operational feasibility but also across various technical dimensions indispensable for its seamless integration into prevailing diagnostic frameworks. Concurrently, an evaluative lens should be directed toward pioneering CAD products that are emergent within the market landscape. This comprehensive inquiry stands to provide a robust foundation for harnessing the maximal potential of CAD, charting its trajectory toward optimized medical diagnostics within the distinctive landscape of low-burden nations.

Conclusion

Combining chest X-ray readings by CAD4TB and symptomatology is extremely valuable for screening a population at risk in a resource-limited country with a high burden of a neglected disease. CAD4TB is noticeably more efficient than other methods for TB screening and early diagnosis in people who would otherwise go undetected. In order to increase case finding and infection control and lower the cost of case detection within triage algorithms, CAD solutions may present an opportunity. This inspires further investigation into the best ways to utilize its potential as a support tool for clinical officers in the diagnostic interpretation of radiographs as well as a stand-alone triage test in systematic screening settings.

Data availability statement

The raw data supporting the conclusions of this article will be made available by the authors, without undue reservation.

Ethics statement

The study protocol was approved by the Palestinian Health Research Council (Helsinki Committee for Ethical Approval research number: PHRC/HC/1175/22). Additional approval was obtained from the included Gaza Strip hospitals. Study participants provided written informed consent for survey activities.

Author contributions

SA: Conceptualization, Data curation, Formal analysis, Funding acquisition, Investigation, Methodology, Project administration, Resources, Software, Supervision, Validation, Visualization, Writing — original draft, Writing — review & editing. KZ: Methodology, Project administration, Software, Validation, Visualization, Writing — original draft, Writing — review & editing.

Funding

This research was funded by the WHO-EMRO, Unit Reference: AP-22-00673.

Acknowledgments

The authors are grateful to the World Health Organization-Regional Office for the Eastern Mediterranean (WHO-EMRO) and Development Pioneers Company for Consultation (Pioneers) for supporting the implementation of the study. The certified radiologist, hospitals, and patients who participated in the study are all thanked for their vital contributions to conducting the study.

Conflict of interest

The authors declare that the research was conducted in the absence of any commercial or financial relationships that could be construed as a potential conflict of interest.

Publisher's note

All claims expressed in this article are solely those of the authors and do not necessarily represent those of their affiliated

organizations, or those of the publisher, the editors and the reviewers. Any product that may be evaluated in this article, or claim that may be made by its manufacturer, is not guaranteed or endorsed by the publisher.

References

1. WHO. *Tuberculosis*. World Health Organization (2022). Available online at: https://www.who.int/en/news-room/fact-sheets/detail/tuberculosis (accessed January 12, 2023).

2. WHO. *Chest Radiography in Tuberculosis Detection -Summary of Current WHO Recommendations and Guidance on Programmatic Approaches*. World Health Organization (2016). p. 1–44. Available online at: https://www.who.int/tb/publications/Radiography_TB_factsheet.pdf?ua=1 (accessed January 14, 2023).

3. WHO. *Global Tuberculosis Report Executive Summary 2020*. World Health Organization(2022). p. 1–11. Available online at: https://www.who.int/tb/publications/global_report/TB20_Exec_Sum_20201014.pdf?ua=1 (accessed January 15, 2023).

4. Bansal G. Digital radiography. A comparison with modern conventional imaging. *Postgr Med J.* (2006) 82:425–8. doi: 10.1136/pgmj.2005.038448

5. Pande T, Pai M, Khan FA, Denkinger CM. Use of chest radiography in the 22 highest tuberculosis burden countries. *Eur Respir J.* (2015) 46:1816–9. doi: 10.1183/13993003.01064-2015

6. Chartrand G, Cheng PM, Vorontsov E, Drozdzal M, Turcotte S, Pal CJ, et al. Deep learning: a primer for radiologists. *Radiographics.* (2017) 37:2113–31. doi: 10.1148/rg.2017170077

7. Lakhani P, Sundaram B. Deep learning at chest radiography: automated classification of pulmonary tuberculosis by using convolutional neural networks. *Radiology.* (2017) 284:574–82. doi: 10.1148/radiol.2017162326

8. Harris M, Qi A, Jeagal L, Torabi N, Menzies D, Korobitsyn A, et al. systematic review of the diagnostic accuracy of artificial intelligence-based computer programs to analyze chest x-rays for pulmonary tuberculosis. *PLoS ONE.* (2019) 14:e0221339. doi: 10.1371/journal.pone.0221339

9. Gonem S, Janssens W, Das N, Topalovic M. Applications of artificial intelligence and machine learning in respiratory medicine. *Thorax.* (2020) 75:695–701. doi: 10.1136/thoraxjnl-2020-214556

10. Khan FA, Pande T, Tessema B, Song R, Benedetti A, Pai M, et al. Computer-aided reading of tuberculosis chest radiography: moving the research agenda forward to inform policy. *Eur Respiratory Soc.* (2017) 50. doi: 10.1183/13993003.00953-2017

11. Pande T, Cohen C, Pai M, Ahmad Khan F. Computer-aided detection of pulmonary tuberculosis on digital chest radiographs: a systematic review. *Int J Tuberc Lung Dis.* (2016) 20:1226–30. doi: 10.5588/ijtld.15.0926

12. Nash M, Kadavigere R, Andrade J, Sukumar CA, Chawla K, Shenoy VP, et al. Deep learning, computer-aided radiography reading for tuberculosis: a diagnostic accuracy study from a tertiary hospital in India. *Sci Rep.* (2020) 10:1–10. doi: 10.1038/s41598-019-56589-3

13. Fehr J, Konigorski S, Olivier S, Gunda R, Surujdeen A. Computer-aided interpretation of chest radiography to detect TB in rural South Africa 1. *Age.* (2021) 4:1–10.

14. Qin ZZ, Sander MS, Rai B, Titahong CN, Sudrungrot S, Laah SN, et al. Using artificial intelligence to read chest radiographs for tuberculosis detection: a multi-site evaluation of the diagnostic accuracy of three deep learning systems. *Sci Rep.* (2019) 9:1–10. doi: 10.1038/s41598-019-51503-3

15. Khan FA, Majidulla A, Tavaziva G, Nazish A, Abidi SK, Benedetti A, et al. Chest x-ray analysis with deep learning-based software as a triage test for pulmonary tuberculosis: a prospective study of diagnostic accuracy for culture-confirmed disease. *Lancet Digital Health.* (2020) 2:e573–81. doi: 10.1016/S2589-7500(20)30221-1

16. Qin ZZ, Ahmed S, Sarker MS, Paul K, Adel ASS, Naheyan T, et al. Can artificial intelligence (AI) be used to accurately detect tuberculosis (TB) from chest X-ray? A multiplatform evaluation of five AI products used for TB screening in a high TB-burden setting. *medRxiv.* (2020). doi: 10.48550/arXiv.2006.05509

17. Gelaw SM, Kik SV, Ruhwald M, Ongarello S, Egzertegegne TS, Gorbacheva O, et al. Diagnostic accuracy of three computer-aided detection systems for detecting pulmonary tuberculosis on chest radiography when used for screening: analysis of an international, multicenter migrants screening study. *medRxiv.* (2022). doi: 10.1101/2022.03.30.22273191

18. WHO. *Chest Radiography in Tuberculosis Detection: Summary of Current WHO Recommendations and Guidance on Programmatic Approaches*. World Health Organization (2016). p. 26–8. Available online at: https://apps.who.int/iris/bitstream/handle/10665/252424/9789241511506-eng.pdf?sequence=1&isAllowed=y (accessed January 15, 2023).

19. Abuzerr S, Nasseri S, Yunesian M, Hadi M, Mahvi AH, Nabizadeh R, et al. Prevalence of diarrheal illness and healthcare-seeking behavior by age-group and sex among the population of Gaza strip: a community-based cross-sectional study. *BMC Public Health.* (2019) 19:1–10. doi: 10.1186/s12889-019-7070-0

20. Abuzerr S, Nasseri S, Yunesian M, Hadi M, Zinszer K, Mahvi AH, et al. Water, sanitation, and hygiene risk factors of acute diarrhea among children under five years in the Gaza Strip. *J Water Sanit Hyg Dev.* (2020) 10:111–23. doi: 10.2166/washdev.2019.072

21. Mungai B, Ong 'angò J, Ku CC, Henrion MY, Morton B, Joekes E, Onyango E, Kiplimo R, Kirathe D, Masini E. Accuracy of computer-aided chest X-ray screening in the Kenya National Tuberculosis Prevalence Survey. *medRxiv.* (2021). doi: 10.1101/2021.10.21.21265321

22. Tavaziva G, Majidulla A, Nazish A, Saeed S, Benedetti A, Khan AJ, et al. Diagnostic accuracy of a commercially available, deep learning-based chest X-ray interpretation software for detecting culture-confirmed pulmonary tuberculosis. *Int J Infect Dis.* (2022) 122:15–20. doi: 10.1016/j.ijid.2022.05.037

23. Breuninger M, van Ginneken B, Philipsen RH, Mhimbira F, Hella JJ, Lwilla F, et al. Diagnostic accuracy of computer-aided detection of pulmonary tuberculosis in chest radiographs: a validation study from sub-Saharan Africa. *PLoS ONE.* (2014) 9:e106381. doi: 10.1371/journal.pone.0106381

24. Murphy K, Habib SS, Zaidi SMA, Khowaja S, Khan A, Melendez J, et al. Computer aided detection of tuberculosis on chest radiographs: An evaluation of the CAD4TB v6 system. *Sci Rep.* (2020) 10:5492. doi: 10.1038/s41598-020-62148-y

25. Zaidi SMA, Habib SS, Van Ginneken B, Ferrand RA, Creswell J, Khowaja S, et al. Evaluation of the diagnostic accuracy of Computer-Aided Detection of tuberculosis on Chest radiography among private sector patients in Pakistan. *Sci Rep.* (2018) 8:12339. doi: 10.1038/s41598-018-30810-1

26. WHO. *Physical Status: The Use and Interpretation of Anthropometry*. Geneva: World Health Organization (1995).

27. Maduskar P, Muyoyeta M, Ayles H, Hogeweg L, Peters-Bax L, Van Ginneken B. Detection of tuberculosis using digital chest radiography: automated reading vs. interpretation by clinical officers. *Int J Tuberc Lung Dis.* (2013) 17:1613–20. doi: 10.5588/ijtld.13.0325

28. Fehr J, Konigorski S, Olivier S, Gunda R, Surujdeen A, Gareta D, et al. Computer-aided interpretation of chest radiography reveals the spectrum of tuberculosis in rural South Africa. *NPJ Dig Med.* (2021) 4:106. doi: 10.1101/2020.09.04.20188045

29. Philipsen R, Sánchez C, Maduskar P, Melendez J, Peters-Bax L, Peter J, et al. Automated chest-radiography as a triage for Xpert testing in resource-constrained settings: a prospective study of diagnostic accuracy and costs. *Sci Rep.* (2015) 5:12215. doi: 10.1038/srep12215

30. WHO. *Systematic Screening for Active Tuberculosis: Principles And Recommendations*. World Health Organization (2013). Available online at: https://books.google.com.pk/books?hl=-en&lr=-&id=-g7EXDAAAQBAJ&oi=-fnd&pg=PP1&dq=-Systematic+screening+for+active+-tuberculosis:+principles+and+recommendations.+&ots=BnNSCcvlv&sig=N5mkmTU0Ke24X9C5Y9Dxw1V83_M#v=onepage&q=Systematic%20screening%20for%20active%20tuberculosis%3A%20principles%20and%20recommendations.&f=false (accessed January 13, 2023).

31. Qin ZZ, Pai M, Van Gemert W, Sahu S, Ghiasi M, Creswell J. How is Xpert MTB/RIF being implemented in 22 high tuberculosis burden countries? *Eur Respir J.* (2015) 45:549–54. doi: 10.1183/09031936.00147714

32. Kagujje M, Kerkhoff AD, Nteeni M, Dunn I, Mateyo K, Muyoyeta M. The performance of computer-aided detection digital chest X-ray reading technologies for triage of active tuberculosis among persons with a history of previous tuberculosis. *Clin Infect Dis.* (2023) 76:e894–901. doi: 10.1093/cid/ciac679

33. Story A, Aldridge RW, Abubakar I, Stagg H, Lipman M, Watson J, et al. Active case finding for pulmonary tuberculosis using mobile digital chest radiography: an observational study. *Int J Tuberc Lung Dis.* (2012) 16:1461–7. doi: 10.5588/ijtld.11.0773

34. Gautam S, Shrestha N, Mahato S, Nguyen TP, Mishra SR, Berg-Beckhoff G. Diabetes among tuberculosis patients and its impact on tuberculosis treatment in South Asia: a systematic review and meta-analysis. *Sci Rep.* (2021) 11:2113. doi: 10.1038/s41598-021-81057-2

35. Khan AH, Sulaiman SAS, Hassali MA, Khan KU, Ming LC, Mateen O, et al. Effect of smoking on treatment outcome among tuberculosis patients in Malaysia; a multicenter study. *BMC Public Health.* (2020) 20:1–8. doi: 10.1186/s12889-020-08856-6

36. WHO. *Xpert MTB/RIF Implementation Manual*. World Health Organization (2014). Available online at: http://apps.who.int/iris/bitstream/handle/10665/112469/9789241506700_eng.pdf (accessed January 12, 2023).

37. Zennaro F, Oliveira Gomes JA, Casalino A, Lonardi M, Starc M, Paoletti P, et al. Digital radiology to improve the quality of

care in countries with limited resources: a feasibility study from Angola. *PLoS ONE.* (2013) 8:e73939. doi: 10.1371/journal.pone.0073939

38. Theron G, Peter J, van Zyl-Smit R, Mishra H, Streicher E, Murray S, et al. Evaluation of the Xpert MTB/RIF assay for the diagnosis of pulmonary tuberculosis in a high HIV prevalence setting. *Am J Respir Crit Care Med.* (2011) 184:132–40. doi: 10.1164/rccm.201101-0056OC

39. van't Hoog AH, Meme H, Van Deutekom H, Mithika A, Olunga C, Onyino F, Borgdorff M. High sensitivity of chest radiograph reading by clinical officers in a tuberculosis prevalence survey. *Int J Tuberc Lung Dis.* (2011) 15:1308-1314. doi: 10.5588/ijtld.11.0004

40. WHO. *High-Priority Target Product Profles for New Tuberculosis Diagnostics: Report of a Consensus Meeting*. Tech. Rep. World Health Organization (2014). Available online at: http://apps.who.int/iris/bitstream/handle/10665/135617/WHO_HTM_TB_2014.18_eng.pdf (accessed January 16, 2023).

41. Fatima R, Qadeer E, Yaqoob A, Haq MU, Majumdar SS, Shewade HD, et al. Extending 'contact tracing'into the community within a 50-metre radius of an index tuberculosis patient using Xpert MTB/RIF in urban, Pakistan: did it increase case detection? *PLoS ONE.* (2016) 11:e0165813. doi: 10.1371/journal.pone.0165813

42. Vo LNQ, Vu TN, Nguyen HT, Truong TT, Khuu CM, Pham PQ, et al. Optimizing community screening for tuberculosis: Spatial analysis of localized case finding from door-to-door screening for TB in an urban district of Ho Chi Minh City, Viet Nam. *PLoS ONE.* (2018) 13:e0209290. doi: 10.1371/journal.pone.0209290

43. Nishtar T, Burki S, Ahmad FS, Ahmad T. Diagnostic accuracy of computer aided reading of chest x-ray in screening for pulmonary tuberculosis in comparison with Gene-Xpert. *Pak J Med Sci.* (2022) 38:62. doi: 10.12669/pjms.38.1.4531

frontiers | Frontiers in Microbiology

TYPE Original Research
PUBLISHED 14 December 2023
DOI 10.3389/fmicb.2023.1257267

OPEN ACCESS

EDITED BY
Lin Fan,
Tongji University, China

REVIEWED BY
Yuan Liang,
Nanjing Medical University, China
Erin J. Van Schaik,
Texas A&M University, United States

*CORRESPONDENCE
Yan Li
✉ liyan.nju@163.com
Limei Zhu
✉ 309122229@qq.com

†These authors have contributed equally to this work and share first authorship

RECEIVED 12 July 2023
ACCEPTED 06 November 2023
PUBLISHED 14 December 2023

CITATION
Li G, Feng Z, Song H, Wang Y, Zhu L and Li Y (2023) Long non-coding RNA expression in PBMCs of patients with active pulmonary tuberculosis.
Front. Microbiol. 14:1257267.
doi: 10.3389/fmicb.2023.1257267

Long non-coding RNA expression in PBMCs of patients with active pulmonary tuberculosis

Guoli Li[2†], Zhelong Feng[3†], Honghuan Song[2], Yajing Wang[3], Limei Zhu[2*] and Yan Li[1,2*]

[1]Integrated Service and Management Office, Jiangsu Provincial Center for Disease Control and Prevention, Nanjing, China, [2]Department of Chronic Communicable Disease, Jiangsu Provincial Center for Disease Control and Prevention, Nanjing, China, [3]School of Basic Medicine and Clinical Pharmacy, China Pharmaceutical University, Nanjing, China

Purpose: *Mycobacterium tuberculosis* (*Mtb*) infection is the primary cause of the chronic infectious illness tuberculosis (TB). Long non-coding RNAs (lncRNAs) are functional RNA molecules that cannot be translated into proteins and play a crucial role in regulating the immune system's innate and adaptive responses. It has been demonstrated that the dysregulation of lncRNA expression is associated with various human diseases. However, the mechanism underlying the involvement of so many lncRNAs in the immune response to TB infection remains unclear. The objective of our current study was to identify a number of significantly differentially expressed lncRNAs in peripheral blood mononuclear cells (PBMCs) from TB patients and to select the most indicative lncRNAs as potential biomarkers for active pulmonary tuberculosis.

Methods: Microarray analysis was performed to determine the lncRNA and mRNA expression profiles in TB patients using a case-control model. The differentially expressed lncRNAs were subjected to gene ontology (GO) and Kyoto Encyclopedia of Genes and Genomes (KEGG) pathway analysis to investigate potential roles and pathways associated with the pathogenesis of TB infection, and to screen lncRNAs specifically linked to TB infection. Using real-time fluorescence quantitative PCR (QRT-PCR), specific lncRNAs were identified in TB patients and latent infections.

Results: Our findings revealed that various signaling pathways were differentially expressed in TB-infected individuals, suggesting a potential role for lncRNAs in the immunological responses driven by TB infection. This study provides crucial guidelines for future functional research. Upregulated lncRNAs were mainly enriched in Neutrophil extracellular trap formation and Chemokine signaling pathways, while downregulated lncRNAs were enriched in Neuroactive ligand-receptor interaction and Cushing syndrome in TB PBMCs. Furthermore, we found that lnc-XPNPEP1-5, lnc-CASKIN2-2, lnc-HSPA13-6, lnc-CLIC5-1, and LINC02502 were significantly downregulated in TB-infected patients, while LINC00528, lnc-SLC45A4-3, and LINC00926 were significantly upregulated in TB patients and latent infections. These eight lncRNAs, identified as novel biological marker candidates for diagnosing TB infection, were validated by real-time fluorescence quantitative PCR (QRT-PCR).

Conclusion: The abnormally expressed lncRNAs identified in this research may provide crucial information for understanding the pathophysiological

characteristics of TB patients and the dysfunction of PBMCs. Our findings reveal potential targets for early TB diagnosis and therapy, as well as offer new insights into the mechanisms underlying TB infection.

KEYWORDS

tuberculosis, latent tuberculosis infection (LTBI), long non-coding RNAs, PBMCs, RRT-PCR, biomarker

Introduction

Tuberculosis (TB) is a grave public health concern that poses significant risks to human health. *Mycobacterium tuberculosis* (*Mtb*), the pathogen responsible for TB, is prevalent among approximately one-third of the global population. Among those infected, roughly 5–10% suffer from active pulmonary tuberculosis. The World Health Organization's (WHO) most recent study estimates that there were 10.6 million new TB cases worldwide in 2021, with an incidence rate of 134 per 100,000. Globally, TB remains one of the leading causes of mortality, and in 2021 it was the second-highest cause of death overall, surpassed only by COVID-19. China ranks third among the 30 nations with the highest TB burden, following India and Indonesia. In 2021, China reported 780,000 new TB cases, with a tuberculosis incidence of 55 per 100,000 individuals. The increasing incidence of multidrug-resistant (MDR), extensively drug-resistant (XDR), and entirely drug-resistant TB is exacerbating the challenges associated with this disease (World Health Organization, 2022). To prevent and control TB and develop novel medications, it is essential to understand the mechanisms of *Mtb* infection and survival within the host (Boro et al., 2016). Following macrophage phagocytosis during host-pathogen interactions, *Mtb's* intracellular survival and reproduction elicit an immunological response that ultimately leads to the development of granulomas and/or disease manifestations (Qian et al., 2018). To facilitate the eradication of active tuberculosis (ATB), host cells have evolved several clearance processes, which include apoptosis, autophagy, inflammation, and macrophage polarization. Concurrently, *Mtb* has developed an array of near-perfect immune evasion mechanisms to help it evade the host immune system (Boro et al., 2016; Healy et al., 2021).

Long-non-coding RNAs (lncRNAs) are a type of RNAs with transcripts longer than 200 nucleotides that do not directly encode proteins but have the ability to regulate chromatin remodeling and transcriptional and post-transcriptional regulation of gene expression (Schwenk and Arnvig, 2018; Li Y. et al., 2019). At the epigenetic, transcriptional, and post-transcriptional levels, lncRNAs have been demonstrated to play crucial roles in controlling gene expression. LncRNAs exert their influence on a broad range of biological processes through intricate and diverse mechanisms, such as participating in the regulation of chromatin's open or closed state prior to transcription, interacting with transcription factors to modulate gene transcription, and engaging in variable shear regulation (Schwenk and Arnvig, 2018; Wang et al., 2019; Fathizadeh et al., 2020). LncRNAs possess the capacity to form hybrid structures with DNA, thereby affecting gene expression. They interact with unstranded DNA bases through complementary pairing to control DNA methylation and transcriptional inhibition (Zhang et al., 2019). Additionally, lncRNAs can alter the binding of transcription factors at promoter regions, impeding their activity or limiting the recruitment of Pol II, thereby modifying the transcription of downstream target genes (Wang and Chang, 2011; Yang et al., 2016; Li Y. et al., 2019). LncRNAs attract transcription regulators to the promoter region of target genes at the RNA level, where they exert control over the target genes' transcription (Ye et al., 2022; Zhang et al., 2022). At the protein level, lncRNAs bind to specific proteins to govern their associated protein activity or modify the cellular localization of these proteins.

According to accumulating evidence, lncRNAs significantly regulate the innate immunological response of host macrophages (Li M. et al., 2019). LncRNAs participate in innate immunity that is regulated by macrophages, and an inducible pattern of inflammatory gene expression is essential for the body's defense against microbes (Hu et al., 2020; Li et al., 2020; Wang et al., 2020). For instance, to control the inflammatory response to *Mtb* infection, lincRNA-Cox2 regulates the activation or repression of immune-related genes, activating NF-κB and STAT (Schwenk and Arnvig, 2018; Yan et al., 2018). Numerous studies indicate that a significant number of lncRNAs likely play a vital role in the pathophysiology of tuberculosis by controlling the apoptosis and autophagy caused by *Mtb* in macrophages (Roy et al., 2018). For example, macrophages infected with BCG induce apoptosis by upregulating the expression of lincRNA-Cox2. Activation of the PERK-eIF-2-CHOP signaling pathway by Cox2 knockdown exacerbates the accumulation of reactive oxygen species (ROS) and initiates apoptosis (Yan et al., 2018).

Most clinical diagnostic techniques currently in use have certain limitations (Healy et al., 2021; Wei et al., 2021). Interferon-gamma release assays (IGRA) are unable to differentiate between latent tuberculosis infection (LTBI) and active tuberculosis (ATB), while sputum smear and culture lack adequate sensitivity, timeliness, and a poor detection rate for smear-negative pulmonary tuberculosis (PTB) (Venkatappa et al., 2019). The World Health Organization (WHO) has recently proposed non-pathogen-based diagnosis as a method to enhance the rapid and universal identification of clinically confirmed TB (Broderick et al., 2021; Jung et al., 2021). As such, biomarkers of the host immune response may provide critical information for addressing this issue (Li et al., 2020; Fang et al., 2021). Various lncRNAs have been proposed as potential biomarkers. An increasing body of research indicates that peripheral blood mononuclear cells (PBMCs) from TB patients exhibit abnormal expression of lncRNAs (Qian et al., 2018; Zhang et al., 2020; Yi et al., 2021).

A study suggests that two highly aberrantly expressed long non-coding RNAs (MIR3945HG V1 and MIR3945HG V2) in PBMC samples from individuals with active PTB could potentially serve as novel diagnostic biomarkers (Kaushik et al., 2021). Additionally, NEAT1 expression—including both NEAT1 1 and NEAT1 2—was found to be elevated in TB patients compared to healthy controls, with the expression declining progressively throughout therapy and returning to normal levels. This dynamic change in NEAT1 expression could potentially indicate the effectiveness of anti-TB treatment, making it a possible biomarker for prognosticating TB patient outcomes (Huang et al., 2018). In this study, we employed microarray detection to identify multiple key lncRNAs that are expressed in PBMCs of TB patients. By selecting the most representative lncRNAs, we aim to establish them as potential biomarkers for active pulmonary tuberculosis. Further research is required to explore the mechanism of these lncRNAs in the immune imbalance that occurs in pulmonary tuberculosis. This understanding may provide valuable insights into their role in the pathogenesis of the disease and could help guide therapeutic interventions. These lncRNAs could serve as biomarkers for biological early warning and precision treatment, enabling more accurate diagnosis, prognosis, and personalized treatment plans for TB patients. This approach has the potential to improve patient outcomes and reduce the burden of tuberculosis worldwide.

Materials and methods

Study cohort

The study group comprised of three subgroups: TB patient group, TB infection group, and healthy control group (HC group).

Tuberculosis patient group: 53 TB patients receiving primary therapy who tested pathogenic positive were enrolled from the Department of TB at Jiangsu Infectious Disease Hospital. All patients were diagnosed according to clinical manifestations, bacteriological identification, and genotyping as *Mycobacterium tuberculosis*, in accordance with the 2017 Chinese Medical Association's Clinical Diagnosis and Treatment Manual (Tuberculosis Branch). The study was approved by the Jiangsu Provincial Center for Disease Control and Prevention, and all patients provided informed consent (Ethics Authorization Number: JSCDCLL (2014)003).

Tuberculosis infection group: Blood specimens from the same period of physical examination, identified as TB infection by the IGRA (T-spot) method, constituted a total of 50 cases. The T-spot Positive result was defined as having $\geq$8 spots in Panel A and/or Panel B.

HC group: Blood specimens from the same period of physical examination, identified as non-TB infected by IGRA (T-spot) method, included a total of 53 cases. The T-spot Negative result was defined as having both Panel A and Panel B spot counts $\leq$4, including values <0.

The differences in age and sex between the above 3 groups were not statistically significant (P-value > 0.05). For the microarray analysis, three samples from the HC group and three samples from the TB Patient group were included. The remaining samples in each group were used for validation (50 samples in each group).

Reagents and instruments

Erythrocyte lysate was purchased from Beijing Tiangen Biotechnology Co., Ltd. Ficoll lymphocyte separation solution was purchased from Sigma Company, and Trizol, Superscript III PlatinumOneStep fluorescent quantitative PCR System reagents were purchased from Invitrogen Company. DX fluorescent quantitative PCR instrument was purchased from ABI company, AII biosafety cabinet was purchased from Thermo company, and CO_2 incubator was purchased from Thermo Fisher.

PBMC collection

In this study, 5 mL of venous blood was collected from research subjects using Vacutainer® CPT™ Mononuclear Cell Preparation Tube (BD, Cat. #362761), which could separate mononuclear cells from whole blood in a fully closed system. Whole blood is drawn directly into the CPT™ tubes using standard phlebotomy techniques and processed in the same tube. To isolate the mononuclear cells, the blood samples were centrifuged within 2 h at room temperature at a speed of 1800 RCF for 20 min. During centrifugation, the gel forms a physical barrier between the mononuclear cells in plasma and the erythrocytes and granulocytes. After centrifugation, the collected mononuclear cells were transferred to 15 mL tubes using a Pasteur pipette. To wash the cells, PBS was added and the mixture was centrifuged for 15 min at 300 RCF. Finally, the cell pellet was resuspended in 1 mL of AIM-V medium for further procedures.

Total RNA extraction

For each RNA preparation, 500 μl of resuspended PBMCs (peripheral blood mononuclear cells) were used. In accordance with the instructions, total RNA was isolated using the mirVana™ RNA Isolation Kit (QIAGEN). The process began by adding an equal volume of chloroform and centrifuging at 10,000 × g for 5 min. The supernatant was then collected. Next, 1.25 times the volume of 100% ethanol was added, the mixture was vortexed, and it was passed through a purification column. The centrifuge was run at 10,000 × g for 15 s, and 350 μL of wash solution was added. The centrifuge was run again at 10,000 g for 15 s. After that, 10 μL of DNase I and 70 μL of Buffer RDD were added, and the mixture was allowed to stand for 15 min at room temperature. It was then washed 2–3 times with 500 μL, with each wash followed by a centrifuge run at 5–10 s. The purification column was washed twice, and the centrifuge was run at 10,000 g for 15 s. The filtrate was discarded, and the centrifuge was run for 1 min. Lastly, 100 μL of pre-warmed eluent at 95°C was added to the center of the column. The centrifuge was run at the highest speed for 30 s at room temperature, and the collected total RNA was stored in a new EP tube at −80°C.

Total RNA and chip quantification

Thermo Scientific's NanoDrop ND-2000 was utilized for RNA quantification, while the Agilent Bioanalyzer 2100

was employed to assess the integrity of the RNA samples (both from Agilent Technologies). The process followed the manufacturers' recommended protocols for sample labeling, microarray hybridization, and washing. Briefly, the whole RNA was first converted to double-stranded cDNA, which was then transcribed into cRNA and tagged with cyanine-3-CTP. The resulting microarray was hybridized with the respective cRNAs. Post-washing, the Agilent Scanner G2505C was used for scanning the arrays.

mRNA chip detection

The GeneChip Human TranscriptomeArray 2.0 chip was employed to detect changes in lncRNA expression. Six qualified RNAs, judged by their RIN score $\geq$7 and 28S/18S ratio $\geq$0.7, were amplified and transcribed into fluorescently labeled cRNA samples. The Agilent Gene Expression Hybridization Kit (Agilent p/n 5188-5242) was used for Fragmentation and Hybridization, with 33045 LncRNA and 30215 mRNA probes (4 replicates per probe per array). Following hybridization, the microarrays were cleaned, fixed, and scanned using a DNA microarray scanner. The Agilent Scanner was used to scan the chip after hybridization, extracting the original signal values. Data normalization and probe filtering were performed prior to screening for differentially expressed genes. At least one group of samples in each comparison group must have 100% of the probes marked as "P" for subsequent analysis. For analysis with biological replicates, the difference in standardized signal values (Fold change) and significant *P*-value from the *T*-test were used for screening, with criteria of Fold change value $\geq$2.0 and *P*-value $\leq$ 0.05.

To search for differentially expressed signaling pathways and functionally forecast the function of the differentially expressed lncRNAs, GO analysis and KEGG pathway analysis were performed. These analyses compared target lncRNAs with genes in databases to obtain information about the biological processes, cellular components, and molecular functions and pathways they participate in. R/Bioconductor packages (GOseq2, KEGG.db3) were used for these analyses. The specific analysis process included Gene annotation, Enrichment analysis, and Functional/Pathway clustering.

Fluorescence quantitative PCR validation

Based on the chip detection results, specific Taqman primers were designed to select 50 healthy controls without *Mtb* infection, 50 latent TB infection, and 50 patients with confirmed pulmonary tuberculosis for correlation analysis. Eight lncRNAs were chosen from the lncRNA profiles due to their strong association with mRNAs that exhibited minimal variation within the group but showed significant differences between groups. By referring to the existing gene nucleotide sequences in the PubMed database, DNASTAR software was employed for homology analysis, and conserved regions were selected. Subsequently, PrimerExpress 3.0 software was used to design primers and probes, respectively. The synthesis of primers and probes was entrusted to Sangon Biotech (Shanghai) Co., Ltd. A fluorescent emitting group FAM was attached to the 5' end of the probe, while the fluorescent emitting group BHQ1 was attached to the 3' end of the probe. **Table 1** presents the primer and probe sequences. The target fragment was amplified using a one-step method. The concentrations of primers and probes are presented in **Table 1**, and a 10 μL reaction system was employed. The system preparation is detailed in **Table 2**. The conditions for fluorescence quantitative PCR reaction were as follows: 52°C for 10 min, 95°C for 5 min; 95°C for 15 s, 58°C for 40 s, 42 cycles; and 25°C for 5 min. The fluorescence signal was detected at the annealing stage at 58°C. Six replicate wells were prepared for all samples, with GAPDH serving as the internal reference gene. The qRT-PCR results were analyzed based on the Ct value of the sample to be tested, using the relative quantitative method. The relative expression of the target gene ($-\Delta\Delta$Ct) represented the relative change in expression of the target gene in each group of PBMC samples.

Statistical analysis

The study results were statistically processed using R Studio version 1.4.1106. The results were expressed as mean $\pm$ standard deviation ($-x \pm s$). The *t*-test was employed to compare the means of two groups, while one-way analysis of variance (ANOVA) was used to compare the data between various groups. A *P*-value of less than 0.05 was considered statistically significant.

Result

Chip quantification results

The lncRNA expression in each group was visually represented by the chip hybridization scan, box plot, scatter plot, and Principal Component Analysis (PCA) plot (**Figure 1**). The chip hybridization scan results demonstrated that the chip hybridization was of good quality, with reliable data signals and distinct expression differences between the two groups. The distribution of data within the case and control groups was more concentrated, and the intergroup difference was more pronounced, indicating that there are significant disparities between the two groups of samples.

Expression signatures of the deregulated lncRNAs

Using human lncRNA arrays, the expression profiles of lncRNAs and mRNAs in peripheral blood mononuclear cells (PBMCs) were investigated. For six samples, the unnormalized raw lncRNA and mRNA data were transformed to log2 values. Unsupervised phylogenetic clustering analysis showed a distinct separation of lncRNAs into two groups (**Figure 2A**). By applying a fold change of 2 and a false discovery rate (FDR) of 0.05, significantly differentially expressed genes were identified. The volcano plot illustrates the lncRNA abundance and distribution (**Figure 2B**).

10.3389/fmicb.2023.1257267

TABLE 1 Gene hybridization primer and probe sequences and working concentrations.

Gene	Primers/probes (5′-3′)	Final conc. (μM)
FR255266-FP	AACCTACAGAGGCAAATCC	40
FR255266-RP	CCATTAGCTTAGCATCTGTCG	40
FR255266-PROBE	FAM-CTGTAGCCTCATCTCATGTGCT-BHQ1	10
NONHSAT006952-FP	CGCAGCCCTGAAGAAACTAC	40
NONHSAT006952-RP	AAGCTTCACTGTCCCTCCAA	40
NONHSAT006952-PROBE	FAM-GCCGGCTCCTTTGAAAACAGGTCATAT-BHQ1	10
TCONS_l2-FP	AGGTGCCAGTAAATGTATGAG	40
TCONS_l2-RP	TCAGGACTGGTTATGACCG	40
TCONS_l2-PROBE	FAM-AGTGGAGTAGTGCCTCCCTGGT-BHQ1	10
β-Catenin-FP	GCTGCTTGTACGAGCACATCA	40
β-Catenin-RP	TGCGT TCCACCCATGGA	40
β-Catenin-PROBE	FAM-ACACCCAACGGCG-BHQ1	10
TCF-FP	CGCCTGAGGGTCCGAGATA	40
TCF-RP	GCACCATACGGCCAAGCT	40
TCF-PROBE	FAM-CGCGACCCGAATTGAGAACCAAGTAATGCGTCGCG-BHQ1	10
GSK-3β-FP	CCCTCTGGCCACCATCCT	40
GSK-3β-RP	CCCTCTGGCCACCATCCT	40
GSK-3β-PROBE	FAM-CCCTCCACATGCTC-BHQ1	10
GAPDH-FP	ATGGAAATCCCA TCACCATCTT	40
GAPDH-RP	CGCCCCACTTGATTTTGG	40
GAPDH-PROBE	FAM-CAGGAGCGAGATCC-BHQ1	10

Expression profile of lncRNAs in PBMCs

The results revealed that 1904 LncRNAs were differentially expressed between health controls and active TB patients (Figure 3). As compared to the control group, the active pulmonary TB group showed up-regulation in 1081 lncRNAs and down-regulation in 823 lncRNAs, among which, the top 10 lncRNAs that were up- and down-regulated are shown in Table 2. NONHSAG003987 was the most upregulated lncRNA gene among them, while linc-SNAP25-1 was the most downregulated gene. The top 10 mRNAs that were up- and down-regulated are listed in Table 3. The most upregulated mRNA gene among them was CHI3L1, whereas the most downregulated gene was FAM177B.

Functional prediction results of the differentially expressed lncRNAs

Gene Ontology (GO)[1] and Kyoto Encyclopedia of Genes and Genomes (KEGG)[2] pathway analyses of the dysregulated mRNAs were performed to elucidate the functions of lncRNAs, with separate analyses conducted for upregulated and downregulated mRNAs. Initially, we identified the co-expressed mRNAs for each differentiated lncRNA and conducted a functional enrichment analysis on this group. The predicted functional term for a specific lncRNA was derived from the enriched functional terms. Co-expressed lncRNA mRNAs were discovered using Pearson Correlation calculations with correlation P-values < 0.05, using R Studio. Subsequently, we employed the hypergeometric cumulative distribution function to determine the enrichment of functional terms in the annotation of co-expressed mRNAs.

The results indicated that PBMCs from TB patients significantly differed from healthy controls in terms of biological processes and signaling pathways. Based on the GO analysis, the majority of biological processes featuring dysregulated lncRNAs were primarily associated with neutrophil activation, immune responses involving neutrophil activation, neutrophil-mediated immunity, and neutrophil degranulation. In contrast, the KEGG analysis revealed that downregulated mRNAs were associated with neuroactive ligand-receptor interaction and olfactory transduction, while upregulated lncRNAs were primarily enriched in neutrophil extracellular trap formation, the chemokine signaling pathway, and FcgammaR-mediated phagocytosis in TB patients. Figure 3 depicts the key functional clusters.

The results indicate that the response of PBMCs during active TB infection is characterized by variable regulation and suppression.

Correlation analysis of lncRNAs and mRNAs

We constructed a lncRNA-mRNA interaction network to explore the regulatory mechanisms of lncRNAs in PTB. We first

1 https://geneontology.org/

2 https://www.genome.jp/kegg/

calculated the Pearson Correlation between the expression values of each lncRNA and each mRNA. Then, we combined the data of differentially expressed (DE) mRNAs and DE lncRNAs after performing correlation analysis on the lncRNA-mRNA pair.

For correlation analysis, we used a total of 198 DE lncRNAs and 392 DE mRNAs obtained from our data. The lncRNA-mRNA interaction network was built according to the interaction mechanism of the two molecules. As a result, we discovered a total of 469 lncRNA-mRNA interactions, including 239 mRNAs and 64 lncRNAs (**Figure 4**).

This network provides valuable insights into the regulatory roles of lncRNAs in PTB. The identified interactions can help researchers understand the molecular pathogenesis of PTB and potentially identify new therapeutic targets for the treatment of the disease. Additionally, these networks can be used to further study the functional roles of lncRNAs in other biological processes and pathological conditions.

qRT-PCR validation

To validate the microarray results, we selected eight lncRNAs for real-time quantitative polymerase chain reaction (QRT-PCR) examination across all samples. The selected lncRNAs were LINC00528, lnc-SLC45A4-3, LINC00926, lnc-XPNPEP1-5, lnc-CASKIN2-2, lnc-HSPA13-6, lnc-CLIC5-1, and LINC02502.

The results showed that the expression of lncRNAs LINC00528, lnc-SLC45A4-3, and LINC00926 was significantly higher in both the latent infection group and the TB patient group compared to the uninfected HC group (P-value < 0.05). On the other hand, the expression of lncRNAs lnc-XPNPEP1-5, lnc-CASKIN2-2, lnc-HSPA13-6, lnc-CLIC5-1, and LINC02502 was significantly reduced in both the latent infection group and the TB patient group compared to the uninfected HC group (all P-values < 0.05).

The findings from the QRT-PCR analysis were consistent with the microarray data, supporting the reliability of our results. This validation process strengthens the evidence for the regulatory roles of these lncRNAs in PTB, providing a basis for further research into their functional roles and potential therapeutic targets (**Figure 5**).

Discussion

In the present study, we employed microarray technology to examine the mRNA and lncRNA expression profiles of peripheral blood mononuclear cells (PBMCs) from tuberculosis (TB) patients and healthy individuals. This was followed by bioinformatics analysis to delve into the functional networks and potential regulatory roles of the differentially expressed lncRNAs and mRNAs. To corroborate our findings, we also used quantitative real-time polymerase chain reaction (qRT-PCR). Through microarray analysis, we were able to compare the lncRNA expression profiles of TB patients and healthy controls. The bioinformatics analysis revealed several lncRNAs and mRNAs with altered expression in PBMCs from TB patients, suggesting that these aberrant long non-coding RNAs (lncRNAs) may play crucial roles in the pathophysiology and progression of tuberculosis. We further identified several

TABLE 2 The top 10 upregulated and downregulated lncRNAs in the PBMCs of ATB patients, compared to the HC group.

lncRNA gene symbol	Regulation	Fold change	*P*-value
NONHSAG003987	Up	171.35942	0.020535182
NONHSAG028745	Up	119.57172	0.00110843
AD000685.1-001	Up	54.02492	0.000188
RP11-678G14.4-002	Up	51.42291	0.0000638
NONHSAG003812	Up	49.56341	0.001218415
CCDC147-AS1	Up	42.48658	0.007961398
NONHSAG054582	Up	40.38269	0.00755706
FR346361	Up	39.48970	0.00795282
RP4-620F22.2-001	Up	38.01553	0.003028001
RP11-925D8.6	Up	35.73091	0.039328746
linc-SNAP25-1	Down	149.43263	0.005198977
NONHSAG029335	Down	135.94028	0.01675956
NONHSAG015932	Down	112.96288	0.006525897
NONHSAG019454	Down	67.02208	0.000506
LOC101927998	Down	51.443554	0.004187135
linc-GRAMD3-2	Down	33.895023	0.019641997
NONHSAG019533	Down	27.05918	0.010219458
NONHSAG020174	Down	18.319973	0.004563094
NONHSAG041748	Down	17.41906	0.0000936
linc-MRPL22	Down	15.715142	0.00137531

dysregulated biological processes in human PBMCs, including "neutrophil extracellular trap formation," "Chemokine signaling pathway," "Fc gamma R-mediated phagocytosis," "Neuroactive ligand-receptor interaction," and "AMPK signaling pathway," using KEGG pathway-based paired-sample analysis. The majority of these dysregulated pathways are essential for the onset and progression of tuberculosis.

Neutrophils play a significant role in the pathogenesis of TB, as they are rapidly recruited to the infection site and capture *Mycobacterium tuberculosis* (*Mtb*) in extracellular traps (NETs) (Borkute et al., 2021; Pellegrini et al., 2021). This occurs due to the release of neutrophil extracellular traps (NETs), which contain antigens that can prime T cells and exacerbate inflammation. Moreover, neutrophils can modulate the immune response by interacting with other immune cells, such as macrophages, dendritic cells, and T cells. Neutrophils have been shown to generate NETs in response to various microbes, TLRs, Fc receptors, chemokine and cytokine receptors, as well as in response to stimulating substances like phorbol myristate acetate (PMA) (Braian et al., 2013; Ravindran et al., 2019). Chemokines produced in response to *Mtb* infection have been shown to efficiently facilitate the trafficking of dendritic cells (DCs) to the lymph nodes, the attraction of activated T cells to the lung, and the proper positioning of T cells within the lung parenchyma to mediate optimal *Mtb* control (Monin and Khader, 2014). These chemokine-dependent pathways facilitate the inhibition of *Mtb* development, although they often do not eradicate the bacteria entirely (Park et al., 2021). The design of vaccines and adjuvants can be significantly

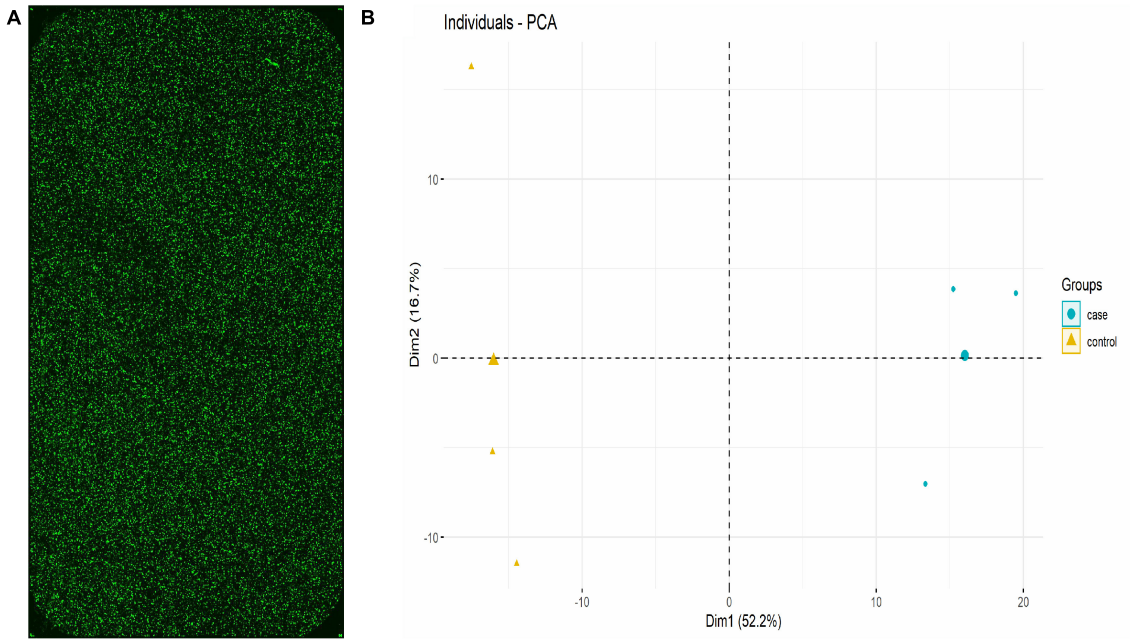

FIGURE 1
lncRNA expression in each group (Three samples in HC group and three samples in TB patients). **(A)** Chip hybridization scan showed that the fluorescence intensity was good, the signal was clear, and the density was uniform, which confirmed that the hybridization was in good condition. **(B)** PCA plot showed the distribution of the samples. The case and control were concentrated in different regions in the two-dimensional space, indicating that the samples are grouped reasonably and the repeatability within the group was good.

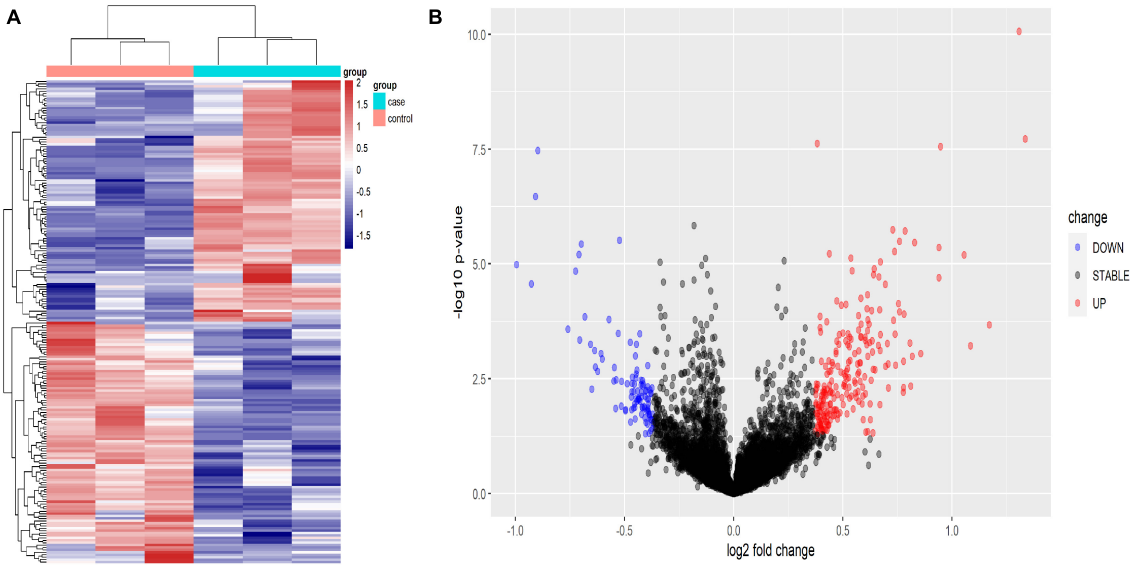

FIGURE 2
Heat map **(A)** and volcano plot presentation **(B)** of the lncRNA expression profiles in the TB patient group and the HC group. **(A)** Each column represents a sample and each row represents a gene. Red represents high relative expression and blue represents low relative expression. **(B)** Red represents significantly up-regulated genes and blue represents significantly down-regulated genes. Genes with an expression fold change >2 and FDR-adjusted *P*-value < 0.05 were considered statistically significant.

improved by gaining a deeper understanding of the mechanisms underlying *Mtb* containment, which will also contribute to the development of novel anti-TB medicines. Several studies have identified *Mtb* lncRNAs that may be involved in regulating the immune response, including those that modulate the function of neutrophils. Studis reported that *Mtb*-lncRNA, a lncRNA encoded by the *Mtb* genome, regulates the expression of various *Mtb* genes involved in metabolism, virulence, and stress response. This lncRNA has also been shown to modulate the expression of pro-inflammatory cytokines in macrophages and neutrophils, suggesting that it may play a role in regulating the immune response against *Mtb*.

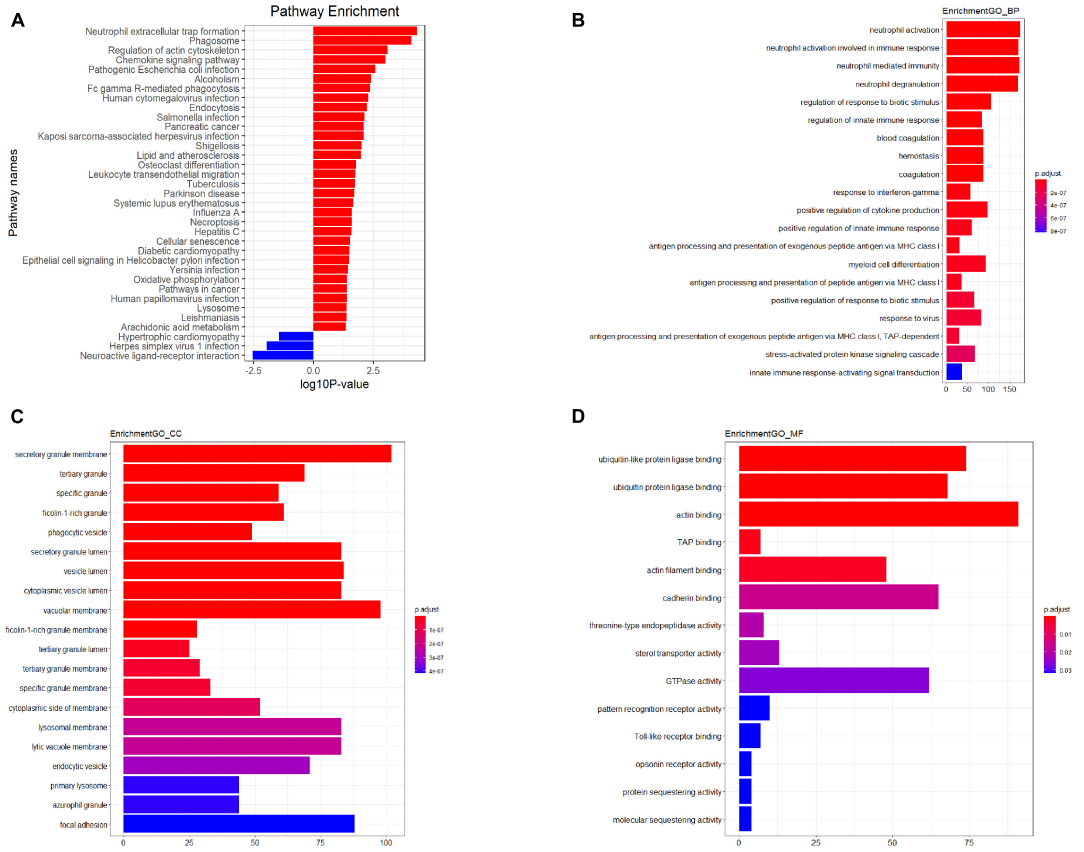

FIGURE 3
Kyoto Encyclopedia of Genes and Genomes (KEGG) pathway analysis **(A)** GO analysis plot–Biological process **(B)** GO analysis plot–Cellular component **(C)** GO analysis plot–Molecular function **(D)**. *P*-value denoted the significance of the GO term and pathway correlated to the conditions. Lower the *P*-value, more significant were the GO term and KEGG pathway.

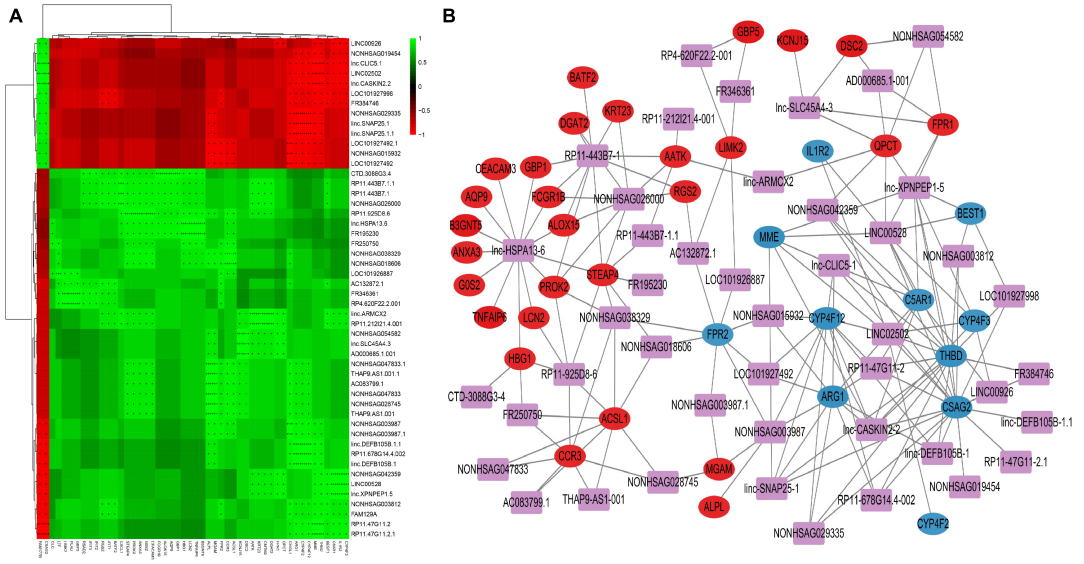

FIGURE 4
Correlation analysis of lncRNA and mRNA **(A)** Correlation heatmap. The horizontal axis represents lncRNA, the vertical axis represents mRNA, the green square represents positive correlation, and the red square represents negative correlation, "+" stands for FDR < 0.1, "++" stands for FDR < 0.01, "+++" stands for FDR < 0.001. **(B)** DE lncRNAs and DE mRNAs co-expression network. The networks were based on lncRNA–mRNA interactions. In the network, purple squares represent lncRNAs, which are located in the center of the network, and circles represent significantly associated mRNAs, which are distributed around lncRNAs. The red circles represent significantly positively associated mRNAs and the blue circles represent significantly negatively associated mRNAs.

TABLE 3 The top 10 upregulated and downregulated mRNAs in the PBMCs of ATB patients, compared to the HC group.

mRNA gene symbol	Regulation	Fold change	*P*-value
CHI3L1	Up	118.88714	0.000487
IL1R2	Up	102.415306	0.000145
KCNJ15	Up	94.443924	0.000000753
CYP4F2	Up	90.364334	0.000926
MME	Up	90.1744	0.00023
MGAM	Up	85.16178	0.000177
TNFRSF10C	Up	76.06052	0.00128015
IFIT3	Up	73.37543	0.002505481
CXCL1	Up	69.12307	0.004915247
CYP4F3	Up	67.52758	0.0000468
FAM177B	Down	294.74496	0.004868665
MADCAM1	Down	17.573362	0.005767919
CSAG2	Down	15.699993	0.013869465
FCRL2	Down	11.852164	0.012213992
CABLES1	Down	11.157983	0.013856612
C10orf114	Down	10.827955	0.00771278
PRR20B	Down	10.800922	0.002674374
NOS2	Down	10.639506	0.002279884
FCRL1	Down	10.294664	0.003636744
GSTM5	Down	10.257128	0.01034451

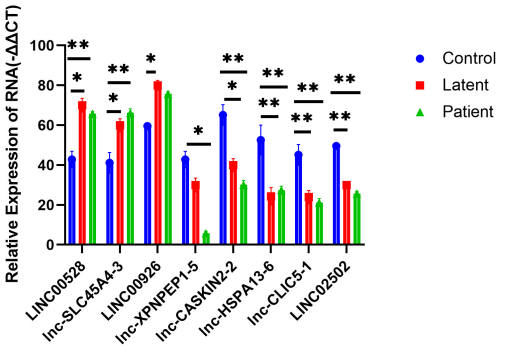

FIGURE 5
Quantitative PCR (QRT-PCR) validation of eight differentially expressed lncRNAs and lncRNA as well as its nearby protein-coding gene. Eight lncRNAs LINC00528, lnc-SLC45A4-3, LINC00926, lnc-XPNPEP1-5, lnc-CASKIN2-2, lnc-HSPA13-6, lnc-CLIC5-1, and LINC02502 were chosen for the validation of the gene chip results using qRT-PCR. LINC00528, lnc-SLC45A4-3, and LINC00926 were upregulated, while lnc-XPNPEP1-5, lnc-CASKIN2-2, lnc-HSPA13-6, lnc-CLIC5-1, and LINC02502 were downregulated in the latent infection group (n = 50) and TB patient group (n = 50) relative to health controls (n = 50). *Response that is significantly different from the HC group ($p < 0.05$). **Response that is significantly different from the HC group ($p < 0.01$).

In the present study, we rigorously controlled the quality of the experimental data. This entailed examining the integrity, purity, and concentration of RNA to ensure the accuracy and repeatability of the experimental procedures. We employed multiple bioinformatic methods to corroborate our findings and elucidate the functional and regulatory relationships of the obtained results in the context of biology. By comparing our results with those of other published studies, we determined whether there was consistency among them. We also validated the differentially expressed lncRNAs through various experiments, such as real-time fluorescent quantitative PCR, to confirm our findings (Song et al., 2019; Huang et al., 2020).

Based on the identified dysregulated pathways, we discovered eight PBMC lncRNAs that displayed different expression patterns in TB patients, thereby creating an 8-lncRNA TB biological signature. This signature was also found to be capable of distinguishing TB patients from healthy controls in an independent cohort. The significant changes in pathway or function which are related Neutrophils suggest that the findings show a strong neutrophil response, which could be due to an infection or inflammation in the sample. The further investigate of the specific pathways and functions is needed to gain a deeper understanding of the neutrophil response and potential causes. Our research clearly suggests that PBMC lncRNAs hold potential as biomarkers for differentiating active TB patients from healthy individuals. For instance, lncRNA LINC00528 functions as a predictive biomarker for myocardial infarction (MI) (Sheng et al., 2020). It regulates myocardial infarction (MI) through the miR-143-3p/COX-2 axis (Liu et al., 2020). LINC00528 is significantly associated with immunological activity, and its target mRNAs are involved in biological processes triggered by various immune cells, including T cells, lymphocytes, and leukocytes. The pathways that positively and negatively regulate leukocyte cell-cell adhesion are highly enriched in LINC00528, which includes multiple molecules of the CD family (Zhang et al., 2021). This indicates that when *Mtb* invades the host, LINC00528 is closely linked to the immunological control of lymphocytes. Another recent study revealed that LINC02502 is directly related to calcium accumulation in mitochondria, suggesting that LINC02502 is connected to TB patients' energy metabolism (Guo et al., 2022).

This study demonstrates a correlation between LINC02502 and the energy metabolism of TB patients. The lncRNA LINC00926 negatively regulates the expression of phosphoglycerate kinase 1 (PGK1) and predicts a favorable clinical outcome for breast cancer. This regulation occurs through an increase in PGK1 ubiquitination, which is mediated by the E3 ligase STUB1 (Chu et al., 2021; Guo et al., 2022). The WNT signaling pathway, crucial for various physiological processes such as cell fate determination, development, differentiation, and more, is dysregulated in PTSD and contributes to the upregulation of pro-inflammatory genes. The promoter of WNT10B's H3K4me3 is regulated by LINC00926, leading to enhanced WNT signaling (Bam et al., 2022). Our study's Gene Set Enrichment Analysis (GSEA) revealed an enrichment of the WNT signaling pathway. Although it is unknown whether elevated WNT10B expression in PBMCs leads to additional lung parenchymal inflammation in TB patients, this research suggests that LINC00926 could serve as a potential TB biomarker and therapeutic target. Unfortunately, most DE lncRNAs, including lnc-SLC45A4-3, LINC00926, lnc-XPNPEP1-5, lnc-CASKIN2-2, lnc-HSPA13-6, and lnc-CLIC5-1, have not yet been investigated; further research is warranted.

In summary, we identified and validated distinct DElncRNAs in TB cases. Our findings suggest that the genes LINC00528, LINC00926, and LINC02502 may play a significant regulatory role in the development of TB. These discoveries provide insights into the etiology of immunoregulatory dysfunction in tuberculosis and could reveal potential molecular pathways and therapeutic targets.

Data availability statement

The datasets presented in this study can be found in online repositories. The names of the repository/repositories and accession number(s) can be found below: GSA–PRJCA019204.

Ethics statement

The studies involving human participants were reviewed and approved by Ethics Review Committee of Jiangsu Provincial Center for Disease Control and Prevention [Ethics Authorization Number: JSCDCLL(2014)003]. The studies were conducted in accordance with the local legislation and institutional requirements. The participants provided their written informed consent to participate in this study.

Author contributions

YL: Conceptualization, Data curation, Formal analysis, Funding acquisition, Investigation, Methodology, Project administration, Resources, Software, Supervision, Validation, Visualization, Writing – original draft, Writing – review and editing. ZF: Data curation, Investigation, Writing – original draft. GL: Methodology, Formal analysis, Writing – original draft, Writing – review and editing. HS: Formal analysis, Investigation, Methodology, Writing – original draft. YW: Methodology, Supervision, Writing – review and editing. LZ: Funding acquisition, Investigation, Methodology, Resources, Supervision, Visualization, Writing – review and editing.

Funding

The authors declare financial support was received for the research, authorship, and/or publication of this article. This work was supported by the National Natural Science Foundation of China Youth Science Foundation Project (grant numbers 8130144 and 81302480), Jiangsu Provincial Medical Key Discipline (ZDXK202250) and Jiangsu Young Medical Talents Project (grant number QNRC2016541). The funding sources had no input into the planning of the study, gathering and analyzing the data, choosing to publish, or writing the manuscript.

Conflict of interest

The authors declare that the research was conducted in the absence of any commercial or financial relationships that could be construed as a potential conflict of interest.

Publisher's note

References

Bam, M., Yang, X., Ginsberg, J. P., Aiello, A. E., Uddin, M., Galea, S., et al. (2022). Long non-coding RNA LINC00926 regulates WNT10B signaling pathway thereby altering inflammatory gene expression in PTSD. *Transl. Psychiatry* 12:200. doi: 10.1038/s41398-022-01971-5

Borkute, R., Woelke, S., Pei, G., and Dorhoi, A. (2021). Neutrophils in tuberculosis: Cell biology, cellular networking and multitasking in host defense. *Int. J. Mol. Sci.* 22:801. doi: 10.3390/ijms22094801

Boro, M., Singh, V., and Balaji, K. (2016). Mycobacterium tuberculosis-triggered Hippo pathway orchestrates CXCL1/2 expression to modulate host immune responses. *Sci. Rep.* 6:37695. doi: 10.1038/srep37695

Braian, C., Hogea, V., and Stendahl, O. (2013). Mycobacterium tuberculosis-induced neutrophil extracellular traps activate human macrophages. *J. Innate Immun.* 5, 591–602. doi: 10.1159/000348676

Broderick, C., Cliff, J., Lee, J., Kaforou, M., and Moore, D. (2021). Host transcriptional response to TB preventive therapy differentiates two sub-groups of IGRA-positive individuals. *Tuberculosis* 127:102033. doi: 10.1016/j.tube.2020.102033

Chu, Z., Huo, N., Zhu, X., Liu, H., Cong, R., Ma, L., et al. (2021). FOXO3A-induced LINC00926 suppresses breast tumor growth and metastasis through inhibition of PGK1-mediated Warburg effect. *Mol. Ther.* 29, 2737–2753. doi: 10.1016/j.ymthe.2021.04.036

Fang, Y., Zhao, J., Wang, X., Wang, X., Wang, L., Liu, L., et al. (2021). Identification of differentially expressed lncRNAs as potential plasma biomarkers for active tuberculosis. *Tuberculosis* 128:102065. doi: 10.1016/j.tube.2021.102065

Fathizadeh, H., Hayat, S. M., Dao, S., Ganbarov, K., Tanomand, A., Asgharzadeh, M., et al. (2020). Long non-coding RNA molecules in tuberculosis. *Int. J. Biol. Macromol.* 156, 340–346. doi: 10.1016/j.ijbiomac.2020.04.030

Guo, D., Zhou, Y., Wei, X., Zhang, S., Jin, T., Zhang, Y., et al. (2022). Preliminary study of genome-wide association identifies novel susceptibility genes for serum mineral elements in the Chinese Han population. *Biol. Trace Elem. Res.* 200, 2549–2555. doi: 10.1007/s12011-021-02854-4

Healy, E., Goering, L., Hauser, C., and King, P. (2021). An immunomodulatory role for the *Mycobacterium tuberculosis* Acr protein in the formation of the tuberculous granuloma. *FEBS Lett.* 595, 284–293. doi: 10.1002/1873-3468.13998

Hu, X., Liao, S., Bai, H., Gupta, S., Zhou, Y., Zhou, J., et al. (2020). Long Noncoding RNA and Predictive Model To Improve Diagnosis of Clinically Diagnosed Pulmonary Tuberculosis. *J. Clin. Microbiol.* 58, e1973–e1919. doi: 10.1128/JCM.01973-19

Huang, S., Huang, Z., Luo, Q., and Qing, C. (2018). The Expression of lncRNA NEAT1 in human tuberculosis and its antituberculosis effect. *Biomed. Res. Int.* 2018:9529072. doi: 10.1155/2018/9529072

Huang, Z., Liu, J., Li, L., Guo, Y., Luo, Q., and Li, J. (2020). Long non-coding RNA expression profiling of macrophage line RAW264.7 infected by *Mycobacterium tuberculosis*. *Biotech. Histochem* 95, 403–410.

Jung, J., Jhun, B. W., Jeong, M., Yoon, S. J., Huh, H. J., Jung, C. W., et al. (2021). Is the new interferon-gamma releasing assay beneficial for the diagnosis of latent and active *Mycobacterium tuberculosis* infections in tertiary care setting? *J. Clin. Med.* 10:1376. doi: 10.3390/jcm10071376

Kaushik, A. C., Wu, Q., Lin, L., Li, H., Zhao, L., Wen, Z., et al. (2021). Exosomal ncRNAs profiling of mycobacterial infection identified miRNA-185-5p as a novel biomarker for tuberculosis. *Brief Bioinform*. 22, bbab210. doi: 10.1093/bib/bbab210

Li, M., Cui, J., Niu, W., Huang, J., Feng, T., Sun, B., et al. (2019). Long non-coding PCED1B-AS1 regulates macrophage apoptosis and autophagy by sponging miR-155 in active tuberculosis. *Biochem. Biophys. Res. Commun*. 509, 803–809. doi: 10.1016/j.bbrc.2019.01.005

Li, Y., Yin, Z., Fan, J., Zhang, S., and Yang, W. (2019). The roles of exosomal miRNAs and lncRNAs in lung diseases. *Signal Transduct. Target Ther*. 4:47. doi: 10.1038/s41392-019-0080-7

Li, Z., Han, Y., Wei, L., Shi, L., Yi, W., Chen, J., et al. (2020). Screening and identification of plasma lncRNAs uc.48+ and NR_105053 as potential novel biomarkers for cured pulmonary tuberculosis. *Int. J. Infect. Dis*. 92, 141–150. doi: 10.1016/j.ijid.2020.01.005

Liu, K., Zhao, D., and Wang, D. (2020). LINC00528 regulates myocardial infarction by targeting the miR-143-3p/COX-2 axis. *Bioengineered* 11, 11–18. doi: 10.1080/21655979.2019.1704535

Monin, L., and Khader, S. (2014). Chemokines in tuberculosis: the good, the bad and the ugly. *Semin. Immunol*. 26, 552–558. doi: 10.1016/j.smim.2014.09.004

Park, J., Park, S., Park, H., Kim, J., Kim, Y., and Kim, S. (2021). Cytokine and Chemokine MRNA expressions after mycobacterium tuberculosis-specific antigen stimulation in whole blood from hemodialysis patients with latent tuberculosis infection. *Diagnostics* 11:595. doi: 10.3390/diagnostics11040595

Pellegrini, J. M., Sabbione, F., Morelli, M. P., Tateosian, N. L., Castello, F. A., Amiano, N. O., et al. (2021). Neutrophil autophagy during human active tuberculosis is modulated by SLAMF1. *Autophagy* 17, 2629–2638. doi: 10.1080/15548627.2020.1825273

Qian, Z., Liu, H., Li, M., Shi, J., Li, N., Zhang, Y., et al. (2018). Potential diagnostic power of blood circular RNA expression in active pulmonary tuberculosis. *EBioMedicine* 27, 18–26. doi: 10.1016/j.ebiom.2017.12.007

Ravindran, M., Khan, M., and Palaniyar, N. (2019). Neutrophil extracellular trap formation: Physiology, pathology, and pharmacology. *Biomolecules* 9:365. doi: 10.3390/biom9080365

Roy, S., Schmeier, S., Kaczkowski, B., Arner, E., Alam, T., Ozturk, M., et al. (2018). Transcriptional landscape of *Mycobacterium tuberculosis* infection in macrophages. *Sci. Rep*. 8:6758. doi: 10.1038/s41598-018-24509-6

Schwenk, S., and Arnvig, K. (2018). Regulatory RNA in Mycobacterium tuberculosis, back to basics. *Pathog. Dis*. 76, fty035. doi: 10.1093/femspd/fty035

Sheng, X., Fan, T., and Jin, X. (2020). Identification of key genes involved in acute myocardial infarction by comparative transcriptome analysis. *Biomed. Res. Int*. 2020:1470867. doi: 10.1155/2020/1470867

Song, J., Liu, T., Zhao, Z., Hu, X., Wu, Q., Peng, W., et al. (2019). Genetic polymorphisms of long noncoding RNA RP11-37B2.1 associate with susceptibility of tuberculosis and adverse events of antituberculosis drugs in west China. *J. Clin. Lab. Anal.* 33:e22880.

Venkatappa, T. K., Punnoose, R., Katz, D. J., Higgins, M. P., Banaei, N., Graviss, E. A., et al. (2019). Comparing QuantiFERON-TB gold plus with other tests to diagnose mycobacterium tuberculosis infection. *J. Clin. Microbiol*. 57, e985–e919. doi: 10.1128/JCM.00985-19

Wang, K., and Chang, H. (2011). Molecular mechanisms of long noncoding RNAs. *Mol. Cell* 43, 904–914. doi: 10.1016/j.molcel.2011.08.018

Wang, L., Xie, B., Zhang, P., Ge, Y., Wang, Y., and Zhang, D. (2019). LOC152742 as a biomarker in the diagnosis of pulmonary tuberculosis infection. *J. Cell Biochem*. 120, 8949–8955. doi: 10.1002/jcb.27452

Wang, Z., Xu, H., Wei, Z., Jia, Y., Wu, Y., Qi, X., et al. (2020). The role of non-coding RNA on macrophage modification in tuberculosis infection. *Microb. Pathog*. 149:104592. doi: 10.1016/j.micpath.2020.104592

Wei, L., Liu, K., Jia, Q., Zhang, H., Bie, Q., and Zhang, B. (2021). The roles of host noncoding RNAs in *Mycobacterium tuberculosis* infection. *Front. Immunol*. 12:664787. doi: 10.3389/fimmu.2021.664787

World Health Organization (2022). *Global tuberculosis report*. Geneva: World Health Organization.

Yan, H., Xu, R., Zhang, X., Wang, Q., Pang, J., Zhang, X., et al. (2018). Identifying differentially expressed long non-coding RNAs in PBMCs in response to the infection of multidrug-resistant tuberculosis. *Infect. Drug Resist*. 11, 945–959. doi: 10.2147/IDR.S154255

Yang, X., Yang, J., Wang, J., Wen, Q., Wang, H., He, J., et al. (2016). Microarray analysis of long noncoding RNA and mRNA expression profiles in human macrophages infected with Mycobacterium tuberculosis. *Sci. Rep*. 6:38963. doi: 10.1038/srep38963

Ye, T., Zhang, J., Zeng, X., Xu, Y., and Li, J. (2022). LncRNA CCAT1 is overexpressed in tuberculosis patients and predicts their survival. *Immun. Inflamm. Dis*. 10, 218–224. doi: 10.1002/iid3.565

Yi, F., Hu, J., Zhu, X., Wang, Y., Yu, Q., Deng, J., et al. (2021). Transcriptional profiling of human peripheral blood mononuclear cells stimulated by *Mycobacterium tuberculosis* PPE57 identifies characteristic genes associated With Type I interferon signaling. *Front. Cell Infect Microbiol*. 11:716809. doi: 10.3389/fcimb.2021.716809

Zhang, Q., Chao, T., Patil, V. S., Qin, Y., Tiwari, S. K., Chiou, J., et al. (2019). The long noncoding RNA ROCKI regulates inflammatory gene expression. *EMBO J*. 38:41. doi: 10.15252/embj.2018100041

Zhang, X., Chen, C., and Xu, Y. (2022). Long non-coding RNAs in tuberculosis: from immunity to biomarkers. *Front. Microbiol*. 13:883513. doi: 10.3389/fmicb.2022.883513

Zhang, X., Liang, Z., Zhang, Y., Dai, K., Zhu, M., Wang, J., et al. (2020). Comprehensive analysis of long non-coding RNAs expression pattern in the pathogenesis of pulmonary tuberculosis. *Genomics* 112, 1970–1977. doi: 10.1016/j.ygeno.2019.11.009

Zhang, X., Zhang, H., Li, J., Ma, X., He, Z., Liu, C., et al. (2021). 6-lncRNA assessment model for monitoring and prognosis of HER2-positive breast cancer: based on transcriptome data. *Pathol. Oncol. Res*. 27:609083. doi: 10.3389/pore.2021.609083

frontiers | Frontiers in Microbiology

TYPE Original Research
PUBLISHED 07 February 2024
DOI 10.3389/fmicb.2024.1287806

OPEN ACCESS

EDITED BY
Ranjan Nanda,
International Centre for Genetic Engineering and Biotechnology (India), India

REVIEWED BY
Swati Jaiswal,
University of Massachusetts Medical School, United States
Jitendra Narain Singh,
National Institute of Pharmaceutical Education and Research, Mohali, India
Newton Valerio Verbisck,
Brazilian Agricultural Research Corporation (EMBRAPA), Brazil

*CORRESPONDENCE
Hongfei Duan
✉ duanhongfei@hotmail.com
Hairong Huang
✉ huanghairong@tb123.org

†These authors have contributed equally to this work

RECEIVED 02 September 2023
ACCEPTED 22 January 2024
PUBLISHED 07 February 2024

CITATION
Liang R, Li J, Zhao Y, Qi H, Bao S, Wang F, Duan H and Huang H (2024) A comparative study of MassARRAY and GeneXpert assay in detecting rifampicin resistance in tuberculosis patients' clinical specimens.
Front. Microbiol. 15:1287806.
doi: 10.3389/fmicb.2024.1287806

A comparative study of MassARRAY and GeneXpert assay in detecting rifampicin resistance in tuberculosis patients' clinical specimens

Ruixia Liang[1†], Jiankang Li[1†], Yue Zhao[2†], Haoran Qi[3], Shengjuan Bao[4], Fen Wang[3], Hongfei Duan[4*] and Hairong Huang[3*]

[1]Tuberculosis Department, Henan Chest Hospital, Zhengzhou, China, [2]Clinical Laboratory, Henan Chest Hospital, Zhengzhou, China, [3]National Clinical Laboratory on Tuberculosis, Beijing Key Laboratory for Drug-Resistant Tuberculosis Research, Beijing Chest Hospital, Beijing Tuberculosis and Thoracic Tumor Institute, Capital Medical University, Beijing, China, [4]Tuberculosis Department, Beijing Chest Hospital, Capital Medical University, Beijing, China

Objectives: Matrix-assisted laser desorption ionization-time of flight mass spectrometry (MALDI-TOF MS) has emerged as a potent tool for detecting drug resistance in tuberculosis (TB); however, concerns about its reliability have been raised. In this study, we assessed the reliability of MassARRAY (Sequenom, Inc.), which is a MALDI-TOF MS-based method, by comparing it to the well-established GeneXpert assay (Cepheid) as a reference method.

Methods: A retrospective study was conducted using laboratory data retrieved from Henan Chest Hospital (Zhengzhou, China). To ensure a rigorous evaluation, we adopted a comprehensive assessment approach by integrating multiple outcomes of the Xpert assay across various specimen types.

Results: Among the 170 enrolled TB cases, MassARRAY demonstrated significantly higher sensitivity (85.88%, 146 of 170) compared to the Xpert assay (76.62%, 118 of 154) in TB diagnosis ($p < 0.05$). The concordance in detecting rifampicin resistance between MassARRAY and the combined outcomes of the Xpert assay was 90%, while it was 97.37% (37 of 38) among smear-positive cases and 89.06% (57 of 64) among culture-positive cases. When compared to the phenotypic susceptibility outcomes of the 12 included drugs, consistency rates of 81.8 to 93.9% were obtained, with 87.9% for multiple drug resistance (MDR) identification.

Conclusion: MassARRAY demonstrates high reliability in detecting rifampicin resistance, and these findings may offer a reasonable basis for extrapolation to other drugs included in the test panel.

KEYWORDS

tuberculosis, MALDI-TOF MS, MassARRAY, Xpert assay, drug resistance, reliability

Introduction

Tuberculosis (TB) remains a significant contributor to infectious disease-related mortality worldwide. In 2022, an estimated 10.6 million individuals were diagnosed with TB. Among them, the rate of multiple drug-resistant (MDR, defined as simultaneous resistance to at least isoniazid and rifampin)/rifampin-resistant (RR)-TB was 3.3% among new cases and 17% among previously treated cases (World Health Organization, 2023). TB drug resistance is broadly categorized as RR, MDR, or extensively drug-resistant (XDR). Leveraging the rapid, sensitive, and reliable features of the molecular diagnostics of TB, many more drug-resistant patients have been diagnosed timely. However, the complete drug resistance patterns exhibited by individual patients can vary widely and often go undetected. This significant detection gap is primarily caused by the shortage and limitations of available diagnostics.

Conventional phenotypic drug susceptibility testing (pDST) provides coverage for a wide range of drugs; however, the complexity associated with this technique has limited its widespread application. Additionally, the long turnaround time hampers its effectiveness in guiding the establishment of an appropriate treatment regimen. Concerns about its reliability and reproducibility further constrain its use as a diagnostic tool for drug resistance (van Deun et al., 2011). Commercial PCR-based molecular testing addresses the prolonged time delay inherent in pDST while also exhibiting reduced technical complexity. However, it has an obvious drawback in that the targeted genes, i.e., the drugs covered, are limited (World Health Organization, 2021). For instance, the Xpert MTB/RIF assay (Xpert) (Cepheid Inc., Sunnyvale, CA, USA) solely identifies rifampin resistance associated with the *rpoB* mutation. The GenoType MTBDRplus (Hain Lifescience) can only detect mutations in genes related to resistance to rifampin (*rpoB*) and isoniazid (*inhA* and *katG*) (Gu et al., 2015). Even though the Xpert MTB/XDR (Cepheid, USA) covers six drugs, this number remains insufficient (Xie et al., 2017). Without knowledge of the complete drug resistance pattern, drugs (without information on their susceptibility) must be selected without a clear understanding for establishing a regimen for drug-resistant cases. Reliable, rapid, and accessible diagnostics that can provide susceptibility information for every candidate anti-TB drug would undoubtedly facilitate the establishment of an appropriate treatment regimen.

Matrix-assisted laser desorption ionization-time of flight mass spectrometry (MALDI-TOF MS) has recently been employed for single nucleic acid polymorphism (SNP) detection, leveraging its simple workflow, short turnaround time, high accuracy, and low cost (Tsai et al., 2012). MALDI-TOF MS utilizes a single-base extension method similar to the Sanger sequencing method, employing dideoxynucleotides (ddNTPs) to extend a single base after the primer. Hence, nucleic acid mass spectrometry is often referred to as a mass spectrometry-based sequencing technique (Hsu et al., 2015). The application of MALDI-TOF MS in pharmacogenomics and the identification of genetic predisposition have validated its reliability and feasibility in SNP detection (Venkatesh et al., 2014; Williams et al., 2020). In 2017, Su et al. (2017) pioneered the detection of drug-resistant TB via the MALDI-TOF MS platform using clinical isolates and specimens. The detection process could be completed within a few hours, with an accuracy comparable to the Sanger sequencing method. In comparison to other detection systems, MALDI-TOF MS acquires the absolute mass value, representing an intrinsic property of a molecule, while others depend on signals of relative electrophoretic mobility or a hybridization event. This disparity enhances the accuracy of the detection outcomes obtained through MALDI-TOF MS.

MassARRAY® (Sequenom, Inc., San Diego, United States) is a MALDI-TOF MS-based method with robust capabilities for detecting drug resistance in tuberculosis (Bouakaze et al., 2011; Su et al., 2017). MassARRAY offers the ability to analyze multiple drug resistance-associated genes in a single reaction, providing the convenience of incorporating additional genes when needed. For instance, the current MassARRAY version covers all 5 first-line anti-TB drugs and more than 10 s-line drugs, including novel anti-TB drugs such as bedaquiline and linezolid (Table 1). However, despite the excitement surrounding this technique, concerns and suspicions have also emerged. The drug resistance detected by MassARRAY in a given patient often cannot be corroborated by another test. This is either because these drugs are not covered by other methods or because the negative results of these tests are due to their less sensitive performance. A few published studies have compared the concordance among MassARRAY, pDST, and DNA sequencing outcomes on strains. Good consistency was achieved for most of the drugs, with some exceptions (Shi et al., 2022; Wu et al., 2022). One study conducted on sputum using MassARRAY and pDST showed good consistency only with rifampin (RIF) and isoniazid (INH) but poor outcomes for kanamycin (KAN) (Wu et al., 2022). These studies could only include culture-positive cases

TABLE 1 Targeted drug-resistant genes and loci of the MassARRAY platform.

Drug*	Targeted gene	Included locus
Rifampin (RIF)	*rpoB*	511, 513, 516, 522, 526, 531, 533
Isoniazid (INH)	*inhA*	−15
	katG	315, 316
Pyrazinamide (PZA)	*pncA*	57
Ethambutol (EMB)	*embB*	306, 406
Fluoroquinolones (FQs)	*gyrA*	90, 94,
	gyrB	538
Streptomycin (Sm)	*rpsL*	43, 48
Amikacin (AK)	*rrs*	1,401, 1,484
Kanamycin (Kan)	*eis*	−15
	rrs	1,401, 1,402, 1,408
Capreomycin (Cm)	*rrs*	1,401, 1,402, 1,408
Ethionamide (ETO) /protionamide (PTO)	*inhA*	−15
Cycloserine (Cs)	*alr*	261
p-aminosalicylic acid (PAS)	*folC*	43
	thyA	202, 75
Bedaquiline (BDQ)	*Rv0678*	193, 466
Clofazimine (CFZ)	*Rv0678*	193, 466
Linezolid (LZD)	*rplC*	450

*Drug in bold indicating the drug that included in a routine pDST.

with available pDST outcomes, potentially introducing bias toward patients with a higher acid-fast bacilli (AFB) load in sputum. Furthermore, the low reliability of pDST for TB could lead to misleading outcomes, especially for second-line anti-TB drugs (Xie et al., 2017; Penn-Nicholson et al., 2022). Consequently, relatively lower concordance rates were often observed when using pDST outcomes as a reference compared to DNA sequencing. Therefore, accurately interpreting the resistance outcomes generated by MassARRAY poses a significant challenge.

In this study, we sought to address this dilemma by comparing the results of MassARRAY with another widely recognized molecular test, the Xpert MTB/RIF assay (Lawn et al., 2013). Our objective was to furnish objective evidence that could aid healthcare providers in comprehending the practical utility of the MALDI-TOF MS technique. Through this, we aimed to empower them to judiciously leverage the outcomes of this technique in clinical practice.

Materials and methods

Ethical approval

This study received approval from the Ethics Committees of Henan Chest Hospital (Zhengzhou, China), and written informed consent was obtained from each participant.

Study design and participants

Participants were consecutively enrolled from July 2021 to November 2022. The patient recruitment criteria were as follows: the patient exhibited symptoms or signs suggestive of TB (World Health Organization, 2013); any of the following tests conducted during this episode of disease yielded positive results, including smear microscopy examination, culture, Xpert assay, or other molecular tests; or all the aforementioned tests yielded negative results, but the patient had a history of TB and was diagnosed with relapse; with a sufficient volume of the clinical specimen; and the patient expressed willingness to undergo MassARRAY testing to detect drug resistance. For pulmonary TB patients, bronchoalveolar lavage fluid (BALF) was the preferred specimen when the patient consented to the invasive bronchoscopic examination. The clinical specimen underwent smear, culture, Xpert assay, and other routine molecular tests for TB diagnosis. Multiple specimens could be tested for the same patient, and various specimen types might be included for patients with involvement of multiple organs. If any of the above assays yielded a positive result, the case was classified as positive with the corresponding test. If the Xpert assay indicated rifampicin resistance, the case was categorized as rifampicin-resistant. A specific specimen was collected separately for MassARRAY testing. Additionally, pDST and species identification were performed once the isolate was successfully recovered.

Smear and culture

A direct smear was prepared and stained with auramine, then examined using light-emitting diode microscopy. Liquid culture was conducted using the MGIT 960 system (BD Diagnostic Systems, NJ, USA). For all recovered isolates, MPT64 antigen testing (Kaibili Ltd., Hangzhou, China) was employed to confirm the presence of the *Mycobacterium tuberculosis* (Mtb) complex. Non-tuberculous mycobacteria (NTM) were confirmed through molecular testing (Chen et al., 2022).

Xpert assay

The Xpert assays were conducted following the manufacturer's instructions. In brief, 1 mL of sputum specimen was processed and detected using the GeneXpert instrument (Cepheid Inc., Sunnyvale, CA, USA).

Phenotypic drug susceptibility testing

Culture-positive samples underwent pDST using the 96-well microtiter plate assay (manufactured by Zhuhai Yinke Ltd., China). The assay covered 16 drugs, and testing was conducted following the manufacturer's instructions. The critical concentrations used were based on the guidelines of the Clinical and Laboratory Standards Institute (CLSI, USA) (Gail, 2018).

MassARRAY testing

All specimens were processed according to a standardized procedure previously outlined by Conlight TB&DR® Detection (Shanghai Conlight Medical Laboratory Co., Ltd., Shanghai, China) (Shi et al., 2022; Wu et al., 2022). The specimens were transported under appropriate cold chain conditions. Subsequently, DNA was extracted from the specimens and used in PCR reactions targeting 15 drug-resistant genes associated with 15 anti-TB drugs. Another extension reaction was conducted with the product from the previous PCR, designed to detect the mutated loci in each targeted gene. Following desalting, the products were spotted onto the chip using the MassARRAY® Nanodispenser, and the chip was inserted into the MassARRAY® Analyzer for detection and analysis.

Statistical analyses

The sensitivity and specificity of various assays were determined in comparison to the reference standard. The McNemar test was employed to assess the sensitivity and specificity of Mtb or RIF detection between MassARRAY and the Xpert assay. Statistical analysis was conducted using SPSS version 19.0, with differences considered statistically significant at a p-value of <0.05.

Results

Patient characteristics

A total of 186 participants were enrolled, and 16 of them were subsequently identified as having NTM infections, leading to their

exclusion from further analysis. More than one-third of the enrolled cases underwent multiple Xpert assay tests, with a significant number using different specimen types for the repeated assays. Additionally, multiple tests were conducted using smear and culture methods. The reported outcomes of the Xpert assay, smear, and culture hereafter may represent combined results from multiple tests. Among the 170 TB patients, 101 were men, with a median age of 45 years (ranging from 13 to 84). All patients were HIV-negative. The study included 118 pulmonary TB cases, 20 bone and joint TB cases, 15 pleural TB cases, 11 lymph node TB cases, 4 tuberculous meningitis cases, and 2 kidney TB cases. Based on all laboratory testing outcomes except MassARRAY, 130 cases were defined as confirmed TB, while 40 others were clinically diagnosed with TB without any supporting bacterial evidence (Figure 1).

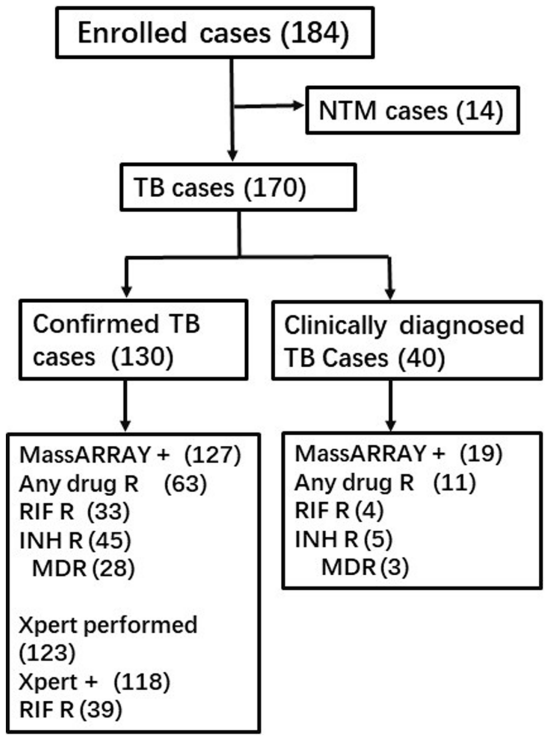

FIGURE 1
Enrolled patients and the outcomes of MassARRAY and Xpert assay.

The overall performance of each diagnostic method in TB diagnosis

Among all the enrolled TB cases, MassARRAY exhibited better sensitivity (85.88%, 146/170) than Xpert assay (76.62%, 118/154), culture (48.91%, 67/137), and smear (25.85%, 38/147) ($p = 0.032$, $p < 0.001$, $p < 0.001$, respectively). In the subset of 130 confirmed TB cases where the diagnosis was established based on the outcomes of different methods, excluding MassARRAY, the sensitivity of MassARRAY was 97.69% (127/130). This was followed by the Xpert assay with a sensitivity of 95.94% (118/123), culture (58.56%, 65/111), and smear (33.23%, 38/111). MassARRAY showed comparable sensitivity to the Xpert assay ($p = 0.425$) but exhibited higher sensitivity than culture and smear testing ($p < 0.001$, $p < 0.001$) (Table 2).

The performance of MassARRAY and Xpert assay in smear-positive cases

A total of 40 patients had positive smear outcomes, and 2 of them were identified as NTM and were subsequently excluded. Both MassARRAY and the Xpert assay detected TB DNA from all the specimens in these 38 cases. Among them, 28 sensitive cases and 9 RIF-resistant cases were uniformly detected by both methods, whereas one case was found to have a *rpoB* mutation by Xpert only but not by MassARRAY, and the outcome from pDST for this case indicated it as RIF-sensitive. The concordance rate between MassARRAY and Xpert assay for *rpoB* mutation detection was 97.37% (37/38).

The performance of MassARRAY and Xpert assay in culture-positive cases

A total of 75 patients yielded positive culture outcomes, and 8 of them were excluded because of NTM identification, while the Xpert assay was not performed for 3 other cases. Therefore, 64 patients had comparable outcomes. Both MassARRAY and the Xpert assay detected TB DNA from all the specimens in these 64 cases. Among them, 30 were reported to be sensitive to RIF by both methods, whereas 27 had detectable *rpoB* mutations using both methods. Five cases detected *rpoB* mutations by Xpert only, and another two detected *rpoB* mutations by MassARRAY only. Out of the seven cases with discrepant outcomes, only three had pDST results available. Among these, one case showed resistance to RIF and

TABLE 2 Performance of different diagnostics in 130 confirmed TB*

TB location	Specimen type (*n*)	MassARRAY+	Smear+	Culture+	Xpert +
Pulmonary	BALF (78)	75/78	22/70	37/66	69/72
	Sputum (20)	20/20	10/17	14/19	18/19
Bone and joint	Pus (14)	14/14	3/12	6/13	13/14
Pleura	Pleural fluid (9)	9/9	2/5	5/6	9/9
Lymph node	Tissue (7)	7/7	1/6	2/5	7/7
Kidney	Urine (2)	2/2	0/1	1/2	2/2
Total specimens		127/130	38/111[&]	65/111[&]	118/123[$]

*Denominator indicates the number of specimens performed the corresponding assay, and the numerator indicates the number of specimens yielded positive outcome. [&]Compared with the MassARRAY, the difference was significant ($p < 0.001$). [$]Compared with the MassARRAY, the difference was not significant ($p > 0.05$).

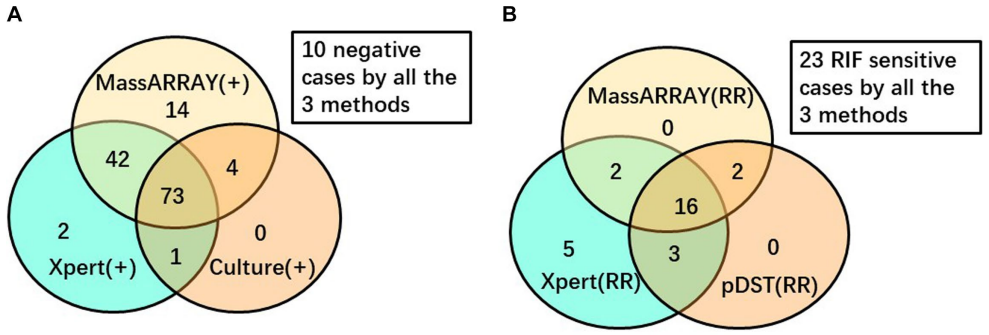

FIGURE 2
Venn diagram to depict the performance of different diagnostic methods. **(A)** Among 146 cases performed all the 3 tests for TB diagnosis. **(B)** Among 51 cases performed all the 3 tests for RIF resistance detection.

aligned with the Xpert outcome, while the remaining two cases were sensitive to RIF, contradicting the Xpert outcome. The concordance rate between these two tests for *rpoB* mutation detection was 89.06% (57/64).

MassARRAY outcome among patients with positive Xpert assay outcomes

Out of the 154 patients who underwent the Xpert assay, 118 patients had positive outcomes, but only 102 had determined RIF outcomes. Among these positive cases, 64 were identified as RIF-sensitive by both methods, whereas 31 exhibited the *rpoB* mutation using both methods. Additionally, seven cases were found to have the *rpoB* mutation solely by the Xpert assay. Only two of these seven cases had pDST outcomes, and both were RIF-resistant. The overall concordance rate between these two tests for *rpoB* mutation detection was 93.14% (95/102).

The head-to-head comparison of different methods in TB diagnosis and detecting RIF resistance

To enhance the objectivity of the comparison, a stratified analysis was conducted (Figure 2). Among the 170 analyzed TB cases, 146 underwent MassARRAY testing, Xpert assay, and culture testing. Out of these, a total of 136 yielded positive results for TB diagnosis. The Venn diagram illustrates that 53.68% (73/136) of these cases were consistently detected by all three methods, while an additional 34.56% (47/136) cases were identified as positive by two of these three methods. In contrast, 14 cases were detected as positive by MALDI-TOF MS only, with 2 and 0 cases detected by Xpert assay or culture only, respectively. Regarding RIF-resistant cases, among the 51 cases that underwent MALDI-TOF MS, Xpert, and pDST for RIF resistance detection, 28 were reported to have RIF resistance by any method. Out of these 28 cases, 16 (57.14%) were consistently detected by all three methods, while another 7 (25%) cases were identified as RIF-resistant by two of these three methods. Additionally, five cases were reported as RIF-resistant by the Xpert assay only.

The 12 drug resistance detection comparison between MassARRAY and pDST

A total of 33 cases had both MALDI and pDST outcomes, with consistency rates ranging from 78.8 to 93.9% for different drugs (Table 3). Some drugs included in pDST were analyzed as a group due to the over-cross resistance between analog drugs, such as thioacetazone, fluoroquinolone, and second-line injectables. Amikacin exhibited the highest consistency rate at 93.9%, while ethambutol demonstrated the lowest consistency between MassARRAY and pDST.

Discussion

Tuberculosis necessitates treatment regimens that encompass multiple drugs (World Health Organization, 2022). Therefore, identifying the complete spectrum of drug resistance is a prerequisite for establishing a personalized anti-TB regimen. However, physicians often face challenges in determining an appropriate treatment regimen for the patient due to the absence of drug susceptibility information. While pDST can cover multiple drugs, its value is limited by the fact that outcomes may take months to be obtained. Moreover, growing concerns have been raised about its reproducibility and reliability, as various factors could impact its performance (Yu et al., 2011). Next-generation sequencing (NGS) is a robust platform for detecting mutations in drug resistance-associated genes (Shendure and Ji, 2008). It can simultaneously analyze all genes of interest from clinical specimens and clinical strains within a few days (Goig et al., 2020), and WHO released its guidelines for this promising technique in 2018 (Word Health Organization, 2018). However, due to the expensive equipment required, the complex processing method, low throughput, and the challenging interpretation of sequencing data, NGS is still a few steps away from routine clinical application. MALDI-TOF-MS directly detects the molecular weight of molecules without the need for fluorescent-labeled dye. This feature allows for a higher multiplex of up to 30 targets in one reaction and significantly reduces reagent costs compared to the NGS platform, which requires expensive dye.

WHO recommended the Xpert assay as the initial test for pulmonary TB in 2010 (World Health Organization, 2010). The Xpert

TABLE 3 Concordance between pDST and MassARRAY in resistance detection.

Drug	MassARRAY	pDST R	pDST S	Concordance rate (%)
RIF	R	16	1	87.9%
	S	3	13	
Isoniazid (INH)	R	17	1	87.9%
	S	3	12	
RIF + INH (MDR)	R	16	1	87.9%
	S	3	13	
Ethambutol	R	6	2	78.8%
	S	5	20	
Fluoroquinolone	R	7	1	87.9%
	S	3	22	
Kanamycin	R	2	2	87.9%
	S	2	27	
Cycloserine	R	0	0	81.8%
	S	6	27	
p-aminosalicylic acid (PAS)	R	0	2	84.8%
	S	3	28	
Streptomycin	R	11	2	87.9%
	S	2	18	
Ethionamide/protionamide	R	1	1	90.0%
	S	2	29	
Amikacin	R	3	1	93.9%
	S	1	28	
Capreomycin	R	2	2	90.9%
	S	1	28	
Second-line injectable reagent	R	3	1	90.9%
	S	2	27	

assay has demonstrated excellent performance in TB diagnosis and RIF resistance detection (Steingart et al., 2014). Therefore, in this study, we selected the Xpert assay as a reference standard to evaluate the reliability of MassARRAY in TB diagnosis and the detection of RIF resistance. However, for other drugs, the absence of a standardized method, coupled with the limited sensitivity or reproducibility of available pDST or molecular tests, makes it challenging to establish a reliable benchmark for evaluation. Among the enrolled cases, MassARRAY, Xpert assay, and culture all exhibited high reliability, as positive outcomes were observed in 88.24% (120 of 136) of cases that underwent all three tests, and these positive results could be confirmed by at least one of the other two methods. The concordance rate between MassARRAY and the Xpert assay was higher in smear-positive cases than in culture-positive cases, but the difference was not statistically significant (97.37% vs. 89.06%, $p = 0.259$). Smear positivity indicates a high bacilli load in the specimen. The reliability of RIF resistance outcomes in the Xpert assay is associated with the bacilli load, and studies have reported lower reliability of RIF resistance with a "very low" level readout (Wang et al., 2018; Hu et al., 2019). The discrepancy between the MassARRAY and Xpert assay in detecting RIF resistance may mainly be due to the different bacilli loads in different specimens and the heterogeneous nature of resistance. Another advantage of MALDI-TOF MS in mutation detection is that MassARRAY can differentiate heterogeneity of drug resistance genes with higher sensitivity, very independent of the constitution ratio of these sequence types. Among the 28 cases that underwent MassARRAY testing, Xpert, and pDST and demonstrated RIF resistance, 20 cases with RIF-resistant outcomes by MassARRAY were confirmed by at least one of the Xpert assays or pDSTs (Figure 2B). These findings strongly suggest the high reliability of MassARRAY testing in detecting RIF resistance.

In addition to RIF, other drugs detectable by pDST also showed a high level of agreement with the results obtained through MassARRAY analysis, with consistency rates ranging from 81.8 to 93.9%. Furthermore, a concordance rate of 87.9% was achieved for the identification of MDR cases. These concordance rates are generally about 5% lower than those reported by Wu et al. (2022), who conducted their evaluation using clinical isolates. They also obtained the best concordance for kanamycin but the lowest for ethambutol. We hypothesize that the paucibacillary status of the specimens we tested may have influenced the drug detection outcomes in some way (Wang et al., 2018). Many studies focusing on the discrepancy between molecular tests and pDST for drug resistance diagnosis have demonstrated that molecular tests have much better reproducibility

than phenotypic DST, meaning the adjusted outcomes after repeated tests favor the molecular test results (Gu et al., 2015; Wu et al., 2022). Hence, we presume that a better authentic performance for MassARRAY could be expected.

Pulmonary TB patients were recommended to collect BALF instead of sputum to enhance the success rate of detection; however, similar positive rates were observed for both groups [63.89% (69 of 108) vs. 66.67% (16 of 24), $p > 0.05$]. This observation may suggest a bias in which patients with higher bacterial loads in sputum are less likely to be advised for an invasive bronchoscopy examination. Further analysis revealed that more than half of the tested sputa were smear-positive, while only 15% showed smear positivity with BALF. This difference might justify considering bronchoscopy examination as a measure for sample collection, particularly for patients with a low AFB load in their sputum. In this study, good performance of MassARRAY was observed for all specimen types except CSF. However, due to the limited number of these extra-pulmonary specimens, it is challenging to draw reliable conclusions.

MALDI-TOF MS is renowned for its high sensitivity in detecting small molecules (Roskey et al., 1996; World Health Organization, 2017). In this study, MassARRAY outperformed the Xpert assay in the etiological diagnosis of TB, even when the Xpert assay outcomes of many patients were a composite result of multiple tests. Su et al. reported that the limit of detection (LOD) of MassARRAY is 5 CFU/mL (Hsu et al., 2015), which is significantly lower than the reported LOD of the Xpert assay (114 CFU/mL) and even lower than the new generation Xpert assay, i.e., Xpert MTB/RIF Ultra (16 CFU/mL) (Chakravorty et al., 2017). More than one-third of the enrolled cases yielded negative outcomes in their initial Xpert tests in this study, while the majority of these cases were successfully detected by MassARRAY. However, based on the principle of MALDI-TOF MS in mutation detection, it may not provide comprehensive coverage for resistant genes lacking mutation hotspots, such as the pyrazinamide (PZA) resistant gene *pncA*. Dozens of *pncA* mutation types related to PZA resistance have been reported, but only one locus of the *pncA* gene was included in the panel of MassARRAY. This limited coverage diminishes the practical value of PZA resistance detection in MassARRAY, so we did not analyze the detection outcome of the *pncA* mutation in this study.

The strength of our study is that we concentrated on the reliability evaluation of MassARRAY against a very stringent reference standard, and our outcomes favor the application of this technique. Although we only extensively analyzed the reliability of RIF resistance detection by MassARRAY, owing to the same rationale for drug resistance detection, the same specimen used, and the same detection reaction performed, we propose that the high reliabilities of other drug resistance detection could be expected. However, as a retrospective study, its limitations should also be noted. First, as the focal control method, the outcomes of the Xpert assay for more than one-third of the enrolled patients were integrations of outcomes of several tests and even on different specimen types in this near episode. Consequently, the performance of the Xpert assay was overstated in this study. Second, we focused on the drug resistance detection capability of MassARRAY; therefore, patients with bacteriological evidence of TB were favored in enrollment, and hence the performance of each involved method for TB diagnosis could not be extrapolated to all TB patients. Third, due to the accessibility of the molecular test, only the Xpert assay was used as a reference in this study. We suggest more comparative studies using MTBDRplus, Xpert MTB/XDR (Cepheid, USA), and other molecular tests as references to better understand the reliability of MALDI-TOF MS in drug resistance detection of other drugs. Finally, the targets of MassARRAY are gene mutations, and their authentic significance in drug resistance indication was not discussed in this study.

In conclusion, MassARRAY was demonstrated as a highly sensitive method in TB diagnostics and a powerful tool for comprehensive TB resistance detection. Given its high consistency in RIF resistance detection compared with the Xpert assay, it is reasonable to speculate that resistant outcomes of other drugs detected by the MassARRAY assay, which often pose difficulty in verification, could be highly predictive of actual drug resistance.

Data availability statement

The raw data supporting the conclusions of this article will be made available by the authors, without undue reservation.

Ethics statement

The studies involving humans were approved by Ethics Committees of Henan Chest Hospital (Zhengzhou, China). The studies were conducted in accordance with the local legislation and institutional requirements. The participants provided their written informed consent to participate in this study. Written informed consent was obtained from the individual(s) for the publication of any potentially identifiable images or data included in this article.

Author contributions

RL: Data curation, Writing – original draft. JL: Data curation, Writing – original draft, Investigation, Methodology. YZ: Methodology, Writing – original draft. HQ: Methodology, Writing – original draft. SB: Writing – original draft, Data curation. FW: Writing – original draft, Methodology. HD: Writing – original draft, Data curation, Writing – review & editing. HH: Data curation, Writing – review & editing, Writing – original draft, Conceptualization, Funding acquisition.

Funding

The author(s) declare financial support was received for the research, authorship, and/or publication of this article. This study was supported by the Beijing High-Level Public Health Talent Program (G2023-2-002) and the Beijing Tongzhou Yunhe Project (YH201917).

Conflict of interest

The authors declare that the research was conducted in the absence of any commercial or financial relationships that could be construed as a potential conflict of interest.

Publisher's note

References

Bouakaze, C., Keyser, C., Gonzalez, A., Sougakoff, W., Veziris, N., Dabernat, H., et al. (2011). Matrix-assisted laser desorption ionization-time of flight mass spectrometry-based single nucleotide polymorphism genotyping assay using iPLEX gold technology for identification of *Mycobacterium tuberculosis* complex species and lineages. *J. Clin. Microbiol.* 49, 3292–3299. doi: 10.1128/JCM.00744-11

Chakravorty, S., Simmons, A. M., Rowneki, M., Parmar, H., Cao, Y., Ryan, J., et al. (2017). The new Xpert MTB/RIF ultra: improving detection of mycobacterium tuberculosis and resistance to rifampin in an assay suitable for point-of-care testing. *MBio* 8, e00812–e00817. doi: 10.1128/mBio.00812-17

Chen, S., Wang, F., Xue, Y., Huo, F., Jia, J., Dong, L., et al. (2022). Doubled nontuberculous mycobacteria isolation as a consequence of changes in the diagnosis algorithm. *Infect. Drug Resist.* 15, 3347–3355. doi: 10.2147/IDR.S368671

Gail. Clinical and Laboratory Standards Institute. *CLSI M24-A2: Susceptibility testing of mycobacteria, Nocardiae, And Other Aerobic Actinomycetes, Approved Standard-Third Edition*. (2018). Wayne, PA: Clinical And Laboratory Standards Institute.

Goig, G. A., Torres-Puente, M., Mariner-Llicer, C., Villamayor, L. M., Chiner-Oms, Á., Gil-Brusola, A., et al. (2020). Towards next-generation diagnostics for tuberculosis: identification of novel molecular targets by large-scale comparative genomics. *Bioinformatics* 36, 985–989. doi: 10.1093/bioinformatics/btz729

Gu, Y., Wang, G., Dong, W., Li, Y., Ma, Y., Shang, Y., et al. (2015). Xpert MTB/RIF and Geno type MTBDRplus assay for rapid diagnosis of bone and joint tuberculous. *Int. J. Infect. Dis.* 36, 27–30. doi: 10.1016/j.ijid.2015.05.014

Hsu, K. H., Ho, C. C., Hsia, T. C., Tseng, J. S., Su, K. Y., Wu, M. F., et al. (2015). Identification of five driver gene mutations in patients with treatment-naive lung adenocarcinoma in Taiwan. *PLoS One* 10:e0120852. doi: 10.1371/journal.pone.0120852

Hu, P., Zhang, H., Fleming, J., Zhu, G., Zhang, S., Wang, Y., et al. (2019). Retrospective analysis of false-positive and disputed rifampin resistance Xpert MTB/RIF assay results in clinical samples from a referral hospital in Hunan, China. *J. Clin. Microbiol.* 57, e01707–e01718. doi: 10.1128/JCM.01707-18

Lawn, S. D., Mwaba, P., Bates, M., Piatek, A., Alexander, H., Marais, B. J., et al. (2013). Advances in tuberculosis diagnostics: the Xpert MTB/RIF assay and future prospects for a point-of-care test. *Lancet Infect. Dis.* 13, 349–361. doi: 10.1016/S1473-3099(13)70008-2

Penn-Nicholson, A., Georghiou, S., Ciobanu, N., Kazi, M., Bhalla, M., David, A., et al. (2022). Detection of isoniazid, fluoroquinolone, ethionamide, amikacin, kanamycin, and capreomycin resistance by the Xpert MTB/XDR assay: a cross-sectional multicentre diagnostic accuracy study. *Lancet Infect. Dis.* 22, 242–249. doi: 10.1016/S1473-3099(21)00452-7

Roskey, M., Juhasz, P., Smirnov, I., Takach, E. J., Martin, S. A., Haff, L. A., et al. (1996). DNA sequencing by delayed extraction-matrix-assisted laser desorption/ionization time of flight mass spectrometry. *Proc. Natl. Acad. Sci. USA* 93, 4724–4729. doi: 10.1073/pnas.93.10.4724

Shendure, J., and Ji, H. (2008). Next-generation DNA sequencing. *Nat. Biotechnol.* 26, 1135–1145. doi: 10.1038/nbt1486

Shi, J., He, G., Ning, H., Wu, L., Wu, Z., Ye, X., et al. (2022). Application of matrix-assisted laser desorption ionization time-of-flight mass spectrometry (MALDI-TOF MS) in the detection of drug resistance of *Mycobacterium tuberculosis* in re-treated patients. *Tuberculosis (Edinb.)* 135:102209. doi: 10.1016/j.tube.2022.102209

Steingart, K. R., Schiller, I., Horne, D. J., Pai, M., Boehme, C. C., Dendukuri, N., et al. (2014). Xpert (R) MTB/RIF assay for pulmonary tuberculosis and rifampicin resistance in adults. *Cochrane Database Syst. Rev.* 1:CD009593. doi: 10.1002/14651858.CD009593.pub3

Su, K. Y., Yan, B. S., Chiu, H. C., Yu, C. J., Chang, S. Y., Jou, R., et al. (2017). Rapid sputum multiplex detection of the *M. tuberculosis* complex (MTBC) and resistance mutations for eight antibiotics by nucleotide MALDI-TOF MS. *Sci. Rep.* 7:41486. doi: 10.1038/srep41486

Tsai, T. H., Su, K. Y., Wu, S. G., Chang, Y. L., Luo, S. C., Jan, I. S., et al. (2012). RNA is favourable for analysing EGFR mutations in malignant pleural effusion of lung cancer. *Eur. Respir. J.* 39, 677–684. doi: 10.1183/09031936.00043511

van Deun, A., Wright, A., Zignol, M., Weyer, K., and Rieder, H. L. (2011). Drug susceptibility testing proficiency in the network of supranational tuberculosis reference laboratories. *Int. J. Tuberc. Lung Dis.* 15, 116–124.

Venkatesh, S. K., Siddaiah, A., Padakannaya, P., and Ramachandra, N. B. (2014). Association of SNPs of DYX1C1 with developmental dyslexia in an Indian population. *Psychiatr. Genet.* 24, 10–20. doi: 10.1097/YPG.0000000000000009

Wang, G., Dong, W., Lan, T., Fan, J., Tang, K., Li, Y., et al. (2018). Diagnostic accuracy evaluation of the conventional and molecular tests for spinal tuberculosis in a cohort, head-to-head study. *Emerg. Microbes Infect.* 7, 1–8. doi: 10.1038/s41426-018-0114-1

Williams, G. R., Cook, L., Lewis, L. D., Tsongalis, G. J., and Nerenz, R. D. (2020). Clinical validation of a 106-SNV MALDI-ToF MS Pharmacogenomic panel. *J. Appl. Lab. Med.* 5, 454–466. doi: 10.1093/jalm/jfaa018

Word Health Organization. *The use of next-generation sequencing technologies for the detection of mutations associated with drug resistance in Mycobacterium tuberculosis complex: Technical guide*. (2018). Geneva: Word Health Organization.

World Health Organization. *WHO endorses new rapid tuberculosis test*. (2010). Geneva: Word Health Organization.

World Health Organization. *Systematic screening for active tuberculosis: Principles and recommendations*. (2013). Geneva: World Health Organization.

World Health Organization. *WHO Meeting Report for a Technical Expert Consultation: No-Inferiority Analysis of Xpert MTB/RIF Ultra Compared to Xpert MTB/RIF*. (2017). Geneva: World Health Organization.

World Health Organization. *WHO consolidated guidelines on tuberculosis: Module 3: Diagnosis – rapid diagnostics for tuberculosis detection*. (2021). Geneva: World Health Organization.

World Health Organization. *WHO operational handbook on tuberculosis. Module 4: Treatment – drug-resistant tuberculosis treatment, 2022 update*. (2022). Geneva: World Health Organization.

World Health Organization. *Global tuberculosis report*. (2023). Geneva: World Health Organization.

Wu, X., Tan, G., Yang, J., Guo, Y., Huang, C., Sha, W., et al. (2022). Prediction of *Mycobacterium tuberculosis* drug resistance by nucleotide MALDI-TOF-MS. *Int. J. Infect. Dis.* 121, 47–54. doi: 10.1016/j.ijid.2022.04.061

Xie, Y., Chakravorty, S., Armstrong, D., Hall, S. L., Via, L. E., Song, T., et al. (2017). Evaluation of a rapid molecular drug-susceptibility test for tuberculosis. *N. Engl. J. Med.* 377, 1043–1054. doi: 10.1056/NEJMoa1614915

Yu, X., Jiang, G., Li, H., Zhao, Y., Zhang, H., Zhao, L., et al. (2011). Rifampicin stability in 7H9 broth and Lowenstein-Jensen medium. *J. Clin. Microbiol.* 49, 784–789. doi: 10.1128/JCM.01951-10

frontiers | Frontiers in Microbiology

TYPE Original Research
PUBLISHED 08 February 2024
DOI 10.3389/fmicb.2024.1335526

OPEN ACCESS

EDITED BY
Axel Cloeckaert,
Institut National de recherche pour l'agriculture, l'alimentation et l'environnement (INRAE), France

REVIEWED BY
Aliabbas A. Husain,
Central India Institute of Medical Sciences, India
Basem Battah,
Syrian Private University (SPU), Syria

*CORRESPONDENCE
Liping Pan
✉ panliping2006@163.com
Dailun Hou
✉ hou.dl@mail.ccmu.edu.cn

†These authors have contributed equally to this work

RECEIVED 09 November 2023
ACCEPTED 29 January 2024
PUBLISHED 08 February 2024

CITATION
Li Z, Wang B, Du B, Sun Q, Wang D, Wei R, Li C, Zhu C, Jia H, Xing A, Zhang Z, Pan L and Hou D (2024) The incremental value of *Mycobacterium tuberculosis* trace nucleic acid detection in CT-guided percutaneous biopsy needle rinse solutions for the diagnosis of tuberculosis. *Front. Microbiol.* 15:1335526. doi: 10.3389/fmicb.2024.1335526

The incremental value of *Mycobacterium tuberculosis* trace nucleic acid detection in CT-guided percutaneous biopsy needle rinse solutions for the diagnosis of tuberculosis

Zihui Li[1†], Bing Wang[2†], Boping Du[1], Qi Sun[1], Dongpo Wang[2], Rongrong Wei[1], Chenghai Li[2], Chuanzhi Zhu[1], Hongyan Jia[1], Aiying Xing[1], Zongde Zhang[1], Liping Pan[1*] and Dailun Hou[2*]

[1]Laboratory of Molecular Biology, Beijing Key Laboratory for Drug Resistant Tuberculosis Research, Beijing Chest Hospital, Capital Medical University, Beijing Tuberculosis and Thoracic Tumor Research Institute, Beijing, China, [2]Department of Radiology, Beijing Chest Hospital, Capital Medical University, Beijing Tuberculosis and Thoracic Tumor Research Institute, Beijing, China

Introduction: Tuberculosis (TB) diagnosis still faces challenges with high proportion of bacteriologic test negative incidences worldwide. We assessed the diagnostic value of digital PCR (dPCR) analysis of ultramicro *Mycobacterium tuberculosis* (*M.tb*) nucleic acid in CT-guided percutaneous biopsy needle rinse solution (BNRS) for TB.

Methods: BNRS specimens were consecutively collected and total DNA was purified. The concentrations of *M.tb*-specific IS*6110* and IS*1081* were quantified using droplet dPCR. The diagnostic performances of BNRS-dPCR and its sensitivity in comparison with conventional tests were analyzed.

Results: A total of 106 patients were enrolled, 63 of whom were TB (48 definite and 15 clinically suspected TB) and 43 were non-TB. The sensitivity of BNRS IS*6110* OR IS*1081*-dPCR for total, confirmed and clinically suspected TB was 66.7%, 68.8% and 60.0%, respectively, with a specificity of 97.7%. Its sensitivity was higher than that of conventional etiological tests, including smear microscopy, mycobacterial culture and Xpert using sputum and BALF samples. The positive detection rate in TB patients increased from 39.3% for biopsy AFB test alone to 73.2% when combined with BNRS-dPCR, and from 71.4% for biopsy *M.tb* molecular detection alone to 85.7% when combined with BNRS-dPCR.

Conclusion: Our results preliminarily indicated that BNRS IS*6110* OR IS*1081*-dPCR is a feasible etiological test, which has the potential to be used as a supplementary method to augment the diagnostic yield of biopsy and improve TB diagnosis.

KEYWORDS

tuberculosis, biopsy, biopsy needle rinse solution, digital PCR, diagnosis, computed tomography (CT)

1 Introduction

Tuberculosis (TB) was the predominant cause of mortality attributable to a single infectious agent prior to the coronavirus (COVID-19) pandemic. Globally in 2021, an estimated 10.6 million people fell ill with TB, and 1.6 million people died from the disease (World Health Organization, 2022).

An essential step in the pathway of global TB infection control is rapid and accurate testing to diagnose TB. Currently, laboratory diagnosis of *Mycobacterium tuberculosis* (*M.tb*) infection primarily relies on the detection of *M.tb* and *M.tb* -specific immune responses. The latter, such as tuberculin skin test (TST) and interferon-γ release assay (IGRA), serves as an auxiliary diagnostic tool for TB but possess limitations when applied to immunocompromised individuals (Redelman-Sidi and Sepkowitz, 2013; Nguyen et al., 2018). Testing for *M.tb* or its nucleic acids or antigens is crucial as it allows people to get an etiological diagnosis and start on effective treatment regimen as early as possible. The traditional smear microscopy with Ziehl-Nielsen staining is widely used with low sensitivity. Mycobacterial culture is more sensitive, but its application is greatly limited by the longtime of return results (10 days - 8 weeks) and biosafety requirements. In recent years, the development and application of nucleic acid amplification-based tests (NAATs) of *M.tb*, such as conventional polymerase chain reaction (PCR), quantitative real-time PCR (qPCR), loop-mediated isothermal amplification (LAMP), as well as Xpert MTB/RIF (Xpert) and Xpert Ultra recommended by WHO, have improved the microbiological diagnosis of TB (Lawn et al., 2013; Detjen et al., 2015; Dorman et al., 2018; Sabi et al., 2018; Gong et al., 2023). However, despite the availability of these methods, the worldwide percentage of bacteriological confirmation of pulmonary TB remains at only 63% in 2021 due to complex factors such as sensitivity, testing cost and experimental facilities (World Health Organization, 2022). Therefore, more etiological methods are urgently needed to enhance TB diagnosis.

Biopsy plays a crucial role in establishing a definitive diagnosis for patients who have undergone all routine procedures but remain undiagnosed (Xu et al., 2023; Zhao et al., 2023). Usually, the minimal cellular residues adhering to the puncture needle are discarded along with the used needle following the biopsy operation. Considering the trajectory of the puncture needle, the outer surface of the needle contacts a larger area of lesion tissue compared to the needle groove housing the biopsy tissue. Consequently, residual cells on needle's outer wall may harbor pathogenic evidence that differs from the biopsy tissue. Previous studies have demonstrated the role of this kind of biopsy needle rinse solutions (BNRS) in enhancing lung cancer diagnosis and multiple genetic analyses (Sakairi et al., 2014; Lan et al., 2021). Whether this type of ultra-microsample can be used to provide the etiological evidence of TB has not been reported.

Digital PCR (dPCR) is a robust technique employed for the absolute quantification of trace amounts of nucleic acids. Compared to qPCR, dPCR offers advantages such as quantification without the need for a standard curve, improved precision, and enhanced tolerance to PCR inhibitors (Kuypers and Jerome, 2017). It has demonstrated good efficacy in improving the diagnosis of paucibacillary TB, including tuberculous meningitis and pleurisy (Li et al., 2020, 2022). The aim of this study was to assess the value of computed tomography (CT) - guided percutaneous BNRS-dPCR analysis in the diagnosis of TB.

2 Materials and methods

2.1 Study participants

We conducted the cross-sectional study from 2021 to 2022 at Beijing Chest Hospital, Beijing, China. Patients who met the inclusion and exclusion criteria were consecutively enrolled. The inclusion criteria were as follows: (1) age $\geq$ 18 years; (2) imaging showed isolated or multiple lesions suggesting TB; (3) received doctor's advice for CT-guided percutaneous biopsy to confirm diagnosis; (4) provided informed consent for the study. The exclusion criteria were as follows: (1) uncorrectable coagulation abnormalities; (2) severe pulmonary arterial hypertension; (3) anatomically or functionally isolated lung; (4) pulmonary bulla, chronic obstructive pulmonary disease, emphysema, and pulmonary fibrosis; (5) mechanical ventilation; (6) imaging findings of pulmonary hydatidosis, which may increase the risk of allergy; (7) uncontrolled cough or other conditions that may affect biopsy. The sample size was calculated using PASS 11 software, with area under curve (AUC) 0 (H0) = 0.5, AUC1 (H1) = 0.7 (set according to preliminary experimental results), $\alpha = 0.025$, $\beta = 0.1$, sample allocation ratio = 1.0 and one-sided test. At least 41 cases needed to be included in each group. Some of the following tests were performed to help make a final diagnosis: formalin-fixed paraffin-embedded (FFPE) biopsy tissue tests including routine pathology, acid-fast bacilli (AFB) detection and molecular pathology (detection of *M.tb* nucleic acids) (Shengxiang, Changsha, Hunan, China); *M.tb* tests including smear microscopy for AFB, mycobacterial culture and Xpert (Cepheid, Sunnyvale, CA, USA) using sputum, bronchoalveolar lavage fluid (BALF) or pus samples; blood tests related to *M.tb* infection including IGRA (X.DOT-TB; Signature Biotechnology, Foshan, Guangdong, China) and *M.tb* antibody detection (Huian, Shenzhen, Guangdong, China). All of the commercial assays were performed according to the manufacturer's instructions. This study was approved by the Ethics Committee of Beijing Chest Hospital, Capital Medical University (ethical approval number: 2021 clinical trial review-scientific research-no. 37). Written informed consent was acquired from each participant before enrollment or any study procedure.

2.2 Categorization of patients

Patients were divided into two groups: (1) TB group: composite reference standard (CRS) was used as gold standard according to the diagnostic criteria (WS288-2017) (National Health and Family Planning Commission of the People's Republic of China, 2018), which was composed of clinical, laboratory, histopathological and radiological features. Confirmed TB: imaging examination was positive, at least one etiological test was positive, and nontuberculous mycobacterial disease was excluded by species identification or *M.tb*-specific molecular detection. Clinically suspected TB: with positive imaging findings and positive immunological results or typical clinical manifestations. Confirmed TB by molecular pathology: confirmed TB with positive *M.tb* molecular detection using FFPE biopsy tissue. Etiological tests

included AFB detection, mycobacterial culture or commercial NAAT for *M.tb* using sputum, BALF, pus or biopsy samples. Immunological tests included blood IGRA or *M.tb* antibody detection. (2) Non-TB group: an alternative diagnosis was made, without convincing signs of *M.tb* infection.

2.3 CT-guided percutaneous biopsy

Percutaneous biopsy was performed by radiologists under the guidance of a 64-detector row CT scanner (Light Speed, VCT, GE, Milwaukee, WI, USA). Depending on the location of the lesion, the patient was placed in the supine or prone position and instructed to remain motionless throughout the entire puncture process. After the patient was in a stable state, the needle entry point was selected under the guidance of CT. Following skin disinfection, the patient was locally anesthetized with 2% lidocaine. Then a small incision at the injection point was made using a disposable core biopsy instrument (MC1810, MC1816, BARD, Murray Hill, NJ, USA) to retrieve specimens. After the biopsy procedure, all visible tissue specimens were removed and placed in formalin for routine histopathological examination. The front part of the used needle was rinsed in a 10-mL aseptic phosphate buffered saline (PBS) tube several times without touching the tube wall. This tube containing BNRS was then sent to the laboratory for further testing.

2.4 BNRS sample processing and DNA extraction

The tubes containing BNRS were centrifuged at 4000 rpm for 10 min at room temperature, and the sediments and 800 μL supernatant were frozen at −80 °C. They were mixed and transferred into a 2 ml Lysing Matrix B tubes (116911050, MP, California, USA) and added 200 μL Buffer ATL (939011, Qiagen, Hilden, Germany) with 0.67% Reagent DX (19088, Qiagen, Hilden, Germany). The tubes were vortexed on the FastPrep-24 instrument (116004500, MP, California, USA) applying a velocity of 6.5 m/s for three times 45 s with a 5 min intermission. After centrifugation, 400 μL supernatants were transferred into fresh tubes for DNA extraction using DNeasy Blood and Tissue Kits (69506, Qiagen, Hilden, Germany) with an elution volume of 50 μL. DNA samples were extracted in batches and stored at −80 °C until dPCR detection.

2.5 Digital PCR analysis

Conserved DNA sequences in *M.tb* complex, insertion sequence IS*6110* and IS*1081*, were used as detection targets in this study. The primers for amplification, oligonucleotide probes and dPCR assay procedures have been previously optimized and described in Li et al. (2022). The 20-μL reaction mixtures (10 μL ddPCR^{TM} supermix for probes, 0.9 μM each primer, 0.2 μM each probe, 0.3 U uracil-N-glycosylase, DNA samples without dilution) and 70-μL droplet generation oil were added in cartridges and droplets were generated using QX200 Droplet Generator (Bio-Rad). After droplet emulsions were transferred into the 96-well plate and PCR procedure, the fluorescence signals of each droplet in each well was acquired using QX200 Droplet Reader (BioRad) with FAM and HEX/VIC channels. Data analysis was performed using QuantaSoft Version 1.7.4.0917 (BioRad) and the absolute quantity of target DNA in each well were automatically calculated based on the Poisson distribution. No-template negative control and *M.tb* H37Rv DNA positive control were adopted in each assay, which was used to set the threshold manually based on their fluorescence amplitudes. The number of copies per 20-μL reaction mixture was calculated as the average of two independent dPCR results, with each result in duplicate.

2.6 Statistical analysis

All statistical analysis was performed using the software SPSS version 25.0 (IBM, Armonk, NY, USA). Continuous variables were compared using Mann-Whitney *U*-test or Wilcoxon test, as appropriate. Categorical variables were tested by Chi-square test. Receiver operating characteristic (ROC) curves were constructed by plotting the rate of sensitivity against the rate of (1-specificity) over a range of cut-off values of dPCR. Diagnostic performance was expressed in terms of sensitivity, specificity, positive likelihood ratio (LR+), negative likelihood ratio (LR-), positive predictive value (PPV), negative predictive value (NPV) and AUC. All tests were two-sided and $P < 0.05$ were considered statistically significant.

3 Results

3.1 Participant characteristics

A total of 165 subjects who underwent CT-guided percutaneous biopsy were prospectively enrolled and 30 patients were excluded due to undetermined diagnosis. Among the 135 patients, 63 were diagnosed as TB and 72 as non-TB. Twenty-nine patients were excluded from non-TB group due to positive IGRA result indicating concurrent infection with *M.tb*. Therefore, the final sample size for analysis comprised 106 patients, including 63 TB patients (48 definite TB cases and 15 clinically suspected TB cases) and 43 non-TB patients without *M.tb* infection. Among the 43 non-TB patients, there were 38 cases of tumor, 3 cases of pneumonia, 1 case of pneumoconiosis, and 1 case of non-tuberculous mycobacterial pulmonary disease (Figure 1). Overall, the study population consisted of 65 male patients (61%), with a median age of 53.5 years (range: 18 to 83). TB patients were younger than non-TB patients ($P < 0.0001$). The biopsy tissues primarily originated from the lungs, as well as the pleura, peritoneum, chest wall, and mediastinum. Demographic and basic clinical characteristics of the study population are presented in Table 1.

3.2 Results of dPCR in detection of *M.tb* nucleic acids in BNRS

The IS*6110*- and IS*1081*- targeted tests exhibited a strong positive correlation ($r = 0.793$, $P < 0.0001$, Figure 2A). In most cases, the number of IS*6110* detected was higher than that of IS*1081*

10.3389/fmicb.2024.1335526

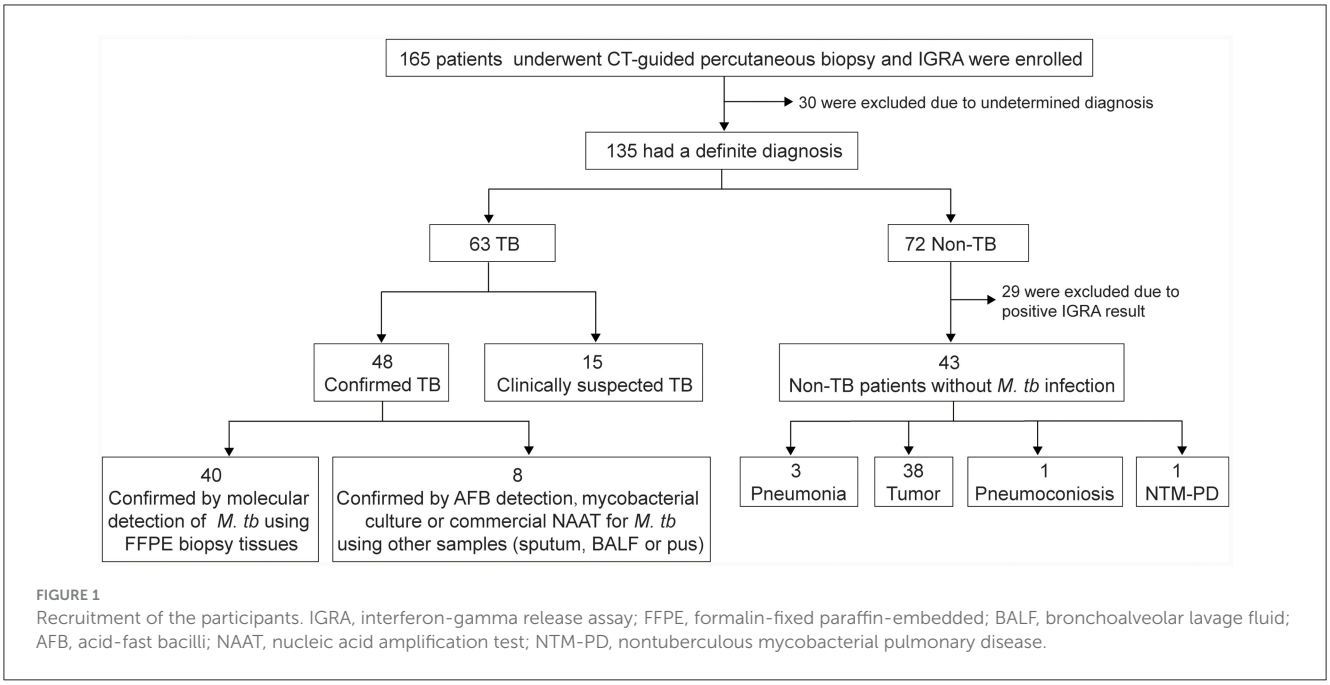

FIGURE 1
Recruitment of the participants. IGRA, interferon-gamma release assay; FFPE, formalin-fixed paraffin-embedded; BALF, bronchoalveolar lavage fluid; AFB, acid-fast bacilli; NAAT, nucleic acid amplification test; NTM-PD, nontuberculous mycobacterial pulmonary disease.

TABLE 1 Demographic and clinical characteristics of the participants.

Characteristics	Total patients ($N = 106$)	TB ($N = 63$)	Non-TB ($N = 43$)	*P*-value
Age - median (range), yr	53.5 (18, 83)	44 (18, 80)	64 (32, 83)	< 0.0001
Male sex - no. (%)	65 (61)	41 (65)	24 (56)	0.336
BMI [a] - mean ± SD	22.8 ± 3.8	22.3 ± 3.3	23.5 ± 4.2	0.097
Biopsy site				0.082 [b]
Lung	88	49	39	
Pleura	11	10	1	
Peritoneum	2	2	0	
Chest wall	2	2	0	
Mediastinum	3	0	3	

[a]BMI, body-mass index, is the weight in kilograms divided by the square of the height in meters. [b]Comparison of the proportion of biopsy sites in lung and non-lung between TB and non-TB group (Pearson's Chi-square test).

($P < 0.0001$, Figure 2B). The number of copies detected in TB group was significantly higher than that in non-TB group: median (25% percentile, 75% percentile), IS*6110*, 7.8 (2.2, 58.0) vs. 1.3 (0.4, 2.9) copies/20 μL reaction mixture, $P < 0.0001$; IS*1081*, 2.7 (1.0, 19.1) vs. 0.5 (0.0, 0.9) copies/20 μL reaction mixture, $P < 0.0001$ (Figure 2C). The number of copies detected in confirmed TB group was slightly higher than that in clinically suspected TB group; however, the difference was not significant due to a relatively small number of cases (Figure 2D).

3.3 Performance of BNRS-dPCR in the diagnosis of TB

The ability to detect *M.tb* DNA in BNRS was assessed using ROC analysis. The overall area under the ROC curve (AUC) of IS*6110*-dPCR was nearly identical to that of IS*1081*-dPCR [both 0.84, 95% confidence interval (CI): 0.76-0.91, $P = 0.93$, Figure 2E]. There was no significant difference in the AUC of dPCR between patients with confirmed TB and those with clinically suspected TB (Figures 2F, G). The AUC of dPCR in patients with confirmed TB by molecular pathology was the highest (IS*6110*, 0.90, 95% CI 0.84-0.97; IS*1081*, 0.89, 95% CI 0.81-0.96, Figure 2H). The diagnostic performance of BNRS-dPCR assay for TB is presented in Table 2. In this study, the optimal cut-off values to ensure high specificity and then the maximum sum of sensitivity and specificity were defined as 4.2 (IS*6110*) and 1.7 (IS*1081*) copies/20 μL reaction mixture, respectively. An IS*6110* OR IS*1081*-dPCR result was considered "positive" if either IS*6110* or IS*1081* > their cut-off values, and 'negative' if both IS*6110* and IS*1081* ≤ their cut-off values. Its sensitivity was higher than that of single target-dPCR and IS*6110 and* IS*1081*-dPCR, while maintaining a relatively high specificity. The sensitivity of IS*6110* OR IS*1081*-dPCR for

10.3389/fmicb.2024.1335526

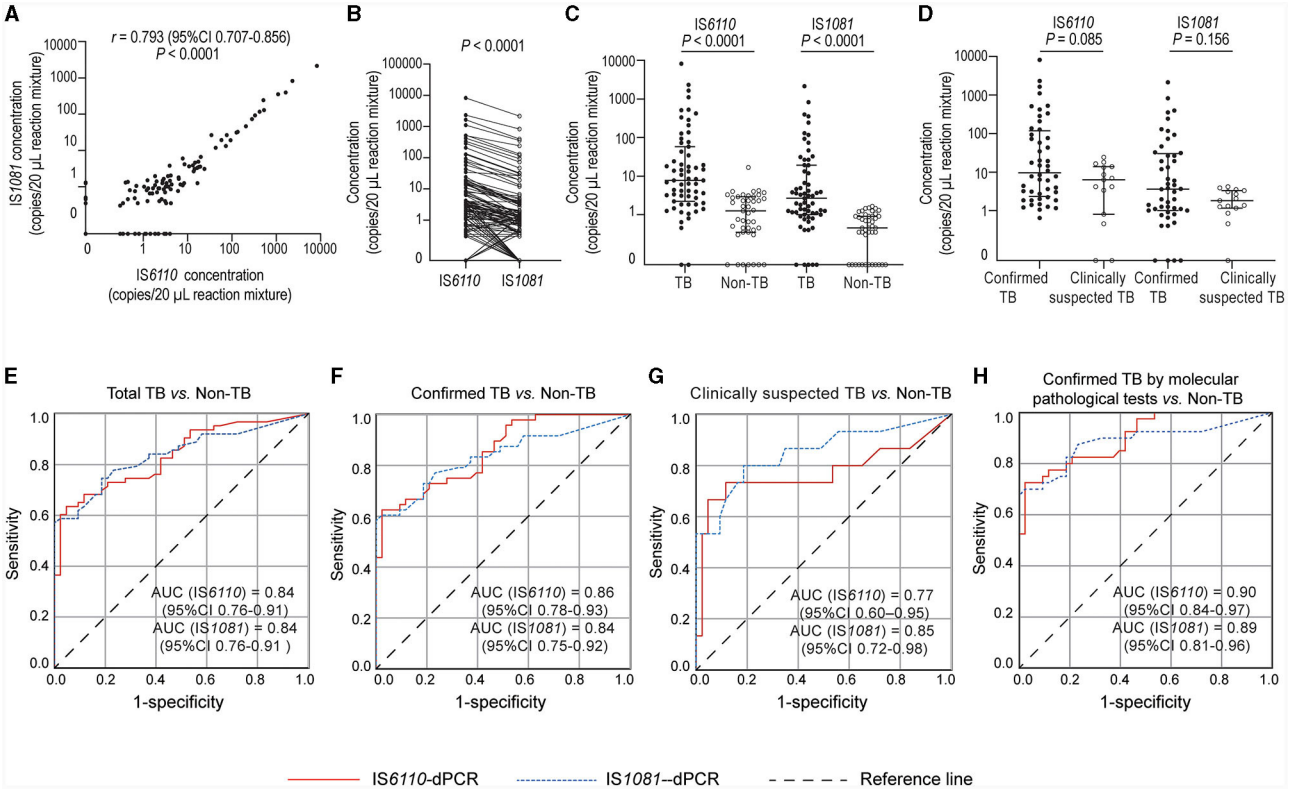

FIGURE 2
Quantification of *M.tb* nucleic acids in biopsy needle rinse solutions (BNRS) samples by dPCR and receiver operating characteristic (ROC) curves analysis. **(A, B)** show the correlation (Spearman correlation test) and the differences (Wilcoxon test) in the number of copies detected between IS*6110*- and IS*1081*- dPCR, respectively. **(C)** shows IS*6110* and IS*1081* copies detected in TB and non-TB group, respectively (Mann–Whitney *U*-test). **(D)** shows IS*6110* and IS*1081* copies detected in confirmed and clinically suspected TB patients, respectively (Mann–Whitney *U*-test). All copy numbers are obtained from the average of two independent dPCR results, with each result in duplicate. Results are considered significant when $P < 0.05$. **(E–H)** ROC curve analysis of IS*6110*- and IS*1081*- dPCR for the diagnosis of total TB, confirmed TB, clinically suspected TB and confirmed TB by molecular pathological tests, respectively. AUC, area under ROC curve; CI, confidence interval.

total, confirmed and clinically suspected TB was 66.7%, 68.8% and 60.0%, respectively, with a specificity of 97.7%. Its sensitivity in diagnosing confirmed TB patients by molecular pathology reached 77.5%.

3.4 Sensitivity comparison of BNRS-dPCR assay with routine diagnostic tests

The positive detection rates of different tests in TB patients are listed in Table 3. BNRS IS*6110* OR IS*1081*-dPCR showed comparable sensitivity to *M.tb* molecular detection using FFPE biopsy tissue (69.6% vs.71.4%, $P = 1.000$), and significantly higher sensitivity than AFB test using FFPE biopsy tissue (69.6% vs. 39.3%, $P < 0.001$). It exhibited higher sensitivity compared to routine etiological tests, including smear microscopy (58.8% vs. 5.9%), mycobacterial culture (52.9% vs. 17.6%), and Xpert (67.9% vs. 21.4%) using sputum samples, as well as smear microscopy (66.7% vs. 8.3%), mycobacterial culture (66.7% vs. 25.0%), and Xpert (72.2% vs. 22.2%) using BALF samples. When compared with immunological tests, the sensitivity of BNRS IS*6110* OR IS*1081*-dPCR was slightly lower than that of peripheral blood IGRA (66.7% vs. 81.3%, $P = 0.143$), and slightly higher than that of TB antibody detection in peripheral blood (60.0% vs. 40.0%, $P = 0.289$).

3.5 Incremental diagnostic value of BNRS-dPCR in TB patients underwent biopsy

The positive proportion of BNRS IS*6110* OR IS*1081*-dPCR in TB cases with negative AFB test results and negative *M.tb* molecular detection results using FFPE biopsy tissue was 55.9% (19/34) and 50.0% (8/16), respectively. Combination of conventional biopsy pathology and BNRS-dPCR increased the positive detection rate in TB patients, with 39.3% for biopsy AFB test alone and 73.2% for it plus BNRS-dPCR, and 71.4% for biopsy *M.tb* molecular detection alone and 85.7% for it plus BNRS-dPCR (Table 4).

4 Discussion

As shown in the results, BNRS IS*6110* OR IS*1081*-dPCR demonstrated considerable sensitivity in comparison with conventional diagnostic tests. We also assessed the agreement

TABLE 2 Diagnostic performances of BNRS-dPCR assay for TB.

	AUC (95% CI)	Criterion (copies/20 μL reaction mixture)	Sensitivity (%) (95% CI)	Specificity (%) [c] (95% CI)	LR+ (95% CI)	LR- (95% CI)	PPV (%) (95% CI)	NPV (%) (95% CI)
Total TB ($n = 63$)								
IS*6110*-dPCR	0.84 (0.76–0.91)	> 4.2	60.3 (47.2–72.4)	97.7 (87.7–99.9)	25.9 (3.7–181.8)	0.4 (0.3–0.6)	97.4 (86.5–99.9)	62.7 (50.0–74.2)
IS*1081*-dPCR	0.84 (0.76–0.91)	> 1.7	57.1 (44.0–69.5)	100.0 (91.8–100.0)	–	0.4 (0.3–0.6)	100.0 (90.3–100.0)	61.4 (49.0–72.8)
IS*6110* and IS*1081*-dPCR[a]	0.75 (0.66–0.85)	> 4.2 and > 1.7	50.8 (37.9–63.6)	100.0 (91.8–100.0)	–	0.5 (0.4–0.6)	100.0 (89.1–100.0)	58.1 (46.1–69.5)
IS*6110* OR IS*1081*-dPCR[b]	0.82 (0.74–0.90)	> 4.2 or > 1.7	66.7 (53.7–78.0)	97.7 (87.7–99.9)	28.7 (4.1–200.5)	0.3 (0.2–0.5)	97.7 (87.7–99.9)	66.7 (53.7–78.0)
Confirmed TB ($n = 48$)								
IS*6110*-dPCR	0.86 (0.78–0.93)	> 4.2	62.5 (47.4–76.0)	97.7 (87.7–99.9)	26.9 (3.8–188.8)	0.4 (0.3–0.6)	96.8 (83.3 – 99.9)	70.0 (56.8–81.2)
IS*1081*-dPCR	0.84 (0.75–0.92)	> 1.7	58.3 (43.2–72.4)	100.0 (91.8–100.0)	–	0.4 (0.3–0.6)	100.0 (87.7–100.0)	68.3 (55.3–79.4)
IS*6110* and IS*1081*-dPCR	0.76 (0.66–0.86)	> 4.2 and > 1.7	52.1 (37.2–66.7)	100.0 (91.8–100.0)	–	0.5 (0.4–0.6)	100.0 (86.3–100.0)	65.2 (52.4–76.5)
IS*6110* OR IS*1081*-dPCR	0.83 (0.75–0.92)	> 4.2 or > 1.7	68.8 (53.7–81.3)	97.7 (87.7–99.9)	29.6 (4.2–207.0)	0.3 (0.2–0.5)	97.1 (84.7–99.9)	73.7 (60.3–84.5)
Clinically suspected TB ($n = 15$)								
IS*6110*-dPCR	0.77 (0.60–0.95)	> 4.2	53.3 (26.6–78.7)	97.7 (87.7–99.9)	22.9 (3.1–168.5)	0.5 (0.3–0.8)	88.9 (51.8–99.7)	85.7 (72.8–94.1)
IS*1081*-dPCR	0.85 (0.72–0.98)	> 1.7	53.3 (26.6–78.7)	100.0 (91.8–100.0)	–	0.5 (0.3–0.8)	100.0 (63.1–100.0)	86.0 (73.3–94.2)
IS*6110* and IS*1081*-dPCR	0.73 (0.56–0.91)	> 4.2 and > 1.7	46.7 (21.3–73.4)	100.0 (91.8–100.0)	–	0.5 (0.3–0.9)	100.0 (59.0–100.0)	84.3 (71.4–93.0)
IS*6110* OR IS*1081*-dPCR	0.79 (0.63–0.95)	> 4.2 or > 1.7	60.0 (32.3–83.7)	97.7 (87.7–99.9)	25.8 (3.6–187.0)	0.4 (0.2–0.8)	90.0 (55.5–99.7)	87.5 (74.8–95.3)
Confirmed TB by molecular pathology ($n = 40$)								
IS*6110*-dPCR	0.90 (0.84–0.97)	> 4.2	72.5 (56.1–85.4)	97.7 (87.7–99.9)	31.2 (4.5–218.3)	0.3 (0.2–0.5)	96.7 (82.8–99.9)	79.2 (65.9–89.2)
IS*1081*-dPCR	0.89 (0.81–0.96)	> 1.7	67.5 (50.9–81.4)	100.0 (91.8–100.0)	–	0.3 (0.2–0.5)	100.0 (87.2–100.0)	76.8 (63.6–87.0)
IS*6110* and IS*1081*-dPCR	0.81 (0.71–0.89)	> 4.2 and > 1.7	62.5 (45.8–77.3)	100.0 (91.8–100.0)	–	0.4 (0.3–0.6)	100.0 (85.8–100.0)	74.1 (61.0–84.7)
IS*6110* OR IS*1081*-dPCR	0.88 (0.79–0.94)	> 4.2 or > 1.7	77.5 (61.5–89.2)	97.7 (87.7–99.9)	33.2 (4.8–232.9)	0.2 (0.1–0.4)	96.9 (83.8–99.9)	82.4 (69.1–91.6)

[a]IS*6110* and IS*1081*-dPCR is positive if both IS*6110* and IS*1081* > their cut-off values, and negative if either IS*6110* or IS*1081* ≤ their cut-off values. [b]IS*6110* OR IS*1081*-dPCR is positive if either IS*6110* or IS*1081* > their cut-off values, and negative if both IS*6110* and IS*1081* ≤ their cut-off values. [c]Specificity was calculated in the non-TB group (N = 43). AUC, area under curve; CI, confidence interval; LR+, positive likelihood ratio; LR-, negative likelihood ratio; PPV, positive predictive value; NPV, negative predictive value.

10.3389/fmicb.2024.1335526

TABLE 3 Sensitivity comparisons of BNRS-dPCR assay with conventional tests in diagnosis of TB.

Tests	Number of TB patients	Sensitivity % (n/N)			*P*-value [b]
BNRS IS*6110* OR IS*1081*-dPCR[a] compared with biopsy pathology					
BNRS IS*6110* OR IS*1081*-dPCR vs. *M.tb* molecular detection using FFPE biopsy tissue	56	69.6% (39/56)	vs.	71.4% (40/56)	1.000
BNRS IS*6110* OR IS*1081*-dPCR vs. AFB test using FFPE biopsy tissue	56	69.6% (39/56)	vs.	39.3% (22/56)	< 0.001
BNRS IS*6110* OR IS*1081*-dPCR compared with routine etiological tests					
BNRS IS*6110* OR IS*1081*-dPCR vs. sputum smear microscopy	17	58.8% (10/17)	vs.	5.9% (1/17)	0.004
BNRS IS*6110* OR IS*1081*-dPCR vs. sputum mycobacterial culture	17	52.9% (9/17)	vs.	17.6% (3/17)	0.109
BNRS IS*6110* OR IS*1081*-dPCR vs. sputum Xpert MTB/RIF	28	67.9% (19/28)	vs.	21.4% (6/28)	0.002
BNRS IS*6110* OR IS*1081*-dPCR vs. BALF smear microscopy	12	66.7% (8/12)	vs.	8.3% (1/12)	0.039
BNRS IS*6110* OR IS*1081*-dPCR vs. BALF culture	12	66.7% (8/12)	vs.	25.0% (3/12)	0.063
BNRS IS*6110* OR IS*1081*-dPCR vs. BALF Xpert MTB/RIF	18	72.2% (13/18)	vs.	22.2% (4/18)	0.035
BNRS IS*6110* OR IS*1081*-dPCR compared with immunological tests					
BNRS IS*6110* OR IS*1081*-dPCR vs. peripheral blood IGRA	48	66.7% (32/48)	vs.	81.3% (39/48)	0.143
BNRS IS*6110* OR IS*1081*-dPCR vs. TB antibody in peripheral blood	20	60.0% (12/20)	vs.	40.0% (8/20)	0.289

[a]The cut-off values of BNRS IS*6110* OR IS*1081*-dPCR assay were 4.2 and 1.7 copies/20μL reaction mixture, respectively. One of them was positive meant the dPCR result was positive. [b]McNemar test was used to determine the significance between BNRS IS*6110* OR IS*1081*-dPCR assay and other tests. FFPE, formalin-fixed paraffin-embedded; AFB, acid-fast bacilli; BALF, bronchoalveolar lavage fluid; IGRA, interferon-gamma release assays; n/N, the number of samples tested positive/the total number of samples.

between BNRS IS*6110* OR IS*1081*-dPCR and these tests. The results indicated that BNRS IS*6110* OR IS*1081*-dPCR exhibited a higher agreement with biopsy pathology, with a *Kappa* value of 0.270 and 0.308 for agreement with molecular detection of *M.tb* and AFB detection using FFPE biopsy tissue, respectively (P = 0.043 and 0.005, respectively) (Supplementary Table S1). This can be attributed to the fact that BNRS is most similar to biopsy samples in terms of location and type compared to sputum, blood and BALF samples.

Considering that approximately a quarter of the global population is estimated to be affected by latent tuberculosis infection (LTBI), the detection results of BNRS IS*6110* OR IS*1081*-dPCR in the LTBI population are also a significant concern. IGRA is one of the effective methods recommended by WHO guidelines for LTBI detection, but it cannot distinguish between LTBI and active TB. Our findings revealed that the positive rate of BNRS IS*6110* OR IS*1081*-dPCR assay was significantly higher in non-TB patients with positive IGRA results (37.9%, 11/29) compared to those with negative IGRA results (2.3%, 1/43) ($P < 0.001$). This result suggests that the small amount of *M.tb* nucleic acid in the lung tissue of LTBI cases can be detected by the ultra-sensitive digital PCR method. Additionally, we observed that the number of target copies detected in 63 TB patients was significantly higher than that in 29 non-TB patients with positive IGRA results: median (25% percentile, 75% percentile), IS*6110*, 7.8 (2.2, 58.0) vs. 3.0 (0.9, 8.1) copies/20 μL reaction mixture, P = 0.005; IS*1081*, 2.7 (1.0, 19.1) vs. 0.9 (0.4, 2.2) copies/20 μL reaction mixture, P = 0.001. This finding is consistent with previous research suggesting that there is a pathogenetic continuum from *M.tb* exposure to infection to TB disease, individuals in different states have different bacterial loads, the trend of infection outcome depends on changes in the host immunity, and TB transmission can occur during the subclinical period (Pai and Behr, 2016; Wang et al., 2023). Subsequent in-depth research with larger sample size is needed to ascertain whether the copy number of target genes detected by dPCR can differentiate between LTBI and TB, appropriate threshold, and specific discriminative performance. Hence, patients with TB or other diseases combined with TB or LTBI may yield positive results in BNRS IS*6110* OR IS*1081*-dPCR testing. Healthcare professionals should make comprehensive judgments by considering other test results such as histopathology to avoid overlooking other serious conditions like lung cancer.

The results of BNRS IS*6110* OR IS*1081*-dPCR in non-TB patients with a history of TB are also noteworthy. In this study, ten non-TB patients with a known TB history were excluded due to positive IGRA results (1 case had completed at least 1 year of anti-TB treatment, while the other 9 cases had completed anti-TB treatment for decades). After analyzing the BNRS IS*6110* OR IS*1081*-dPCR results of these patients, we found that the positive rate was 50% (5/10) with low target level in most cases. Another

TABLE 4 BNRS-dPCR combined with conventional biopsy pathology increased the detection rate of TB.

Tests	Specimens examined	Positive cases	Increased positive cases	Positive rate
BNRS IS*6110* OR IS*1081*-dPCR assay[a] in TB patients with negative biopsy results for *M.tb*				
BNRS IS*6110* OR IS*1081*-dPCR assay in TB patients with negative AFB test results using FFPE biopsy tissue	34	19	-	55.9%
BNRS IS*6110* OR IS*1081*-dPCR assay in TB patients with negative *M.tb* molecular detection results using FFPE biopsy tissue	16	8	-	50.0%
Combination of BNRS IS*6110* OR IS*1081*-dPCR assay with conventional biopsy pathology in TB patients				
AFB test using FFPE biopsy tissue	56	22	-	39.3%
AFB test using FFPE biopsy tissue + BNRS IS*6110* OR IS*1081*-dPCR assay	56	41	19	73.2%
M.tb molecular detection using FFPE biopsy tissue	56	40	-	71.4%
M.tb molecular detection using FFPE biopsy tissue + BNRS IS*6110* OR IS*1081*-dPCR assay	56	48	8	85.7%

[a]The cut-off values of BNRS IS*6110* OR IS*1081*-dPCR assay were 4.2 and 1.7 copies/20 μL reaction mixture, respectively. One of them was positive meant the dPCR result was positive. AFB, acid-fast bacilli; FFPE, formalin-fixed paraffin-embedded.

study also reported that a small percentage (4%, 3/82) of non-TB participants with a known TB history yielded Xpert MTB/RIF Ultra trace outcomes from sputum samples (Wang et al., 2022). Furthermore, it was reported that non-TB patients with a previous TB history exhibited a significantly higher positive rate of IGRA compared to those without (84.3% vs. 26.9%, $P < 0.001$) (Kim et al., 2011). It remains unclear whether these non-TB patients had newly acquired *M.tb* infection or if there were still replicating or dormant *M.tb* bacteria and its nucleic acid fragments in the lung tissue due to incomplete anti-TB treatment in the past.

In this study, although BNRS IS*6110* OR IS*1081*-dPCR showed comparable sensitivity to molecular methods in FFPE biopsy samples (69.6% vs. 71.4%, $P = 1.000$), BNRS-dPCR yielded positive results in some patients with negative biopsy pathological results but diagnosed as TB through other tests. Specifically, among TB cases with negative molecular detection of *M.tb* results and negative AFB test results using FFPE biopsy tissue, the positive proportion of BNRS-dPCR was 50.0% and 55.9% respectively, suggesting that combination of conventional biopsy pathology and BNRS IS*6110* OR IS*1081*-dPCR has the potential to increase the etiological diagnosis rate in TB patients. Indeed, in this study, the rate increased from 39.3% for biopsy AFB test alone to 73.2% when combined with BNRS-dPCR, and from 71.4% for biopsy *M.tb* molecular detection alone to 85.7% when combined with BNRS-dPCR, respectively. This ability can be partly attributed to the utilization of robust physical lysis methods for *M.tb* DNA extraction along with the application of ultra-sensitive digital PCR technology. But more importantly, as previously mentioned, the outer wall of the puncture needle had a larger surface area compared to the needle groove containing the biopsy tissue. This difference enabled the cellular residues adhered to the outer wall of the needle to offer supplementary diagnostic value.

In conclusion, our study preliminarily revealed that the CT-guided percutaneous BNRS IS*6110* OR IS*1081*-dPCR test is an effective auxiliary diagnostic approach for TB. The utilization of this method can convert previously discarded materials into valuable resources, augment the diagnostic yield of biopsy procedures, and improve the diagnosis of TB. This holds great significance for patients whose diagnosis is still ambiguous despite undergoing multiple examinations including biopsy. However, due to the limited sample size in this study, further research with larger sample size and encompassing different infection stages is needed to better elucidate its potential application value in diagnosis and pathogenesis of TB.

Data availability statement

The raw data supporting the conclusions of this article will be made available by the authors, without undue reservation.

Ethics statement

The studies involving humans were approved by Ethics Committee of Beijing Chest Hospital, Capital Medical University. The studies were conducted in accordance with the local legislation and institutional requirements. The participants provided their written informed consent to participate in this study.

Author contributions

ZL: Data curation, Formal analysis, Funding acquisition, Investigation, Methodology, Project administration, Writing—original draft, Conceptualization, Writing—review & editing. BW: Data curation, Investigation, Resources, Writing—original draft, Writing—review & editing, Methodology. BD: Investigation, Writing—review & editing. QS: Investigation, Writing—review & editing. DW: Resources, Writing—review & editing. RW: Investigation, Writing—review & editing. CL: Resources, Writing—review & editing. CZ: Funding acquisition, Investigation, Writing—review & editing. HJ: Investigation, Writing—review & editing. AX: Investigation, Writing—review & editing. ZZ:

Supervision, Writing—review & editing. LP: Conceptualization, Funding acquisition, Methodology, Supervision, Writing—review & editing. DH: Conceptualization, Resources, Supervision, Writing—review & editing, Methodology.

Funding

The author(s) declare financial support was received for the research, authorship, and/or publication of this article. This work was supported by National Natural Science Foundation of China (82070012 and 82172279), Beijing Municipal Natural Science Foundation (7212012), Tongzhou District Science and Technology Commission of Beijing Municipality (KJ2023CX046), Beijing Municipal Science and Technology Commission (Z201100005520067), Tongzhou Yunhe Plan Project (YH201908), and Beijing Hospitals Authority Innovation Studio of Young Staff Funding (202136).

Acknowledgments

We sincerely acknowledge the patients for their participation in this study.

Conflict of interest

The authors declare that the research was conducted in the absence of any commercial or financial relationships that could be construed as a potential conflict of interest.

Publisher's note

Supplementary material

The Supplementary Material for this article can be found online at: https://www.frontiersin.org/articles/10.3389/fmicb.2024.1335526/full#supplementary-material

References

Detjen, A. K., DiNardo, A. R., Leyden, J., Steingart, K. R., Menzies, D., Schiller, I., et al. (2015). Xpert MTB/RIF assay for the diagnosis of pulmonary tuberculosis in children: a systematic review and meta-analysis. *Lancet Respir. Med.* 3, 451–461. doi: 10.1016/S2213-2600(15)00095-8

Dorman, S. E., Schumacher, S. G., Alland, D., Nabeta, P., Armstrong, D. T., King, B., et al. (2018). Xpert MTB/RIF Ultra for detection of *Mycobacterium tuberculosis* and rifampicin resistance: a prospective multicentre diagnostic accuracy study. *Lancet Infect. Dis.* 18, 76–84. doi: 10.1016/S1473-3099(17)30691-6

Gong, X., He, Y., Zhou, K., Hua, Y., and Li, Y. (2023). Efficacy of Xpert in tuberculosis diagnosis based on various specimens: a systematic review and meta-analysis. *Front. Cell. Infect. Microbiol.* 13, 1149741. doi: 10.3389/fcimb.2023.1149741

Kim, H. J., Yoon, H. I., Park, K. U., Lee, C. T., and Lee, J. H. (2011). The impact of previous tuberculosis history on T-SPOT.TB(R) interferon-gamma release assay results. *Int. J. Tuberc. Lung. Dis.* 15, 510–516. doi: 10.5588/ijtld.10.0520

Kuypers, J., and Jerome, K. R. (2017). Applications of digital PCR for clinical microbiology. *J. Clin. Microbiol.* 55, 1621–1628. doi: 10.1128/JCM.00211-17

Lan, Z., Zhang, X., Ma, X., Hu, Y., Zhang, J., Yang, F., et al. (2021). Utility of liquid-based cytology on residual needle rinses collected from core needle biopsy for lung nodule diagnosis. *Cancer Med.* 10, 3919–3927. doi: 10.1002/cam4.3949

Lawn, S. D., Mwaba, P., Bates, M., Piatek, A., Alexander, H., Marais, B. J., et al. (2013). Advances in tuberculosis diagnostics: the Xpert MTB/RIF assay and future prospects for a point-of-care test. *Lancet Infect. Dis.* 13, 349–361. doi: 10.1016/S1473-3099(13)70008-2

Li, Z., Pan, L., Lyu, L., Li, J., Jia, H., Du, B., et al. (2020). Diagnostic accuracy of droplet digital PCR analysis of cerebrospinal fluid for tuberculous meningitis in adult patients. *Clin. Microbiol. Infect.* 26, 213–219. doi: 10.1016/j.cmi.2019.07.015

Li, Z., Sun, Q., Du, B., Jia, H., Dong, J., Lyu, L., et al. (2022). Use of pleural fluid digital PCR analysis to improve the diagnosis of pleural tuberculosis. *Microbiol. Spectr.* 10, e0163222. doi: 10.1128/spectrum.01632-22

National Health and Family Planning Commission of the People's Republic of China. (2018). Dignosis for pulmonary tuberculosis (WS288-2017). *Electron. J. Emerg. Infect. Dis.* 3, 59–61. doi: 10.3877/j.issn.2096-2738.2018.01.017

Nguyen, D. T., Teeter, L. D., Graves, J., and Graviss, E. A. (2018). Characteristics associated with negative interferon-gamma release assay results in culture-confirmed tuberculosis patients, Texas, USA, 2013-2015. *Emerg. Infect. Dis.* 24, 534–540. doi: 10.3201/eid2403.171633

Pai, M., and Behr, M. (2016). Latent *Mycobacterium tuberculosis* infection and interferon-gamma release assays. *Microbiol. Spectr.* 4, 2016. doi: 10.1128/microbiolspec.TBTB2-0023-2016

Redelman-Sidi, G., and Sepkowitz, K. A. (2013). IFN-gamma release assays in the diagnosis of latent tuberculosis infection among immunocompromised adults. *Am. J. Respir. Crit. Care. Med.* 188, 422–431. doi: 10.1164/rccm.201209-1621CI

Sabi, I., Rachow, A., Mapamba, D., Clowes, P., Ntinginya, N. E., Sasamalo, M., et al. (2018). Xpert MTB/RIF Ultra assay for the diagnosis of pulmonary tuberculosis in children: a multicentre comparative accuracy study. *J. Infect.* 77, 321–327. doi: 10.1016/j.jinf.2018.07.002

Sakairi, Y., Sato, K., Itoga, S., Saegusa, F., Matsushita, K., Nakajima, T., et al. (2014). Transbronchial biopsy needle rinse solution used for comprehensive biomarker testing in patients with lung cancer. *J. Thorac. Oncol.* 9, 26–32. doi: 10.1097/JTO.0000000000000024

Wang, G., Huang, M., Jing, H., Jia, J., Dong, L., Zhao, L., et al. (2022). The practical value of Xpert MTB/RIF Ultra for diagnosis of pulmonary tuberculosis in a high tuberculosis burden setting: a prospective multicenter diagnostic accuracy study. *Microbiol. Spectr.* 10, e0094922. doi: 10.1128/spectrum.00949-22

Wang, Z., Li, H., Song, S., Sun, H., Dai, X., Chen, M., et al. (2023). Transmission of tuberculosis in an incarcerated population during the subclinical period: a cross-sectional study in Qingdao, China. *Front. Public Health* 11, 1098519. doi: 10.3389/fpubh.2023.1098519

World Health Organization. (2022). *Global Tuberculosis Report 2022*. Geneva: World Health Organization.

Xu, J. C., Shi, X., Ma, X., Gu, W. F., Fang, Z. X., Zhang, H., et al. (2023). Diagnosis of extrapulmonary tuberculosis by ultrasound-guided biopsy: a retrospective comparison study. *Front. Cell. Infect. Microbiol.* 13, 1154939. doi: 10.3389/fcimb.2023.1154939

Zhao, J., Pu, D., Zhang, Y., Qu, J., Lu, B., Cao, B., et al. (2023). Comparison of performances of GeneXpert MTB/RIF, Bactec MGIT 960, and Bactec Myco/F Systems in detecting *Mycobacterium tuberculosis* in biopsy tissues: a retrospective study. *Microbiol. Spectr.* 11, e0141422. doi: 10.1128/spectrum.01414-22

frontiers | Frontiers in Microbiology

TYPE Original Research
PUBLISHED 08 February 2024
DOI 10.3389/fmicb.2024.1354190

OPEN ACCESS

EDITED BY
Robert Jansen,
Radboud University, Netherlands

REVIEWED BY
Dharmendra Kumar Soni,
Uniformed Services University of the Health Sciences, United States
Yadong Zhang,
Boston Children's Hospital and Harvard Medical School, United States

*CORRESPONDENCE
Liping Pan
✉ panliping2006@163.com
Zongde Zhang
✉ zzd417@ccmu.edu.cn

†These authors have contributed equally to this work

RECEIVED 12 December 2023
ACCEPTED 23 January 2024
PUBLISHED 08 February 2024

CITATION
Dong J, Song R, Shang X, Wang Y, Liu Q, Zhang Z, Jia H, Huang M, Zhu C, Sun Q, Du B, Xing A, Li Z, Zhang L, Pan L and Zhang Z (2024) Identification of important modules and biomarkers in tuberculosis based on WGCNA.
Front. Microbiol. 15:1354190.
doi: 10.3389/fmicb.2024.1354190

Identification of important modules and biomarkers in tuberculosis based on WGCNA

Jing Dong[1,2,3†], Ruixue Song[1,2,3†], Xuetian Shang[1,2,3], Yingchao Wang[1,2,3], Qiuyue Liu[3,4], Zhiguo Zhang[5], Hongyan Jia[1,2,3], Mailing Huang[3,6], Chuanzhi Zhu[1,2,3], Qi Sun[1,2,3], Boping Du[1,2,3], Aiying Xing[1,2,3], Zihui Li[1,2,3], Lanyue Zhang[1,2,3], Liping Pan[1,2,3]* and Zongde Zhang[1,2,3]*

[1]Beijing Chest Hospital, Capital Medical University, Beijing, China, [2]Beijing Key Laboratory for Drug Resistant Tuberculosis Research, Beijing, China, [3]Beijing Tuberculosis and Thoracic Tumor Research Institute, Beijing, China, [4]Department of Intensive Care Unit, Beijing Chest Hospital, Capital Medical University, Beijing, China, [5]Changping Tuberculosis Prevent and Control Institute of Beijing, Beijing, China, [6]Department of Tuberculosis, Beijing Chest Hospital, Capital Medical University, Beijing, China

Background: Tuberculosis (TB) is a significant public health concern, particularly in China. Long noncoding RNAs (lncRNAs) can provide abundant pathological information regarding etiology and could include candidate biomarkers for diagnosis of TB. However, data regarding lncRNA expression profiles and specific lncRNAs associated with TB are limited.

Methods: We performed ceRNA-microarray analysis to determine the expression profile of lncRNAs in peripheral blood mononuclear cells (PBMCs). Weighted gene co-expression network analysis (WGCNA) was then conducted to identify the critical module and genes associated with TB. Other bioinformatics analyses, including Kyoto Encyclopedia of Genes and Genomes (KEGG), Gene Ontology (GO), and co-expression networks, were conducted to explore the function of the critical module. Finally, real-time quantitative polymerase chain reaction (qPCR) was used to validate the candidate biomarkers, and receiver operating characteristic analysis was used to assess the diagnostic performance of the candidate biomarkers.

Results: Based on 8 TB patients and 9 healthy controls (HCs), a total of 1,372 differentially expressed lncRNAs were identified, including 738 upregulated lncRNAs and 634 downregulated lncRNAs. Among all lncRNAs and mRNAs in the microarray, the top 25% lncRNAs (3729) and top 25% mRNAs (2824), which exhibited higher median expression values, were incorporated into the WGCNA. The analysis generated 16 co-expression modules, among which the blue module was highly correlated with TB. GO and KEGG analyses showed that the blue module was significantly enriched in infection and immunity. Subsequently, considering module membership values (>0.85), gene significance values (>0.90) and fold-change value (>2 or < 0.5) as selection criteria, the top 10 upregulated lncRNAs and top 10 downregulated lncRNAs in the blue module were considered as potential biomarkers. The candidates were then validated in an independent validation sample set (31 TB patients and 32 HCs). The expression levels of 8 candidates differed significantly between TB patients and HCs. The lncRNAs ABHD17B (area under the curve [AUC] = 1.000) and ENST00000607464.1 (AUC = 1.000) were the best lncRNAs in distinguishing TB patients from HCs.

Conclusion: This study characterized the lncRNA profiles of TB patients and identified a significant module associated with TB as well as novel potential biomarkers for TB diagnosis.

KEYWORDS

tuberculosis, lncRNA, mRNA, WGCNA, diagnosis

1 Introduction

Tuberculosis (TB), which is caused by infection with *Mycobacterium tuberculosis* (*M.tb*), is an epidemic disease of global health concern. Approximately one-fourth of the global population is estimated to have been infected with *M.tb*, but only a small number of people develop active tuberculosis (ATB) each year (Bagcchi, 2023). Nevertheless, TB remains a leading cause of death worldwide. Although numerous mechanistic studies have examined *M.tb* infection and TB development in recent years, the role and mechanism of important molecules remain largely unexplored (Fathizadeh et al., 2020). Obtaining a better understanding of the underlying pathogenesis and regulatory network may facilitate the development of methods to prevent or control TB.

Recently, the development of high-throughput genome-wide gene analysis technologies, such as microarray, next-generation sequencing, and single-cell transcriptome and novel microarray-based integrated bioinformatics analyses, have helped promote the screening and identification of pivotal biomarkers associated with diseases and further elucidate the mechanisms underlying TB occurrence and development (Li et al., 2022; Salmen et al., 2022; Zhu et al., 2023). Until now, the Xpert MTB Host response assay [including Dual specificity phosphatase 3 (DUSP3), Guanylate-binding protein (GBP5), Krupple-like factor 2 (KLF2) genes] which was developed by Cepheid (Sunnyvale, CA, United States) has been recommended in TB screening by WHO (Sodersten et al., 2021; Wu et al., 2023). Other transcriptomic signatures, such as RISK6 Host response assay (QuantuMDx, United Kingdom), IRISA-TB (Antrum Biotech, South Africa), T cell activation marker (TAM-TB) assay (Ludwig-Maximilians-University, Germany), and so on, were also in development (Penn-Nicholson et al., 2020). Therefore, there is no doubt that transcriptomic signatures based on host immune response to *M.tb* or other mechanisms have the potential in diagnosis of TB, and WHO has also recommended to develop the host biomarker-based assay for TB diagnosis (Penn-Nicholson et al., 2020). In the human genome, most nucleic acids are noncoding RNAs (ncRNA), which are thought to play important roles in various biological processes. Furthermore, based on the developed technologies, it is possible to quantify the specific ncRNA molecules in cellular and subcellular compartments of diseased cells, as well as in extracellular compartments (such as exosomes and body fluids), which makes these molecules suitable for liquid biopsy utility (Nemeth et al., 2023). Approximately three-fourths of ncRNAs are long noncoding RNAs (lncRNAs), which have a length of over 200 nucleotides and tissue/cell-specific expression patterns. Previous research has suggested that lncRNAs are involved in regulating gene expression via interactions with common biological macromolecules, forming a complex network that regulates multiple normal biological and disease processes (Fathizadeh et al., 2020; Liang et al., 2022). A number of studies have examined the expression and function of lncRNAs in various diseases based on co-expression analyses (Liu et al., 2022; Wen et al., 2022). Although there is no commercial assay based on lncRNAs in TB diagnosis, many researches have confirmed that the abnormal expression of lncRNAs are associated with TB occurrence, development and prognosis, and have the potentials as diagnostic, prognostic biomarkers and therapeutic targets in TB (Chen et al., 2017; Zhang et al., 2022; Xu et al., 2023). However, the expression patterns and pathogenesis of host lncRNAs in TB patients have not yet been fully elucidated, and mechanistic details regarding the regulatory network involving lncRNAs in TB remain unclear (Chen et al., 2017; Agliano et al., 2019; Liang et al., 2022). Uncovering the expression profile and co-expression relationship between ncRNAs and mRNA in the host could facilitate the development of novel strategies for TB prevention and therapy (Xia et al., 2023).

In the present study, we performed a genome-wide ceRNA microarray analysis of peripheral blood mononuclear cells (PBMCs) from TB patients and health controls (HCs) to elucidate lncRNAs profile associated with TB. We also performed a weighted gene co-expression network analysis (WGCNA) to identify important expression modules associated with TB. The results of this study shed light on the gene expression profile in TB patients and provide new clues for exploring the regulatory mechanisms of lncRNAs in the pathogenesis of TB.

2 Materials and methods

2.1 Ethical approval

This study was performed in accordance with the guidelines of the Helsinki Declaration and was approved by the Ethics Committee of the Beijing Chest Hospital, Capital Medical University. Written informed consents were obtained from each participant before blood collection.

2.2 Participants information

TB patients in the discovery set were recruited from Beijing Chest Hospital between January 2019 and May 2019. HCs in the discovery set were enrolled from a TB screening campaign in Beijing Changping District between October 2019 and December 2019. TB patients in the validation set were recruited from Beijing Chest Hospital between December 2021 and August 2022, and HCs in the validation set were enrolled from a physical examination program conducted at Beijing Chest Hospital between October 2021 and December 2021. TB

patients were diagnosed based on positive *M.tb* culture, positive Xpert MTB/RIF, positive microscopy, or positive histology. All enrolled HCs were confirmed as not infected with *M.tb* based on normal computed tomography results and negative T-SPOT.TB results (Kruse et al., 2021). Individuals positive for human immunodeficiency virus (HIV), hepatitis B virus (HBV), hepatitis C virus (HCV), diabetes, severe autoimmune diseases, or those who took immunosuppressive or immunopotentiator agents, received anti-TB treatment, or were pregnant or lactating were excluded.

2.3 Blood sample collection

Peripheral blood (3 mL) was collected from each individual into heparin-containing vacutainer tubes. PBMCs were isolated by density gradient using Lympholyte Cell Separation Media (HY2015, Tianjin Haoyang Biological Manufacture Co., Ltd., China) within 4 h after blood collection. The isolated PBMCs were lysed with TRIzol reagent (Invitrogen, Carlsbad, CA, United States) and stored at −80°C to avoid RNA degradation. The samples were not thawed repeatedly.

2.4 RNA extraction

Total RNA was extracted from PBMCs using a miRNeasy Mini kit (217004, QIAGEN, Germany) according to the protocols recommended by the manufacturer. RNase-free DNase I (79254, QIAGEN) was added to remove genomic or cell-free DNA contamination. The integrity and quality of RNA from PBMCs were evaluated using an Agilent 2,100 Bioanalyzer (Agilent Technology, Palo Alto, CA, United States). RNA with a 2,100 RNA integrity number ≥ 7.0 and 28S/18S > 0.7 was used for the microarray study and qPCR validation.

2.5 Microarray study

Each slide was hybridized with 1.65 μg of Cy3-labeled cRNA using a Gene Expression Hybridization kit (5188-5242, Agilent Technologies, Santa Clara, CA, United States) and hybridization oven (G2545A, Agilent Technologies) according to the manufacturer's instructions. After 17 h of hybridization, slides were washed in staining dishes (121, Thermo Shandon, Waltham, MA, United States) using a Gene Expression Wash Buffer kit (5188-5327, Agilent Technologies) according to the manufacturer's instructions. The slides were then scanned using an Agilent Microarray Scanner (G2565CA, Agilent Technologies) with the following default settings: dye channel, Green; scan resolution, 3 μm; PMT, 100%; 20 bit. Data were extracted using Feature Extraction software 10.7 (Agilent Technologies), and raw data were normalized using the Quantile algorithm and limma packages in R.

2.6 Reverse transcription and qPCR

A total of 200 ng of purified RNA was reverse transcribed to cDNA using a ReverTra Ace qPCR RT kit (FSQ-101, TOYOBO Co., Ltd., Life Science Department, Osaka, Japan) according to the protocols recommended by the manufacturer. Two microliters of cDNA was mixed with 10 μL of PowerUp™ SYBR™ Green Master Mix (A25742, Thermo Fisher Scientific, Waltham, MA, United States) and 2 μL of primers mix. qPCR was performed on a QuantStudio 7 Flex Real-time PCR System (Thermo Fisher Scientific) as follows: 50°C for 2 min, 95°C for 10 min, followed by 40 cycles of 95°C for 15 s and 60°C for 1 min, following the melting curve stage. The expression threshold for each lncRNA detector was automatically determined.

We calculated $2^{(-\Delta CT)}$ and used this statistic to determine relative gene expression values. The relative amount of lncRNA in PBMCs was normalized against GAPDH. The primer sequences for qPCR used in this study are shown in Supplementary Table 1.

2.7 WGCNA

The WGCNA package (R 4.2.1) was used to construct a gene co-expression network and screen crucial genes significantly associated with TB. Among the expression profiles, the top 25% of genes with higher median expression values were used as the input (Chen et al., 2022). In the present study, we firstly used the function pickSoftThreshold and chose a soft-threshold R^2 value of 0.85. An adjacency matrix was performed into a topological overlap matrix (TOM) as well as the corresponding dissimilarity. Then, a hierarchical clustering tree diagram of the corresponding dissimilarity matrix was constructed to classify similar gene expression into different gene coexpression modules. Moreover, module-trait associations between modules and clinical feature information were calculated to selected the optimum module. Then, we estimated the gene significance (GS) value for each gene's traits and module membership (MM) in the hub module. Finally, genes in the module were screened as potential TB-related genes based on a GS value > 0.90 and MM value > 0.85 as thresholds (Ling et al., 2023).

2.8 Enrichment analysis

Gene ontology (GO) and Kyoto Encyclopedia of Genes and Genomes (KEGG) analyses were performed using the Database for Annotation Visualization and Integrated Discovery[1](Sherman et al., 2022). Figures and graphics to display the resulting data were generated using tools from the website[2] (Tang et al., 2023).

2.9 Statistical analysis

More details regarding statistical methods for transcriptome data processing and module establishment are covered in the above sections. Demographic information and qPCR data were calculated using SPSS software (v.4.0.1). Parametric data are expressed as the mean ± standard deviation, and differences were assessed using the Student's *t*-test. Non-parametric data are expressed as median (range), and differences were assessed using the Mann–Whitney *U*-test. Receiver operating characteristic (ROC) curves were constructed to determine the area

1 https://david.ncifcrf.gov/home.jsp/

2 www.bioinformatics.com.cn

10.3389/fmicb.2024.1354190

TABLE 1 Demographic characteristics of the study population.

Study complex	Variables	TB	HCs	*p*-value
Discovery set	n[a]	8	9	
	Age (mean ± SD[b])	59 ± 18	57 ± 12	0.790
	Male/female	6/2	4/5	0.335
Validation set	n	31	32	
	Age (mean ± SD)	57 ± 19	52 ± 17	0.300
	Male/female	26/5	16/16	0.007

[a]n, number of subjects. [b]SD, standard deviation.

under the curve (AUC) and evaluate the diagnostic value of biomarkers. Principal component analysis was performed in Python (v3.9.6). The regulation network was generated using Cytoscape (v3.10.1). Differences were considered statistically significant at $p < 0.05$.

3 Results

3.1 Characteristics of the study population

A total of 10 TB patients and 10 age- and gender-matched HCs who satisfied the inclusion and exclusion criteria were included in the discovery set for high-throughput ceRNA microarray analysis. Three of the samples (2 TB and 1 HC) were excluded from final analysis because of inferior raw microarray data quality. In addition, another 31 TB patients and 32 HCs were enrolled in the validation set for candidate biomarker validation and diagnostic performance analysis. Demographic information regarding the study population is summarized in Table 1. The work flow of this study is shown in Figure 1 (Created with BioRender.com).

3.2 Overview of differential lncRNA expression profiles

Raw microarray data from 17 samples, including samples from 8 TB patients and 9 HCs, were finally normalized. The cluster of 17 samples based on lncRNA expression levels is shown by principal component analysis in a two-dimensional coordinate system (Figure 2A). A total of 1,372 lncRNAs differentially expressed between the TB patients and HCs were identified (fold-change >2 or <0.5 and $p < 0.05$), including 738 upregulated lncRNAs and 634 downregulated lncRNAs in the TB group (Figure 2B). The top 20 differentially expressed lncRNAs, including 10 upregulated and 10 downregulated, are listed in Supplementary Table 2. Furthermore, the results showed that average expression levels of lncRNAs in human PBMCs were lower than those of mRNAs (Figure 2C), in agreement with previous research (Mo et al., 2019).

3.3 Identification of key modules by WGCNA and enrichment analysis

To further understand the gene expression patterns in TB patients, a gene co-expression network was built using WGCNA (Supplementary Figure S1A). The top 25% of genes with higher median expression values were incorporated into the WGCNA (including 3,729 lncRNAs and 2,824 mRNAs). A power of $\beta = 8$ ($R^2 = 0.85$) was selected as the soft-thresholding parameter for scale-free network construction (Supplementary Figure S1B). Next, an adjacency matrix and topological overlap matrix were constructed. All genes were divided into different modules, and each module was assigned a different color. Sixteen modules were identified based on average hierarchical clustering and dynamic tree clipping (Supplementary Figure S1C). The correlation between each module and TB was assessed based on module-trait relationship. The results of the module-trait relationship analyses were shown in Figure 3A and indicated that the blue module had the highest correlation with TB ($r = 0.95$, $p = 4 \times 10^{-9}$), which indicated the genes in the blue module were highly associated with TB. The blue module was therefore selected as the meaningful module for further analysis.

In the blue module, correlations between MM and GS (Cor = 0.95) were observed by scatter plot analysis and cluster analysis (Figures 3B,C). Finally, lncRNAs in the blue module were screened as potential TB-related genes based on the criteria MM > 0.85, GS > 0.90, and $p < 0.05$ as thresholds. All of the selected lncRNAs also showed significantly different expression levels ($p < 0.05$ and fold-change >2 or < 0.5) between the TB and HC groups in the microarray results. Accordingly, we screened the top 10 significantly upregulated and 10 significantly downregulated genes for further validation, as shown in Table 2 and Figure 3D.

GO and KEGG analyses were performed in order to predict the biological function of the critical module. The results of GO enrichment analysis are shown in Figure 3E. In the Biological Process category, most genes were enriched in regulation of apoptotic processes. In the Cellular Component category, most genes were enriched in the cytosol. In the Molecular Function category, most genes were enriched in protein binding. KEGG pathway analysis indicated that the genes in the blue module were enriched in many pathways, including *Salmonella* infection, lysosome, phagosome, acute myeloid leukemia, TB, and chemical carcinogenesis–reactive (Figure 3F). The result of GO and KEGG analyses showed that most genes in blue module enriched in immune-related biological process and pathway, such as apoptosis, autophagy and so on. The above results suggest that genes in blue module may play an important role in host immunity against tuberculosis infection.

3.4 Verification of lncRNAs by qPCR in the discovery and validation sets

Among the top 10 upregulated and top 10 downregulated lncRNAs in the blue module that were associated with TB, 12 lncRNAs were selected for further validation in the discovery set. The other 8 lncRNAs were not validated due to the highly conserved sequence relative to the encoding gene or a lack of specific primers for validation. Among the 12 differentially expressed genes, there were 3 upregulated lncRNAs (lncRNA GBA, lncRNA FBXL5 and lncRNA KRT8) and 9 downregulated lncRNAs (lncRNA periodic tryptophan protein 1 [PWP1], ENST00000620744.1, NR_003000, ENST00000417346.1, lncRNA BCL2L10, ENST00000516057.1, lncRNA ABHD17B,

10.3389/fmicb.2024.1354190

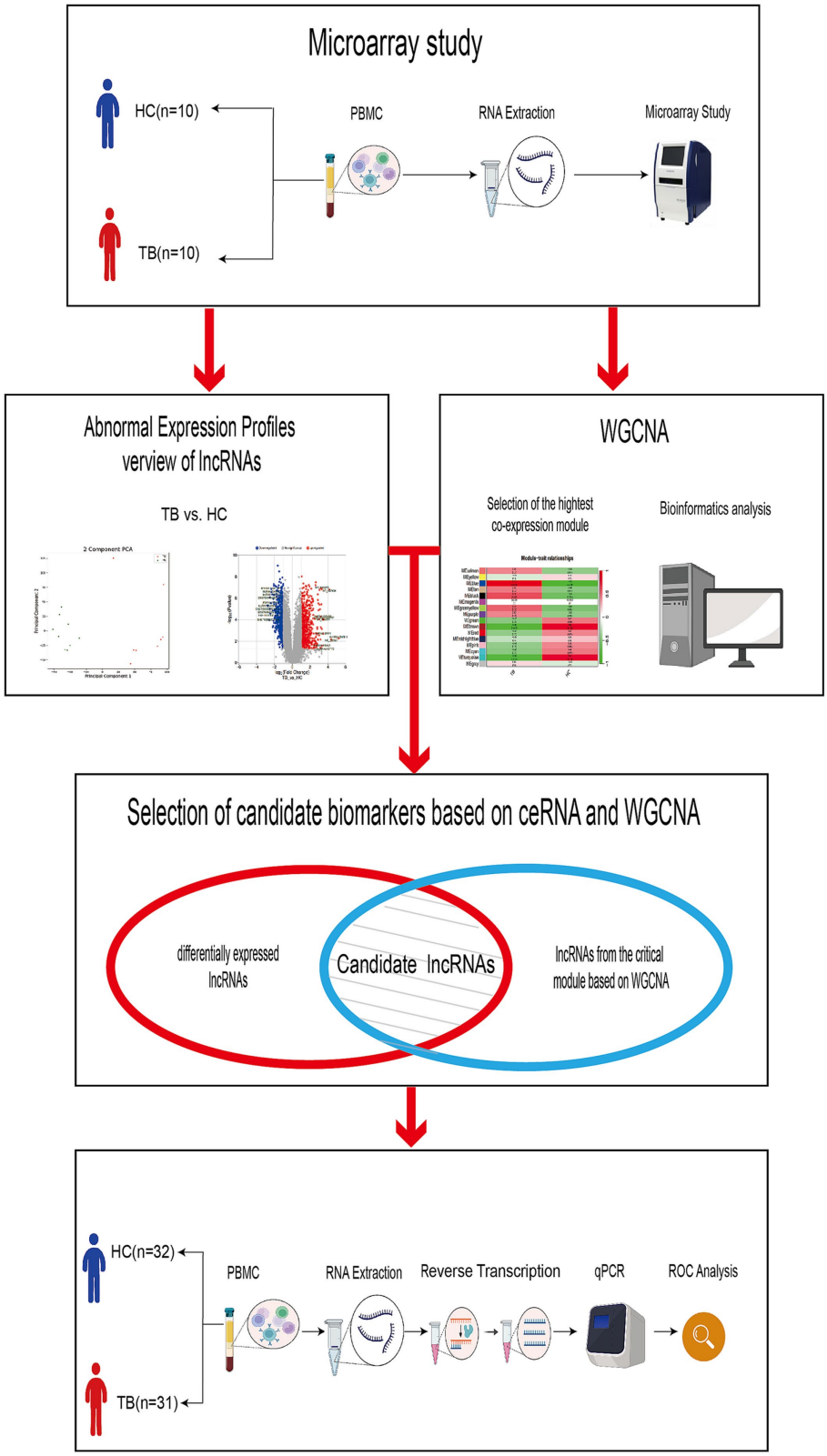

FIGURE 1
Work flow of the study. The discovery set included 8 TB patients and 9 HCs. The validation set included 31 TB patients and 32 HCs.

ENST00000607464.1 and ENST00000583184.1) in the TB group in the microarray analysis. qPCR analysis showed that the expression levels of 9 lncRNAs differed significantly and were consistent with the microarray results, whereas the expression patterns of lncRNA FBXL5 and lncRNA KRT8 were not consistent with the microarray results; there was no significant difference in

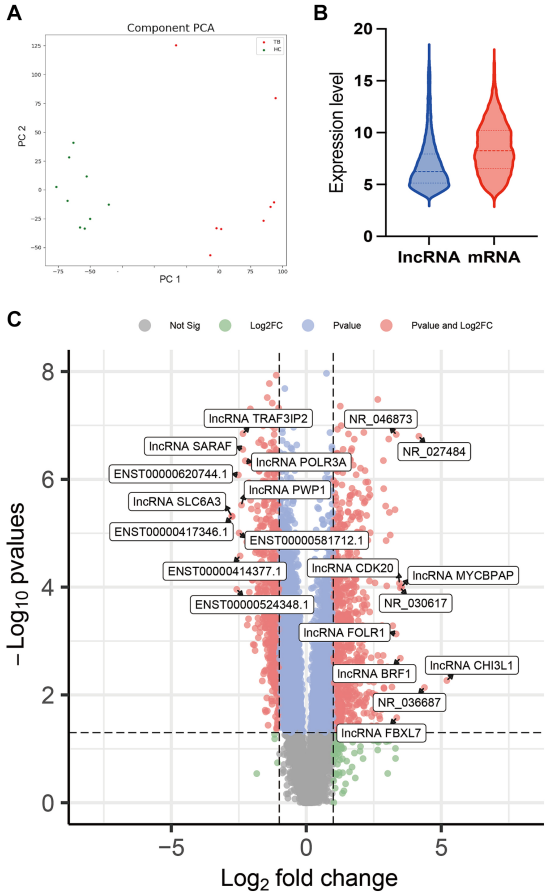

FIGURE 2
Comparison of lncRNA expression data between TB patients and HCs. **(A)** Principal component analysis of lncRNA expression profile in TB patients and HCs. **(B)** Volcano plot of the differentially expressed lncRNAs. **(C)** Expression patterns of lncRNAs and mRNAs in PBMCs.

the expression levels of lncRNA GBA between the TB and HC groups (Figure 4; Table 3).

The 9 lncRNAs were further validated by qPCR in the validation sample set (31 TB patients and 32 HCs). As shown in Figure 5 and Table 4, the expression levels of lncRNA PWP1, ENST00000620744.1, ENST00000417346.1, lncRNA BCL2L10, ENST00000516057.1, lncRNA ABHD17B, ENST00000607464.1 and ENST00000583184.1 were significantly lower in the TB group than that in HC group. Furthermore, the expression patterns of 8 lncRNAs were consistent with the microarray results, whereas the expression pattern of lncRNA NR_003000 was not consistent with the microarray results.

3.5 Diagnostic performance of the differentially expressed lncRNAs

To evaluate the diagnostic accuracy of the 8 lncRNAs, an ROC curve was generated to determine the AUC, sensitivity, and specificity of each lncRNA in discriminating TB patients from HCs in the discovery and validation sets. As shown in Table 4 and Figure 5J, the ROC curve for the validation set showed that lncRNA ABHD17B (AUC = 1.000) and ENST00000607464.1 (AUC = 1.000) were the best lncRNAs in distinguishing the TB and HC groups, followed by ENST00000620744.1 (AUC = 0.998) and the lncRNA BCL2L10 (AUC = 0.967). As each lncRNA showed excellent diagnostic performance in differentiating TB patients and HCs, we did not analyze whether combining these differentially expressed lncRNAs would provide better diagnostic accuracy.

4 Discussion

TB remains a serious public health problem, particularly in China, due to the large number of TB patients, which generates a great burden and risk of transmission. Furthermore, common methods to diagnose TB depend on clinical, immunological, microscopic, radiographic, and bacterial culture (Acharya et al., 2020). However, due to equipment, technology, and sensitivity limitations, the common methods can not satisfy the requirements for TB diagnosis in clinical practice. Even the utility of the molecular diagnostic techniques, including GeneXpert/MTB, also have limitations in clinical application, since the utility rate of these molecular diagnostic tests was limited (47%) in people newly diagnosed with TB (World Health Organization, 2023). Therefore, novel and rapid diagnosis methods, including the host biomarkers-based assay, which present higher analytical sensitivity and reduce assay times, remain to be explored. One type of target molecule is lncRNAs, which act through a plethora of different mechanisms and interactors and function as important regulators in many aspects of biology. lncRNAs play important roles in a variety of biological processes, including development and immune responses (Jonas and Izaurralde, 2015; Marchese et al., 2017; McDonel and Guttman, 2019). A broader and more in-depth understanding of the regulatory mechanisms of host lncRNAs could contribute to the identification of novel targets for TB diagnosis or development of host-directed anti-TB therapies.

Characterizing the lncRNA-mRNA interaction patterns and connection between gene modules and TB could provide criteria for identifying functional lncRNA-mRNA relationships. However, the lncRNA-mRNA correlation patterns are far from clear. With the development of bioinformatics techniques, all types of expression profile data, such as transcriptome and single-cell sequencing data, can be re-analyzed from different dimensions. The identification of differentially expressed genes is the most classical and fundamental analyses and commonly used in screening novel biomarkers via a series of statistical algorithms to identify differentially expressed genes between subgroups. WGCNA is a topological network analysis approach that can establish the linkage between gene modules and clinical traits; genes classified into the same module are all linked to the selected clinical traits, which can then be used for subsequent analysis and experiments. Because it can be linked with clinical information, immunological state, biological function, and other specific characteristics, WGCNA can be used to efficiently screen biomarkers. As such, WGCNA has been used in numerous studies to identify biomarkers associated with other diseases. For example, Wen et al. used WGCNA to preliminarily screen protein biomarkers, and the results were then combined with enzyme-linked immunosorbent assay results to verify CCL19, C1Qb, CCL5, and HLA-DMB as

10.3389/fmicb.2024.1354190

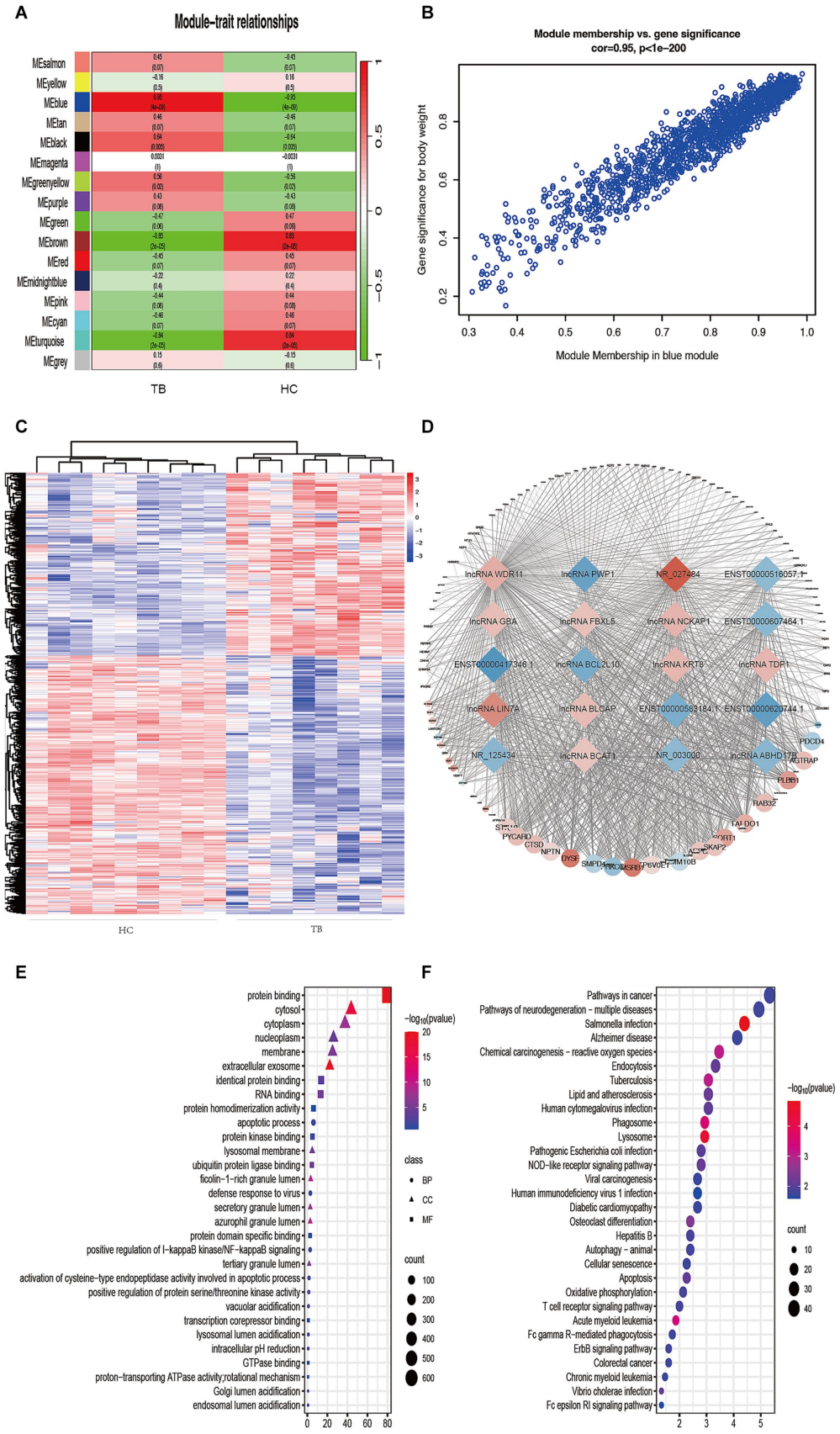

FIGURE 3
Identification of TB-related modules and key genes. **(A)** Analysis of correlations between the modules and TB; *p*-values are shown. **(B)** Scatter plot analysis of the blue module. Key genes were screened out in the upper-right area where GS > 0.90 and MM > 0.85. **(C)** Cluster analysis of the

(Continued)

FIGURE 3 (Continued)
differentially expressed lncRNAs in the blue module. The samples were successfully clustered into 2 groups based on the lncRNA profile, and each group matched exactly to the clinical groupings of the TB patients and HCs. **(D)** Co-expression networks of selected genes in the blue module. Diamonds indicate lncRNAs. Circles indicate mRNAs. Red indicates upregulation. Blue indicates downregulation. **(E)** GO enrichment analysis. BP, biological process; MF, molecular function; CC, cellular component. **(F)** KEGG enrichment analysis. Colors indicate the *p*-value for each term.

potentially effective biomarkers for TB diagnosis (Wen et al., 2022). A study on pediatric sepsis verified that 4 lncRNAs (GSEC, NONHSAT160878.1, XR_926068.1, and RARA-AS1) identified by WGCNA were linked to prognosis based on function (Zhang et al., 2021). A large number of studies based on WGCNA have suggested that the unique algorithm tends to cause the expression network to be distributed, which is of paramount importance in the screening of biomarkers.

In the present study, we analyzed the expression profiles of lncRNAs in PBMCs from TB patients and HCs using a ceRNA microarray. A total of 1,372 differentially expressed genes were identified in TB patients, suggesting that the gene expression regulation network of lncRNAs is altered in individuals with TB. A subsequent WGCNA further identified the critical module and specific biomarkers. In addition, KEGG analysis showed that the blue module was significantly enriched in infection and immunity-related processes, including autophagy and apoptosis. Some lncRNAs in the blue module in our study, have been previously confirmed to participate in apoptosis by experiments, including the promotion of apoptosis by lncRNA PAXIP1 (Ma and Zheng, 2021) and lncRNA SLC9A3 (Li et al., 2021), while the inhibition of apoptosis by lncRNA EZR-AS1 (Yu et al., 2023). Meanwhile, recent studies have also shown that lncRNA EGOT (Liu et al., 2020) can inhibit autophagy, either by ceRNA interactive patterns or by posttranscriptional regulation of the ATG7/16 L1 (Wang I. K. et al., 2020). Autophagy and apoptosis are common kinds of programmed cell death to regulate inflammation and injury which played significant roles in anti-TB immune response (Liu et al., 2018). Increasing evidence suggests that not only mRNA, but also ncRNAs, participate in autophagy and apoptosis in TB occurrence and development (Wang Y. et al., 2020). For instance, it was proved that the lncRNA MIAT could regulate autophagy and apoptosis in macrophages infected by BCG through the miR-665/ULK1 signaling axis (Jiang et al., 2021). Furthermore, PCED1B-AS1, as an endogenous sponge, was involved in TNF-α-induced apoptosis and autophagy by targeting the miR-155/FOXO3 (Rheb) axis (Li et al., 2019). Therefore, these results indicated it was the genes in the blue module that associated with host anti-TB immune response, which were promising potential biomarkers and targets for TB diagnosis and treatment. In addition, the result of the Molecular Function category in GO analyses showed genes in blue module were most enriched in protein binding. As we known, the important function of the lncRNA was binding with RNA-binding proteins to regulate gene expression. For example, lncRNA EST12 suppresses antimycobacterial innate immunity through interaction with FUBP3 in *M.tb* infection (Yao et al., 2022). Therefore, these results also confirmed the reliability of our analysis.

Ultimately, 8 of the lncRNAs were selected to validate by qPCR, which exhibited superior diagnostic performance in the validation sample set, especially 2 of the 8 lncRNAs showed an AUC value of 1 in discriminating TB patients from HCs. Nevertheless, we also screened the differentially expressed lncRNAs using differential gene analysis based on fold-change, and also detected another group of top 10 up-regulated lncRNAs and top 10 down-regulated lncRNAs. Two of them (lncRNA MYCBPAP and lncRNA CHI3L1) were validated by qPCR and the diagnostic performance of these two lncRNAs were decreased (AUC = 0.915 and AUC = 0.656), respectively, indicating less ability to discriminate TB patients from HCs. These results suggest that WGCNA is a more beneficial tool for biomarker screening, than the traditional differential gene analysis.

The present study confirmed that lncRNAs aberrantly expressed in PBMCs of TB patients are potentially useful biomarkers for diagnosis of TB and also appear to be associated with regulating the host immune response to TB infection. Some research has identified critical lncRNA and further focused on the role of lncRNAs in the immune regulation of *M.tb* infection. For example, lncRNA EST12, which is found mainly in the cytoplasm, interacted with the transcription factor far upstream element-binding protein 3 (FUEBP3) to suppresses the NLRP3 inflammasome assembly and gasdermin D–mediated pyroptosis–IL-1β immune pathway (Yao et al., 2022). Furthermore, in $CD8^+$ T cells, CD244 signaling drives lncRNA-CD244 expression which was selected based on microarray and lncRNA-CD244 inhibits IFN-γ/TNF-α expression by mediates H3K27 trimethylation at infg/tnfa loci (Wang et al., 2015). Therefore, further in-depth analyses of the functions and regulatory mechanisms of the crucial lncRNAs in the blue module that were screened in this study may provide clues to elucidate the pathogenesis of TB occurrence and to develop new TB treatment strategy.

Eight differentially expressed lncRNAs identified in our study have not been reported elsewhere to date in TB field, although there was a research on lncRNA WDR11 divergent transcript (lncRNA WDR11-AS1) suggested that the lncRNA WDR11-AS1 had an effect on inflammation (Huang et al., 2023). In contrast to miRNAs and mRNA, there are no standard rules for naming lncRNAs, and the most commonly used naming methods are primarily based on the function or origin of the encoding gene. For example, lncRNA BC050410, which is derived by CD244 signaling in $CD8^+$ T cells, is located nearby the 5′ UTR of Glutathione S-transferase T 1 (GSTT1), so it is named as lncRNA AS-GSTT1 due to its genomic context, and also can be termed as lncRNA-CD244 that is associated with its function (Wang et al., 2015). Although the varied methods of naming brought inconvenience for research on lncRNA, there was no doubt that lncRNAs played an important role in TB related immune response and researches on lncRNAs needs to be further refined and enriched (Yan et al., 2018).

There are some limitations to our study. First, the sample size in the discovery set for the microarray analysis was moderate. Although we enrolled an independent sample set to validate the differentially expressed lncRNAs, we cannot rule out the potential for bias resulting from sample heterogeneity. Second, this microarray analysis was performed in 2019. Although we ultimately identified 8 candidate

TABLE 2 The top 20 differentially expressed lncRNAs identified in blue module.

Genes	*p*-values	FC[a](TB[b]/HC[c])	Chromosome	Start	End	Relation	Associated_gene	Associated_gene_description
ENST00000417346.1	4.88E-06	0.149	chr20	57,384,160	57,393,062	antisense	RAE1	Ribonucleic acid export 1 [Source:HGNC Symbol;Acc:HGNC:9828]
ENST00000620744.1	8.32E-07	0.175	chr18	32,031,035	32,031,359	sense_intronic	RNF125	ring finger protein 125, E3 ubiquitin protein ligase [Source:HGNC Symbol;Acc:HGNC:21150]
lncRNA PWP1	3.00E-06	0.189	chr12	107,333,942	107,335,261	sense_intronic_ncRNA	BTBD11	BTB (POZ) domain containing 11 [Source:HGNC Symbol;Acc:HGNC:23844]
lncRNA BCL2L10	1.15E-06	0.230	chr15	52,123,558	52,128,273	sense_intronic_ncRNA	GNB5	Guanine nucleotide binding protein (G protein), beta 5 [Source:HGNC Symbol;Acc:HGNC:4401]
ENST00000583184.1	6.96E-08	0.236	chr18	32,018,829	32,111,779	processed_transcript	RNF125	Ring finger protein 125, E3 ubiquitin protein ligase [Source:HGNC Symbol;Acc:HGNC:21150]
NR_125434	9.83E-06	0.281	NT_187607.1	560,536	575,265	bidirectional	-	-
lncRNA ABHD17B	3.09E-06	0.286	chr9	71,750,000	71,768,513	sense_intronic_ncRNA	TMEM2	Transmembrane protein 2 [Source:HGNC Symbol;Acc:HGNC:11869]
ENST00000607464.1	4.14E-07	0.293	chr3	16,314,439	16,314,987	antisense	OXNAD1	Oxidoreductase NAD-binding domain containing 1 [Source:HGNC Symbol;Acc:HGNC:25128]
NR_003000	7.07E-07	0.298	chr17	7,906,122	7,906,260	intronic_sense	CHD3	Chromodomain helicase DNA binding protein 3 [Source:HGNC Symbol;Acc:HGNC:1918]
ENST00000516057.1	7.05E-07	0.299	chr1	15,542,165	15,542,304	scaRNA	DNAJC16	DnaJ heat shock protein family (Hsp40) member C16 [Source:HGNC Symbol;Acc:HGNC:29157]
lncRNA BCAT1	7.51E-07	2.547	chr12	24,967,126	24,967,504	lincRNA	-	-
lncRNA FBXL5	5.37E-07	2.660	chr4	15,492,728	15,492,972	antisense_lncRNA	CC2D2A	Coiled-coil and C2 domain containing 2A [Source:HGNC Symbol;Acc:HGNC:29253]
lncRNA GBA	6.78E-06	2.865	chr1	155,231,271	155,233,637	lincRNA	GBA	Glucosidase, beta, acid [Source:HGNC Symbol;Acc:HGNC:4177]
lncRNA BLCAP	1.18E-05	2.931	chr20	37,602,851	37,603,185	lincRNA	-	-
lncRNA KRT8	2.69E-07	3.220	chr12	52,949,215	52,949,954	sense_intronic_ncRNA	KRT18	Keratin 18, type I [Source:HGNC Symbol;Acc:HGNC:6430]
lncRNA TDP1	4.93E-06	3.260	chr14	90,107,674	90,107,995	sense_intronic_ncRNA	KCNK13	potassium channel, two pore domain subfamily K, member 13 [Source:HGNC Symbol;Acc:HGNC:6275]
lncRNA NCKAP1	1.80E-07	3.427	chr2	184,596,216	184,599,048	antisense_lncRNA	ZNF804A	Zinc finger protein 804A [Source:HGNC Symbol;Acc:HGNC:21711]
lncRNA WDR11	1.83E-06	3.803	chr10	120,843,216	120,844,603	lincRNA	WDR11	WD repeat domain 11 [Source:HGNC Symbol;Acc:HGNC:13831]
lncRNA LIN7A	1.49E-06	7.294	chr12	80,792,519	80,795,906	sense_intronic_ncRNA	LIN7A	Lin-7 homolog A (*C. elegans*) [Source:HGNC Symbol;Acc:HGNC:17787]
NR_027484	1.59E-07	18.012	chr1	143,874,742	143,883,733	exonic_sense	HIST2H2BB	Histone cluster 2, H2bb (pseudogene) [Source:HGNC Symbol;Acc:HGNC:20654]

[a]FC, Fold change; [b]TB, Tuberculosis; [c]HC, Health control.

10.3389/fmicb.2024.1354190

10.3389/fmicb.2024.1354190

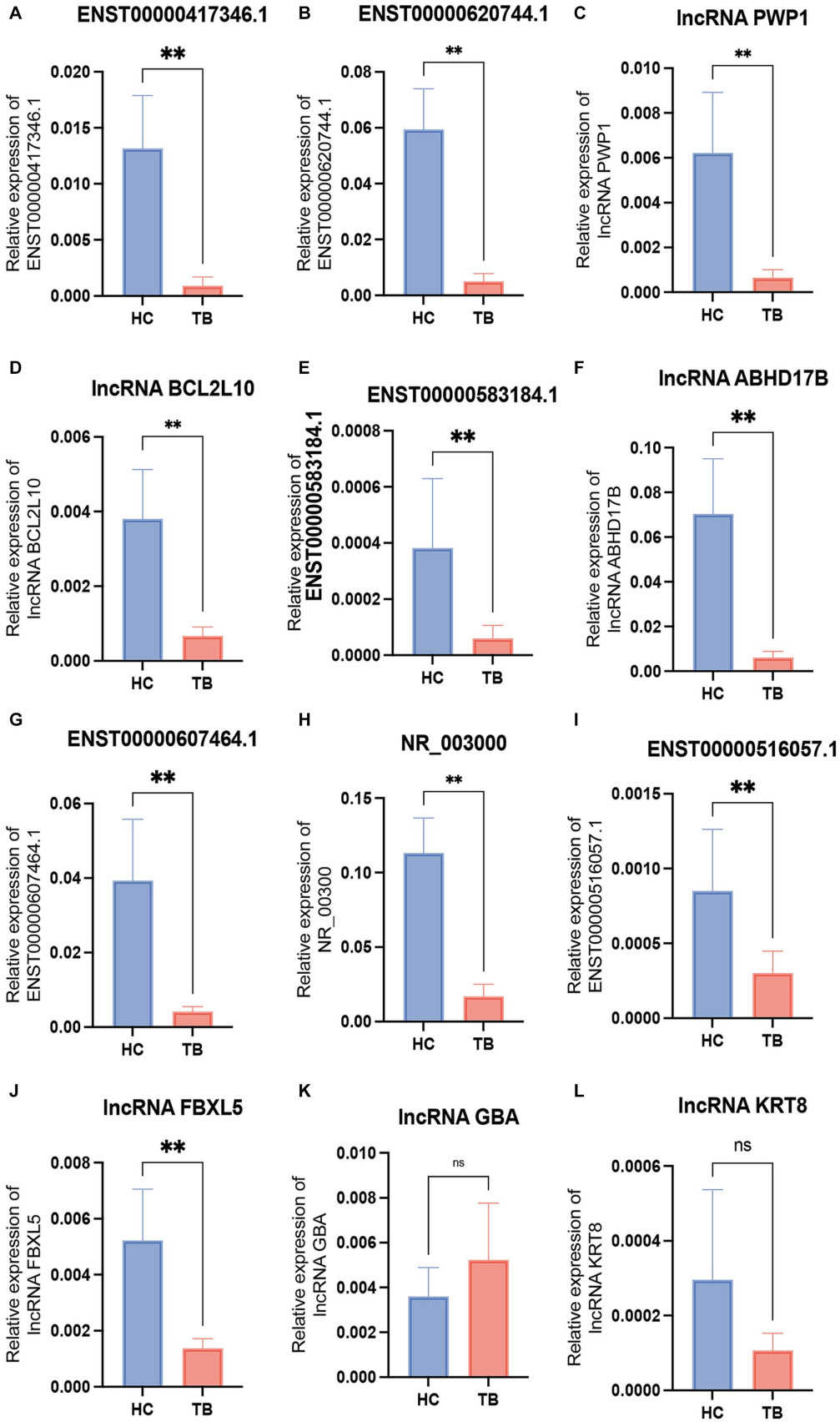

FIGURE 4
Validation of the differentially expressed lncRNAs by qPCR in the discovery set. The 12 differential lncRNAs were validated by qPCR in the discovery set. Ten of these lncRNAs showed the same expression pattern as in the microarray analysis **(A–L)**. NS, not significant; $^{**}p < 0.01$. Data presented as mean ± standard deviation.

TABLE 3 Differentially expressed lncRNAs identified by qPCR.

Gene	Discovery sample set		Validation sample set	
lncRNAs	*P*-value	FC[a](TB[b]/HC[c])	*P*-value	FC(TB/HC)
lncRNA ABHD17B	0.000	0.086	<0.0001	0.092
ENST00000516057.1	0.030	0.354	<0.0001	0.289
ENST00000583184.1	0.030	0.156	<0.0001	0.386
ENST00000620744.1	0.004	0.085	<0.0001	0.071
lncRNA KRT8	0.116	0.361	-	-
NR_003000	0.000	0.150	0.037	1.864
lncRNA PWP1	0.002	0.104	<0.0001	0.162
ENST00000607464.1	0.000	0.246	<0.0001	0.060
LncRNA GBA	0.159	1.420	-	-
LncRNA BCL2L10	0.001	0.463	<0.0001	0.533
ENST00000417346.1	0.001	0.181	<0.0001	0.166
LncRNA FBXL5	0.033	0.442	-	-

[a]FC, Fold change; [b]TB, Tuberculosis; [c]HC, Health control.

TABLE 4 The AUC, sensitivity and specificity of the 8 differentially expressed lncRNAs in validation sample set.

Genes	Validation sample set			
	Cut-off	Sensitivity[a] (95% CI[b])	Specificity	AUC(95% CI)
lncRNA ABHD17B	0.0307	1.000 (0.943–1.000)	1.000 (0.9431.000)	1.000 (1.000–1.000)
ENST00000516057.1	0.0004	0.969 (0.892–0.991)	0.871 (0.769–0.934)	0.968 (0.932–1.000)
ENST00000583184.1	0.0002	0.844 (0.732–0.912)	0.742 (0.627–0.837)	0.842 (0.740–0.944)
ENST00000620744.1	0.0144	1.000 (0.943–1.000)	0.968 (0.892–0.991)	0.998 (0.993–1.000)
lncRNA PWP1	0.0008	1.000 (0.943–1.000)	0.903 (0.807–0.956)	0.948 (0.878–1.000)
ENST00000607464.1	0.0138	1.000 (0.943–1.000)	1.000 (0.943–1.000)	1.000 (1.000–1.000)
LncRNA BCL2L10	0.0034	1.000 (0.943–1.000)	0.968 (0.892–0.991)	0.968 (0.906–1.000)
ENST00000417346.1	0.0050	0.938 (0.848–0.975)	0.935 (0.848–0.975)	0.961 (0.899–1.000)

[a]AUC, Area under curve; [b]CI, Confidence intervals.

biomarkers, the molecular characteristics of the lncRNAs need to be verified by in-depth experiments, and as the database iterates, the types and quantities of lncRNAs may update, which could result in an alteration of the TB-specific lncRNA profile, more or less. However, the major types of RNAs identified in our study are very similar to those reported in previous studies, which confirms the accuracy of our microarray results (Mo et al., 2019).

In conclusion, our study characterized the lncRNA profiles in PBMCs of TB patients, resulting in the identification of a critical module associated with TB. Furthermore, a total of 8 lncRNAs differentially expressed between the TB and HC groups were identified and were shown as promising biomarkers for discriminating TB from HCs.

Data availability statement

The datasets presented in this study can be found in online repositories. The names of the repository/repositories and accession number (s) can be found at: https://www.ncbi.nlm.nih.gov/, GSE249824.

Ethics statement

The studies involving humans were approved by Ethics Committee of the Beijing Chest Hospital, Capital Medical University. The studies were conducted in accordance with the local legislation and institutional requirements. The participants provided their written informed consent to participate in this study.

Author contributions

JD: Data curation, Writing – original draft. RS: Validation, Writing – original draft. XS: Validation, Writing – original draft. YW: Validation, Writing – original draft. QL: Resources, Writing – original draft. ZhZ: Resources, Writing – original draft. HJ: Resources, Writing – original draft. MH: Resources, Writing – original draft. CZ: Supervision, Writing – original draft. QS: Resources, Writing – original draft. BD: Resources, Writing – original draft. AX: Resources, Writing – original draft. ZL: Supervision, Writing – original draft. LZ: Supervision, Writing – original draft. LP: Project administration, Supervision, Writing – review & editing. ZoZ: Project administration, Supervision, Writing – review & editing.

10.3389/fmicb.2024.1354190

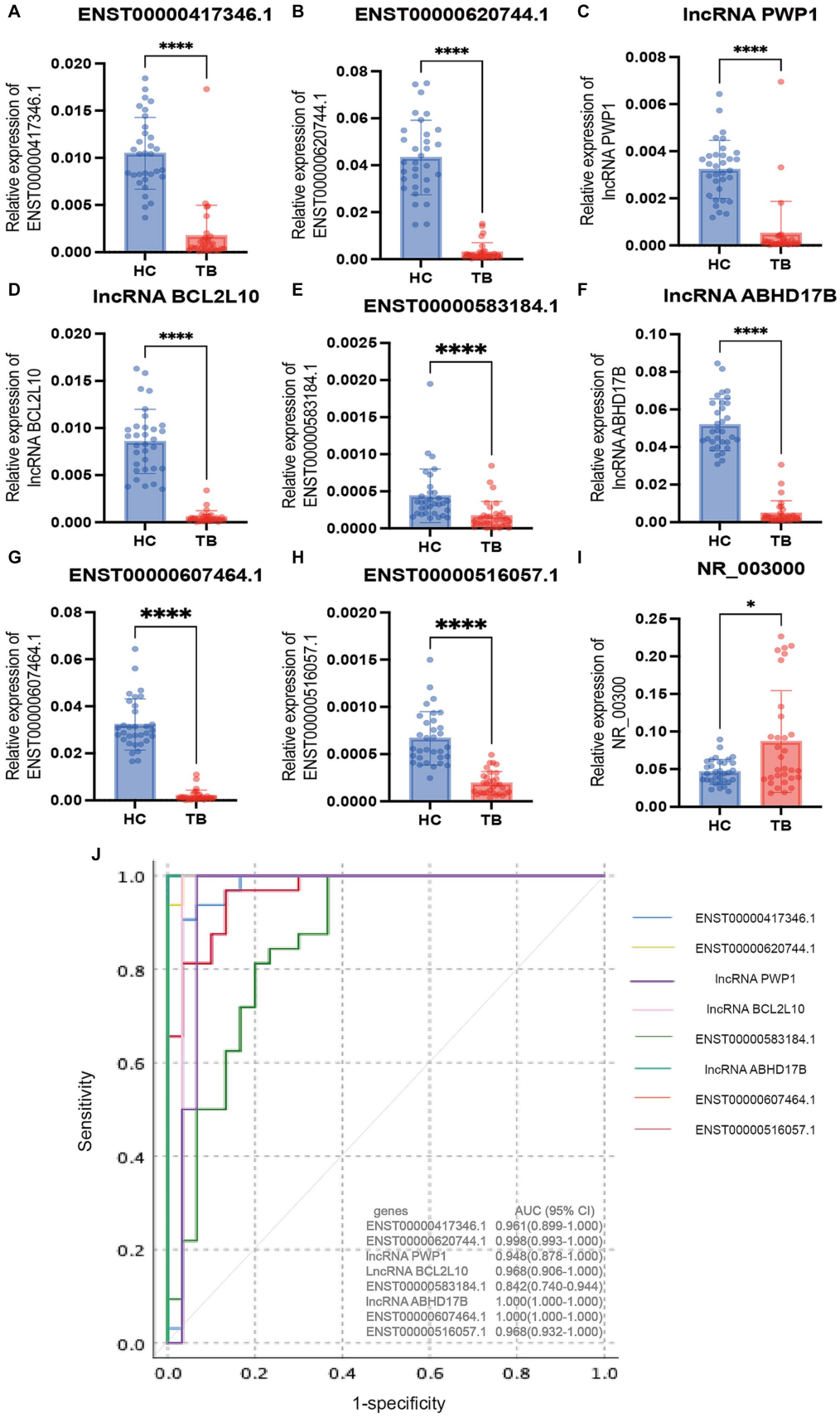

FIGURE 5
Validation of the differentially expressed lncRNAs by qPCR in the validation set. The 9 differential lncRNAs were validated by qPCR in the validation set **(A–I)**. Eight of these lncRNAs showed the same expression pattern as in the microarray analysis. The expression levels of lncRNA PWP1,

(Continued)

FIGURE 5 (Continued)
ENST00000620744.1, ENST00000417346.1, lncRNA BCL2L10, ENST00000516057.1, lncRNA ABHD17B, ENST00000607464.1 and ENST00000583184.1 in the TB group were significantly lower than in the HC group, in which the expression patterns were consistent with the microarray results. The expression pattern of lncRNA NR_003000 was not consistent with the microarray results. The AUC values of the 8 lncRNAs are shown in **(J)**. *$p < 0.05$; ****$p < 0.0001$. Data presented as mean ± standard deviation.

Funding

The author(s) declare financial support was received for the research, authorship, and/or publication of this article. This work was supported by grants from the National Natural Science Foundation (82172279 and 82100011), the Beijing Natural Science Foundation (L234055), Tongzhou Science and Technology Project (KJ2022CX042), and Tongzhou Yunhe Project (YH201807 and YH202001).

Conflict of interest

The authors declare that the research was conducted in the absence of any commercial or financial relationships that could be construed as a potential conflict of interest.

Publisher's note

Supplementary material

The Supplementary material for this article can be found online at: https://www.frontiersin.org/articles/10.3389/fmicb.2024.1354190/full#supplementary-material

References

Acharya, B., Acharya, A., Gautam, S., Ghimire, S. P., Mishra, G., Parajuli, N., et al. (2020). Advances in diagnosis of tuberculosis: an update into molecular diagnosis of *Mycobacterium tuberculosis*. *Mol. Biol. Rep.* 47, 4065–4075. doi: 10.1007/s11033-020-05413-7

Agliano, F., Rathinam, V. A., Medvedev, A. E., Vanaja, S. K., and Vella, A. T. (2019). Long noncoding Rnas in host-pathogen interactions. *Trends Immunol.* 40, 492–510. doi: 10.1016/j.it.2019.04.001

Bagcchi, S. (2023). Who's global tuberculosis report 2022. *Lancet Microbe* 4:e20. doi: 10.1016/S2666-5247(22)00359-7

Chen, Y., Liao, R., Yao, Y., Wang, Q., and Fu, L. (2022). Machine learning to identify immune-related biomarkers of rheumatoid arthritis based on Wgcna network. *Clin. Rheumatol.* 41, 1057–1068. doi: 10.1007/s10067-021-05960-9

Chen, Z. L., Wei, L. L., Shi, L. Y., Li, M., Jiang, T. T., Chen, J., et al. (2017). Screening and identification of lncrnas as potential biomarkers for pulmonary tuberculosis. *Sci. Rep.* 7:16751. doi: 10.1038/s41598-017-17146-y

Fathizadeh, H., Hayat, S., Dao, S., Ganbarov, K., Tanomand, A., Asgharzadeh, M., et al. (2020). Long non-coding Rna molecules in tuberculosis. *Int. J. Biol. Macromol.* 156, 340–346. doi: 10.1016/j.ijbiomac.2020.04.030

Huang, H., Yan, J., Lan, X., Guo, Y., Sun, M., Zhao, Y., et al. (2023). Lncrna Wdr 11-As1 promotes extracellular matrix synthesis in osteoarthritis by directly interacting with Rna-binding protein Pabpc 1 to stabilize Sox9 expression. *Int. J. Mol. Sci.* 24:817. doi: 10.3390/ijms24010817

Jiang, F., Lou, J., Zheng, X. M., and Yang, X. Y. (2021). Lncrna Miat regulates autophagy and apoptosis of macrophage infected by *Mycobacterium tuberculosis* through the miR-665/Ulk1 signaling axis. *Mol. Immunol.* 139, 42–49. doi: 10.1016/j.molimm.2021.07.023

Jonas, S., and Izaurralde, E. (2015). Towards a molecular understanding of microrna-mediated gene silencing. *Nat. Rev. Genet.* 16, 421–433. doi: 10.1038/nrg3965

Kruse, M., Dark, C., Aspden, M., Cochrane, D., Competiello, R., Peltz, M., et al. (2021). Performance of the T-Spot(®).Covid test for detecting Sars-CoV-2-responsive T cells. *Int. J. Infect. Dis.* 113, 155–161. doi: 10.1016/j.ijid.2021.09.073

Li, M., Cui, J., Niu, W., Huang, J., Feng, T., Sun, B., et al. (2019). Long non-coding Pced1B-As1 regulates macrophage apoptosis and autophagy by sponging miR-155 in active tuberculosis. *Biochem. Biophys. Res. Commun.* 509, 803–809. doi: 10.1016/j.bbrc.2019.01.005

Li, J., Li, D., Zhang, X., Li, C., and Zhu, F. (2021). Long noncoding Rna Slc9A3-As1 increases E2F6 expression by sponging microrna-486-5p and thus facilitates the oncogenesis of nasopharyngeal carcinoma. *Oncol. Rep.* 46:165. doi: 10.3892/or.2021.8116

Li, B., Zhao, R., Qiu, W., Pan, Z., Zhao, S., Qi, Y., et al. (2022). The N (6)-methyladenosine-mediated lncrna Wee2-As1 promotes glioblastoma progression by stabilizing Rpn2. *Theranostics* 12, 6363–6379. doi: 10.7150/thno.74600

Liang, S., Ma, J., Gong, H., Shao, J., Li, J., Zhan, Y., et al. (2022). Immune regulation and emerging roles of noncoding Rnas in *Mycobacterium tuberculosis* infection. *Front. Immunol.* 13:987018. doi: 10.3389/fimmu.2022.987018

Ling, X., Zhang, L., Fang, C., Liang, H., Zhu, J., and Ma, J. (2023). Development of a cuproptosis-related signature for prognosis prediction in lung adenocarcinoma based on Wgcna. *Transl Lung Cancer Res* 12, 754–769. doi: 10.21037/tlcr-23-157

Liu, F., Chen, J., Wang, P., Li, H., Zhou, Y., Liu, H., et al. (2018). Microrna-27a controls the intracellular survival of *Mycobacterium tuberculosis* by regulating calcium-associated autophagy. *Nat. Commun.* 9:4295. doi: 10.1038/s41467-018-06836-4

Liu, S. L., Sun, X. S., Chen, Q. Y., Liu, Z. X., Bian, L. J., Yuan, L., et al. (2022). Development and validation of a transcriptomics-based gene signature to predict distant metastasis and guide induction chemotherapy in locoregionally advanced nasopharyngeal carcinoma. *Eur. J. Cancer* 163, 26–34. doi: 10.1016/j.ejca.2021.12.017

Liu, Y., Zhang, B., Cao, W. B., Wang, H. Y., Niu, L., and Zhang, G. Z. (2020). Study on clinical significance of Lncrna Egot expression in Colon Cancer and its effect on autophagy of Colon Cancer cells. *Cancer Manag Res* 12, 13501–13512. doi: 10.2147/CMAR.S285254

Ma, Y., and Zheng, W. (2021). H3K27ac-induced lncrna Paxip1-As1 promotes cell proliferation, migration, Emt and apoptosis in ovarian cancer by targeting miR-6744-5p/Pcbp2 axis. *J. Ovarian Res.* 14:76. doi: 10.1186/s13048-021-00822-z

Marchese, F. P., Raimondi, I., and Huarte, M. (2017). The multidimensional mechanisms of long noncoding Rna function. *Genome Biol.* 18:206. doi: 10.1186/s13059-017-1348-2

Mcdonel, P., and Guttman, M. (2019). Approaches for understanding the mechanisms of long noncoding Rna regulation of gene expression. *Cold Spring Harb. Perspect. Biol.* 11:2151. doi: 10.1101/cshperspect.a032151

Mo, X. B., Wu, L. F., Lu, X., Zhu, X. W., Xia, W., Wang, L., et al. (2019). Detection of lncrna-mrna interaction modules by integrating eqtl with weighted gene co-expression network analysis. *Funct. Integr. Genomics* 19, 217–225. doi: 10.1007/s10142-018-0638-4

Nemeth, K., Bayraktar, R., Ferracin, M., and Calin, G. A. (2023). Non-coding Rnas in disease: from mechanisms to therapeutics. *Nat. Rev. Genet.* doi: 10.1038/s41576-023-00662-1 [Online ahead of print].

Penn-Nicholson, A., Mbandi, S. K., Thompson, E., Mendelsohn, S. C., Suliman, S., Chegou, N. N., et al. (2020). Risk6, a 6-gene transcriptomic signature of Tb disease risk, diagnosis and treatment response. *Sci. Rep.* 10:8629. doi: 10.1038/s41598-020-65043-8

Salmen, F., De Jonghe, J., Kaminski, T. S., Alemany, A., Parada, G. E., Verity-Legg, J., et al. (2022). High-throughput total Rna sequencing in single cells using vasa-seq. *Nat. Biotechnol.* 40, 1780–1793. doi: 10.1038/s41587-022-01361-8

Sherman, B. T., Hao, M., Qiu, J., Jiao, X., Baseler, M. W., Lane, H. C., et al. (2022). David: a web server for functional enrichment analysis and functional annotation of gene lists (2021 update). *Nucleic Acids Res.* 50, W216–W221. doi: 10.1093/nar/gkac194

Sodersten, E., Ongarello, S., Mantsoki, A., Wyss, R., Persing, D. H., Banderby, S., et al. (2021). Diagnostic accuracy study of a novel blood-based assay for identification of tuberculosis in people living with Hiv. *J. Clin. Microbiol.* 59:20. doi: 10.1128/JCM.01643-20

Tang, D., Chen, M., Huang, X., Zhang, G., Zeng, L., Zhang, G., et al. (2023). Srplot: a free online platform for data visualization and graphing. *PloS One* 18:e0294236. doi: 10.1371/journal.pone.0294236

Wang, I. K., Palanisamy, K., Sun, K. T., Yu, S. H., Yu, T. M., Li, C. H., et al. (2020). The functional interplay of lncrna Egot and HuR regulates hypoxia-induced autophagy in renal tubular cells. *J. Cell. Biochem.* 121, 4522–4534. doi: 10.1002/jcb.29669

Wang, Z., Xu, H., Wei, Z., Jia, Y., Wu, Y., Qi, X., et al. (2020). The role of non-coding Rna on macrophage modification in tuberculosis infection. *Microb. Pathog.* 149:104592. doi: 10.1016/j.micpath.2020.104592

Wang, Y., Zhong, H., Xie, X., Chen, C. Y., Huang, D., Shen, L., et al. (2015). Long noncoding Rna derived from Cd244 signaling epigenetically controls Cd8+ T-cell immune responses in tuberculosis infection. *Proc. Natl. Acad. Sci. U. S. A.* 112, E3883–E3892. doi: 10.1073/pnas.1501662112

Wen, Z., Wu, L., Wang, L., Ou, Q., Ma, H., Wu, Q., et al. (2022). Comprehensive genetic analysis of tuberculosis and identification of candidate biomarkers. *Front. Genet.* 13:832739. doi: 10.3389/fgene.2022.832739

World Health Organization. (2023). World health organization: global tuberculosis report 2022.

Wu, X., Tan, G., Ma, J., Yang, J., Guo, Y., Lu, H., et al. (2023). Assessment of the Cepheid 3-gene host response Fingerstick blood test (Mtb-Hr) on rapid diagnosis of tuberculosis. *Emerg Microbes Infect* 12:2261561. doi: 10.1080/22221751.2023.2261561

Xia, J., Liu, Y., Ma, Y., Yang, F., Ruan, Y., Xu, J. F., et al. (2023). Advances of long non-coding Rnas as potential biomarkers for tuberculosis: new Hope for diagnosis? *Pharmaceutics* 15:2096. doi: 10.3390/pharmaceutics15082096

Xu, X., Liang, Y., Gareev, I., Liang, Y., Liu, R., Wang, N., et al. (2023). Lncrna as potential biomarker and therapeutic target in glioma. *Mol. Biol. Rep.* 50, 841–851. doi: 10.1007/s11033-022-08056-y

Yan, H., Xu, R., Zhang, X., Wang, Q., Pang, J., Zhang, X., et al. (2018). Identifying differentially expressed long non-coding Rnas in Pbmcs in response to the infection of multidrug-resistant tuberculosis. *Infect drug resist* 11, 945–959. doi: 10.2147/IDR.S154255

Yao, Q., Xie, Y., Xu, D., Qu, Z., Wu, J., Zhou, Y., et al. (2022). Lnc-Est12, which is negatively regulated by mycobacterial Est12, suppresses antimycobacterial innate immunity through its interaction with Fubp3. *Cell. Mol. Immunol.* 19, 883–897. doi: 10.1038/s41423-022-00878-x

Yu, X., Wu, L., Lu, Z., Zhang, J., and Zhou, Y. (2023). Silencing lncrna Ezr-As1 induces apoptosis and attenuates the malignant properties of lung adenocarcinoma cells. *Acta Biochim. Pol.* 70, 713–719. doi: 10.18388/abp.2020_6754

Zhang, X., Chen, C., and Xu, Y. (2022). Long non-coding Rnas in tuberculosis: from immunity to biomarkers. *Front. Microbiol.* 13:883513. doi: 10.3389/fmicb.2022.883513

Zhang, X., Cui, Y., Ding, X., Liu, S., Han, B., Duan, X., et al. (2021). Analysis of mrna-lncrna and mrna-lncrna-pathway co-expression networks based on Wgcna in developing pediatric sepsis. *Bioengineered* 12, 1457–1470. doi: 10.1080/21655979.2021.1908029

Zhu, P., Pei, Y., Yu, J., Ding, W., Yang, Y., Liu, F., et al. (2023). High-throughput sequencing approach for the identification of lncrna biomarkers in hepatocellular carcinoma and revealing the effect of Zfas1/miR-150-5p on hepatocellular carcinoma progression. *PeerJ* 11:e14891. doi: 10.7717/peerj.14891

Glossary

ATB	Active tuberculosis
AUC	Area under curve
DUSP3	Dual specificity phosphatase 3
GSTT1	Glutathione S-transferase T 1
GO	Gene Ontology
GS	Gene significance
GBP5	Guanylate-binding protein
HBV	Hepatitis B virus
HC	Health control
HCV	Hepatitis C virus
HIV	Human immunodeficiency virus
KEGG	Kyoto Encyclopedia of Genes and Genomes
KLF2	Krupple-like factor 2
lncRNAs	Long noncoding RNAs
lncRNA WDR11-AS1	lncRNA WDR11 divergent transcript
M.tb	*Mycobacterium tuberculosis*
MM	Module membership
ncRNA	Noncoding RNA
PBMC	Peripheral blood mononuclear cell
qPCR	Real-time quantitative polymerase chain reaction
ROC	Receiver operating characteristic
RT	Reverse transcription
TB	Tuberculosis
WGCNA	Weighted gene co-expression network analysis

frontiers | Frontiers in Microbiology

TYPE Original Research
PUBLISHED 20 February 2024
DOI 10.3389/fmicb.2024.1367092

OPEN ACCESS

EDITED BY
Robert Jansen,
Radboud University, Netherlands

REVIEWED BY
Johid Malik,
University of Nebraska Medical Center, United States
Jason L. Cantera,
Global Health Labs, United States

*CORRESPONDENCE
Guanghong Bai
baiguanghong1966@163.com

RECEIVED 08 January 2024
ACCEPTED 09 February 2024
PUBLISHED 20 February 2024

CITATION
Gao M, Wu Q, Wang X, Sun X, Li M and Bai G (2024) Advancements in LAM-based diagnostic kit for tuberculosis detection: enhancing TB diagnosis in HIV-negative individuals.
Front. Microbiol. 15:1367092.
doi: 10.3389/fmicb.2024.1367092

Advancements in LAM-based diagnostic kit for tuberculosis detection: enhancing TB diagnosis in HIV-negative individuals

Man Gao[1], Qianhong Wu[2], Xinhong Wang[2], Xiuli Sun[3], Meng Li[1] and Guanghong Bai[1]*

[1]Department of Clinical Laboratory, Shaanxi Provincial Tuberculosis Prevention and Control Hospital, Xi'an, China, [2]Department of Tuberculosis, Shaanxi Provincial Tuberculosis Prevention and Control Hospital, Xi'an, China, [3]Department of Surgery, Shaanxi Provincial Tuberculosis Prevention and Control Hospital, Xi'an, China

Objective: The purpose of this study was to investigate the diagnostic value of urine lipoarabinomannan (LAM) detection based on chemiluminescence assay for pulmonary tuberculosis (PTB) and extrapulmonary tuberculosis (EPTB) in HIV-negative individuals.

Methods: A total of 215 patients and 37 healthy individuals were included according to inclusion and exclusion criteria, including 173 cases of PTB and 42 cases of EPTB. Sputum smears, sputum culture, TB-RNA, GeneXpert, and urine LAM results were obtained from all patients before treatment. Using the composite reference standard as the reference, the diagnostic performance of these methods for PTB and EPTB was evaluated, and the diagnostic performance and cost-effectiveness of different combinations were analyzed.

Results: In PTB, LAM exhibited the highest sensitivity (55.49%), followed by GeneXpert (44.51%). In EPTB, LAM also had the highest sensitivity (40.48%), followed by GeneXpert (33.33%). When combined with one method, LAM combined with GeneXpert showed the highest sensitivity for both PTB (68.79%) and EPTB (61.9%). When combined with two methods, culture, GeneXpert, and LAM showed the highest sensitivity for both PTB (73.99%) and EPTB (69.05%). In terms of cost-effectiveness analysis, the price of LAM was significantly lower than that of GeneXpert ($129.82 vs. $275.79 in PTB and 275.79 vs. 502.33 in EPTB). Among all combinations, the combination of LAM and sputum smear had the lowest cost, with prices of $124.94 for PTB and $263.72 for EPTB.

Conclusion: Urine LAM detection based on chemiluminescence assay can be used as an adjunct diagnostic tool for PTB and EPTB in HIV-negative individuals. This facilitates expanding the current application of urine LAM from solely HIV-positive populations to the general population. LAM detection can overcome the limitations of obtaining clinical samples, and its ease of sample acquisition will be beneficial for its broader application in a larger scope. For economically better-off areas, we recommend using a combination of LAM + GeneXpert+culture for higher sensitivity; for economically disadvantaged areas, LAM + smear microscopy combination can provide a quick and accurate diagnosis of tuberculosis at a lower cost.

KEYWORDS

pulmonary tuberculosis, extrapulmonary tuberculosis, lipoarabinomannan, chemiluminescence, diagnostic value

1 Introduction

Tuberculosis is a disease that plagues all of humanity. According to the Global Tuberculosis Report 2023, there were a total of 10.6 million tuberculosis infections worldwide, an incidence rate of 133 per 100,000 population, and 1.3 million deaths. Tuberculosis is the second largest single infectious cause of death globally, second only to COVID-19 (World Health Organization, 2023).

Traditional diagnostic methods for tuberculosis are time-consuming (sputum culture) or insensitive (sputum smear) (Nicol et al., 2021). Molecular diagnostics, like GeneXpert and TB-RNA, have improved sensitivity, but they have high laboratory requirements and cost, limiting their use in low-income countries (Pang et al., 2014; Zou et al., 2023). These methods primarily rely on the detection of *Mycobacterium tuberculosis* (MTB) in sputum or tissue fluid, which poses significant limitations for patients who do not produce sufficient sputum or have minimal sputum, particularly in the case of pediatric patients (Grant et al., 2012) or severe cases. Additionally, invasive procedures for obtaining tissue fluid samples can cause discomfort to patients. There is a clinical need for a rapid, non-invasive, easily sampled, and highly sensitive and specific diagnostic product for tuberculosis.

Lipoarabinomannan (LAM) is a major component of the cell wall of MTB, accounting for approximately 15% of the bacterial mass (Correia-Neves et al., 2019). LAM is heat and protease stable, and possesses unique structural epitopes specific to MTB (Sigal et al., 2018). LAM can modulate host immunity and plays an important role in the pathogenesis of tuberculosis (Briken et al., 2004). Following MTB degradation, the remaining LAM in the blood is filtered through the glomerular basement membrane into the urine (Bulterys et al., 2019). LAM testing is promising for tuberculosis diagnosis, especially in HIV-positive and disseminated tuberculosis patients (Lawn, 2012). It is a non-invasive test that does not require sputum, and the samples are easy to obtain (Gupta-Wright et al., 2016).

Currently, the Alere Determine TB LAM test is the only commercially available LAM test. It is only recommended by the World Health Organization for the diagnosis of active tuberculosis in HIV-positive individuals (World Health Organization, 2019). However, the sensitivity of AlereLAM varies across different patient groups. Specifically, it is only 16% in patients with a CD4+ T cell count greater than 200 cells/μl, but increases to 45% in those with CD4 counts less than 200 cells/μl (Bjerrum et al., 2020). Within the HIV-positive population, the sensitivity rate of AlereLAM is 42% (Bjerrum et al., 2020), whereas in the HIV-negative population, it is only 18% (Minion et al., 2011).

The HIV attacks the human immune system, ultimately leading to immune deficiency. As a result, MTB can replicate extensively within the body, leading to an increased circulation of LAM. In addition to promoting the replication of MTB, immune suppression also reduces the formation of antigen–antibody complexes, resulting in more free LAM present in the circulation (Lawn, 2012). In late-stage HIV patients, podocyte function is impaired, which leads to an increase in filtered LAM (Minion et al., 2011). Therefore, in patients with co-infection of tuberculosis and HIV, the concentration of LAM in the urine is much higher. In HIV-negative patients, most individuals have normal immune function, which inhibits the replication of MTB and promotes the formation of antigen–antibody complexes. This results in lower concentrations of LAM in the urine. AlereLAM uses immunochromatographic assay based on colloidal gold, with a detection limit of 500 pg./mL (García et al., 2019). This may partially explain why sensitivity of AlereLAM is low, especially in HIV-negative population. FujiLAM uses high-affinity monoclonal antibodies and silver-based amplification, which lowered the detection limit of LAM to 30 pg./mL (Broger et al., 2019). The sensitivity of FujiLAM in the HIV-positive population has reached 70.7% (Broger et al., 2020). However its stability is not satisfactory (Huerga et al., 2023), the utilization of this test kit has not been widespread.

The majority of tuberculosis-infected cases are HIV-negative, resulting in a greater demand for a more stable and sensitive LAM test kit. Chemiluminescence does not require an external light source for excitation, which can reduce background interference and enhance the sensitivity of diagnostics (Roda and Guardigli, 2012). Due to the high technical barriers, there have been limited developments and market promotions of LAM test kits based on the chemiluminescent platform. The reagent kit used in this study is the only commercially available LAM test kit developed on a chemiluminescent platform worldwide (Peng et al., 2023), significantly enhances the sensitivity and stability of LAM detection through urine concentration and chemiluminescent detection method. The limit of detection has been improved to reach 1 pg./mL (according to the user manual provided by the manufacturer).

The purpose of this study is to compare the accuracy of the chemiluminescent-based LAM with other methods for diagnosing tuberculosis, conduct an economic cost-effectiveness analysis of LAM in diagnosing tuberculosis.

2 Methods

2.1 Study design and population

This is a retrospectively diagnostic study. 256 patients who were firstly treated during hospitalization in Shaanxi Provincial Tuberculosis Control Hospital from June 2022 to August 2022 were selected for the study. Eligibility criteria were as follows: (1) Patients suffering from pulmonary tuberculosis (PTB) or extra-pulmonary tuberculosis (EPTB) must meet "Diagnosis for pulmonary tuberculosis (WS 288–2017)" (People's Republic of China state health and Family Planning Commission, 2018) and WHO tuberculosis guideline

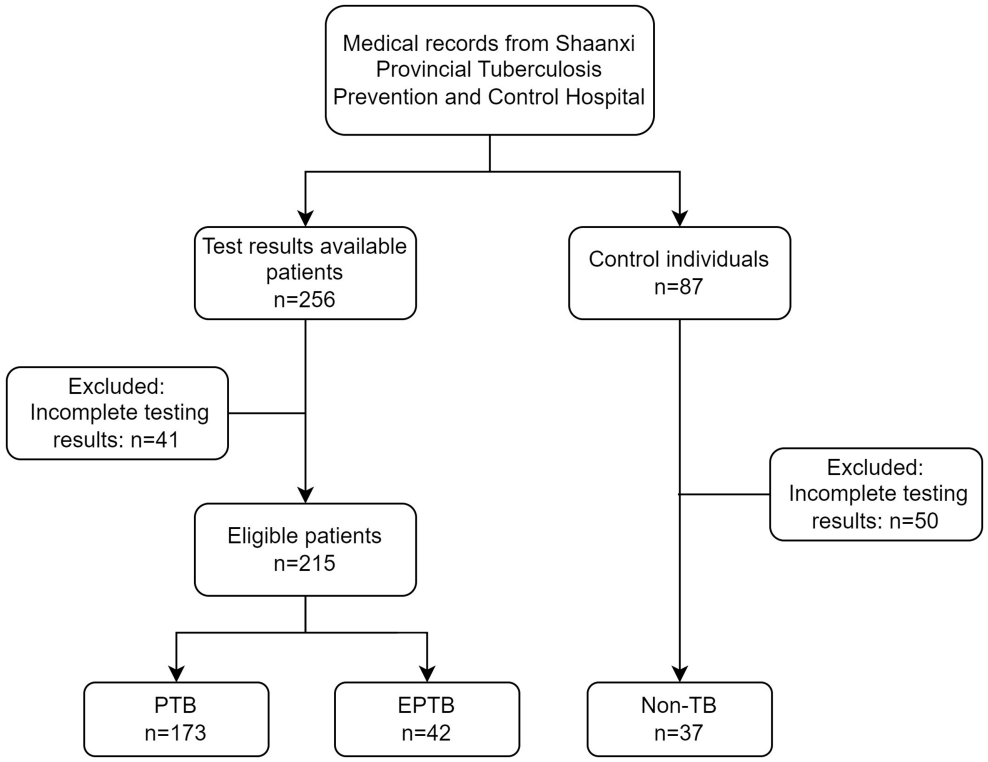

FIGURE 1
Flow chart of included participants.

(World Health Organization, 2022); (2) availability of sputum smears, sputum culture, GeneXpert and urine LAM results. Patients with HIV infection were excluded. 41 cases were excluded from the analysis due to incomplete testing results. The study finally included 215 cases of active tuberculosis patients, including 173 cases of PTB and 42 cases of EPTB. 87 individuals without symptoms related to tuberculosis infection were enrolled from physical examination population in our hospital during the same period, 50 cases were excluded from the analysis due to incomplete testing results. 37 cases were included as the non-TB group (Figure 1). This study adhered to the Helsinki Declaration and was approved by the Medical Ethics Committee of Shaanxi Provincial Tuberculosis Prevention and Control Hospital with the ethics number (2023) LSH-1.

2.2 Sample collection

2.2.1 Sputum collection

Sputum was collected from patients during their visit, using sterile physiological saline for mouth rinsing. Sputum was collected in plastic containers or wax-coated paper-sealed containers. Three samples of sputum, collected at night, in the morning, and immediately, were mixed. The volume of each sample was between 2 and 5 mL. The collection was supervised by laboratory personnel. For patients who had difficulty expectorating sputum, sputum induction using hypertonic saline nebulization or bronchoalveolar lavage was employed. The collected sputum specimens were stored at room temperature for up to 2 h before testing or refrigerated at 4°C and were used for testing within 24 h.

2.2.2 Urine collection

Midstream urine was collected to ensure cleanliness, with a minimum volume of 5 mL. After sample collection, it was stored at room temperature and testing was completed within 72 h. The sample should not have undergone more than three freeze–thaw cycles.

2.2.3 Other samples

Other samples mainly included pleural effusion, cerebrospinal fluid, and pus. The puncture was performed under strict aseptic conditions. For pleural effusion, the puncture position was between the 7th and 8th ribs on the scapular line, between the 6th and 7th ribs on the axillary line, or at the 5th rib on the anterior axillary line. For cerebrospinal fluid, the puncture position was between the 3rd and 4th lumbar vertebrae or between the 4th and 5th lumbar vertebrae. First, disinfection was carried out, and then local anesthetics were used for infiltration anesthesia. A puncture needle was used to enter the chest cavity, and pleural effusion was extracted. Finally, the puncture site was covered with sterile dressing.

2.3 Laboratory test protocol

2.3.1 Sputum smear

Sputum smear test was conducted using acid-fast stain (AFS) and microscopy. AFB was performed according to the protocol previous reported (Van Deun et al., 2008) followed by microscopical examination. At least 100 visual fields were observed with a "100×" oil microscope, and continued observation of 300 visual fields was performed if no bacilli were found. A negative result was defined as

300 consecutive visual fields with no acid-fast bacilli detected, while the detection of acid-fast bacilli was considered positive.

2.3.2 Sputum culture

Sputum culture was performed according to protocol (Hanna et al., 1999) previously established based on BACTEC™ MGIT ™ 960 TB system (BD Diagnostic Systems, Sparks, MD, USA). NALC+4% NaOH was used to free MTB from the mucus for sputum sample (Wang et al., 2022), tissue specimens were lysed using NALC for tissue lysis. After the pretreatment was completed. Samples were incubated into the BBL MGIT culture tube and then tested. The interpretation of the results was also conducted following the aforementioned protocol.

2.3.3 TB-RNA

TB-RNA testing was performed using simultaneous amplification and testing (SAT) method (Qiu et al., 2022) according to the manufacturer's instructions (Shanghai Rendu Biological Technology Co., Ltd., China). All samples were diluted with 4% NaOH solution. Diluted sample was centrifuged at 13,000 × g for 5 min then supernatant removed. The resulting pellet was subjected to ultrasound treatment at 300 W for 15 min and then centrifuged to obtain the supernatant. The supernatant was used for the SAT test according to the manufacturer's instruction.

2.3.4 Urinary LAM detection (chemiluminescence)

Urinary LAM detection was conducted using AIMLAM kits (Leide Biosciences Co., Ltd., China) according to user's manual (Zhang et al., 2023). This kit uses chemiluminescent immunoassay to detect LAM content in human urine. LAM-captured antibodies on magnetic beads bind to LAM in the test sample, forming a magnetic bead-antibody–antigen complex. After binding with the luminescent label, a magnetic bead-antibody–antigen-aminoluciferin label complex is formed for detection of LAM immune complexes. After separation and washing, the pre-triggering solution and the triggering solution are added to the reaction mixture, and the LAM content in the test substance is proportional to the relative light unit value.

The operating procedure is as follows: 5 mL of midstream urine was collected from the patient and the test was performed according to the instructions. 1.5 mL of the test sample was transferred to a 2 mL centrifuge tube. Then, 50 μL of the magnetic bead reagent (containing LAM-capturing antibodies) was added to the centrifuge tube and mixed. The tube was labeled for identification. The labeled centrifuge tube was placed in a rotating mixer and incubated at room temperature with a rotation speed of 30 rpm/min for 2 h. After incubation, the centrifuge tube was placed on a magnetic rack for adsorption. Once the components were fully separated, the supernatant was discarded. To each tube, 200 μL of sample dilution solution was added. The mixture was thoroughly mixed using a vortex mixer and within 5 min, the sample was processed according to the operation manual of the LAM detection chemiluminescence analyzer SMART 500S (Chongqing Keysmile Biological Technology Co., Ltd., China). If the time exceeded 5 min, the sample needed to be mixed again before testing.

2.3.5 GeneXpert

One mL of sample was collected into a disposable leak-proof 50 mL pre-treatment container. For sputum and lavage fluid samples, a two-fold volume of Sample Reagent (SR) was added (equal volume of SR for body fluid samples). The sample and SR were mixed by shaking for 10–20 times or vortexing for at least 10 s. Subsequently, the mixture was incubated for 15 min at 20–30°C, with another round of mixing at 5–10 min into the incubation period. The processed samples were pipetted into the cartridge using the special sterile pipette provided in the kit, the cartridge was placed in the instrument (Cepheid, USA), and the reading was done by referring to the instructions provided by the manufacturer.

2.3.6 Statistical analysis

The data were analyzed using SPSS 26.0 statistical software (SPSS Inc., Chicago, IL). Qualitative data, such as positive detection rate and sensitivity, were presented as frequencies and percentages (%) and the chi-square test were used. All analyses were two-tailed, and a value of p <0.05 was considered statistically significant for differences. According to the composite reference standard, the sensitivity, specificity, positive predictive value (PPV) negative predictive value (NPV), and Kappa value were used to evaluate different methods and consistency. Cost-effectiveness analysis was calculated by dividing the total cost of each diagnostic method by the number of true positive cases diagnosed. The costs were reported in 2022 U.S. dollars, using an exchange rate of 6.74 Chinese yuan to 1 U.S. dollar.[1]

3 Results

3.1 Demographic data of the participants

A total of 215 patients were included in this study. There were no significant differences in age (p = 0.096) and gender (p = 0.506) among the PTB, EPTB and Non-TB groups. Regarding comorbidities, there were no significant differences in the prevalence of diabetes (p = 0.158), hypertension (p = 0.358), coronary heart disease (CHD) (p = 0.074), and chronic obstacle pulmonary disease (COPD) (p = 0.631). Among PTB patients, 9.25% had a history of tuberculosis (p = 0.02), which is higher than that of EPTB patients and Non-TB group (Table 1).

3.2 Diagnostic performance of the five methods compared to CRS

In PTB, the sensitivity of LAM (55.49%) is significantly higher than that of other methods (p < 0.05). The specificity and PPV of all five methods reached 100%. LAM demonstrates the highest NPV (32.46%), slightly higher than Xpert (27.82%). The kappa value for LAM is also the highest (0.305), higher than Xpert (0.220) (Table 2). In EPTB, LAM shows the highest sensitivity, NPV, and kappa value (40.48, 59.68%, 0.389, respectively), followed by GeneXpert (33.33, 56.92%, 0.319, respectively). The sensitivity of LAM is higher than smear (7.14%, p < 0.05) and RNA (9.52%, p < 0.05). The specificity and PPV for all five methods were 100% (Table 3). Positive results of PTB and EPTB patients' tests are shown in Figure 2.

3.3 Diagnostic performance of LAM in combination of other methods

In PTB, LAM combined with another diagnostic method showed the highest sensitivity when combined with GeneXpert (68.79%),

1 https://wdi.worldbank.org/table/4.16

TABLE 1 Demographics of participants.

Variables	All (*N*)	PTB (*N*, %)	EPTB (*N*, %)	Non-TB (*N*, %)	x^2	*p*
total	252	173 (68.65%)	42 (16.67%)	37 (14.68%)		
gender(male)	131 (51.98%)	90 (52.02%)	17 (40.48%)	24 (64.86%)	4.688	0.096
age					3.319	0.506
<30	56	41 (23.70%)	9 (21.43%)	6 (16.22%)		
30–60	124	83 (47.98%)	24 (57.14%)	17 (45.95%)		
>60	72	49 (28.32%)	9 (21.43%)	14 (37.84%)		
DM	35	28 (16.18%)	2 (4.76%)	5 (13.51%)	3.692	0.158
hypertension	30	24 (13.87%)	3 (7.14%)	3 (8.11%)	2.056	0.358
CHD	20	18 (10.40%)	2 (4.76%)	0 (00.00%)	5.211	0.074
COPD	3	2 (1.16%)	0 (00.00%)	0 (00.00%)	0.921	0.631
history of TB	16	16 (9.25%)	0 (00.00%)	0 (00.00%)	7.802	0.020

PTB, pulmonary tuberculosis; EPTB, extrapulmonary tuberculosis; DM, diabetes mellitus; CHD, chronic heart disease; COPD, chronic obstacle pulmonary disease; TB, tuberculosis.

TABLE 2 The diagnostic performance of five methods in PTB.

Methods	Results	CRS		Sensitivity	Specificity	PPV	NPV	Kappa
		PTB	Non-TB					
smear	positive	21	0	12.14%*	100.00%	100.00%	19.58%	0.046
	negative	152	37					
culture	positive	63	0	36.42%*	100.00%	100.00%	25.17%	0.168
	negative	110	36					
RNA	positive	46	0	26.59%*	100.00%	100.00%	22.56%	0.113
	negative	127	37					
Xpert	positive	77	0	44.51%*	100.00%	100.00%	27.82%	0.220
	negative	96	37					
LAM	positive	96	0	55.49%	100.00%	100.00%	32.46%	0.305
	negative	77	37					

CRS, composite reference standard; PTB, pulmonary tuberculosis; PPV, positive predictive value; NPV, negative predictive value; RNA, ribonucleic acid; TB: tuberculosis; LAM, lipoarabinomannan; *$p < 0.05$, Compared to LAM.

TABLE 3 The diagnostic performance of five methods in EPTB.

Methods	Results	CRS		Sensitivity	Specificity	PPV	NPV	Kappa
		EPTB	Non-TB					
smear	positive	3	0	7.14%*	100.00%	100.00%	48.68%	0.067
	negative	39	37					
culture	positive	11	0	26.19%	100.00%	100.00%	54.41%	0.249
	negative	31	37					
RNA	positive	4	0	9.52%*	100.00%	100.00%	49.33%	0.090
	negative	38	37					
Xpert	positive	14	0	33.33%	100.00%	100.00%	56.92%	0.319
	negative	28	37					
LAM	positive	17	0	40.48%	100.00%	100.00%	59.68%	0.389
	negative	25	37					

CRS, composite reference standard; EPTB, extrapulmonary tuberculosis; PPV, positive predictive value; NPV, negative predictive value; RNA, ribonucleic acid; TB, tuberculosis; LAM, lipoarabinomannan; *$p < 0.05$, Compared to LAM.

followed by combination with sputum culture (63.58%), RNA (60.69%), and sputum smear (58.38%). The sensitivity of LAM in combination with the other four methods was significantly higher than when they were individually tested ($p < 0.05$). The sensitivity of LAM in combination with Xpert was higher than when LAM was tested alone ($p < 0.05$). Compared to individual detection methods, LAM detection in combination with sputum smear, sputum culture, RNA, and GeneXpert showed higher sensitivity, increasing by 46.24, 27.17, 34.10 and 24.28%, respectively, (Table 4). When LAM, Xpert were combined with another methods for diagnosing PTB, the combination of culture, Xpert, and LAM showed the highest sensitivity (73.99%) (Table 5). The sensitivity of all three combination approaches was higher than that of using LAM alone ($p < 0.05$). In EPTB, the combined use of LAM with other diagnostic methods can significantly improve sensitivity. According to the data provided, the combination of LAM with GeneXpert showed the highest sensitivity (61.90%), followed by the combination of LAM with sputum culture (52.38%), RNA (45.24%), and sputum smear (42.86%). The sensitivity of LAM in combination with the other four methods was significantly higher than when they were individually tested ($p < 0.05$). The sensitivity of LAM in combination with Xpert was higher than when LAM was tested alone ($p < 0.05$). Compared to individual detection methods, the combination of LAM with sputum smear, sputum culture, RNA, and GeneXpert can increase sensitivity by 35.71, 26.19, 35.71, and 28.57%, respectively (Table 6). When LAM is combined with two other methods (culture and Xpert) for the diagnosis of EPTB, the sensitivity is highest at 69.05% (Table 7). The sensitivity of all three combination approaches was higher than that of using LAM alone ($p < 0.05$).

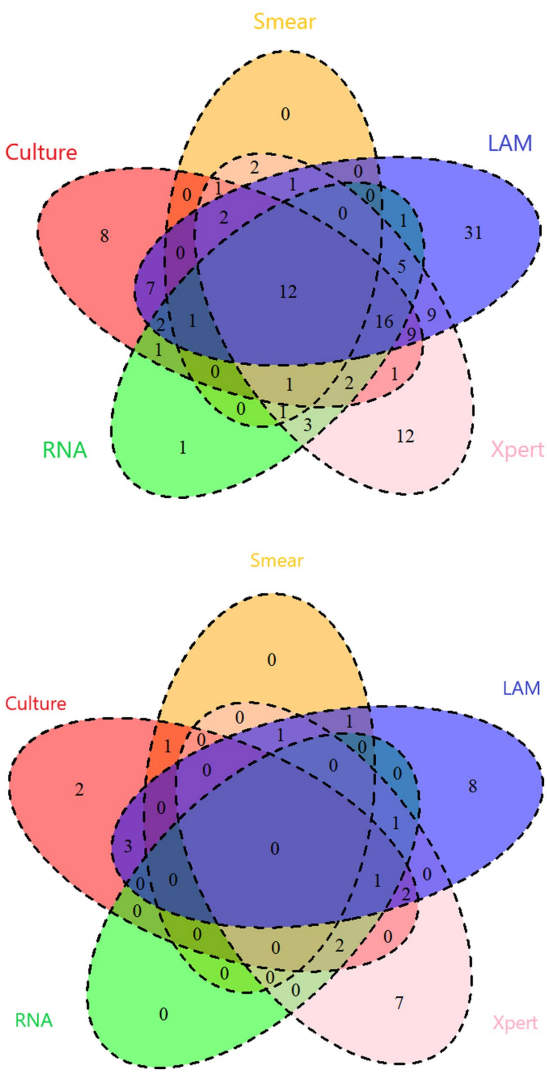

FIGURE 2
Venn diagram of number of positive individuals of PTB and EPTB.

3.4 Cost-effective analysis of different combination

The calculation method for cost-effectiveness is to divide the total cost (unit price multiplied by the number of participants) by the number of true positive cases. An analysis of the economic benefits of the aforementioned combination approaches reveals that when used alone for the diagnosis of PTB, the *per capita* cost of LAM is lower than Xpert ($129.82 vs. $242.78) but higher than other methods. When using the lowest national price, LAM is priced lower than Xpert and RNA, but higher than others. When using the highest national price, LAM is priced lower than Xpert but higher than others. For EPTB, the *per capita* cost of LAM is lower than RNA and Xpert ($275.79, $468.84 and $502.33respectively), but still higher

TABLE 4 Diagnostic performance of LAM in combination of 1 other method in PTB.

Methods	Results	CRS		Sensitivity	Increment	Specificity	PPV	NPV	Kappa
		PTB	Non-TB						
LAM + smear	positive	101	0	58.38%#	46.24%	100.00%	100.00%	33.94%	0.331
	negative	72	37						
LAM + culture	positive	110	0	63.58%#	27.17%	100.00%	100.00%	37.00%	0.381
	negative	63	37						
LAM + RNA	positive	105	0	60.69%#	34.10%	100.00%	100.00%	35.24%	0.352
	negative	68	37						
LAM + Xpert	positive	119	0	68.79%*#	24.28%	100.00%	100.00%	40.66%	0.437
	negative	54	37						

CRS, composite reference standard; PTB, pulmonary tuberculosis; PPV, positive predictive value; NPV, negative predictive value; RNA, ribonucleic acid; TB, tuberculosis; LAM, lipoarabinomannan; *$p < 0.05$, Compared to LAM; #$p < 0.05$, compared to single detection.

TABLE 5 Diagnostic performance of LAM in combination of 2 other methods in PTB.

Methods	Results	CRS		Sensitivity	Increment	Specificity	PPV	NPV	Kappa
		PTB	Non-TB						
LAM + Xpert+smear	positive	119	0	68.79%*	13.29%	100.00%	100.00%	40.66%	0.437
	negative	54	37						
LAM + Xpert+culture	positive	128	0	73.99%*	18.50%	100.00%	100.00%	45.12%	0.501
	negative	45	37						
LAM + Xpert+RNA	positive	121	0	69.94%*	14.45%	100.00%	100.00%	41.57%	0.451
	negative	52	37						

CRS, composite reference standard; PTB, pulmonary tuberculosis; PPV, positive predictive value; NPV, negative predictive value; RNA, ribonucleic acid; TB, tuberculosis; LAM, lipoarabinomannan; *$p < 0.05$, Compared to LAM.

TABLE 6 Diagnostic performance of LAM in combination of 1 other method in EPTB.

Methods	Results	CRS		Sensitivity	Increment	Specificity	PPV	NPV	Kappa
		EPTB	Non-TB						
LAM + smear	positive	18	0	42.86%#	35.71%	100.00%	100%	60.66%	0.413
	negative	24	37						
LAM + culture	positive	22	0	52.38%#	26.19%	100.00%	100%	64.91%	0.507
	negative	20	37						
LAM + RNA	positive	19	0	45.24%#	35.71%	100.00%	100%	61.67%	0.436
	negative	23	37						
LAM + Xpert	positive	26	0	61.90%*#	28.57%	100.00%	100%	69.81%	0.604
	negative	16	37						

CRS, composite reference standard; EPTB, extrapulmonary tuberculosis; PPV, positive predictive value; NPV, negative predictive value; RNA, ribonucleic acid; TB, tuberculosis; LAM, lipoarabinomannan; *$p < 0.05$, Compared to LAM; #$p < 0.05$, compared to single detection.

TABLE 7 Diagnostic performance of LAM in combination of 2 other method in EPTB.

Methods	Results	CRS		Sensitivity	Specificity	PPV	NPV	Kappa
		EPTB	Non-TB					
LAM + Xpert+RNA	positive	26	0	61.90%*	100.00%	100.00%	69.81%	0.604
	negative	16	37					
LAM + Xpert+culture	positive	29	0	69.05%*	100.00%	100.00%	74.00%	0.676
	negative	13	37					
LAM + Xpert +smear	positive	27	0	64.29%*	100.00%	100.00%	71.15%	0.628
	negative	15	37					

CRS, composite reference standard; EPTB, extrapulmonary tuberculosis; PPV, positive predictive value; NPV, negative predictive value; RNA, ribonucleic acid; TB, tuberculosis; LAM, lipoarabinomannan; *$p < 0.05$, Compared to LAM.

than other methods. The same applies when using the highest and lowest national prices. When combined with another method for PTB diagnosis, the combination of LAM and smear has the lowest cost ($124.94). The same applies when using the highest and lowest national prices. Similarly, for EPTB, the combination of LAM and smear also has the lowest cost ($263.72). The same applies when using the highest and lowest national prices. When combined with Xpert and another method for PTB diagnosis, the combination of Xpert, RNA, and LAM has the lowest cost ($258.78). The combination of Xpert, smear, and LAM has the lowest cost ($436.28) in EPTB diagnosis. When using the highest and lowest national prices, Xpert, smear, and LAM has the lowest cost (Table 8).

4 Discussion

This study investigated the diagnostic value of LAM, sputum culture, sputum smear, RNA, and GeneXpert for the diagnosis of PTB and EPTB. We also compared the diagnostic efficacy of LAM in combination with other diagnostic methods. The main finding of this study is that chemiluminescent-based LAM achieved a sensitivity of 55.49% in PTB and 40.48% in EPTB (Tables 2, 3), Which is higher than the sensitivity of other diagnostic methods, in this study, the sensitivity of sputum smear microscopy is 12.14%, sputum culture approximately 36.42%, and GeneXpert 44.51%, exhibiting relatively lower levels when compared to other institutions (Sorsa and Kaso, 2021). This difference

TABLE 8 The cost-effectiveness analysis [$, price in Shaanxi (lowest nationally, highest nationally)].

Methods	Price	PTB	EPTB
smear	0.74 (0.74,2.23)	7.42 (7.42,22.26)	19.54 (19.54,58.61)
culture	20.77 (9.29,29.67)	69.24 (30.96,98.91)	149.18 (66.7,213.11)
RNA	23.74 (11.19,23.74)	108.37 (51.07,108.37)	468.84 (220.94,468.84)
Xpert	89.02 (69.44,90.5)	242.78 (189.37,246.83)	502.33 (391.82,510.7)
LAM	59.35 (22.26,59.35)	129.82 (48.68,129.82)	275.79 (103.42,275.79)
LAM+ smear	60.09 (23,61.57)	124.94 (47.82,128.02)	263.72 (100.93,270.24)
LAM+ culture	80.12 (31.54,89.02)	152.95 (60.22,169.95)	287.7 (113.27,319.67)
LAM+ RNA	83.09 (33.44,83.09)	166.17 (66.88,166.17)	345.46 (139.05,345.46)
LAM+ Xpert	148.37 (91.69,149.85)	261.83 (161.81,264.44)	450.81 (278.6,455.32)
LAM + Xpert+RNA	172.11 (102.88,173.59)	258.78 (178.55,301.27)	453.06 (312.59,527.45)
LAM + Xpert+culture	169.14 (100.98,179.53)	277.49 (165.67,294.53)	460.76 (275.08,489.05)
LAM + Xpert +smear	149.11 (92.43,152.08)	263.14 (163.12,268.37)	436.28 (270.45,444.97)

PTB, pulmonary tuberculosis; EPTB, extrapulmonary tuberculosis; RNA, ribonucleic acid; LAM, lipoarabinomannan.

in sensitivity might be attributed to variances in sample collection and testing procedures among individual laboratories.

Moreover, a meta-analysis reported that the sensitivity of LAM detection for PTB in HIV-negative populations was only about 31% (Yin et al., 2022). The currently available commercial LAM detection method, Alere's Determine TB LAM, has limitations in methodology, resulting in lower sensitivity in HIV-negative populations. Therefore, it is not suitable for TB diagnosis in HIV-negative individuals (Suwanpimolkul et al., 2017). Our study significantly improves the sensitivity of LAM detection in PTB or EPTB. To enhance the sensitivity of LAM detection, raising the detection limit is crucial. Chemiluminescence has a high signal-to-noise ratio and is one of the methods with the highest analytical sample concentration (Green et al., 2017). Additionally, the use of high-affinity monoclonal antibodies and magnetic bead concentration technology in the kit significantly enhances the detection limit of LAM (Peng et al., 2023). Our findings exhibit a similar sensitivity and specificity compared to those reported in prior studies employing the same LAM testing method (Huang et al., 2023; Zhang et al., 2023).

In clinical practice, multiple diagnostic methods are often used in combination to improve the detection rate of TB patients. Therefore, we conducted a comparative analysis of the diagnostic performance of combining LAM with other methods for TB diagnosis. When combined with another method for TB diagnosis, the sensitivity of several other methods was significantly improved. In PTB (Table 4), the combination of LAM with smear increased the sensitivity by over 23 to 40% compared to using smear alone, and the sensitivity of combinations with four other methods exceeded 50%. The combination of LAM with Xpert showed the highest sensitivity (68.79%). The research results of Shah et al. also showed that the sensitivity of combined detection using Xpert and LAM was superior to using either detection method alone (Shah et al., 2014). The result is similar to Zhang et al. (2023). In EPTB (Table 6), the sensitivity was increased by 26 to 36%, and again, the combination of LAM with Xpert showed the highest sensitivity (61.90%). When combined with two other diagnostic methods for pulmonary TB (Table 5), the combination of culture, Xpert, and LAM exhibited the highest sensitivity at 73.99%. Similarly, in EPTB (Table 7), the combination of culture, Xpert, and LAM also demonstrated the highest sensitivity at 69.05%. From the perspective of improving sensitivity, the combination of LAM, Xpert, and culture is the optimal approach for both EPTB and PTB patients.

The incidence of tuberculosis is positively correlated with the economic level of countries and regions, with higher rates observed in economically disadvantaged areas. According to the Global Tuberculosis Report of 2023, geographically, the regions with the highest number of tuberculosis patients in 2022 were the WHO Southeast Asia region (46%), Africa (23%), and the Western Pacific region (18%), primarily concentrated in areas with poor economic development (World Health Organization, 2023). In western China, a region characterized by economic underdevelopment, the burden of tuberculosis is particularly heavy (Hu et al., 2022). Therefore, reducing the cost-effectiveness ratio of tuberculosis diagnosis is essential for ending the tuberculosis epidemic.

The significant cost disparity among various diagnostic techniques, with a nominal expense of $0.74 for sputum smear compared to the higher cost of $89.02 for GeneXpert, underscores the need for judicious selection of diagnostic methods, especially in resource-constrained settings and screening initiatives. Taking into account the price variations for each diagnostic test across different regions in the country, we conducted a cost-effectiveness analysis using pricing standards specific to Shaanxi Province, the highest national pricing, and the lowest national pricing.

To address this, we conducted a comprehensive cost-effectiveness analysis encompassing diverse diagnostic methods and combinations for both PTB and EPTB. Sputum smear emerges as the most economically viable single detection method, with costs amounting to $7.42 for PTB and $19.54 for EPTB, respectively. Among combinations exhibiting sensitivity surpassing 50%, the most cost-effective option is the combination of sputum smear with LAM, incurring expenses of $124.94 for PTB and $263.72 for EPTB. These results hold consistent when considering both the lowest and highest national pricing standards. Given the shorter time requirements for LAM detection and smear microscopy, these

methods play a crucial role in expediting the diagnosis of tuberculosis patients. Furthermore, if combined with sputum culture for diagnosis, a marginal cost increase is observed, significantly augmenting diagnostic capabilities. When the price of LAM is as low as $22.26 or even lower, its cost-effectiveness for diagnosing PTB ($48.68) and EPTB ($103.42) is only secondary to sputum smear and sputum culture. This further emphasizes the importance of LAM, especially in resource-limited settings. By using LAM in combination with sputum smear, diagnostic accuracy can be significantly improved while saving time and costs during the diagnosis process. Furthermore, although it may slightly increase the cost, combining with sputum culture for diagnosis can significantly enhance diagnostic capabilities. Therefore, when formulating diagnostic strategies and allocating resources, the pricing of LAM and cost-effectiveness ratios of other diagnostic methods should be taken into account to ensure optimal diagnostic outcomes in resource-limited settings.

This study has the following limitations: On the one hand, it is a single-center retrospective study, which is subject to inherent biases associated with retrospective studies. Future research could be conducted as multi-center and prospective studies. On the other hand, given the complexity of medical activities, such as the different operation and interpretation times required for different diagnostic methods, our cost-effectiveness analysis did not take these factors into account. Future research can use more comprehensive methods, such as decision tree models, to analyze the cost-effectiveness of different diagnostic methods.

5 Conclusion

Urine LAM detection based on chemiluminescence assay can be used as an adjunct diagnostic tool for PTB and EPTB in HIV-negative individuals. This facilitates expanding the current application of urine LAM from solely HIV-positive populations to the general population. LAM detection can overcome the limitations of obtaining clinical samples, and its ease of sample acquisition will be beneficial for its broader application in a larger scope. For economically better-off areas, we recommend using a combination of LAM + Xpert+culture for higher sensitivity; for economically disadvantaged areas, LAM + smear microscopy combination can provide a quick and accurate diagnosis of tuberculosis at a lower cost.

Data availability statement

The raw data supporting the conclusions of this article will be made available by the authors, without undue reservation.

Ethics statement

The studies involving humans were approved by Ethics Committee, Shaanxi Provincial Tuberculosis Prevention and Control Hospital. The studies were conducted in accordance with the local legislation and institutional requirements. The human samples used in this study were acquired from a by-product of routine care or industry. Written informed consent for participation was not required from the participants or the participants' legal guardians/next of kin in accordance with the national legislation and institutional requirements.

Author contributions

MG: Conceptualization, Formal analysis, Writing – original draft. QW: Investigation, Methodology, Writing – review & editing. XW: Data curation, Writing – review & editing. XS: Validation, Visualization, Writing – review & editing. ML: Software, Writing – review & editing. GB: Conceptualization, Project administration, Writing – review & editing.

Funding

The author(s) declare that no financial support was received for the research, authorship, and/or publication of this article.

Acknowledgments

We would like to express our gratitude to Xiaotan Wang and Hongxia Wei for their assistance in data analysis and editing.

Conflict of interest

The authors declare that the research was conducted in the absence of any commercial or financial relationships that could be construed as a potential conflict of interest.

Publisher's note

References

Bjerrum, S., Broger, T., Székely, R., Mitarai, S., Opintan, J. A., Kenu, E., et al. (2020). Diagnostic accuracy of a novel and rapid Lipoarabinomannan test for diagnosing tuberculosis among people with human immunodeficiency virus. Open forum. *Infect. Dis.* 7:ofz530. doi: 10.1093/ofid/ofz530

Briken, V., Porcelli, S. A., Besra, G. S., and Kremer, L. (2004). Mycobacterial lipoarabinomannan and related lipoglycans: from biogenesis to modulation of the immune response. *Mol. Microbiol.* 53, 391–403. doi: 10.1111/j.1365-2958.2004.04183.x

Broger, T., Nicol, M. P., Sigal, G. B., Gotuzzo, E., Zimmer, A. J., Surtie, S., et al. (2020). Diagnostic accuracy of 3 urine lipoarabinomannan tuberculosis assays in HIV-negative outpatients. *J. Clin. Invest.* 130, 5756–5764. doi: 10.1172/JCI140461

Broger, T., Sossen, B., du Toit, E., Kerkhoff, A. D., Schutz, C., Ivanova Reipold, E., et al. (2019). Novel lipoarabinomannan point-of-care tuberculosis test for people with HIV: a diagnostic accuracy study. *Lancet Infect. Dis.* 19, 852–861. doi: 10.1016/S1473-3099(19)30001-5

Bulterys, M. A., Wagner, B., Redard-Jacot, M., Suresh, A., Pollock, N. R., Moreau, E., et al. (2019). Point-of-care urine LAM tests for tuberculosis diagnosis: a status update. *J. Clin. Med.* 9:111. doi: 10.3390/jcm9010111

People's Republic of China state health and Family Planning Commission. (2018). Tuberculosis classification (WS196—2017). *Electron. J. Emerg. Infect. Dis.* 3, 191–192. doi: 10.19871/j.cnki.xfcrbzz.2018.03.018

Correia-Neves, M., Froberg, G., Korshun, L., Viegas, S., Vaz, P., Ramanlal, N., et al. (2019). Biomarkers for tuberculosis: the case for lipoarabinomannan. *ERJ Open Res.* 5, 00115–02018. doi: 10.1183/23120541.00115-2018

García, J. I., Kelley, H. V., Meléndez, J., de León, R. A. A., Castillo, A., Sidiki, S., et al. (2019). Improved Alere determine Lipoarabinomannan antigen detection test for the diagnosis of human and bovine tuberculosis by manipulating urine and Milk. *Sci. Rep.* 9:18012. doi: 10.1038/s41598-019-54537-9

Grant, L. R., Hammitt, L. L., Murdoch, D. R., O'Brien, K. L., and Scott, J. A. (2012). Procedures for collection of induced sputum specimens from children. *Clin. Infect. Dis.* 54, S140–S145. doi: 10.1093/cid/cir1069

Green, O., Eilon, T., Hananya, N., Gutkin, S., Bauer, C. R., and Shabat, D. (2017). Opening a gateway for Chemiluminescence cell imaging: distinctive methodology for design of bright Chemiluminescent Dioxetane Probes. *ACS Cent Sci.* 3, 349–358. doi: 10.1021/acscentsci.7b00058

Gupta-Wright, A., Peters, J. A., Flach, C., and Lawn, S. D. (2016). Detection of lipoarabinomannan (LAM) in urine is an independent predictor of mortality risk in patients receiving treatment for HIV-associated tuberculosis in sub-Saharan Africa: a systematic review and meta-analysis. *BMC Med.* 14:53. doi: 10.1186/s12916-016-0603-9

Hanna, B. A., Ebrahimzadeh, A., Elliott, L. B., Morgan, M. A., Novak, S. M., Rusch-Gerdes, S., et al. (1999). Multicenter evaluation of the BACTEC MGIT 960 system for recovery of mycobacteria. *J. Clin. Microbiol.* 37, 748–752. doi: 10.1128/JCM.37.3.748-752.1999

Hu, M., Feng, Y., Li, T., Zhao, Y., Wang, J., Xu, C., et al. (2022). Unbalanced risk of pulmonary tuberculosis in China at the subnational scale: spatiotemporal analysis. *JMIR Public Health Surveill.* 8:e36242. doi: 10.2196/36242

Huang, L., Niu, Y., Zhang, L., Yang, R., and Wu, M. (2023). Diagnostic value of chemiluminescence for urinary lipoarabinomannan antigen assay in active tuberculosis: insights from a retrospective study. *Front. Cell. Infect. Microbiol.* 13:13. doi: 10.3389/fcimb.2023.1291974

Huerga, H., Bastard, M., Lubega, A. V., Akinyi, M., Antabak, N. T., Ohler, L., et al. (2023). Novel FujiLAM assay to detect tuberculosis in HIV-positive ambulatory patients in four African countries: a diagnostic accuracy study. *Lancet Glob. Health* 11, e126–e135. doi: 10.1016/S2214-109X(22)00463-6

Lawn, S. D. (2012). Point-of-care detection of lipoarabinomannan (LAM) in urine for diagnosis of HIV-associated tuberculosis: a state of the art review. *BMC Infect. Dis.* 12:103. doi: 10.1186/1471-2334-12-103

Minion, J., Leung, E., Talbot, E., Dheda, K., Pai, M., and Menzies, D. (2011). Diagnosing tuberculosis with urine lipoarabinomannan: systematic review and meta-analysis. *Eur. Respir. J.* 38, 1398–1405. doi: 10.1183/09031936.00025711

Nicol, M. P., Schumacher, S. G., Workman, L., Broger, T., Baard, C., Prins, M., et al. (2021). Accuracy of a novel urine test, Fujifilm SILVAMP tuberculosis Lipoarabinomannan, for the diagnosis of pulmonary tuberculosis in children. *Clin. Infect. Dis.* 72, e280–e288. doi: 10.1093/cid/ciaa1052

Pang, Y., Wang, Y., Zhao, S., Liu, J., Zhao, Y., and Li, H. (2014). Evaluation of the Xpert MTB/RIF assay in gastric lavage aspirates for diagnosis of smear-negative childhood pulmonary tuberculosis. *Pediatr. Infect. Dis. J.* 33, 1047–1051. doi: 10.1097/INF.0000000000000403

Peng, L., Dai, L., Zhu, M., Fang, T., Sun, H., Shao, Y., et al. (2023). Developing a method to detect lipoarabinomannan in pleural fluid and assessing its diagnostic efficacy for tuberculous pleural effusion. *Heliyon* 9:e18949. doi: 10.1016/j.heliyon.2023.e18949

Qiu, X., Zheng, S., Yang, J., Yu, G., and Ye, Y. (2022). Comparing *Mycobacterium tuberculosis* RNA accuracy in various respiratory specimens for the rapid diagnosis of pulmonary tuberculosis. *Infect. Drug Resist.* 15, 4195–4202. doi: 10.2147/IDR.S374826

Roda, A., and Guardigli, M. (2012). Analytical chemiluminescence and bioluminescence: latest achievements and new horizons. *Anal. Bioanal. Chem.* 402, 69–76. doi: 10.1007/s00216-011-5455-8

Shah, M., Ssengooba, W., Armstrong, D., Nakiyingi, L., Holshouser, M., Ellner, J. J., et al. (2014). Comparative performance of urinary lipoarabinomannan assays and Xpert MTB/RIF in HIV-infected individuals. *AIDS* 28, 1307–1314. doi: 10.1097/QAD.0000000000000264

Sigal, G. B., Pinter, A., Lowary, T. L., Kawasaki, M., Li, A., Mathew, A., et al. (2018). A novel sensitive immunoassay targeting the 5-Methylthio-d-Xylofuranose-Lipoarabinomannan epitope meets the WHO's performance target for tuberculosis diagnosis. *J. Clin. Microbiol.* 56, e01338–e01318. doi: 10.1128/JCM.01338-18

Sorsa, A., and Kaso, M. (2021). Diagnostic performance of GeneXpert in tuberculosis-HIV co-infected patients at Asella teaching and referral hospital, southeastern Ethiopia: a cross sectional study. *PLoS One* 16:e0242205. doi: 10.1371/journal.pone.0242205

Suwanpimolkul, G., Kawkitinarong, K., Manosuthi, W., Sophonphan, J., Gatechompol, S., Ohata, P. J., et al. (2017). Utility of urine lipoarabinomannan (LAM) in diagnosing tuberculosis and predicting mortality with and without HIV: prospective TB cohort from the Thailand big City TB research network. *Int. J. Infect. Dis.* 59, 96–102. doi: 10.1016/j.ijid.2017.04.017

Van Deun, A., Hossain, M. A., Gumusboga, M., and Rieder, H. L. (2008). Ziehl-Neelsen staining: theory and practice. *Int. J. Tuberc. Lung Dis.* 12, 108–110.

Wang, J., Wang, Y., Ling, X., Zhang, Z., Deng, Y., and Tian, P. (2022). Comparison of sputum treated with power ultrasound and routine NALC-NaOH methods for mycobacterial culture: a prospective study. *J. Clin. Med.* 11:4694. doi: 10.3390/jcm11164694

World Health Organization (2019). *Lateral flow urine Lipoarabinomannan assay (LF-LAM) for the diagnosis of active tuberculosis in people living with HIV. Policy update 2019*, Geneva: World Health Organization.

World Health Organization. *WHO consolidated guidelines on tuberculosis. Module 3: diagnosis. Tests for TB infection.* (2022). Geneva: World Health Organization.

World Health Organization (2023). *Global tuberculosis report 2023*, Geneva: World Health Organization.

Yin, X., Ye, Q. Q., Wu, K. F., Zeng, J. Y., Li, N. X., Mo, J. J., et al. (2022). Diagnostic value of Lipoarabinomannan antigen for detecting *Mycobacterium tuberculosis* in adults and children with or without HIV infection. *J. Clin. Lab. Anal.* 36:e24238. doi: 10.1002/jcla.24238

Zhang, Y., Chen, S., Wei, H., Zhong, Q., Yuan, Y., Wang, Y., et al. (2023). Breakthrough of chemiluminescence-based LAM urine test beyond HIV-positive individuals: clinical diagnostic value of pulmonary tuberculosis in the general population. *Medicine (Baltimore)* 102:e36371. doi: 10.1097/MD.0000000000036371

Zou, X., Zhu, Y., Qin, Y., Fei, F., Chen, Y., Wang, P., et al. (2023). Value analysis of next-generation sequencing combined with Xpert in early precise diagnosis of pulmonary tuberculosis. *Diagn. Microbiol. Infect. Dis.* 107:115921. doi: 10.1016/j.diagmicrobio.2023.115921

frontiers | Frontiers in Medicine

TYPE Systematic Review
PUBLISHED 11 March 2024
DOI 10.3389/fmed.2023.1278716

OPEN ACCESS

EDITED BY
Xueqiong Wu,
The 8th Medical Center of Chinese PLA General Hospital, China

REVIEWED BY
Quanxin Long,
Chongqing Medical University, China
Jana Amlerova,
University Hospital in Pilsen, Czechia

*CORRESPONDENCE
Yu Pang
✉ pangyupound@163.com
Liang Li
✉ liliang69@tb123.org

†These authors have contributed equally to this work and share first authorship

RECEIVED 23 August 2023
ACCEPTED 26 December 2023
PUBLISHED 11 March 2024

CITATION
Zhang F, Wang Y, Zhang X, Liu K, Shang Y, Wang W, Liu Y, Li L and Pang Y (2024) Diagnostic accuracy of oral swab for detection of pulmonary tuberculosis: a systematic review and meta-analysis. *Front. Med.* 10:1278716. doi: 10.3389/fmed.2023.1278716

Diagnostic accuracy of oral swab for detection of pulmonary tuberculosis: a systematic review and meta-analysis

Fuzhen Zhang[1,2†], Yilin Wang[2†], Xuxia Zhang[2†], Kewei Liu[2], Yuanyuan Shang[2], Wei Wang[2], Yuanyuan Liu[2], Liang Li[1,2*] and Yu Pang[2*]

[1]Department of Epidemiology, School of Public Health, Cheeloo College of Medicine, Shandong University, Jinan, China, [2]Department of Bacteriology and Immunology, Beijing Chest Hospital, Capital Medical University/Beijing Tuberculosis and Thoracic Tumor Research Institute, Beijing, China

Objectives: Tuberculosis (TB) remains a significant concern in terms of public health, necessitating the timely and accurate diagnosis to impede its advancement. The utilization of oral swab analysis (OSA) presents a promising approach for diagnosing pulmonary TB by identifying *Mycobacterium tuberculosis* (MTB) within oral epithelial cells. Due to disparities in the diagnostic performance of OSA reported in the original studies, we conducted a meticulous meta-analysis to comprehensively assess the diagnostic efficacy of OSA in pulmonary TB.

Methods: We conducted a comprehensive investigation across multiple databases, namely PubMed, Cochrane Library, Embase, Web of Science, ClinicalTrials.gov, Chinese BioMedical Literature Database (CBM), China National Knowledge Infrastructure Database (CNKI), and Wanfang China Science and Technology Journal Database to identify relevant studies. Out search query utilized the following keywords: oral swab, buccal swab, tongue swab, tuberculosis, and TB. Subsequently, we employed STATA 16.0 to compute the combined sensitivity, specificity, positive likelihood ratio, negative likelihood ratio, and diagnostic odds ratio for both the overall and subgroup analyses.

Results: Our findings indicated that OSA has a combined sensitivity of 0.67 and specificity of 0.95 in individuals with pulmonary TB. Subgroup analysis further revealed that among adult individuals with pulmonary TB, the sensitivity and specificity of OSA were 0.73 and 0.93, respectively. In HIV-negative individuals with pulmonary TB, the sensitivity and specificity were 0.68 and 0.98, respectively. The performance of OSA in detecting pulmonary TB correlated with the bacteria load in sputum. Additionally, the sensitivity for diagnosing pulmonary TB using tongue specimens was higher (0.75, 95% CI: 0.65–0.83) compared to cheek specimens (0.52, 95% CI: 0.34–0.70), while both types of specimens demonstrated high specificity.

Conclusions: To conclude, oral swabs serve as a promising alternative for diagnosing pulmonary TB, especially in adult patients. In addition, tongue swabs yield better sensitivity than cheek swabs to identify pulmonary TB patients.

Systematic review registration: identifier: CRD42023421357.

KEYWORDS

oral swab analysis, tuberculosis, diagnostic accuracy, systematic review, meta-analysis

Introduction

Tuberculosis (TB), caused by *Mycobacterium tuberculosis* (MTB), remains a major significant contributor to mortality resulting from chronic infectious diseases, especially in immunodeficiency patients with HIV (1). The emergence of drug-resistant TB (DR-TB), encompassing extensively drug-resistant TB (XDR-TB) and pre-XDR-TB, has posed a substantial threat to TB control efforts in recent years (2). Timely and early diagnosis, along with prompt treatment, plays a crucial role in preventing the dissemination of drug-resistant TB (3). Currently, the majority of confirmed TB cases rely on the detection of MTB in sputum specimens, such as sputum smear, sputum culture, and MTB molecular in sputum (4–6). However, the reliance on sputum specimens presents limitations, particularly in pediatric patients and those who are unable to produce sputum (7). Additionally, the collection of sputum can cause potentially infectious aerosols that are harmful to healthcare workers and other patients (8). Moreover, the efficacy of TB diagnostic tests is contingent upon the quality of the sputum collected (9). Therefore, there is a pressing need for non-invasive alternatives to sputum-based testing that are easier, safer, and more efficient in diagnosing TB.

Several human samples, including exhaled breath condensate, saliva, urine, blood and stool, have been explored as alternatives to sputum for evaluating the diagnostic performance of TB (10, 11). Unfortunately, these alternative samples have demonstrated lower sensitivity or specificity than sputum. Recently, an oral (buccal) swab has emerged as a more encouraging alternative to sputum specimens for TB diagnosis. Previous studies have shown that oral swab analysis (OSA) can detect MTB DNA present in oral epithelial cells (12–15). OSA involves the utilization of a sterile brush to gently scrape cells from the dorsal surface of the tongue. This procedure is simple, quick, painless, non-invasive and does not generate aerosols, making it suitable for implementation in various healthcare settings, including tertiary hospitals, outpatient clinics, and community settings. Consequently, OSA holds particular value in identifying TB cases within diverse populations.

A series of studies examining the efficacy of OSA for diagnosing pulmonary TB have yielded inconsistent findings. For instance, one study conducted in South Africa evaluated swabs from adult subjects and found that OSA exhibited a sensitivity of 92.8% and specificity of 91.5% when compared to sputum GeneXpert testing (14). Similarly, another study involving 201 South African children with suspected pulmonary TB revealed that OSA demonstrated greater sensitivity than sputum testing in children who were negative for sputum, although its sensitivity was lower in sputum-positive children (16). By contrast, conflicting outcomes were noted in other studies, reporting lower sensitivity for detecting tubercle bacilli using oral swabs (13, 15, 17, 18). The limited sample sizes in previous studies undermine the confidence of these conclusions. Therefore, we conducted a meta-analysis to investigate the diagnostic value of OSA in detecting pulmonary TB while also conducting a comprehensive analysis of its diagnostic accuracy across different populations.

Materials and methods

Protocol registration

This systematic review and meta-analysis were conducted according to the Preferred Reporting Items for Systematic Reviews and meta-Analyses (PRISMA) statement. The protocol has been registered in PROSPERO (Number: CRD42023421357).

Search strategy

We conducted a comprehensive and systematic search for relevant studies in electronic databases, including PubMed, Cochrane Library, Embase, Web of Science, ClinicalTrials.gov, Chinese BioMedical Literature Database (CBM), China National Knowledge Infrastructure Database (CNKI), and Wanfang China Science and Technology Journal Database, based on our review protocol. The most recent searches performed on 12 March 2023 used the following terms: ("oral swab" or "buccal swab" or "tongue swab") and ("tuberculosis" or "TB"). No geographical or demographic restrictions were imposed during the search process, including the race or age of study participants. We considered studies published in both English and Chinese languages, and only included relevant data for our analysis.

Eligibility criteria

We enrolled records that met the following eligibility criteria, which involved studies designed as diagnostic accuracy studies aiming to assess the diagnostic value of oral swabs for TB in human subjects. We exclusively considered studies that provided sufficient data for computing pooled sensitivity and specificity in human populations, including the count of true positives and negatives, as well as false positives and negatives. Only studies with complete data were included to avoid duplications. We excluded studies that lacked adequate data for calculating effect size or were missing other essential information. Moreover, publications encompassing reviews, case reports, abstracts, guidelines, and recommendations were also excluded, as they did not present primary results. Furthermore, studies lacking research indicators necessary for meta-analysis were also excluded.

Data extraction

The study selection process was conducted independently by two investigators. In case of any discrepancies, a third author reviewed the articles, and a final consensus was reached through discussion. Initially, the investigators screened the literature based on titles and abstracts to exclude articles that did not meet the inclusion criteria. Subsequently, the remaining articles were re-evaluated by reading their full texts. Detailed information and data from the identified studies were extracted by the two investigators using a standardized data extraction form that had been pre-constructed. The following information was extracted

for each study: the first author's name, year of publication, place of study, study population, population size, age, and sex distribution of participants, method of diagnosis, TB type, sensitivity, and specificity values with their corresponding 95% confidence intervals (CI), as well as the number of true positives, false positives, false negatives, and true negatives. The investigators extracted data according to various subgroups, including adults and children, TB patients with and without HIV and smear-positive and smear-negative TB. Furthermore, OSA samples collected from the tongue and cheek were evaluated in the diagnosis of TB.

Statistical analysis

The quality of the included studies was evaluated using the widely Quality Assessment of Diagnostic Accuracy Studies-2 (QUADAS-2) tool (19). This tool assesses diagnostic accuracy based on four main points: selection of patients, index criteria, reference standard and flow and timing in the preliminary study. The quality rating scale is based on risk bias. Additionally, applicability concerns were taken into account when assessing the first three domains.

For the meta-analysis, STATA software version 16.0 was utilized. Heterogeneity was evaluated using both the chi-square and the I^2 statistical tests. A significant level of heterogeneity was considered when P is greater or equal to 0.10, accompanied by an I^2 values of 50% or higher. Acceptable inter-study heterogeneity was determined when the I^2 value was equal to or $<$50%. To mitigate the potential impact of the heterogeneity on the final conclusion, a random effects model was employed combine data from individual studies. This approach allowed for the estimation of sensitivity, specificity, positive/negative likelihood ratio and diagnostic odds ratio. The receiver operator characteristic (ROC) curve was utilized to obtain the area under the curve, providing a measure of the diagnostic accuracy. Publication bias was assessed using Deek's funnel plot methodology.

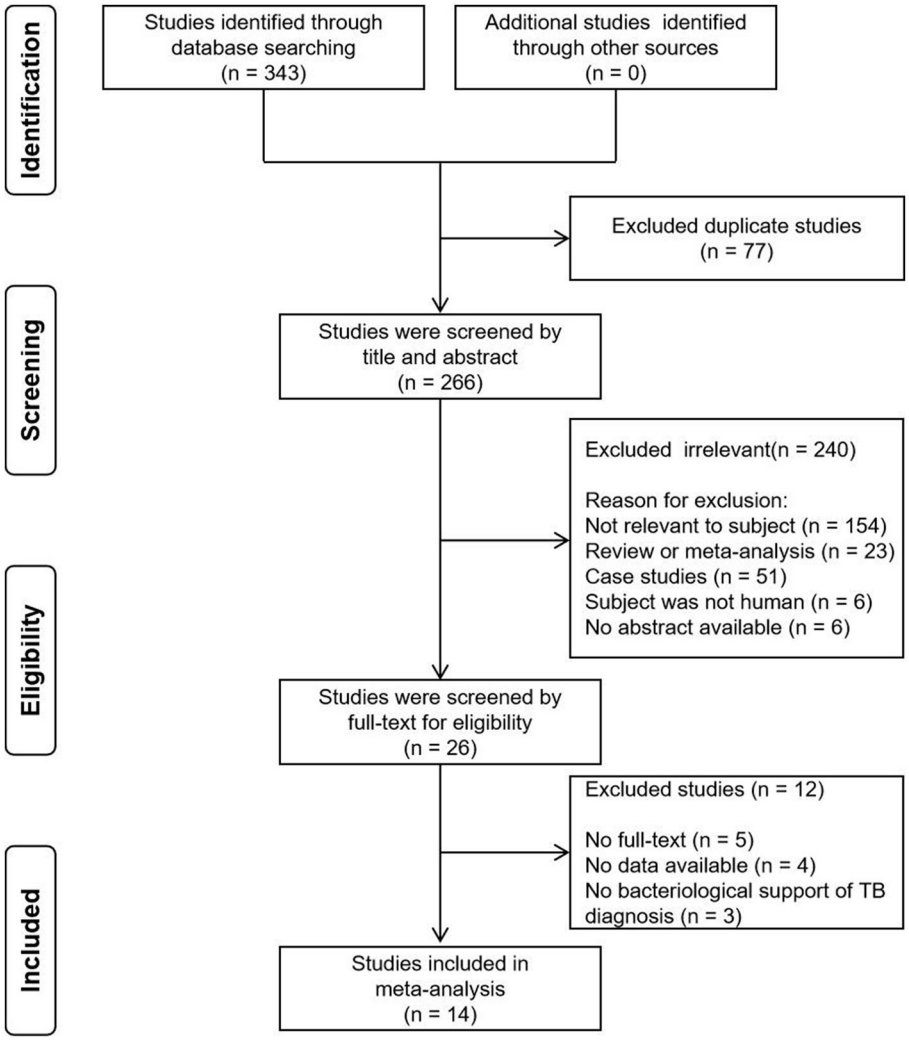

FIGURE 1
PRISMA flow diagram of the studies selection process.

Results

Study characteristics

Initially, a total of 343 records were identified, out of which 77 duplicates were removed. Subsequently, a screening process based on titles and abstracts was carried out, resulting in the exclusion of 240 irrelevant records. This narrowed down the selection to 26 articles, which were then assessed based on full-text contents. Among these, 12 articles were excluded due to reasons such as unavailability of full-text, absence of data and lack of bacteriological support of pulmonary TB diagnosis. Eventually, a systematic review was conducted, including 14 studies that fulfilled the inclusion criteria (Figure 1). Notably, two studies were included twice in separate records. In one study, TB was diagnosed using either culture or GeneXpert MTB/RIF as reference standards, resulting in two records being incorporated for this study (20). In the other study, two methods were employed in the OSA experiment. One used the double swab GeneXpert sample reagent method for GeneXpert MTB/RIF Ultra, while the other used the boil method for GeneXpert MTB/RIF Ultra, with two records also being included in this study (17). Among the remaining 16 records, two reported the diagnostic effectiveness of OSA in children with pulmonary TB, twelve explored the diagnostic effectiveness of OSA in adults with pulmonary TB, while the age range of the study population in two records could not be determined. Table 1 provides a concise summary of the key characteristics of the included studies. It is important to note that the diagnosis of pulmonary TB in all the included studies was based on confirmed cases using the reference standard.

Risk of bias within studies

The 14 studies included in this research were assessed for risk of bias by using the QUADAS-2 tool. Among them, ten studies were found to have a low risk of selection bias, while 4 studies had an unclear risk of selection bias. Furthermore, eight studies exhibited a high risk of bias in the index test, as the interpretation of OSA results was influenced by prior knowledge of the reference standard results. In contrast, the reference standard and flow and timing displayed a low risk across all 14 studies. Lastly, two studies had unclear applicability concerns regarding patient selection. A detailed summary of the results can be found in Supplementary Table 1.

Overall diagnostic accuracy of OSA in pulmonary TB

A total of 16 records were examined to assess the diagnostic value of OSA in pulmonary TB. Analysis of the results revealed that despite the heterogeneity resulting from variations in the operational processing of OSA among the studies (see Supplementary Table 3), OSA showed an overall pooled sensitivity of 0.67 (95% CI: 0.55–0.77, $I^2 = 88.94\%$) and an overall pooled specificity of 0.95 (95% CI: 0.88–0.96, $I^2 = 91.09\%$) in the diagnosis of pulmonary TB (Figure 2). Further subgroup analysis supported the overall findings, indicating a high specificity and diagnostic sensitivity of OSA in TB.

Subgroups diagnostic accuracy of OSA in pulmonary TB

The meta-analysis findings demonstrated that OSA exhibits sensitivity of 0.73 (95% CI: 0.61–0.82, $I^2 = 90.08\%$) and specificity of 0.93 (95% CI: 0.83–0.97, $I^2 = 88.07\%$) for diagnosing adults with pulmonary TB (Figure 3A). In HIV-negative individuals with pulmonary TB, the sensitivity and specificity of OSA were 0.68 (95% CI: 0.42–0.86, $I^2 = 88.69\%$) and 0.98 (95% CI: 0.91–1.00, $I^2 = 90.03\%$), respectively (Figure 3B). However, due to the limited number of studies available, a meta-analysis could not be conducted to evaluate the effectiveness of OSA in diagnosing children and HIV-positive individuals with pulmonary TB. Therefore, the diagnosis of OSA in these populations remains uncertain. Details are listed in Supplementary Table 2. Furthermore, for individuals with smear-positive pulmonary TB, OSA demonstrated a sensitivity and specificity of 0.58 (95% CI: 0.47–0.68, $I^2 = 20.99\%$) and 0.98 (95% CI: 0.88–1.00, $I^2 = 88.80\%$), respectively (Figure 3C). For smear-negative individuals with pulmonary TB, OSA exhibited a sensitivity and specificity of 0.30 (95% CI: 0.11–0.59, $I^2 = 84.78\%$) and 0.97 (95% CI: 0.88–0.99, $I^2 = 89.17\%$), respectively (Figure 3D). Moreover, we investigated the performance of OSA in diagnosing pulmonary TB using tongue and cheek specimens. The sensitivity of tongue and cheek specimens was 0.75 (95% CI: 0.65–0.83, $I^2 = 85.34\%$) and 0.52 (95% CI: 0.34–0.70, $I^2 = 79.28\%$), while the specificity was 0.95 (95% CI: 0.77–0.99, $I^2 = 91.81\%$) and 0.97 (95% CI: 0.89–0.99, $I^2 = 90.34\%$), respectively (Figure 4). Supplementary Table 2 displays all subgroup analyses of OSA in diagnosing pulmonary TB. Table 2 provides a summary of the meta-analysis results.

Publication bias assessment

To assess publication bias, a funnel plot was employed (Supplementary Figure 1). The funnel plot clearly indicated the absence of significant publication bias in this meta-analysis ($P = 0.99$).

Discussion

TB continues to pose a significant public health challenge, necessitating early detection and prompt treatment to curb its spread (3, 28). In recent years, researchers have developed oral swabs, as a non-invasive method for detecting MTB DNA, which can be obtained from the tongue, cheek or gums (14). While obtaining samples directly from the lower respiratory tract is of paramount importance and demonstrates superior efficacy in diagnosing TB, oral swabs present a more accessible alternative approach for TB diagnosis (17, 25). They have also been widely utilized in diagnosing TB in animals (29–31). Furthermore, the development of oral swabs aimed to mitigate the health

TABLE 1 Baseline characteristics of OSA in the diagnosis of TB included in our analysis.

References	Location	Study population	Sample size	Age, year	Sex (M/F)	No. of participants				Diagnostic method	Sensitivity (95% CI), %	Specificity (95% CI), %	TP	FP	FN	TN
						HIV positive	Confirmed TB	Suspected TB	Unlikely TB							
Wood et al. (21)	South African; USA	Adult	40	NA	24/16	0	20		20	Xpert	90.0 (66.9–98.2)	100.0 (80.0–100.0)	18	0	2	20
Luabeya et al. (14)	South African	Adult	219	NA	NA	NA	148		71	Xpert or Culture	83.1 (70.6–91.1)	91.5 (81.9–96.5)	49	6	10	65
Nicol et al. (16)	South African	Children	165	2.5 (1.1–6.7)[a]	78/87	18	40	81	44	Xpert or Culture	42.5 (27.4–59.0)	93.2 (80.3–98.2)	17	3	23	41
Mesman et al. (15)	Peru	Adult	63	NA	NA	NA	33		30	Culture	45.5 (28.5–63.4)	100.0 (84.0–100.0)	15	0	18	26
Lima et al. (22)	Brazil	NA	256	NA	NA	NA	128		128	Xpert	51.6 (42.6–60.4)	100.0 (96.4–100.0)	66	0	62	128
Molina-Moya et al. (12)	Spain	Adult	266	48.8 ± 14.4[b]	157/109	NA	80	34	152	Xpert or Culture	36.3 (26.0–47.8)	79.6 (72.9–85.0)	29	38	51	148
Mesman et al. (23)	Peru	Adult	153	NA	NA	4	123		30	Culture	51.2 (42.1–60.3)	96.7 (80.9–99.8)	63	1	60	29
Flores et al. (13)	Peru	Children	288	NA	148/140	0	24	65	199	Culture	20.8 (7.9–42.7)	99.0 (96.0–99.8)	5	2	19	197
Wood et al. (20)[d]	Uganda; USA	Adult	194	NA	124/70	55	142		52	Xpert	88.0 (75.0–95.0)	79.2 (65.5–88.7)	44	11	6	42
Wood et al. (20)[e]	Uganda; USA	Adult	194	NA	124/70	55	142		52	Culture	91.5 (78.7–97.2)	66.1 (52.1–77.8)	43	19	4	37
Song et al. (24)	China	Adult	101	43.5 (17–88)[c]	69/32	0	46		55	Xpert and/or Culture	82.6 (71.7–93.6)	94.5 (88.5–100)	38	3	8	52
Shapiro et al. (25)	South African	Adult	131	36 (31–46)[a]	72/59	121	64		67	Xpert Ultra or Culture	65.7 (52.7–76.8)	77.6 (65.5–86.5)	42	15	22	52
Andama et al. (17)[f]	Uganda	Adult	183	33 (26–43)[a]	107/76	58	58		125	Xpert Ultra or Culture	72.4 (58.9–83.0)	100.0 (96.1–100.0)	42	0	16	119
Andama et al. (17)[g]	Uganda	Adult	183	33 (26–43)[a]	107/76	58	58		125	Xpert Ultra or Culture	77.1 (59.4–89.0)	100.0 (19.8–100.0)	27	0	8	2
Kang et al. (26)	Korea	Adult	272	58.8 ± 15.2[b]	174/98	1	99	29	144	Culture	64.6 (54.3–73.8)	86.1 (79.1–91.1)	64	20	35	124
LaCourse et al. (27)	Kenya	≥13 years	100	38 (30–44)[a]	52/48	54	20		80	Xpert or Culture	65.0 (40.9–83.7)	81.3 (70.6–88.8)	13	15	7	65

HIV, human immunodefificiency virus; Xpert, GeneXpert MTB/RIF; Xpert Ultra, GeneXpert MTB/RIF Ultra; IQR, interquartile range; SD, standard deviation; NA, not available applicable; TP, true positive; FP, false positive; FN, false negative; TN, true negative. [a]Median ± IQR; [b]mean ± SD; [c]median ± range; [d]TB Diagnosis using Xpert; [e]TB Diagnosis using Culture; [f]Xpert Ultra testing using the double swab GeneXpert sample reagent method; [g]Xpert Ultra testing using the boil method.

10.3389/fmed.2023.1278716

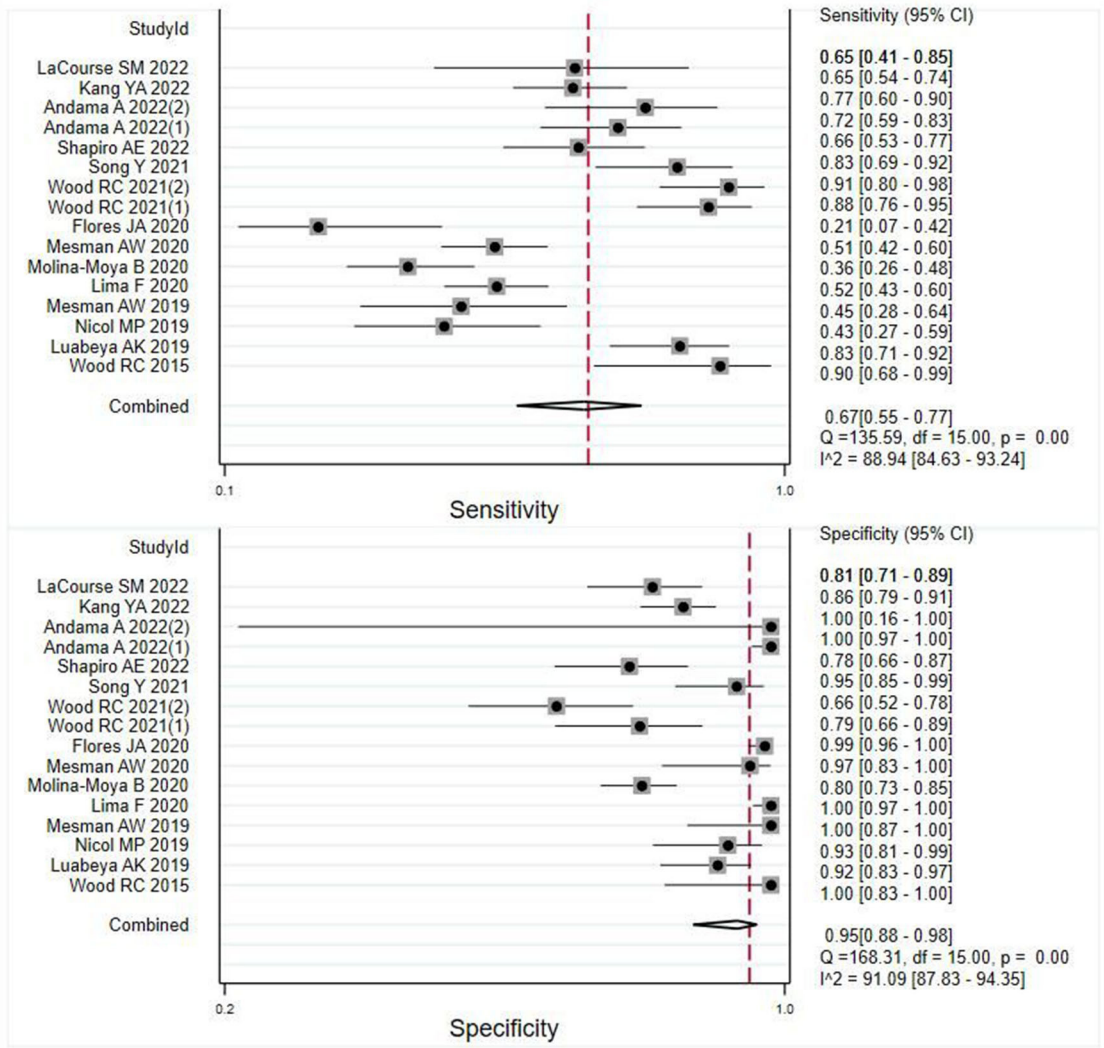

FIGURE 2
Meta-analysis results of the sensitivity and specificity of OSA in the diagnosis of individuals with pulmonary TB.

risks associated with collecting sputum, which poses potential hazards for healthcare providers (32). In our meta-analysis, we comprehensively evaluated the diagnostic efficacy of oral swabs for pulmonary TB, providing novel insights into its potential utility. We observed that while the sensitivity of oral swabs for TB diagnosis was moderate, the specificity was notably high, yielding an overall favorable diagnostic effect. These findings suggest that oral swabs may serve as suitable specimens for rule-in testing in the diagnosis of pulmonary TB. Nonetheless, the records included exhibited considerable heterogeneity. This was mainly due to variations in the collection process of oral swabs and the number of participants in the studies. For instance, in a study by Wood et al. (21) found that oral swabs had high sensitivity and specificity for the diagnosis of pulmonary TB. However, the sample size was small, and the set positive threshold was larger than other studies (21). Another study by Wood et al. (20) revealed that increasing the number of participants and lowering the positive threshold of OSA resulted in a reduced specificity and slightly decreased sensitivity for diagnosing pulmonary TB. Nevertheless, the sensitivity still remained high in such instances, with Xpert-positive TB as the reference standard (20). Notably, when using the TB-LAMP method (24) or combining samples from two consecutive days (14) for OSA, both sensitivity and specificity were improved. These results highlight the presence of heterogeneity in the available data, emphasizing the need for further investigation into improving the implementation methodology of OSA and establishing appropriate thresholds to enhance sensitivity and specificity. Consequently, conducting more robust studies in this area becomes imperative.

In this study, we performed a subgroup analysis of various factors related to OSA for diagnosing individuals with pulmonary TB. Our finding revealed a high specificity of OSA for diagnosing pulmonary TB across various subgroups. Specifically, our analysis

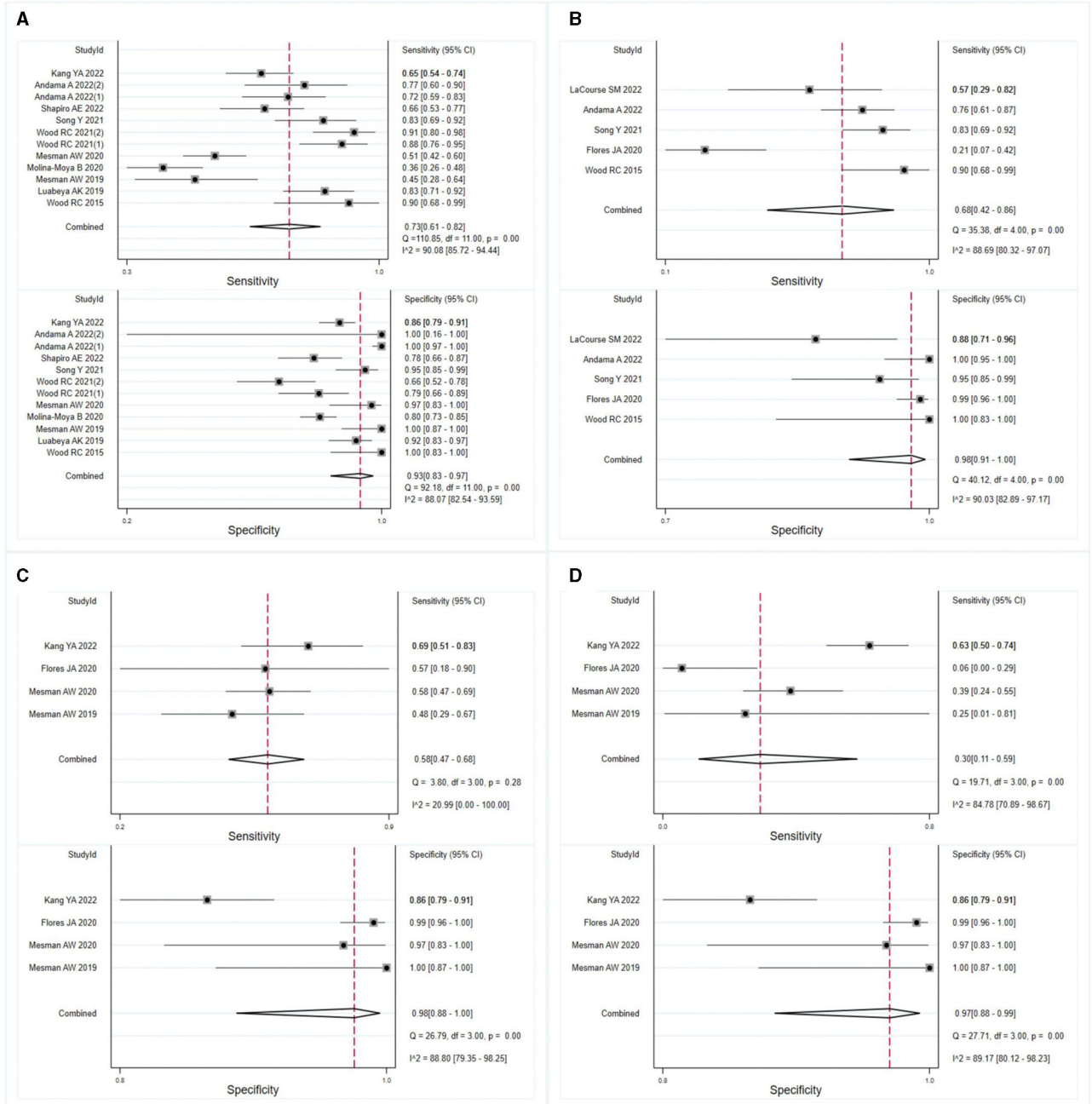

FIGURE 3
Meta-analysis assessed the sensitivity and specificity of OSA in diagnosing individuals with pulmonary TB. The results were stratified by **(A)** adult individuals with pulmonary TB, **(B)** HIV-negative individuals with pulmonary TB, **(C)** smear-positive individuals with pulmonary TB, and **(D)** smear-negative individuals with pulmonary TB.

revealed a higher combined sensitivity of OSA for diagnosing pulmonary TB in adults compared to in children, as observed in studies by Nicol et al. (16) and Flores et al. (13). However, the sensitivity was lower for diagnosing pulmonary TB in HIV-negative individuals compared to HIV-positive individuals, according to LaCourse et al. (27), but higher than in the study by Andama et al. (17). These results suggest that OSA is a reliable method for diagnosing pulmonary TB in adults. However, caution is warranted in the case of HIV-positive individuals with pulmonary TB. Notably, Cox et al. found that the yield of microbiologic confirmation using oral swab specimens in children with pulmonary TB was suboptimal (18). Flores et al. demonstrated that tongue swabs can be employed for diagnosing TB in children who are clinically diagnosed with TB but are unable to produce sputum samples (33). Nevertheless, interpretation of these results requires caution as the number of studies on diagnosing OSA in children with pulmonary TB and HIV-positive individuals with pulmonary TB is limited. Further investigations are necessary to

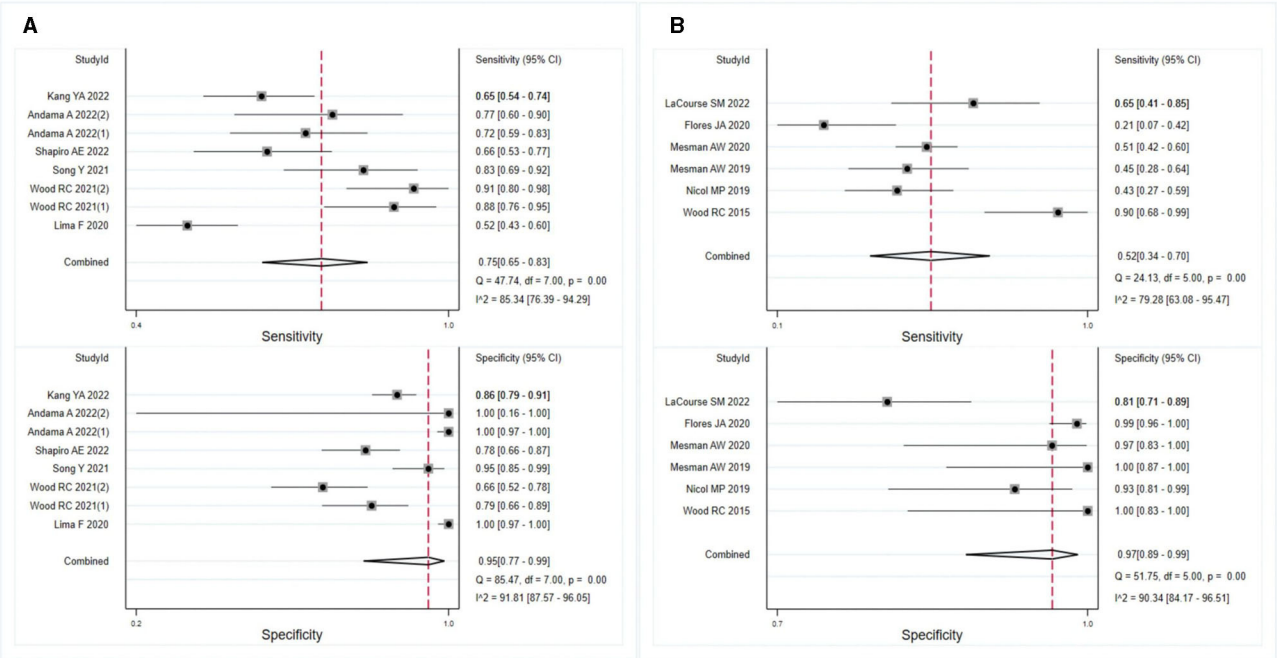

FIGURE 4
Meta-analysis of the sensitivity and specificity of tongue and cheek specimens of OSA in diagnosing pulmonary TB. **(A)** Results of meta-analysis on tongue specimens in diagnosing pulmonary TB; **(B)** results of meta-analysis on cheek specimens in diagnosing pulmonary TB.

TABLE 2 **Pooled results of OSA in the diagnosis of TB patients.**

Group	Sensitivity (95% CI)	Specificity (95% CI)	Positive LR (95% CI)	Negative LR (95% CI)	Diagnostic OR (95% CI)	SROC (95% CI)
Overall	0.67 (0.55–0.77)	0.95 (0.88–0.98)	12.6 (5.4–29.0)	0.35 (0.26–0.48)	36 (14–89)	0.88 (0.85–0.91)
Adult	0.73 (0.61–0.82)	0.93 (0.83–0.97)	10.4 (4.2–25.7)	0.29 (0.20–0.43)	35 (12–102)	0.89 (0.86–0.92)
HIV negative	0.68 (0.42–0.86)	0.98 (0.91–1.00)	34.4 (7.3–162.5)	0.32 (0.15–0.67)	107 (17–690)	0.96 (0.94–0.98)
Smear positive TB	0.58 (0.47–0.68)	0.98 (0.88–1.00)	23.1 (5.0–107.0)	0.43 (0.34–0.54)	53 (12–244)	0.73 (0.69–0.76)
Smear negative TB	0.30 (0.11–0.59)	0.97 (0.88–0.99)	9.6 (3.5–26.5)	0.73 (0.52–1.01)	13 (5–38)	0.83 (0.79–0.86)
Tongue	0.75 (0.65–0.83)	0.95 (0.77–0.99)	13.8 (3.1–61.8)	0.26 (0.19–0.37)	53 (12–233)	0.87 (0.84–0.90)
Cheek	0.52 (0.34–0.70)	0.97 (0.89–0.99)	15.9 (4.6–54.8)	0.49 (0.34–0.72)	32 (8–124)	0.88 (0.85–0.91)

LR, likelihood ratio; OR, odds ratio; SROC, summary receiver operator characteristic curve; HIV, human immunodefificiency virus.

validate these findings. Moreover, in this meta-analysis, we assessed the diagnostic efficacy of OSA in individuals with pulmonary TB who had positive and negative sputum smear test results. Our analysis revealed that OSA exhibited a higher sensitivity in diagnosing pulmonary TB in individuals with positive sputum smear test results compared to those with negative test results. Flores et al. observed a positive correlation between positive sputum smear results and the detection of MTB in oral specimens (13). This suggests that the detection rate of MTB by oral swabs is proportional to the amount of MTB present in sputum. Consequently, oral swabs can serve as a viable substitute for sputum specimens in the diagnosis of TB.

While OSA can be utilized for diagnosing TB, it is important to note that their sensitivity is lower compared to the detection of TB using sputum specimens with the Xpert MTB/RIF and Xpert MTB/RIF Ultra methods, as indicated by previous study (34). However, in children with suspected pulmonary TB, OSA exhibits higher diagnostic sensitivity in comparison to using Xpert MTB/RIF for detecting sputum specimens and is comparable to the sensitivity of Xpert MTB/RIF Ultra for sputum specimen detection (35). Moreover, the sensitivity of OSA in diagnosing HIV-positive individuals with pulmonary TB (27) is similar to that of TB detection using Xpert MTB/RIF and Xpert MTB/RIF Ultra methods for sputum specimens (36). It is crucial to note that these conclusions are based on a limited number of studies examining the use of OSA as a diagnostic tool for pulmonary TB, highlighting the necessity for additional high-quality studies to confirm its utility in the future. To enhance the diagnostic effectiveness of OSA in pulmonary TB, optimization tests can be conducted. Supplementary Table 3 provides a comprehensive

overview of the data we used from OSA in this study. Our previous research demonstrated that the TB-LAMP method we utilized to detect MTB in tongue swabs for diagnosing pulmonary TB yielded high sensitivity and specificity (24). Additionally, Andama et al. demonstrated that the sensitivity of Xpert MTB/RIF Ultra method for detecting MTB in tongue swabs was also relatively high, with a specificity of 100% (17). We recommend conducting further studies employing different methods to detect MTB in tongue swabs, thereby improving the sensitivity and specificity of OSA.

Tongue and cheek swabs are oral specimens commonly employed for the diagnosis of TB, although their exact diagnostic value remains uncertain. In this study, we conducted a meta-analysis focusing on tongue and cheek swabs collected via the use of OSA to diagnose pulmonary TB. The results of the meta-analysis revealed that tongue swabs exhibited higher sensitivity than cheek swabs when utilizing OSA for TB diagnosis, while their specificity remained comparable. The summary findings strongly underscore the importance of utilizing tongue swabs for the diagnosis of pulmonary TB, attributing their superior sensitivity to the fact that MTB primarily colonize the epithelial cells on the surface of the tongue. For future developments in the field of OSA-based diagnosis of pulmonary TB, we highly recommend the utilization of tongue swabs. However, it is crucial to note that despite conducting a subgroup analysis, the presence of substantial heterogeneity observed amongst the results emphasizes significant variability across the studies included in the analysis. Hence, there is a pressing need to establish standardized protocols for conducting OSA to ensure consistency and reliability in its diagnostic applications.

A limitation of the current work is the relatively small number of publications available on this particular topic. Despite ongoing and extensive research in the field of OSA for diagnosing TB, only a limited number of articles met our eligibility criteria. Adding complexity to the analysis is the lack of methodological consistency across studies and insufficient reporting of methods and outcome parameters. Additionally, there are several other confounding factors that might have affected the diagnostic effectiveness of OSA in pulmonary TB, including the method of sample collection, swab storage buffer, storage period before testing, DNA extraction method and detection method. Consequently, the heterogeneity among the included studies was significant, thereby impacting the analysis in this study.

In conclusion, our findings suggest that oral swabs serve as a promising alternative for diagnosing pulmonary TB, particularly in adult patients. Notably, tongue swabs exhibit superior sensitivity compared to cheek swabs in detecting individuals with pulmonary TB. However, further rigorous assessment with a larger sample size, focusing on populations such as HIV-positive individuals and children, is warranted to validate the diagnostic performance of OSA. Furthermore, we strongly advocate for future studies to offer comprehensive information regarding collection procedures, enabling the field to better comprehend the necessary trade-offs required for the successful implementation and scalability of OSA in TB diagnosis.

Data availability statement

The original contributions presented in the study are included in the article/Supplementary material, further inquiries can be directed to the corresponding authors.

Author contributions

FZ: Writing – original draft, Data curation, Formal analysis, Investigation, Methodology, Software. YW: Data curation, Formal analysis, Investigation, Validation, Writing – review & editing. XZ: Data curation, Formal analysis, Investigation, Writing – review & editing, Supervision. KL: Formal analysis, Supervision, Writing – review & editing, Methodology. YS: Formal analysis, Methodology, Supervision, Writing – review & editing. WW: Formal analysis, Methodology, Supervision, Writing – review & editing. YL: Formal analysis, Methodology, Supervision, Writing – review & editing. LL: Conceptualization, Funding acquisition, Writing – original draft. YP: Conceptualization, Funding acquisition, Writing – original draft.

Funding

The author(s) declare financial support was received for the research, authorship, and/or publication of this article. This work was supported by the Beijing Hospitals Authority Ascent Plan (DFL20191601 & DFL20221401).

Conflict of interest

The authors declare that the research was conducted in the absence of any commercial or financial relationships that could be construed as a potential conflict of interest.

Publisher's note

Supplementary material

The Supplementary Material for this article can be found online at: https://www.frontiersin.org/articles/10.3389/fmed.2023.1278716/full#supplementary-material

References

1. World Health Organization. *Global tuberculosis report 2022*. Geneva: World Health Organization (2022). Available online at: https://www.who.int/teams/global-tuberculosis-programme/data (accessed October 27, 2022).

2. Chakaya J, Khan M, Ntoumi F, Aklillu E, Fatima R, Mwaba P, et al. Global Tuberculosis Report 2020 - Reflections on the Global TB burden, treatment and prevention efforts. *Int J Infect Dis.* (2021) 113:S7–S12. doi: 10.1016/j.ijid.2021.02.107

3. van Cutsem G, Isaakidis P, Farley J, Nardell E, Volchenkov G, Cox H. Infection control for drug-resistant tuberculosis: early diagnosis and treatment is the key. *Clin Infect Dis.* (2016) 62:S238–S43. doi: 10.1093/cid/ciw012

4. Denkinger CM, Pai M. Point-of-care tuberculosis diagnosis: are we there yet? *Lancet Infect Dis.* (2012) 12:169–70. doi: 10.1016/S1473-3099(11)70257-2

5. Ryu YJ. Diagnosis of pulmonary tuberculosis: recent advances and diagnostic algorithms. *Tuberc Respir Dis.* (2015) 78:64–71. doi: 10.4046/trd.2015.78.2.64

6. Acharya B, Acharya A, Gautam S, Ghimire SP, Mishra G, Parajuli N, et al. Advances in diagnosis of Tuberculosis: an update into molecular diagnosis of *Mycobacterium tuberculosis*. *Mol Biol Rep.* (2020) 47:4065–75. doi: 10.1007/s11033-020-05413-7

7. Bulterys MA, Wagner B, Redard-Jacot M, Suresh A, Pollock NR, Moreau E, et al. Point-of-care urine LAM tests for tuberculosis diagnosis: a status update. *J Clin Med.* (2020) 9:111. doi: 10.3390/jcm9010111

8. Klompas M, Baker M, Rhee C. What is an aerosol-generating procedure? *JAMA Surg.* (2021) 156:113–4. doi: 10.1001/jamasurg.2020.6643

9. Alisjahbana B, van Crevel R, Danusantoso H, Gartinah T, Soemantri ES, Nelwan RHH, et al. Better patient instruction for sputum sampling can improve microscopic tuberculosis diagnosis. *Int J Tuberc Lung Dis.* (2005) 9:814–7.

10. Shenai S, Amisano D, Ronacher K, Kriel M, Banada PP, Song T, et al. Exploring alternative biomaterials for diagnosis of pulmonary tuberculosis in HIV-negative patients by use of the GeneXpert MTB/RIF assay. *J Clin Microbiol.* (2013) 51:4161–6. doi: 10.1128/JCM.01743-13

11. Nicol MP, Spiers K, Workman L, Isaacs W, Munro J, Black F, et al. Xpert MTB/RIF testing of stool samples for the diagnosis of pulmonary tuberculosis in children. *Clin Infect Dis.* (2013) 57:E18–21. doi: 10.1093/cid/cit230

12. Molina-Moya B, Ciobanu N, Hernandez M, Prat-Aymerich C, Crudu V, Adams ER, et al. Molecular detection of *Mycobacterium tuberculosis* in oral mucosa from patients with presumptive tuberculosis. *J Clin Med.* (2020) 9:4124. doi: 10.3390/jcm9124124

13. Flores JA, Calderon R, Mesman AW, Soto M, Coit J, Aliaga J, et al. Detection of *Mycobacterium tuberculosis* DNA in buccal swab samples from children in Lima, Peru. *Pediatr Infect Dis J.* (2020) 39:E376–E80. doi: 10.1097/INF.0000000000002828

14. Luabeya AK, Wood RC, Shenje J, Filander E, Ontong C, Mabwe S, et al. Noninvasive detection of tuberculosis by oral swab analysis. *J Clin Microbiol.* (2019) 57:10–1128. doi: 10.1128/JCM.01847-18

15. Mesman AW, Calderon R, Soto M, Coit J, Aliaga J, Mendoza M, et al. *Mycobacterium tuberculosis* detection from oral swabs with Xpert MTB/RIF ULTRA: a pilot study. *BMC Res Notes.* (2019) 12:349. doi: 10.1186/s13104-019-4385-y

16. Nicol MP, Wood RC, Workman L, Prins M, Whitman C, Ghebrekristos Y, et al. Microbiological diagnosis of pulmonary tuberculosis in children by oral swab polymerase chain reaction. *Sci Rep.* (2019) 9:10789. doi: 10.1038/s41598-019-47302-5

17. Andama A, Whitman GR, Crowder R, Reza TF, Jaganath D, Mulondo J, et al. Accuracy of tongue swab testing using Xpert MTB-RIF ultra for tuberculosis diagnosis. *J Clin Microbiol.* (2022) 60:e0042122. doi: 10.1128/jcm.00421-22

18. Cox H, Workman L, Bateman L, Franckling-Smith Z, Prins M, Luiz J, et al. Oral swab specimens tested with xpert MTB/RIF ultra assay for diagnosis of pulmonary tuberculosis in children: a diagnostic accuracy study. *Clin Infect Dis.* (2022) 75:2145–52. doi: 10.1093/cid/ciac332

19. Whiting PF, Rutjes AW, Westwood ME, Mallett S, Deeks JJ, Reitsma JB, et al. QUADAS-2: a revised tool for the quality assessment of diagnostic accuracy studies. *Ann Intern Med.* (2011) 155:529–36. doi: 10.7326/0003-4819-155-8-201110180-00009

20. Wood RC, Andama A, Hermansky G, Burkot S, Asege L, Job M, et al. Characterization of oral swab samples for diagnosis of pulmonary tuberculosis. *PLoS ONE.* (2021) 16:e0251422. doi: 10.1371/journal.pone.0251422

21. Wood RC, Luabeya AK, Weigel KM, Wilbur AK, Jones-Engel L, Hatherill M, et al. Detection of *Mycobacterium tuberculosis* DNA on the oral mucosa of tuberculosis patients. *Sci Rep.* (2015) 5:8668. doi: 10.1038/srep08668

22. Lima F, Santos AS, Oliveira RD, Silva CCR, Goncalves CCM, Andrews JR, et al. Oral swab testing by Xpert(R) MTB/RIF Ultra for mass tuberculosis screening in prisons. *J Clin Tuberc Other Mycobact Dis.* (2020) 19:100148. doi: 10.1016/j.jctube.2020.100148

23. Mesman AW, Calderon RI, Pollock NR, Soto M, Mendoza M, Coit J, et al. Molecular detection of *Mycobacterium tuberculosis* from buccal swabs among adult in Peru. *Sci Rep-Uk.* (2020) 10:22231. doi: 10.1038/s41598-020-79297-9

24. Song Y, Ma Y, Liu R, Shang Y, Ma L, Huo F, et al. Diagnostic yield of oral swab testing by TB-LAMP for diagnosis of pulmonary tuberculosis. *Infect Drug Resist.* (2021) 14:89–95. doi: 10.2147/IDR.S284157

25. Shapiro AE, Olson AM, Kidoguchi L, Niu X, Ngcobo Z, Magcaba ZP, et al. Complementary nonsputum diagnostic testing for tuberculosis in people with HIV using oral swab PCR and urine Lipoarabinomannan detection. *J Clin Microbiol.* (2022) 60:e0043122. doi: 10.1128/jcm.00431-22

26. Kang YA, Koo B, Kim OH, Park JH, Kim HC, Lee HJ, et al. Gene-based diagnosis of tuberculosis from oral swabs with a new generation pathogen enrichment technique. *Microbiol Spectr.* (2022) 10:e0020722. doi: 10.1128/spectrum.00207-22

27. LaCourse SM, Seko E, Wood R, Bundi W, Ouma GS, Agaya J, et al. Diagnostic performance of oral swabs for non-sputum based TB diagnosis in a TB/HIV endemic setting. *PLoS ONE.* (2022) 17:e0262123. doi: 10.1371/journal.pone.0262123

28. Jo KW. Preventing the transmission of tuberculosis in health care settings: administrative control. *Tuberc Respir Dis.* (2017) 80:21–6. doi: 10.4046/trd.2017.80.1.21

29. Wilbur AK, Engel GA, Rompis A, Ig AP, Lee BP, Aggimarangsee N, et al. From the mouths of monkeys: detection of *Mycobacterium tuberculosis* complex DNA from buccal swabs of synanthropic macaques. *Am J Primatol.* (2012) 74:676–86. doi: 10.1002/ajp.22022

30. Meesawat S, Warit S, Hamada Y, Malaivijitnond S. Prevalence of *Mycobacterium tuberculosis* complex among wild rhesus macaques and 2 subspecies of long-tailed macaques, Thailand, 2018-2022. *Emerg Infect Dis.* (2023) 29:551–60. doi: 10.3201/eid2903.221486

31. Rosenbaum M, Mendoza P, Ghersi BM, Wilbur AK, Perez-Brumer A, Cavero Yong N, et al. Detection of *Mycobacterium tuberculosis* complex in new world monkeys in Peru. *Ecohealth.* (2015) 12:288–97. doi: 10.1007/s10393-014-0996-x

32. Valinetz ED, Cangelosi GA. A look inside: oral sampling for detection of non-oral infectious diseases. *J Clin Microbiol.* (2021) 59:e0236020. doi: 10.1128/JCM.02360-20

33. Ealand C, Peters J, Jacobs O, Sewcharran A, Ghoor A, Golub J, et al. Detection of *Mycobacterium tuberculosis* complex bacilli and nucleic acids from tongue swabs in young, hospitalized children. *Front Cell Infect Microbiol.* (2021) 11:696379. doi: 10.3389/fcimb.2021.696379

34. Horne DJ, Kohli M, Zifodya JS, Schiller I, Dendukuri N, Tollefson D, et al. Xpert MTB/RIF and Xpert MTB/RIF Ultra for pulmonary tuberculosis and rifampicin resistance in adults. *Cochrane Database Syst Rev.* (2019) 6:CD009593. doi: 10.1002/14651858.CD009593.pub4

35. Pradhan NN, Paradkar MS, Kagal A, Valvi C, Kinikar A, Khwaja S, et al. Performance of Xpert® MTB/RIF and Xpert® Ultra for the diagnosis of tuberculous meningitis in children. *Int J Tuberc Lung Dis.* (2022) 26:317–25. doi: 10.5588/ijtld.21.0388

36. Esmail A, Tomasicchio M, Meldau R, Makambwa E, Dheda K. Comparison of Xpert MTB/RIF (G4) and Xpert Ultra, including trace readouts, for the diagnosis of pulmonary tuberculosis in a TB and HIV endemic setting. *Int J Infect Dis.* (2020) 95:246–52. doi: 10.1016/j.ijid.2020.03.025

frontiers | Frontiers in Microbiology

TYPE Original Research
PUBLISHED 25 March 2024
DOI 10.3389/fmicb.2024.1301204

OPEN ACCESS

EDITED BY
Robert Jansen,
Radboud University, Netherlands

REVIEWED BY
Khushboo Borah Slater,
University of Surrey, United Kingdom
Martin S. Pavelka,
University of Rochester, United States

*CORRESPONDENCE
Yu Lu
✉ luyu4876@hotmail.com
Xuefu You
✉ xuefuyou@imb.pumc.edu.cn
Xinyi Yang
✉ xinyiyang@imb.cams.cn

†These authors have contributed equally to this work

RECEIVED 24 September 2023
ACCEPTED 01 March 2024
PUBLISHED 25 March 2024

CITATION
Lu Y, Chen H, Shao Z, Sun L, Li C, Lu Y, You X and Yang X (2024) Deletion of the *Mycobacterium tuberculosis cyp138* gene leads to changes in membrane-related lipid composition and antibiotic susceptibility. *Front. Microbiol.* 15:1301204. doi: 10.3389/fmicb.2024.1301204

Deletion of the *Mycobacterium tuberculosis cyp138* gene leads to changes in membrane-related lipid composition and antibiotic susceptibility

Yun Lu[1,2†], Hongtong Chen[1,2,3†], Zhiyuan Shao[1,2,3], Lang Sun[1,2,3], Congran Li[1,2], Yu Lu[4*], Xuefu You[1,2,3*] and Xinyi Yang[1,2*]

[1]Beijing Key Laboratory of Antimicrobial Agents, Institute of Medicinal Biotechnology, Chinese Academy of Medical Sciences and Peking Union Medical College, Beijing, China, [2]Division for Medicinal Microorganisms-related Strains, CAMS Collection Center of Pathogenic Microorganisms, Beijing, China, [3]State Key Laboratory of Bioactive Substances and Functions of Natural Medicines, Institute of Medicinal Biotechnology, Chinese Academy of Medical Sciences & Peking Union Medical College, Beijing, China, [4]Beijing Key Laboratory of Drug Resistance Tuberculosis Research, Beijing Tuberculosis and Thoracic Tumor Research Institute, and Beijing Chest Hospital, Capital Medical University, Beijing, China

Introduction: *Mycobacterium tuberculosis* (*Mtb*), the main cause of tuberculosis (TB), has brought a great burden to the world's public health. With the widespread use of *Mtb* drug-resistant strains, the pressure on anti-TB treatment is increasing. Anti-TB drugs with novel structures and targets are urgently needed. Previous studies have revealed a series of CYPs with important roles in the survival and metabolism of *Mtb*. However, there is little research on the structure and function of CYP138.

Methods: In our study, to discover the function and targetability of CYP138, a *cyp138*-knockout strain was built, and the function of CYP138 was speculated by the comparison between *cyp138*-knockout and wild-type strains through growth curves, growth status under different carbon sources, infection curves, SEM, MIC tests, quantitative proteomics, and lipidomics.

Results and discussion: The knockout of *cyp138* was proven to affect the *Mtb*'s macrophage infection, antibiotics susceptibility, and the levels of fatty acid metabolism, membrane-related proteins, and lipids such as triacylglycerol. We proposed that CYP138 plays an important role in the synthesis and decomposition of lipids related to the cell membrane structure as a new potential anti-tuberculosis drug target.

KEYWORDS

***Mycobacterium tuberculosis*, CYP138, gene knock-out, membrane-related lipids, antibiotics susceptibility, triacylglycerol**

1 Introduction

Tuberculosis (TB), caused mainly by *Mycobacterium tuberculosis* (*Mtb*), is the leading cause of death from a single infection. WHO reported that an estimated 10.6 million people (95% UI: 9.9–11.4 million) fell ill with TB in 2022 worldwide, and China was one of the highest TB burden countries (World Health Organization, 2023). With the continuous and widespread use of first-line anti-tuberculosis drugs, multidrug-resistant (MDR) and extensively drug-resistant (XDR) TB appeared and posed great threats to public health (Mabhula and Singh, 2019). Anti-TB drugs with novel structures and targets are urgently needed to prevent the prevalence of drug-resistant strains.

Cytochromes P450s (CYPs) are monooxygenases that usually interact with flavoprotein and/or iron-sulfur central redox partners to perform catalysis (Lu et al., 2017). They are found in diverse species, from bacteria to vertebrates, and are known to be involved in the primary and secondary metabolisms of organisms (Nelson, 2018). CYPs from humans are closely related to the metabolism of numerous exogenous (i.e., drugs and polycyclic aromatic hydrocarbons) and endogenous molecules (i.e., steroids, vitamins, eicosanoids, and neurotransmitters), while CYPs from bacteria were found to be involved in species-specific biological processes such as antibiotic synthesis and nitric oxide reduction (Munro et al., 2003; McLean et al., 2010; Elfaki et al., 2018; Msomi et al., 2021).

The determination of the *Mtb* H37Rv genome sequence has revealed that 20 different CYP genes exist, indicating their vital roles in the survival or pathogenicity of *Mtb* H37Rv (McLean et al., 2006; Hudson et al., 2012). For the past few decades, *Mtb* CYPs have attracted lots of attention from researchers, and some of them have been structurally and functionally characterized. CYP51B1 (the first revealed prokaryotic sterol demethylase in prokaryotes) has been proven to be a promising anti-TB drug target (Podust et al., 2001). CYP124, CYP125, and CYP142 were found to be related to cholesterol metabolism (Johnston et al., 2012). CYP121 is shown to be essential for the viability of *Mtb*, and screening has been performed to find inhibitors (Kavanagh et al., 2016). CYP130 has been identified as an individually expressed protein, along with CYP51 and CYP121 (Ouellet et al., 2008). CYP128 is sufficient for the biosynthesis of sulfomenaquinone from menaquinone, which is related to *Mtb* virulence (Sogi et al., 2016). CYP141 is an intermediary metabolic and respiratory protein, whose gene was proved to be a good genotypic marker for direct detection of *Mtb* (Darban-Sarokhalil et al., 2011). Furthermore, CYP126, CYP143, and CYP144 were also purified and crystallized (Swami, 2015; Chenge et al., 2016). CYP139 was predicted to play a role in the synthesis of secondary metabolites in mycobacterial species (Syed et al., 2019).

CYP138 belongs to the *Mtb* CYPs, whose structures and functions are still unclear. Although transposon insertion mutagenesis (TRaSH)-based gene-deficient screening tentatively suggested that *cyp138* is non-essential for the survival of *Mtb* (Murphy and Brown, 2007), phylogenetic tree analysis of the amino acid sequences of CYP138 from the NCBI protein database revealed it highly conserved (99%) across *Mtb* complex species, including *Mycobacterium canettii*, *Mtb* variant bovis BCG, etc. (Supplementary Figure S1), suggesting the possibility of species-specific functions that we do not yet know. In addition, in a study on the influence of HIV on the evolution of *Mtb*, it was vaguely mentioned that CYP138 may indirectly interact with human proteins, thereby functionally interacting with HIV proteins (Koch et al., 2017). However, to date, little is known about the more detailed roles of the CYP enzyme.

To better understand the function and roles of CYP138 in *Mtb*, in our study, *cyp138* was knocked out from the *Mtb* genome by homologous recombination, and differences in the surface morphology, growth curve, growth status under different carbon sources, ability to infect macrophages, and antimicrobial susceptibility among *Mtb* H37Rv (wild-type), *cyp138*-knockout (Δ138), and *cyp138* complementary strains (Δ138-C) were evaluated. Proteomics and lipidomics were helpful tools for investigating mechanisms and elucidating the functions and roles of targeted proteins or genes (Jain et al., 2007; Qin et al., 2023). A more diverse dataset of molecular changes can be acquired by a multi-omics approach, which can help us with the functional clarification of targeted proteins or genes. Thus, to further characterize the specific effects or consequences of *cyp138*-knockout on profiles of protein expression and lipid production in *Mtb*, quantitative proteomes and lipidomes were used for large-scale comparative analysis of protein and lipid metabolite changes in the *cyp138*-knockout strain, and targeted proteomes based on parallel reaction monitoring (PRM) and thin layer chromatography (TLC) were used to confirm the changes.

2 Materials and methods

2.1 Bacterial strains and growth conditions

The wild-type and Δ138 strains were grown in the 7H9 medium supplemented with 0.2% (v/v) glycerol, 0.05% (v/v) Tween 80, and 10% (v/v) oleic acid albumin dextrose catalase [OADC, Becton, Dickinson, and Company (BD), United States] at 37°C. The Δ138-C was cultured in the 7H9 broth mentioned above, supplemented with an additional 10 $\mu g \cdot ml^{-1}$ (Gentamicin, GM). All strains were cultured on the 7H10 culture plate supplemented with 10% OADC at 37°C for 14 days.

2.2 Vector construction

Gene deletion was achieved by overlap extension PCR (Lee et al., 2004), as shown in Figure 1A. Through a two-step PCR process, only the 493-bp fragment of the *Rv0136* coding gene (with a full length of 1,326 bp) was retained. A suicide vector was generated by amplifying the flanking gene of *Rv0136* (*cyp138*) using primer pairs Fa 5′-ACAAGCTT TTCAGACCAGGGAAATGC-3′, Rb 5′-ATGGCTTACGGAACCGAACATCCGACT-3′, Fc 5′-TTCGGTTCC GTAAGCCATCCCCGTTTG-3′, and Rd 5′-ATGCGGCCGC ATCACCGACCACAGCGAC-3′ and cloned into p2NIL by HindIII-NotI restriction sites. Then the hygR, lacZ, and sacB cassettes from pGOAL19 were inserted into the p2NIL-Δ*cyp138* plasmid by Pac I to generate the suicide vector pGNL138. A complementing vector pCM138 was generated by amplifying the gene of *Rv0136*(*cyp138*) using primers 5′-GATTAATTAAGATCGAGGCGACCAGGCC-3′ and 5′-ATC TTAATTAAGGTGACCGAGGTCAGCCC-3′ and cloned into pAPA3 by Pac I restriction site (Brown, 2009). For the PCR of gene sequences with high GC abundance, GC buffer (Takara-Bio, Dalian, China) was used to reduce non-specific amplification.

2.3 Gene switching and essentiality testing

The single crossover strain (SCO) was generated by transforming the suicide vector pGNL138 carrying the in-frame deletion into the *Mtb* H37Rv strain. Double crossover strain (DCO) was then generated by transforming the complementing vector pCM138 into SCO, and sucrose with gradient concentrations was

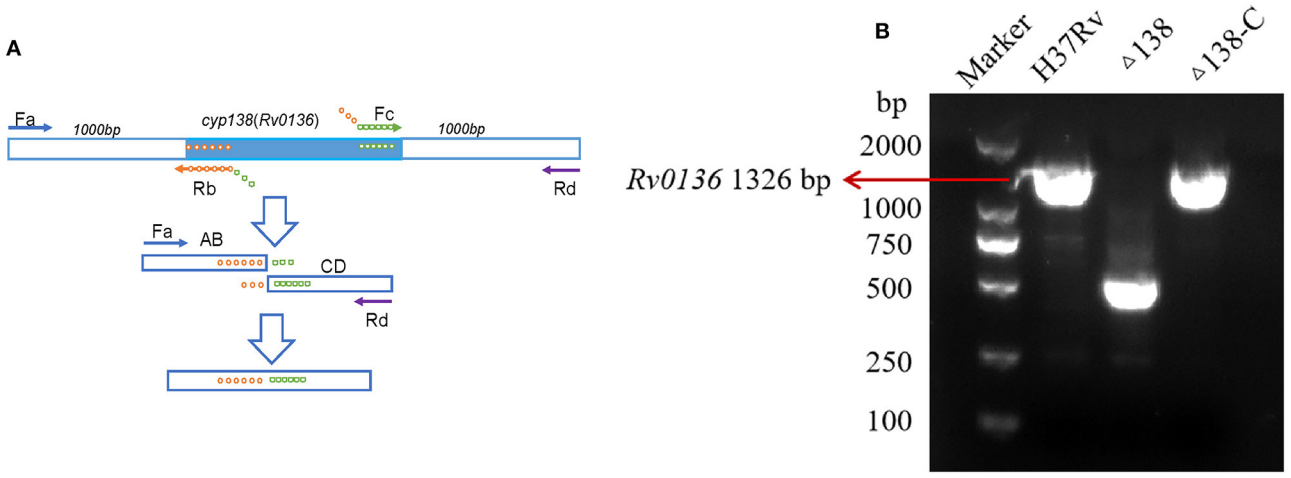

FIGURE 1
(A) Gene deletion by overlap extension PCR. For the first step, four primers were needed; the products of the first step were used for the template of the second step. **(B)** Primers that can replicate gene ORF, also used to construct complementary plasmids, were used for the PCR confirmation of wild-type, Δ138, and Δ138-C strains. PCR results of the *cyp138* gene in the wild-type, Δ138 (*cyp138*-knockout), and complementary strains (Δ138-C).

used to screen positive strains. DCO was then electroporated with a pUC-Hyg-Int plasmid to switch the complementing vector for essentiality confirmation (Brown, 2009).

2.4 Evaluation of bacterial growth status

The growth curves of the wild-type, Δ138, and Δ138-C were measured as previously reported (Penuelas-Urquides et al., 2013). Briefly, the bacterial suspension was diluted using 7H9 medium to $OD_{600} = 0.01$ and then cultured at 37°C with 5% CO_2 for 3 weeks. Three biological replicates were measured for each group, and the same volume of suspension was taken and measured at OD_{600}.

For growth on defined carbon sources, strains were grown in minimal medium (0.5 g·L^{-1} asparagine, 1.0 g·L^{-1} KH_2PO_4, 2.5 g·L^{-1} Na_2HPO_4, 50 mg·L^{-1} ferric ammonium citrate, 0.5 g·L^{-1} $MgSO_4{\cdot}7H_2O$, 0.5 mg·L^{-1} $CaCl_2$, 0.1 mg·L^{-1} $ZnSO_4$, and 0.05% tyloxapol) containing 0.1% glycerol (v/v) or 0.01% cholesterol (wt/v). Before addition, cholesterol was dissolved to 100 mg·ml^{-1} in a solution of tyloxapol/ethanol (1:1) at 80°C for 30 min (Lee et al., 2013). Bacterial growth under different carbon source conditions was monitored by measuring the optical density at 600 nm of strains on days 0, 7, and 14.

2.5 Macrophage infection

The macrophage infection experiment for *Mtb* was performed as previously reported, with slight changes (Hu et al., 2006; Xu et al., 2017). The wild-type, Δ138, and Δ138-C strains were grown at 37°C in 7H9 broth for 21 days. The J774A.1 macrophage cell line was cultured in DMEM medium (Gibco, United States), supplemented with 10% fetal bovine serum (FBS) at 37°C with 5% CO_2. Macrophages were seeded in 24-well culture plates at a density of 4×10^5 cells per well in DMEM medium with 10% FBS and incubated for 16 h at 37°C with 5% CO_2. Infection of J774A.v1 cells with wild-type, Δ138, and Δ138-C strains was performed at a multiplicity of infection (MOI) of 1:1 (bacteria/macrophage). After incubation for 4 h, cells were washed twice with a fresh medium to remove extracellular bacteria. Fresh DMEM medium containing 10% FBS was added per well, and the cells were cultured at 37°C with 5% CO_2. Macrophages were lysed with 200 μl 0.1% SDS at 37°C for 5 min separately at 0, 1, 3, 5, and 7 days after infection, and a fresh medium was added to terminate lysis. The mixture was diluted to a proper concentration by serial dilutions, and then 100 μl of samples were spread onto the 7H10 culture plate and incubated at 37°C with 5% CO_2. After 3 weeks, the colonies' numbers of the wild-type, Δ138, and Δ138-C strains were counted, respectively.

2.6 Scanning electron microscope

The wild-type, Δ138, and Δ138-C strains were cultured in the Middlebrook 7H9 medium supplemented with 0.2% glycerol, 10% OADC, and 0.05% tyloxapol for 14 days. One ml of bacteria cultures were collected by centrifugation at 5,000 × *g* for 5 min, and 1 × PBS buffer was used to wash the collected bacteria. 2.5% glutaraldehyde solution was added, and samples were kept at RT for 1 h, and then at 4°C overnight. The prepared samples were then examined using a scanning electron microscope (SU8020).

2.7 Minimum inhibitory concentration tests

The MIC of different antimicrobials against the wild-type, Δ138, and Δ138-C strains were measured using the micro-dilution method. The strains were cultured in 7H9 medium. Antimicrobials including ampicillin, polymyxin B, trimethoxil, actinomycin, rifampicin, isoniazid, ethambutol, streptomycin, levofloxacin,

erythromycin, tetracycline, minocycline, D-cycloserine, and vancomycin were included in the test. Results were measured by the microplate alamar blue assay (MABA) and were performed in 96-well black microplates (Collins and Franzblau, 1997). Antimicrobials in gradient concentrations were prepared from 2-fold serial dilutions in the 7H9 medium. The same volume of diluted bacterial samples was transferred to the wells of a 96-well plate to obtain a final density of 5×10^5 CFU·ml^{-1}. Three biological replicates were performed for all the groups. Microplates were then incubated at 37°C for 7 days. Alamar blue and 20% Tween-80 were added, and microplates were incubated at 37°C for 1 day. Alamar color will change from blue to purple with bacteria growth. The minimum drug concentration that inhibits bacterial growth is the MIC value.

2.8 Protein extraction and TMTsixplex quantitative proteomics analysis

The wild-type and Δ138 strains were cultured as mentioned above. Three biological replicates were prepared, and bacteria of different groups were harvested at the logarithmic ($OD_{600} = 0.6$) phase. The same amounts of bacteria were collected and suspended in SDC buffer (50 mM NH_4HCO_3, 2% sodium deoxycholate, 75 mM NaCl, pH 8.5). Then ultrasonication (3s on, 6s rest, 30%) was used to help lysis. Protein solutions were heated at 95°C for 20 min, and their concentrations were determined using a BCA protein quantification kit. Two hundred μg of proteins from each sample were reduced by 10 mM dithiothreitol (DTT) and digested by trypsin (1:50 (w/w), Promega, Madison, WI, United States) overnight at 37°C. SDC was removed by 1% formic acid (FA), and the sample was desalted by C18 reverse-phase tips (Reprosil-Pur Basic C18, 5 μm, Dr. Maisch GmbH). Peptides were frozen-dried and resuspended in 50 mM HEPES (pH 8.5). Equal amounts of peptides from each sample were used for 6-plex TMT labeling (Thermo Fisher Scientific, United States). Wild-type replicates were labeled with TMT^{TM}-126, TMT^{TM}-127, and TMT^{TM}-128, and Δ138 replicates were labeled with TMT^{TM}-129, TMT^{TM}-130, and TMT^{TM}-131, respectively. Labeled processes were performed by incubating the samples for 1 h at RT (pH = 8.0–8.5). Reactions were quenched by 8 μl of 5% hydroxylamine and incubated for 15 min. Label efficiency was tested, and equal amounts of peptides from different groups were mixed and fractionated using the C18 column (Durashell C18, 3 μm, 150 Å). Peptides were serially eluted by 6%, 9%, 12%, 15%, 18%, 21%, 25%, 30%, 35%, and 50% ACN (50 mM NH_4CO_3, pH 10). The fractions were then mixed into seven fractions and vacuum-dried. The peptides were resuspended in water with 0.1% FA and subjected to LC-MS/MS analysis.

The fractions were analyzed on a Nano LC 1200-Orbitrap Fusion Lumos platform with a trap column [ReproSil-Pur 120 C18-AQ (3 μm, Dr. Maisch GmbH, Germany); 20 × 0.05 mm] and a C18 column [ReproSil-Pur 120 C18 (1.9 μm, Dr. Maisch GmbH); 150 × 0.15 mm] at a flow rate of 600 μl·min^{-1}. Seven different Nano LC methods with a liner gradient of 15%−95% solvent B (80% acetonitrile with 0.1% FA) over 75 min were used, and data-dependent acquisition with full scans in the 350–1,550 m/z range was carried out using an Orbitrap mass analyzer at a mass resolution of 120,000 at 200 m/z. Parameters were set as follows: cycle time, 3 s; charge, 2–7; intensity threshold, $5.0e^3$; MS2 OT (HCD, collision energy, 38%; isolation window, 0.7; orbitrap resolution, 15,000).

Peptide and protein identification was acquired through Thermo Scientific^{TM} Proteome Discoverer^{TM} version 2.2 (PD2.2). The protein database used for searching was downloaded from UniProt[1] Protein digestion with two missed cleavages was allowed for each peptide. The search parameters were set as follows: MS accuracy, 10 ppm; MS/MS accuracy, 0.6 Da; dynamic modification (protein terminus) for acetyl; dynamic modification for oxidation; and static modification for carbamidomethyl on cysteine and TMTsixplex were set as fixed modifications. In all cases, the FDR for peptide identification was limited to a maximum of 0.01 by using a decoy database and the percolator algorithm. A hypothetical test (*t*-test) was applied, and proteins with a fold change >1.2 and $p < 0.05$ were considered significantly changed proteins. Functional annotation and clustering enrichment of differentially expressed proteins were conducted using the Gene Ontology (GO) enrichment tool. KEGG pathway enrichment and STRING analysis were also used to find the relationship between proteins. All data have been deposited with the ProteomeXchange Consortium via the PRIDE (Perez-Riverol et al., 2022) partner repository with the dataset identifier PXD045505.

2.9 Lipidomic analysis by LipidSearch

The same amounts of bacteria were collected as described in the proteomic analysis. Six biological replicates were prepared for each group. Bacteria were washed with pre-cooled PBS and water. A volume of 240 μl pre-cooled methanol, 200 μl water, and 800 μl MTBE were added before ultrasound in a low-temperature water bath for 20 min. After standing at RT for 30 min, samples were centrifuged at a speed of 14,000 × *g* at 10°C for 15 min. The organic phase was collected and dried. Samples were resuspended in 200 μl of 90% isopropanol/acetonitrile and centrifuged at a speed of 14,000 × *g* for LC-MS/MS analysis.

The samples were separated using the UHPLC Nexera LC-30A system at 45°C with a flow rate of 300 μl·min^{-1}. Solvent A is composed of 10 mM ammonium formate and acetonitrile aqueous solution (acetonitrile: water = 6:4, v/v), and solvent B is composed of 10 mM ammonium formate and acetonitrile isopropanol solution (acetonitrile: isopropanol = 1:9, v/v). The gradient elution procedure was set as follows: solvent B was maintained at 30% for 2 min, then solvent B was raised linearly from 30% to 100% in 23 min, and finally, solvent B was maintained at 30% for 10 min. Positive ion and negative ion modes of electrospray ionization (ESI) were used for detection. The samples were analyzed using a Q Exactive plus mass spectrometer (Thermo Fisher Scientific, United States). The ESI source conditions are as follows: for positive: heater temperature, 300°C; sheath gas flow rate, 45 arb; auxiliary gas flow rate,15 arb; sweep gas flow

1 https://www.uniprot.org/

rate, 1 arb; spray voltage, 3.0 KV; capillary temperature, 350°C; S-Lens RF level, 50%; MS1 scan ranges, 200–1,800 m/z. For negative: heater temperature, 300°C; sheath gas flow rate, 45 arb; auxiliary gas flow rate, 15 arb; sweep gas flow rate, 1 arb; spray voltage, 2.5 KV; capillary temperature, 350°C; S-Lens RF level, 60%; MS1 scan ranges, 250–1,800 m/z. In total, 10 fragment patterns (MS2 scan, HCD) are collected after each full scan. MS1 has a resolution of 70,000 at 200 m/z, and MS2 has a resolution of 17,500 at 200 m/z.

The LipidSearch version 4.1 software (Thermo Fisher Scientific, United States) was used for peak identification, lipid identification (secondary identification), peak extraction, peak alignment, and quantification. The main parameters were set as follows: precise tolerance, 5 ppm; product tolerance, 5 ppm; and product ion threshold, 5%. The abundance of lipid molecules with an RSD >30% was deleted. Lipid molecules with missing values >50% in each group were deleted. All the data were normalized by the total peak area. SIMCA-P 14.1 (Umetrics, Umea, Sweden) was used for pattern recognition. After the data were preprocessed by Pareto-scaling, multi-dimensional statistical analysis was performed, including unsupervised PCA analysis and orthogonal partial least squares discriminant analysis (OPLS-DA). One-dimensional statistical analysis was also performed, including the Student's *t*-test and fold change analysis. Volcano diagrams, hierarchical cluster analysis, and correlation analysis were analyzed using the R software.

2.10 Lipidomic analysis by MS-LAMP

The LipidSearch version 4.1 software (Thermo Fisher Scientific, USA) was used for peak extraction and quantification. The abundance of lipid molecules with an RSD >30% was deleted. Lipid molecules with missing values >50% in each group were deleted. All the data were normalized by the total peak area. The "Wu Kong" platform (https://www.omicsolution.com/wkomics/main/) (Zhou et al., 2023) was used for multi-dimensional statistical analysis, including Student's *t*-test, PCA, OPLS-DA, and fold change analysis. The data were then interpreted by "*Mtb* LipidDB" of MS-LAMP (Sabareesh and Singh, 2013), and [M+H]+, [M+NH4]+, and [M+Na]+ ions were searched with a mass window range as 0.5.

2.11 Targeted proteomics

To confirm the expression of proteins, a targeted proteomics method based on parallel reaction monitoring (PRM) was used to validate the expression differences of proteins as previously reported (Lu et al., 2021a,b). The sample preparation process was the same as that of the DDA method. Unique peptides were chosen to quantify proteins. Raw data were analyzed by Skyline, and the spectral library was built from label-free DDA results. The data were filtered by CV (coefficient of variation) < 30%. Peptides were selected by a *t*-test with a *p*-value < 0.05.

2.12 TLC analysis

The extraction and purification of lipids were performed as described previously (Siméone et al., 2010; Janagama et al., 2013). *Mtb* strains were cultured in Middlebrook 7H9 medium supplemented with 0.2% glycerol, 10% OADC, and 0.05% tyloxapol. An additional 0.05 mM propionate was added to study the generation of pthiocerol dimycoserosate (PDIM) and triacylglycerols (TG) under the propionate condition. The bacterial count was kept consistent across all groups, and all *Mtb* strains were harvested by centrifugation at 5,000 × *g* for 5 min and sterilized by adding $CHCl_3/CH_3OH$ (1:2, v/v) for 1 day at room temperature. Lipids were extracted with $CHCl_3/CH_3OH$ (2:1, v/v) and $CHCl_3/CH_3OH$ (1:1, v/v) for 1 h at room temperature, respectively. Then, it was washed twice with water and dried before analysis. After resuspension in an equal volume of $CHCl_3$, the extracted lipids were analyzed by TLC. Equivalent amounts of lipids from each extraction were spotted onto silica gel G60 plates (20 × 20 cm, Shanghai Titan Scientific Co., Ltd.) and separated with petroleum ether/diethyl ether (90:10, v/v) for PDIM and TG analysis. PDIM and TG were visualized by spraying the plates with 10% phosphomolybdic acid in ethanol, followed by heating at 120°C.

3 Results

3.1 Essentiality testing and construction of knockout and complementary strains

Gene knockout was performed using the overlap extension PCR method shown in Figure 1A, and the gene non-essentiality of *cyp138* was confirmed by gene switching. A two-step homologous recombination procedure was combined with complemented *cyp138* encoded on an integrated vector derived from the L5 mycobacteriophage to generate the merodiploid strain. The resident integrated vector was removed and replaced by an alternative version carrying a different antibiotic selection marker for gene switching. DCO with complemented *cyp138* was obtained, and *cyp138* was proved to be a non-essential gene. In the meantime, the complementary strain was also obtained. Primers used to construct the complementary plasmid were used for the PCR confirmation of wild-type, Δ138, and Δ138-C strains (Figure 1B).

3.2 Evaluation of growth status in different culture conditions and infection ability in macrophages

The growth status of H37Rv strains was evaluated by monitoring the absorbance of bacterial culture at OD_{600}. As shown in Figure 2A, the absorbance values of the wild-type, Δ138, and Δ138-C increased continuously. Similar growth curves were observed among the wild-type, Δ138, and Δ138-C groups.

As glycerol and cholesterol are important carbon and energy sources of *Mtb* (Pandey and Sassetti, 2008; Martinez et al., 2023), and CYP125 was previously proved to be essential for cholesterol catabolism (Johnston et al., 2012), we performed the sole carbon

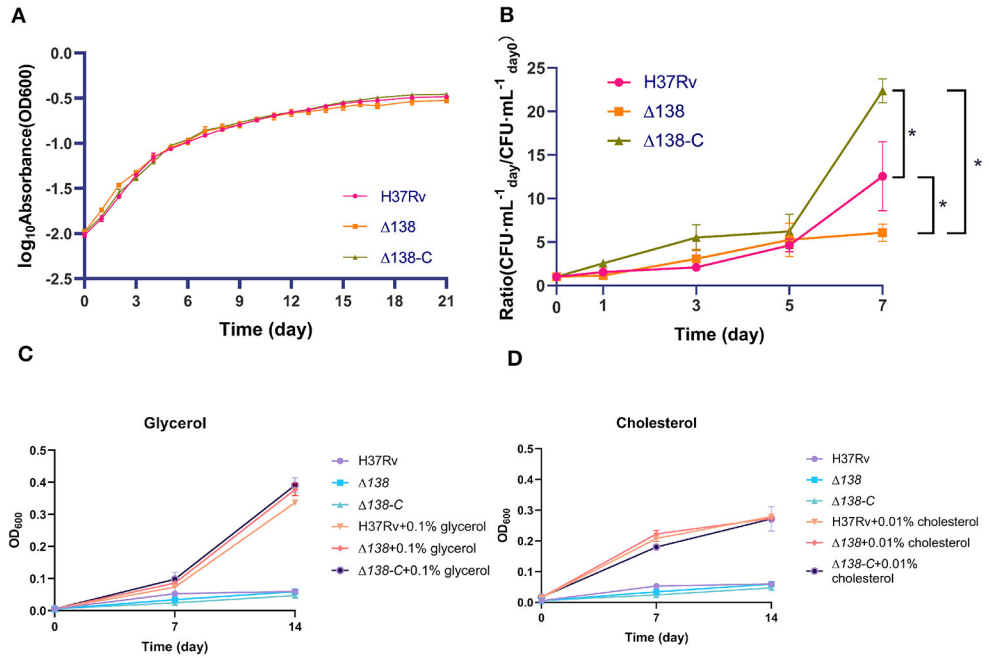

FIGURE 2
(A) The growth status of the wild-type, Δ138, and Δ138-C strains in the 7H9 medium supplemented with 0.2% (v/v) glycerol, 0.05% (v/v) Tween 80, and 10% (v/v) OADC at 37°C. The Δ138-C was cultured in the 7H9 broth mentioned above, supplemented with an additional 10 $\mu g \cdot ml^{-1}$ gentamicin, with three replicates per group, and the bacteria density was monitored at OD_{600}. A two-way ANOVA analysis was used for the statistical analysis among groups and no significant difference was observed; **(B)** intracellular counts of the wild-type, Δ138, and Δ138-C strains in macrophages after infection by culturing on the 7H10 culture plate supplemented with 10% OADC at 37°C for 14 days with three replicates per group, and a rank-sum test was used for the statistical analysis; **(C, D)** the indicated strains were cultured in defined medium containing 0.1% glycerol **(C)** or 0.01% cholesterol **(D)** as the sole carbon source.

source experiments to explore whether CYP138 was involved in the carbon source utilization. As shown in Figures 2C, D, no growth was observed without the addition of a carbon source, and there was no significant difference in the growth rate of the wild-type H37Rv, Δ138, and Δ138-C strains, whether supplementing with 0.1% glycerol or 0.01% cholesterol in the medium.

Compared with the increasing trend of intracellular counts of the wild-type and Δ138-C, that of the Δ138 in macrophages was relatively gentler (Figure 2B). After 7 days of infection, the CFU number of the Δ138 collected from cells was significantly lower than that of the wild-type and Δ138-C in macrophages ($p < 0.05$).

3.3 Evaluation of antimicrobial susceptibility

To further investigate the effect of *cyp138*-knockout on the susceptibility of *Mtb* to antibiotics, 14 antimicrobial drugs (as shown in Table 1) were selected for MIC tests of the wild-type, Δ138, and Δ138-C strains, respectively. Compared with the wild-type and Δ138-C strains, Δ138 showed similar susceptibility to actinomycin, isoniazid, ethambutol, streptomycin, levofloxacin, tetracycline, erythromycin, D-cycloserine, and minocycline. It is worth noting that compared to the wild-type strain, the MIC values of ampicillin and vancomycin against the Δ138 strain decreased by eight times and four times, respectively, while the MIC values of polymyxin B against the Δ138 strain increased by four times.

3.4 Effects of *cyp138*-knockout on protein expression

To identify proteins that may be potentially associated with CYP138, we compared the proteome of the wild-type with the Δ138 strains using a 6-plex TMT-labeling-based quantitative proteomic approach. Bacteria cells, harvested at their logarithmic phases in three biological replicates, were analyzed by Nano LC-MS/MS. In total, 2,726 bacterial proteins were identified in both groups. As shown in Figure 3A, good stability and reproducibility were observed in both groups. Based on $p < 0.05$ and fold change >1.2, the expression levels of 109 proteins were finally identified to be significantly different in the Δ138 group. Among these, 37 proteins exhibited decreased accumulation and 72 proteins exhibited increased accumulation (as shown in Figure 3B and Supplementary Table S1).

By using GO annotation enrichment analysis, as shown in Supplementary Figure S2, the expression levels of proteins related to oxidation-reduction process, pathogenesis, growth of symbiont in the host cell, valine catabolic process response to hypoxia, etc. in biological process (BP); plasma membrane, an integral component of membrane, extracellular region, cytosol, cytoplasm, etc. in cellular component (CC); and DNA binding, metal ion binding, iron ion binding, flavin adenine dinucleotide binding, etc. in molecular function (MF) were observed to be significantly changed. According to the KEGG pathway enrichment results shown in Supplementary Figure S3, 20 significantly expressed proteins were

10.3389/fmicb.2024.1301204

involved in metabolic pathways. The expression levels of prpC, leuD, leuC, and metA in the biosynthesis of amino acids pathway were all increased, and that of argD decreased. FadA2, prpC, argD, KorB, and MymA were involved in microbial metabolism in diverse environmental pathways. FadA2, prpC, and KorB also belonged to the carbon metabolism pathway. FadA2, fadE19, scoB, scoA, and fadE23 were involved in the valine, leucine, and isoleucine degradation pathways. FabG4, moaE2, moaX, and folB were involved in the biosynthesis of the cofactors pathway. FadA2, KorB, scoB, and scoA were involved in the butanoate metabolism pathway. FabG4, fadA2, fadE23, and desA3 (Rv3230c) were involved in the fatty acid metabolism pathway, and the expression levels of all these proteins were increased. FadA2 and FadE23 also belong to the fatty acid degradation pathway. PrpC, argD, leuD, and leuC belonged to the 2-oxocarboxylic acid metabolism pathway. LeuD and leuC also belonged to the C5-branched dibasic acid metabolism and valine, leucine, and isoleucine biosynthesis pathway. FadA2, glinD, and devR belonged to the two-component system pathway. MoaE2, moaX, and folB belonged to the folate biosynthesis pathway. MoaE2 and moaX were also related to the sulfur relay system pathway. Protein–protein interaction analysis by STRING (Figure 4) revealed that clusters were found, and core proteins such as prpC, fadA2, fadG4, fadE23, scoB, desA3, cyp138, fadD26, Rv2499c, and sigB were acquired, indicating the important roles they played in the network.

TABLE 1 Results of MIC tests of the wild-type, Δ138, and Δ138-C strains.

Strains	MIC ($\mu g \cdot ml^{-1}$)		
	Wild type	Δ138	Δ138-C
Polymyxin B	512	2,048	1,024
Ampicillin	128	16	128
Actinomycin	1,024	1,024	1,024
Trimethoprim	1,024	512	1,024
Rifampicin	0.125	0.0625	0.125
Isoniazid	0.0625	0.0625	0.0625
Ethambutol	0.0625	0.0625	0.0625
Streptomycin	0.5	0.5	0.5
Levofloxacin	0.125	0.125	0.125
Tetracycline	16	16	16
Erythromycin	512	512	1,024
D-cycloserine	4	4	4
Vancomycin	512	128	512
Minocycline	4	4	4

3.5 Differences in lipid metabolism annotated by LipidSearch

To investigate the effects of the *cyp138*-knockout on the production of lipids, lipidomics based on LC-MS/MS were performed. A total of 241 lipid species among 16 lipid classes were identified by LipidSearch in total. The PCA results of the control and gene knockout groups are shown in Supplementary Table S2 and Supplementary Figure S4A. In summary, the data of the samples in the same group were stable and reliable, and differences between the groups could be observed. The data acquired were analyzed using OPLS-DA. It can be seen that the OPLS-DA model can distinguish two sets of samples

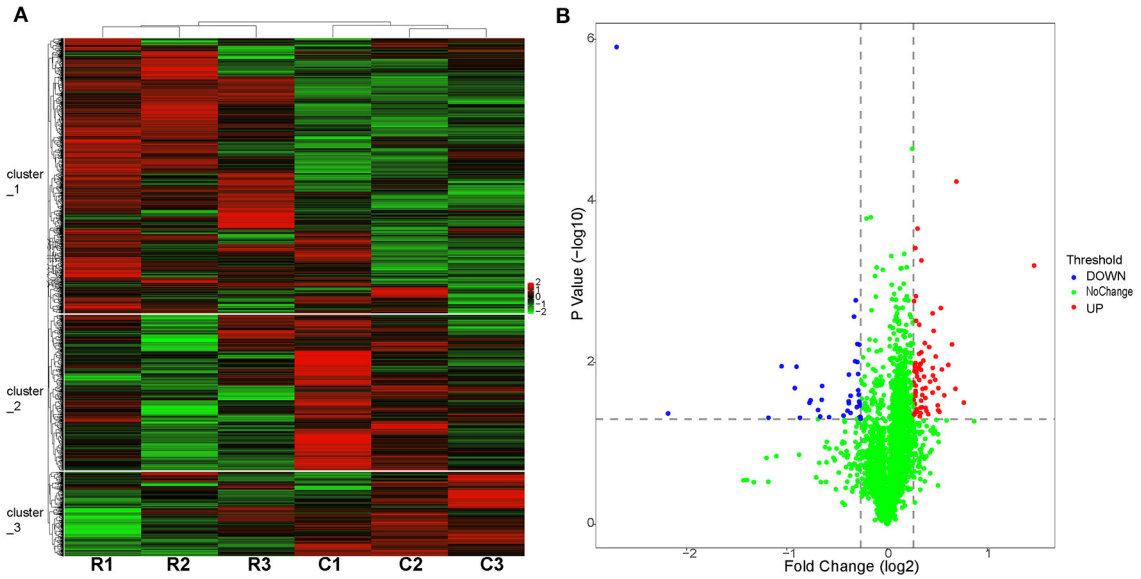

FIGURE 3
Proteome profiles of the wild-type or *cyp138*-knockout *Mtb* H37Rv. **(A)** Hierarchical clustering of proteomes with three biological replicates. Red represents the highest relative expression, and green represents the lowest. C1, C2, and C3 (the wide-type); R1, R2, and R3 (the *cyp138*-knockout). **(B)** Volcano distribution of proteins divided by $p < 0.05$ and fold change >1.2; red represents downregulated, and blue represents upregulated.

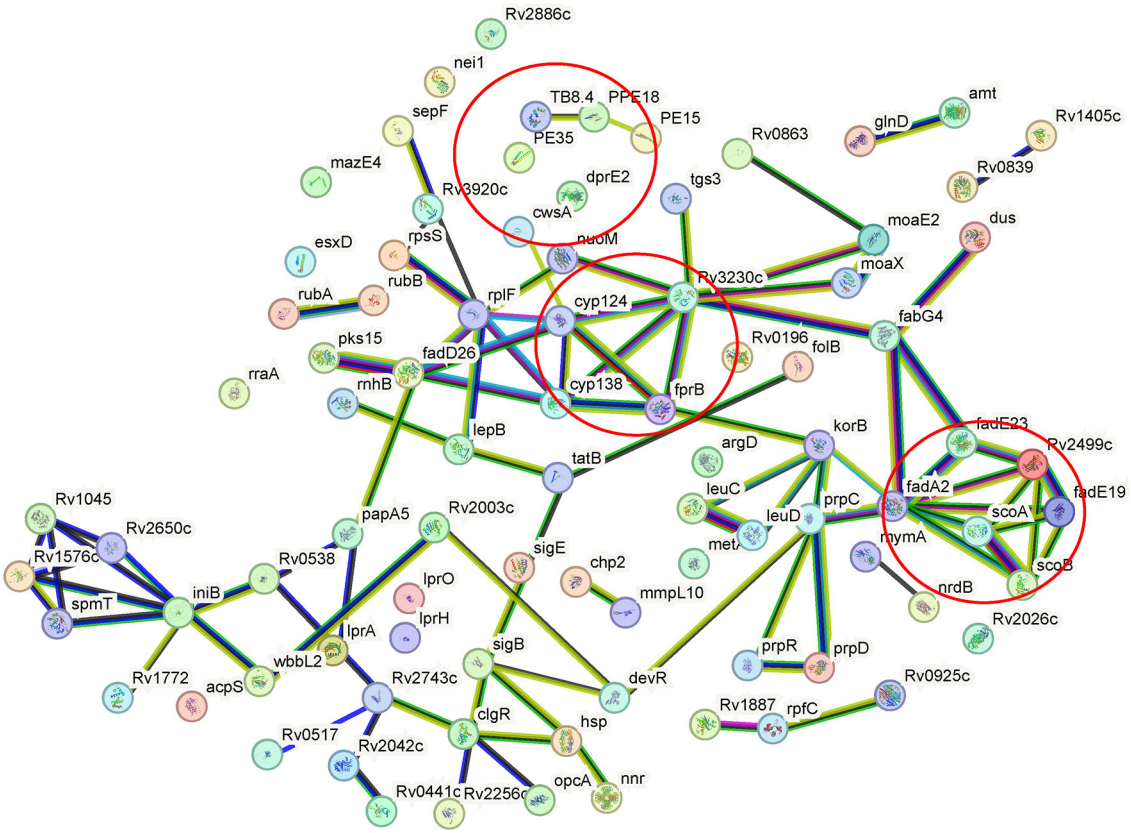

FIGURE 4
Protein–protein interaction networks of differentially expressed proteins of the wild-type or *cyp138*-knockout *Mtb* H37Rv. Nodes represent proteins, while edges represent protein–protein interactions. Colored nodes represent clusters. Colored edges: known interactions from: teal, curated databases; magenta, experimentally determined; predicted interactions: green, gene neighborhood; red, gene fusions; blue, gene co-occurrence; others: yellow, text mining; black, coexpression; purple, protein homology. Partial KEGG pathways were marked by a circle.

(Supplementary Figure S4B). According to the VIP values (variable importance for the projection) obtained by the OPLS-DA model, differentially produced lipids with biological significance are discovered. Volcano plots are shown in Supplementary Figure S5A. In this experiment, lipids with VIP $>$ 1 and p-value $<$ 0.05 were selected as the lipids with significant differences, and 15 lipids belonging to the TG class were acquired, as shown in Table 2 and Supplementary Figure S5B.

3.6 Differences in lipid metabolism annotated by *Mtb* LipidDB (MS-LAMP)

We also analyzed the lipidomic data with another database, *Mtb* LipidDB (Sartain et al., 2011), reported by Sartain et al. through *Mtb* Lipidome MS-LAMP. Only data acquired in positive mode were analyzed. In total, 20,911 ions were identified and further analyzed by Student's t-test and OPLS-DA (Supplementary Figure S6). After filtering by VIP $>$ 1, p $<$ 0.05, and fold change $>$ 1.5, 1,814 ions were identified as significantly changed lipid molecules. These ions were then annotated by *Mtb* LipidDB through MS-LAMP, and 5,344 lipid molecules were matched with a mass window range of 0.5 (Supplementary Table S3). As shown in Figure 5A, glycerophospholipids (GP), fatty acyls (FA), and glycerolipids (GL) have the highest quantity of ions. The levels of most molecules in the FA and GP groups decreased in the Δ138 groups, while the levels of more than half of the GL molecules increased (shown in Figure 5B). Most of these lipids in the FA and GP groups were important molecules of membrane structure.

3.7 Verification of targeted proteins

To verify the differently expressed proteins in the wild-type, Δ138, and Δ138-C strains separately, targeted proteomics based on the PRM approach was applied. In total, we reliably quantified two proteins with six peptides (Supplementary Table S4) as significantly expressed proteins filtered by p $<$ 0.05 and fold change $>$ 1.5.

3.8 Verification of lipids composition by TLC analysis

TLC analysis was performed to verify the influence of the *cyp138*-knockout on the lipid composition. As shown in Figures 6A, B, similar amounts of TG were observed in the Δ*138*

TABLE 2 Lipids with significant differences affected by *cyp138*-knockout and selected by VIP>1 and *p*-value < 0.05.

Lipid Ion	Class	Fatty Acid	Ion Formula	CalcMz	RT(min)	VIP	Fold change	*P*-Value
TG(16:1/18:2/18:3)+NH4	TG	(16:1/18:2/18:3)	C55 H98 O6 N1	868.7388655	18.50068935	1.51277	0.575183456	0.027456008
TG(20:0/16:0/18:1)+NH4	TG	(20:0/16:0/18:1)	C57 H112 O6 N1	906.8484155	23.65975995	1.69167	1.443537104	0.031452067
TG(18:0/18:1/18:2)+NH4	TG	(18:0/18:1/18:2)	C57 H108 O6 N1	902.8171155	21.50437738	4.63207	1.550719532	0.024463195
TG(16:0/18:1/22:1)+NH4	TG	(16:0/18:1/22:1)	C59 H114 O6 N1	932.8640655	23.03547947	1.78592	1.79253124	0.002596323
TG(20:1/18:1/18:1)+NH4	TG	(20:1/18:1/18:1)	C59 H112 O6 N1	930.8484155	22.30441518	2.94074	1.868213222	0.00336453
TG(20:1/18:1/18:2)+NH4	TG	(20:1/18:1/18:2)	C59 H110 O6 N1	928.8327655	21.51308038	2.96771	1.991436574	0.008196598
TG(26:0/16:0/16:0)+NH4	TG	(26:0/16:0/16:0)	C61 H122 O6 N1	964.9266655	25.05756867	1.48333	1.562056334	0.023229385
TG(16:0/18:1/24:1)+NH4	TG	(16:0/18:1/24:1)	C61 H118 O6 N1	960.8953655	23.73997583	1.43663	1.794524514	0.005769944
TG(18:1/18:1/22:1)+NH4	TG	(18:1/18:1/22:1)	C61 H116 O6 N1	958.8797155	23.08435855	1.06999	1.76465305	0.016931395
TG(26:0/16:0/18:1)+NH4	TG	(26:0/16:0/18:1)	C63 H124 O6 N1	990.9423155	24.56273872	2.00241	1.523469872	0.03224491
TG(26:0/16:1/18:1)+NH4	TG	(26:0/16:1/18:1)	C63 H122 O6 N1	988.9266655	24.15275172	1.65893	1.538378437	0.012527172
TG(18:1/18:1/24:1)+NH4	TG	(18:1/18:1/24:1)	C63 H120 O6 N1	986.9110155	23.72456073	1.20174	1.673546326	0.025807869
TG(26:0/18:1/18:2)+NH4	TG	(26:0/18:1/18:2)	C65 H124 O6 N1	1014.942315	24.24900233	1.4178	1.598777179	0.013215417
TG(28:0/16:0/24:0)+NH4	TG	(28:0/16:0/24:0)	C71 H142 O6 N1	1105.083165	26.56641218	1.28293	2.766283949	0.003271675
TG(28:0/18:1/24:0)+NH4	TG	(28:0/18:1/24:0)	C73 H144 O6 N1	1131.098815	26.56063782	1.22111	1.865395521	0.001405548

strain compared to those of wild-type and Δ138-C strains, and an obvious reduction was observed in the culture group with additional propionate supplementation. No significant changes were observed for the levels of PDIMA and PDIMB in the regular culture conditions and the propionate group.

4 Discussion

Recently, much more attention has been drawn to the CYPs of *Mtb* due to their unexpected number and important function in cell survival, virulence, and metabolism (Ortega Ugalde et al., 2019). Some of them, such as CYP121 and CYP125, were developed as promising anti-*Mtb* drug targets. However, there is little or no research for almost half of the CYPs in *Mtb*, and CYP138 is one of them. In our study, preliminary explorations on the function of CYP138 were conducted by comparing several properties of the *cyp138*-knockout and wild-type strains.

In this study, we successfully constructed a *cyp138*-knockout strain by homologous recombination and confirmed *cyp138* as a non-essential gene for *in vitro* growth for the first time. Initially, by comparison of the growth curves and macrophage infection status among the wild-type, Δ138, and Δ138-C strains, we found that although there is no significant difference in the 21-day growth *in vitro* among the three strains, the intracellular Δ138 bacterial count on the 7th day after macrophage infection was significantly lower than that of wild-type and Δ138-C strains. Thus, we speculated that *cyp138* might play an important role in maintaining the normal growth and replication of bacteria in the later cellular infection process. The growth experiments on medium using glycerol and cholesterol as the sole carbon sources proved that the knockout of *cyp138* does not affect the utilization of glycerol and cholesterol. SEM results provided us with no changes in bacterial surface morphology (Supplementary Figure S7).

To further investigate the effects of *cyp138*-knockout on the susceptibility of *Mtb* to antimicrobial drugs, 14 antibiotics were used for the MIC test. Interestingly, compared to the wild-type strain, the susceptibility of the Δ138 strain to ampicillin and vancomycin increased. Studies have reported that the action mechanism of ampicillin is binding to primary receptors called membrane-bound penicillin-binding proteins (PBPs) and preventing the late stages of peptidoglycan synthesis in the cell wall (Peechakara et al., 2021). The action mechanism of vancomycin is to inhibit the polymerization of peptidoglycans in the bacterial cell wall (Patel et al., 2021). According to the cell wall structure of *Mtb* reported (Batt et al., 2020), the peptidoglycan layer is located inside the arabinan and mycolic acid layers. The exposure of the peptidoglycan layer, which is the target of ampicillin and vancomycin, indicates damage to the cell wall structure, especially the arabinan and mycolic acid layers. Besides, compared with the wild-type strain, the Δ138 strain had a reduced susceptibility to polymyxin B, which may be due to the loss of some targets or changes in membrane components. Interestingly, ampicillin and vancomycin were not on the list of commonly used anti-TB drugs in clinical practice. The increased susceptibility of the Δ138 strain to them indicated that the absence of *cyp138* can promote the possible application of these drug classes in the fight against TB.

A quantitative proteomics method based on the TMTsixplex-labeled technique was used to discover the differences in proteomes between the wild-type and Δ138 strains. Among the 72 proteins with increased expression levels, fadA2 is involved in 17 pathways, indicating its basic and important roles in metabolism as an acetyl-CoA acyltransferase. Given the increased expression level of fabG4, fadA2, fadE23, and desA3, which are associated with the fatty acid metabolism pathway (as shown in Supplementary Figure S8),

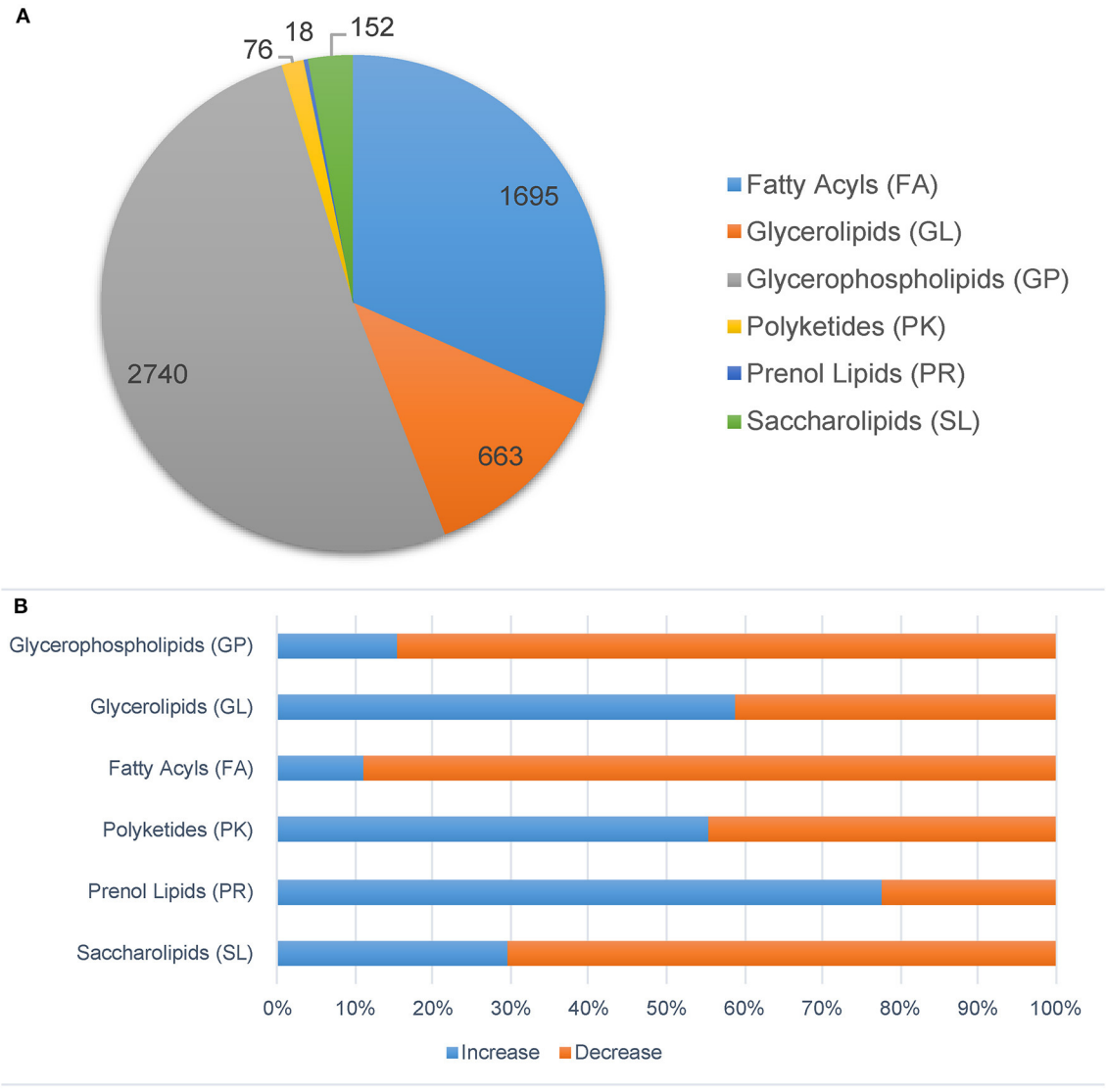

FIGURE 5
Significantly changed lipids molecules in the *cyp138*-knockout *Mtb* H37Rv filtered by $p < 0.05$, VIP > 1, and fold change > 1.5. Ions were annotated by MS-LAMP. **(A)** Lipid categories. **(B)** The increased and decreased molecules numbers in each category.

fatty acid biosynthesis, elongation, and beta-oxidation would be promoted. PrpR, prpC, and prpD are key enzymes of methylcitrate, which are essential for the growth of mycobacteria on propionate as a sole carbon source *in vitro*. The increased expression of these enzymes also indicated the increased production of propionyl-CoA, the product of odd-chain-length fatty acid metabolism (Masiewicz et al., 2012). MmpL10 is likely responsible for the translocation of diacyl trehalose (DAT) and the biosynthesis of pentacyl trehalose (PAT) (Bailo et al., 2015). Chp2 is essential for the final steps of PAT biosynthesis and is regulated by MmpL10 (Touchette et al., 2015b). The increased expression of MmpL10 and Chp2 might indicate the increased biosynthesis of PAT. Isopropylmalate isomerase (IPMI), a complex of two subunits, namely, LeuC and LeuD, is an enzyme of the leucine biosynthesis pathway, which is absent in humans (Manikandan et al., 2011). The increased expression of LeuC and LeuD indicates an increased level of leucine. The isoniazid-induced protein IniB was reported to respond to cell wall stress (Alland et al., 2000). MymA, also a target of isoniazid, was reported to be required for maintaining the appropriate mycolic acid composition and permeability of *Mtb* on its exposure to acidic pH (Singh et al., 2005). The increased expression of IniB and MymA represents the changes in the cell wall. The expression level of stress-regulated proteins such as sigB and sigE also responds to surface stress (Kundu and Basu, 2021). A previous study reported that over-expression of ClgR also indicated threats to the stability of the cell membrane (Sawicki et al., 2018). Nnr, FprB, and CYP124 are all electron transfer chain-related proteins. As shown in Figure 4, cyp124, FprB, and desA3 showed strong connections with each other, and all of these proteins showed increased levels in the Δ138 strain, indicating the possibility of functional correlation or compensation between them and *cyp*138. Among the 37 proteins with decreased expression

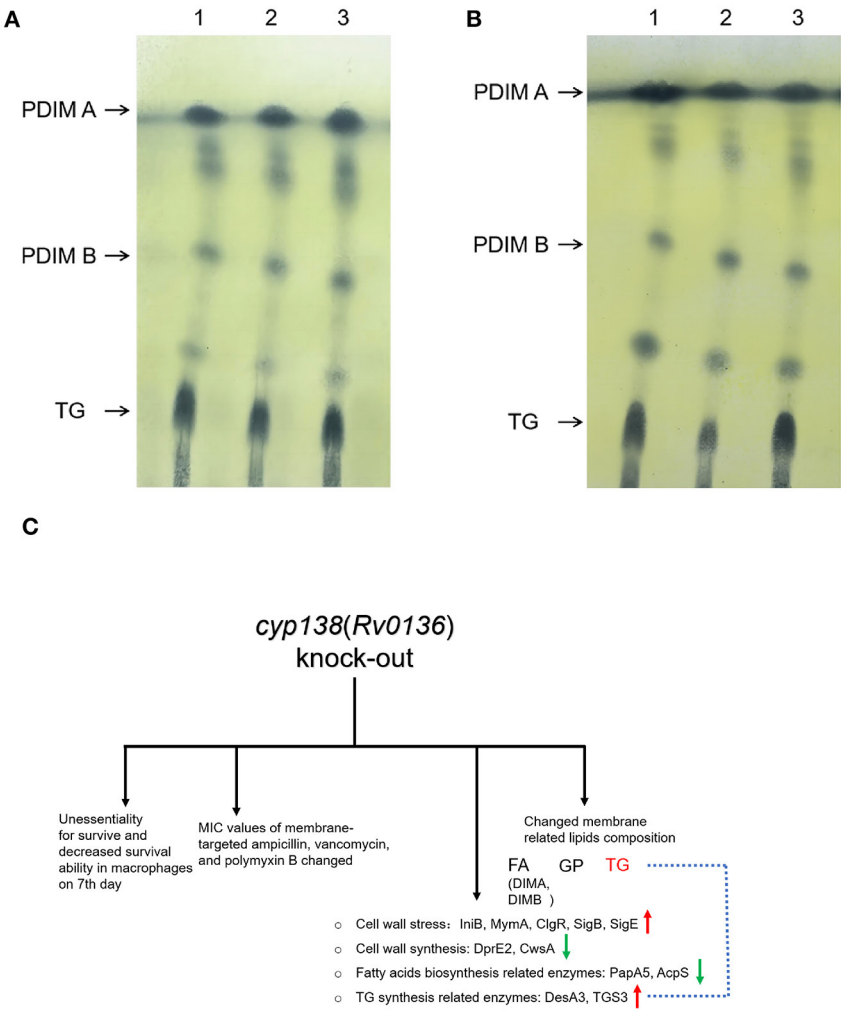

FIGURE 6
TLC analysis of PDIMs and TG extracted from the wild-type H37Rv, Δ138, and Δ138-C strains. **(A)** The strains were cultured in 7H9 medium. **(B)** The strains were cultured in 7H9 medium supplemented with 0.05 mM propionate. Lane 1, the wild-type H37Rv strain; Lane 2, the Δ138 strain; Lane 3, the Δ138-C strain. **(C)** A general view of the effects of *cyp138*-knockout on *Mtb* H37Rv.

levels, fadE19, OXCT A (scoA), and OXCT B (scoB) are involved in the valine, leucine, and isoleucine degradation pathways, while OXCT A (scoA) and OXCT B (scoB) are involved in the butanoate metabolism pathway. Acetylornithine aminotransferase (ACOAT) and the 2-oxoglutarate oxidoreductase subunit KorB are involved in several pathways related to metabolism. DNA-binding transcriptional activator DevR/DosR was reported to participate in the virulence, dormancy adaptation, and antibiotic tolerance mechanisms of *Mtb* (Sharma et al., 2021).

Among these significantly expressed proteins, 48 membrane-related (cell wall, plasma membrane, cell surface, integral component of plasma membrane, integral component of membrane, cell surface, cell outer membrane, etc.) proteins were acquired, while the expression level of 18 membrane-related proteins increased and that of 30 membrane-related proteins decreased. Among the membrane-related proteins with reduced expression levels, DprE2 (P9WGS9) is required for the synthesis of cell-wall arabinans (Manina et al., 2010), and CwsA (P9WJF3) is involved in peptidoglycan synthesis and cell shape determination (Plocinski et al., 2012). The decreased expression levels of these two proteins will affect the cell wall composition and explain the MIC results to some extent. In addition, the decreased expression level of cell division protein SepF (P9WGJ5) will affect cell division and ultimately affect cell proliferation (Gupta et al., 2018). The expression levels of membrane proteins related to immunity, such as LprA (P9WK55), LprH (P9WK43), PPE18, PE35, and TB8.4, all decreased (Skerry et al., 2016).

Mtb is abnormally rich in lipids, which are mainly distributed on the cell envelope. TG (also known as TAG) and PDIM (also known as DIMs) were proven to be important components of the *Mtb* membrane (Ortalo-Magné et al., 1996; Daffé and Marrakchi, 2019). TG serves as a dependable, long-term energy source, which is associated with the long-term persistence of *Mtb* (Maurya et al., 2018). According to the omics results, the

quantity of 15 TG molecules and TG-related proteins such as desA3 and TGS3 changed. DesA3 is a membrane-bound stearoyl-CoA delta (9)-desaturase that produces oleic acid, a precursor of mycobacterial membrane phospholipids and TG (Chang and Fox, 2006). Triacylglycerol synthase TGS3 is an enzyme that can synthesize TG (Supplementary Figure S9). The levels of TG molecules changed in the Δ138 strain according to the lipidomic data, which might not be apparent in the TLC image as TLC is a relatively rough separation method. The addition of propionate makes this change more pronounced (Figures 6A, B). However, identifying the specific step at which TG synthesis inhibition occurs due to the cyp138-knockout may necessitate additional research. Studies have proven that the addition of a low concentration of propionate can promote the levels of PDIM (Mulholland et al., 2023). Our proteomics results showed that the levels of PapA5 and fadD26, both critical enzymes in PDIM biosynthesis (Onwueme et al., 2005; Touchette et al., 2015a), decreased in the Δ138 strain. The levels of 97% of PDIM molecules were decreased in the lipidomic data shown in Supplementary Table S3. However, no obvious changes in PDIM were observed in the subsequent TLC analysis. Therefore, given the crucial role of TG in cell membrane integrity and long-term cell viability, variations in its content may account for the observed differences in macrophage infection on day 7, as well as changes in cell wall composition and susceptibility to several antibiotics.

Besides, by being reannotated by MS-LAMP, the levels of diacylglycerols (DG) and monoacylglycerols (MG) molecules in the Δ138 group were also changed. GP, like TG, has glycerol as its basic skeleton. For the Δ138 strain, the levels of most molecules in the GP group decreased. PIM, which belongs to GP, serves as the anchor for the biologically important lipoglycans lipoarabinomannan and lipomannan (Pitarque et al., 2008). The level changes of PIM will influence the membrane structure and function. In addition, the changed level of DAT confirmed the increased expression level of MmpL10 and Chp2 and indicated the increased biosynthesis of DAT and PAT. Consistent with the fatty acid metabolism-related proteome dataset, the levels of most FA ions changed, such as MA, GMM, TMM, and PDIM, indicating changes in membrane composition. However, due to the incompleteness of the *Mtb* lipidomic spectrum library, the same ion was matched with multiple molecules by MS-LAMP. With the development of technology, the *Mtb* lipid and KEGG pathway libraries will become more complete, which will improve the clarification of gene function.

5 Conclusion

As shown in Figure 6C, the knockout of the *cyp138* gene leads to decreased survival ability within macrophages on the 7th day, changes in susceptibilities to membrane-targeted ampicillin, vancomycin, and polymyxin B, changed levels of membrane-related and lipids metabolism-related proteins, as well as membrane-related lipids composition, especially TG. Besides, it is worth noting that the deletion of *cyp138* significantly improved the susceptibility of the pathogen to ampicillin and vancomycin, which gives us a hint that the development of *cyp138* inhibitors may promote the potential use of β-lactams and glycopeptides in anti-TB treatment. In addition, how CYP138 participates in and affects the synthesis and metabolism of TG and how propionate promotes this effect is still not clear to us. More work needs to be done to further reveal the function, the substrate, and the redox partner of the CYP enzyme.

Data availability statement

The datasets presented in this study can be found in online repositories and Supplementary material. The names of the repository/repositories and accession number(s) can be found in the article.

Author contributions

YunL: Conceptualization, Funding acquisition, Methodology, Software, Visualization, Writing—original draft. HC: Formal analysis, Methodology, Validation, Writing—original draft. ZS: Methodology, Validation, Writing—original draft. LS: Software, Writing—review & editing. CL: Supervision, Writing—review & editing. YuL: Project administration, Resources, Writing—review & editing. XYo: Funding acquisition, Project administration, Writing—review & editing. XYa: Conceptualization, Funding acquisition, Project administration, Writing—review & editing.

Funding

The author(s) declare financial support was received for the research, authorship, and/or publication of this article. This study was supported by the National Natural Science Foundation of China (grant number 32141003, 81803593, and 81273427), the CAMS Innovation Fund for Medical Sciences (CIFMS) (grant number 2021-I2M-1-030 and 2021-I2M-1-039), the Fundamental Research Funds for the Central Universities (grant number 2021-PT350-001), and the National Science and Technology Infrastructure of China (grant Project No. National Pathogen Resource Center-NPRC-32).

Conflict of interest

The authors declare that the research was conducted in the absence of any commercial or financial relationships that could be construed as a potential conflict of interest.

The author(s) declared that they were an editorial board member of Frontiers, at the time of submission. This had no impact on the peer review process and the final decision.

Publisher's note

All claims expressed in this article are solely those of the authors and do not necessarily represent those of

their affiliated organizations, or those of the publisher, the editors and the reviewers. Any product that may be evaluated in this article, or claim that may be made by its manufacturer, is not guaranteed or endorsed by the publisher.

Supplementary material

The Supplementary Material for this article can be found online at: https://www.frontiersin.org/articles/10.3389/fmicb.2024.1301204/full#supplementary-material

References

Alland, D., Steyn, A. J., Weisbrod, T., Aldrich, K., and Jacobs, W. R. (2000). Characterization of the *Mycobacterium tuberculosis* iniBAC promoter, a promoter that responds to cell wall biosynthesis inhibition. *J. Bacteriol.* 182, 1802–1811. doi: 10.1128/JB.182.7.1802-1811.2000

Bailo, R., Bhatt, A., and Ainsa, J. A. (2015). Lipid transport in *Mycobacterium tuberculosis* and its implications in virulence and drug development. *Biochem. Pharmacol.* 96, 159–167. doi: 10.1016/j.bcp.2015.05.001

Batt, S. M., Burke, C. E., Moorey, A. R., and Besra, G. S. (2020). Antibiotics and resistance: the two-sided coin of the mycobacterial cell wall. *Cell Surf.* 6:100044. doi: 10.1016/j.tcsw.2020.100044

Brown, A. C. (2009). Gene switching and essentiality testing. *Methods Mol. Biol.* 465, 337–352. doi: 10.1007/978-1-59745-207-6_23

Chang, Y., and Fox, B. G. (2006). Identification of Rv3230c as the NADPH oxidoreductase of a two-protein DesA3 acyl-CoA desaturase in *Mycobacterium tuberculosis* H37Rv. *Biochemistry* 45, 13476–13486. doi: 10.1021/bi0615285

Chenge, J., Kavanagh, M. E., Driscoll, M. D., McLean, K. J., Young, D. B., Cortes, T., et al. (2016). Structural characterization of CYP144A1 - a cytochrome P450 enzyme expressed from alternative transcripts in *Mycobacterium tuberculosis*. *Sci. Rep.* 6:26628. doi: 10.1038/srep26628

Collins, L., and Franzblau, S. G. (1997). Microplate alamar blue assay versus BACTEC 460 system for high-throughput screening of compounds against *Mycobacterium tuberculosis* and Mycobacterium avium. *Antimicrob. Agents Chemother.* 41, 1004–1009. doi: 10.1128/AAC.41.5.1004

Daffé, M., and Marrakchi, H. (2019). Unraveling the structure of the mycobacterial envelope. *Microbiol. Spectr.* 7, 7–14. doi: 10.1128/microbiolspec.GPP3-0027-2018

Darban-Sarokhalil, D., Fooladi, A. A., Bameri, Z., Nasiri, M. J., and Feizabadi, M. M. (2011). Cytochrome CYP141: a new target for direct detection of *Mycobacterium tuberculosis* from clinical specimens. *Acta Microbiol. Immunol. Hung.* 58, 211–217. doi: 10.1556/amicr.58.2011.3.4

Elfaki, I., Mir, R., Almutairi, F. M., and Duhier, F. M. A. (2018). Cytochrome P450: polymorphisms and roles in cancer, diabetes and atherosclerosis. *Asian Pac. J. Cancer Prev.* 19, 2057–2070. doi: 10.22034/APJCP.2018.19.8.2057

Gupta, S., Banerjee, S. K., Chatterjee, A., Sharma, A. K., Kundu, M., and Basu, J. (2018). Corrigendum: Essential protein SepF of mycobacteria interacts with FtsZ and MurG to regulate cell growth and division. *Microbiology (Reading)* 164:1326. doi: 10.1099/mic.0.000712

Hu, Y., Movahedzadeh, F., Stoker, N. G., and Coates, A. R. (2006). Deletion of the *Mycobacterium tuberculosis* alpha-crystallin-like hspX gene causes increased bacterial growth in vivo. *Infect. Immun.* 74, 861–868. doi: 10.1128/IAI.74.2.861-868.2006

Hudson, S. A., McLean, K. J., Munro, A. W., and Abell, C. (2012). *Mycobacterium tuberculosis* cytochrome P450 enzymes: a cohort of novel TB drug targets. *Biochem. Soc. Trans.* 40, 573–579. doi: 10.1042/BST20120062

Jain, M., Petzold, C. J., Schelle, M. W., Leavell, M. D., Mougous, J. D., Bertozzi, C. R., et al. (2007). Lipidomics reveals control of *Mycobacterium tuberculosis* virulence lipids via metabolic coupling. *Proc. Natl. Acad. Sci. U S A.* 104, 5133–5138. doi: 10.1073/pnas.0610634104

Janagama, H. K., Tounkang, S., Cirillo, S. L., Zinniel, D. K., Barletta, R. G., and Cirillo, J. D. (2013). Molecular analysis of the *Mycobacterium tuberculosis* lux-like mel2 operon. *Tuberculosis (Edinb)* 93, S83–87. doi: 10.1016/S1472-9792(13)70016-7

Johnston, J. B., Singh, A. A., Clary, A. A., Chen, C. K., Hayes, P. Y., Chow, S., et al. (2012). Substrate analog studies of the omega-regiospecificity of *Mycobacterium tuberculosis* cholesterol metabolizing cytochrome P450 enzymes CYP124A1, CYP125A1 and CYP142A1. *Bioorg. Med. Chem.* 20, 4064–4081. doi: 10.1016/j.bmc.2012.05.003

Kavanagh, M. E., Coyne, A. G., McLean, K. J., James, G. G., Levy, C. W., Marino, L. B., et al. (2016). Fragment-Based Approaches to the Development of *Mycobacterium tuberculosis* CYP121 Inhibitors. *J. Med. Chem.* 59, 3272–3302. doi: 10.1021/acs.jmedchem.6b00007

Koch, A. S., Brites, D., Stucki, D., Evans, J. C., Seldon, R., Heekes, A., et al. (2017). The Influence of HIV on the Evolution of *Mycobacterium tuberculosis*. *Mol. Biol. Evol.* 34, 1654–1668. doi: 10.1093/molbev/msx107

Kundu, M., and Basu, J. (2021). Applications of transcriptomics and proteomics for understanding dormancy and resuscitation in *Mycobacterium tuberculosis*. *Front. Microbiol.* 12:642487. doi: 10.3389/fmicb.2021.642487

Lee, J., Lee, H. J., Shin, M. K., and Ryu, W. S. (2004). Versatile PCR-mediated insertion or deletion mutagenesis. *Biotechniques* 36, 398–400. doi: 10.2144/04363BM04

Lee, W., VanderVen, B. C., Fahey, R. J., and Russell, D. G. (2013). Intracellular *Mycobacterium tuberculosis* exploits host-derived fatty acids to limit metabolic stress. *J. Biol. Chem.* 288, 6788–6800. doi: 10.1074/jbc.M112.445056

Lu, Y., Hu, X., Nie, T., Yang, X., Li, C., and You, X. (2021a). Strategies for rapid identification of acinetobacter Baumannii membrane proteins and polymyxin B's effects. *Front. Cell. Infect. Microbiol.* 11:896. doi: 10.3389/fcimb.2021.734578

Lu, Y., Pang, J., Wang, G., Hu, X., Li, X., Li, G., et al. (2021b). Quantitative proteomics approach to investigate the antibacterial response of Helicobacter pylori to daphnetin, a traditional Chinese medicine monomer. *RSC Adv.* 11, 2185–2193. doi: 10.1039/D0RA06677J

Lu, Y., Qiao, F., Li, Y., Sang, X. H., Li, C. R., Jiang, J. D., et al. (2017). Recombinant expression and biochemical characterization of *Mycobacterium tuberculosis* 3Fe-4S ferredoxin Rv1786. *Appl. Microbiol. Biotechnol.* 101, 7201–7212. doi: 10.1007/s00253-017-8454-7

Mabhula, A., and Singh, V. (2019). Drug-resistance in *Mycobacterium tuberculosis*: where we stand. *Medchemcomm* 10, 1342–1360. doi: 10.1039/C9MD00057G

Manikandan, K., Geerlof, A., Zozulya, A. V., Svergun, D. I., and Weiss, M. S. (2011). Structural studies on the enzyme complex isopropylmalate isomerase (LeuCD) from *Mycobacterium tuberculosis*. *Proteins* 79, 35–49. doi: 10.1002/prot.22856

Manina, G., Pasca, M. R., Buroni, S., De Rossi, E., and Riccardi, G. (2010). Decaprenylphosphoryl-beta-D-ribose 2′-epimerase from *Mycobacterium tuberculosis* is a magic drug target. *Curr. Med. Chem.* 17, 3099–3108. doi: 10.2174/092986710791959693

Martinez, N., Smulan, L. J., Jameson, M. L., Smith, C. M., Cavallo, K., Bellerose, M., et al. (2023). Glycerol contributes to tuberculosis susceptibility in male mice with type 2 diabetes. *Nat. Commun.* 14, 5840. doi: 10.1038/s41467-023-41519-9

Masiewicz, P., Brzostek, A., Wolanski, M., Dziadek, J., and Zakrzewska-Czerwinska, J. (2012). A novel role of the PrpR as a transcription factor involved in the regulation of methylcitrate pathway in *Mycobacterium tuberculosis*. *PLoS ONE* 7:e43651. doi: 10.1371/journal.pone.0043651

Maurya, R. K., Bharti, S., and Krishnan, M. Y. (2018). Triacylglycerols: Fuelling the Hibernating *Mycobacterium tuberculosis*. *Front. Cell Infect. Microbiol.* 8:450. doi: 10.3389/fcimb.2018.00450

McLean, K. J., Belcher, J., Driscoll, M. D., Fernandez, C. C., Le Van, D., Bui, S., et al. (2010). The *Mycobacterium tuberculosis* cytochromes P450: physiology, biochemistry and molecular intervention. *Future Med. Chem.* 2, 1339–1353. doi: 10.4155/fmc.10.216

McLean, K. J., Clift, D., Lewis, D. G., Sabri, M., Balding, P. R., Sutcliffe, M. J., et al. (2006). The preponderance of P450s in the *Mycobacterium tuberculosis* genome. *Trends Microbiol.* 14, 220–228. doi: 10.1016/j.tim.2006.03.002

Msomi, N. N., Padayachee, T., Nzuza, N., Syed, P. R., Kryś, J. D., Chen, W., et al. (2021). In Silico Analysis of P450s and their role in secondary metabolism in the bacterial class gammaproteobacteria. *Molecules* 26:1538. doi: 10.3390/molecules26061538

Mulholland, C. V., Wiggins, T. J., Cui, J., Vilchèze, C., Rajagopalan, S., Shultis, M. W., et al. (2023). The PDIM paradox of *Mycobacterium tuberculosis*: new solutions to a persistent problem. *bioRxiv*. doi: 10.1101/2023.10.16.562559

Munro, A. W., McLean, K. J., Marshall, K. R., Warman, A. J., Lewis, G., Roitel, O., et al. (2003). Cytochromes P450: novel drug targets in the war against multidrug-resistant *Mycobacterium tuberculosis*. *Biochem. Soc. Trans.* 31, 625–630. doi: 10.1042/bst0310625

Murphy, D. J., and Brown, J. R. (2007). Identification of gene targets against dormant phase *Mycobacterium tuberculosis* infections. *BMC Infect. Dis.* 7:84. doi: 10.1186/1471-2334-7-84

Nelson, D. R. (2018). Cytochrome P450 diversity in the tree of life. *Biochim. Biophys. Acta Proteins Proteom.* 1866, 141–154. doi: 10.1016/j.bbapap.2017.05.003

Onwueme, K. C., Vos, C. J., Zurita, J., Ferreras, J. A., and Quadri, L. E. (2005). The dimycocerosate ester polyketide virulence factors of mycobacteria. *Prog. Lipid Res.* 44, 259–302. doi: 10.1016/j.plipres.2005.07.001

Ortalo-Magné, A., Lemassu, A., Lanéelle, M. A., Bardou, F., Silve, G., Gounon, P., et al. (1996). Identification of the surface-exposed lipids on the cell envelopes of *Mycobacterium tuberculosis* and other mycobacterial species. *J. Bacteriol.* 178, 456–461. doi: 10.1128/jb.178.2.456-461.1996

Ortega Ugalde, S., Boot, M., Commandeur, J. N. M., Jennings, P., Bitter, W., and Vos, J. C. (2019). Function, essentiality, and expression of cytochrome P450 enzymes and their cognate redox partners in *Mycobacterium tuberculosis*: are they drug targets? *Appl. Microbiol. Biotechnol.* 103, 3597–3614. doi: 10.1007/s00253-019-09697-z

Ouellet, H., Podust, L. M., and de Montellano, P. R. (2008). *Mycobacterium tuberculosis* CYP130: crystal structure, biophysical characterization, and interactions with antifungal azole drugs. *J. Biol. Chem.* 283, 5069–5080. doi: 10.1074/jbc.M708734200

Pandey, A. K., and Sassetti, C. M. (2008). Mycobacterial persistence requires the utilization of host cholesterol. *Proc. Natl. Acad. Sci. U S A.* 105, 4376–4380. doi: 10.1073/pnas.0711159105

Patel, S., Preuss, C. V., and Bernice, F. (2021). *Vancomycin.* Treasure Island, FL: StatPearls.

Peechakara, B. V., Basit, H., and Gupta, M. (2021). *Ampicillin.* Treasure Island, FL: StatPearls.

Penuelas-Urquides, K., Villarreal-Trevino, L., Silva-Ramirez, B., Rivadeneyra-Espinoza, L., Said-Fernandez, S., and de Leon, M. B. (2013). Measuring of *Mycobacterium tuberculosis* growth. A correlation of the optical measurements with colony forming units. *Braz. J. Microbiol.* 44, 287–289. doi: 10.1590/S1517-83822013000100042

Perez-Riverol, Y., Bai, J., Bandla, C., Garcia-Seisdedos, D., Hewapathirana, S., Kamatchinathan, S., et al. (2022). The PRIDE database resources in 2022: a hub for mass spectrometry-based proteomics evidences. *Nucleic. Acids Res.* 50, D543–D552. doi: 10.1093/nar/gkab1038

Pitarque, S., Larrouy-Maumus, G., Payré, B., Jackson, M., Puzo, G., and Nigou, J. (2008). The immunomodulatory lipoglycans, lipoarabinomannan and lipomannan, are exposed at the mycobacterial cell surface. *Tuberculosis (Edinb)* 88, 560–565. doi: 10.1016/j.tube.2008.04.002

Plocinski, P., Arora, N., Sarva, K., Blaszczyk, E., Qin, H., Das, N., et al. (2012). *Mycobacterium tuberculosis* CwsA interacts with CrgA and Wag31, and the CrgA-CwsA complex is involved in peptidoglycan synthesis and cell shape determination. *J. Bacteriol.* 194, 6398–6409. doi: 10.1128/JB.01005-12

Podust, L. M., Poulos, T. L., and Waterman, M. R. (2001). Crystal structure of cytochrome P450 14alpha -sterol demethylase (CYP51) from *Mycobacterium tuberculosis* in complex with azole inhibitors. *Proc. Natl. Acad. Sci. U S A.* 98, 3068–3073. doi: 10.1073/pnas.061562898

Qin, H., Zhuang, W., Liu, X., Wu, J., Li, S., Wang, Y., et al. (2023). Targeting CXCR1 alleviates hyperoxia-induced lung injury through promoting glutamine metabolism. *Cell Rep.* 42, 112745. doi: 10.1016/j.celrep.2023.112745

Sabareesh, V., and Singh, G. (2013). Mass spectrometry based lipid(ome) analyzer and molecular platform: a new software to interpret and analyze electrospray and/or matrix-assisted laser desorption/ionization mass spectrometric data of lipids: a case study from *Mycobacterium tuberculosis*. *J. Mass Spectrom.* 48, 465–477. doi: 10.1002/jms.3163

Sartain, M. J., Dick, D. L., Rithner, C. D., Crick, D. C., and Belisle, J. T. (2011). Lipidomic analyses of *Mycobacterium tuberculosis* based on accurate mass measurements and the novel "Mtb LipidDB". *J. Lipid Res.* 52, 861–872. doi: 10.1194/jlr.M010363

Sawicki, R., Golus, J., Przekora, A., Ludwiczuk, A., Sieniawska, E., and Ginalska, G. (2018). Antimycobacterial activity of cinnamaldehyde in a *Mycobacterium tuberculosis*(H37Ra) model. *Molecules* 23:2381. doi: 10.3390/molecules23092381

Sharma, S., Kumar, R., Jain, A., Kumar, M., Gauttam, R., Banerjee, R., et al. (2021). Functional insights into *Mycobacterium tuberculosis* DevR-dependent transcriptional machinery utilizing *Escherichia coli*. *Biochem. J.* 478, 3079–3098. doi: 10.1042/BCJ20210268

Siméone, R., Léger, M., Constant, P., Malaga, W., Marrakchi, H., Daffé, M., et al. (2010). Delineation of the roles of FadD22, FadD26 and FadD29 in the biosynthesis of phthiocerol dimycocerosates and related compounds in *Mycobacterium tuberculosis*. *Febs J.* 277, 2715–2725. doi: 10.1111/j.1742-464X.2010.07688.x

Singh, A., Gupta, R., Vishwakarma, R. A., Narayanan, P. R., Paramasivan, C. N., Ramanathan, V. D., et al. (2005). Requirement of the mymA operon for appropriate cell wall ultrastructure and persistence of *Mycobacterium tuberculosis* in the spleens of guinea pigs. *J. Bacteriol.* 187, 4173–4186. doi: 10.1128/JB.187.12.4173-4186.2005

Skerry, C., Klinkenberg, L. G., Page, K. R., and Karakousis, P. C. (2016). TLR2-modulating lipoproteins of the mycobacterium tuberculosis complex enhance the HIV infectivity of CD4+ T cells. *PLoS ONE* 11:e0147192. doi: 10.1371/journal.pone.0147192

Sogi, K. M., Holsclaw, C. M., Fragiadakis, G. K., Nomura, D. K., Leary, J. A., and Bertozzi, C. R. (2016). Biosynthesis and regulation of sulfomenaquinone, a metabolite associated with virulence in *Mycobacterium tuberculosis*. *ACS Infect. Dis.* 2, 800–806. doi: 10.1021/acsinfecdis.6b00106

Swami, S. (2015). *Structure and Biochemistry of the Orphan Cytochrome P450s CYP126A1 and CYP143A1 from the Human Pathogen Mycobacterium tuberculosis.* Manchester, UK: University of Manchester.

Syed, P. R., Chen, W., Nelson, D. R., Kappo, A. P., Yu, J. H., Karpoormath, R., et al. (2019). Cytochrome P450 Monooxygenase CYP139 family involved in the synthesis of secondary metabolites in 824 mycobacterial species. *Int. J. Mol. Sci.* 20:2690. doi: 10.3390/ijms20112690

Touchette, M. H., Bommineni, G. R., Delle Bovi, R. J., Gadbery, J. E., Nicora, C. D., Shukla, A. K., et al. (2015a). Diacyltransferase activity and chain length specificity of mycobacterium tuberculosis PapA5 in the synthesis of alkyl beta-diol lipids. *Biochemistry* 54, 5457–5468. doi: 10.1021/acs.biochem.5b00455

Touchette, M. H., Holsclaw, C. M., Previti, M. L., Solomon, V. C., Leary, J. A., Bertozzi, C. R., et al. (2015b). The rv1184c locus encodes Chp2, an acyltransferase in *Mycobacterium tuberculosis* polyacyltrehalose lipid biosynthesis. *J. Bacteriol.* 197, 201–210. doi: 10.1128/JB.02015-14

World Health Organization (2023). *Global Tuberculosis Report 2023*. World Health Organization.

Xu, J., Wang, J. X., Zhou, J. M., Xu, C. L., Huang, B., Xing, Y., et al. (2017). A novel protein kinase inhibitor IMB-YH-8 with anti-tuberculosis activity. *Sci. Rep.* 7:5093. doi: 10.1038/s41598-017-04108-7

Zhou, W., Li, W., Wang, S., Salovska, B., Hu, Z., Tao, B., et al. (2023). An optogenetic-phosphoproteomic study reveals dynamic Akt1 signaling profiles in endothelial cells. *Nat. Commun.* 14:3803. doi: 10.1038/s41467-023-39514-1

frontiers | Frontiers in Microbiology

TYPE Original Research
PUBLISHED 10 May 2024
DOI 10.3389/fmicb.2024.1372647

OPEN ACCESS

EDITED BY
Ranjan Nanda,
International Centre for Genetic Engineering and Biotechnology (India), India

REVIEWED BY
Monique Williams,
University of Cape Town, South Africa
Philippe Clevenbergh,
CHU Brugmann, Belgium

*CORRESPONDENCE
Akterono Dwi Budiyati
akteronodwib@gmail.com

RECEIVED 18 January 2024
ACCEPTED 11 April 2024
PUBLISHED 10 May 2024

CITATION
Parwati I, Chaidir L, Yunus M, Montain MM, Budhiarko D, Selasih SF, Ristandi RB, Rachman RW, Nurhayati RD, Pambudi I and Budiyati AD (2024) Evaluation of a real-time PCR assay performance to detect *Mycobacterium tuberculosis*, rifampicin, and isoniazid resistance in sputum specimens: a multicenter study in two major cities of Indonesia.
Front. Microbiol. 15:1372647.
doi: 10.3389/fmicb.2024.1372647

Evaluation of a real-time PCR assay performance to detect *Mycobacterium tuberculosis*, rifampicin, and isoniazid resistance in sputum specimens: a multicenter study in two major cities of Indonesia

Ida Parwati[1], Lidya Chaidir[2], Muhammad Yunus[3], Maya Marinda Montain[4], Dini Budhiarko[3], Siti Fatimah Selasih[3], Ryan Bayusantika Ristandi[5], Rifky Waluyajati Rachman[5], Raden Desy Nurhayati[6], Imran Pambudi[7] and Akterono Dwi Budiyati[3]*

[1]Department of Clinical Pathology, Faculty of Medicine, Universitas Padjadjaran/Dr. Hasan Sadikin General Hospital, Bandung, Indonesia, [2]Department of Biomedical Sciences, Faculty of Medicine, Universitas Padjadjaran, Bandung, Indonesia, [3]Stem Cell and Cancer Institute, PT. Kalbe Farma, Jakarta, Indonesia, [4]Unit Pelayanan Fungsional Balai Besar Kesehatan Paru Masyarakat Bandung (UPF BBKPM), Bandung, Indonesia, [5]West Java Provincial Health Laboratory, Bandung, Indonesia, [6]Dr. H. A. Rotinsulu Lung Hospital, Bandung, Indonesia, [7]Directorate General of Diseases Prevention and Control, Ministry of Health of the Republic of Indonesia, Jakarta, Indonesia

Background: Tuberculosis (TB) is one of the major global health issues due to its high mortality rate, especially in low- and middle-income countries. One of the key success points of the TB eradication program is early TB diagnosis, which requires rapid and accurate diagnostic testing. This study aimed to evaluate the performance of a newly developed RT-PCR kit (Indigen MTB/DR-TB RT-PCR) in a routine TB clinical setting.

Method: A multi-fluorescence RT-PCR assay was designed and developed to detect regions within *IS6110*, *rpoB, katG*, and *inhA* of the *Mycobacterium tuberculosis* (MTB) genes. Sputum specimens were obtained from suspected TB patients who visited TB healthcare facilities in two major cities of Indonesia from September 2022 to May 2023. Specimens were assessed using Indigen MTB/DR-TB RT-PCR, acid-fast bacillus (AFB) smear microscopy, MTB culture, and drug susceptibility testing (DST) methods. Fisher's exact test (χ^2) was used to analyze the Indigen performance relative to culture methods.

Result: The performance of Indigen MTB/DR-TB RT-PCR to detect MTB was assessed using 610 sputum specimens obtained from suspected patients. The overall sensitivity and specificity were 94.12% (95% CI: 90.86–96.48%) and 98.32% (95% CI: 96.20–99.46%), respectively. When the analysis was performed on AFB smear-negative TB subjects (386 subjects), a lower sensitivity level was found at 78.57% (95% CI: 68.26–86.78%), while the specificity level remained similar at 98.34% (95% CI: 96.18–99.46%). The overall performance of Indigen MTB/DR-TB RT-PCR to detect MTB showed substantial agreement with the MTB culture method (kappa value 0.93). In comparison to DST, the sensitivity

and specificity levels of Indigen to detect RIF resistance or INH resistance were 78.2% (95% CI: 61.8–90.2%) and 82.8% (95% CI: 64.2–94.2%), respectively, while the specificity level for both groups was at 100% (95% CI, 87.7–100%).

Conclusion: Indigen MTB/DR-TB RT-PCR demonstrated reliable performance for TB molecular diagnostic testing and can be implemented in routine TB diagnostic settings.

KEYWORDS

***Mycobacterium tuberculosis*, real-time PCR, diagnostic, Indigen, RIF resistance, INH resistance**

1 Introduction

Tuberculosis (TB) remains the leading cause of death by a single infectious agent globally. The World Health Organization (WHO) reported that there were an estimated 10.6 million new cases of disease and 1.6 million deaths from TB in 2022 (World Health Organization, 2023). Most of the cases were contributed by low- and middle-income countries, which accounted for two-thirds of the global total cases (Chakaya et al., 2020). Of those countries, Indonesia ranked as having the second highest burden of TB behind India. Indonesia was estimated to have 969,000 TB cases in 2023 (Ministry of Health Republic Indonesia, 2020), and two-thirds of the cases were found in Java and Bali, predominantly in urban areas (Ministry of Health Republic Indonesia, 2023).

Early TB diagnosis followed by precise treatment is critical to stopping the transmission of the disease. Substantial efforts have been made by Indonesia's national program to find TB cases in the last 5 years, including scaling up the TB diagnostic technology with a nucleic acid amplification test (NAAT)-based platform. Currently, the GeneXpert MTB/RIF assay is being used by the Indonesian government as the recommended NAAT-based diagnostic testing in the TB national program (Ministry of Health Republic Indonesia, 2023). This kit allows completely automated nucleic acid preparation and amplification in a simple and rapid TB detection process. The efforts successfully increased the case notification from 360,000 cases in 2016 to 570,000 cases in 2018. However, there were an estimated 275,000 cases in 2018 (Ministry of Health Republic Indonesia, 2020) that were still underreported, and unfortunately, the gap remains unchanged at 244,691 in 2023 (Ministry of Health Republic Indonesia, 2023).

Despite the advantages offered by GeneXpert/MTB/RIF assay, it also has shortcomings such as high cost, closed system, and requirement for imported material that need to be addressed. Given the circumstances, implementing local NAAT testing to cover the underreported gap in TB case notification is imperative. Meanwhile, there was a considerable increase in the number of laboratories equipped with advanced real-time polymerase chain reaction (RT-PCR) machines and molecular infrastructure readiness as an impact of the COVID-19 pandemic situation (Ministry of Health Republic Indonesia, 2023) waiting to be leveraged. RT-PCR itself has been accepted as a robust method for detecting *Mycobacterium tuberculosis* (MTB), making its implementation highly recommended (Espy et al., 2006; Babafemi et al., 2017).

To address the abovementioned issue, we developed an open platform RT-PCR assay that can be run on the same RT-PCR instruments that have been placed in several healthcare facilities across Indonesia, including labs that use COVID-19 diagnostic testing facilities. The assay was designed to detect the region within the insertion sequence of the *IS6110*, *rpoB*, *katG*, and *inhA* (*C15T*) genes of MTB. The *IS6110* region has been widely used as a target for MTB detection due to its relatively high sensitivity related to its presence in multiple copies (ranging from 1 to 25 copies depending on bacterial strains) within the MTB genome (Eisenach et al., 1990; Peng et al., 2017). Meanwhile, mutations within the 81-base pair core region of rpoB, corresponding to codons 507–533, are associated with resistance to rifampicin (RIF), the first-line and most common antibiotic for treating TB. Within this *rpoB* hot spot region, we targeted two of the most prevalent mutations, which are mutations at codons 531 and 526 (Ramaswamy and Musser, 1998; Peng et al., 2017). On the other hand, mutations at codon 315 of *katG* and codon 15 of *Inh* genes were known to be the most prevalent hot spot mutations related to resistance to isoniazid (INH), the other first-line drug against TB worldwide (Ramaswamy and Musser, 1998). Harnessing the ability of Indigen MTB/DR-TB RT-PCR to detect MTB while at the same time detecting MTB RIF-resistant and INH-resistant strains, as well as common NTM infections, would be the strongest value proposition of the kit for leveraging TB capacity testing in Indonesia.

We evaluated the Indigen MTB/DR-TB RT-PCR assay performance by conducting a clinical validation study in Jakarta and Bandung, the two major cities in Indonesia with more than 250 TB incidences per 100,000 (Alisjahbana et al., 2021; Ministry of Health Republic Indonesia, 2023). In order to assess the use of Indigen in the routine clinical TB setting, the protocol was applied in such a way that the workflow and diagnostic methodologies were maintained as recommended by national TB guidelines.

2 Methods

2.1 Study design, clinical specimens, and ethics consideration

The clinical performance study was designed as a non-interventional and multicenter study from September 2022 to May 2023. Sputum specimens were obtained from suspected TB patients who visited primary healthcare facilities in Bandung, i.e., UPF BBKPM and Dr. H. A. Rotinsulu Pulmonary Hospital, or from routine sputum specimens that were sent to the national referral TB diagnostic laboratory at Bandung (West Java Provincial Health Laboratory/

WJPHL) and Jakarta (BBLK Jakarta). Only raw sputum with a minimum volume of 4 mL was included in this study. In addition to these, we assessed archived specimen leftovers from the Research Center for Care and Control of Infectious Disease (RC3ID) Universitas Padjadjaran Bandung. Acid-fast bacilli (AFB) smears and culture assays were performed at the respective laboratories, whereas Indigen RT-PCR was performed at Stem Cell and Cancer Institute (SCI) Jakarta, WJPHL in Jakarta, and BBLK in Jakarta. Each sputum sample represented one subject. In order to obtain sufficient power to determine sensitivity and specificity to the 95% confidence interval level for this study, we were targeting to get as few as 300 MTB positive and 300 MTB negative sputum samples based on MTB culture as reference method (Mattocks et al., 2010). All the testing methods were performed blindly between methods and between sites to obtain accountable results.

This study was approved by the Ethics Committee at the Universitas Padjadjaran Bandung, under ethical approval number 876/UN6.KEP/EC/2022. The specimen collection process was a part of the TB-routine clinical diagnostic setting; therefore, informed consent was not required.

2.2 Acid-fast bacilli (AFB) smear microscopy and culture

The presence of AFB was assessed using the Ziehl–Neelsen staining method. It was performed directly in unprocessed sputum at each laboratory site, and the remaining samples were then processed for MTB culture and RT-PCR procedure. In brief, the sputum samples were decontaminated and homogenized using NaLC-4% NaOH according to the protocol recommended by the Ministry of Health for TB diagnostic laboratory guidelines (Ministry of Health Republic of Indonesia, 2021). Following sediment resuspension with phosphate-buffered saline (PBS), the suspension was inoculated into a Lowenstein–Jensen (LJ) tube (0.5 mL) or inoculated into a liquid Bactec mycobacteria growth indicator tube (MGIT) 960 (0.2 mL) (Becton Dickinson, Sparks, MD, USA) at 37°C or at 35°C for 8 weeks, respectively (Vinuesa et al., 2018; Ministry of Health Republic of Indonesia, 2021). Every positive culture was subjected to Ziehl–Neelsen staining to confirm the presence of AFB and cord formation and to exclude contamination. Drug susceptibility testing (DST) was conducted to determine the phenotype of mycobacterial strains against RIF and INH and used as the gold standard reference for Indigen DR/MDR-TB RT-PCR performance to detect MTB RIF- or INH-resistance strains (Ministry of Health Republic of Indonesia, 2021).

2.3 Indigen MTB/TB-DR RT-PCR assay

The Indigen MTB/TB-DR RT-PCR assay was designed to detect key mutations in four gene regions associated with RIF/INH resistance as well as MTB presence. Five dually labeled probes and four pairs of primers have been designed based on (Peng et al., 2017, Supplementary Table 1). Since most of the RT-PCR machines placed in laboratories are available in a 4-channel model, we designed the assay to have two PCR reactions for each sample. Four fluorophores (FAM, HEX, ROX, and Cy5) are attached at the 5′ end of probes, which allows the detection of the target biomarkers in a single PCR reaction simultaneously. In brief, 750 µL of raw sputum or decontaminated or sediment sputum was mixed with an equal volume of lysis buffers in a microcentrifuge tube. The mixture was incubated at room temperature for 30 min with intermittent agitation. Following centrifugation at 14,000 rpm for 3 min, the supernatant was discarded and replaced by 1 mL of saline buffer. The mixture was centrifuged at 14,000 rpm for 3 min, and the supernatant was discarded. A measure of 200 µL of Chelex® solution was added, followed by incubation at 100°C and then centrifugation at 14,000 rpm for 10 min. The supernatant was transferred to a new microcentrifuge tube and used directly as a PCR template or stored at -20°C. All reagents for the DNA extraction procedure were provided in the kit. PCR mixture contained 2 µL of 10 × PCR buffer, 1.6 µL of dNTP (each 2.5 µM), 0.8 µL of MgCl2 (25 mM), 0.2 µL of Taq-polymerase (5 U/ul), 2 µL of primers and probes extracted DNA template of 1 µL, and Milli-Q H_2O to make up the whole PCR mixture volume to 20 µL for each PCR reaction. The PCR cycle was run in a Rotor-Gene Q real-time rotary analyzer (Qiagen, Hilden, Germany) or in a LightCycler instrument (Roche). Cycling parameters consist of denaturation denaturation at 95°C for 15 min, followed by 45 cycles of amplification at 95°C for 15 s, and elongation at 60°C for 1 min. An internal extraction control (IC) for each sample, as well as a negative and positive control for each run, were also included.

Result interpretation was performed based on a simple algorithm. First, the positive signal at the IS6110 probe represents MTB positivity. Second, signals of the other four drug-resistant probes were investigated. When all RIF and INH probes show a negative signal, it is classified as MTB drug-susceptible. On the other hand, when the RIF probes show positive signals, either at S531L and/or H526Y, the sample is classified as RIF resistance. Similarly, the sample is classified as INH resistance when katG and/or inhA probes are positive. Drug-susceptible TB patients can be treated with first-line TB therapy, while TB patients with RIF-mono resistance or INH-mono resistance are considered to receive first-line anti-TB drugs, except RIF or INH, respectively. In addition to this, when both RIF and INH resistance are present, the TB patients are classified as multi-drug resistant and considered to receive a combination of second-line anti-TB drugs (Ministry of Health Republic of Indonesia, 2021).

2.4 Limit of detection and analytical specificity of Indigen MTB/DR-TB RT-PCR

We prepared solution of each bacterial isolate (MTB HRa37, MTB with rpoB S531L, MTB with rpoB H526Y, MTB with katG S315T, MTB with inhA C15T, and *M. smegmatis*) corresponding to McFarland standard no. 1. The limit of detection (LoD) was initially performed by 10-fold dilution of each bacterial isolate in triplicates. The expected LoD was determined, and all replicates were positive. The LoD was then confirmed by repeating the assay using five different serial dilutions of concentration covering the expected range of LoD, which was performed in 20 replicates for each dilution. Final LoD was determined based on the lowest colony forming unit per milliliter (CFU/mL) at ≥95% positivity rate of each bacterial isolate.

The analytical specificity of the probe sequence of *IS6110* was conducted *in silico*. Sequence alignment was performed against PCR products and surrounding sequences of 35 types of mycobacteria, 66

types of non-mycobacteria bacteria, 12 types of fungi, and 14 types of viruses. All sequences were downloaded from https://blast.ncbi.nlm.nih.gov/Blast.cgi. If the designed probes have less than 80% homology in terms of the matched base pair amount with target organisms, potential cross-reactivity may be prevented.

2.5 Sequencing

Bidirectional sequencing was performed on samples with discrepant results using the BigDye Terminator Cycle Sequencing kit, according to the manufacturer's recommendations in a 3130xl Genetic Analyzer (Applied Biosystems). Traces were analyzed with BioEdit v7 2.5.

2.6 Statistical analysis

Fisher's exact test (χ^2) was used to analyze the sensitivity and specificity level of Indigen MTB RT-PCR assay on sputum samples compared to culture, which is considered the TB gold standard method for TB diagnosis. The kappa test was used to measure agreement between the two methods (MedCalc Software Ltd, 2023).

3 Results

3.1 Sputum samples and phenotypic analysis based on AFB smears and MTB culture

A total of 610 sputum samples from 610 TB-suspected subjects were collected from our five study sites. Most of our prospectively collected samples were collected from WJPHL (305 samples), followed by UPF BBKPM, BBLK Jakarta, and Dr. H. A. Rotinsulu Pulmonary Hospital with 105, 89, and 22 samples, respectively. Meanwhile, our archived samples from RC3ID Laboratory were 89 samples. Overall, our cohort samples consist of 306 MTB culture-positive and 304 MTB culture-negative samples. Stratification of samples based on the AFB smear method resulted in 224 smear-positive samples and 386 smear-negative samples, as described in Table 1.

3.2 Limit of detection and analytical specificity of Indigen MTB/DR-TB RT-PCR

The LoD of Indigen MTB/TB DR RT-PCR is 400 CFU/mL for the IS6110 detection, 6,000 CFU/mL for the *rpoB* S531L and *rpoB* H526Ydetection, 400 CFU/mL for the *katG* S315T detection, and 6,000 CFU/mL for the *inhA* C15T detection (Supplementary Data 1). Analytical specificity test demonstrated that the *IS6110* probe has no homology with greater or equal to 80% against listed bacteria (mycobacteria and non-mycobacteria), fungi, and viruses (Supplementary Data 2).

3.3 Performance of Indigen MTB/DR-TB RT-PCR on detecting MTB in sputum

The results of culture, AFB smear microscopy, and Indigen MTB/DR-TB RT-PCR are given in Table 1. Compared to culture, the overall sensitivity and specificity of Indigen MTB/DR-TB RT-PCR in detecting MTB were 94.12% (95% CI 90.86–96.48) and 98.36% (95% CI 96.20–99.46), respectively. The positive predictive value (PPV) and negative predictive value (NPV) were 98.29% (95% CI 96.02–99.28) and 94.41% (95% CI 91.39–96.30). However, when the analysis was stratified based on AFB smear-negative samples (386 samples), a lower sensitivity level was found at 78.57% (95% CI, 68.26–86.78%), while the specificity remained similar at 98.34% (95% CI, 96.18–99.46%). On the other hand, the PPV and NPV levels for these AFB smear-negative samples were 92.96% (95% CI 84.60–96.94) and 94.29% (95% CI 91.63–96.13). Corresponding values for sensitivity, specificity, PPV, and NPV of the other 224 AFB smear-positive samples were 100 (95% CI 98.35–100.00), 100 (95% CI 15.8–100.00), 100 (95% CI 98.35–100.00), and 100 (95% CI 15.81–100.00), respectively. Overall agreement between culture and Indigen MTB/DR-TB RT-PCR was 96.23% (95% CI 94.40–97.60).

TABLE 1 Performance of Indigen MTB/DR-TB RT-PCR for detecting MTB in all sputum samples and in samples stratified according to smear results.

AFB smear microscopy result	Indigen MTB/DR-TB	MTB culture positive	MTB culture negative	Sensitivity, % (95% CI)	Specificity, % (95% CI)	PPV (95% CI)	NPV (95% CI)	Accuracy (95% CI)	κ-value ± SE
Overall ($N = 610$)	MTB positive	288	5	94.1 (90.9–96.5)	98.4 (96.2–99.5)	98.3 (96.0–99.3)	94.4 (91.4–96.3)	96.2 (94.4–97.6)	0.9 ± 0.02 0.9–1
	MTB negative	18	299						
Positive ($N = 224$)	MTB positive	222	0	100 (98.4–100)	100 (15.8–100)	100 (98.4–100)	100 (15.8–100)	100 (98.4–100)	1 ± 0 1–1
	MTB negative	0	2						
Negative ($N = 386$)	MTB positive	66	5	78.6 (68.3–86.8)	98.3 (96.2–99.5)	93 (84.6–97)	94.3 (91.6–96.1)	94 (91.2–96.2)	0.8 ± 0.04 0.7 ± 0.9
	MTB negative	18	297						

PPV, positive predictive value; NPV, negative predictive value.

3.4 Performance of Indigen MTB/DR-TB RT-PCR on detecting MTB RIF/INH resistance in sputum

We assessed the Indigen MTB/DR-TB RT-PCR ability to detect drug-resistant (MTB DR) on 65 samples that already had DST results and sufficient volume for RT-PCR. Of these samples, 28 were MTB drug-susceptible, and the remaining 37 samples were MTB DR samples. Based on the DST result, the MTB DR samples mainly consisted of 78.4% (29/37) double RIF- and INH-resistant and 21.6% (8/37) RIF-mono-resistant. Our result showed that the sensitivity and specificity levels of Indigen MTB/DR-TB RT-PCR to detect RIF resistance and INH resistance were 78.2% (95% CI, 61.8–90.2%) and 82.8% (95% CI, 64.2–94.2%), respectively, while the specificity level for both groups is at 100% (95% CI, 87.7–100%) (Table 2).

We found eight samples with false-susceptible results for RIF resistance. These samples contained MTB with mutations other than the targets of Indigen TB DR/MDR RT-PCR. Of these samples, three contained MTB with single amino acid substitutions at D526Y/H526D/H526H, while five contained multiple amino acid substitutions, including G523G, D516Y, H526N, H526Q, L521L, L524L, L530L, P520P, R528R, R529R, S522A, S522G, S531F, S531N, and 518-Del (Table 3). Meanwhile, we found five false-susceptible samples for INH resistance. Of these samples, four were confirmed susceptible, while one sample contained amino acid substitution at *katG* (S315T) (Table 3).

4 Discussion

Early TB diagnosis followed by precise treatment is critical to stopping the transmission of TB disease. Despite a significant increase in NAAT implementation for TB diagnosis such as GeneXpert MTB/RIF in Indonesia, considerable underreporting of TB cases remains to be addressed (Ministry of Health Republic Indonesia, 2020, 2023). In this study, we demonstrated the clinical performance of a newly

TABLE 2 Performance of Indigen MTB/DR-TB RT-PCR based on rifampicin and isoniazid phenotypic susceptibility testing.

Target drug	Indigen MTB/DR-TB results	Phenotypic DST testing results (n = 65)		Sensitivity, % (95% CI)	Specificity, % (95% CI)	PPV (95% CI)	NPV (95% CI)	Accuracy (95% CI)	κ-value
		Resistant	Susceptible						
Rifampicin	Resistant	29	0	78.4 (61.8–90.2)	100 (87.7–100)	100 (88.1–100)	77.8 (65.5–86.6)	87.7 (77.2–94.5)	0.8 ± 0.08 0.6–0.9
	Susceptible	8	28						
Isoniazid	Resistant	24	0	82.8 (64.2–94.2)	100 (90.3–100)	100 (85.8–100)	87.8 (76.4–94.1)	92.3 (83–97.5)	0.8 ± 0.07 0.7–1
	Susceptible	5	36						

DR, drug resistance to RIF- or INH; PPV, positive predictive value; NPV, negative predictive value.

TABLE 3 Sanger sequencing analysis for samples with discordant susceptibility results.

ID	Indigen MTB/DR-TB RT-PCR	Phenotypic DST		RIF sequencing results
		RIF	INH	
2400214	TB+, INH Resistance	Resistant	Resistant	P520P, L521L, S522A, G523G, L524L, R529R
2400297	TB+, INH resistance	Resistant	Resistant	P520P, L521L, S522A, G523G, R528R
2400284	TB+, INH resistance	Resistant	Resistant	P520P, L521L, S522G, L530L, S531F
2400301	TB+, INH resistance	Resistant	Resistant	D516Y
2400184	TB+, INH resistance	Resistant	Resistant	L521L, G523G, L524L, R528R, R529R
2400182	TB+, INH resistance	Resistant	Resistant	H526D
2400197	TB+, INH resistance	Resistant	Resistant	P520P, G523G, R529R
2400185	TB+, INH resistance	Resistant	Resistant	518_Del, H526N
ID	Indigen MTB/DR-TB RT-PCR	Phenotypic DST		INH sequencing result
		RIF	INH	
2400189	TB+, RIF resistance	Resistant	Resistant	Wild type
2400208	TB+, RIF resistance	Resistant	Resistant	Wild type
2400162	TB+, RIF resistance	Resistant	Resistant	Wild type
2400210	TB+, RIF resistance	Resistant	Resistant	Wild type
2400214	TB+, RIF-sensitive, INH-sensitive	Resistant	Resistant	S315T

developed TB NAAT, the Indigen DR/MDR RT-PCR, on 610 sputum samples obtained from 610 TB-suspected patients. This kit was designed as an open-system RT-PCR that can be implemented in any molecular laboratory equipped with an RT-PCR machine. The clinical performance of Indigen DR/MDR RT-PCR on detecting MTB, RIF, and INH resistance was almost in perfect agreement with MTB culture and DST, as shown by a kappa value of ≥0.8 in all analyses: overall samples, stratified based on AFB smear microscopy results, DR samples, and MDR samples. The findings support the potential use of Indigen MTB/DR-TB RT-PCR as an early TB diagnostic in clinical laboratory settings.

The gold standard technique for TB diagnostics is culture; however, the process requires 2–8 weeks to complete. NAAT-based testing, such as RT-PCR, has been widely accepted for TB diagnosis as it offers great robustness and a shorter turnaround time. However, to be accepted as a TB diagnosis NAAT, an assay should demonstrate high reliability, sensitivity, specificity, and accessibility levels. To achieve those requirements, one of the most determining factors is primers specific to target sequences within the MTB genome. Most TB PCR-based assays target *IS6110* to detect MTB in pulmonary and extra-pulmonary specimens (Noordhoek et al., 1994; Lee et al., 2014; Araya et al., 2021). It has been reported that the sensitivity and specificity of *IS6110* sequence-based PCR for the detection of MTB differ among trials, ranging from 50 to 90% and 60 to 100%, respectively, compared to culture (Noordhoek et al., 1994). Despite this wide range of performance, our study demonstrated that the overall sensitivity and specificity of the Indigen MTB/DR-TB RT-PCR assay to detect MTB in sputum were 94.1 and 98.1%, respectively, in comparison to the standard TB culture method, along with a kappa value of ≥0.9. Concordant with our results, studies on the performance of a commercial IS6110 sequence-based PCR assay, Abbot Real-Time RIF/INH, reported a sensitivity level of 92.4% (Araya et al., 2021), while another meta-analysis study confirmed that the assay had sensitivity and specificity levels of 96 and 97%, respectively (Wang et al., 2019). Moreover, another comparison study between the *IS6110*-Taq Man-based PCR assay and GeneXpert RIF/INH reported that *IS6110*-Taq Man-based had better sensitivity (84% vs. 79%, respectively, 19). All these findings support that multicopy target *IS6110*, which is present at 10 to 15 copies in most genomes of MTB, contributes to the better sensitivity of the TB PCR-based assay (Eisenach et al., 1990; Araya et al., 2021).

Approximately 17% of TB transmission was attributable to the presence of AFB smear-negative, culture-positive TB patients. It was estimated that 20 to 50% of pulmonary TB patients are AFB smear negative (Sarmiento et al., 2003). The TB diagnostic assay should overcome this low-load AFB specimen to deliver good performance, allowing clinicians to deliver early correct treatment to patients and prevent disease transmission. The proportion of AFB smear-negative among culture-positive TB samples in our cohort was 84/310 (27.1%), and Indigen MTB/DR-TB was able to detect 66 of them (78.6% sensitivity) with a kappa value of ≥0.8. In line with our results, a meta-analysis approach on six studies by Sarmiento et al. (2003) reported that the sensitivity of PCR-based testing for the diagnosis of MTB in AFB smear-negative sputum was 70% compared to the standard culture method. Contrarily, the same study also reported that the sensitivity ranged between 32 and 92% depending on the type of sample and the type of study design. Another study demonstrated that the performance of an IS6110 sequence-based PCR on AFB smear-negative sputum was 64.5% (Lodha et al., 2022). In addition, another previous study revealed that IS6110-TaqMan assay performed better sensitivity than GeneXpert MTB/RIF on AFB smear-negative sputum (69 vs. 48%, 19), while another study demonstrated GeneXpert MTB/RIF had a sensitivity level of 73.1% compared to culture (Lombardi et al., 2017).

Several factors might contribute to the variability in the sensitivity of *IS6110* sequence-based PCR found in different studies. Regarding this, apart from the target sequence used, the diagnosis performance might depend on the efficiency of the DNA extraction process. The Indigen MTB/DR-TB RT-PCR involves simple steps, including a lysis procedure, a heating process, followed by sedimentation through centrifugation. Although the process requires more time to complete, these manual steps could be more reliable for AFB smear-negative samples due to their better efficiency in eliminating the inhibiting substances and allowing optimal bacterial lysis compared to the cartridge-based GeneXpert MTB/RIF system (Kolia-Diafouka et al., 2018). Furthermore, a study by Tan et al. (1997) showed that a simple DNA release method did not seem to impair the sensitivity of PCR assays. This simple procedure could be easily integrated into the routine schedule of a mycobacteriology laboratory without changing the existing TB workflow. In general, the abovementioned factors might support the Indigen MTB/DR-TB's good performance in detecting MTB in this study.

Indigen MTB/DR-TB RT-PCR discrepant results for MTB detection were observed in 18 (5.88%) false-negative MTB samples. As expected, they were included in the AFB smear-negative samples. Of these samples, 13 showed a late cycle threshold between 35 and 37 cycles, while the remaining gave an undetectable amplification signal. Adjusting the Ct threshold value up to 40 cycles would have eliminated 13 of the 18 samples; however, this would simultaneously decrease the specificity level. Since the Indigen MTB/DR-TB assay demonstrated specificity above 97% in all analysis categories, the assay was considered to have optimum performance.

The prevalence of drug-resistant MTB strains can vary between and within countries. According to the WHO's Global Tuberculosis Report, the prevalence of RIF-resistant TB in new cases was estimated to be approximately 3.4% in 2020 (World Health Organization, 2023), while a lower prevalence of 1.3% (12,531/969,000) was reported by the government of Indonesia in 2023 (Ministry of Health Republic Indonesia, 2023). INH resistance is often closely associated with RIF resistance, and their co-occurrence is commonly defined as MDR (Armand et al., 2011; World Health Organization, 2023). Detecting resistance mutations in primary samples enables the immediate initiation of the correct treatment. In order to support early diagnosis in DR/MDR cases, Indigen MTB/DR-TB RT-PCR was designed to detect two frequent mutations related to RIF resistance and two frequent mutations related to INH resistance. In this study, its performance was compared to DST on 65 samples. In terms of detecting RIF resistance, Indigen was able to detect 29 of 37 RIF-resistant samples (78.4% sensitivity) and correctly detect 28 MTB-susceptible samples (100% specificity). The performance was considered lower than previously established TB assays, such as Abbot Real-Time RIF/INH (Wang et al., 2019) or GeneXpert MTB/RIF

(Boehme et al., 2010). The discrepant results for false RIF-susceptible were observed in 22% (8/37) of DR/MDR cases, and these were mainly because of mutations within 81-rpoB hotspot regions that were out of the target range of Indigen DR/MDR RT-PCR (Table 3). In addition to this, Indigen was able to detect 24 of 29 INH-resistant samples (82.8% sensitivity) and correctly detect 36 INH-susceptible samples (100% specificity). The sensitivity was lower than Abbot Real-Time RIF/INH[18] but higher than other PCR assays that also cover INH-resistance mutations (FT-MTBDR; Hain Lifescience; 26).

Four of five false-susceptible INH discrepant results were confirmed to harbor wild-type sequences at *katG* and *inhA* (C15T). The reason for the lack of detection based on Indigen was unknown because Sanger sequencing results support our findings. One sample harbored a mutation at the *katG* (S315T) sequence that was actually detected nearly above our Ct value threshold. In this case, adjusting the Ct value threshold up to 40 might increase the sensitivity level; however, this would require another DR study to confirm the validity of the adjusted Ct value threshold and would be considered for our future research.

There are limitations to the current study that should be considered. First, a relatively small number of samples were included for DR-TB analysis. This may have limited the statistical power of the assessment of the Indigen MTB/DR-TB RT-PCR analysis. Second, we included archived, decontaminated frozen samples in this study. Therefore, the length of storage time might affect the quality of isolated nucleic acids, thus lowering the quantity of targeted DNA. Finally, we are fully aware of the limited coverage of the MTB RIF-resistance region of Indigen MTB/DR-TB RT-PCR; however, the kit is also equipped with probes targeting frequent INH-resistant MTB, which enable MDR detection in samples simultaneously.

5 Conclusion

The Indigen MTB/DR-TB RT-PCR assay evaluated in this study demonstrated reliable sensitivity compared to the gold standard method of culture. The Indigen MTB/DR-TB RT-PCR detects RIF resistance as well as INH resistance, providing clinicians with more resistance information to deliver prompt treatment early. Further studies are required to evaluate the performance of this kit in more clinical sputum from suspected DR-TB patients.

Data availability statement

The original contributions presented in the study are included in the article/Supplementary material, further inquiries can be directed to the corresponding author.

Author contributions

IPar: Conceptualization, Resources, Writing – review & editing. LC: Conceptualization, Resources, Supervision, Writing – review & editing. MY: Conceptualization, Data Curation, Formal analysis, Investigation, Writing – original draft, Writing – review & editing. MM: Resources, Supervision, Writing – review & editing. DB: Conceptualization, Data Curation, Formal analysis, Writing – original draft, Writing – review & editing. SS: Conceptualization, Data Curation, Writing – original draft, Writing - review & editing. RRi: Resources, Supervision, Writing – review & editing. RRa: Resources, Supervision, Writing – review & editing. RN: Resources, Supervision, Writing – review & editing. IPam: Resources, Supervision, Writing – review & editing. AB: Conceptualization, Supervision, Data Curation, Formal analysis, Writing – original draft, Writing – review & editing.

Ethics statement

The studies involving humans were approved by the Ethics Committee at Universitas Padjadjaran Bandung, ethical approval number 876/UN6.KEP/EC/2022. The studies were conducted in accordance with the local legislation and institutional requirements. The participants provided their written informed consent to participate in this study.

Funding

The author(s) declare financial support was received for the research, authorship, and/or publication of this article. This study was funded by PT. Kalbe Farma Tbk.

Acknowledgments

The authors thank Tri Fajari Agustini, director of H. A. Rotinsulu Pulmonary Hospital, Eka Jusup Singka, director of BBLK, Jakarta, and Andi Utama, director of KALGen Innolab Clinical Laboratorium for accommodating research in their institutions. The authors also thank Retno Ambarwati, director of PT. Kalgen DNA, for providing the Indigen MTB/DR-TB RT-PCR for this research.

Conflict of interest

The authors declare that the research was conducted in the absence of any commercial or financial relationships that could be construed as a potential conflict of interest.

Publisher's note

Supplementary material

The Supplementary material for this article can be found online at: https://www.frontiersin.org/articles/10.3389/fmicb.2024.1372647/full#supplementary-material

References

Alisjahbana, B., Koesoemadinata, R. C., Hadisoemarto, P. F., Lestari, B. W., Hartati, S., Chaidir, L., et al. (2021). Are neighbourhoods of tuberculosis cases a high-risk population for active intervention? A protocol for tuberculosis active case finding. *PLoS One* 16:e0256043. doi: 10.1371/journal.pone.0256043

Araya, B. T., Ali, K. E., Geleta, D. A., Tekele, S. G., and Tulu, K. D. (2021). Performance of the Abbott RealTime MTB and RIF/INH resistance assays for the detection of *mycobacterium tuberculosis* and resistance markers in sputum specimens. *PLoS One* 16:e0251602. doi: 10.1371/journal.pone.0251602

Armand, S., Vanhuls, P., Delcroix, G., Courcol, R., and Lemaître, N. (2011). Comparison of the Xpert MTB/RIF test with an IS6110-TaqMan real-time PCR assay for direct detection of *Mycobacterium tuberculosis* in respiratory and nonrespiratory specimens. *J. Clin. Microbiol.* 49, 1772–1776. doi: 10.1128/JCM.02157-10

Babafemi, E. O., Cherian, B. P., Banting, L., Mills, G. A., and Ngianga, K. (2017). Effectiveness of real-time polymerase chain reaction assay for the detection of *Mycobacterium tuberculosis* in pathological samples: a systematic review and meta-analysis. *Syst. Rev.* 6:215. doi: 10.1186/s13643-017-0608-2

Boehme, C. C., Nabeta, P., Hillemann, D., Nicol, M. P., Shenai, S., Krapp, F., et al. (2010). Rapid molecular detection of tuberculosis and rifampin resistance. *N. Engl. J. Med.* 363, 1005–1015. doi: 10.1056/NEJMoa0907847

Chakaya, J., Khan, M., Ntoumi, F., Aklillu, E., Fatima, R., Mwaba, P., et al. (2020). Reflections on the global TB burden, treatment and prevention efforts. *Int. J. Infect. Dis.* 113 Suppl 1, S7–S12. doi: 10.1016/j.ijid.2021.02.107

Eisenach, K. D., Cave, M. D., Bates, J. H., and Crawford, J. T. (1990). Polymerase chain reaction amplification of a repetitive DNA sequence specific for *Mycobacterium tuberculosis*. *J. Infect. Dis.* 161, 977–981. doi: 10.1093/infdis/161.5.977

Espy, M. J., Uhl, J. R., Sloan, L. M., Buckwalter, S. P., Jones, M. F., Vetter, E. A., et al. (2006). Real-time PCR in clinical microbiology: applications for routine laboratory testing. *Clin. Microbiol. Rev.* 19, 165–256. doi: 10.1128/CMR.19.1.165–256

Kolia-Diafouka, P., Godreuil, S., Bourdin, A., Carrère-Kremer, S., Kremer, L., Van de Perre, P., et al. (2018). Optimized lysis-extraction method combined with IS6110-amplification for detection of *Mycobacterium tuberculosis* in Paucibacillary sputum specimens. *Front. Microbiol.* 9:9. doi: 10.3389/fmicb.2018.02224

Lee, H., Park, K. G., Lee, G., Park, J., Park, Y. G., and Park, Y. J. (2014). Assessment of the quantitative ability of AdvanSure TB/NTM real-time PCR in respiratory specimens by comparison with phenotypic methods. *Ann. Lab. Med.* 34, 51–55. doi: 10.3343/alm.2014.34.1.51

Lodha, L., Mudliar, S. R., Singh, J., Maurya, A., Khurana, A. K., Khadanga, S., et al. (2022). Diagnostic performance of multiplex PCR for detection of *Mycobacterium tuberculosis* complex in presumptive pulmonary tuberculosis patients and its utility in smear negative specimens. *J. Lab. Physicians.* 14, 403–411. doi: 10.1055/s-0042-1757231

Lombardi, G., Di Gregori, V., Girometti, N., Tadolini, M., Bisognin, F., and Dal Monte, P. (2017). Diagnosis of smear-negative tuberculosis is greatly improved by Xpert MTB/RIF. *PLoS One* 12:e0176186. doi: 10.1371/journal.pone.0176186

Mattocks, C. J., Morris, M. A., Matthijs, G., Swinnen, E., Corveleyn, A., Dequeker, E., et al. (2010). A standardized framework for the validation and verification of clinical molecular genetic tests. *Eur. J. Hum. Genet.* 18, 1276–1288. doi: 10.1038/ejhg.2010.101

MedCalc Software Ltd. Diagnostic test evaluation calculator. (2023). Available at: https://www.medcalc.org/calc/diagnostic_test.php (Version 22.014); Accessed October 18, 2023).

Ministry of Health Republic Indonesia (2020). *The Republic of Indonesia joint external monitoring Mission for tuberculosis*. Indonesia: Ministry of Health Republic of Indonesia.

Ministry of Health Republic Indonesia. *Dashboard data kondisi TB di Indonesia*. (2023). Available at: https://tbindonesia.or.id/pustaka-tbc/dashboard/. (Accessed on November 9, 2023).

Ministry of Health Republic of Indonesia. *Petunjuk teknis dan pemantapan mutu: pemeriksaan biakan, identifikasi, dan uji kepekaan Mycobacterium tuberculosis complex terhadap obat anti Tuberkulosis pada media padat dan media cair*. Indonesia: Ministry of Health of the Republic of Indonesia. (2021).

Noordhoek, G. T., Kolk, A., Bjune, G., Catty, D., Dale, J. W., Fine, P., et al. (1994). Sensitivity and specificity of PCR for detection of *Mycobacterium tuberculosis*: a blind comparison study among seven laboratories. *J. Clin. Microbiol.* 32, 277–284. doi: 10.1128/jcm.32.2.277-284.1994

Peng, J., Yu, X., Cui, Z., Xue, W., Luo, Z., Wen, Z., et al. (2017). Multi-fluorescence real-time PCR assay for detection of RIF and INH resistance of *M.Tuberculosis*. *Front. Microbiol.* 7:7618. doi: 10.3389/fmicb.2016.00618

Ramaswamy, S., and Musser, J. M. (1998). Molecular genetic basis of antimicrobial agent resistance in *Mycobacterium tuberculosis*: 1998 update. *Tuber. Lung Dis.* 79, 3–29. doi: 10.1054/tuld.1998.0002

Sarmiento, O. L., Weigle, K. A., Alexander, J., Weber, D. J., and Miller, W. C. (2003). Assessment by meta-analysis of PCR for diagnosis of smear-negative pulmonary tuberculosis. *J. Clin. Microbiol.* 41, 3233–3240. doi: 10.1128/JCM.41.7.3233-3240.2003

Svensson, E., Folkvardsen, D. B., Rasmussen, E. M., and Lillebaek, T. (2021). Detection of *Mycobacterium tuberculosis* complex in pulmonary and extrapulmonary samples with the FluoroType MTBDR assay. *Clin. Microbiol. Infect.* 27, 1514.e1–1514.e4. doi: 10.1016/j.cmi.2020.12.020

Tan, M. F., Ng, W. C., Chan, S. H., and Tan, W. C. (1997). Comparative usefulness of PCR in the detection of *Mycobacterium tuberculosis* in different clinical specimens. *J. Med. Microbiol.* 46, 164–169. doi: 10.1099/00222615-46-2-164

Vinuesa, V., Borras, R., Brionnes, M. L., Clari, M. A., Cresencio, V., Gimenez, E., et al. (2018). Performance of highly sensitive *Mycobacterium tuberculosis* complex real-time PCR assay for diagnosis of pulmonary tuberculosis in a low-prevalence setting: a prospective intervention study. *J. Clin. Microbiol.* 56, e00116–e00118. doi: 10.1128/JCM.00116-18

Wang, M. G., Xue, M., Wu, S. Q., Zhang, M. M., Wang, Y., Liu, Q., et al. (2019). Abbott RealTime MTB and MTB RIF/INH assays for the diagnosis of tuberculosis and rifampicin/isoniazid resistance. *Infect. Genet. Evol.* 71, 54–59. doi: 10.1016/j.meegid.2019.03.012

World Health Organization (2023). *Global tuberculosis report*. Geneva: WHO.

frontiers | Frontiers in Microbiology

TYPE Original Research
PUBLISHED 17 May 2024
DOI 10.3389/fmicb.2024.1374458

OPEN ACCESS

EDITED BY
Lin Fan,
Tongji University, China

REVIEWED BY
Valeria Cavalcanti Rolla,
Instituto Nacional de Infectologia Evandro Chagas (INI), Brazil
Rizaldy Taslim Pinzon,
Duta Wacana Christian University, Indonesia
Ahmad Rizal Ganiem,
Padjadjaran University, Indonesia

*CORRESPONDENCE
Ting Wang
✉ pengjinli@126.com
Gang Zhao
✉ zhaogang@nwu.edu.cn

†These authors have contributed equally to this work

RECEIVED 22 January 2024
ACCEPTED 24 April 2024
PUBLISHED 17 May 2024

CITATION
Wang T, Li M-y, Cai X-s, Cheng Q-s, Li Z, Liu T-t, Zhou L-f, Wang H-h, Feng G-d, Marais BJ and Zhao G (2024) Disease spectrum and prognostic factors in patients treated for tuberculous meningitis in Shaanxi province, China.
Front. Microbiol. 15:1374458.
doi: 10.3389/fmicb.2024.1374458

Disease spectrum and prognostic factors in patients treated for tuberculous meningitis in Shaanxi province, China

Ting Wang[1*†], Meng-yan Li[1†], Xin-shan Cai[2†], Qiu-sheng Cheng[1], Ze Li[1], Ting-ting Liu[3], Lin-fu Zhou[4], Hong-hao Wang[1], Guo-dong Feng[5], Ben J. Marais[6] and Gang Zhao[3,4*]

[1]Department of Neurology, Guangzhou First People's Hospital, School of Medicine, South China University of Technology, Guangzhou, China, [2]Department of Clinical Laboratory, Guangzhou Chest Hospital, Guangzhou, China, [3]Department of Neurology, Xijing Hospital, The Air Force Medical University, Xi'an, China, [4]Department of Neurology, Northwestern University School of Medicine, Xi'an, China, [5]Department of Neurology, Zhongshan Hospital, Fudan University, Shanghai, China, [6]Sydney Infectious Diseases Institute (Sydney ID) and the WHO Collaborating Centre in Tuberculosis, University of Sydney, Sydney, NSW, Australia

Background: Tuberculous meningitis (TBM) is the most severe form of tuberculosis (TB) and can be difficult to diagnose and treat. We aimed to describe the clinical presentation, diagnosis, disease spectrum, outcome, and prognostic factors of patients treated for TBM in China.

Methods: A multicenter retrospective study was conducted from 2009 to 2019 enrolling all presumptive TBM patients referred to Xijing tertiary Hospital from 27 referral centers in and around Shaanxi province, China. Patients with clinical features suggestive of TBM (abnormal CSF parameters) were included in the study if they had adequate baseline information to be classified as "confirmed," "probable," or "possible" TBM according to international consensus TBM criteria and remained in follow-up. Patients with a confirmed alternative diagnosis or severe immune compromise were excluded. Clinical presentation, central nervous system imaging, cerebrospinal fluid (CSF) results, TBM score, and outcome—assessed using the modified Barthel disability index—were recorded and compared.

Findings: A total of 341 presumptive TBM patients met selection criteria; 63 confirmed TBM (25 culture positive, 42 Xpert-MTB/RIF positive), 66 probable TBM, 163 possible TBM, and 49 "not TBM." Death was associated with BMRC grade III (OR = 5.172; 95%CI: 2.298–11.641), TBM score ≥ 15 (OR = 3.843; 95%CI: 1.372–10.761), age > 60 years (OR = 3.566; 95%CI: 1.022–12.442), and CSF neutrophil ratio ≥ 25% (OR = 2.298; 95%CI: 1.027–5.139). Among those with confirmed TBM, nearly one-third (17/63, 27.0%) had a TBM score < 12; these patients exhibited less classic meningitis symptoms and signs and had better outcomes compared with those with a TBM score ≥ 12. In this group, signs of disseminated/miliary TB (OR = 12.427; 95%CI: 1.138–135.758) and a higher TBM score (≥15, OR = 8.437; 95%CI: 1.328–53.585) were most strongly associated with death.

Conclusion: TBM patients who are older (>60 years) have higher TBM scores or CSF neutrophil ratios, have signs of disseminated/miliary TB, and are at greatest risk of death. In general, more effort needs to be done to improve early diagnosis and treatment outcome in TBM patients.

KEYWORDS
tuberculous meningitis, prognostic factors, disease spectrum, diagnostic, CSF

Introduction

Tuberculous meningitis (TBM) is the most severe form of tuberculosis (TB). The best way to improve TBM outcome is early diagnosis and timely effective treatment (Donovan et al., 2020). Most patients with TBM are diagnosed based on their clinical features, neuroimaging findings, and characteristic changes in their cerebrospinal fluid (CSF). The methods that are currently available for diagnosis (Wang et al., 2016) have their strengths and weaknesses (Marais et al., 2010) but remain sub-optimal (Ho et al., 2013; Seddon and Thwaites, 2019). Difficulties include frequent atypical clinical manifestations, the need for invasive CSF sampling, and poor microbiological yield (Arshad et al., 2020). Therefore, early diagnosis and timely treatment of TBM remains challenging (Huynh et al., 2022).

Microbiological confirmation requires *M. tuberculosis* to be cultured from CSF or a positive World Health Organization (WHO)-approved commercial nucleic acid amplification test (NAAT) (Marais et al., 2010). CSF culture is limited by low sensitivity and slow turn-around time. Liquid culture using the mycobacteria growth indicator tube (MGIT) method is more sensitive and faster than traditional Lowenstein–Jensen (LJ) solid medium used in most TB endemic settings (Koh et al., 2012; Tayyab et al., 2018). Commercial NAATs, such as Xpert MTB/RIF and Xpert MTB/RIF Ultra (Dorman et al., 2018; Kohli et al., 2021), have sensitivity comparable to culture and can be completed within 2 h, but it is relatively expensive. Although it is extremely useful as a 'rule in' test, its sensitivity is too low to serve as a reliable 'rule out' test (Kohli et al., 2021). Microscopic acid-fast staining, including modified Ziehl–Neelsen (MZN) staining (Chen et al., 2012), is convenient and fast but hampered by poor accuracy (Wang et al., 2016).

To improve TBM management in China, it is important for doctors to consider the relative value of different diagnostic approaches and the factors associated with poor outcome. Therefore, we conducted a study to describe the clinical presentation and outcome of patients treated for TBM, with specific emphasis on diagnostic approaches and prognostic factors.

Materials and methods

Study design, setting, and ethics approval

We performed a multicenter retrospective study from May 2009 to April 2019, including all patients with presumptive TBM referred to Xijing tertiary Hospital from 27 referral centers in and around Shaanxi province, China, which was coordinated by Xijing hospital of the Air Force Medical University; one of the largest medical centers in China (a 3,218-bed university-affiliated hospital). All patients underwent chest X-ray (CXR), lumber puncture, brain magnetic resonance imaging (MRI), and/or computed tomography (CT) scanning and were tested for human immunodeficiency virus (HIV) using an enzyme-linked immunosorbent assay. The study protocol was approved by the Ethics Committee of Xijing Hospital of Air Force Medical University (Study No. KY20105255-1 and No. KY20163367-1) and the Ethics Committee of Guangzhou First People's Hospital (Study No. K-2022-054-01).

Clinical data

Clinical data (including demographics, clinical, radiological, and routine CSF laboratory results) were collected through medical record review using a standard data capture tool, while trained interviewers completed telephone follow-ups after the patient was discharged from hospital on TB treatment using a standard questionnaire. Patients with clinical signs and symptoms and abnormal CSF parameters (pleocytosis or elevated protein levels) suggestive of TBM are classified as "confirmed," "probable," or "possible" TBM based on international uniform consensus diagnostic criteria for TBM research (Marais et al., 2010) (Supplementary Panel S1). Patients were only included if meet minimum data quality and completeness criteria were met. Confirmed TBM required a positive *M. tuberculosis* culture or Xpert MTB/RIF on CSF, and given that all patients received brain imaging, probable TBM required a TBM score of ≥12 and possible TBM score of 6–11. Severity grading was done using revised British Medical Research Council (BMRC, 1948) TBM severity grade criteria (Solomons et al., 2015). MZN was not considered as evidence of microbiological confirmation given sub-optimal specificity and the possibility of false positives (Wang et al., 2016; Heemskerk et al., 2018). Patients with confirmed viral, cryptococcal, or bacterial meningitis, intracranial tumor, intracranial hematoma, underlying malignancy, or HIV infection were excluded from the study (Figure 1). People living with HIV were excluded because there were only a small number representing a very specific subgroup with unique and well-described risk factors (Marais et al., 2011).

The modified Barthel Index assesses a person's functional independence in daily activities and is useful to track neurological recovery over time (Collin et al., 1988). The Barthel Index consists of 10 items with a designated numerical value that corresponds to the level of assistance required to perform specific tasks. The total score ranges from 0 to 20, with higher scores indicating greater independence. We conducted telephonic outcome assessments, utilizing the modified Barthel Index (Supplementary Panel S2) (Collin et al., 1988), 9–24 months post treatment completion (Jha et al., 2015). Patients who were 'lost to follow up' after completing TBM treatment were excluded from comparative outcome analyses. A modified Bathel Index score of <12 was categorized as "poor outcome," indicating diminished functional status. Poor outcome was only measured in those in whom an outcome was recorded. In general, TB treatment was only commenced after diagnostic work-up and collection of CSF samples, but in some instances, documentation was unclear.

All patients received standard WHO-recommended TBM treatment with isoniazid (300 mg/d), rifampicin (450–600 mg/d),

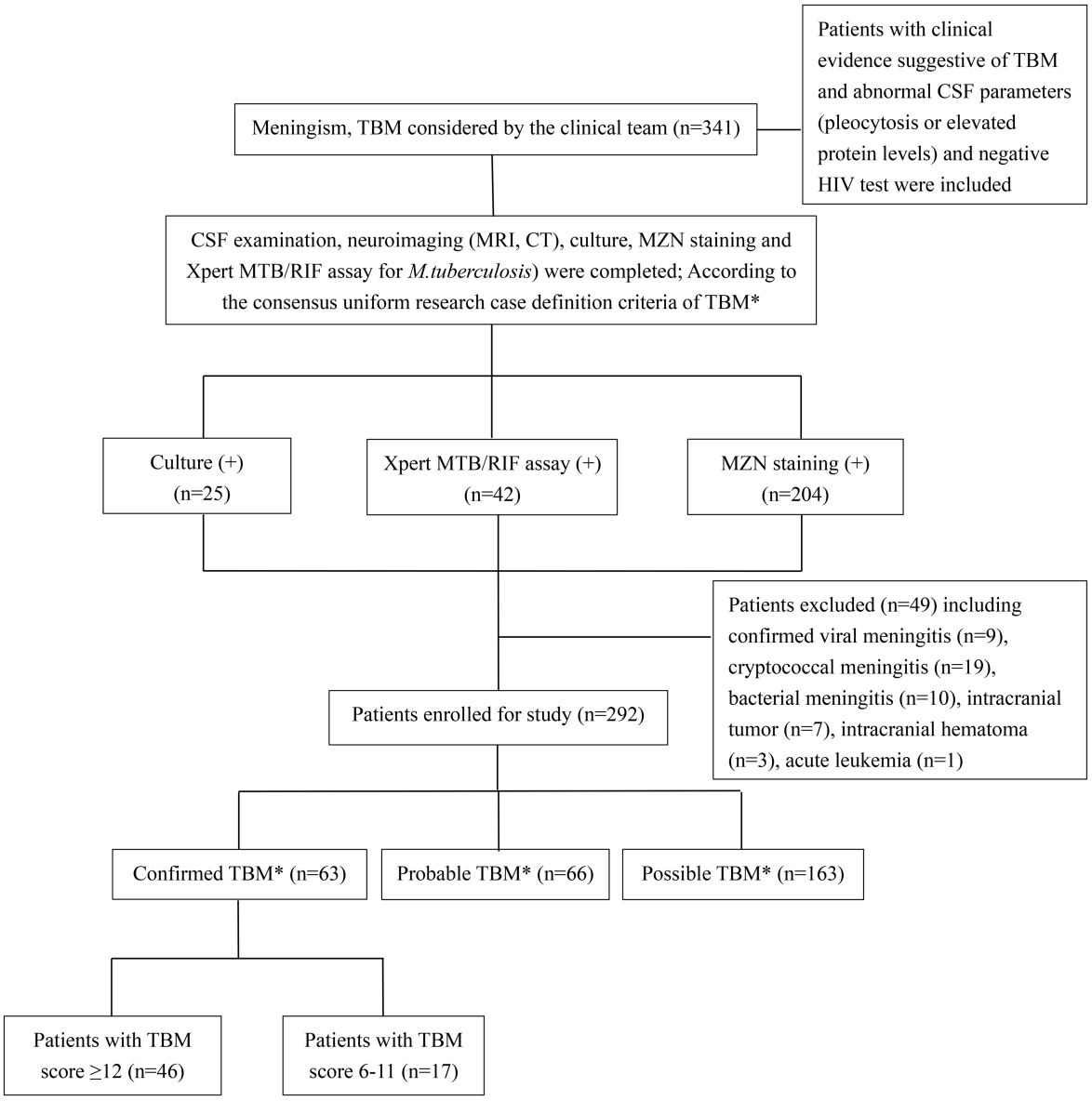

FIGURE 1
Flow diagram of patients with presumptive tuberculous meningitis included in the study. TBM, tuberculous meningitis; CSF, cerebrospinal fluid; MZN, modified Ziehl–Neelsen staining; HIV, human immunodeficiency virus. *According to consensus uniform research case definition criteria (Marais et al., 2010) (Supplementary Panel S1).

pyrazinamide (20–30 mg/kg/d), and ethambutol (15–20 mg/kg/d) orally during the 2-month intensive phase (World Health Organization, 2010; Thwaites, 2013), with isoniazid and rifampicin during the 7–12 month continuation phase (Thwaites, 2013; Thwaites et al., 2013; Jullien et al., 2016; Falzon et al., 2017). Intravenous dexamethasone (0.4 mg/kg/day) or oral prednisone (40 mg/day) was given for severe disease at baseline (judged by the treating clinician), if a patient's condition worsened after the start of treatment (Gilpin et al., 2018; Mirzayev et al., 2021). Additional adjuvant treatments, including mannitol, hypertonic saline, acetazolamide, and external CSF drainage or ventriculoperitoneal shunt, were used as clinically indicated. A combination of rifampicin (600 mg/kg/d) and levofloxacin (500–1,000 mg/d) or moxifloxacin (400–800 mg/d) was given intravenously if patients were unable to take oral medication or worsened on treatment. Patients with drug-resistant TBM received standard treatment since drug susceptibility testing (DST) was conducted retrospectively. Response to treatment was assessed by clinical examination during treatment and telephone follow-up 9–24 months after treatment completion.

Specimen collection and testing

CSF was collected for routine, biochemical, cytological, and microbiological analyses. CSF protein and glucose were determined by immunoturbidimetry (Beckman Coulter DXA5000). CSF cell counts included total white blood cells, lymphocytes, neutrophils, and monocytes. CSF microscopy and MZN staining were performed using

0.5 mL of CSF loaded into a cytospin chamber with poly-lysine-coated slides and centrifuged at 70×*g* for 5 min, according to a standard protocol (Wang et al., 2016). The slide was fixed with 4% paraformaldehyde for 15 min at room temperature and sent to Xijing Hospital of the Fourth Military Medical University for reading. They were permeabilized with 0.3% TritonX-100 for 30 min, before staining with carbolfuchsin containing 0.3% TritonX-100 and counterstained with methylene blue. All slides stained by the modified method were observed under oil immersion at a magnification of 1,000 (Chen et al., 2012). Three hundred fields on each slide were examined documenting the number of fields in which acid-fast bacilli and their intracellular or extracellular location were observed. All positive slides were confirmed by an experienced technician, and 25% of slides were selected for random quality assurance review (Feng et al., 2014; Wang et al., 2016).

A WHO-approved NAAT (Xpert MTB/RIF, Cepheid, Sunnyvale, CA, United States) (Boehme et al., 2010) or *M. tuberculosis* culture (BACTEC MGIT 960, Bio-Rad Laboratories, Hercules, CA, United States) using standard operating procedures (Krüüner et al., 2006) was performed on all patients. At least 2 mL of CSF was collected. This was first sent to Xijing Hospital where MGIT 960 culture was performed on all specimens. Xpert MTB/RIF was performed at the same time if locally available, but there were periods of interruption when the test was unavailable or unfunded. Remaining CSF and cultured strains were stored at −80°C before transfer to the National Tuberculosis Reference Laboratory of the Chinese Center for Disease Control and Prevention (CDC) in Beijing, where batch Xpert MTB/RIF testing was performed on frozen CSF specimens if an adequate volume was available, and no previous Xpert MTB/RIF test result recorded. Phenotypic DST, as well as gene sequencing and spoligotyping were performed on all viable strains if an adequate amount of DNA could be harvested. Batched phenotypic DST was performed for isoniazid (H), rifampin (R), ethambutol (E), streptomycin (S), kanamycin (K), amikacin (A), capreomycin (C), moxifloxacin (Mfx), levofloxacin (Lfx), para-aminosalicylic acid (PAS), and prothionamide (Pto) on solid LJ medium, according to standard protocols (World Health Organization, 2011). Following resistance detection, the MGIT 960 system (Krüüner et al., 2006) was used to determine the mean inhibitory drug concentration (MIC) (Woods et al., 2011). DNA was extracted from freshly cultured colonies on LJ medium and processed using standard methodology for gene sequencing and spoligotyping (Gori et al., 2005). Strains were identified by *16–23467, rrs1690, and 16s555* gene sequencing (Supplementary Panel S3) (Clarridge, 2004), compared with the *M. tuberculosis* reference strain H37Rv, and deposited in GenBank[1] (Wang et al., 2016); whole genome sequencing was not performed. Genotypic DST was performed using standard primers for the *inhA, katG, rpoB, embB, gyrA, gyrB, rrs-KAN, eis, rpsL,* and *gidB* genes (Supplementary Panel S4) (Maus et al., 2005; Avalos et al., 2015; Cohen et al., 2015).

Statistical analyses

Continuous variables (age, TBM score, leukocytes, lymphocytes, neutrophils, monocytes, protein, glucose, intracranial pressure, and Barthel score) were expressed as the median and interquartile range (IQR). Categorical variables (female sex, fever, headache, vomiting, neck stiffness, seizures, BMRC grade, CXR suggestive of active cavitating disease or disseminated/miliary TB, reported diabetes, hydrocephalus, infarcts, basal meningeal enhancement, granulomas/tuberculomas, any drug resistance detected, Beijing genotype, TBM treatment completed, lost to follow-up, death, and poor outcome) were expressed as counts and proportions. Differences between microbiologically confirmed TBM cases that had a TBM score of ≥12 and <12 were assessed by the χ^2 test for categorical variables, and the Mann–Whitney U test was performed to assess continuous variables. Continuous variables were also assessed using the Kruskal–Wallis test (non-parametric one-way analysis of variance, ANOVA), and categorical variables were assessed using the χ^2 test, with Bonferroni adjustments. Multivariate logistic regression was used to analyze risk factors for poor outcome, including all factors significantly associated ($p < 0.05$) with univariate analyses. Comparative results were presented as odds ratios (ORs) with 95% confidence interval (CI). Receiver operating characteristic (ROC) curves were constructed to assess diagnostic accuracy. All statistical analyses were performed using statistical package for social sciences (SPSS) version 20.0 and GraphPad Prism 7.0. Instances with missing data ($n = 42$) were excluded from the particular analysis, instead of imputing missing values.

Results

A total of 341 presumptive TBM patients met selection criteria; 63 confirmed TBM (25 culture positive, 42 Xpert-MTB/RIF positive), 66 probable TBM, 163 possible TBM, and 49 "not TBM" according to uniform research TBM case definition criteria (Marais et al., 2010) (Figure 1). Among 292 patients started on TBM treatment, 93.1% (270/292) had an outcome reported and were included in comparative analyses. In total, 83.3% (50/60) confirmed TBM, 64.6% (42/65) probable TBM, and 33.1% (48/145) possible TBM patients completed TBM treatment. The 49 patients with presumptive TBM who were excluded had an alternative cause (9 viral meningitis, 19 cryptococcal meningitis, 10 bacterial meningitis, 7 intracranial tumor, 1 intracranial hematoma, an 1 acute leukemia) identified. Table 1 provides an overview of the TBM cohort comparing patients with confirmed, probable, and possible TBM. Key differences are shown in Figure 2. Female sex, CXR suggestive of active cavitating disease, hydrocephalus, basal meningeal enhancement, CSF neutrophils, all death, and all poor outcomes were significantly associated with confirmed TBM compared with probable or possible TBM.

Table 2 compares the baseline characteristics of patients with confirmed TBM (culture and/or Xpert MTB/RIF positive) with those who were MZN-positive, but culture and Xpert-MTB/RIF-negative, on CSF. A chest X-ray suggestive of active cavitating disease, hydrocephalus, basal meningeal enhancement, CSF protein ≥1.4 mg/dL, CSF glucose <2.2 mmol/L, TBM score ≥ 12, and all poor outcomes was significantly associated with confirmed TBM compared with MZN staining-positive but culture and Xpert MTB/RIF-negative cases. Nearly one-third (17 of 63; 27.0%) of patients with confirmed TBM had a TBM score of <12. Since no patients with a TBM score of <6 were included in the study, we can only compare those with a score of ≥12 and 6–11. Supplementary Table S1 compares the characteristics of patients with confirmed TBM who had a TBM score of ≥12 and 6–11. Among confirmed TBM patients, those with a TBM score of

1 http://www.ncbi.nlm.nih.gov/BLAST/

TABLE 1 Comparison of baseline characteristics between confirmed, probable, and possible TBM patients.

Characteristic	Confirmed TBM[a], *N* = 63(%)	Probable TBM[b], *N* = 66(%)	Possible TBM[c], *N* = 163(%)	*p*	Multiple comparisons
Median age-years (IQR)	26 (3–82)	34.5(2–64)	29 (1–80)	0.513	–
Female sex	35 (55.6)	32 (48.5)	53 (32.5)	**0.003**	**a > b > c**
Median TBM score (IQR)[d]	14 (6–20)	13 (12–19)	8 (6–11)	**<0.001**	**a = b > c**
Reported diabetes	1 (1.6)	2 (3.0)	1 (0.6)	0.357	–
History					
Fever	43 (68.3)	54 (81.8)	113 (69.3)	0.125	–
Headache	48 (76.2)	56 (84.9)	109 (66.9)	**0.017**	**b > a > c**
Vomiting	27 (42.9)	39 (59.1)	85 (52.2)	0.180	–
Neck stiffness	24 (38.1)	45 (68.2)	95 (58.3)	**0.002**	**a < b = c**
Seizures	6 (9.5)	10 (15.2)	27 (16.6)	0.405	–
BMRC grading[e]					
I	32 (50.8)	23 (34.9)	72 (44.2)	0.182	–
II	21 (33.3)	24 (36.4)	67 (41.1)	0.521	–
III	10 (15.9)	19 (28.8)	24 (14.7)	**0.038**	**b > a > c**
Imaging					
CXR suggestive of active cavitating disease	27 (42.9)	15 (22.7)	18 (11.0)	**<0.001**	**a > b = c**
CXR indicative of disseminated/miliary TB	6 (9.5)	8 (12.1)	1 (0.6)	**<0.001**	**a = b > c**
Hydrocephalus	20 (31.8)	13 (19.7)	15 (9.20)	**<0.001**	**a > b > c**
Infarcts	15 (23.8)	17 (25.8)	17 (10.4)	**0.005**	**a = b > c**
Basal meningeal enhancement	18 (28.6)	13 (19.7)	14 (8.6)	**0.001**	**a > b > c**
Granulomas/tuberculomas	1 (1.6)	1 (1.5)	0	0.280	–
CSF findings					
Median leukocyte count—cells/μL (IQR)	141.5 (0–6,100)	94.0 (0–1,355)	96.0 (0–5,450)	0.360	–
Leukocyte (50–500)—cells/μL	43 (68.3)	42 (63.6)	85 (52.2)	0.053	–
Median lymphocytes—% (IQR)	60.8 (1.0–98.0)	77.0 (3.5–98.5)	74.0 (2.0–99.0)	0.053	–
Lymphocytes >50 (%)	38 (60.3)	52 (78.8)	112 (68.7)	0.074	–
Median neutrophils—% (IQR)	26.0 (0–94.5)	5.5 (0–95)	1.5 (0–94)	**<0.001**	**a > b = c**
Median monocytes—% (IQR)	8.5 (0–53)	7.5 (0–47)	10.5 (0–85)	**0.014**	**b < c**
Median protein—mg/dL (IQR)	1.5 (0.2–7.4)	1.3 (0.07–9.3)	0.8 (0.04–6.0)	**<0.001**	**a = b > c**
Protein >1.0 mg/dL	37 (58.7)	41 (62.1)	47 (28.8)	**<0.001**	**a = b > c**
Median glucose—mmol/L (IQR)	1.8 (0.4–4.5)	2.1 (0.4–5.2)	2.5 (0.03–6.2)	**<0.001**	**a = b < c**
Glucose <2.2 mmoL/L	37 (58.7)	38 (57.6)	36 (22.1)	**<0.001**	**a = b > c**
Median intracranial pressure (mmH_2O) (IQR)	260 (100–400)	240 (60–600)	190 (60–400)	**<0.001**	**a = b > c**
Intracranial hypertension (>180 mmH_2O)[f]	43 (68.3)	47 (71.2)	76 (46.6)	**<0.001**	**a = b > c**
Outcome	N = 60 (95.2)	N = 65 (98.5)	N = 145 (89.0)	**0.030**	–
TBM treatment completed[g]	50 (83.3)	42 (64.6)	48 (33.1)	**<0.001**	**a = b > c**
Lost to follow up	3 (5.0)	1 (1.5)	18 (12.4)	**0.017**	–
Death (on treatment)	5 (8.3)	5 (7.7)	16 (11.0)	0.696	–
Death (post treatment)[h]	12 (20.0)	1 (1.5)	2 (1.4)	**<0.001**	**a > b = c**
All death	17 (28.3)	6 (9.2)	18 (12.4)	**0.005**	**a > b = c**
Alive with poor outcome[i]	6 (10.0)	9 (13.8)	7 (4.8)	0.073	–
Median Barthel score (IQR)[j]	14 (2–20)	14 (2–20)	16 (2–20)	**<0.001**	**a = b < c**
All Poor outcome[k]	23 (38.3)	15 (23.1)	25 (17.2)	**0.005**	**a > b > c**

CXR, chest X-ray; TBM, tuberculous meningitis; TB, tuberculosis; CSF, cerebrospinal fluid; BMRC, British Medical Research Council; IQR, interquartile range.
Continuous variables are presented as median (interquartile range), and categorical variables are presented as counts (proportions). The Bonferroni method was used to adjust the significance level to perform multiple testing. If statistically significant, continuous variables were analyzed by the Kruskal–Wallis test followed by post-hoc analysis with Bonferroni adjustment to compare differences between confirmed TBM, probable TBM, and possible TBM. Categorical parameters were analyzed using χ^2 test with Bonferroni adjustment for multiple testing. *p*-values < 0.05 were considered statistically significant (shown with bold). [a]Confirmed TBM defined by a positive M. tuberculosis culture or Xpert MTB/RIF on CSF (Marais et al., 2010).
[b]Probable TBM required a TBM score of ≥12 given that all patients received brain imaging (3).
[c]Patients with a TBM score of 6–11 was classified as possible TBM (3).
[d]According to the consensus uniform research case definition criteria (Marais et al., 2010) (see Supplementary Panel S1).
[e]TBM severity grade according to the revised British Medical Research Council disease severity grade (BMRC 1948) with stage 3 being most severe (Solomons et al., 2015).
[f]Normal intracranial pressure typically ranges between 80 and 180 mmH_2O. Values exceeding 180 mmH_2O are indicative of intracranial hypertension (Gomez-Beldarrain and García-Moncó, 2018; Wang et al., 2023).
[g]Patients were treated for TBM for 9–12 months.
[h]Assessed 9–24 months after treatment completion.
[i]Modified Barthel Index score < 12 (excluding dead); assessed 9–24 months after treatment completion.
[j]See Supplementary Panel S2 for calculation of Modified Barthel Index score (excluding dead) (Collin et al., 1988).
[k]Death during or after treatment or Barthel index score < 12; assessed 9–24 months after treatment completion. Only reported for those in whom an outcome was reported; lost to follow-up excluded.

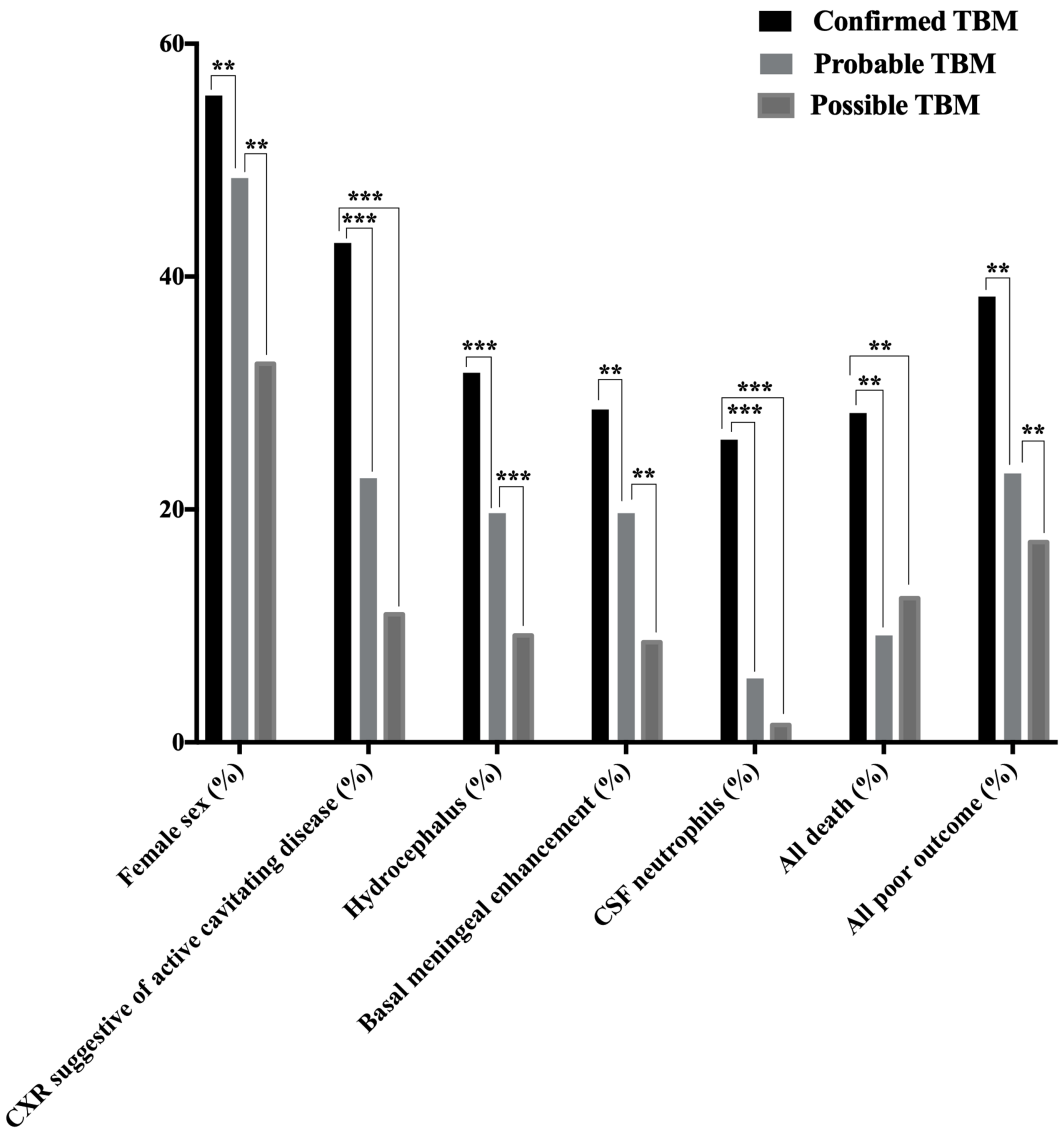

FIGURE 2
Disease characteristics observed among patients with confirmed, probable, and possible TBM[a]. TBM, tuberculous meningitis; CSF, cerebrospinal fluid; CXR, chest X-ray; TB, tuberculosis. Female sex, CXR suggestive of active cavitating disease, hydrocephalus, basal meningeal enhancement, CSF neutrophils, all death[b], and all poor outcome[c] were significantly associated with confirmed TBM compared with probable or possible TBM. *$p < 0.05$, **$p < 0.01$, and ***$p < 0.001$. [a]According to the consensus uniform research case definition criteria (Marais et al., 2010) (Supplementary Panel S1). [b]Death during or after treatment; assessed 9–24 months after treatment completion (Supplementary Panel S2) (Collin et al., 1988). [c]Death during or after treatment or Barthel index score <12; assessed 9–24 months after treatment completion (Supplementary Panel S2) (Collin et al., 1988). "Confirmed TBM" required a positive *M. tuberculosis* culture or Xpert MTB/RIF on CSF. "Probable TBM" required a TBM score of ≥12 given that all patients received brain imaging, while patients with a TBM score of 6–11 was classified as "possible TBM."

<12 exhibited less classic meningitis symptoms and signs and had better outcomes compared with those with a TBM score of ≥12. Interestingly, two patients (1 male of 23 years with fever, headache, vomiting, and reduced consciousness and 1 female of 47 years without any classic meningitis symptoms) with confirmed TBM (both CSF Xpert MTB/RIF positive, but culture-negative) had pristine CSF (total leukocyte count $<1 \times 10^6$ cells/L, normal protein, and glucose levels) and normal CNS imaging. One had a good outcome without completing TBM treatment and one was lost to follow up.

All 341 presumed TBM patients underwent CSF culture, and 323 underwent Xpert-MTB/RIF testing. Figure 3A reflects the concordance of CSF culture and Xpert-MTB/RIF results (282 of 323; 87.3%), among all patients who underwent both tests. Figure 3B shows the overlap of positive culture and Xpert-MTB/RIF and MZN results. Among 63 confirmed TBM patients, 21 (33.3%) were culture-positive and Xpert-MTB/RIF-negative, while 38 (60.3%) were Xpert-MTB/RIF-positive and culture-negative. Among those who had both tests performed at the same time, 57.1% (4/7) culture-positive CSF specimens tested Xpert MTB/RIF-positive compared with zero (0/18) when tests were performed more than 30 days apart. While 95.2% (60/63) of confirmed TBM cases were MZN-positive, only 29.3% (60 of 204) of MZN-positive cases were culture or Xpert MTB/RIF-positive. Using data from all 341 presumptive TBM cases, with confirmed TBM as the reference standard, the ROC area under the

curve (AUC) for MZN was 0.71 (95% CI: 0.66–0.78) with diagnostic sensitivity of 95.2% and specificity of 48.2%. The AUC for TBM score ≥ 12 was 0.74 (95% CI: 0.67–0.81) with diagnostic sensitivity of 73.0% and specificity of 75.5%. The AUC for TBM score ≥ 12 and positive MZN combined using binary logistic prediction was 0.81 (95%CI: 0.76–0.86), with diagnostic sensitivity of 70.0% and specificity of 79.1% (Figure 3C and Supplementary Table S2).

Table 3 reflects the multivariable logistic regression analysis of risk factors associated with poor outcome (including death) in 270 patients treated for TBM. BMRC grade III (OR = 4.369; 95%CI: 1.949–9.792) and hydrocephalus (OR = 2.520; 95%CI: 1.044–6.084) were associated with poor outcome, while BMRC grade III (OR = 5.172; 95%CI: 2.298–11.641), TBM score ≥ 15 (OR = 3.843; 95%CI: 1.372–10.761), age > 60 years (OR = 3.566; 95%CI: 1.022–12.442), and CSF neutrophil ratio ≥ 25% (OR = 2.298; 95%CI: 1.027–5.139) were most strongly associated with death (Table 4). Among those with confirmed TBM, CXR signs indicating disseminated/miliary TB (OR = 19.183; 95%CI: 1.601–229.896) was mostly associated with poor outcome (Supplementary Table S3). Moreover, CXR signs indicating disseminated/miliary TB (OR = 12.427; 95%CI: 1.138–135.758) and a higher TBM score (≥15, OR = 8.437; 95%CI: 1.328–53.585) were most strongly associated with death (Supplementary Table S4). In addition, BMRC grade III (OR = 5.129; 95%CI: 2.152–12.222), which essentially reflects a depressed level of consciousness, was strongly associated with poor outcome in probable and possible TBM cases (Supplementary Table S5). However, detected drug resistance was not associated with poor outcome or death in those with confirmed TBM (Supplementary Tables S3, S4).

Resistance to at least one TB drug was documented in nearly one-third (16 of 63; 25.4%) of confirmed TBM cases (Supplementary Table S1), and 50% (8 of 16) had rifampicin resistance identified by Xpert-MTB/RIF. Drug resistance was detected in 48.0% (12 of 25) of all cultured strains and 3 had multidrug-resistance (MDR; resistance to isoniazid and rifampicin). All four strains with phenotypic isoniazid resistance had high-level resistance with mutations in the *katG* gene (S315T, R463L). One case with phenotypic low-level rifampin resistance was not detected by Xpert MTB/RIF, and no mutations could be identified upon *rpoB* gene sequencing. Notably, there was no phenotypic fluoroquinolone resistance detected, despite the presence of non-synonymous mutations in the *gyrA* gene (Supplementary Table S6). All cultured strains belonged to *M. tuberculosis* complex, with the Beijing lineage being most common (20 of 25; 80%), including 80.0% (10 of 12) of all drug-resistant strains detected by culture.

TABLE 2 Comparison of baseline characteristics in patients with confirmed TBM[a] and those that were MZN staining-positive but culture and Xpert-MTB/RIF-negative on cerebrospinal fluid.

Characteristic	Confirmed TBM (culture or Xpert positive)	MZN positive; culture and Xpert negative	*p*
	N = 63 (%)	*N* = 130 (%)	
Median age-years (IQR)	26 (3–82)	33 (1–74)	0.263
Female sex	35 (55.6)	58 (44.6)	0.154
Median TBM score (IQR)[b]	14 (6–20)	10 (6–19)	**<0.001**
TBM score ≥ 12	46 (73.0)	57 (43.8)	**<0.001**
Reported diabetes	1 (1.6)	2 (1.5)	0.979
History			
Fever	43 (68.3)	98 (75.4)	0.295
Headache	48 (76.2)	98 (75.4)	0.903
Vomiting	27 (42.9)	72 (55.4)	0.103
Neck stiffness	24 (38.1)	81 (62.3)	**0.002**
Seizures	6 (9.5)	14 (10.8)	0.790
BMRC grading[c]			
I	32 (50.8)	52 (40.0)	0.156
II	21 (33.3)	52 (40.0)	0.371
III	10 (15.9)	26 (20.0)	0.490
Imaging			
CXR suggestive of active cavitating disease	27 (42.9)	18 (13.8)	**<0.001**
CXR indicative of disseminated/ miliary TB	6 (9.5)	8 (6.2)	0.415
Hydrocephalus	20 (31.7)	20 (15.4)	**0.009**
Infarcts	15 (23.8)	22 (16.9)	0.254
Basal meningeal enhancement	18 (28.6)	17 (13.1)	**0.009**
Granulomas/tuberculomas	1 (1.6)	1 (0.8)	0.599
CSF findings			
Median total leukocyte count—cells/μL (IQR)	141.5 (0–6,100)	110 (0–5,450)	0.857
Median lymphocytes—% (IQR)	60.8 (1.0–98.0)	69.8 (2.0–98.5)	0.272
Median neutrophils—% (IQR)	26.0 (0–94.5)	7.3 (0–95.0)	0.093
Median monocytes—% (IQR)	8.5 (0–53.0)	8.3 (0–62.5)	0.896
Median protein—mg/dL (IQR)	1.5 (0.2–7.4)	1.0 (0.04–9.3)	**0.029**
Protein ≥1.4 mg/dL	33 (52.4)	41 (31.5)	**0.005**
Median glucose—mmol/L (IQR)	1.8 (0.4–4.5)	2.3 (0.3–6.2)	**0.012**
Glucose <2.2 mmoL/L	37 (58.7)	56 (43.1)	**0.041**
Median intracranial pressure—mmH_2O (IQR)	260 (100–400)	210 (60–600)	**0.001**
Intracranial hypertension (>180 mmH_2O)[d]	43 (68.3)	75 (57.7)	0.158
Outcome	N = 60 (95.2)	N = 123 (94.6)	0.855

(Continued)

Discussion

This study represents the most comprehensive investigation of demographic, clinical, radiological, and laboratory descriptors associated with TBM diagnosis and outcome in Shaanxi province, China. The detailed description of prognostic factors in an HIV-uninfected population provides valuable new insight, especially in an Asian context. The fact that nearly one-third (27.0%) of confirmed TBM cases had a TBM score of <12, highlighting the difficulty of early accurate diagnosis and the shortcoming of traditional diagnostic methods. Our results indicate that a high TBM score (≥12) combined with a positive MZN result indicates reasonable diagnostic accuracy compared with a reference

TABLE 2 (Continued)

Characteristic	Confirmed TBM (culture or Xpert positive)	MZN positive; culture and Xpert negative	*p*
	N = 63 (%)	*N* = 130 (%)	
TBM treatment completed[e]	50 (83.3)	63 (51.2)	**<0.001**
Lost to follow-up	3 (5.0)	7 (5.7)	0.847
Death (on treatment)	5 (8.3)	11 (8.9)	0.891
Death (post treatment)[f]	12 (20.0)	2 (1.6)	**<0.001**
Alive with poor outcome[g]	6 (10.0)	12 (9.8)	0.959
Median Barthel score (IQR)[h]	14 (2–20)	16 (2–20)	**<0.001**
All poor outcome[i]	23 (38.3)	25 (20.3)	**0.009**

CXR, chest X-ray; TBM, tuberculous meningitis; MZN, modified Ziehl–Neelsen staining; TB, tuberculosis; CSF, cerebrospinal fluid; BMRC, British Medical Research Council; IQR, interquartile range.

Continuous variables are presented as median (IQR), and categorical variables are presented as counts (proportions). Differences were assessed by the χ^2-test for categorical variables and the Mann-Whitney U test for continuous variables. *p*-values <0.05 were considered statistically significant (shown with bold). [a]Confirmed TBM defined by a positive M. tuberculosis culture or Xpert MTB/RIF on CSF (Marais et al., 2010).

[b]According to consensus uniform research case definition criteria (Marais et al., 2010) (see Supplementary Panel S1).

[c]TBM severity grade according to the revised British Medical Research Council disease severity grade (BMRC 1948) with stage 3 being most severe (Solomons et al., 2015).

[d]Normal intracranial pressure typically ranges between 80 and 180 mmH_2O. Values exceeding 180 mmH_2O are indicative of intracranial hypertension (Gomez-Beldarrain and García-Moncó, 2018; Wang et al., 2023).

[e]Patients were treated for TBM for 9–12 months.

[f]Assessed 9–24 months after treatment completion.

[g]Modified Barthel Index score < 12 (excluding dead); assessed 9–24 months after treatment completion.

[h]See Supplementary Panel S2 for calculation of Modified Barthel Index score (excluding dead) (Collin et al., 1988).

[i]Death during or after treatment or Barthel index score < 12; assessed 9–24 months after treatment completion. Only reported for those in whom an outcome was reported; lost to follow-up excluded.

of confirmed TBM (as defined), but poor specificity remains a particular limitation of MZN (Wang et al., 2016; Heemskerk et al., 2018). A definitive CSF test with high sensitivity, such as Xpert-MTB/RIF Ultra (Cresswell et al., 2020) or culture (Hannan et al., 2010), should always be included in the diagnostic work-up. A study of 204 Ugandan adults with meningitis reported that the sensitivity of Xpert MTB/RIF Ultra was 76.5% (95% CI: 62.5–87.2) while that of Xpert MTB/RIF was 55.6% (44.0–70.4; $p = 0.001$ for the comparison of sensitivity between tests) compared with a reference standard of definite or probable TBM. The reduced sensitivity of Xpert MTB/RIF compared with Ultra is well established (Donovan et al., 2020) and also corresponds to our findings, where only 57.1% of culture-positive CSF specimens were Xpert MTB/RIF-positive if both tests were performed at the same time. Negative cultures in the presence of a positive Xpert MTB/RIF result might be related to low CSF bacillary load and sample processing that affected viability (Thuong et al., 2019). Samples were generally collected before TB treatment initiation, but this was not accurately recorded in all instances, and discrepancies may also represent a treatment effect.

Several studies served to highlight the key distinguishing features of TBM, including non-acute symptom onset (>5 days), low CSF leukocytes (<1,000 cells per mm^3), elevated CSF protein (>100 mg/dL), and a low CSF: blood glucose ratio (<0.5) (Wilkinson et al., 2017). The association of a CSF glucose level of <2.2 mmol/L with confirmed TBM supports the findings from a UK study (Heemskerk et al., 2018), although comparative assessment of CSF and serum glucose is considered most informative (Solomons et al., 2016). Basal meningeal exudates, identified on contrast enhanced CT imaging, have been found to be highly specific for TBM and predictive of poor outcome (Bullock and Welchman, 1982). Although it was significantly associated with both confirmed TBM and probable TBM in our study, it was present in less than one-third of cases.

Unfortunately, TBM treatment outcomes remain poor outcome despite some recent treatment improvement (Méchaï and Bouchaud, 2019; Donovan et al., 2020; Huynh et al., 2022). In a study from Singapore, 38.9% (7 of 18) of TBM patients had a poor outcome (Modi et al., 2017), which was similar to a large series from India where 32.5% (165 of 507) had poor outcomes, 17.0% (86 of 507) died, and 15.6% (79 of 507) suffered from severe neurological sequelae (Erdem et al., 2015). In our study, 38.3% (23 of 60) of those with confirmed TBM had a poor outcome and 28.3% (17 of 60) died. Interestingly, only 31.3% (5 of 16) and 25% (4 of 16) of drug-resistant TBM patients died despite receiving suboptimal therapy. Similar to our findings TBM prognosis has been associated with old age, disease severity (Schoeman and Donald, 2013), hydrocephalus, disseminated/miliary TB (Gu et al., 2015), and a high neutrophil-to-lymphocyte ratio (Chan et al., 2003; Török, 2015; Li et al., 2017; Kamat et al., 2018; Gu et al., 2023). Detected drug resistance was not associated with poor outcome in our study, aligning with some past observations (Seddon et al., 2012), but in contrasts to studies where multidrug resistance (combined resistance to isoniazid and rifampicin) was strongly associated with mortality (Thwaites et al., 2005). This discrepancy could be attributed to the small number of drug-resistant strains, and the predominance of mono-resistant strains in our study.

In our study, Beijing lineage strains were predominated, broadly reflecting the percentage (990 of 1,189; 83.3%) of *M. tuberculosis* isolates obtained from pulmonary TB patients in another study from China (Liu et al., 2018) and in 71.1% (32 of 45) of isolates from relapsed TB cases in Singapore (Sun et al., 2006). These data is very different from India where only 8.9% (11/124) of isolates from North India (Mathuria et al., 2017), were identified as Beijing genotype and most strains were from lineage 3 (Singh et al., 2021). Beijing lineage strains have been associated with poor TB treatment outcome in some studies (Feng et al., 2008; Liu et al., 2020), but the association with TBM has been variable (Maree et al., 2007; Buu et al., 2010; Liu et al., 2018). Our analysis was limited by small sample size, but we could not demonstrate an association between Beijing genotype and TBM outcome.

It is important to acknowledge major study limitations. Retrospective data collection was conducted over an extended observation period, with risk of missing data and data inconsistency. These risks were minimized by comprehensive assessment of all clinical notes using a standard data collection template. We excluded those cases in whom baseline data was inadequate for accurate disease classification and those in whom outcomes could not be assessed. This excluded many patients and may have introduced selection bias, with the outcomes representative of those who received optimal care under the local circumstances. While adjunctive corticosteroid use is recommended by WHO guidelines (World Health Organization, 2010; Thwaites, 2013) during the initial

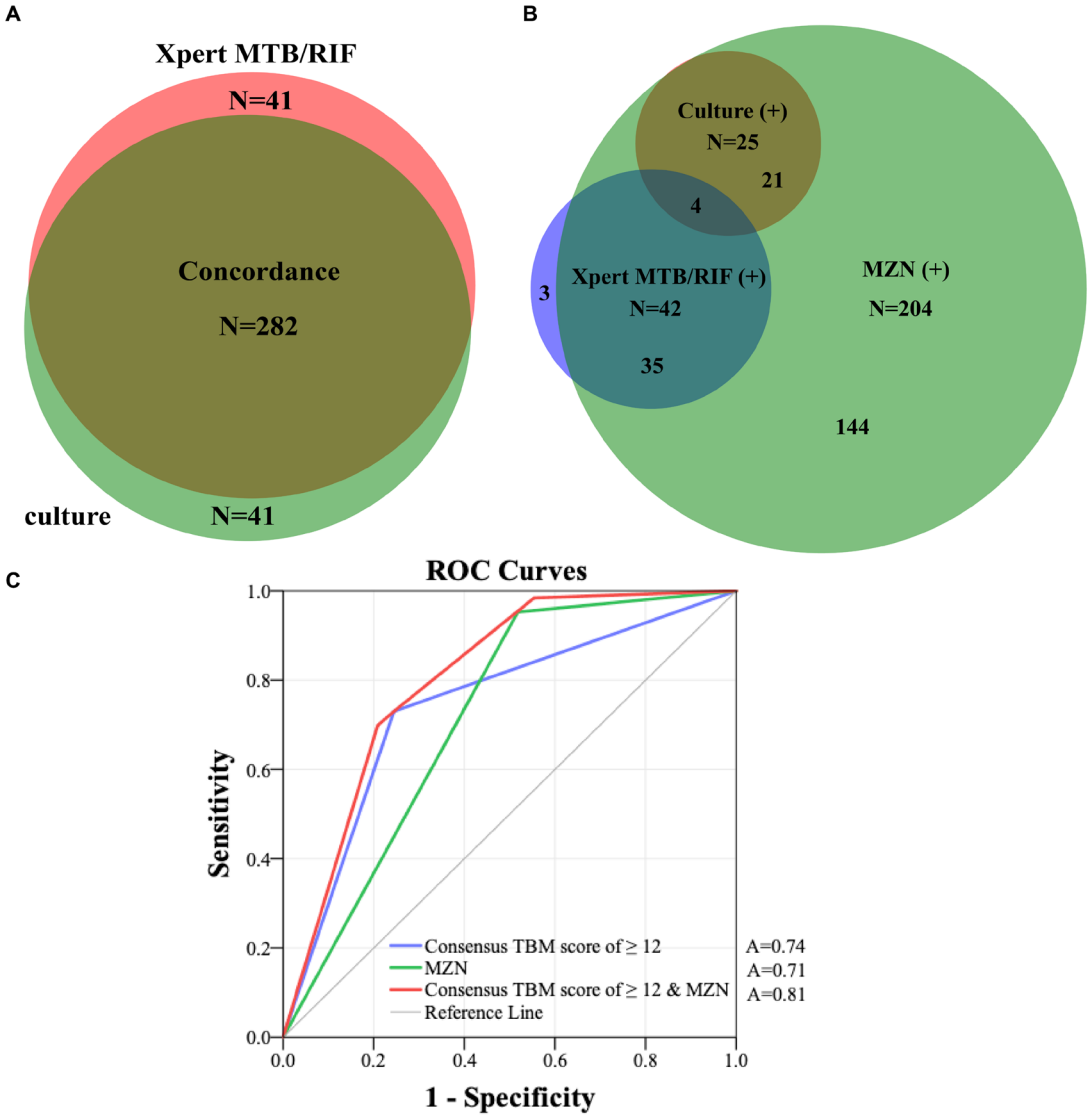

FIGURE 3
(A) Concordance of all CSF Xpert MTB/RIF and culture results in patients who had both tests performed. **(B)** The overlap of positive culture, Xpert-MTB/RIF and MZN results. **(C)** ROC curves of consensus TBM score of ≥12 and MZN with confirmed TBM as the reference standard in 341 presumptive TBM patients who had at least a CSF culture or Xpert MTB/RIF performed. MZN, modified Ziehl–Neelsen staining; TBM, tuberculous meningitis; CSF, cerebrospinal fluid; A, area under the curve; ROC, receiver operating characteristic.

6–8 weeks of TBM treatment, there is currently no consensus on its routine use in China (Prasad et al., 2016; Brett et al., 2020; Huynh et al., 2022). Some clinicians argue that adjunctive corticosteroid use does not significantly improve the prognosis in mild cases (Schoeman et al., 1997), and that the risk of complications such as infection resulting from immune compromise, hyperglycemia, and stress ulcers (Török, 2015; Wilkinson et al., 2017) may outweigh the benefit. A Cochrane systematic review concluded that adjunctive corticosteroids reduce death from TBM by almost a quarter, but no effect on disabling neurological deficits could be demonstrated (Wilkinson et al., 2017; Huynh et al., 2022). In addition, due to variations in the LHA4 genotype, certain patients may experience worsening symptoms after corticosteroid administration (Donovan et al., 2018), and at present, we do not have a mechanism to identify this risk group.

Since MGIT 960 culture and Xpert MTB/RIF were not consistently performed at the same time and before TB treatment initiation, it is difficult to compare between diagnostic yield and accuracy. However, at least one confirmatory test (MGIT 960 culture or Xpert MTB/RIF) was performed in all cases included in the comparative analyses. Unfortunately, Xpert MTB/RIF Ultra®, which is the most sensitive NAAT for CSF diagnosis (Donovan et al., 2020), was not available at the time of the study. WHO first recommended the use of the Xpert MTB/RIF assay in the diagnosis of TB and extrapulmonary TB in 2013 (World Health Organization, 2014), while the Xpert-MTB/RIF Ultra only became available in 2017 (Chakravorty et al., 2017). Since our data collection period extended from May 2009 to April 2019, and in order to ensure internal consistency, we only performed the Xpert MTB-RIF test. Finally, since DST was only performed

TABLE 3 Multivariable logistic regression analysis for risk factors of poor outcome[a] in 270 patients treated for TBM[b].

Characteristic	Univariate		Multivariate model	
	OR (95%CI)	*p*	Adjusted OR (95% CI)	*p*
Neck stiffness	**2.146 (1.072–4.294)**	**0.031**	–	0.396
Seizures	**2.502 (1.252–4.998)**	**0.009**	–	0.072
BMRC grading[c]				
I	**0.214 (0.106–0.432)**	**<0.001**	**0.332 (0.136–0.810)**	**0.015**
III	**6.307 (3.238–12.283)**	**<0.001**	**4.369 (1.949–9.792)**	**<0.001**
TBM score[d] ≥ 12	**2.558 (1.437–4.552)**	**0.001**	–	0.193
TBM score[d] ≥ 15	**3.657 (1.763–7.584)**	**<0.001**	–	0.623
Imaging				
Hydrocephalus	**3.735 (1.928–7.237)**	**<0.001**	**2.520 (1.044–6.084)**	**0.040**
Basal meningeal enhancement	**3.006 (1.527–5.917)**	**0.001**	–	0.618
CXR suggestive of active cavitating disease	–	0.729	–	–
CXR indicative of disseminated/miliary TB	–	0.125	–	–
CSF findings				
Total leukocyte count >100 (cells/μL)	–	0.798	–	–
Lymphocytes (%)	–	0.144	–	–
Neutrophils (%)	–	0.143	–	–
Glucose <2.2 mmoL/L	**1.819 (1.030–3.213)**	**0.039**	–	0.404
Protein >1 mg/dL	–	0.810	–	–
Intracranial pressure (mmH_2O)	**1.004 (1.001–1.007)**	**0.009**	–	–
Intracranial hypertension (>180mmH_2O)[e]	**1.942 (1.014–3.719)**	**0.045**		0.319

CXR, chest X-ray; TBM, tuberculous meningitis; OR, odds ratio; CI, confidence interval; BMRC grade, British Medical Research Council disease severity grade; CSF, cerebrospinal fluid; TB, tuberculosis. Age, Female sex, BMRC grade II, fever, headache, vomiting, CXR suggestive of active cavitating disease or disseminated/miliary TB, infarcts, granulomas/tuberculomas, CSF total leukocyte count, lymphocytes, monocytes, neutrophils, and protein were non-significant controlled covariates. *p*-values <0.05 were considered statistically significant (shown with bold).
[a]Death during or after treatment or Barthel index score < 12; assessed 9–24 months after treatment completion (see Supplementary Panel S2) (Collin et al., 1988).
[b]Among 292 patients started on TBM treatment, 270 patients followed for outcome (22 patients lost to follow-up) and included in comparative analyses.
[c]TBM severity grade according to the revised British Medical Research Council disease severity grade (BMRC 1948) with stage 3 being most severe (Solomons et al., 2015).
[d]According to the consensus uniform research case definition criteria (Marais et al., 2010) (see Supplementary Panel S1).
[e]Normal intracranial pressure typically ranges between 80 and 180 mmH_2O. Values exceeding 180 mmH_2O are indicative of intracranial hypertension (Gomez-Beldarrain and García-Moncó, 2018; Wang et al., 2023).

at the end of the study, these results could not inform patient management and treatment was empirical. Patients who did not improve on standard therapy were treated with high-dose rifampicin and moxifloxacin, which does not represent optimal treatment in cases with drug resistant TBM. In addition, we were unable to correlate HIV infection (excluded), hyponatremia, and other unmeasured risk factors potentially associated with prognosis. Despite these limitations, the data obtained from this study offer valuable insights into TBM clinical presentation and prognostic factors in China.

Conclusion

TBM patients have variable presentations and those with a TBM score of <12 may be missed by traditional diagnostic approaches. Early TBM diagnosis remains challenging, but ready access to Xpert MTB/RIF Ultra should improve the accuracy of CSF testing. TBM patients that are older (>60 years) have higher TBM scores or CSF neutrophil ratios, have signs of disseminated/miliary TB, and are at greatest risk of death. In general, more effort needs to be done to improve early diagnosis and treatment outcome in TBM patients.

Data availability statement

The original contributions presented in the study are publicly available. This data can be found in the NCBI BioProject repository (accession number PRJNA1069020) and in the article/Supplementary material.

Ethics statement

The studies involving humans were approved by the Ethics Committee of Xijing Hospital of Air Force Medical University (Study No. KY20105255-1 and No. KY20163367-1) and the Ethics Committee of Guangzhou First People's Hospital (Study No. K-2022-054-01). The studies were conducted in accordance with the local legislation and institutional requirements. Written

TABLE 4 Multivariable logistic regression analysis of risk factors for death[a] in 270 patients treated for TBM[b].

Characteristic	Univariate		Multivariate model	
	OR (95%CI)	*p*	Adjusted OR (95% CI)	*p*
Headache	**0.389 (0.190–0.798)**	**0.010**	**0.378 (0.161–0.888)**	**0.026**
Seizures	**3.002 (1.401–6.432)**	**0.005**	–	0.058
Age (years)	**1.023 (1.004–1.043)**	**0.019**	–	–
<15	–	0.055	–	–
15–60	**0.374 (0.186–0.752)**	**0.006**	–	–
>60	**5.687 (1.938–16.693)**	**0.002**	**3.566 (1.022–12.442)**	**0.046**
Consensus TBM score[c]	**1.154 (1.042–1.277)**	**0.006**	–	–
≥15	**4.158 (1.894–9.129)**	**<0.001**	**3.843 (1.372–10.761)**	**0.010**
≥12	–	0.079	–	–
BMRC grading[d]				
III	**6.568 (3.179–13.571)**	**<0.001**	**5.172 (2.298–11.641)**	**<0.001**
Imaging				
Hydrocephalus	**2.573(1.216–5.447)**	**0.013**	–	0.598
Infarcts	1.572 (0.712–3.469)	0.263	–	–
Basal meningeal enhancement	**2.458 (1.141–5.293)**	**0.022**	–	0.752
CXR suggestive of active cavitating disease	–	0.442	–	–
CXR indicative of disseminated/miliary TB	–	0.212	–	–
CSF findings				
Neutrophils (%)	**1.011 (1.001–1.022)**	**0.034**	–	–
Neutrophils ≥25 (%)	**3.049 (1.529–6.080)**	**0.002**	**2.298 (1.027–5.139)**	**0.043**
Intracranial pressure—mmH_2O	–	0.200	–	–

CXR, chest X-ray; OR, odds ratio; CI, confidence interval; BMRC grade, British Medical Research Council disease severity grade; TBM, tuberculous meningitis; CSF, cerebrospinal fluid; TB, tuberculosis. Female, fever, vomiting, neck stiffness, BMRC grading I, II, CXR suggestive of active cavitating disease or disseminated/miliary TB, granulomas/tuberculomas, CSF leukocyte, CSF lymphocyte, CSF monocytes, CSF protein, CSF glucose, and intracranial pressure were non-significant controlled covariates. *p*-values <0.05 were considered statistically significant (shown with bold). [a]Death during or after treatment; assessed 9–24 months after treatment completion (see Supplementary Panel S2) (Collin et al., 1988).
[b]Among 292 patients started on TBM treatment, 270 patients followed for outcome (22 patients lost to follow-up) and included in the comparative analyses.
[c]According to the consensus uniform research case definition criteria (Marais et al., 2010) (see Supplementary Panel S1).
[d]TBM severity grade according to the revised British Medical Research Council disease severity grade (BMRC 1948) with stage 3 being most severe (Solomons et al., 2015).

informed consent for participation in this study was provided by the participants' legal guardians/next of kin.

Author contributions

TW: Conceptualization, Data curation, Formal analysis, Funding acquisition, Investigation, Methodology, Project administration, Resources, Software, Supervision, Validation, Visualization, Writing – original draft, Writing – review & editing. M-yL: Conceptualization, Data curation, Formal analysis, Funding acquisition, Writing – review & editing. X-SC: Data curation, Methodology, Resources, Supervision, Writing – review & editing. Q-sC: Conceptualization, Methodology, Supervision, Visualization, Writing – review & editing. ZL: Supervision, Validation, Visualization, Writing – review & editing. T-tL: Data curation, Supervision, Validation, Writing – review & editing. L-fZ: Data curation, Methodology, Supervision, Writing – review & editing. H-hW: Data curation, Methodology, Supervision, Writing – review & editing. G-dF: Data curation, Methodology, Supervision, Writing – review & editing. BM: Conceptualization, Data curation, Formal analysis, Investigation, Validation, Visualization, Writing – review & editing. GZ: Conceptualization, Data curation, Formal analysis, Funding acquisition, Investigation, Methodology, Project administration, Resources, Supervision, Validation, Visualization, Writing – review & editing.

Funding

The author(s) declare financial support was received for the research, authorship, and/or publication of this article. This work was supported by the National Natural Science Foundation of China (No: 82101430) to TW, the Science and Technology Projects in Guangzhou to TW (No: 202201010610), the start-up funding for doctoral research of Guangzhou First People's Hospital (No: KY09050006) to TW, the Science and Technology Projects in Guangzhou (No: 202102080086) to MY-L and the National Natural Science Foundation of China (81371334) to GZ.

Acknowledgments

The authors thank all of the clinical and laboratory staff of Xijing Hospital, the CDC, and all the district hospitals for their assistance in patient recruitment, isolate collection, and identification.

Conflict of interest

The authors declare that the research was conducted in the absence of any commercial or financial relationships that could be construed as a potential conflict of interest.

Publisher's note

All claims expressed in this article are solely those of the authors and do not necessarily represent those of their affiliated organizations, or those of the publisher, the editors and the reviewers. Any product that may be evaluated in this article, or claim that may be made by its manufacturer, is not guaranteed or endorsed by the publisher.

Supplementary material

The Supplementary material for this article can be found online at: https://www.frontiersin.org/articles/10.3389/fmicb.2024.1374458/full#supplementary-material

References

Arshad, A., Dayal, S., Gadhe, R., Mawley, A., Shin, K., Tellez, D., et al. (2020). Analysis of tuberculosis meningitis pathogenesis, diagnosis, and treatment. *J. Clin. Med.* 9:2962. doi: 10.3390/jcm9092962

Avalos, E., Catanzaro, D., Catanzaro, A., Ganiats, T., Brodine, S., Alcaraz, J., et al. (2015). Frequency and geographic distribution of gyrA and gyrB mutations associated with fluoroquinolone resistance in clinical *Mycobacterium tuberculosis* isolates: a systematic review. *PLoS One* 10:e0120470. doi: 10.1371/journal.pone.0120470

Boehme, C. C., Nabeta, P., Hillemann, D., Nicol, M. P., Shenai, S., Krapp, F., et al. (2010). Rapid molecular detection of tuberculosis and rifampin resistance. *N. Engl. J. Med.* 363, 1005–1015. doi: 10.1056/NEJMoa0907847

Brett, K., Dulong, C., and Severn, M. (2020). *Treatment of tuberculosis: a review of guidelines*. Ottawa ON: Canadian Agency for Drugs and Technologies in Health.

Bullock, M. R., and Welchman, J. M. (1982). Diagnostic and prognostic features of tuberculous meningitis on CT scanning. *J. Neurol. Neurosurg. Psychiatry* 45, 1098–1101. doi: 10.1136/jnnp.45.12.1098

Buu, T. N., Huyen, M. N., van Soolingen, D., Lan, N. T., Quy, H. T., Tiemersma, E. W., et al. (2010). The *Mycobacterium tuberculosis* Beijing genotype does not affect tuberculosis treatment failure in Vietnam. *Clin. Infect. Dis.* 51, 879–886. doi: 10.1086/656410

Chakravorty, S., Simmons, A. M., Rowneki, M., Parmar, H., Cao, Y., Ryan, J., et al. (2017). The new Xpert MTB/RIF ultra: improving detection of mycobacterium tuberculosis and resistance to rifampin in an assay suitable for point-of-care testing. *MBio* 8:e00812-17. doi: 10.1128/mBio.00812-17

Chan, K. H., Cheung, R. T., Fong, C. Y., Tsang, K. L., Mak, W., and Ho, S. L. (2003). Clinical relevance of hydrocephalus as a presenting feature of tuberculous meningitis. *QJM* 96, 643–648. doi: 10.1093/qjmed/hcg108

Chen, P., Shi, M., Feng, G. D., Liu, J. Y., Wang, B. J., Shi, X. D., et al. (2012). A highly efficient Ziehl-Neelsen stain: identifying de novo intracellular mycobacterium tuberculosis and improving detection of extracellular *M. tuberculosis* in cerebrospinal fluid. *J. Clin. Microbiol.* 50, 1166–1170. doi: 10.1128/JCM.05756-11

Clarridge, J. E. 3rd. (2004). Impact of 16S rRNA gene sequence analysis for identification of bacteria on clinical microbiology and infectious diseases. *Clin. Microbiol. Rev.* 17, 840–862. doi: 10.1128/CMR.17.4.840-862.2004

Cohen, K. A., Abeel, T., Manson McGuire, A., Desjardins, C. A., Munsamy, V., Shea, T. P., et al. (2015). Evolution of extensively drug-resistant tuberculosis over four decades: whole genome sequencing and dating analysis of *Mycobacterium tuberculosis* isolates from KwaZulu-Natal. *PLoS Med.* 12:e1001880. doi: 10.1371/journal.pmed.1001880

Collin, C., Wade, D. T., Davies, S., and Horne, V. (1988). The Barthel ADL index: a reliability study. *Int. Disabil. Stud.* 10, 61–63. doi: 10.3109/09638288809164103

Cresswell, F. V., Tugume, L., Bahr, N. C., Kwizera, R., Bangdiwala, A. S., Musubire, A. K., et al. (2020). Xpert MTB/RIF ultra for the diagnosis of HIV-associated tuberculous meningitis: a prospective validation study. *Lancet Infect. Dis.* 20, 308–317. doi: 10.1016/S1473-3099(19)30550-X

Donovan, J., Cresswell, F. V., Thuong, N. T. T., Boulware, D. R., Thwaites, G. E., and Bahr, N. C. (2020). Xpert MTB/RIF ultra for the diagnosis of tuberculous meningitis: a small step forward. *Clin. Infect. Dis.* 71, 2002–2005. doi: 10.1093/cid/ciaa473

Donovan, J., Phu, N. H., Thao, L. T. P., Lan, N. H., Mai, N. T. H., Trang, N. T. M., et al. (2018). Adjunctive dexamethasone for the treatment of HIV-uninfected adults with tuberculous meningitis stratified by leukotriene A4 hydrolase genotype (LAST ACT): study protocol for a randomised double blind placebo controlled non-inferiority trial. *Wellcome Open Res.* 3:32. doi: 10.12688/wellcomeopenres.14007.1

Donovan, J., Thwaites, G. E., and Huynh, J. (2020). Tuberculous meningitis: where to from here? *Curr. Opin. Infect. Dis.* 33, 259–266. doi: 10.1097/QCO.0000000000000648

Dorman, S. E., Schumacher, S. G., Alland, D., Nabeta, P., Armstrong, D. T., King, B., et al. (2018). Xpert MTB/RIF ultra for detection of mycobacterium tuberculosis and rifampicin resistance: a prospective multicentre diagnostic accuracy study. *Lancet Infect. Dis.* 18, 76–84. doi: 10.1016/S1473-3099(17)30691-6

Erdem, H., Ozturk-Engin, D., Tireli, H., Kilicoglu, G., Defres, S., Gulsun, S., et al. (2015). Hamsi scoring in the prediction of unfavorable outcomes from tuberculous meningitis: results of Haydarpasa-II study. *J. Neurol.* 262, 890–898. doi: 10.1007/s00415-015-7651-5

Falzon, D., Schünemann, H. J., Harausz, E., González-Angulo, L., Lienhardt, C., Jaramillo, E., et al. (2017). World Health Organization treatment guidelines for drug-resistant tuberculosis, 2016 update. *Eur. Respir. J.* 49:1602308. doi: 10.1183/13993003.02308-2016

Feng, G. D., Shi, M., Ma, L., Chen, P., Wang, B. J., Zhang, M., et al. (2014). Diagnostic accuracy of intracellular *mycobacterium tuberculosis* detection for tuberculous meningitis. *Am. J. Respir. Crit. Care Med.* 189, 475–481. doi: 10.1164/rccm.201309-1686OC

Feng, J. Y., Su, W. J., Tsai, C. C., and Chang, S. C. (2008). Clinical impact of *Mycobacterium tuberculosis* W-Beijing genotype strain infection on aged patients in Taiwan. *J. Clin. Microbiol.* 46, 3127–3129. doi: 10.1128/JCM.01132-08

Gilpin, C., Korobitsyn, A., Migliori, G. B., Raviglione, M. C., and Weyer, K. (2018). The World Health Organization standards for tuberculosis care and management. *Eur. Respir. J.* 51:1800098. doi: 10.1183/13993003.00098-2018

Gomez-Beldarrain, M., and García-Moncó, J. C. (2018). "Lumbar puncture and CSF analysis and interpretation" in *CNS infections: a clinical approach*. ed. J. C. García-Moncó (London: Springer-Verlag), 1–17.

Gori, A., Bandera, A., Marchetti, G., Degli Esposti, A., Catozzi, L., Nardi, G. P., et al. (2005). Spoligotyping and *Mycobacterium tuberculosis*. *Emerg. Infect. Dis.* 11, 1242–1248. doi: 10.3201/eid1108.040982

Gu, Z., Liu, B., Yu, X., Cheng, T., Han, T., Tong, L., et al. (2023). Association of blood neutrophil-lymphocyte ratio with short-term prognosis and severity of tuberculosis meningitis patients without HIV infection. *BMC Infect. Dis.* 23:449. doi: 10.1186/s12879-023-08438-y

Gu, J., Xiao, H., Wu, F., Ge, Y., Ma, J., and Sun, W. (2015). Prognostic factors of tuberculous meningitis: a single-center study. *Int. J. Clin. Exp. Med.* 8:4487-93.

Hannan, A., Hafeez, A., Chaudary, S., and Rashid, M. (2010). Rapid confirmation of tuberculous meningitis in children by liquid culture media. *J. Ayub Med. Coll. Abbottabad* 22:171-5.

Heemskerk, A. D., Donovan, J., Thu, D. D. A., Marais, S., Chaidir, L., Dung, V. T. M., et al. (2018). Improving the microbiological diagnosis of tuberculous meningitis: a prospective, international, multicentre comparison of conventional and modified Ziehl-Neelsen stain, GeneXpert, and culture of cerebrospinal fluid. *J. Infect.* 77, 509–515. doi: 10.1016/j.jinf.2018.09.003

Ho, J., Marais, B. J., Gilbert, G. L., and Ralph, A. P. (2013). Diagnosing tuberculous meningitis – have we made any progress? *Trop. Med. Int. Health* 18, 783–793. doi: 10.1111/tmi.12099

Huynh, J., Donovan, J., Phu, N. H., Nghia, H. D. T., Thuong, N. T. T., and Thwaites, G. E. (2022). Tuberculous meningitis: progress and remaining questions. *Lancet Neurol.* 21, 450–464. doi: 10.1016/S1474-4422(21)00435-X

Jha, S. K., Garg, R. K., Jain, A., Malhotra, H. S., Verma, R., and Sharma, P. K. (2015). Definite (microbiologically confirmed) tuberculous meningitis: predictors and prognostic impact. *Infection* 43, 639–645. doi: 10.1007/s15010-015-0756-z

Jullien, S., Ryan, H., Modi, M., and Bhatia, R. (2016). Six months therapy for tuberculous meningitis. *Cochrane Database Syst. Rev.* 9:CD012091. doi: 10.1002/14651858.CD012163

Kamat, A. S., Gretschel, A., Vlok, A. J., and Solomons, R. (2018). CSF protein concentration associated with ventriculoperitoneal shunt obstruction in tuberculous meningitis. *Int. J. Tuberc. Lung Dis.* 22, 788–792. doi: 10.5588/ijtld.17.0008

Koh, W. J., Ko, Y., Kim, C. K., Park, K. S., and Lee, N. Y. (2012). Rapid diagnosis of tuberculosis and multidrug resistance using a MGIT 960 system. *Ann. Lab. Med.* 32, 264–269. doi: 10.3343/alm.2012.32.4.264

Kohli, M., Schiller, I., Dendukuri, N., Yao, M., Dheda, K., Denkinger, C. M., et al. (2021). Xpert MTB/RIF ultra and Xpert MTB/RIF assays for extrapulmonary tuberculosis and rifampicin resistance in adults. *Cochrane Database Syst. Rev.* 1:CD012768. doi: 10.1002/14651858.CD012768.pub3

Krüüner, A., Yates, M. D., and Drobniewski, F. A. (2006). Evaluation of MGIT 960-based antimicrobial testing and determination of critical concentrations of first- and second-line antimicrobial drugs with drug-resistant clinical strains of *Mycobacterium tuberculosis*. *J. Clin. Microbiol.* 44, 811–818. doi: 10.1128/JCM.44.3.811-818.2006

Li, K., Tang, H., Yang, Y., Li, Q., Zhou, Y., Ren, M., et al. (2017). Clinical features, long-term clinical outcomes, and prognostic factors of tuberculous meningitis in West China: a multivariate analysis of 154 adults. *Expert Rev. Anti-Infect. Ther.* 15, 629–635. doi: 10.1080/14787210.2017.1309974

Liu, Q., Wang, D., Martinez, L., Lu, P., Zhu, L., Lu, W., et al. (2020). *Mycobacterium tuberculosis* Beijing genotype strains and unfavourable treatment outcomes: a systematic review and meta-analysis. *Clin. Microbiol. Infect.* 26, 180–188. doi: 10.1016/j.cmi.2019.07.016

Liu, H., Zhang, Y., Liu, Z., Liu, J., Hauck, Y., Liu, J., et al. (2018). Associations between *Mycobacterium tuberculosis* Beijing genotype and drug resistance to four first-line drugs: a survey in China. *Front. Med.* 12, 92–97. doi: 10.1007/s11684-017-0610-z

Liu, Y., Zhang, X., Zhang, Y., Sun, Y., Yao, C., Wang, W., et al. (2018). Characterization of *Mycobacterium tuberculosis* strains in Beijing, China: drug susceptibility phenotypes and Beijing genotype family transmission. *BMC Infect. Dis.* 18:658. doi: 10.1186/s12879-018-3578-7

Marais, S., Pepper, D. J., Schutz, C., Wilkinson, R. J., and Meintjes, G. (2011). Presentation and outcome of tuberculous meningitis in a high HIV prevalence setting. *PLoS One* 6:e20077. doi: 10.1371/journal.pone.0020077

Marais, S., Thwaites, G., Schoeman, J. F., Török, M. E., Misra, U. K., Prasad, K., et al. (2010). Tuberculous meningitis: a uniform case definition for use in clinical research. *Lancet Infect. Dis.* 10, 803–812. doi: 10.1016/S1473-3099(10)70138-9

Maree, F., Hesseling, A. C., Schaaf, H. S., Marais, B. J., Beyers, N., van Helden, P., et al. (2007). Absence of an association between *Mycobacterium tuberculosis* genotype and clinical features in children with tuberculous meningitis. *Pediatr. Infect. Dis. J.* 26, 13–18. doi: 10.1097/01.inf.0000247044.05140.c7

Mathuria, J. P., Srivastava, G. N., Sharma, P., Mathuria, B. L., Ojha, S., Katoch, V. M., et al. (2017). Prevalence of *Mycobacterium tuberculosis* Beijing genotype and its association with drug resistance in North India. *J. Infect. Public Health* 10, 409–414. doi: 10.1016/j.jiph.2016.06.007

Maus, C. E., Plikaytis, B. B., and Shinnick, T. M. (2005). Molecular analysis of cross-resistance to capreomycin, kanamycin, amikacin, and viomycin in *Mycobacterium tuberculosis*. *Antimicrob. Agents Chemother.* 49, 3192–3197. doi: 10.1128/AAC.49.8.3192-3197.2005

Méchaï, F., and Bouchaud, O. (2019). Tuberculous meningitis: challenges in diagnosis and management. *Rev. Neurol. (Paris)* 175, 451–457. doi: 10.1016/j.neurol.2019.07.007

Mirzayev, F., Viney, K., Linh, N. N., Gonzalez-Angulo, L., Gegia, M., Jaramillo, E., et al. (2021). World Health Organization recommendations on the treatment of drug-resistant tuberculosis, 2020 update. *Eur. Respir. J.* 57:2003300. doi: 10.1183/13993003.03300-2020

Modi, M., Sharma, K., Prabhakar, S., Goyal, M. K., Takkar, A., Sharma, N., et al. (2017). Clinical and radiological predictors of outcome in tubercular meningitis: a prospective study of 209 patients. *Clin. Neurol. Neurosurg.* 161, 29–34. doi: 10.1016/j.clineuro.2017.08.006

Prasad, K., Singh, M. B., and Ryan, H. (2016). Corticosteroids for managing tuberculous meningitis. *Cochrane Database Syst. Rev.* 4:CD002244. doi: 10.1002/14651858.CD002244.pub4

Schoeman, J. F., and Donald, P. R. (2013). Tuberculous meningitis. *Handb. Clin. Neurol.* 112, 1135–1138. doi: 10.1016/B978-0-444-52910-7.00033-7

Schoeman, J. F., Van Zyl, L. E., Laubscher, J. A., and Donald, P. R. (1997). Effect of corticosteroids on intracranial pressure, computed tomographic findings, and clinical outcome in young children with tuberculous meningitis. *Pediatrics* 99, 226–231. doi: 10.1542/peds.99.2.226

Seddon, J. A., and Thwaites, G. E. (2019). Tuberculous meningitis: new tools and new approaches required. *Wellcome Open Res.* 4:181. doi: 10.12688/wellcomeopenres.15591.1

Seddon, J. A., Visser, D. H., Bartens, M., Jordaan, A. M., Victor, T. C., van Furth, A. M., et al. (2012). Impact of drug resistance on clinical outcome in children with tuberculous meningitis. *Pediatr. Infect. Dis. J.* 31, 711–716. doi: 10.1097/INF.0b013e318253acf8

Singh, A. V., Singh, S., Yadav, A., Kushwah, S., Yadav, R., Sai, D. K., et al. (2021). Genetic variability in multidrug-resistant *Mycobacterium tuberculosis* isolates from patients with pulmonary tuberculosis in North India. *BMC Microbiol.* 21:123. doi: 10.1186/s12866-021-02174-6

Solomons, R. S., Visser, D. H., Donald, P. R., Marais, B. J., Schoeman, J. F., and van Furth, A. M. (2015). The diagnostic value of cerebrospinal fluid chemistry results in childhood tuberculous meningitis. *Childs Nerv. Syst.* 31, 1335–1340. doi: 10.1007/s00381-015-2745-z

Solomons, R. S., Visser, D. H., Marais, B. J., Schoeman, J. F., and van Furth, A. M. (2016). Diagnostic accuracy of a uniform research case definition for TBM in children: a prospective study. *Int. J. Tuberc. Lung Dis.* 20, 903–908. doi: 10.5588/ijtld.15.0509

Sun, Y. J., Lee, A. S., Wong, S. Y., and Paton, N. I. (2006). Association of *Mycobacterium tuberculosis* Beijing genotype with tuberculosis relapse in Singapore. *Epidemiol. Infect.* 134, 329–332. doi: 10.1017/S095026880500525X

Tayyab, N., Zaman, G., Satti, L., Ikram, A., Gardezi, A. H., and Khadim, M. T. (2018). Direct susceptibility testing on MGIT 960 TB system: a rapid method for detection of drug resistant tuberculosis. *J. Coll. Physicians Surg. Pak.* 28, 590–593. doi: 10.29271/jcpsp.2018.08.590

Thuong, N. T. T., Vinh, D. N., Hai, H. T., Thu, D. D. A., Nhat, L. T. H., Heemskerk, D., et al. (2019). Pretreatment cerebrospinal fluid bacterial load correlates with inflammatory response and predicts neurological events during tuberculous meningitis treatment. *J. Infect. Dis.* 219, 986–995. doi: 10.1093/infdis/jiy588

Thwaites, G. E. (2013). Advances in the diagnosis and treatment of tuberculous meningitis. *Curr. Opin. Neurol.* 26, 295–300. doi: 10.1097/WCO.0b013e3283602814

Thwaites, G. E., Lan, N. T., Dung, N. H., Quy, H. T., Oanh, D. T., Thoa, N. T., et al. (2005). Effect of antituberculosis drug resistance on response to treatment and outcome in adults with tuberculous meningitis. *J. Infect. Dis.* 192, 79–88. doi: 10.1086/430616

Thwaites, G. E., van Toorn, R., and Schoeman, J. (2013). Tuberculous meningitis: more questions, still too few answers. *Lancet Neurol.* 12, 999–1010. doi: 10.1016/S1474-4422(13)70168-6

Török, M. E. (2015). Tuberculous meningitis: advances in diagnosis and treatment. *Br. Med. Bull.* 113, 117–131. doi: 10.1093/bmb/ldv003

Wang, T., Feng, G. D., Pang, Y., Liu, J. Y., Zhou, Y., Yang, Y. N., et al. (2016). High rate of drug resistance among tuberculous meningitis cases in Shaanxi province, China. *Sci. Rep.* 6:25251. doi: 10.1038/srep25251

Wang, T., Feng, G. D., Pang, Y., Yang, Y. N., Dai, W., Zhang, L., et al. (2016). Sub-optimal specificity of modified Ziehl-Neelsen staining for quick identification of tuberculous meningitis. *Front. Microbiol.* 7:2096. doi: 10.3389/fmicb.2016.02096

Wang, S., Yang, W., Zhu, M., Wang, X., Pan, L., Jin, T., et al. (2023). Cerebrospinal fluid protein levels are elevated 100 times in a leptomeningeal metastasis patient: a case report and literature review. *Front. Neurosci.* 17:1174309. doi: 10.3389/fnins.2023.1174309

Wilkinson, R. J., Rohlwink, U., Misra, U. K., van Crevel, R., Mai, N. T. H., Dooley, K. E., et al. (2017). Tuberculous meningitis. *Nat. Rev. Neurol.* 13, 581–598. doi: 10.1038/nrneurol.2017.120

Woods, G. L., Brown-Elliott, B. A., Conville, P. S., Desmond, E. P., Hall, G. S., Lin, G., et al. Susceptibility Testing of Mycobacteria, Nocardiae, and Other Aerobic Actinomycetes [Internet]. 2nd ed. Wayne (PA): Clinical and Laboratory Standards Institute. (2011).

World Health Organization (2010). *Treatment of tuberculosis: guidelines*. Geneva: World Health Organization.

World Health Organization (2011). *Guidelines for the programmatic Management of Drug-Resistant Tuberculosis: 2011 update*. Geneva: World Health Organization.

World Health Organization (2014, 2014). *Xpert MTB/RIF Implementation Manual: Technical and operational 'how-to'; practical considerations*. Geneva: World Health Organization.

10.3389/fmicb.2024.1374458

Glossary

MZN	modified Ziehl–Neelsen staining
TBM	tuberculous meningitis
CSF	cerebrospinal fluid
AUC	area under the curve
TB	tuberculosis
M. tuberculosis	*Mycobacterium tuberculosis*
MGIT	mycobacteria growth indicator tube
BMRC	British Medical Research Council
H	isoniazid
R	rifampin
E	ethambutol
S	streptomycin
K	kanamycin
A	amikacin
C	capreomycin
Mfx	moxifloxacin
Lfx	levofloxacin
PAS	para-aminosalicylic acid
Pto	prothionamide
DST	drug sensitivity test
HIV	human-immunodeficiency-virus
CXR	chest X-ray
OR	odds ratio
CI	confidence interval
SPSS	statistical package for social sciences

frontiers | Frontiers in Microbiology

TYPE Original Research
PUBLISHED 30 May 2024
DOI 10.3389/fmicb.2024.1409552

OPEN ACCESS

EDITED BY
Ranjan Nanda,
International Centre for Genetic Engineering and Biotechnology, India

REVIEWED BY
Yuhang Wang,
The University of Iowa, United States
Joaquin Pellegrini,
INSERM U1104 Centre d'immunologie de Marseille-Luminy (CIML), France

*CORRESPONDENCE
Lingna Lyu
✉ lvlingna003@163.com
Liping Pan
✉ panliping2006@163.com
Xiuli Zhang
✉ zhxiuli@gmail.com

RECEIVED 02 April 2024
ACCEPTED 06 May 2024
PUBLISHED 30 May 2024

CITATION
Lyu L, Jia H, Liu Q, Ma W, Li Z, Pan L and Zhang X (2024) Individualized lipid profile in urine-derived extracellular vesicles from clinical patients with *Mycobacterium tuberculosis* infections.
Front. Microbiol. 15:1409552.
doi: 10.3389/fmicb.2024.1409552

Individualized lipid profile in urine-derived extracellular vesicles from clinical patients with *Mycobacterium tuberculosis* infections

Lingna Lyu[1,2]*, Hongyan Jia[2], Qiuyue Liu[2], Wenxia Ma[1], Zihui Li[2], Liping Pan[2]* and Xiuli Zhang[3]*

[1]Department of Gastroenterology and Hepatology, Beijing You'an Hospital Affiliated to Capital Medical University, Beijing, China, [2]Beijing Key Laboratory for Drug Resistant Tuberculosis Research, Beijing Chest Hospital Affiliated to Capital Medical University, Beijing Tuberculosis and Thoracic Tumor Research Institute, Beijing, China, [3]The Chinese Academy of Sciences (CAS) Center for Excellence in Nanoscience, National Center for Nanoscience and Technology of China, Beijing, China

Background: Lipids are a key nutrient source for the growth and reproduction of *Mycobacterium tuberculosis* (*Mtb*). Urine-derived extracellular vesicles (EVs), because of its non-invasive sampling, lipid enrichment, and specific sorting character, have been recognized as a promising research target for biomarker discovery and pathogenesis elucidation in tuberculosis (TB). We aim to profile lipidome of *Mtb*-infected individuals, offer novel lipid signatures for the development of urine-based TB testing, and provide new insights into the lipid metabolism after *Mtb* infection.

Methods: Urine-derived extracellular vesicles from 41 participants (including healthy, pulmonary tuberculosis, latent tuberculosis patients, and other lung disease groups) were isolated and individually detected using targeted lipidomics and proteomics technology platforms. Biomarkers were screened by multivariate and univariate statistical analysis and evaluated by SPSS software. Correlation analyses were performed on lipids and proteins using the R Hmisc package.

Results: Overall, we identified 226 lipids belonging to 14 classes. Of these, 7 potential lipid biomarkers for TB and 6 for latent TB infection (LTBI) were identified, all of which were classified into diacylglycerol (DAG), monoacylglycerol (MAG), free fatty acid (FFA), and cholesteryl ester (CE). Among them, FFA (20:1) was the most promising biomarker target in diagnosing TB/LTBI from other compared groups and also have great diagnostic performance in distinguishing TB from LTBI with AUC of 0.952. In addition, enhanced lipolysis happened as early as individuals got latent *Mtb* infection, and ratio of raft lipids was gradually elevated along TB progression.

Conclusion: This study demonstrated individualized lipid profile of urinary EVs in patients with *Mtb* infection, revealed novel potential lipid biomarkers for TB/LTBI diagnosis, and explored mechanisms by which EV lipid raft-dependent bio-processes might affect pathogenesis. It lays a solid foundation for the subsequent diagnosis and therapeutic intervention of TB.

KEYWORDS

***Mycobacterium tuberculosis*, extracellular vesicles, lipidome, proteome, biomarker, lipid raft, immune response**

Introduction

Tuberculosis (TB) remains one of the most lethal infectious diseases in the world, posing a grave threat to public health. According to World Health Organization [WHO]'s (2023) global TB report, an estimated 10.6 million people were infected by *M. tuberculosis* (*Mtb*) and 1.3 million died from TB (World Health Organization [WHO], 2023). New TB cases in China for 2022 were approximately 748,000 with an estimated 30,000 deaths (World Health Organization [WHO], 2023). The burden for TB prevention and control was even more rigorous as a direct result of COVID-19 pandemic (Pai et al., 2022).

Currently, sputum smear and sputum culture are the gold standards for clinical TB diagnosis, which are time-consuming, less sensitive, and out of reach for many TB patients (Hepple et al., 2021). The limitations are even more apparent in children and the elderly, who cannot cooperate with sputum coughing for specimen collection. If methods for rapid testing by using body fluids can be developed, it would be a valuable addition to the diagnostic toolkit. Urine has been recognized as an ideal body fluid because it can be collected in large quantities without invasion, simple to handle, and low risk of infection when compared with other biofluids including serum, plasma, and saliva. In addition, urine-based TB testing is more affordable and device-free for allowing rapid TB diagnosis than blood-based testing (Hwang et al., 2022). In the past decades, high-throughput technology and multi-omic analysis have facilitated potential biomarker discovery in TB urine samples (Nogueira et al., 2022; Chen et al., 2023; Kim et al., 2023; Singh et al., 2023); we still face with great challenges for the disease-specific biomarker identification because of the huge number, broad range, and complexity of the components in human urine.

Extracellular vesicles (EVs), mainly exosomes, microvesicles (MVs), and apoptotic bodies, are nano-sized, double-membraned cup-like vesicles that were actively secreted from cells both under physiological and pathological conditions (Doyle and Wang, 2019). They can mediate signal transmission between cells by trafficking bio-active molecules including nucleic acids, proteins, and lipids (Singh et al., 2012; Lv et al., 2017; Lyu et al., 2019; Biadglegne et al., 2021). EVs are extensively present in various body fluids such as blood, urine, ascites, amniotic fluid, milk, cerebrospinal fluid, and bronchoalveolar lavage fluid (Singh et al., 2012; Biadglegne et al., 2021). Due to their lipid composition, EV lipids, apart from proteins and nucleic acids, have been recognized as a promising biomarker targets in a variety of diseases, including TB (Lam et al., 2021; Su et al., 2021; Yu et al., 2021). For instance, plasma exosomes from TB patients under different disease states (positive TB and TB lymphadenitis) showed distinct changes in the TAG and CE profiles compared with healthy controls, and their lipid spectrum was reorganized after TB treatment (Biadglegne et al., 2022). In addition, lipids are a key nutrient source for the growth and reproduction of *Mtb* (Maurya et al., 2019). Previous studies have indicated that *Mtb* can apply host fatty acids as their primary carbon source to enhance their survival *in vitro* and *in vivo* (Daniel et al., 2011; Maurya et al., 2019). However, research studies on lipidome of EVs from urine of TB have not been reported up to now. Therefore, revealing the lipid expression profile of urinary EVs from TB is of great value for biomarker discovery and pathogenesis elucidation.

This study examined the changes in lipid metabolism of the EVs derived from urine samples of healthy control (HC), latent TB infection (LTBI), tuberculosis (TB), and other non-TB lung diseases (Other) by using the targeted lipidomics technology platform (UPLC-TQMS). Furthermore, we analyzed and screened the characteristic lipid biomarkers for the TB/LTBI diagnosis. Finally, correlation analysis of lipids and lipid-associated proteins were carried out to obtain metabolic response networks in TB pathogenesis. Our study will offer novel lipid signatures with potential diagnostic value for the development of urine-based TB testing and provide new insights into the functions of disease-specific metabolism after *Mtb* infection.

Materials and methods

Participants and collection of samples

Urine samples from 41 participants including HC (healthy control, $n = 10$), LTBI (latent TB Infection, $n = 7$), TB (Tuberculosis, $n = 10$), and other (other lung diseases, $n = 14$, including 10 patients with lung cancer and 4 patients with pneumonia) were collected at initial diagnosis. All subjects were 18-year-old adults with HIV negative and signed the written informed consent form according to the Declaration of Helsinki, which was approved by the Ethics Committee of the Beijing Chest Hospital, Capital Medical University (number of ethical approvals: BJXK-2017-40-01). The HC individuals were recruited during annual health examination, and they have normal computed tomography (CT) chest films, negative tuberculin skin test (TST), and interferon-gamma release assay (IGRA) results. For LTBI individuals, they were diagnosed based on positive TST and IGRA results, but their other indicators were the same as healthy controls. All the TB patients were enrolled with positive *Mtb* culture and smear test results, and severe TB was identified with three or more lung lobe alterations observed in the CT scan and accompanied respiratory failure. Lung cancer and pneumonia patients were clinically newly diagnosed with negative IGRA results, and lung cancer patients had not received preoperative chemotherapy or radiotherapy. The clinical characteristics of the participants are shown in Supplementary Table S1.

Urine-derived EV isolation and identification

EVs from urine were isolated by using exo-Easy Maxi Kit according to the manufacturer's instructions (QIAGEN, Cat.76064). Transmission electron microscopy (TEM) was employed to visualize EVs using a JEM-1400 TEM (JEOL, Japan). Western blot was performed to detect EV surface marker CD9 and TSG101 with rabbit anti-human antibodies of anti-CD9 (SBI, United States) and anti-TSG101 (SBI, United States), and an endoplasmic reticulum marker protein, Calnexin, as negative control was detected with anti-Calnexin antibody (Abcam, United States). The size distribution of EVs was also measured through nanoparticle tracking analysis (NTA, Malvern, United Kingdom).

Lipidomic analysis

Using high-performance liquid chromatography coupled with triple quadrupole mass spectrometry (UPLC-TQMS) (TACQUITY

UPLCXevo TQ- S, Waters Corp., Milford, MA, USA), lipids from urine samples were detected and processed using MassLynx software (Waters, Milford, MA, USA) for peak extraction, integration, and quantification of each lipid, according to a set of standard samples of known concentration (Quantitative Curve, QC).

Profiling of lipidome in different groups

Heatmap was plotted based on z-scores of mean of lipid levels expressed by R.pheatmap (version 1.0.12), k-means clustering was performed to aggregate lipids that exhibited similar patterns of change, and lipids levels in each group were presented as line plots. Classes of the detected lipids were shown as follows: FFA, free fatty acid; LPA, lysophosphatidic acid; PA, phosphatidic acid; PE, phosphatidylethanolamine; PG, phosphatidylglycerol; CE, cholesterylester; Cer, ceramide; DAG, diacylglycerol; HexCer, Hexosylceramide; LPC, lysophosphatidylcholine; LPE, lysophosphatidylethanolamine; MA, monoacylglycerol; PC, phosphatidylcholine; SM, sphingomyelin; TAG, triacylglycerol; PS, phosphatidylserine; PI, phosphatidylinositol.

Differential expressed lipid analysis and biomarker selection

Multivariate statistical analysis of orthogonal partial least squares discriminant analysis (OPLS-DA) and univariate statistical analysis of *t*-test or Mann–Whitney–Wilcoxon (*U*-test) based on normality and chi-square of data were used to obtain differential expressed lipids (DELs) between two groups. Threshold value for potential biomarkers selection in this project is: VIP > 1 in multi-dimensional statistics and/or $p < 0.05$ and $|\log2FC| >= 0$ in univariate statistics. SPSS version 13.0 software (SPSS Inc., Chicago, IL, USA) was used for receiver operating characteristic (ROC) curve analysis to evaluate the diagnostic performance of potential biomarkers. The following analysis was conducted using these DELs.

Analysis of lipolysis and ratio of raft lipids

Method used to illustrate TAG lipolysis, and the ratio of raft lipids was applied as Lam SM reported with minor revisions according to detectability and replaceability of lipid species based on our actual data: TAG lipolysis = TAGs/(DAGs+MAGs+FFAs); proportion of raft lipids = ((SM + CE)/PC) (Lam et al., 2021).

Lipid pathway enrichment analysis

Pathway enrichment analysis was carried out using the pathway-associated metabolite sets (SMPDB) with fold changes (FC) and *p*-value, and pathway analysis was performed using hsa set with pathway impact factor and *p*-value. Pathways with *p*-value<0.05 were plotted in this study.

Proteomic LC–MS/MS and correlation analysis of DELs and DEPs

protein samples (100 μg) from urinary EVs were digested and desalted and then dried by SpeedVac for mass spectrometry. LC–MS/MS was run on the EASY-nLC 1,000 (Thermo Scientific, USA) using an analytical column (C18, 1.9 μm, 75 μm*20 cm) at a flow rate of 200 nL/min. The *Homo sapiens* proteome sequence database containing 20,417 entries downloaded from UniProt was used for the database searching. Normalization was performed against the total peptide intensity of each sample. At least two mapping peptides were used as cutoff for protein identification. Statistical analysis of differential expressed proteins (DEPs) was assessed using t-test for pairwise comparisons. $p < 0.05$ and $|\log2FC| >= 0$ were considered to be statistically significant. Among the DEPs, lipid-associated proteins were manually selected according to published data (Boerke et al., 2014; Sobocińska et al., 2018; Biadglegne et al., 2022; Franco Fontes et al., 2023). Correlation analyses (Pearson's method) were performed on the selected lipid APs and DELs using the R Hmisc package (version 5.1–0).

Results

Characteristics of EVs from HC, LTBI, TB, and other groups

To explore the expression profiles of lipids in urine-derived EVs derived from HC, LTBI, TB, and other individuals, we isolated the urinary EVs using exoEasy maxi kit (Qiagen, 76064) and then visualized them by transmission electron microscopy (TEM) (Figure 1). A characteristic cup-shaped vesicle morphology was showed with the diameter approximately 100 nm (Figure 1A). Western blot analysis detected the expression of EV-specific markers of CD9 and TSG101 on them, with an endoplasmic reticulum marker protein Calnexin as negative control to exclude the contamination of cellular components (Figure 1B). The size distribution of the isolated EVs by nanoparticle tracking analysis (NTA) was in agreement with theoretical size of EVs ranging from 50 nm to 200 nm with the peaks at ~100 nm (Figure 1C).

Lipid profiles and differential expression patterns in urine-derived EVs from HC, LTBI, TB, and other groups

Using high-performance liquid chromatography coupled with triple quadrupole mass spectrometry (UPLC-TQMS), we profiled the lipidome of isolated urinay EVs from HC, LTBI, TB, and other groups (Figure 2A). Finally, up to 226 lipids belonging to 14 classes were detected among them with free fatty acids (FFA, 56.94%), phosphatidylcholine (PC, 21.89%), sphingomyelins (SM, 12.29%), phosphatidylethanolamine (PE, 3.94%), and diacylglycerol (DAG, 2.20%) as the top five classes (Figure 2B). Then, a global *k*-means clustering heatmap was constructed, and line plots were drawn on the basis of z scores of the mean of lipid levels, to illustrate the expression patterns of changes in the lipidome of EVs in different groups (Figure 2A). We showed that all the lipids were aggregated in four clusters with different KEGG pathway enrichment by functional and lipid gene enrichment analysis. Notably, there was the greatest proportion of lipids classified into clusters 1 and 2, in which LTBI had the most upregulated lipids compared with other control groups (Figure 2A). Moreover, as expected, glycerolipid metabolism and glycerophospholipid metabolism were the most enriched pathways across the clusters 1, 2, and 4, while substantial lipids were also enriched in KEGG pathway of sphingolipid metabolism in cluster 1 (Figure 2A). Accordingly, it has been reported that abnormalities in phospholipid, triglyceride, and sphingolipid metabolism were present in plasma exosomes derived from TB patients (Biadglegne et al., 2022). Interestingly, we noticed that pathway of

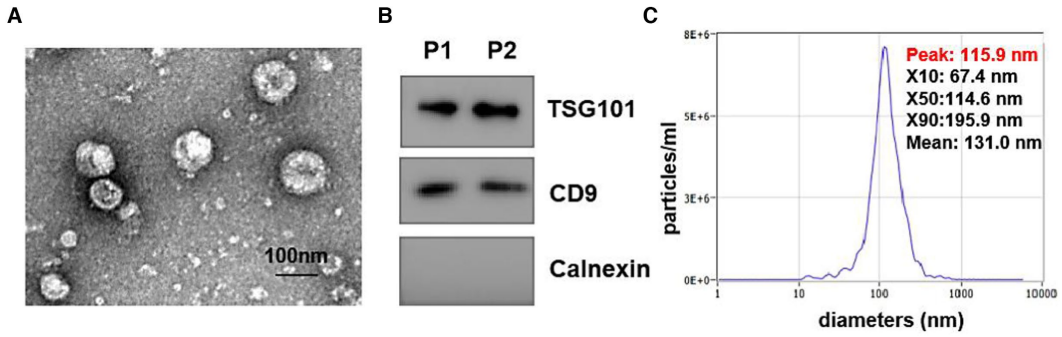

FIGURE 1
Identification of isolated urine-derived EVs. **(A)** Transmission electron microscopy (TEM) Image of EVs (magnification scale bar = 100 nm). **(B)** Western blot examined the EV surface marker of TSG101 and CD9, the expression of calreticulin (an endoplasmic reticulum marker protein) in vesicles. **(C)** Nanoparticle tracking analysis (NTA) showed the size distribution of isolated EVs, Y-axis present concentrations (particles/ml), the X-axis presented diameters (nm). The distribution peaks of EVs are at ~100 nm.

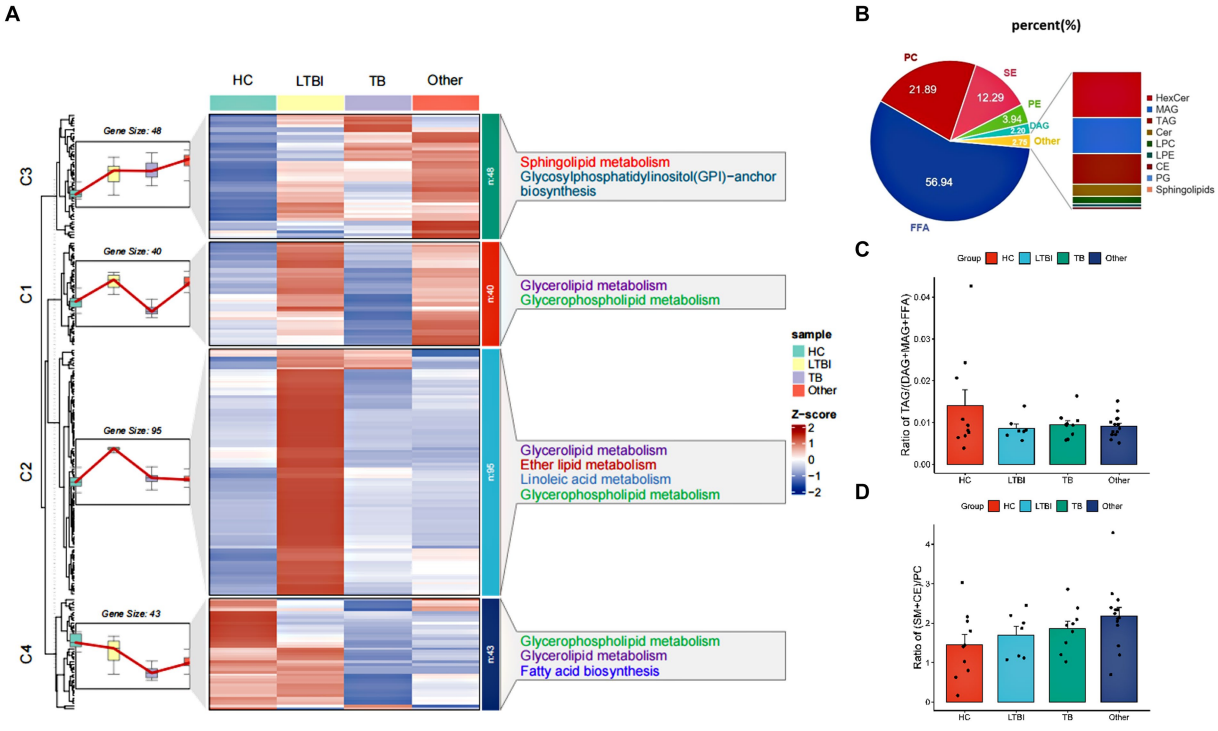

FIGURE 2
Profiling and different expression patterns of change in the lipidome of urine-derived EVs from LTBI and TB patients. **(A)** Heatmap was plotted based on z-scores of mean of lipid levels expressed, k-means clustering was performed to aggregate lipids that exhibited similar patterns of change in the LTBI, TB, an other. Lipids in four clusters were examined by KEGG Pathway Enrichment analysis. **(B)** Bar plot showed the distribution of different classes of lipids in each group. **(C)** Changes in the proportion of raft lipids ((SM + CE)/PC) across four groups. **(D)** Lipolysis was shown by the ratio of TAGs to their lipolytic substrates (DAGs) and free fatty acids (FFAs).

glycosylphosphatidylinositol (GPI)-anchor biosynthesis was enriched in cluster 3, and it has been indicated that GPI-anchor proteins (GPI-APs) are key components of lipid raft, involving in key signal transduction such as T-cell activation and other immune responses (Simons and Toomre, 2000; Hou et al., 2016; Gagliardi et al., 2021).

To further address the lipolysis and raft lipid level in the tested groups, we examined the ratio of TAGs to their lipolytic substrates (DAGs) and free fatty acids (FFA), and it was reduced obviously in LTBI, TB, and other groups compared with HC, indicating enhanced lipolysis after *Mtb* infection and in individuals with lung diseases (Figure 2C). Moreover, we observed elevated proportion of raft lipids ((SM + CE)/PC) (Figure 2D) in the LTBI, TB, and other groups compared with HC, suggesting a role of lipid raft-mediated immune processes in TB pathogenesis and/or after lung injuries.

Differentially expressed lipids in TB and LTBI indicate potential biomarkers for disease diagnosis

Next, we examined the differential expression profiles among the four groups by pairwise comparison based on OPLS-DA and univariate analysis (VIP > 1 and/or $|\log_2(FC)| \geq 0$, $p < 0.05$) and identified 118 differentially expressed lipids (DELs) in TB and 107 DELs in LTBI compared with the other three control groups (Supplementary Figure S1; Figures 3A,C). Interestingly, 113/118 DELs were dramatically downregulated in TB, while 101/107 DELs were significantly upregulated in LTBI (Figures 3A,C). By constructing Venn plot, we identified seven overlapped DELs, including MAG (18:2), MAG (16:1), FFA (22:5), FFA (16:1), DAG (18:1/18:2), FFA (20:1), and DAG (18:0/18:0) in TB and six overlapped DELs including DAG (16:1/18:1), FFA (20:1), CE (18:2), DAG (18:0/20:1), DAG (18:2/18:2), and FFA (12:1) in LTBI, which could be served as potential biomarkers to differentiate TB or LTBI from other control groups (Figures 3B,D; Supplementary Tables S2, S3). Notably, FFA (20:1) was found in both TB and LTBI overlapped lipids, which has the remarkable expression in LTBI and the lowest levels in TB (Figure 4A). We then performed receiver operating characteristic (ROC) curve analysis to evaluate the ability to detect FFA (20:1) in LTBI/TB and each compared group. The AUC of FFA (20:1) in distinguishing LTBI from HC/other was 0.825 (specificity of 88.9% and sensitivity of 85.7%) and 0.837 (specificity of 85.7% and sensitivity of 85.7%), respectively (Figure 4B; Table 1). Meanwhile, the AUC of FFA (20:1) in diagnosing TB from HC/other was 0.852 (specificity of 88.9% and sensitivity of 88.9%) and 0.857 (specificity of 92.9% and sensitivity of 88.9%) (Figure 4C; Table 1). Importantly, the AUC of FFA (20:1) was 0.952, the highest in distinguishing TB versus LTBI, with specificity of 100% and sensitivity of 88.9%, respectively (Table 1).

Characteristics of lipid expression changes along the different stages of *Mtb* (LTBI/TB) infection

Our previous study has reported a gradually deteriorated progression with LTBI developing to the active TB (Lv et al., 2017; Lyu et al., 2019). Together with the probable dysfunction of lipid metabolism across TB progression, as shown in Figure 2, we then focused on the DEL profiles in HC, LTBI, and TB and their changes in LTBI versus HC and TB versus LTBI (Figure 5). DELs in both TB versus HC and LTBI versus HC were enriched in "glycerolipid metabolism" and "glycerophospholipid metabolism" (Figures 5A,B); besides, DELs in TB versus HC also played a role in "fatty acid biosynthesis" and "ether lipid metabolism," while DELs in LTBI versus HC also gathered in specific pathways of "sphingolipid metabolism" and "inositol phosphate metabolism" (Figure 5B). Interestingly, there were 8 overlapped DELs between LTBI versus HC and TB versus LTBI, all of which were upregulated in LTBI but downregulated in stage of TB (Figures 5C,D). It showed that TB group has some

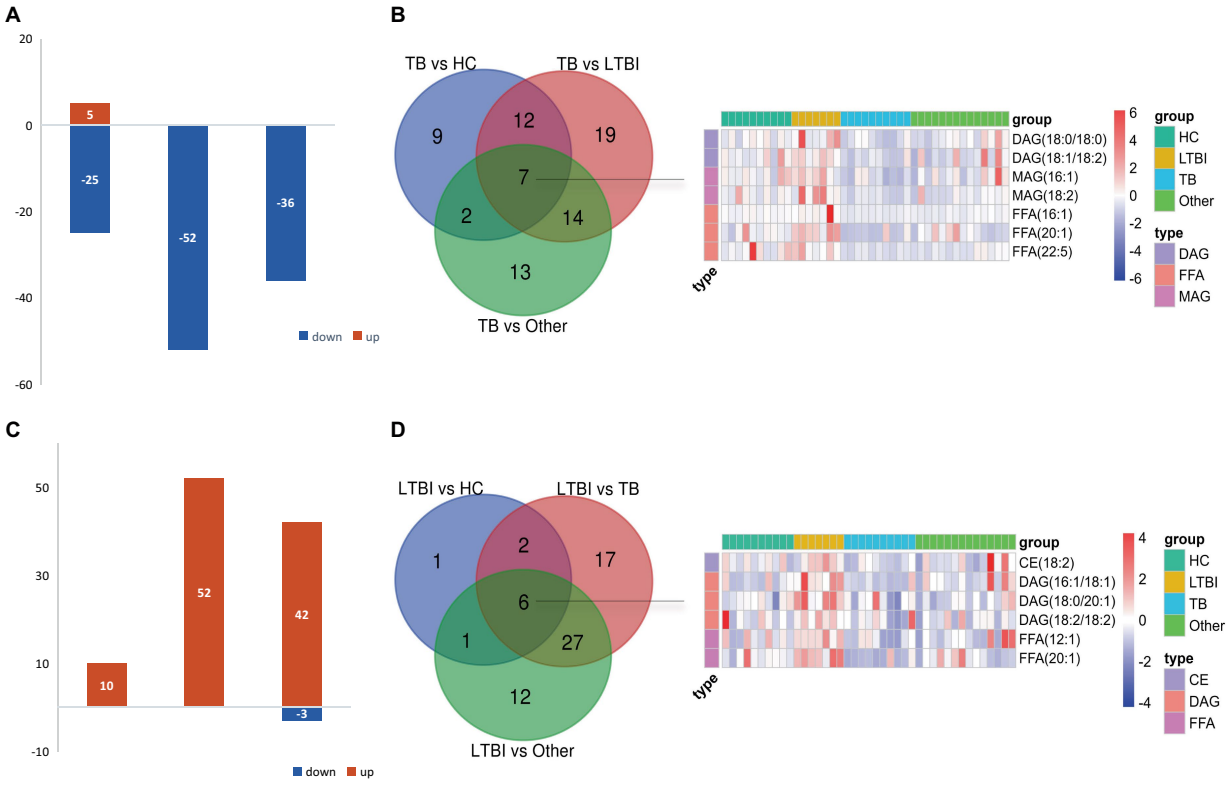

FIGURE 3
Differentially expressed lipids in LTBI/TB compared with control groups. **(A)** Bar plot showed significantly upregulated (red) or downregulated (green) lipids in TB. **(B)** Venn diagram presented overlapped lipids distinguishing TB from each control group and heatmap showed expression profile of overlapped seven lipids in each group. **(C)** Bar plot showed significantly upregulated (red) or downregulated (green) lipids in LTBI. **(D)** Venn diagram presented overlapped lipids distinguishing LTBI from each control group and heatmap showed expression profile of overlapped six lipids in each group.

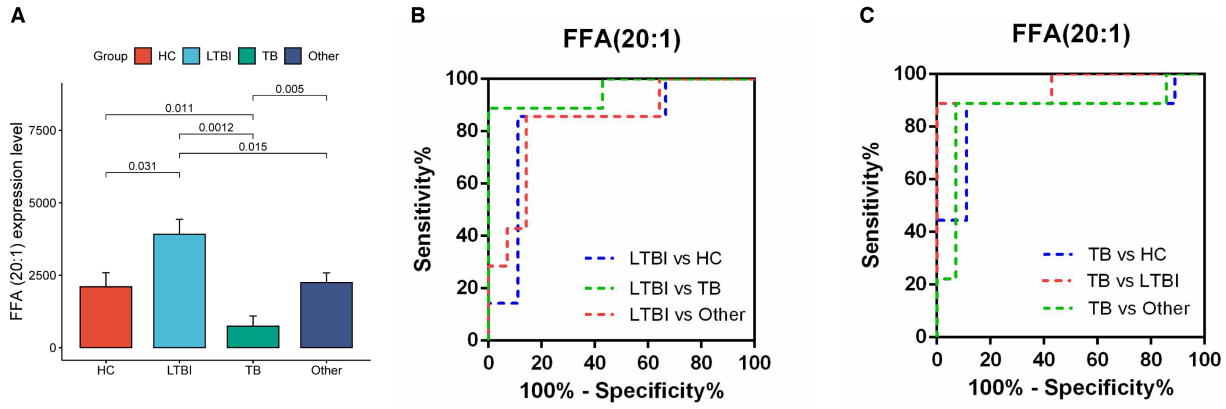

FIGURE 4
Diagnostic performance of lipid FFA (20:1) in distinguishing TB and LTBI from other control groups. **(A)** Expression level of FFA (20:1) in HC, LTBI, TB, and other, *p*-values were showed between LTBI/TB and each compared group. **(B,C)** Receiver operating characteristic (ROC) curve of the ability to detect FFA (20:1) in LTBI/TB and each compared group, respectively.

TABLE 1 Statistics of FFA (20:1) distinguished TB/LTBI from compared groups.

Groups	AUC	95% CI	Specificity (%)	Sensitivity (%)	SE	*P*-value
LTBI vs. HC	0.825	0.597 to 1.054	88.9	85.7	0.116	0.031
LTBI vs. Other	0.837	0.645 to 1.029	85.7	85.7	0.098	0.015
LTBI vs. TB	0.952	0.848 to 1.057	100	88.9	0.053	0.001
TB vs. HC	0.852	0.648 to 1.055	88.9	88.9	0.104	0.011
TB vs. Other	0.857	0.664 to 1.050	92.9	88.9	0.099	0.005

differential regulation of lipids compared with HC rather than the changed lipids in progress of LTBI from HC (Figure 5D, the third graph).

Correlation network of the differentially expressed lipids and lipid-related proteins in TB pathogenesis

A combination of lipidomics and proteomics may identify the composition of EVs and reveal the metabolism specific to the parent cells of origin or discover unique biological functions that elicit a coordinated metabolic response at a system level (Xue et al., 2022). We then performed proteomics with the same samples for lipidomics and applied two omics data to perform correlation network analysis with all the DELs and DEPs identified in patients with *Mtb* infection. It has been reported that apolipoproteins were dysregulated in TB patients (Biadglegne et al., 2022). Meanwhile, there are some clues that lipid raft might play a role in TB progression; we thus screened lipid-related proteins from DEPs including apolipoprotein-asscociated proteins (Apo-APs) and lipid raft-asscociated proteins (lipid raft-APs) (Boerke et al., 2014; Sobocińska et al., 2018; Biadglegne et al., 2022; Franco Fontes et al., 2023) and constructed a correlation network which was displayed with *p*-value (≤0.05) and correlation coefficient (>0.3 or <−0.3) (Figures 6A,B). Among them, CD59, CD55, and CD14 were the top three highlighted lipid raft-APs with broader connections with DELs, and APOA1BP, APOC1, and LPA were the top three important Apo-APs (Figures 6C,D). Notably, nearly all of them were positively correlated with DELs in our experimental system (Figures 6C,D).

Discussion

Lipids are significant components in the formation of foamy macrophages and tuberculous granuloma, both of which were favorable for the growth and reproduction of *Mtb* in host cells (Cronan, 2022; Florance and Ramasubbu, 2022). It has been reported that *Mtb* infection could lead to the accumulation of cholesteryl ester (CE) and triglyceride (TAG), promoted lipid droplet formation, and then used them as a long-term nutrition source (Daniel et al., 2011; Maurya et al., 2019). Previous studies also showed that mutations of genes in the specific pathway of lipid metabolism would recover the TB symptoms (Gioffré et al., 2005; Nazarova et al., 2017). Taken together, lipid homeostasis was of great value for TB research.

EVs are released from various human cells into the periphery, providing a potential source of tissue and disease-specific lipid biomarkers (Su et al., 2021; Yu et al., 2021). Our previous study has revealed potential miRNA and mRNA biomarkers for LTBI and TB by analyzing the transcriptome of their serum exosomes (Lv et al., 2017; Lyu et al., 2019). Importantly, we have identified exosomal genes from TB patients that enriched in GO terms of "lipid metabolism," but the changes of the lipid metabolism in TB excreting EVs are largely unexplored (Lv et al., 2017). In the current study, we collected the promising testing sample of urine from TB patients and control groups and used large-scaled targeted lipidomic platform

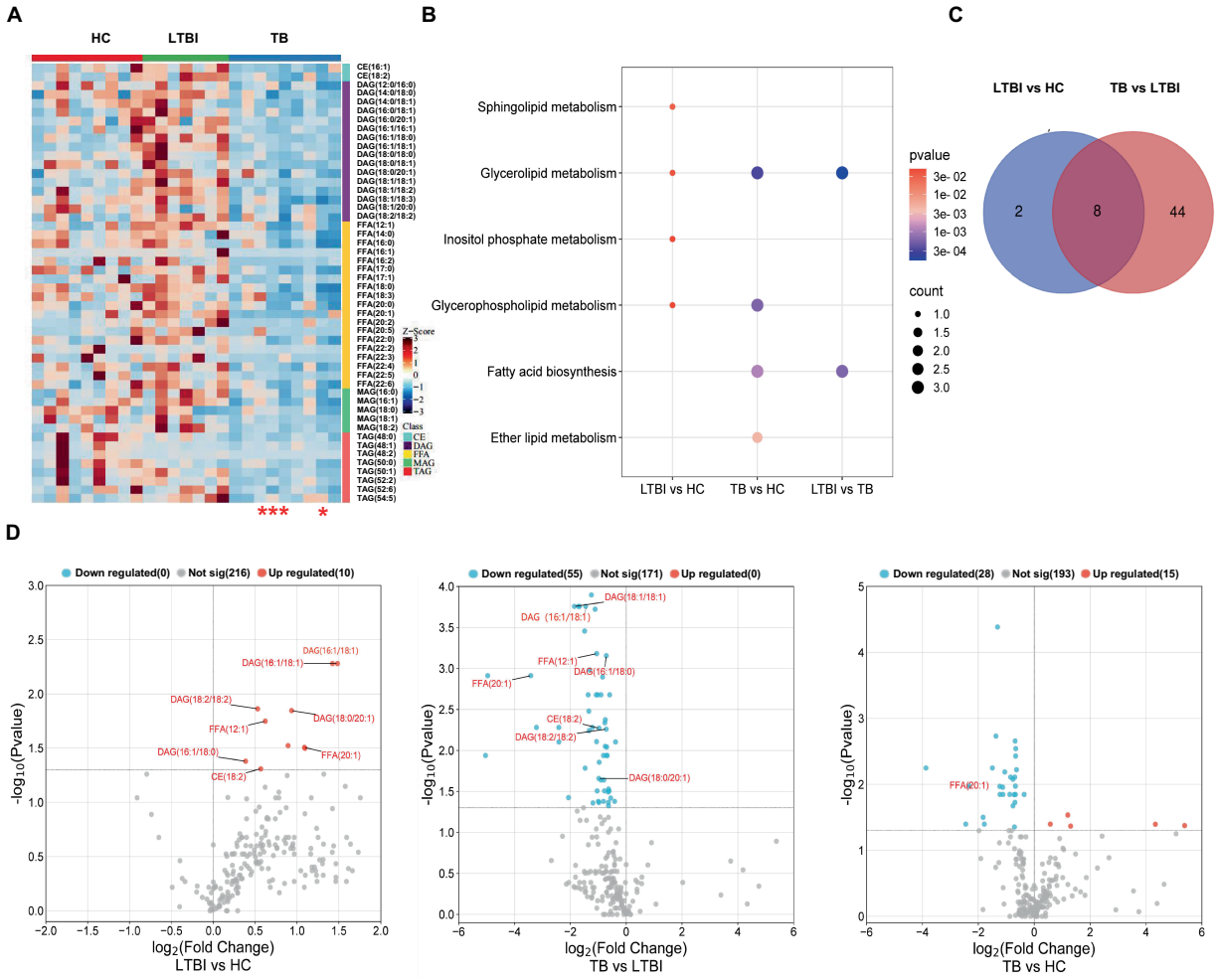

FIGURE 5
Distinct expression changes in lipids along the different stages of *Mtb* (LTBI and TB) infection. **(A)** Heatmap showing the differentially expressed lipids from HC, LTBI, and TB groups (VIP score > 1, p-value <0.05, |log2 (FC)| > 0). The color key indicates the expression level of the lipids. The four red stars mark severe TB patients. **(B)** KEGG pathway analysis and lipid enrichment were shown in compared groups ($p \leq 0.05$). **(C)** Venn diagram showed the shared lipids altered over the courses of LTBI to TB. **(D)** Volcano plots showed significantly regulated lipids in compared groups. Red represented upregulation, blue represented downregulation. Shared lipids were labeled in red.

(UPLC-TQMS) to profile the distinct lipid expression spectrum in different stages of TB (LTBI and TB) and compared groups. Further analysis screened seven potential lipid biomarkers (downregulated) for TB and six lipid biomarkers (upregulated) for LTBI, all of which were classified into TAG lipolytic substrates (DAG, MAG), FFA and CE, in accordance with a recent study that reported decreased levels of certain types of TAG and FFA in the plasma of TB patients (Chen et al., 2021). Notably, we identified FFA (20:1) as the most promising biomarker target in diagnosing TB/LTBI from other compared groups with dramatic upregulation in LTBI but remarkable downregulation in TB. Specifically, it ranked the highest diagnostic performance in distinguishing TB versus LTBI with AUC of 0.952 (specificity of 100% and sensitivity of 88.9%). It has been demonstrated that FFA is accumulated in *Mtb*-infected macrophages, which mediates metabolic adaptation of host cells to anti-Mtb response and forces bacteria to become fat-fueled (Akaki et al., 2000; Taslim et al., 2017), explaining higher FFA (20:1) levels in LTBI at this critical turning point for the transition after *Mtb* infection but before active TB stage. Although there were several publications conducted lipid biomarker identification in TB prediction, diagnosis, or disease monitoring, all of them applied invasive plasma samples or plasma-isolated EVs, and there were also discrepancies for the classes and amounts of certain lipids among them and compared with ours (Chen et al., 2021; Biadglegne et al., 2022; Shivakoti et al., 2022; Anh et al., 2023). For example, by using UPLC–MS/MS, two lysophosphatidic acid (LPA) species of LPA (0:0, 16:0) and LPA (0:0, 18:0) in plasma were identified as potential biomarkers for early diagnosis and treatment efficacy of TB (Chen et al., 2021); however, LPA was not detected in our experiment system that might stem from different lipidomics platform and sample specimens. Meanwhile, another two metabolites of glycerophospholipid such as LPC and LPE were targeted by us but with no significant differences between TB and control groups.

Lipid metabolism was closely associated with host metabolic and immune alterations in TB pathogenesis (Shivakoti et al., 2022; Anh et al., 2023). Our results revealed distinct metabolism of glycerolipid, glycerophospholipid, and sphingolipid in LTBI and TB groups. In addition, the lipolysis presented by the ratio of TAGs/(DAGs+MAGs+FFAs) obviously increased from HC to LTBI stage and

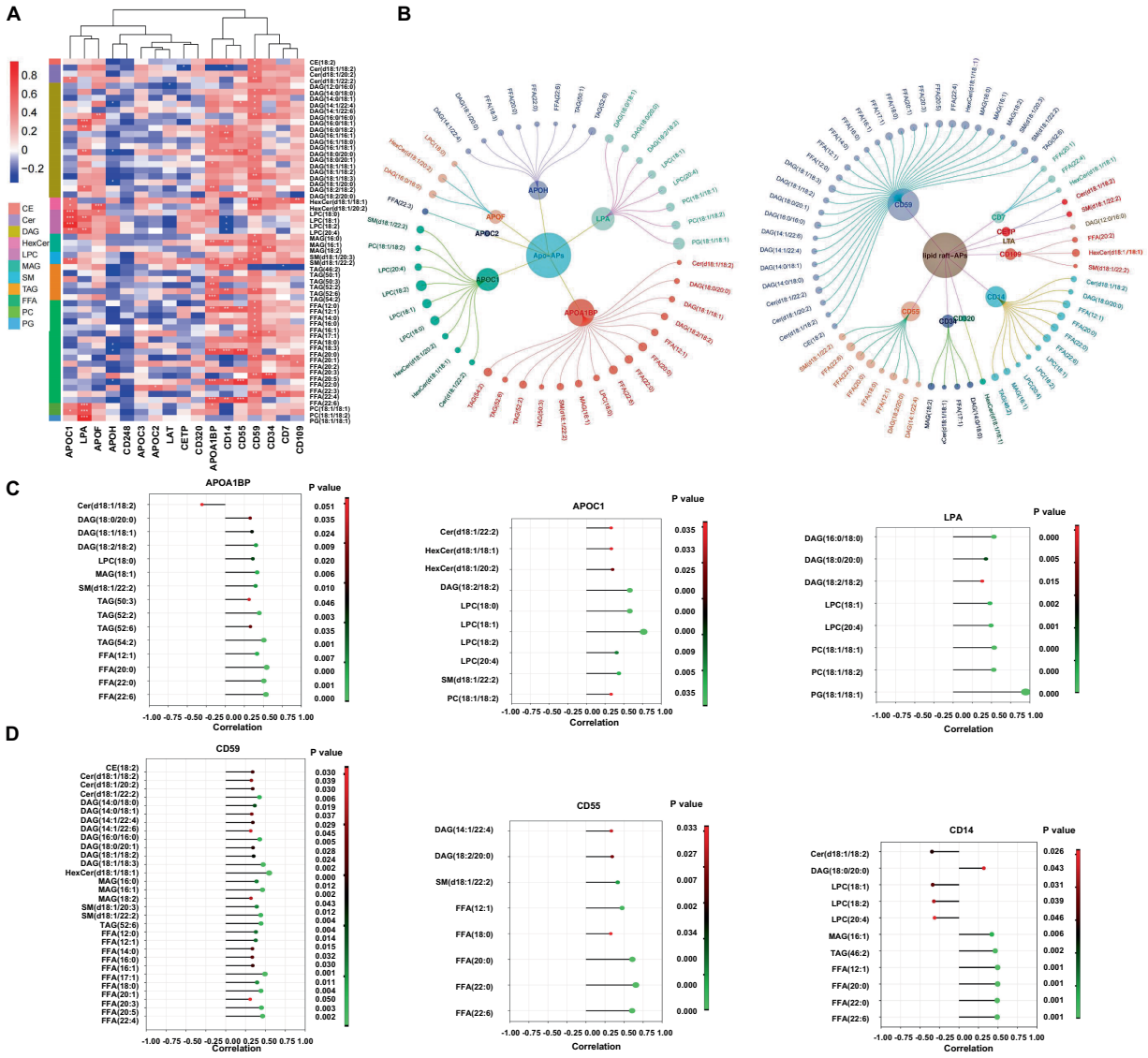

FIGURE 6
Correlation network of the differentially expressed lipids and lipid-related proteins in EVs from LTBI and TB. **(A,B)** Screened EVs apolipoprotein and associated proteins (Apo-APs) and lipid raft-associated proteins (lipid raft-APs) from LC–MS/MS proteome (unpublished data) were applied for Pearson correlation analysis with differentially expressed lipids. Inner dots presented proteins and outer dots presented lipids with larger sizes showing greater correlation coefficient (>0.3 or < −0.3). **(C)** Top 3 broadly correlated Apo-APs and **(D)** top 3 correlated lipid raft-APs and corresponding lipids were displayed with *p*-value (≤0.05) and correlation coefficient (>0.3 or < −0.3).

went slightly higher in TB stage, suggesting that enhanced lipolysis happened as early as individuals got latent *Mtb* infection so as to aid *Mtb* to survive dormancy (Daniel et al., 2011). In addition, the ratio of raft lipid was gradually elevated from HC to LTBI and then to TB, illustrating a potential role of lipid raft-associated process in TB progression. Lipid rafts refer to the formation of ordered, discrete microdomains enriched with cholesterol, sphingolipids, and GPI-anchored proteins within the membranes and has been discovered to be involved in the mechanisms of exosome biogenesis and secretion (de Gassart et al., 2003; Lingwood and Simons, 2010). So as to examine the biological processes related to lipid rafts, we further performed proteomics and conducted combinatorial analysis of lipidomics and proteomics (unpublished data) to build a correlation network between DELs and their related proteins such as Apo-APs and lipid raft-APs (GPI-anchored proteins) including CD59, CD55, and CD14 in lipid raft-APs and APOA1BP, APOC1, and LPA (APOA1) in Apo-APs, respectively. It has been reported that GPI-anchored proteins such as CD55 and CD59 were selectively sorted into exosomes (Rabesandratana et al., 1998). Their loss in red blood cells causes upregulated complement activation (Colden et al., 2022). CD59 was also required by pathogenic bacteria in cholesterol-dependent cytolysins by using virulence factors to punch holes in lipid bilayers (Parker and Feil, 2005; Boyd et al., 2016; Voisin et al., 2023). In addition, CD14 was also founded as immune activation markers on plasma exosomes from HIV patients (Chettimada et al., 2018). Recently, it was reported that trafficking of bacterial endotoxin lipopolysaccharide (LPS) by CD14 could modulate inflammatory responses of murine macrophages (Ciesielska et al., 2022). Thus, these GPI-APs, together with raft lipids, might be responsible for *Mtb* evading into cells and regulating EV-mediated immune signaling processes toward *Mtb*. As for lipids

carrying apolipoproteins, APOA1, APOB, and APOC1 have been detected in plasma exoxomes from drug-resistant TB patients, and APOC1 was found to be deleted in patients after *Mtb* infection (Biadglegne et al., 2022; Wu et al., 2023). Consistently, we also identified LPA (APOA1)/binding protein (APOA1BP) and APOC1 in *Mtb*-infected patients, suggesting their possible involvement in the pathogenesis of TB by regulating lipid metabolism via EVs.

Taken together, our study has confirmed previous discoveries on aberrant lipid spectrum in circulating urine-derived EVs from individuals after *Mtb* infection, uncovered novel potential lipid biomarkers for TB/LTBI diagnosis with non-invasive sampling in a clinical setting, and revealed integral role of lipid metabolism and lipid raft-dependent processes in TB pathogenesis. However, some limitations in our work should be noted: firstly, we did not detect any *Mtb* virulent lipids such as reported sulfoglycolipid (SL) (Mishra et al., 2019), mannose-capped lipoarabinomannan (LAM) (Welin et al., 2008), trehalose dimycolate (TDM) (Spargo et al., 1991), glycopeptidolipids (GPL) (Sut et al., 1990), and phthiocerol dimycocerosate (PDIM) (Quigley et al., 2017) because they were not in the pool of our lipid targets, however, untargeted metabolomics applied by Biadglegne et al. did not report any *Mtb* lipids either, indicating their low levels beyond the detection capacity of current metabolomics platform. Second, the sample size of this study is relatively small, and further validation using larger, multi-center cohorts is needed to verify the diagnostic value of potential biomarkers for TB/LTBI and ravel the regulatory role of lipid-raft engaged biological processes in TB pathogenesis.

Data availability statement

Metabolomics raw data have been deposited at EMB-MetaboLights (accession number MTBLS9666). Proteomics raw data have been deposited at ProteomeXchange (accession number PXD050345).

Ethics statement

All the participants signed the written informed consent forms according to the Declaration of Helsinki, which was approved by the Ethics Committee of the Beijing Chest Hospital, Capital Medical University (number of ethical approvals: BJXK-2017-40-01).

Author contributions

LL: Conceptualization, Data curation, Formal analysis, Funding acquisition, Writing – original draft, Writing – review & editing. HJ: Data curation, Resources, Writing – original draft. QL: Data curation, Funding acquisition, Writing – review & editing. WM: Formal analysis, Software, Writing – original draft. ZL: Data curation, Methodology, Writing – review & editing. LP: Methodology, Supervision, Writing – review & editing. XZ: Investigation, Methodology, Supervision, Writing – original draft, Writing – review & editing.

Funding

The author(s) declare financial support was received for the research, authorship, and/or publication of this article. This study was supported by the National Natural Science Foundation of China (82372260, 82100011) and Beijing Natural Science Foundation Haidian Original Innovation Joint Fund (L202023).

Conflict of interest

The authors declare that the research was conducted in the absence of any commercial or financial relationships that could be construed as a potential conflict of interest.

Publisher's note

Supplementary material

The Supplementary material for this article can be found online at: https://www.frontiersin.org/articles/10.3389/fmicb.2024.1409552/full#supplementary-material

References

Akaki, T., Tomioka, H., Shimizu, T., Dekio, S., and Sato, K. (2000). Comparative roles of free fatty acids with reactive nitrogen intermediates and reactive oxygen intermediates in expression of the anti-microbial activity of macrophages against *Mycobacterium tuberculosis*. *Clin. Exp. Immunol.* 121, 302–310. doi: 10.1046/j.1365-2249.2000.01298.x

Anh, N. K., Phat, N. K., Yen, N. T. H., Jayanti, R. P., Thu, V. T. A., Park, Y. J., et al. (2023). Comprehensive lipid profiles investigation reveals host metabolic and immune alterations during anti-tuberculosis treatment: implications for therapeutic monitoring. *Biomed. Pharmacother.* 158:114187. doi: 10.1016/j.biopha.2022.114187

Biadglegne, F., König, B., Rodloff, A. C., Dorhoi, A., and Sack, U. (2021). Composition and clinical significance of exosomes in tuberculosis: a systematic literature review. *J. Clin. Med.* 10:145. doi: 10.3390/jcm10010145

Biadglegne, F., Schmidt, J. R., Engel, K. M., Lehmann, J., Lehmann, R. T., Reinert, A., et al. (2022). *Mycobacterium tuberculosis* affects protein and lipid content of circulating exosomes in infected patients depending on tuberculosis disease state. *Biomedicines* 10:783. doi: 10.3390/biomedicines10040783

Boerke, A., van der Lit, J., Lolicato, F., Stout, T. A., Helms, J. B., and Gadella, B. M. (2014). Removal of GPI-anchored membrane proteins causes clustering of lipid microdomains in the apical head area of porcine sperm. *Theriogenology* 81, 613–624. doi: 10.1016/j.theriogenology.2013.11.014

Boyd, C., Parsons, E., Smith, R., Seddon, J. M., Ces, O., and Bubeck, D. (2016). Disentangling the roles of cholesterol and CD59 in intermedilysin pore formation. *Sci. Rep.* 6:38446. doi: 10.1038/srep38446

Chen, J. X., Han, Y. S., Zhang, S. Q., Li, Z. B., Chen, J., Yi, W. J., et al. (2021). Novel therapeutic evaluation biomarkers of lipid metabolism targets in uncomplicated pulmonary tuberculosis patients. *Signal Transduct. Target. Ther.* 6:22. doi: 10.1038/s41392-020-00427-w

Chen, P., Meng, Y., Liu, T., Peng, W., Gao, Y., He, Y., et al. (2023). Sensitive urine immunoassay for visualization of Lipoarabinomannan for noninvasive tuberculosis diagnosis. *ACS Nano* 17, 6998–7006. doi: 10.1021/acsnano.3c01374

Chettimada, S., Lorenz, D. R., Misra, V., Dillon, S. T., Reeves, R. K., Manickam, C., et al. (2018). Exosome markers associated with immune activation and oxidative stress in HIV patients on antiretroviral therapy. *Sci. Rep.* 8:7227. doi: 10.1038/s41598-018-25515-4

Ciesielska, A., Krawczyk, M., Sas-Nowosielska, H., Hromada-Judycka, A., and Kwiatkowska, K. (2022). CD14 recycling modulates LPS-induced inflammatory responses of murine macrophages. *Traffic* 23, 310–330. doi: 10.1111/tra.12842

Colden, M. A., Kumar, S., Munkhbileg, B., and Babushok, D. V. (2022). Insights into the emergence of paroxysmal nocturnal Hemoglobinuria. *Front. Immunol.* 12:830172. doi: 10.3389/fimmu.2021.830172

Cronan, M. R. (2022). In the thick of it: formation of the tuberculous granuloma and its effects on host and therapeutic responses. *Front. Immunol.* 13:820134. doi: 10.3389/fimmu.2022.820134

Daniel, J., Maamar, H., Deb, C., Sirakova, T. D., and Kolattukudy, P. E. (2011). *Mycobacterium tuberculosis* uses host triacylglycerol to accumulate lipid droplets and acquires a dormancy-like phenotype in lipid-loaded macrophages. *PLoS Pathog.* 7:e1002093. doi: 10.1371/journal.ppat.1002093

de Gassart, A., Géminard, C., Février, B., and Raposo, G. (2003). Michel Vidal; lipid raft-associated protein sorting in exosomes. *Blood* 102, 4336–4344. doi: 10.1182/blood-2003-03-0871

Doyle, L. M., and Wang, M. Z. (2019). Overview of extracellular vesicles, their origin, composition, purpose, and methods for exosome isolation and analysis. *Cells* 8:727. doi: 10.3390/cells8070727

Florance, I., and Ramasubbu, S. (2022). Current understanding on the role of lipids in macrophages and associated diseases. *Int. J. Mol. Sci.* 24:589. doi: 10.3390/ijms24010589

Franco Fontes, C., Silva Bidu, N., Rodrigues Freitas, F., Maranhão, R. C., Santos Monteiro, A. S., David Couto, R., et al. (2023). Changes in serum amyloid a, plasma high-density lipoprotein cholesterol and apolipoprotein A-I as useful biomarkers for *Mycobacterium tuberculosis* infection. *J. Med. Microbiol.* 72:1726. doi: 10.1099/jmm.0.001726

Gagliardi, M. C., Iwabuchi, K., and Lai, C. H. (2021). Editorial: role of lipid rafts in anti-microbial immune response. *Front. Immunol.* 12:654776. doi: 10.3389/fimmu.2021.654776

Gioffré, A., Infante, E., Aguilar, D., Santangelo, M. P., Klepp, L., Amadio, A., et al. (2005). Mutation in mce operons attenuates *Mycobacterium tuberculosis* virulence. *Microbes Infect.* 7, 325–334. doi: 10.1016/j.micinf.2004.11.007

Hepple, P., Ford, N., and McNerney, R. (2021). Microscopy compared to culture for the diagnosis of tuberculosis in induced sputum samples: a systematic review. *Int. J. Tuberc. Lung Dis.* 16, 579–588. doi: 10.5588/ijtld.11.0617

Hou, T. Y., McMurray, D. N., and Chapkin, R. S. (2016). Omega-3 fatty acids, lipid rafts, and T cell signaling. *Eur. J. Pharmacol.* 785, 2–9. doi: 10.1016/j.ejphar.2015.03.091

Hwang, C., Lee, W. J., Kim, S. D., Park, S., and Kim, J. H. (2022). Recent advances in biosensor Technologies for Point-of-Care Urinalysis. *Biosensors (Basel)* 12:1020. doi: 10.3390/bios12111020

Kim, T., Kim, J., Kim, T., Oak, C. H., and Ryoo, S. (2023). Transrenal DNA detection of *Mycobacterium tuberculosis* in patients with pulmonary tuberculosis. *Int. J. Mycobacteriol.* 12, 66–72. doi: 10.4103/ijmy.ijmy_12_23

Lam, S. M., Zhang, C., Wang, Z., Ni, Z., Zhang, S., Yang, S., et al. (2021). A multi-omics investigation of the composition and function of extracellular vesicles along the temporal trajectory of COVID-19. *Nat. Metab.* 3, 909–922. doi: 10.1038/s42255-021-00425-4

Lingwood, D., and Simons, K. (2010). Lipid rafts as a membrane-organizing principle. *Science* 327, 46–50. doi: 10.1126/science.1174621. PMID: 20044567

Lv, L., Li, C., Zhang, X., Ding, N., Cao, T., Jia, X., et al. (2017). RNA profiling analysis of the serum exosomes derived from patients with active and latent *Mycobacterium tuberculosis* infection. *Front. Microbiol.* 8:1051. doi: 10.3389/fmicb.2017.01051

Lyu, L., Zhang, X., Li, C., Yang, T., Wang, J., Pan, L., et al. (2019). Small RNA profiles of serum exosomes derived from individuals with latent and active tuberculosis. *Front. Microbiol.* 10:1174. doi: 10.3389/fmicb.2019.01174

Maurya, R. K., Bharti, S., and Krishnan, M. Y. (2019). Triacylglycerols: fuelling the hibernating *Mycobacterium tuberculosis*. *Front. Cell. Infect. Microbiol.* 8:450. doi: 10.3389/fcimb.2018.00450

Mishra, M., Adhyapak, P., Dadhich, R., and Kapoor, S. (2019). Dynamic Remodeling of the host cell membrane by virulent mycobacterial Sulfoglycolipid-1. *Sci. Rep.* 9:12844. doi: 10.1038/s41598-019-49343-2

Nazarova, E. V., Montague, C. R., La, T., Wilburn, K. M., Sukumar, N., Lee, W., et al. (2017). Rv3723/LucA coordinates fatty acid and cholesterol uptake in *Mycobacterium tuberculosis*. *eLife* 6:e26969. doi: 10.7554/eLife.26969

Nogueira, B. M. F., Krishnan, S., Barreto-Duarte, B., Araújo-Pereira, M., Queiroz, A. T. L., Ellner, J. J., et al. (2022). Diagnostic biomarkers for active tuberculosis: progress and challenges. *EMBO Mol. Med.* 14:e14088. doi: 10.15252/emmm.202114088

Pai, M., Kasaeva, T., and Swaminathan, S. (2022). COVID-19's devastating effect on tuberculosis care: a path to recovery. *N. Engl. J. Med.* 386, 1490–1493. doi: 10.1056/NEJMp2118145

Parker, M. W., and Feil, S. C. (2005). Pore-forming protein toxins: from structure to function. *Prog. Biophys. Mol. Biol.* 88, 91–142. doi: 10.1016/j.pbiomolbio.2004.01.009

Quigley, J., Hughitt, V. K., Velikovsky, C. A., Mariuzza, R. A., el-Sayed, N. M., and Briken, V. (2017). The Cell Wall lipid PDIM contributes to Phagosomal escape and host cell exit of *Mycobacterium tuberculosis*. *MBio* 8:148. doi: 10.1128/mBio.00148-17

Rabesandratana, H., Toutant, J. P., Reggio, H., and Vidal, M. (1998). Decay-accelerating factor (CD55) and membrane inhibitor of reactive lysis (CD59) are released within exosomes during in vitro maturation of reticulocytes. *Blood* 91, 2573–2580. doi: 10.1182/blood.V91.7.2573

Shivakoti, R., Newman, J. W., Hanna, L. E., Queiroz, A. T. L., Borkowski, K., Gupte, A. N., et al. (2022). Host lipidome and tuberculosis treatment failure. *Eur. Respir. J.* 59:2004532. doi: 10.1183/13993003.04532-2020

Simons, K., and Toomre, D. (2000). Lipid rafts and signal transduction. *Nat. Rev. Mol. Cell Biol.* 1, 31–39. doi: 10.1038/35036052, Erratum in: Nat Rev Mol Cell Biol 2001;2(3):216

Singh, U. B., Angitha, K. P., Bhatnagar, A., Sharma, S., Bir, R., Singh, K., et al. (2023). GeneXpert ultra in urine samples for diagnosis of extra-pulmonary tuberculosis. *Curr. Microbiol.* 80:361. doi: 10.1007/s00284-023-03503-w. PMID: 37796343

Singh, P. P., Smith, V. L., Karakousis, P. C., and Schorey, J. S. (2012). Exosomes isolated from mycobacteria-infected mice or cultured macrophages can recruit and activate immune cells in vitro and in vivo. *J. Immunol.* 189, 777–785. doi: 10.4049/jimmunol.1103638

Sobocińska, J., Roszczenko-Jasińska, P., Zaręba-Kozioł, M., Hromada-Judycka, A., Matveichuk, O. V., Traczyk, G., et al. (2018). Lipopolysaccharide upregulates Palmitoylated enzymes of the phosphatidylinositol cycle: an insight from proteomic studies. *Mol. Cell. Proteomics* 17, 233–254. doi: 10.1074/mcp.RA117.000050

Spargo, B. J., Crowe, L. M., Ioneda, T., Beaman, B. L., and Crowe, J. H. (1991). Cord factor (alpha,alpha-trehalose 6,6′-dimycolate) inhibits fusion between phospholipid vesicles. *Proc. Natl. Acad. Sci. USA* 88, 737–740. doi: 10.1073/pnas.88.3.737

Su, H., Rustam, Y. H., Masters, C. L., Makalic, E., McLean, C. A., Hill, A. F., et al. (2021). Characterization of brain-derived extracellular vesicle lipids in Alzheimer's disease. *J. Extracell Vesicles.* 10:e12089. doi: 10.1002/jev2.12089

Sut, A., Sirugue, S., Sixou, S., Lakhdar-Ghazal, F., Tocanne, J. F., and Laneelle, G. (1990). Mycobacteria glycolipids as potential pathogenicity effectors: alteration of model and natural membranes. *Biochemistry* 29, 8498–8502. doi: 10.1021/bi00488a042

Taslim, N. A., Virani, D., Sumartini, N. K., Karmila, B. A., As'ad, S., Satriono, R., et al. (2017). Energy regulation in newly diagnosed TB with chronic energy deficiency: free fatty acids and RBP4. *Asia Pac. J. Clin. Nutr.* 26, S73–S78. doi: 10.6133/apjcn.062017.s9

Voisin, T. B., Couves, E. C., Tate, E. W., and Bubeck, D. (2023). Dynamics and molecular interactions of GPI-anchored CD59. *Toxins (Basel)* 15:430. doi: 10.3390/toxins15070430

Welin, A., Winberg, M. E., Abdalla, H., Särndahl, E., Rasmusson, B., Stendahl, O., et al. (2008). Incorporation of *Mycobacterium tuberculosis* lipoarabinomannan into macrophage membrane rafts is a prerequisite for the phagosomal maturation block. *Infect. Immun.* 76, 2882–2887. doi: 10.1128/IAI.01549-07

World Health Organization [WHO] (2023). *Global Tuberculosis Report 2022*. Geneva: World Health Organization.

Wu, M., Yang, Q., Yang, C., Han, J., Liu, H., Qiao, L., et al. (2023). Characteristics of plasma exosomes in drug-resistant tuberculosis patients. *Tuberculosis (Edinb.)* 141:102359. doi: 10.1016/j.tube.2023.102359

Xue, M., Yao, T., Xue, M., Francis, F., Qin, Y., Jia, M., et al. (2022). Mechanism analysis of metabolic fatty liver on largemouth bass (*Micropterus salmoides*) based on integrated Lipidomics and proteomics. *Meta* 12:759. doi: 10.3390/metabo12080759

Yu, W., Hurley, J., Roberts, D., Chakrabortty, S. K., Enderle, D., Noerholm, M., et al. (2021). Exosome-based liquid biopsies in cancer: opportunities and challenges. *Ann. Oncol.* 32, 466–477. doi: 10.1016/j.annonc.2021.01.074

frontiers | Frontiers in Microbiology

TYPE Original Research
PUBLISHED 14 June 2024
DOI 10.3389/fmicb.2024.1397792

OPEN ACCESS

EDITED BY
Robert Jansen,
Radboud University, Netherlands

REVIEWED BY
Siamak Heidarzadeh,
Zanjan University of Medical Sciences, Iran
Mudit Chandra,
Guru Angad Dev Veterinary and Animal Sciences University, India
Tais Ramalho Dos Anjos,
Federal Institute of Education, Science and Technology of Mato Grosso, Brazil

*CORRESPONDENCE
Xiaoxu Fan
✉ fanxiaoxu@cahec.cn
Haobo Zhang
✉ zhanghaobo@cahec.cn
Shufang Sun
✉ sunshufang@cahec.cn

†These authors have contributed equally to this work

RECEIVED 08 March 2024
ACCEPTED 31 May 2024
PUBLISHED 14 June 2024

CITATION
Qu Y, Liu M, Sun X, Liu Y, Liu J, Hu L, Jiang Z, Qi F, Nan W, Yan X, Sun M, Shao W, Li J, Sun S, Zhang H and Fan X (2024) Development and evaluation of a triplex droplet digital PCR method for differentiation of *M. tuberculosis*, *M. bovis* and BCG. *Front. Microbiol.* 15:1397792. doi: 10.3389/fmicb.2024.1397792

Development and evaluation of a triplex droplet digital PCR method for differentiation of *M. tuberculosis*, *M. bovis* and BCG

Yao Qu[1,2†], Mengda Liu[1,3†], Xiangxiang Sun[1,3,4], Yongxia Liu[2], Jianzhu Liu[2], Liping Hu[5], Zhiqiang Jiang[1], Fei Qi[1], Wenlong Nan[1,3], Xin Yan[1,4], Mingjun Sun[1], Weixing Shao[1], Jiaqi Li[1], Shufang Sun[1,3]*, Haobo Zhang[1,3]* and Xiaoxu Fan[1,3]*

[1]National Animal Tuberculosis Reference Laboratory, Division of Zoonoses Surveillance, China Animal Health and Epidemiology Center, Qingdao, Shandong, China, [2]College of Animal Technology, Shandong Agricultural University, Taian, Shandong, China, [3]Key Laboratory of Major Ruminant Infectious Disease Prevention and Control (East) of Ministry, Agriculture and Rural Affairs, Qingdao, Shandong, China, [4]Key Laboratory of Animal Biosafety Risk Warning Prevention and Control (South) of Ministry, Agriculture and Rural Affairs, Qingdao, Shandong, China, [5]Shandong Center for Animal Disease Prevention and Control, Jinan, Shandong, China

Introduction: Tuberculosis, caused by *Mycobacterium tuberculosis* complex (MTBC), remains a global health concern in both human and animals. However, the absence of rapid, accurate, and highly sensitive detection methods to differentiate the major pathogens of MTBC, including *M. tuberculosis*, *M. bovis*, and BCG, poses a potential challenge.

Methods: In this study, we have established a triplex droplet digital polymerase chain reaction (ddPCR) method employing three types of probe fluorophores, with targets *M. tuberculosis* (targeting CFP-10-ESAT-6 gene of RD1 and Rv0222 genes of RD4), *M. bovis* (targeting CFP-10-ESATs-6 gene of RD1), and BCG (targeting Rv3871 and Rv3879c genes of ΔRD1), respectively.

Results: Based on optimization of annealing temperature, sensitivity and repeatability, this method demonstrates a lower limit of detection (LOD) as 3.08 copies/reaction for *M. tuberculosis*, 4.47 copies/reaction for *M. bovis* and 3.59 copies/reaction for BCG, without cross-reaction to *Mannheimia haemolytica*, *Mycoplasma bovis*, *Haemophilus parasuis*, *Escherichia coli*, *Pasteurella multocida*, *Ochrobactrum anthropi*, *Salmonella choleraesuis*, *Brucella melitensis*, and *Staphylococcus aureus*, and showed repeatability with coefficients of variation (CV) lower than 10%. The method exhibits strong milk sample tolerance, the LOD of detecting in spike milk was 5×10^3 CFU/mL, which sensitivity is ten times higher than the triplex qPCR. 60 clinical DNA samples, including 20 milk, 20 tissue and 20 swab samples, were kept in China Animal Health and Epidemiology Center were tested by the triplex ddPCR and triplex qPCR. The triplex ddPCR presented a higher sensitivity (11.67%, 7/60) than that of the triplex qPCR method (8.33%, 5/60). The positive rates of *M. tuberculosis*, *M. bovis*, and BCG were 1.67, 10, and 0% by triplex ddPCR, and 1.67, 6.67, and 0% by triplex qPCR, with coincidence rates of 100, 96.7, and 100%, respectively.

Discussion: Our data demonstrate that the established triplex ddPCR method is a sensitive, specific and rapid method for differentiation and identification of *M. tuberculosis*, *M. bovis*, and BCG.

KEYWORDS

molecular diagnosis, multiplex droplet digital PCR, tuberculosis, *M. tuberculosis*, *M. bovis*, BCG

Introduction

Tuberculosis (TB) is a zoonotic disease that leads to the formation of caseous necrotic nodules in multiple organs of both humans and animals (Vielmo et al., 2020). According to the WHO TB report 2022, there were 10.6 million new cases of tuberculosis and 1.6 million tuberculosis-related deaths in 2021 (World Health Organization, 2022). TB is primarily caused by the *Mycobacterium tuberculosis* complex (MTBC), which consists of several members including the *Mycobacterium tuberculosis* (*M. tuberculosis*), *Mycobacterium bovis* (*M. bovis*) and Bacillus Calmette-Guérin (BCG) (Lekko et al., 2020). Despite the genetic similarity, ranging from 99.97 to 99.99%, these members are different microorganisms exhibit different host preferences and pathogenicity resulting in a limited availability of methods for making a differential diagnosis (Pinsky and Banaei, 2008; Kanabalan et al., 2021). MTBC can infect humans and a variety of animals, posing a threat to the concept of "one health" (Marais et al., 2019). For MTBC not only effects domestic animals such as cattle (Gutierrez Reyes et al., 2012) and goats (Quintas et al., 2010), companion animals such as cats (Cerna et al., 2019) and dogs (Rocha et al., 2017), but also affects wildlife including elephants (Maslow and Mikota, 2015), badgers (Smith and Budgey, 2021), deer (Amato et al., 2016), etc. Notably, *M. tuberculosis* is the primary pathogen responsible for human TB, resulting in millions of deaths annually (Rahlwes et al., 2023). While human TB is primarily caused by *M. tuberculosis* (Ehrt et al., 2018), a small percentage is attributed to *M. bovis* due to their high genetic similarity, with approximately 0.5–7% of cases resulting from human contact with infected cattle or related products (Vayr et al., 2018). Furthermore, BCG remains the sole TB vaccine available since the 20th century (Tran et al., 2014). Already, 4 billion people have been vaccinated against TB with the BCG vaccine, resulting in a 60–80% reduction in the incidence of active TB (Kuan et al., 2020). Although BCG greatly reduces the virulence of *M. bovis* as a live vaccine, it occasionally causes local or disseminated disease in immunocompromised individuals (World Health Organization, 2020). Extensive research has been conducted on BCG immunization in domestic and wild animals (such as badgers) over the past 10–20 years. While it may not complete prevent the occurrence of TB, the protection it provides could significantly reduce transmission from infected animals to other animals (Buddle et al., 2018).

In recent years, *M. bovis* has shown a tendency of extensive and multi-drug resistance. The treatment protocols of tuberculosis caused by *M. bovis* and *M. tuberculosis* should be differentiated (El-Sayed et al., 2016). Compared with *M. tuberculosis* and *M. bovis,* there are 2,437 SNPs differences (Garnier et al., 2003). The emergence of point mutations in *M. bovis* could result in the development of drug resistance, with drug-resistant mutants potentially proliferating due to irregular medication in cattle feeding, ultimately leading to multiple drug resistance. This scenario poses significant challenges to the effective treatment of TB resulting from *M. bovis* infection in humans, particularly considering the increased difficulty in treating *M. bovis* strains compared to *M. tuberculosis* due to their multiple drug resistance. As a result, early identification of the pathogen during infection becomes paramount (Kabir et al., 2020; Vazquez-Chacon et al., 2021; Dos Anjos et al., 2022). Moreover, by accurately distinguishing between infections caused by *M. tuberculosis*, *M. bovis*, and the BCG strains, the clinical epidemiology of bovine tuberculosis can be improved (Pfeiffer, 2013). All in all, rapid and accurate identification of these bacteria from suspected samples is crucial for early pathogen identification, contact tracing, detecting latent infection, distinguishing nature infection with vaccine immunity, and differential diagnosis. Despite their differences of genome less than 0.05%, these strains can be distinguished based on their different characteristics (Bigi et al., 2016). Comparative genomic analysis of *M. tuberculosis*, *M. bovis*, and BCG strains has revealed the presence or absence of certain regions of difference (RDs) in their genomes (Brosch et al., 2007; Bespiatykh et al., 2021). Notably, RD1 is absent in all BCG strains, resulting in a deletion of approximately 9.5kb, forming ΔRD1. Additionally, the RD4 fragment was absent in all *M. bovis* strains and BCG strains. The presence of these RDs distinguishes *M. tuberculosis* (RD1 and RD4), from *M. bovis* (RD1), and BCG strains (ΔRD1).

Droplet Digital Polymerase Chain Reaction (ddPCR), a third-generation PCR technique, has emerged as an advancement of the traditional PCR method, enabling the absolute quantification of nucleic acids through the isolation and amplification of individual DNA molecules and calculated by Poisson distribution (Li et al., 2018). In comparison to PCR and quantitative polymerase chain reaction (qPCR), ddPCR demonstrates unique sensitivity for samples with low copy numbers and overcomes the limitations of standard curves, leading to higher accuracy (Huggett and Whale, 2013). Additionally, multiplex ddPCR allows for the simultaneous detection of multiple targets using multiple fluorescent channels, while maintaining high sensitivity and specificity (Ganova et al., 2021). Previous studies have showcased the superior detection capabilities of multiplex ddPCR in complex matrices such as food (McMahon et al., 2017), fecal matter (Chen et al., 2023), aquaculture water (Lewin et al., 2020), and mutation detection with extremely low DNA concentrations (de Kock et al., 2021). Therefore, multiplex ddPCR has been identified as a crucial direction for future diagnostic methods. While the utilization of ddPCR in diagnosing *M. tuberculosis* in infected humans (Lyu et al., 2020) and macaques (Song et al., 2018) have been demonstrated,

and PCR has been employed in the differential diagnosis of MTBC pathogens (Krysztopa-Grzybowska et al., 2014), few studies on dPCR have specifically addressed the differential diagnosis of pathogens within MTBC. *M. tuberculosis, M. bovis*, and other numbers of MTBC such as *M. canetti* share a common progenitor. Through evolutionary processes, their genomes have occurred mutations that facilitate for inter-species transmission, leading to the formation of regions of difference known as RDs. Compared to *M. tuberculosis*, *M. africanum* exhibits the absence of region RD9 and the presence of region TbD1. *M. microti* demonstrates deletions in RD7, RD9 and RD10, along with specific absences in called RD1^{mic}, RD5^{mic}, MiD1, MiD2 and MiD3, as compared to *M. tuberculosis*. *M. caprae* is characterized by the absence of RD7-RD10, RD12 and RD13, with 1,577 gene variants distinguishing it from *M. tuberculosis*. *M. bovis* exhibits the absence of RD4-RD10 compared to *M. tuberculosis,* and BCG further lacks RD1-RD3 based on *M. bovis*. Moreover, *M. bovis* and BCG possess TbD1, which is not present in *M. tuberculosis*. *M. pinnipedii* lacks RD7-RD10 and is missing PiD1 and PiD2 compared to *M. tuberculosis*. Lastly, *M canettii* has all RD regions except phiRv1, phiRv2, and a segment of RD12 (Gonzalo-Asensio et al., 2014; Malone and Gordon, 2017; Kanipe and Palmer, 2020; Romano et al., 2022). Consequently, various methods can be established to distinguish members of MTBC based on these distinctive RDs.

In this study, we have developed a triplex ddPCR-based method for highly sensitive and simultaneous differential detection of *M. tuberculosis*, *M. bovis*, and BCG. The three target genes or fragments are concurrently detected using three fluorescent probes: 6-Carboxyfluorescein (FAM), 5-VIC phosphoramidite (VIC), and Cy5 phosphoramidite (CY5), within a five-color ddPCR system (Sniper DQ24pro^{TM}). This method was comprehensively evaluated alongside qPCR methods. Its ability to identify three pathogens DNA in milk samples was tested, demonstrating its suitability for rapid and sensitive detection of bio-threatening pathogens in suspicious milk samples. Although the high level of genetic similarity within the MTBC complex poses a challenge in distinguishing between different species, the advancement of ddPCR methods that target specific genetic regions, the accurate diagnosis of *M. tuberculosis*, *M. bovis*, and BCG has become achievable, resulting in an anticipated improvement in the differential diagnosis of TB in the future.

Materials and methods

Genomic DNA samples and inactivated bacteria samples

All DNA samples, including *M. tuberculosis* C2, *M. bovis* XJ/18/97 (Xu et al., 2021) and BCG Tokyo 172, *Mannheimia haemolytica*, *Mycoplasma bovis*, *Haemophilus parasuis*, *Escherichia coli*, *Pasteurella multocida*, *Ochrobactrum anthropi*, *Salmonella choleraesuis*, *Brucella melitensis* and *Staphylococcus aureus* used in this study were obtained among previous studies and kept in the National Animal Tuberculosis Reference Laboratory of China Animal Health and Epidemiology Center (Qingdao, China). The DNA and plasmids used in this study are listed in **Supplementary Table 1**. The DNA extraction method is detailed in the **Supplementary Material**.

Inactivated bacteria (*M. tuberculosis* C2, *M. bovis* XJ/18/97 and BCG Tokyo 172) in spiked milk and water were also kept in the National Animal Tuberculosis Reference Laboratory of China Animal Health and Epidemiology Center (Qingdao, China). The concentration ranged from 5×10^1 to 5×10^6 CFU/mL. DNA from spiked milk and water samples were extracted using a Milk Bacterial DNA Isolation kit (Norgen Biotek, Canada).

Primers and probes

According to previous studies, there are 16 different regions of MTBC (RD1-16) (Qu et al., 2020), RD1 is present in *M. tuberculosis* and *M. bovis*, while RD4 solely exists in *M. tuberculosis*. Moreover, the presence of ΔRD1 is exclusive to BCG strains. Thus, triplex ddPCR relies on the targeting of specific sequences, namely CFP-10 and ESAT-6 of RD1, Rv0222 of RD4, as well as the upstream Rv3871 and downstream Rv3879c of ΔRD1. The design of all primers and Taqman® probes was carried out using the PrimerQuest^{TM} Tool (Integrated DNA Technologies, US), while their synthesis was performed by Shanghai Sangon Biotech (China). The RD1 probe was labeled with FAM, the RD4 probe with VIC, and the ΔRD1 probe with CY5. All primers and Taqman@ probes used in this study is shown in **Supplementary Table 2**.

Preparation of recombinant standard plasmids

Recombinant standard plasmids were engineered to contain specific regions: 623bp of RD1, 789bp of RD4, and 1000bp (500bp upstream Rv3871 and 500bp downstream Rv3879c) of ΔRD1. These plasmids were individually constructed within the pUC57 vector and designated as p-RD1, p-RD4, and p-ΔRD1. All recombinant standard plasmids were synthesized by Shanghai Sangon Biotech (China). The concentrations of these plasmids were determined to be 4.8×10^9 copies/μL and were stored at −20°C until required for use. Plasmids were isolated from *E. coli* DH5α culture medium using an E.Z.N.A. HP Plasmid DNA Mini kit (Omega Bio-Tek, US).

Real-time quantitative PCR

The qPCR mixture consisted of 10 μL of Takara Premix Ex Taq^{TM} Probe qPCR Mix, along with 400 nM primers, 200 nM probes, 1 μL DNA sample, and nuclease-free water to reach a final volume of 20 μL. The thermal cycling program was set at 95°C for 10 min, followed by 40 cycles of denaturation at 94°C for 15 s and annealing at 60°C for 30 s. All qPCR reactions were conducted using the Applied Biosystems QuantStudio 5 system (Thermo Fisher United States).

Triplex droplet digital PCR

The triplex ddPCR reaction mixtures were prepared by combining 11 μL of 2 × dPCR probe Master mix plus (Sniper, China), along with 455 nM specific primers for each target, 150 nM

RD1 probe (FAM-labeled), 500 nM RD4 probe (VIC-labeled), 250 nM ΔRD1 probe (CY5-labeled), 1 μL DNA sample, and nuclease-free water to a final volume of 22 μL. All ddPCR assays were performed using the Sniper DQ24pro^{TM} dPCR systems, which includes a droplet generator and an automated reader. The reaction mixture was transferred to the internal stent of the integrated machine, followed by the installation of the droplet reaction plate, droplet reaction plate cover, and droplet generation kit onto the corresponding stent. The droplet generation oil was connected to the integrated machine, generating up to 20,000 nanoliter-sized droplets. The thermal cycle program was performed for 5 min at 60°C with a ramp rate of 2°C/s at each step; followed by 40 cycles of 95°C for 20 s, 60°C for 30 s, and held at 12°C. Data analysis was performed using the SightPro (x64) software.

Analysis of sensitivity, specificity and repeatability of the triplex ddPCR

The sensitivity of the assay was assessed using bacteria DNA and standard plasmids. Bacteria DNA were diluted in nuclease-free water, ranging from 3×10^4 to 3×10^0 copies/μL, while standard plasmids were diluted in nuclease-free water, ranging from 4.8×10^5 to 4.8×10^0 copies/μL. The bacteria DNA samples were tested in triplicate using the triplex ddPCR assay, while the standard plasmid samples were tested using the single-target ddPCR assay. To determine the limit of blank (LOB) for each channel, 8 nuclease-free water samples were tested as blank samples based on a previous study. Samples with copy numbers above the LOB were considered positive, which was calculated as LOB = $\text{mean}_{\text{blank}}$ + 1.645 (SD_{blank}). The lowest DNA concentration that could be detected was defined as the limit of detection (LOD). Quantitative curves were constructed for each target, with $\log_{10}$ (theoretical copies/reaction) as the *x*-axis, and $\log_{10}$ (copies/reaction measured) or Ct value as the *y*-axis. The linear fitting coefficient (R^2) was calculated using GraphPad Prism 10.0.

The specificity of the assay was assessed using a total of 9 other pathogenic bacteria, including *Mannheimia haemolytica*, *Mycoplasma bovis*, *Haemophilus parasuis*, *Escherichia coli*, *Pasteurella multocida*, *Ochrobactrum anthropi*, *Salmonella choleraesuis*, *Brucella melitensis*, and *Staphylococcus aureus*. Each DNA was tested three times independently.

The bacterial DNA samples with different concentrations of 3×10^4, 3×10^3, 3×10^2 copies/μL were tested 8 times to determine the coefficient of variation (CV) for intra-assay repeatability.

Detection of clinical samples

All clinical DNA samples, including 20 milk, 20 tissue and 20 from swab samples were extracted in previous studies and kept in the National Animal Tuberculosis Reference Laboratory of China Animal Health and Epidemiology Center (Qingdao, China), and tested by the established triplex ddPCR and the triplex qPCR methods. In each reaction, nuclease-free water was used as a negative control, while *M. tuberculosis*, *M. bovis*, and BCG DNA served as positive controls. The DNA extraction method is detailed in the **Supplementary Material**.

Results

Optimization of reaction conditions for establishing the triplex ddPCR

The p-RD1, p-RD4, and p-ΔRD1 standard plasmids were utilized to optimize the primers and probe sets, annealing temperature, probe concentrations of the triplex ddPCR. To accomplish this, the standard plasmids were 10-fold serially diluted, ranging from 4.8×10^7 to 4.8×10^0 copies/μL for each plasmid, and served as the template. For each target, three sets of primers and probes were designed (**Supplementary Table 2**), and the best set was determined using both qPCR and ddPCR methods. The qPCR results revealed that primers and probes from RD1 set3, RD4 set3 and ΔRD1 set2 exhibited superior amplification curves and the highest fluorescence amplitude (**Supplementary Figure 1**). For ddPCR, each plasmid with a concentration of 4.8×10^2 copies/μL, the result showed that the most noticeable difference in fluorescence amplitude between negative and positive droplets was observed within the same sets of primers and probes, and the number of positive droplets was the highest (**Figure 1**). Consequently, RD1 set3, RD4 set3, and ΔRD1 set2 were selected as the primer and probe combinations for further experiments (**Table 1**).

The primer and probe concentrations were optimized using standard plasmids, each with a concentration of 4.8×10^3 copies/μL. The arrangement and combination of different concentrations of primers and probes were analyzed using SightPro software (Sniper Technologies, China). The concentration combinations that displayed the most pronounced fluorescence amplitude interval between negative (gray) and positive (color) with distinct boundaries were determined as the optimal primer and probe concentrations (**Figure 2**). The optimal probe concentrations, detailed in **Table 2**, were determined to be 150 nM for RD1, 500 nM for RD4, and 250 nM for ΔRD1.

To determine the optimal ddPCR annealing temperature, each plasmid with a concentration of 4.8×10^2 copies/μL was utilized at annealing temperatures from 55 to 62°C. The result showed that the optimal annealing temperature was 60°C, which could generate the highest fluorescence amplitude (**Figure 3**).

After optimizing the reaction conditions, the triplex ddPCR assay was successfully established (**Table 2**). The total volume of the 22 μL reaction mixtures consisted of 11 μL of Sniper 2 × dPCR probe Master mix plus (Sniper Biotechnology, China), 1 μL of each primer RD1 F/R (10 μM), 0.33 μL of probe RD1-P (10 μM), 1 μL of each primer RD4 F/R (10 μM), 1.1 μL of probe RD4-P (10 μM), 1 μL of each primer ΔRD1 F/R (10 μM), 0.55 μL of probe ΔRD1-P (10 μM), 1 μL of DNA template, and 2.02 μL of nuclease-free water. The ddPCR amplifications were conducted as follows: initial denaturation at 60°C for 5 min, denaturation at 95°C for 5 min, followed by 40 cycles of 95°C for 20 s and 60°C for 30 s. Subsequent to amplification, the absolute copies of each sample were automatically reported by the Sniper System.

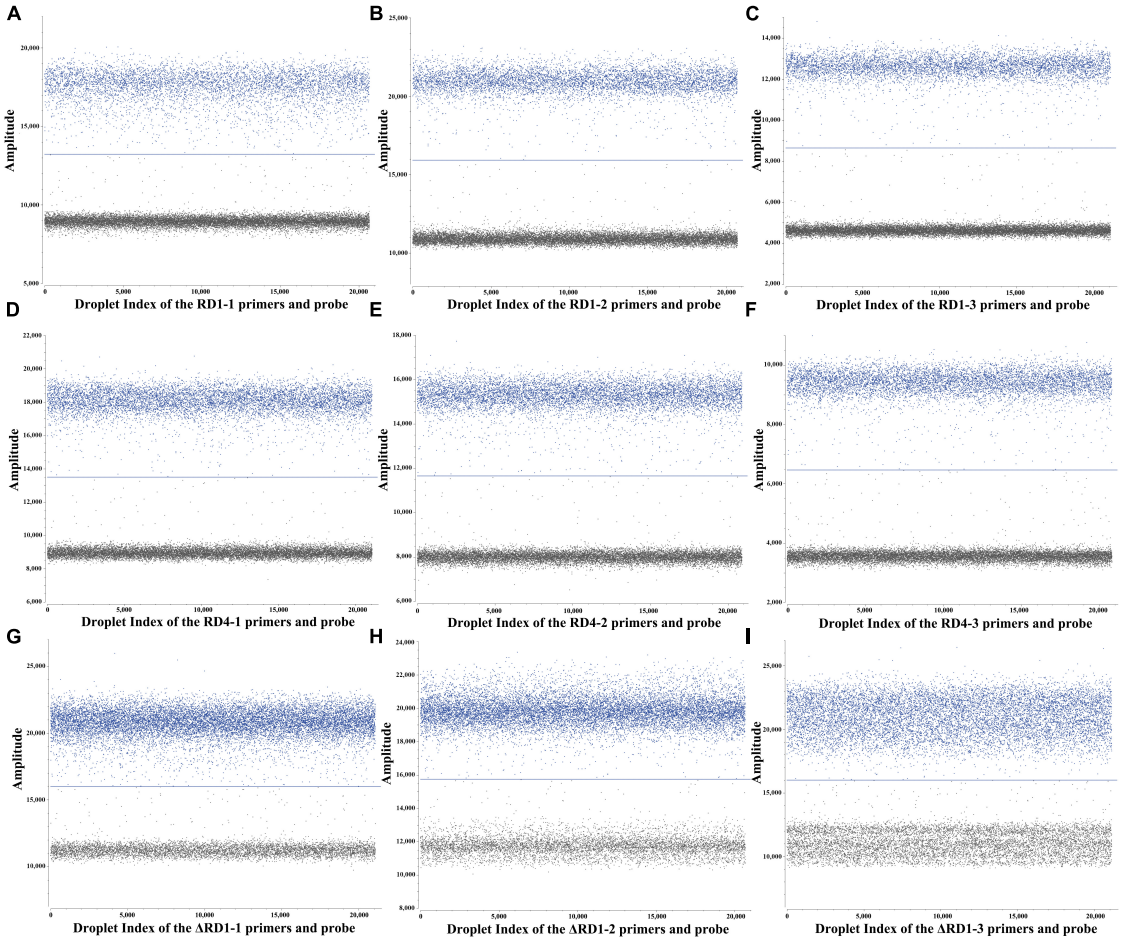

FIGURE 1
ddPCR assay for primers and probes screening. **(A–C)** 3 sets primers and probes screening for RD1. **(D–F)** 3 sets primers and probes screening for RD4. **(G–I)** 3 sets primers and probes screening for ΔRD1.

TABLE 1 Primers and probes sequences were chosen for three targets.

Target gene	RD region	Fragment length	Design sequence 5′–3′
CFP-10 to ESAT-6	RD1	623	F:CCTCGCAAATGGGCTTCT
			R:GACGTGACATTTCCCTGGATT
			P:FAM-AGTGGAATTTCGCGGGTATCGAGG-DHQ1
Rv0222	RD4	789	F:TATGCGATAGCCATGGAGTTG
			R:CCATTGGCGGTGATCTTCT
			P:VIC-TCGATGCTGCGATCGCGTTG-DHQ1
Rv3871 and Rv3879c	ΔRD1	996	F:GGATTTGACGTCGTGCTTCT
			R:CGATCTGGCGGTTTGGG
			P:CY5-ATCCAGCATCTGTCTGGCATAGCT-DHQ2

Evaluation of the triplex ddPCR method with DNA samples

LOBs were established by testing eight blank samples and calculating the average and standard deviation (SD) of their copy numbers, with a confidence interval set at 95%. The determined LOBs for the FAM, VIC, and CY5 channels in the blank samples were 1.07, 0.74, and 1.31 copies/reaction, respectively. Subsequently, copies below the LOBs in the experiments were considered negative. The sensitivity of the triplex ddPCR assay for each target was assessed by testing a range of diluted *M. tuberculosis*, *M. bovis*, and BCG DNA solutions (from 3×10^4 to 3×10^0 copies/μL). When the test yields positive results for both RD1 and RD4, it indicates the sample is *M. tuberculosis*. If only RD1 is positive, the sample is *M. bovis*, and only when ΔRD1 is positive, it signifies BCG. The results indicated that the

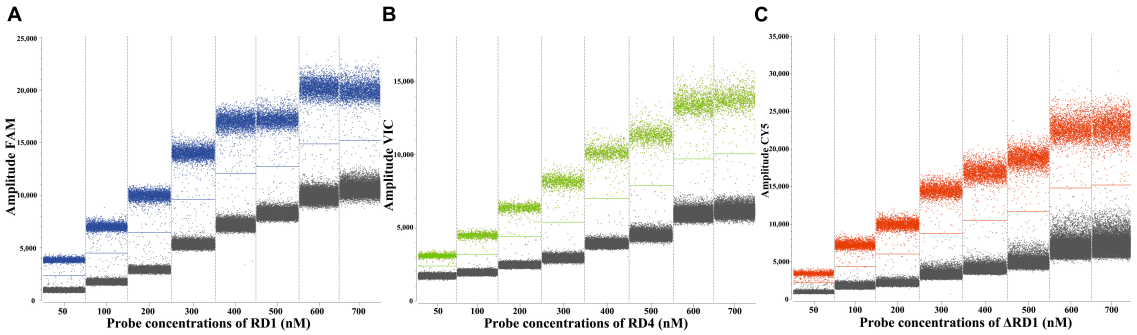

FIGURE 2
Determination of the optimal probe concentrations of the ddPCR of RD1 **(A)**, RD4 **(B)**, ΔRD1 **(C)**.

TABLE 2 The reaction mix of the triplex ddPCR and the triplex qPCR.

	Triplex ddPCR reaction		Triplex qPCR reaction	
	Volume (μL)	Final concentration (nM)	Volume (μL)	Final concentration (nM)
2 × dPCR probe Master mix	11	1×	/	/
2 × Premix Ex Tag (Probe qPCR)	/	/	10	1×
pRD1-F(10 μM)	1	455	0.8	400
pRD1-R(10 μM)	1	455	0.8	400
pRD1-P(10 μM)	0.33	150	0.4	200
pRD4-F(10 μM)	1	455	0.8	400
pRD4-R(10 μM)	1	455	0.8	400
pRD4-P(10 μM)	1.1	500	0.4	200
pΔRD1-F(10 μM)	1	455	0.8	400
pΔRD1-R(10 μM)	1	455	0.8	400
pΔRD1-P(10 μM)	0.55	250	0.4	200
Template	1	/	1	/
RNase Free H_2O	Up to 22	/	Up to 20	/

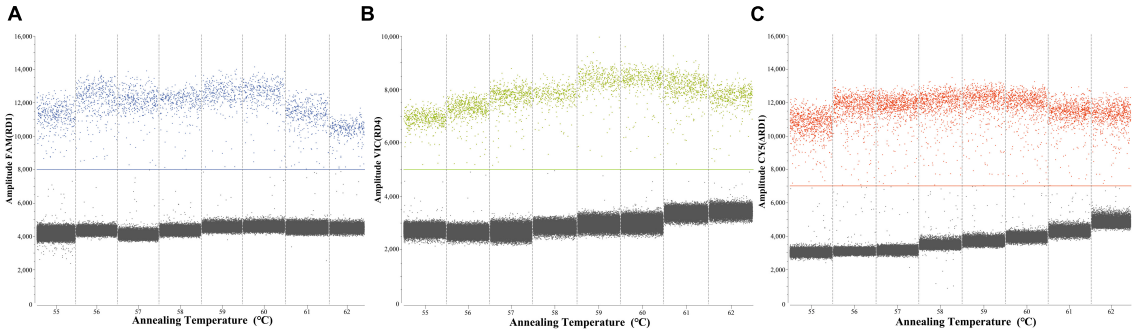

FIGURE 3
Screening the optimum annealing temperature from 55 to 62°C of RD1 **(A)**, RD4 **(B)**, ΔRD1 **(C)**.

LODs for *M. tuberculosis* were 3.08 copies/reaction, for *M. bovis* were 4.47 copies/reaction, and for BCG were 3.59 copies/reaction (Figure 4). These results indicate that accurate detection can be achieved when the target gene content in the sample is above the LOD. Quantitative curves were generated with $\log_{10}$ (theoretical copies/reaction) plotted on the *x*-axis and $\log_{10}$ (copies/reaction measured) plotted on the *y*-axis. Each target exhibited a strong quantitative linearity ($R^2 > 0.99$) within the theoretical range of 3×10^0 to 3×10^4 copies/reaction (Figure 5).

Specificity tests were performed using 9 nucleic acids from other pathogens, including *Mannheimia haemolytica*, *Mycoplasma bovis*, *Haemophilus parasuis*, *Escherichia coli*, *Pasteurella multocida*, *Ochrobactrum anthropi*, *Salmonella choleraesuis*, *Brucella melitensis*, and *Staphylococcus aureus*. As depicted in

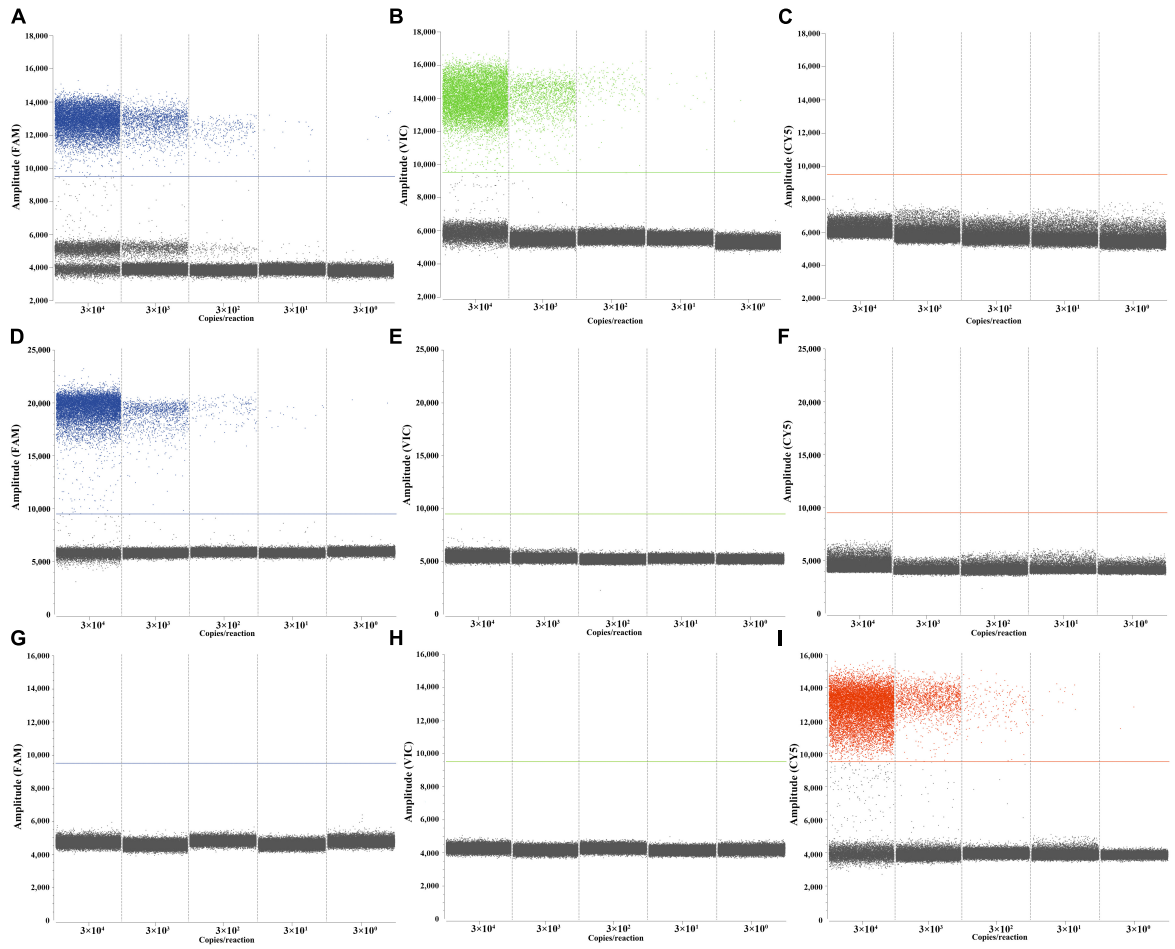

FIGURE 4
Performances of the triplex ddPCR assay by target DNA from 3×10^4 to 3×10^0 copies/μL. **(A–C)** Detection results of the target *M. tuberculosis*. **(D–F)** Detection results of the target *M. bovis*. **(G–I)** Detection results of the target BCG.

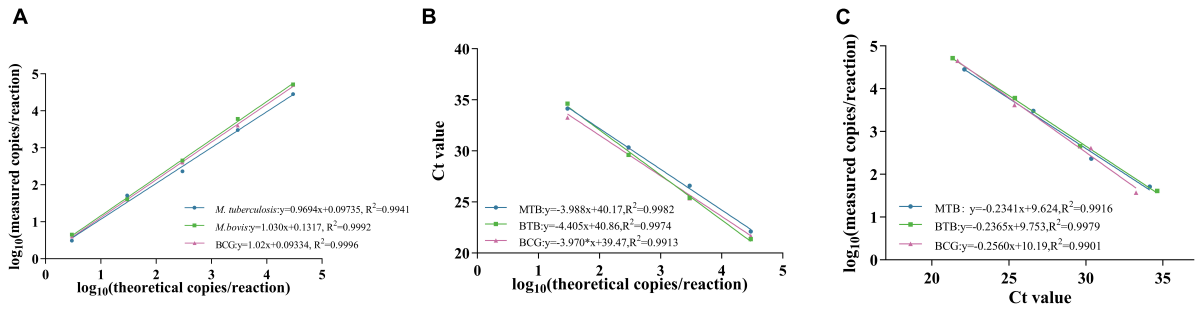

FIGURE 5
Standard curve of *M. tuberculosis*, *M.bovis* and BCG. **(A,B)** show the standard curves of triplex ddPCR and triplex qPCR, respectively, and **(C)** indicates the correlation between them.

Supplementary Figure 2, no cross-amplification was observed for these bacterial DNA (3×10^2 copies/μL), confirming the specificity of our triplex ddPCR method (Supplementary Figure 2).

Three concentrations of 3×10^3 to 3×10^1 copies/μL for each bacteria DNA were used as templates to evaluate the repeatability. The results showed that the CVs of intra-assay ranged from 1.93 to 4.74%, 0.92–9.15%, and 3.13–9.26%, respectively (Table 3).

Comparison analysis of the sensitivity and standard curves between the triplex ddPCR and triplex qPCR

Sensitivity tests were performed on *M. tuberculosis*, *M. bovis*, and BCG DNA templates from 3×10^4 to 3×10^0 copies/μL using triplex ddPCR and triplex qPCR. The results revealed that ddPCR

TABLE 3 Analysis of the repeatability of the triplex ddPCR.

DNA	Final concentration (copies/μL)	Repeatability assay		
		SD	AVG	CV%
M. tuberculosis	3×10^4	283.18	14646.28	1.93%
	3×10^3	74.68	1574.18	4.74%
	3×10^2	6.17	175.95	3.50%
M. bovis	3×10^4	178.50	19320.18	0.90%
	3×10^3	29.31	1338.84	2.19%
	3×10^2	10.76	117.62	9.15%
BCG	3×10^4	769.98	24532.97	3.14%
	3×10^3	98.09	2365.36	4.15%
	3×10^2	22.10	238.48	9.27%

could detect samples containing as few as 3×10^0 copies of the target DNA, whereas qPCR could only detect samples containing 3×10^1 copies of the target DNA (Table 4). The correlation coefficients between the triplex ddPCR and the triplex qPCR were 0.9916 for *M. tuberculosis*, 0.9979 for *M. bovis*, and 0.9901 for BCG (Figure 5), indicating a positive association between these two methods.

The performance of comparison analysis was also evaluated using known bacterial concentrations in spiked milk and water samples to mimic real clinical samples. The spiked milk samples and water at concentrations of 5×10^3 and 5×10^2 CFU/mL could be identified by triplex ddPCR, respectively. In contrast, triplex qPCR could detect concentration of 5×10^4 and 5×10^3 CFU/mL for spiked milk and water samples, respectively (Tables 5, 6). These results all suggested that the sensitivity of triplex ddPCR was ten times higher than the triplex qPCR.

Clinical performance of triplex ddPCR

The 60 clinical DNA samples were tested using the triplex ddPCR and the triplex qPCR. The positive rates of *M. tuberculosis*, *M. bovis*, and BCG were 1.67%, 10% and 0%, respectively. In comparison, 1.67%, 6.67% and 0% from the triplex qPCR results, respectively. The results suggested that the sensitivity of the triplex ddPCR were higher than the triplex qPCR, with the coincidence rates of *M. tuberculosis*, *M. bovis*, and BCG were 100%, 96.7% and 100%, respectively (Table 7).

Discussion

Prior to the COVID-19 outbreak, tuberculosis (TB) had the highest mortality rate among single infectious diseases (World Health Organization, 2021). Timely identification of infecting strains and early-stage diagnosis of TB could control the source of infection and enable the implementation of targeted prevention and treatment measures. However, due to the high genetic similarity within MTBC, differentiating its members presents a challenge. After years of research, the discovery of RDs has helped us understand the genetic differences within MTBC genomes, allowing us to distinguish among *M. tuberculosis*, *M. bovis* and BCG strains. In this study, we developed and evaluated a triplex ddPCR method for the identification of *M. tuberculosis*, *M. bovis* and BCG using RD1, RD4, and ΔRD1 with a three-color ddPCR system. For the first time, the triplex ddPCR method for differentially detecting *M. tuberculosis*, *M. bovis* and BCG was successfully developed, and has the potential to be used in the differential identification of MTBC in early or latent TB infection due to its high sensitivity and accuracy.

Conventional differentiation of members within MTBC relies on a combination of tests that assess the growth characteristics

TABLE 4 Comparison analysis of the sensitivity between the triplex ddPCR and triplex qPCR assay.

Theoretical copies/μl	Copies/reaction in triplex ddPCR			CT in triplex qPCR		
	M. tuberculosis	*M. bovis*	BCG	*M. tuberculosis*	*M. bovis*	BCG
3×10^4	2.8×10^4	5.2×10^4	4.5×10^4	22.10	21.35	21.67
3×10^3	3.0×10^3	6.0×10^3	4.1×10^3	26.59	25.39	25.36
3×10^2	2.3×10^2	4.5×10^2	4.1×10^2	30.34	29.62	30.32
3×10^1	5.1×10^1	4.1×10^1	3.7×10^1	34.15	34.62	33.25
3×10^0	3.1×10^0	4.5×10^0	3.6×10^0	NA	NA	NA

TABLE 5 Estimated the sensitivity of three bacteria in spiked nuclease-free water samples by triplex ddPCR.

CFU/mL	Copies/reaction in triplex ddPCR			CT in triplex qPCR		
	M. tuberculosis	*M. bovis*	BCG	*M. tuberculosis*	*M. bovis*	BCG
5×10^6	5.3×10^4	1.0×10^5	2.5×10^4	19.91	21.15	21.00
5×10^5	6.3×10^3	9.7×10^3	2.5×10^3	23.94	25.13	25.33
5×10^4	5.6×10^2	6.9×10^2	1.7×10^2	28.17	29.56	29.04
5×10^3	4.1×10^1	6.7×10^1	1.0×10^1	32.34	34.43	33.25
5×10^2	1.8×10^0	6.7×10^0	3.1×10^0	NA	NA	NA
5×10^1	NA	NA	NA	NA	NA	NA

TABLE 6 Estimated the sensitivity of three bacteria in spiked milk samples by triplex ddPCR.

CFU/mL	Copies/reaction in triplex ddPCR			CT in triplex qPCR		
	M. tuberculosis	*M. bovis*	BCG	*M. tuberculosis*	*M. bovis*	BCG
5×10^6	6.1×10^3	2.2×10^3	1.9×10^3	24.24	26.72	25.56
5×10^5	3.6×10^2	1.7×10^2	1.5×10^2	27.26	29.65	29.77
5×10^4	3.3×10^1	1.7×10^1	2.1×10^1	32.09	33.41	34.17
5×10^3	5.9×10^0	3.0×10^0	4.1×10^0	NA	NA	NA
5×10^2	NA	NA	NA	NA	NA	NA
5×10^1	NA	NA	NA	NA	NA	NA

and biochemical properties of the strains. However, this approach is time-consuming, taking 2–3 weeks, and can sometimes yield indeterminate results (Bolanos et al., 2017). Additionally, molecular methods like PCR have been developed for differentiating members of MTBC. Although PCR allows for qualitative analysis, its sensitivity limits prevent accurate quantification and early diagnosis of TB (Owusu et al., 2023). In the initial or latent stages of infection, the qPCR method is constrained by standard curve and Ct value considerations, as well as its susceptibility to PCR reaction inhibitors, thus limiting its ability to detect very low sample concentrations. Conversely, ddPCR makes use of the Poisson distribution to determine positive sample copy numbers, allowing for absolute quantification of nucleic acids without reliance on a standard curve, effectively circumventing this issue (Quan et al., 2018). Our comparative analysis focuses on assessing the detection capabilities of triplex qPCR and triplex ddPCR. Findings from DNA and spiked milk samples reveal that ddPCR demonstrates heightened sensitivity in comparison to qPCR, capable of detecting nucleic acids at a minimum concentration ten times lower than qPCR. Furthermore, this method holds promise for simultaneous differential diagnosis of mixed infection samples. The extensive genetic similarity and evolutionary connections within MTBC present challenges in identifying unique regions exclusive to *M. bovis* but absent in BCG strains or *M. tuberculosis*. Consequently, our method currently lacks the capability to differentiate between *M. tuberculosis* and *M. tuberculosis-M. bovis* co-infection in complex samples.

Through in-depth exploration of the genome sequences of *M. tuberculosis*, *M. bovis*, and BCG strains, this method can enhance future detection capabilities by incorporating additional genetic fragments, such as *mmpS6* (Ma et al., 2022). This particular gene presents in *M. bovis* and BCG strains but absent in *M. tuberculosis*, thereby enabling a more precise differentiation between infections of *M. tuberculosis* or *M. bovis* and *M. tuberculosis* co-infections. However, it should be noted that this approach also falls short in distinguishing between *M. tuberculosis-M. bovis* co-infections and *M. tuberculosis-M. bovis*-BCG mixed infections. Further analysis and research are warranted to achieve comprehensive differentiation of mixed infections within complex samples.

Compared with traditional diagnostic methods, this established method for identifying *M. tuberculosis*, *M. bovis*, and BCG strains significantly enhances the accuracy and efficiency of diagnosis. It enables the early-stage diagnosis of individual infections, facilitating targeted treatment and vaccination. Furthermore, this study holds the potential for pathogen traceability, epidemic surveillance, and provides a more robust scientific foundation for disease prevention and control.

TABLE 7 Clinical results for triplex ddPCR.

Detection method	Detection results (positive samples/total samples)		
	M. tuberculosis	*M. bovis*	BCG
ddPCR	1/60	6/60	0/60
qPCR	1/60	4/60	0/60
Coincidence rates	100%	96.7%	100%

Conclusion

In this study, we have successfully developed a triplex ddPCR method for the identification of *M. tuberculosis*, *M. bovis*, and BCG strains, utilizing a three-color ddPCR system. Our established method demonstrates remarkable attributes, including low detection limits (ranging from 3.08 to 4.47 copies per reaction) and excellent specificity. Moreover, it exhibits strong resistance to the presence of milk samples, with lower limits of detection (LODs) reaching the concentrations of 5×10^3 CFU/mL in milk. Notably, this assay allows for the simultaneous detection of three targets in a single sample, introducing a novel and rapid method for sensitive detection, enabling the differentiation of the causative agent in tuberculosis cases.

Data availability statement

The original contributions presented in this study are included in this article/**Supplementary material**, further inquiries can be directed to the corresponding authors.

Author contributions

YQ: Writing – original draft. ML: Writing – review and editing. XS: Writing – original draft. YL: Writing – review and editing. JZL: Writing – review and editing. LH: Writing – review and editing. ZJ: Writing – original draft. FQ: Writing – original draft. WN: Writing – original draft. XY: Writing – original draft. MS: Writing – original draft. WS: Writing – review and editing.

JQL: Writing – original draft. SS: Writing – review and editing. HZ: Writing – review and editing. XF: Writing – review and editing.

Funding

The author(s) declare that financial support was received for the research, authorship, and/or publication of this article. This work was supported by the National Key Research and Development Program of China (2022YFD1800702).

Conflict of interest

The authors declare that the research was conducted in the absence of any commercial or financial relationships that could be construed as a potential conflict of interest.

Publisher's note

Supplementary material

The Supplementary Material for this article can be found online at: https://www.frontiersin.org/articles/10.3389/fmicb.2024.1397792/full#supplementary-material

References

Amato, B., Mignacca, S. A., Pacciarini, M. L., Vitale, M., Antoci, S., Cucinotta, S., et al. (2016). An outbreak of bovine tuberculosis in a fallow deer herd (Dama dama) in Sicily. *Res. Vet. Sci.* 106, 116–120. doi: 10.1016/j.rvsc.2016.03.019

Bespiatykh, D., Bespyatykh, J., Mokrousov, I., and Shitikov, E. (2021). A comprehensive map of mycobacterium tuberculosis complex regions of difference. *mSphere* 6:e0053521. doi: 10.1128/mSphere.00535-21

Bigi, M. M., Blanco, F. C., Araujo, F. R., Thacker, T. C., Zumarraga, M. J., Cataldi, A. A., et al. (2016). Polymorphisms of 20 regulatory proteins between *Mycobacterium tuberculosis* and *Mycobacterium bovis*. *Microbiol. Immunol.* 60, 552–560. doi: 10.1111/1348-0421.12402

Bolanos, C. A. D., Paula, C. L., Guerra, S. T., Franco, M. M. J., and Ribeiro, M. G. (2017). Diagnosis of mycobacteria in bovine milk: An overview. *Rev. Inst. Med. Trop. Sao Paulo* 59:e40. doi: 10.1590/S1678-9946201759040

Brosch, R., Gordon, S. V., Garnier, T., Eiglmeier, K., Frigui, W., Valenti, P., et al. (2007). Genome plasticity of BCG and impact on vaccine efficacy. *Proc. Natl. Acad. Sci. U.S.A.* 104, 5596–5601. doi: 10.1073/pnas.0700869104

Buddle, B. M., Vordermeier, H. M., Chambers, M. A., and de Klerk-Lorist, L. M. (2018). Efficacy and safety of BCG vaccine for control of tuberculosis in domestic livestock and wildlife. *Front. Vet. Sci.* 5:259. doi: 10.3389/fvets.2018.00259

Cerna, P., O'Halloran, C., Sjatkovska, J. O., and Gunn-Moore, D. A. (2019). Outbreak of tuberculosis caused by *Mycobacterium bovis* in a cattery of Abyssinian cats in Italy. *Transbound. Emerg. Dis.* 66, 250–258. doi: 10.1111/tbed.13010

Chen, J., Li, D., Xu, Y., Li, Z., Ma, S., Liu, X., et al. (2023). Establishment and application of multiplex droplet digital polymerase chain reaction assay for bovine enterovirus, bovine coronavirus, and bovine rotavirus. *Front. Vet. Sci.* 10:1157900. doi: 10.3389/fvets.2023.1157900

de Kock, R., van den Borne, B., Youssef-El Soud, M., Belderbos, H., Brunsveld, L., Scharnhorst, V., et al. (2021). Therapy monitoring of EGFR-positive non-small-cell lung cancer patients using ddPCR multiplex assays. *J. Mol. Diagn.* 23, 495–505. doi: 10.1016/j.jmoldx.2021.01.003

Dos Anjos, T. R., Castro, V. S., Machado Filho, E. S., Suffys, P. N., Gomes, H. M., Duarte, R. S., et al. (2022). Genomic analysis of *Mycobacterium tuberculosis* variant bovis strains isolated from bovine in the state of Mato Grosso, Brazil. *Front. Vet. Sci.* 9:1006090. doi: 10.3389/fvets.2022.1006090

Ehrt, S., Schnappinger, D., and Rhee, K. Y. (2018). Metabolic principles of persistence and pathogenicity in *Mycobacterium tuberculosis*. *Nat. Rev. Microbiol.* 16, 496–507. doi: 10.1038/s41579-018-0013-4

El-Sayed, A., El-Shannat, S., Kamel, M., Castaneda-Vazquez, M. A., and Castaneda-Vazquez, H. (2016). Molecular epidemiology of *Mycobacterium bovis* in humans and cattle. *Zoonoses Public Health* 63, 251–264. doi: 10.1111/zph.12242

Ganova, M., Zhang, H., Zhu, H., Korabecna, M., and Neuzil, P. (2021). Multiplexed digital polymerase chain reaction as a powerful diagnostic tool. *Biosens. Bioelectron.* 181:113155. doi: 10.1016/j.bios.2021.113155

Garnier, T., Eiglmeier, K., Camus, J. C., Medina, N., Mansoor, H., Pryor, M., et al. (2003). The complete genome sequence of *Mycobacterium bovis*. *Proc. Natl. Acad. Sci. U.S.A.* 100, 7877–7882. doi: 10.1073/pnas.1130426100

Gonzalo-Asensio, J., Malaga, W., Pawlik, A., Astarie-Dequeker, C., Passemar, C., Moreau, F., et al. (2014). Evolutionary history of tuberculosis shaped by conserved mutations in the PhoPR virulence regulator. *Proc. Natl. Acad. Sci. U.S.A.* 111, 11491–11496. doi: 10.1073/pnas.1406693111

Gutierrez Reyes, J. A., Garcia Casanova, L., Romero Torres, C., Sosa Gallegos, S. L., Canto Alarcon, G. J., Mercado Pezzat, M., et al. (2012). Population structure of *Mycobacterium bovis* isolates from cattle in Mexico. *Prev. Vet. Med.* 106, 1–8. doi: 10.1016/j.prevetmed.2012.05.008

Huggett, J. F., and Whale, A. (2013). Digital PCR as a novel technology and its potential implications for molecular diagnostics. *Clin. Chem.* 59, 1691–1693. doi: 10.1373/clinchem.2013.214742

Kabir, S., Tahir, Z., Mukhtar, N., Sohail, M., Saqalein, M., and Rehman, A. (2020). Fluoroquinolone resistance and mutational profile of gyrA in pulmonary MDR tuberculosis patients. *BMC Pulm. Med.* 20:138. doi: 10.1186/s12890-020-1172-4

Kanabalan, R. D., Lee, L. J., Lee, T. Y., Chong, P. P., Hassan, L., Ismail, R., et al. (2021). Human tuberculosis and *Mycobacterium tuberculosis* complex: A review on genetic diversity, pathogenesis and omics approaches in host biomarkers discovery. *Microbiol. Res.* 246:126674. doi: 10.1016/j.micres.2020.126674

Kanipe, C., and Palmer, M. V. (2020). *Mycobacterium bovis* and you: A comprehensive look at the bacteria, its similarities to *Mycobacterium tuberculosis*, and its relationship with human disease. *Tuberculosis* 125:102006. doi: 10.1016/j.tube.2020.102006

Krysztopa-Grzybowska, K., Brzezinska, S., Augustynowicz-Kopec, E., Augustynowicz, E., and Lutynska, A. (2014). PCR-based genomic deletion analysis of RD-regions in the identification of mycobacteria isolated from adverse events following BCG vaccination or TB suspected cases. *Pol. J. Microbiol.* 63, 359–362.

Kuan, R., Muskat, K., Peters, B., and Lindestam Arlehamn, C. S. (2020). Is mapping the BCG vaccine-induced immune responses the key to improving the efficacy against tuberculosis? *J. Intern. Med.* 288, 651–660. doi: 10.1111/joim.13191

Lekko, Y. M., Ooi, P. T., Omar, S., Mazlan, M., Ramanoon, S. Z., Jasni, S., et al. (2020). *Mycobacterium tuberculosis* complex in wildlife: Review of current applications of antemortem and postmortem diagnosis. *Vet. World* 13, 1822–1836. doi: 10.14202/vetworld.2020.1822-1836

Lewin, A. S., Haugen, T., Netzer, R., Tondervik, A., Dahle, S. W., and Hageskal, G. (2020). Multiplex droplet digital PCR assay for detection of *Flavobacterium psychrophilum* and *Yersinia ruckeri* in Norwegian aquaculture. *J. Microbiol. Methods* 177:106044. doi: 10.1016/j.mimet.2020.106044

Li, H., Bai, R., Zhao, Z., Tao, L., Ma, M., Ji, Z., et al. (2018). Application of droplet digital PCR to detect the pathogens of infectious diseases. *Biosci. Rep.* 38:1170. doi: 10.1042/BSR20181170

Lyu, L., Li, Z., Pan, L., Jia, H., Sun, Q., Liu, Q., et al. (2020). Evaluation of digital PCR assay in detection of *M.tuberculosis* IS6110 and IS1081 in tuberculosis patients plasma. *BMC Infect. Dis.* 20:657. doi: 10.1186/s12879-020-05375-y

Ma, R., Farrell, D., Gonzalez, G., Browne, J. A., Nakajima, C., Suzuki, Y., et al. (2022). Corrigendum: The TbD1 locus mediates a hypoxia-induced copper response

in *Mycobacterium bovis*. *Front. Microbiol.* 13:947450. doi: 10.3389/fmicb.2022.947450

Malone, K. M., and Gordon, S. V. (2017). *Mycobacterium tuberculosis* complex members adapted to wild and domestic animals. *Adv. Exp. Med. Biol.* 1019, 135–154. doi: 10.1007/978-3-319-64371-7_7

Marais, B. J., Buddle, B. M., de Klerk-Lorist, L. M., Nguipdop-Djomo, P., Quinn, F., and Greenblatt, C. (2019). BCG vaccination for bovine tuberculosis; Conclusions from the Jerusalem one health workshop. *Transbound. Emerg. Dis.* 66, 1037–1043. doi: 10.1111/tbed.13089

Maslow, J. N., and Mikota, S. K. (2015). Tuberculosis in elephants-a reemergent disease: Diagnostic dilemmas, the natural history of infection, and new immunological tools. *Vet. Pathol.* 52, 437–440. doi: 10.1177/0300985814568357

McMahon, T. C., Blais, B. W., Wong, A., and Carrillo, C. D. (2017). Multiplexed single intact cell droplet digital PCR (MuSIC ddPCR) method for specific detection of enterohemorrhagic *E. coli* (EHEC) in food enrichment cultures. *Front. Microbiol.* 8:332. doi: 10.3389/fmicb.2017.00332

Owusu, W., van Vliet, A. H. M., Riddell, N. E., Stewart, G., Akwani, W. C., Aryeetey, S., et al. (2023). A multiplex PCR assay for the differentiation of *Mycobacterium tuberculosis* complex reveals high rates of mixed-lineage tuberculosis infections among patients in Ghana. *Front. Cell. Infect. Microbiol.* 13:1125079. doi: 10.3389/fcimb.2023.1125079

Pfeiffer, D. U. (2013). Epidemiology caught in the causal web of bovine tuberculosis. *Transbound. Emerg. Dis.* 60, 104–110. doi: 10.1111/tbed.12105

Pinsky, B. A., and Banaei, N. (2008). Multiplex real-time PCR assay for rapid identification of *Mycobacterium tuberculosis* complex members to the species level. *J. Clin. Microbiol.* 46, 2241–2246. doi: 10.1128/JCM.00347-08

Qu, Z., Zhou, J., Zhou, Y., Xie, Y., Jiang, Y., Wu, J., et al. (2020). Mycobacterial EST12 activates a RACK1-NLRP3-gasdermin D pyroptosis-IL-1beta immune pathway. *Sci. Adv.* 6:aba4733. doi: 10.1126/sciadv.aba4733

Quan, P. L., Sauzade, M., and Brouzes, E. (2018). dPCR: A technology review. *Sensors.* 18:1271. doi: 10.3390/s18041271

Quintas, H., Reis, J., Pires, I., and Alegria, N. (2010). Tuberculosis in goats. *Vet. Rec.* 166, 437–438. doi: 10.1136/vr.c1678

Rahlwes, K. C., Dias, B. R. S., Campos, P. C., Alvarez-Arguedas, S., and Shiloh, M. U. (2023). Pathogenicity and virulence of *Mycobacterium tuberculosis*. *Virulence* 14:2150449. doi: 10.1080/21505594.2022.2150449

Rocha, V. C., Figueiredo, S. C., Rosales, C. A., Porto, C. D., Sequeira, J. L., Neto, J. S., et al. (2017). Infection by *Mycobacterium bovis* in a dog from Brazil. *Braz. J. Microbiol.* 48, 109–112. doi: 10.1016/j.bjm.2016.09.001

Romano, G. E., Silva-Pereira, T. T., de Melo, F. M., Sisco, M. C., Banari, A. C., Zimpel, C. K., et al. (2022). Unraveling the metabolism of *Mycobacterium caprae* using comparative genomics. *Tuberculosis* 136:102254. doi: 10.1016/j.tube.2022.102254

Smith, G. C., and Budgey, R. (2021). Simulating the next steps in badger control for bovine tuberculosis in England. *PLoS One* 16:e0248426. doi: 10.1371/journal.pone.0248426

Song, N., Tan, Y., Zhang, L., Luo, W., Guan, Q., Yan, M. Z., et al. (2018). Detection of circulating Mycobacterium tuberculosis-specific DNA by droplet digital PCR for vaccine evaluation in challenged monkeys and TB diagnosis. *Emerg. Microbes. Infect.* 7:78. doi: 10.1038/s41426-018-0076-3

Tran, V., Liu, J., and Behr, M. A. (2014). BCG vaccines. *Microbiol. Spectr.* 2:MGM2–MGM0028. doi: 10.1128/microbiolspec.MGM2-0028-2013

Vayr, F., Martin-Blondel, G., Savall, F., Soulat, J. M., Deffontaines, G., and Herin, F. (2018). Occupational exposure to human *Mycobacterium bovis* infection: A systematic review. *PLoS Negl. Trop. Dis.* 12:e0006208. doi: 10.1371/journal.pntd.0006208

Vazquez-Chacon, C. A., Rodriguez-Gaxiola, F. J., Lopez-Carrera, C. F., Cruz-Rivera, M., Martinez-Guarneros, A., Parra-Unda, R., et al. (2021). Identification of drug resistance mutations among *Mycobacterium bovis* lineages in the Americas. *PLoS Negl. Trop. Dis.* 15:e0009145. doi: 10.1371/journal.pntd.0009145

Vielmo, A., Lopes, B. C., Panziera, W., Bianchi, R. M., Mayer, F. Q., Vielmo, L. A., et al. (2020). Penile tuberculosis in a bull. *J. Comp. Pathol.* 180, 5–8. doi: 10.1016/j.jcpa.2020.08.001

World Health Organization. (2020). *Bacille Calmette-Guérin (BCG) Information sheet*. Available onile at: https://www.who.int/publications/m/item/bcg-information-sheet (accessed May 13, 2020).

World Health Organization. (2021). *Global tuberculosis report 2021*. Available onile at: https://www.who.int/publications/i/item/9789240037021 (accessed October 14, 2021).

World Health Organization. (2022). *Global tuberculosis report 2022*. Available onile at: https://www.who.int/publications/i/item/9789240061729 (accessed October 2022).

Xu, F., Tian, L., Li, Y., Zhang, X., Qi, Y., Jing, Z., et al. (2021). Highprevalence of extrapulmonary tuberculosis in dairy farms: Evidence forpossible gastrointestinal transmission. *PLoS One.* 16:e0249341. doi: 10.1371/journal.pone.0249341

frontiers | Frontiers in Microbiology

TYPE Original Research
PUBLISHED 03 July 2024
DOI 10.3389/fmicb.2024.1403619

OPEN ACCESS

EDITED BY
Robert Jansen,
Radboud University, Netherlands

REVIEWED BY
Emine Ikbal Atli,
Trakya University, Türkiye
Zheng Jin Tu,
Cleveland Clinic, United States
Iordanis Kesisoglou,
Merck & Co., Inc., United States
Rizaldy Taslim Pinzon,
Duta Wacana Christian University, Indonesia

*CORRESPONDENCE
Yi Zeng
960559051@qq.com

†These authors have contributed equally to this work

RECEIVED 20 March 2024
ACCEPTED 18 June 2024
PUBLISHED 03 July 2024

CITATION
Gao WW, Yang C, Wang TZ, Guo YC and Zeng Y (2024) Nanopore-based targeted next-generation sequencing of tissue samples for tuberculosis diagnosis.
Front. Microbiol. 15:1403619.
doi: 10.3389/fmicb.2024.1403619

Nanopore-based targeted next-generation sequencing of tissue samples for tuberculosis diagnosis

Weiwei Gao†, Chen Yang†, Tianzhen Wang, Yicheng Guo and Yi Zeng*

Department of Tuberculosis, The Second Hospital of Nanjing, Nanjing, China

Objective: Diagnosing tuberculosis (TB) can be particularly challenging in the absence of sputum for pulmonary tuberculosis cases and extrapulmonary TB (EPTB). This study evaluated the utility of nanopore-based targeted next-generation sequencing (tNGS) for diagnosing TB in tissue samples, and compared its efficacy with other established diagnostic methods.

Methods: A total of 110 tissue samples from clinical cases were examined. The sensitivity and specificity of tNGS were benchmarked against a range of existing diagnostic approaches including hematoxylin and eosin (HE) staining in conjunction with acid-fast bacilli (AFB) detection, HE staining combined with PCR, HE staining paired with immunohistochemistry (IHC) using anti-MPT64, and the Xpert *Mycobacterium tuberculosis* (MTB)/rifampicin (RIF) assay.

Results: The sensitivity and specificity of tNGS were 88.2 and 94.1%, respectively. The respective sensitivities for HE staining combined with AFB, HE staining combined with PCR, HE staining combined with IHC using anti-MPT64, and Xpert MTB/RIF were 30.1, 49.5, 47.3, and 59.1%. The specificities for these methods were 82.4, 88.2, 94.1, and 94.1%, respectively. Analysis of drug resistance based on tNGS results indicated that 10 of 93 TB patients (10.75%) had potential drug resistance.

Conclusion: Targeted next-generation sequencing achieved higher accuracy than other established diagnostic methods, and can play a crucial role in the rapid and accurate diagnosis of TB, including drug-resistant TB.

KEYWORDS

extrapulmonary tuberculosis, tissue sample, targeted next-generation sequencing (tNGS), TB diagnosis, drugresistant TB, *Mycobacterium tuberculosis*, hematoxylin and eosin staining

1 Introduction

Tuberculosis (TB) is a preventable and curable disease (Wu et al., 2020). However, in 2023, it was the second leading cause of death from a single infectious agent worldwide, causing almost twice as many deaths as HIV/AIDS. More than 10 million people continue to fall ill with tuberculosis every year (World Health Organization, 2011). The pathogen, *Mycobacterium tuberculosis* (MTB), can affect the lungs (pulmonary TB, PTB) and other organs (extrapulmonary TB, EPTB).

Timely diagnosis is paramount for effective management of TB. Traditional diagnostic methods, such as smear and culture tests, often fail to detect PTB in the absence of sputum (Silva et al., 2019), and EPTB with a low bacterial load (Chakravorty et al., 2005). In recent years, tissue biopsy has been increasingly employed for rapid and accurate diagnosis of smear-negative TB and EPTB (Lin et al., 2022; Barker et al., 2023). Current tissue biopsy methods for TB diagnosis include staining techniques such as hematoxylin and eosin (HE) combined with acid-fast staining (AFB), HE combined with PCR, HE combined with immunohistochemistry (IHC) using anti-MPT64, and the Xpert MTB/rifampicin (RIF) assay. However, HE staining lacks specificity and frequently reveals granulomatous inflammation with or without necrosis (Rui-e, 2020). Although AFB staining is a straightforward method for screening mycobacteria, it exhibits low sensitivity and can struggle to distinguish non-TB mycobacteria (NTM) (Jain et al., 2017) and certain leprosy cases (Ghosh et al., 2017). The GeneXpert MTB/RIF (Xpert) assay, recommended by the World Health Organization, has been widely used in clinical practice (World Health Organization, 2023). Although this assay is universally accessible in most clinical settings for identifying RIF resistance, it does not meet the clinical requirements for testing resistance of other anti-TB drugs (Chen and Shen-jie, 2023). Although PCR has potential for diagnosing TB, its sensitivity is curtailed by issues such as non-specific amplification and base mismatch (Callahan et al., 2019), compromising the diagnostic utility of puncture tissues in TB detection (Raveendran and Wattal, 2016). Adoption of IHC for TB as a standard diagnostic technique in histopathology laboratories has been relatively sluggish, likely attributed to the absence of a universally applicable anti-mycobacterial antibody that can be used for all tissue types (Kohli et al., 2014).

Previous studies have demonstrated the high sensitivity and specificity of targeted next-generation sequencing (tNGS) in diagnosing pulmonary TB (Kambli et al., 2021) and NTM strains (Chen et al., 2023), as well as its efficacy in identifying drug-resistant TB (Cabibbe et al., 2020; de Araujo et al., 2023; Mansoor et al., 2023). However, further investigation is needed to determine the performance of tNGS for histopathology samples. To validate the use of tNGS and establish its practicality in the diagnosis of TB using tissue samples, a retrospective study was conducted that compared the outcomes of tNGS with those of HE staining combined with AFB, HE staining paired with PCR, HE staining coupled to IHC using anti-MPT64, and the Xpert MTB/RIF assay.

2 Materials and methods

2.1 Participants

A total of 150 patients suspected of TB were consecutively included in the study at the Second Hospital of Nanjing, China, between January 2021 and October 2023. These patients were sufficiently representative of all TB patients at the hospital. Diagnosis of TB was based on clinical characteristics, microbiological smear and culture, histopathology, cytology, radiology, and response to anti-tubercular therapy. Active TB was diagnosed for 110 patients and all were included in the study. All ultimate clinical diagnoses relied on the two most authoritative health industry standards in China: Diagnosis for pulmonary tuberculosis (WS288-2017) and Classification of tuberculosis (WS196-2017). The results of all diagnostic tests for all patients were compared independently with those of these gold standard techniques (Figure 1). These participants exhibited typical symptoms associated with the site of EPTB; the most common symptoms are fever (36.56%), cough or expectoration (20.43%) and night-sweat (12.90%). The results of the erythrocyte sedimentation rate and C-reactive protein demonstrated a possible inflammation reaction (Table 1).

2.2 Procedures

Tissue samples were obtained through puncture, biopsy, and surgical resection. All specimens underwent various staining techniques including HE staining combined with AFB, HE staining combined with PCR, HE staining combined with IHC using anti-MPT64, Xpert MTB/RIF assay, and tNGS. All specific experimental processes are described below.

2.2.1 HE staining combined with AFB

Tissue specimens were deparaffinized and rinsed with consecutive dilutions of alcohol. After heat fixation, specimens were washed with carbol fuchsin and incubated with HCl. Brilliant Green was used for counterstaining. After rinsing, samples were allowed to dry at room temperature. A positive result was considered positive even if the patient underwent multiple AFB microscopy examinations.

2.2.2 HE staining combined with PCR

The MPB64 gene is widely recognized as a gene target for PCR diagnosis due to its high specificity in detecting extrapulmonary tuberculosis (Chaudhari et al., 2021). Therefore, in this study, DNA was extracted from tissue homogenates and a PCR assay targeting the MPB64 gene was conducted. DNA amplification was performed in the total reaction volume. The amplified product was electrophoresed and visualized after cycles of denaturation, annealing, and extension. A positive test was indicated by the presence of a 240 bp fragment.

2.2.3 HE staining combined with IHC

For IHC staining, 3–4 micron sections were cut from the tissue block and incubated overnight. After deparaffinization, hydration, and microwave antigen retrieval, the endogenous peroxidase activity was inhibited. Subsequently, primary antibody (anti-BCG) and secondary antibody (anti-MPT64) were added. After staining with chromogen, hematoxylin was used as the contrast dye. Each staining included a negative and positive control.

2.2.4 Xpert MTB/RIF assay

The GeneXpert MTB/RIF kits utilized in this study were sourced from Cepheid (City, State, United States). Firstly, the specimen was mixed with sample treatment reagent and incubated for 15 min. Subsequently, the mixture was transferred into a GeneXpert cartridge using the sterile dropper provided with the kit, and then loaded into the GeneXpert machine. Within 2 h, the GeneXpert system automatically displayed the results.

2.2.5 Targeted next-generation sequencing

For sample processing, samples were digested with proteinase K and lysozyme, ground by zirconia grinding beads for 1 min, and

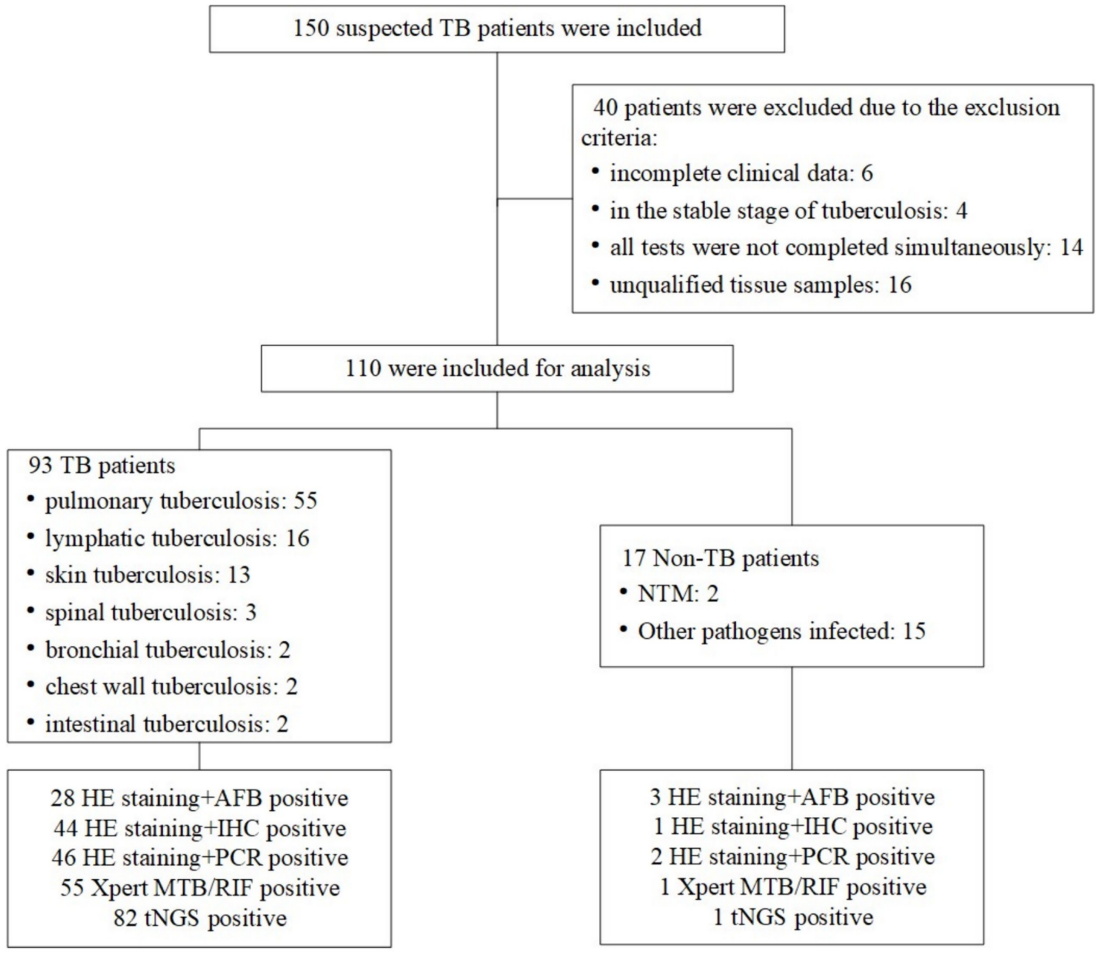

FIGURE 1
Flowchart showing the classification of patients included in the study.

lysozyme solution was added. The resulting lysate was used for subsequent nucleic acid extraction with a QIAamp DNA microbiome kit (Qiagen, City, Canada). Using the non-template control (NTC) method, blank EB buffer was used as a negative control for extracted nucleic acids. The concentration of extracted DNA was measured using a Qubit dsDNA quantification assay kit (Thermo Fisher, City, State, United States). Subsequently, the bacterial 16S rRNA gene was detected using universal primer pair 27F/1492R, and the fungal IST1/2 gene was amplified by PCR using primer pair ITS1/4. PCR amplification was performed using an ABI 2720 thermocycler with an initial denaturation step at 95°C for 3 min, followed by cycles at 95°C for 30 s, 62°C for 60 s, and 72°C for 60 s, and a final extension at 72°C for 3 min. PCR amplification products were purified and quantified using Invitrogen Qubit 4 for subsequent library preparation and TNPseq sequencing.

Nanopore barcode PCR was performed on the aforementioned products according to the instructions supplied with the PCR Barcode Expansion Pack 1–96 (EXP-PBC096) to construct libraries. After chip start-up, ~100 ng library pools were loaded into the nanopore flow cell and sequenced using the GridION platform. MinKNOW version 2.0 software was used to output data for base conditioning, and barcode demultiplexing was performed using Porechop.

Reads of small size (length < 200 bp) were filtered out using NanoFilt, and the remaining high-quality reads were aligned to all targets and potential etiologies using the National Center for Biotechnology Information (NCBI) Basic Local Alignment Search Tool (BLAST). Pathogens were categorized at the species level based on coverage and identity after NTC filtering. In general, the top 10 microorganisms sorted by aligned reads with a relative abundance score > 0.5% were classified as pathogens and further evaluated. MTB was considered positive when at least one sequence was mapped to a species or genus. All these steps in the TNPseq assay were conducted according to a previous report (Liu et al., 2024) with modifications.

2.3 Statistical analysis

In this study, we used R version 4.3.2 for statistical analysis. We calculated the sensitivity, specificity, positive predictive value (PPV), negative predictive value (NPV), and AUC value for the five detection methods using the measured TP, FP, FN, and TN values to evaluate the diagnostic effectiveness of tNGS compared with the other detection methods. Additionally, we used the Chi-square test to compare differences in positive rates for pathogenic identification between tNGS and the other detection methods. Furthermore,

TABLE 1 Clinical characteristics of the included patients.

Characteristics	All (n = 110)	TB (n = 93)	Non-TB (n = 17)
Age (year, mean ± SD)	46.0 ± 18.7	45.0 ± 17.3	48.7 ± 20.0
Male (n, %)	53 (48.2)	45 (48.4)	8 (47.1)
Female (n, %)	57 (51.8)	48 (52.6)	9 (52.9)
BMI (kg/m^2)	21.0 ± 3.5	21.0 ± 3.3	19.5 ± 3.1
Symptoms			
Fever	37 (33.64)	34 (36.56)	3 (17.65)
Cough or expectoration	22 (22.00)	19 (20.43)	3 (17.65)
Night-sweat	20 (18.18)	12 (12.90)	6 (35.29)
Chest and back pain	12 (10.91)	8 (8.60)	0
Physical examination	23 (20.91)	22 (23.66)	2 (11.76)
Other symptoms	29 (23.36)	27 (29.03)	3 (17.65)
Laboratory examination			
Erythrocyte sedimentation rate (mm/h)	53.00 (26.00,88.00)	63.00 (22.00,97.00)	42.00 (26.00,58.00)
C-reactive protein (mg/L)	64.00 (26.34,107.32)	45.32 (17.82,92,16)	66.00 (12.30,77.25)

we compared the etiological positive rates of tNGS and the other detection methods for the three main biopsy tissues using the Chi-square test or Fisher's exact probability method. Additionally, we created Venn and upset diagrams to illustrate the independent positive detection capability and applicability for the joint detection for TB. Finally, a scatter plot was used to demonstrate the diagnostic value of tNGS for clinical specimens with low bacterial load (especially in cases of EPTB).

2.4 Ethics approval

The study was approved by the Ethical and Institutional Review Boards for Human Investigation of the Second Hospital of Nanjing (ID: 2024-LS-ky026). Written informed consent was obtained from the patients themselves.

3 Results

3.1 Overview of clinical specimens from various tissues and detection of TB using tNGS

Histological samples spanned 10 distinct tissues: intestinal mucosa, lung, abdominal wall, spine, lymph node, skin, chest wall, pleura, bronchial mucosa, and paravertebral abscess. As depicted in Figure 2, positive results for TB were obtained from histological samples of all tissues except pleura. The results confirmed the efficacy of tNGS in identifying TB across diverse samples. Notably, 48 of 52 lung specimens and three pleural specimens were positive for PTB, with only seven cases undetected. For lymph node samples, 15 of 16 cases were identified, while 11 of 13 cases were detected for skin samples. In the case of spinal and paravertebral abscess specimens, two of three cases were identified. All cases of bronchial, chest wall, and intestinal TB were successfully detected. Additionally, scatter plots were used to display the number of nucleic acid sequences detected by tNGS in various TB-positive specimens (Figure 3). The median TB sequences of histological specimens of lung, paravertebral abscess, bronchial mucosa, intestinal mucosa, spine, pleura, chest wall, and lymph node were 125.5, 46, 12, 47.5, 4,054, 21,587, 2029.5, 3, and 25, respectively. These results revealed that the majority of histological samples contained few bacteria, demonstrating the utility of tNGS as a potent diagnostic tool for samples with low bacterial load.

3.2 Comparison of sensitivity, specificity, PPV, and NPV for the five detection methods

Table 2 lists the sensitivity, specificity, PPV, and NPV values for the five detection methods employed in the diagnosis of TB. The tNGS method exhibited a sensitivity of 88.2% and a specificity of 94.1%. The sensitivity and specificity values for HE staining combined with AFB were 30.1 and 82.4%; for HE staining combined with PCR they were 49.5 and 88.2%; for HE staining combined with IHC with anti-MPT64 they were 47.3 and 94.1%; and for the Xpert MTB/RIF assay, they were 59.1 and 94.1%, respectively. Across all test methods, tNGS yielded the highest sensitivity and specificity. The positive likelihood ratios for tNGS, Xpert MTB/RIF, HE staining combined with PCR, HE staining paired with IHC, and HE staining coupled with AFB were 14.99 (95% confidence interval [CI], 2.24–100.51), 10.05 (95% CI, 1.49–67.82), 4.20 (95% CI, 1.13–15.71), 8.04 (95% CI, 1.19–54.51), and 1.71 (95% CI, 0.58–4.99), respectively. Receiver operating characteristic (ROC) curves for the five tests are displayed in Figure 4. The area under the curve (AUC) for tNGS in diagnosing TB was 0.91 (95% CI, 0.85–0.98), while that of Xpert MTB/RIF, HE staining combined with PCR, HE staining paired with IHC, and HE staining coupled with AFB was 0.77 (95% CI, 0.69–0.84), 0.69 (95% CI, 0.60–0.79), 0.71 (95% CI, 0.63–0.78), and 0.56 (95% CI, 0.46–0.67), respectively.

3.3 Comparison of the distribution and overlap of positive results from the five tests

In instances where other diagnostic methods yielded negative results, we found that tNGS alone identified 12 specimens as positive, whereas the number of positive specimens detected independently by HE staining combined with AFB, HE staining combined with PCR, Xpert MTB/RIF, and HE staining combined with IHC were 4, 4, 2, and 0, respectively (Figure 5A). Notably, tNGS achieved 100% PPV (12/12), successfully identifying five distinct forms of TB, four cases of PTB, four cases of cutaneous TB, two cases of lymph node TB, one case of tuberculous pleurisy, and one case of intestinal TB. By comparison, PPV for the Xpert MTB/RIF assay was only 50% (1/2), corresponding to one case of tuberculous pleurisy. PPV for HE staining combined with PCR was also only 50% (2/4), correctly identifying one case of lymph node TB and one case of skin

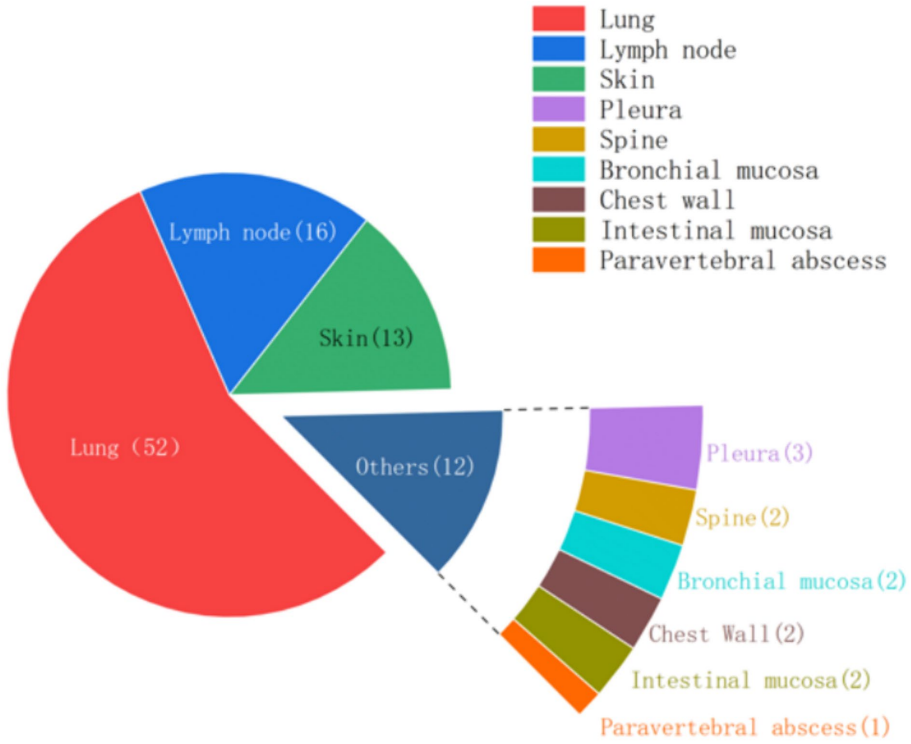

FIGURE 2
Fan chart of positive clinical specimens from various tissues.

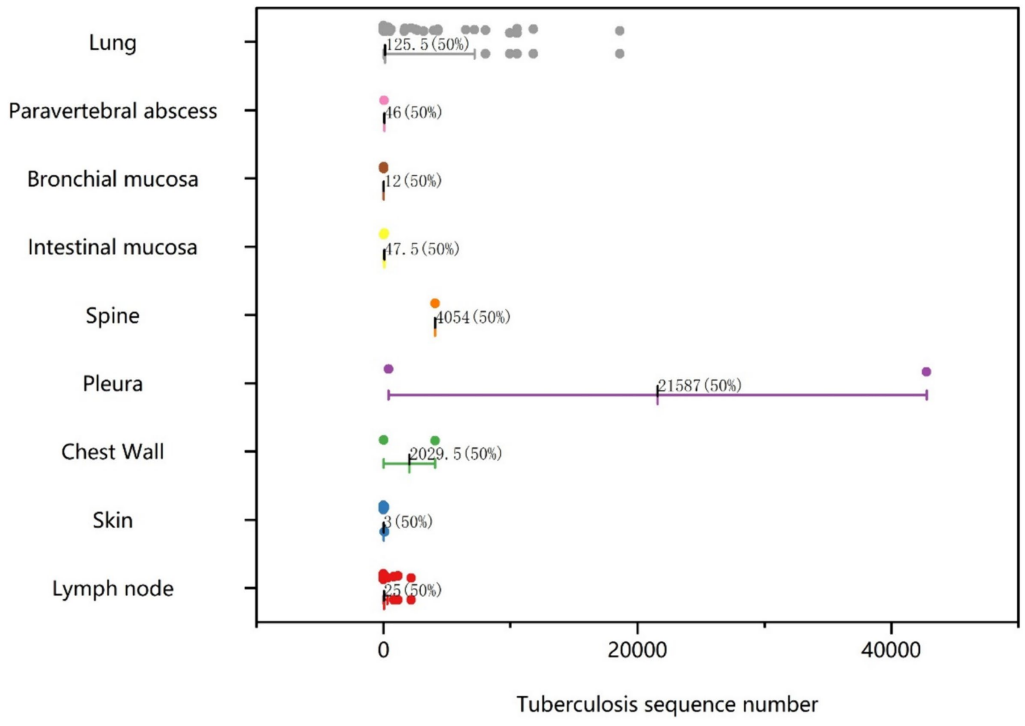

FIGURE 3
Scatter plot of TB sequence numbers for tissue samples testing positive by tNGS.

TABLE 2 Diagnostic efficiency of the five tests for the diagnosis of TB.

Test	Sensitivity (%)	Specificity (%)	PPV (%)	NPV (%)	Positive likelihood ratio
tNGS	**88.2** (95%CI:79.4–93.7)	**94.1** (95%CI:69.2–99.7)	**98.8** (95%CI:92.5–99.9)	**59.3** (95%CI:39.0–77.0)	14.99 (95%CI:2.24–100.51)
Xpert MTB/RIF	**59.1** (95%CI:48.4–69.1)	**94.1** (95%CI:69.2–99.7)	**98.2** (95%CI:89.2–99.9)	**29.6** (95%CI:18.4–43.8)	10.05 (95%CI:1.49–67.82)
HE staining + PCR	**49.5** (95%CI:39.0–60.0)	**88.2** (95%CI:49.8–92.2)	**95.8** (95%CI:84.6–99.3)	**24.2** (95%CI:14.6–37.0)	4.20 (95%CI:1.13–15.71)
HE staining + IHC	**47.3** (95%CI:37.0–57.9)	**94.1** (95%CI:69.2–99.7)	**97.8** (95%CI:86.8–99.9)	**24.6** (95%CI:15.1–37.1)	8.04 (95%CI:1.19–54.51)
HE staining + AFB	**30.1** (95%CI:21.3–40.6)	**82.4** (95%CI:55.8–95.3)	**90.3** (95%CI:73.1–97.5)	**17.7** (95%CI:10.4–28.3)	1.71 (95%CI:0.58–4.99)

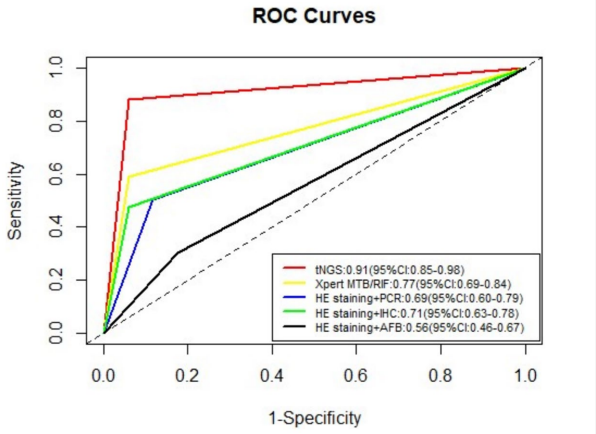

FIGURE 4
ROC curves for the five tests employed the diagnosis of TB.

TB. Similarly, PPV of HE staining combined with AFB was 50% (2/4), detecting one case of skin TB and one case of PTB. In addition, the abilities of tNGS and the other detection methods to identify TB patients were visualized using a Venn diagram (Figure 5B). The results revealed that tNGS shared 11 positive results with Xpert, seven positive results with Xpert and HE staining combined with PCR, 12 positive results with Xpert, HE staining combined with PCR, and HE staining combined with IHC, and nine positive results with all four of the other tests.

3.4 Comparison of pathogenic positivity rate between tNGS and other TB detection methods

For lung tissue samples, tNGS demonstrated statistically significant differences ($p < 0.05$) in pathogenic detection rate compared with three of the other detection methods, while differences between tNGS and Xpert MTB/RIF were not statistically significant ($p = 0.128$, Table 3). Regarding lymph node samples, significant disparities ($p < 0.05$) in pathogenic positivity rate were observed between tNGS and three of the other tests, with no significant differences detected ($p = 0.172$) between tNGS and the combination HE staining and PCR. Concerning skin tissue samples, a remarkable statistical difference ($p < 0.05$) was observed in pathogenic positivity rate between tNGS and all four of the other tests. All p values for tNGS were below the threshold of 0.05 ($p < 0.001$) when compared to the other four detection methods.

3.5 Drug resistance results among 93 TB patients

The tNGS results revealed that variants conferred drug resistance in 10 of 93 (10.75%) TB patients. Specifically, seven patients were resistant to isoniazid (INH), with five cases attributed to mutations in the *katG* gene and two cases due to mutation in the *inhA* gene. Furthermore, six patients demonstrated resistance to RIF, with mutations occurring in the *rpoB* gene. By contrast, the GeneXpert MTB/RIF assay detected resistance to RIF with *rpoB* mutations in only two patients. Additionally, tNGS identified one patient with resistance to fluoroquinolone drugs, specifically due to mutations in the *gyrA* gene, and another patient who showed resistance to pyrazinamide drugs, with mutations in the *pncA* gene.

4 Discussion

Successful treatment of TB depends on widespread access to accurate diagnosis. In general, pathological examination is crucial for confident TB diagnosis, especially when smear and culture tests are negative, and in cases of EPTB (Chen et al., 2024). However, conventional detection methods are deemed inadequate to meet clinical needs due to delayed diagnosis and misdiagnosis (Fan and Xiang, 2021; Ma et al., 2021; Xin, 2021). Although some molecular detection methods such as Xpert can be of remarkable value in TB diagnosis, they perform poorly when assessing paucibacillary specimens (Theron et al., 2011; Ushio et al., 2016). Meanwhile, PCR has drawbacks including a high false positive rate and susceptibility to contamination from the surrounding environment (Guo Li-na et al., 2015). Notably, the applicability of these molecular methods is further limited because patients cannot provide qualified sputum samples, and EPTB patients have limited access to suitable clinical sample types (Chen et al., 2024). Luckily, numerous studies have demonstrated that tNGS is more effective than AFB-based, drug susceptibility testing (DST), and Xpert methods for diagnosing TB in sputum and BALF samples, and it can rapidly detect drug resistance (Daum et al., 2014; Chan et al., 2020; Yu et al., 2022; Liu et al., 2023). Nevertheless, the diagnostic value of tNGS for TB detection in pathological tissues remains unproven, despite its crucial importance in diagnosing EPTB. This is why we compared the diagnostic ability of tNGS for TB detection in pathological tissues with established approaches including HE staining, Ziehl-Neelsen staining, IHC with anti-MPT64, PCR, and Xpert MTB/RIF. We explored the potential clinical significance of tNGS in the diagnosis of TB using various pathological tissue samples.

We assessed the utility of tNGS using tissue samples based on true predictive ability, pathogenic positivity rate, and diagnostic accuracy.

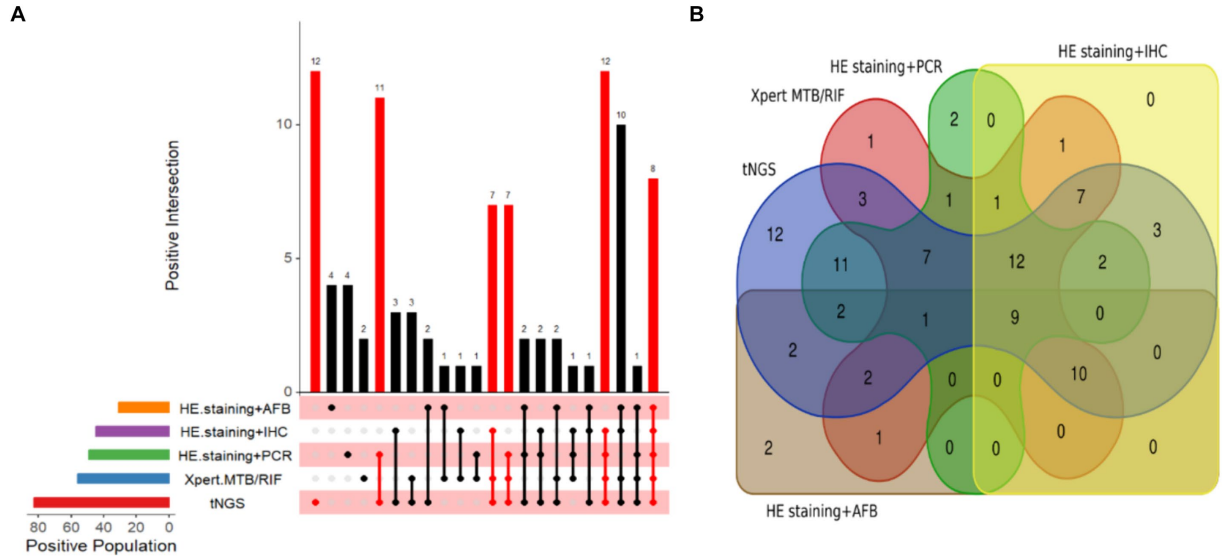

FIGURE 5
Visualization of TB detection test results. **(A)** Upset diagram of positive tests for the included patients. **(B)** Venn diagram of positive tests for TB patients.

TABLE 3 Comparison of pathogenic positivity rate between tNGS and the other four TB detection methods.

Detection method	Lung		Lymph node		Skin		Overall	
	χ^2	*p* value	Odds ratio	*p* value	Odds ratio	*p* value	χ^2	*p* value
Xpert MTB/RIF	2.318	0.128	13.753	0.015	24.624	0.001	13.209	<0.001
HE staining + PCR	16.295	<0.001	6.444	0.172	7.933	0.041	21.813	<0.001
HE staining + IHC	9.805	0.002	22.240	0.002	49.465	<0.001	25.576	<0.001
HE staining + AFB	29.616	<0.001	37.975	<0.001	10.973	0.015	47.354	<0.001

The results showed that tNGS achieved a sensitivity of 88.2% and a specificity of 94.1%, with its sensitivity significantly surpassing that of the other four tests. This suggests that tNGS possesses the benefit of exceptional sensitivity when it comes to identifying TB in tissues. IHC relies on the production of various polyclonal and monoclonal antibodies through tissue reactions. In particular, polyclonal antibodies possess the capacity to attach to various antigenic epitopes of a particular molecule, allowing tNGS to amplify the detection signal and hence the sensitivity when detecting MTB. Li-jing et al. (2014) discovered that the diagnostic efficacy of the polyclonal antibody IHC labeling technique for TB in pathological tissues was markedly superior to that of the acid-fast staining method ($p < 0.005$). This also confirmed why tNGS showed such exceptional sensitivity in our study. Nevertheless, tNGS did not exhibit a remarkable difference in specificity to the other four tests, possibly due to the limited sample size tested in this study, consequently leading to the introduction of statistical errors. Therefore, we integrated sensitivity and specificity to investigate the true predictive ability of tNGS for TB. The results revealed that tNGS surpassed the other four tests, as evidenced by its higher AUC (0.91).

In terms of pathogenic positivity rate, tNGS outperformed the other four testing methods. It consistently detected the highest number of positive cases ($n = 12$), encompassed the widest range of tuberculosis types ($n = 5$), and demonstrated the highest accuracy in terms of PPV (100%). If there was a need to rely on a single method when assessing TB puncture tissues, tNGS would be the optimal assay for TB detection. Additionally, when multiple methods were employed for the simultaneous identification of TB, tNGS always showed the highest overlap in positive detection compared with the other detection methods, indicating the reliability of tNGS in the joint detection of TB.

To delve deeper into the diagnostic performance of the most commonly used puncture tissues in clinical practice (lung, lymph node, and skin), we meticulously assessed the differences in pathogenic positivity rates between tNGS and the other four methods. Prior small-scale studies focusing on non-liquid specimens indicated that Xpert exhibits satisfactory performance in lung biopsy tissues (García-Basteiro et al., 2016), lymph node biopsy tissues (Dhasmana et al., 2014), and joint and bone biopsy tissues (Gu et al., 2015). However, from the CT values, it was considered that most of the tissues examined by Xpert are potentially specimens with high bacterial load (Hanrahan et al., 2014), which limits applicability in complex clinical environments. Thus, we inferred that the negligible discrepancy between tNGS and Xpert in lung puncture tissues ($p = 0.128$) in this study could be attributed to this reason. Lymph nodes are among the most susceptible sites for EPTB, providing niches for MTB growth and persistence (Ganchua et al., 2018). Reactivation of latent TB can initiate disease from lymph nodes and disseminate

MTB to the lungs and various other organs (Ganchua et al., 2020). Additionally, the ability of a drug to reach the lymph nodes is typically significantly lower that its ability to penetrate into the blood, lung tissues, and lung granulomas, resulting in slow progress in drug treatment for lymph node TB (Das et al., 2020). Therefore, the prompt identification and effective management of lymph node TB dissemination are crucial. TB-PCR is a targeted nucleic acid amplification technique for *M. tuberculosis complex IS6110*. Das et al. (2020) employed TB-PCR to evaluate TB patients in low TB incidence areas, and discovered a discrepancy in sensitivity between smear-positive and smear-negative patients (97 vs. 79%). Furthermore, they suggested that despite the favorable performance of TB-PCR in detecting EPTB specimens with low bacterial load, its full potential remains untapped due to the significant false-positive rate resulting from technical characteristics and inadequate negative predictive values in regions with low incidence rates (Das et al., 2020). These findings for PCR are consistent with the detection characteristics observed in our current work (Figure 3).

Furthermore, EPTB poses significant challenges regarding the procurement of pathological tissue samples. For instance, organs such as lymph nodes may be situated in hard-to-reach areas or linked to vital organs, leading to an increased risk of trauma or surgical complexity during resection biopsy (the gold standard; Kiliçarslan et al., 2017). Additionally, the effectiveness of puncture biopsies is dependent on the proficiency and expertise of the operator, with the additional challenge of inadequate sampling impacting the accuracy of detection outcomes (Meng et al., 2022). Considering the aforementioned factors, although our study found no significant difference (p =0.172) between tNGS and PCR for lymph node puncture samples, we remain convinced that PCR-based methods will always struggle to fulfill the clinical requirements for analyzing such pathological tissues. Importantly, obtaining lymph node pathological tissues for clinical diagnosis is not as convenient as obtaining skin samples for detecting skin TB, and inaccurate test results can potentially inflict physical and psychological distress upon patients.

Resistance to anti-TB drugs is a major challenge in the treatment of TB. Recently, a multicenter study used tNGS to evaluate clinical availability for the diagnosis of drug-resistant TB (DR-TB) (Liu et al., 2024). The results showed a remarkable concordance rate of 99.44% (179/180) with the culture assay for identifying the MTB complex. The sensitivity of NanoTNGS for detecting drug resistance was 93.53% for RIF, 89.72% for INH, 85.45% for ethambutol (EMB), 74.00% for streptomycin, and 88.89% for fluoroquinolones. The sensitivity of NanoTNGS for RIF-resistant TB was 9.73% higher than that of Xpert MTB/RIF. Although this study did not conduct phenotypic drug sensitivity testing on punctured tissues, it is known that tNGS can simultaneously detect MTB and assess the sensitivity of >10 anti-TB drugs. Within our study, we employed tNGS to identify resistance to all first-line anti-TB drugs, namely RIF, INH, EMB, and pyrazine (PZA), in pathological tissues. tNGS was particularly effective in detecting PZA resistance, which was challenging to uncover through phenotype drug sensitivity testing (pDST) (Diacon et al., 2012; Zhang et al., 2014). This is because tNGS can selectively amplify drug resistance-related regions of the MTB complex (MTBC) genome, and rapidly provide results directly from clinical specimens, offering higher sensitivity than other detection methods. In conclusion, tNGS offers a hopeful substitute for pDST in high-burden environments. For tissues, ongoing research into drug resistance detection is warranted.

Our current research has some limitations. Firstly, this study was conducted retrospectively, making encountering patient selection bias inevitable. Secondly, considering the diagnostic accuracy of various detection methods, the patients recruited in this study might have a relatively high bacterial load, which prevented us from highlighting the superiority of tNGS in detecting EPTB and specimens with low bacterial load. Thirdly, the absence of phenotypic drug sensitivity testing might undermine the persuasiveness of our resistance results obtained through tNGS. Lastly, there is the possibility of biases in tests conducted by different organizations and personnel, which could potentially impact the applicability of experimental findings.

Our tNGS assay proved to be highly sensitive for detecting TB in tissues, even more so than four established methods, and it has great potential for rapidly defining drug resistance elements. Additionally, we propose that a combination of multiplex PCR and tNGS can be a highly efficacious strategy for identifying EPTB and populations with low bacterial loads. Multiplex PCR can be employed to selectively amplify various antigenic epitopes and resistance sites of MTB. By leveraging the long-read sequencing capabilities of tNGS, challenging and low-load pathogens could be detected, and virulence and resistance genes could be identified.

5 Conclusion

The tNGS assay was more sensitive than four established diagnostic methods for rapidly diagnosing TB in tissues. The assay also has considerable potential for rapidly pinpointing drug resistance elements. Improving the sensitivity of resistance detection, reducing costs, and improving bioinformatics data analysis and integration could further enhance the clinical applicability of this powerful TB diagnostic tool.

Data availability statement

The datasets presented in this study can be found in online repositories. The names of the repository/repositories and accession number(s) can be found here: NCBI BioProject (https://www.ncbi.nlm.nih.gov/bioproject), accession number: PRJNA1127786.

Ethics statement

The studies involving humans were approved by Nanjing Second Hospital Medical Ethics Committee. The studies were conducted in accordance with the local legislation and institutional requirements. The participants provided their written informed consent to participate in this study.

Author contributions

WG: Data curation, Investigation, Validation, Writing – original draft, Writing – review & editing. CY: Data curation, Formal analysis, Methodology, Resources, Writing – original draft. TW: Data curation, Investigation, Methodology, Writing – original draft. YG: Data

curation, Validation, Writing – review & editing. YZ: Writing – original draft.

Funding

The author(s) declare that financial support was received for the research, authorship, and/or publication of this article. This work was supported by the Nanjing Health Science and Technology Development Special Fund (grant number: M2021073) and the Reserve Talent Program of Nanjing Second Hospital (grant number: HBRCYL08).

Acknowledgments

We would like to extend our appreciation to the personnel at the medical record studio for their valuable assistance in gathering data and the technical support provided by Hangzhou Shengting Medical Technology Co., Ltd. in Zhejiang Province. Furthermore, we also thank YZ for her invaluable guidance and support throughout the research process.

Conflict of interest

The authors declare that the research was conducted in the absence of any commercial or financial relationships that could be construed as a potential conflict of interest.

Publisher's note

References

Barker, M., Günther, A., Wurps, H., Gebhardt, A., Schönfeld, N., Polsfuss, S., et al. (2023). Ultrasound-guided lymph node biopsy in smear-negative children and adolescents with suspected TB. *Int. J. Tuberc. Lung Dis.* 27, 164–165. doi: 10.5588/ijtld.22.0364

Cabibbe, A. M., Spitaleri, A., Battaglia, S., Colman, R. E., Suresh, A., Uplekar, S., et al. (2020). Application of targeted next-generation sequencing assay on a portable sequencing platform for culture-free detection of drug-resistant tuberculosis from clinical samples. *J. Clin. Microbiol.* 58:e00632-20e00632-20. doi: 10.1128/jcm.00632-20

Callahan, B. J., Wong, J., Heiner, C., Oh, S., Theriot, C. M., Gulati, A. S., et al. (2019). High-throughput amplicon sequencing of the full-length 16S rRNA gene with single-nucleotide resolution. *Nucleic Acids Res.* 47:e103. doi: 10.1093/nar/gkz569

Chakravorty, S., Sen, M. K., and Tyagi, J. S. (2005). Diagnosis of extrapulmonary tuberculosis by smear, culture, and PCR using universal sample processing technology. *J. Clin. Microbiol.* 43, 4357–4362. doi: 10.1128/jcm.43.9.4357-4362.2005

Chan, W. S., Au, C. H., Chung, Y., Leung, H. C. M., Ho, D. N., Wong, E. Y. L., et al. (2020). Rapid and economical drug resistance profiling with Nanopore MinION for clinical specimens with low bacillary burden of *Mycobacterium tuberculosis*. *BMC. Res. Notes* 13:444. doi: 10.1186/s13104-020-05287-9

Chaudhari, K. V., Toi, P. C., and Joseph, N. M. (2021). Evaluation of real time polymerase chain reaction targeting mpb64 gene for diagnosis of extrapulmonary tuberculosis. *Indian J. Tuberc.* 68, 242–248. doi: 10.1016/j.ijtb.2020.09.009

Chen, H., Chen, P., Li, Y., Deng, Z., Xu, L., Liang, F., et al. (2023). Application value of targeted next-generation sequencing for identification of non-tuberculous mycobacteria strains. *Chin. J. Antituberc.* 45, 362–366. doi: 10.19982/j.issn.1000-6621.20220530

Chen, L., and Shen-jie, T. (2023). Annual progress on molecular biological diagnosis of tuberculosis 2022. *Chin. J. Tubercul. Resp. Dis.* 46, 176–182. doi: 10.3760/cma.j.cn112147-20221030-00857

Chen, S., Wang, C., Zou, Y., Zong, Z., Xue, Y., Jia, J., et al. (2024). Tuberculosis-targeted next-generation sequencing and machine learning: an ultrasensitive diagnostic strategy for paucibacillary pulmonary tuberculosis and tuberculous meningitis. *Clin. Chim. Acta* 553:117697. doi: 10.1016/j.cca.2023.117697

Das, S., Mangold, K. A., Shah, N. S., Peterson, L. R., Thomson, R. B., and Kaul, K. L. (2020). Performance and utilization of a laboratory-developed nucleic acid amplification test (NAAT) for the diagnosis of pulmonary and Extrapulmonary tuberculosis in a low-prevalence area. *Am. J. Clin. Pathol.* 154, 115–123. doi: 10.1093/ajcp/aqaa031

Daum, L. T., Fourie, P. B., Bhattacharyya, S., Ismail, N. A., Gradus, S., Maningi, N. E., et al. (2014). Next-generation sequencing for identifying pyrazinamide resistance in *Mycobacterium tuberculosis*. *Clin. Infect. Dis.* 58, 903–904. doi: 10.1093/cid/cit811

de Araujo, L., Cabibbe, A. M., Mhuulu, L., Ruswa, N., Dreyer, V., Diergaardt, A., et al. (2023). Implementation of targeted next-generation sequencing for the diagnosis of drug-resistant tuberculosis in low-resource settings: a programmatic model, challenges, and initial outcomes. *Front. Public Health* 11:1204064. doi: 10.3389/fpubh.2023.1204064

Dhasmana, D. J., Ross, C., Bradley, C. J., Connell, D. W., George, P. M., Singanayagam, A., et al. (2014). Performance of Xpert MTB/RIF in the diagnosis of tuberculous mediastinal lymphadenopathy by endobronchial ultrasound. *Ann. Am. Thorac. Soc.* 11, 392–396. doi: 10.1513/AnnalsATS.201308-250OC

Diacon, A. H., Dawson, R., von Groote-Bidlingmaier, F., Symons, G., Venter, A., Donald, P. R., et al. (2012). 14-day bactericidal activity of PA-824, bedaquiline, pyrazinamide, and moxifloxacin combinations: a randomised trial. *Lancet* 380, 986–993. doi: 10.1016/s0140-6736(12)61080-0

Fan, L., and Xiang, Z. (2021). The clinical value of loop-mediated isothermal amplification technique, sputum smear microscopy and solid culture method in diagnosis of pulmonary tuberculosis. *Pract. Clin. J. Integr. Tradition. Chin. Western Med.* 21, 9–10. doi: 10.13638/j.issn.1671-4040.2021.06.004

Ganchua, S. K. C., Cadena, A. M., Maiello, P., Gideon, H. P., Myers, A. J., Junecko, B. F., et al. (2018). Lymph nodes are sites of prolonged bacterial persistence during *Mycobacterium tuberculosis* infection in macaques. *PLoS Pathog.* 14:e1007337. doi: 10.1371/journal.ppat.1007337

Ganchua, S. K. C., White, A. G., Klein, E. C., and Flynn, J. L. (2020). Lymph nodes-the neglected battlefield in tuberculosis. *PLoS Pathog.* 16:e1008632. doi: 10.1371/journal.ppat.1008632

García-Basteiro, A. L., Ismail, M. R., Carrilho, C., Ussene, E., Castillo, P., Chitsungo, D., et al. (2016). The role of Xpert MTB/RIF in diagnosing pulmonary tuberculosis in post-mortem tissues. *Sci. Rep.* 6:20703. doi: 10.1038/srep20703

Ghosh, R., Barua, J. K., Garg, A., and Barman, B. P. (2017). Dual infection with Mycobacterium tuberculosis and *Mycobacterium leprae* at same site in an immunocompetent patient: an unusual presentation. *Indian J. Dermatol.* 62:548. doi: 10.4103/ijd.IJD_715_16

Gu, Y., Wang, G., Dong, W., Li, Y., Ma, Y., Shang, Y., et al. (2015). Xpert MTB/RIF and GenoType MTBDRplus assays for the rapid diagnosis of bone and joint tuberculosis. *Int. J. Infect. Dis.* 36, 27–30. doi: 10.1016/j.ijid.2015.05.014

Guo Li-na, X., Ying-chun, S. H.-l., Hong-mei, S., Yao, W., and Ying, Z. (2015). Clinical application of real-time FQ-PCR assay in rapid detection of Mycobacterium spp infection. *Chin. J. Nosocomiol.* 25, 4811–4813. doi: 10.11816/cn.ni.2015-142689

Hanrahan, C. F., Theron, G., Bassett, J., Dheda, K., Scott, L., Stevens, W., et al. (2014). Xpert MTB/RIF as a measure of sputum bacillary burden. Variation by HIV status and immunosuppression. *Am. J. Respir. Crit. Care Med.* 189, 1426–1434. doi: 10.1164/rccm.201312-2140OC

Jain, D., Ghosh, S., Teixeira, L., and Mukhopadhyay, S. (2017). Pathology of pulmonary tuberculosis and non-tuberculous mycobacterial lung disease: facts, misconceptions, and practical tips for pathologists. *Semin. Diagn. Pathol.* 34, 518–529. doi: 10.1053/j.semdp.2017.06.003

Kambli, P., Ajbani, K., Kazi, M., Sadani, M., Naik, S., Shetty, A., et al. (2021). Targeted next generation sequencing directly from sputum for comprehensive genetic information on drug resistant *Mycobacterium tuberculosis*. *Tuberculosis* 127:102051. doi: 10.1016/j.tube.2021.102051

Kiliçarslan, A., Doğan, M., Süngü, N., Karakök, E., Karabekmez, L., Akyol, M., et al. (2017). Can cutting-needle biopsy be an alternative to excisional biopsy in lymph node pathologies? *Turk Patoloji Derg* 1, 235–239. doi: 10.5146/tjpath.2016.01393

Kohli, R., Punia, R. S., Kaushik, R., Kundu, R., and Mohan, H. (2014). Relative value of immunohistochemistry in detection of mycobacterial antigen in suspected cases of tuberculosis in tissue sections. *Ind. J. Pathol. Microbiol.* 57, 574–578. doi: 10.4103/0377-4929.142667

Li-jing, X., Yan, L., Qiao, H., and Xiao-hua, D. (2014). Diagnostic value of polyclonal antibody to *Mycobacterium tuberculosis* in tuberculous. *J. Clin. Pulmon. Med.* 19, 69–72. doi: 10.3969/j.issn.1009-6663.2014.01.024

Lin, C. K., Fan, H. J., Yu, K. L., Chang, L. Y., Wen, Y. F., Keng, L. T., et al. (2022). Effectiveness of Endobronchial ultrasound-guided Transbronchial biopsy combined with tissue culture for the diagnosis of sputum smear-negative pulmonary tuberculosis. *Front. Microbiol.* 13:847479. doi: 10.3389/fmicb.2022.847479

Liu, A., Liu, S., Lv, K., Zhu, Q., Wen, J., Li, J., et al. (2024). Rapid detection of multidrug resistance in tuberculosis using nanopore-based targeted next-generation sequencing: a multicenter, double-blind study. *Front. Microbiol.* 15:1349715. doi: 10.3389/fmicb.2024.1349715

Liu, Z., Yang, Y., Wang, Q., Wang, L., Nie, W., and Chu, N. (2023). Diagnostic value of a nanopore sequencing assay of bronchoalveolar lavage fluid in pulmonary tuberculosis. *BMC Pulm. Med.* 23:77. doi: 10.1186/s12890-023-02337-3

Ma, M., Xiao-cheng, H., and Wei, L. (2021). Clinical significance of bronchoscopic alveolar lavage fluid Xpert MTB/RIF in the diagnosis of early drug-resistant tuberculosis. *Chin. J. Lung Dis.* 14, 626–629. doi: 10.3877/cma.j.issn.1674-6902.2021.05.021

Mansoor, H., Hirani, N., Chavan, V., Das, M., Sharma, J., Bharati, M., et al. (2023). Clinical utility of target-based next-generation sequencing for drug-resistant TB. *Int. J. Tuberc. Lung Dis.* 27, 41–48. doi: 10.5588/ijtld.22.0138

Meng, X., Fu, H., Jia, W., Wang, Y., and Yang, G. (2022). A comparative study of ultrasound-guided puncture biopsy combined with histopathology and Xpert MTB/RIF in the diagnosis of lymph node tuberculosis. *Front. Public Health* 10:1022470. doi: 10.3389/fpubh.2022.1022470

Raveendran, R., and Wattal, C. (2016). Utility of multiplex real-time PCR in the diagnosis of extrapulmonary tuberculosis. *Braz. J. Infect. Dis.* 20, 235–241. doi: 10.1016/j.bjid.2016.01.006

Rui-e, F. (2020). Pay attention to the diagnosis of granulomatous lung disease. *Chin. J. Tubercul. Resp. Dis.* 43, 1004–1008. doi: 10.3760/cma.j.cn112147-20200703-00772

Silva, T. M. D., Soares, V. M., Ramos, M. G., and Santos, A. D. (2019). Accuracy of a rapid molecular test for tuberculosis in sputum samples, bronchoalveolar lavage fluid, and tracheal aspirate obtained from patients with suspected pulmonary tuberculosis at a tertiary referral hospital. *J. Bras. Pneumol.* 45:e20170451. doi: 10.1590/1806-3713/e20170451

Theron, G., Peter, J., van Zyl-Smit, R., Mishra, H., Streicher, E., Murray, S., et al. (2011). Evaluation of the Xpert MTB/RIF assay for the diagnosis of pulmonary tuberculosis in a high HIV prevalence setting. *Am. J. Respir. Crit. Care Med.* 184, 132–140. doi: 10.1164/rccm.201101-0056OC

Ushio, R., Yamamoto, M., Nakashima, K., Watanabe, H., Nagai, K., Shibata, Y., et al. (2016). Digital PCR assay detection of circulating *Mycobacterium tuberculosis* DNA in pulmonary tuberculosis patient plasma. *Tuberculosis* 99, 47–53. doi: 10.1016/j.tube.2016.04.004

World Health Organization (2011). Rapid implementation of the Xpert MTB/RIF diagnostic test: Technical and operational 'How-to'; practical considerations. World Health Organization. Available at: https://www.who.int/publications/i/item/9789241501569 (Accessed February 15, 2011).

World Health Organization (2023). Use of targeted next-generation sequencing to detect drug-resistant tuberculosis. World Health Organization. Available at: https://www.who.int/publications-detail-redirect/9789240076372 (Accessed July 23, 2023).

Wu, Y., Huang, M., Wang, X., Li, Y., Jiang, L., and Yuan, Y. (2020). The prevention and control of tuberculosis: an analysis based on a tuberculosis dynamic model derived from the cases of Americans. *BMC Public Health* 20:1173. doi: 10.1186/s12889-020-09260-w

Xin, W. (2021). Clinical significance of rifampin-resistant real-time fluorescence quantitative nucleic acid amplification detection in the diagnosis of smear-negative pulmonary tuberculosis. *Contemp. Med.* 27, 125–126. doi: 10.3969/j.issn.1009-4393.2021.29.050

Yu, G., Shen, Y., Zhong, F., Zhou, L., Chen, G., Fang, L., et al. (2022). Diagnostic accuracy of nanopore sequencing using respiratory specimens in the diagnosis of pulmonary tuberculosis. *Int. J. Infect. Dis.* 122, 237–243. doi: 10.1016/j.ijid.2022.06.001

Zhang, Y., Shi, W., Zhang, W., and Mitchison, D. (2014). Mechanisms of pyrazinamide action and resistance. *Microbiol Spectr* 2, 1–12. doi: 10.1128/microbiolspec.MGM2-0023-2013

frontiers | Frontiers in Microbiology

TYPE Original Research
PUBLISHED 31 July 2024
DOI 10.3389/fmicb.2024.1398886

OPEN ACCESS

EDITED BY
Axel Cloeckaert,
Institut National de recherche pour l'agriculture, l'alimentation et l'environnement (INRAE), France

REVIEWED BY
Gopinath Chattopadhyay,
University of Zurich, Switzerland
Anwar Alam,
Sharda University, India
Shahbaz Ahmed,
St. Jude Children's Research Hospital, United States
Philip Fowler,
University of Oxford, United Kingdom
Sanjay Gautam,
International Vaccine Institute, Republic of Korea

*CORRESPONDENCE
Yao Liu
✉ doctorliuyao@126.com
Huaichen Li
✉ lihuaichen@163.com
Zhenguo Wang
✉ zhenguow@126.com

RECEIVED 11 March 2024
ACCEPTED 22 July 2024
PUBLISHED 31 July 2024

CITATION
Hou Y, Li Y, Tao N, Kong X, Li Y, Liu Y, Li H and Wang Z (2024) Toxin-antitoxin system gene mutations driving *Mycobacterium tuberculosis* transmission revealed by whole genome sequencing.
Front. Microbiol. 15:1398886.
doi: 10.3389/fmicb.2024.1398886

Toxin-antitoxin system gene mutations driving *Mycobacterium tuberculosis* transmission revealed by whole genome sequencing

Yawei Hou[1], Yifan Li[2], Ningning Tao[3], Xianglong Kong[4], Yameng Li[5], Yao Liu[3]*, Huaichen Li[3]* and Zhenguo Wang[1]*

[1]Institute of Chinese Medical Literature and Culture, Shandong University of Traditional Chinese Medicine, Jinan, Shandong, China, [2]Department of Respiratory and Critical Care Medicine, The Third Affiliated Hospital of Shandong First Medical University (Affiliated Hospital of Shandong Academy of Medical Sciences), Jinan, Shandong, China, [3]Department of Respiratory and Critical Care Medicine, Shandong Provincial Hospital Affiliated to Shandong University, Shandong Provincial Hospital Affiliated to Shandong First Medical University, Jinan, Shandong, China, [4]Artificial Intelligence Institute Qilu University of Technology (Shandong Academy of Sciences), Jinan, Shandong, China, [5]The First Clinical Medical College, Shandong University of Traditional Chinese Medicine, Jinan, Shandong, China

Background: The toxin-antitoxin (TA) system plays a vital role in the virulence and pathogenicity of *Mycobacterium tuberculosis* (*M. tuberculosis*). However, the regulatory mechanisms and the impact of gene mutations on *M. tuberculosis* transmission remain poorly understood.

Objective: To investigate the influence of gene mutations in the toxin-antitoxin system on *M. tuberculosis* transmission dynamics.

Method: We performed whole-genome sequencing on the analyzed strains of *M. tuberculosis*. The genes associated with the toxin-antitoxin system were obtained from the National Center for Biotechnology Information (NCBI) Gene database. Mutations correlating with enhanced transmission within the genes were identified by using random forest, gradient boosting decision tree, and generalized linear mixed models.

Results: A total of 13,518 *M. tuberculosis* isolates were analyzed, with 42.29% (n = 5,717) found to be part of genomic clusters. Lineage 4 accounted for the majority of isolates (n = 6488, 48%), followed by lineage 2 (n = 5133, 37.97%). 23 single nucleotide polymorphisms (SNPs) showed a positive correlation with clustering, including *vapB1* G34A, *vapB24* A76C, *vapB2* T171C, *mazF2* C85T, *mazE2* G104A, *vapB31* T112C, *relB* T226A, *vapB11* C54T, *mazE5* T344C, *vapB14* A29G, *parE1* (C103T, C88T), and *parD1* C134T. Six SNPs, including *vapB6* A29C, *vapB31* T112C, *parD1* C134T, *vapB37* G205C, *Rv2653c* A80C, and *vapB22* C167T, were associated with transmission clades across different countries. Notably, our findings highlighted the positive association of *vapB6* A29C, *vapB31* T112C, *parD1* C134T, *vapB37* G205C, *vapB19* C188T, and *Rv2653c* A80C with transmission clades across diverse regions. Furthermore, our analysis identified 32 SNPs that exhibited significant associations with clade size.

Conclusion: Our study presents potential associations between mutations in genes related to the toxin-antitoxin system and the transmission dynamics of *M. tuberculosis*. However, it is important to acknowledge the presence of confounding factors and limitations in our study. Further research is required to

establish causation and assess the functional significance of these mutations. These findings provide a foundation for future investigations and the formulation of strategies aimed at controlling TB transmission.

KEYWORDS

toxin-antitoxin system, *Mycobacterium tuberculosis*, transmission, whole genome sequencing, single nucleotide polymorphisms

1 Introduction

Tuberculosis (TB) is a global health threat caused by the highly successful human pathogen *Mycobacterium tuberculosis* (*M. tuberculosis*). According to a report by the World Health Organization (WHO), an estimated 10.6 million new TB cases occurred worldwide in 2022, resulting in over 1.3 million deaths (World Health Organization, 2023). Despite the substantial global burden of TB, our knowledge regarding the factors influencing its transmission remains limited. Therefore, it is imperative to delve deeper into the mechanisms underlying the spread of *M. tuberculosis*.

The toxin-antitoxin (TA) system plays a critical biological role in *M. tuberculosis*. Composed of toxins and antitoxins, this system forms a small genetic unit that is widely present in prokaryotes (Schuster and Bertram, 2013; Dai et al., 2022). TA systems have been shown to assist cells in stress adaptation, antibiotic resistance, biofilm formation, persisters, and disease development. Toxins are typically translated into proteins, while antitoxins can be either proteins or RNA (Ogura and Hiraga, 1983; Aizenman et al., 1996; Magnuson, 2007; Fineran et al., 2009; Wang and Wood, 2011; Lobato-Márquez et al., 2016). Based on the nature of antitoxins and the mechanisms which inhibit toxin activity, TA modules can be classified into six distinct types (Page and Peti, 2016). Among these types, type II TA systems are well-characterized, where antitoxins directly interact with toxins to neutralize their effects. Bioinformatics and phylogenetic analyses have revealed the presence of numerous TA systems encoded in the *M. tuberculosis* genome. The retention of these TA systems in members of the *M. tuberculosis* complex suggests their crucial role in regulating metabolic pathways essential for bacterial pathogenesis. Type II TA systems predominate in *M. tuberculosis*. The abundance of TA loci in the *M. tuberculosis* genome raises important questions about their functional diversity (Ramage et al., 2009; Tandon et al., 2019). Previous studies have extensively investigated the various functions of TA systems in *M. tuberculosis* and their potential impact on pathogenic mechanisms (Schippers et al., 2005; Guo et al., 2016). These systems are believed to play a key role in *M. tuberculosis* 's response to stressors such as nutrient starvation and antibiotic treatment, promoting its survival and drug resistance (Kim et al., 2018). Additionally, TA systems are associated with the formation of persistent cells, a subpopulation exhibiting drug tolerance that plays a crucial role in establishing chronic infections in *M. tuberculosis* (Merfa et al., 2016). While the importance of toxin-antitoxin systems in *M. tuberculosis* has been acknowledged, our understanding of their specific mechanisms and functions within this bacterium remains limited. Therefore, comprehensive research is required to explore the roles of TA systems and gain deeper insights into the complex biology of *M. tuberculosis*.

Driven by the need to better understand the mechanisms underlying *M. tuberculosis* transmission, we conducted an extensive study investigating the impact of mutations in TA system genes on its spread. Our research aims to elucidate how genetic variations within this system can influence *M. tuberculosis* strain transmission dynamics. Utilizing whole-genome sequencing (WGS), we analyzed the genetic variations present in *M. tuberculosis* isolates at a high-resolution level. This enabled us to identify specific mutations within the TA system genes that may be associated with *M. tuberculosis* transmission. Advanced statistical and bioinformatics techniques, including random forest, gradient boosting decision tree, and generalized linear mixed models, were employed for comprehensive analyses to identify key genetic variants linked to transmission dynamics. We acknowledge challenges posed by confounding factors and population dynamics in our analysis. Future research should incorporate social networks and regional interactions for a more comprehensive understanding. Limitations of our study include a focus on gene analysis, potentially overlooking other important genetic influences such as drug resistance mutations or virulence determinants. Therefore, more comprehensive studies are needed to address these limitations adequately. Our study has yielded significant results, identifying multiple single nucleotide polymorphisms (SNPs) within the toxin-antitoxin system genes that positively correlate with clustering, suggesting their potential role in *M. tuberculosis* transmission. Furthermore, some of these SNPs were found to be associated with transmission clades across different geographical regions, indicating their potential global impact on the spread of *M. tuberculosis*. These findings provide valuable insights into the transmission dynamics of this pathogen and contribute to a more thorough understanding of *M. tuberculosis* transmission.

2 Materials and methods

2.1 Sample collection

We collected a total of 1,550 samples from patients with culture-positive pulmonary tuberculosis at two medical institutions in China: the Shandong Public Health Clinical Research Center (SPHCC) and Weifang Respiratory Disease Hospital (WRDH). These samples were obtained through analysis of sputum specimens. The sample collection spanned the period from 2011 to 2018. It is important to note that all samples were collected anonymously, and therefore, informed consent was not required as per the approved research protocol. Our study received ethical approval from the Ethics Committee of Shandong Provincial Hospital, which is affiliated with Shandong First Medical University (No.2017-337). This approval ensures that our research

adheres to ethical guidelines and safeguards the rights and privacy of the participants involved in the study.

2.2 DNA extraction and sequencing

Genomic deoxyribonucleic acid (DNA) was successfully extracted from 1,468 of the 1,550 Shandong *M. tuberculosis* isolates. Gene sequencing was performed at the Beijing Genomic Institute. The genomic DNA was sequenced using an Illumina HiSeq 4,000 system. The resulting sequence data were deposited in the National Center for Biotechnology Information (NCBI) BioProject PRJNA1002108. Quality control of the sequence reads was conducted using Fast QC software, and a total of 1,447 samples passed the quality control criteria. Low-quality raw reads with a sequencing base ≤20 or sequencing fragments length ≤ 20 were excluded from the paired-end sequencing process. During the analysis, two isolates were accidentally lost, resulting in 1445 isolates being included for further analysis. The reads of these 1,445 strains, along with 12,132 *M. tuberculosis* isolates downloaded from previous studies and collected from 52 countries and 18 regions worldwide, were aligned to the H37Rv reference genome (NC_000962.3) using BWA-MEM (version 0.7.17-r1188) (Luo et al., 2015; Yang et al., 2017; Coll et al., 2018; Hicks et al., 2018; Koster et al., 2018; Liu et al., 2018; Chen et al., 2019; Huang et al., 2019; Jiang et al., 2020). To improve the alignment quality, clipped alignments and duplicated reads were removed using samclip (v0.4.0) and samtools markdup (v1.15), respectively. Samples with a coverage rate below 98% or a depth less than 20× were excluded from the analysis (Jajou et al., 2019; Yang et al., 2021). Additionally, 55 *Mycobacterium bovis* isolates, one *Mycobacterium caprae* isolate, and three *Mycobacterium orygis* isolates were also excluded. In summary, a total of 13,518 genomes were analyzed in this study. Specific sample numbers can be found in Supplementary Tables 1, 2.

2.3 Single nucleotide polymorphism (SNP) analysis

After performing variant calling, we proceeded with additional filtering steps to enhance the quality of the detected variants. This involved employing Free Bayes (version 1.3.2) with an included filter parameter "FMT/GT = "1/1" && QUAL> = 100 && FMT/DP > = 10 && (FMT/AO)/(FMT/DP) > = 0." and Bcftools (version 1.15.1) for further refinement of the identified variants. To ensure the accuracy of our analysis, we excluded SNPs located within repetitive regions. This includes polymorphic sequences rich in GC found in PE/PPE genes, directly repeated SNPs, and repetitive bases identified using Tandem Repeat Finder (version 4.09) and RepeatMask (version 4.1.2-P1) (Li et al., 2009; Liu et al., 2019). The annotation for each candidate SNP was determined using SnpEff, version 4.11. The resulting output was obtained by utilizing the Python programming language (Cingolani et al., 2012).

2.4 Phylogenetic analysis

Phylogenetic lineages were inferred based on specific SNPs following the methodology described by Coll et al. (2014) (Supplementary Tables 1, 2). Maximum-likelihood phylogenetic and phylogenomic analyses were conducted using IQ-TREE version 1.6.12. The phylogeny was constructed using the general time reversible (GTR) model of nucleotide substitution with the GAMMA model of rate heterogeneity, and bootstrap replicates were performed with 100 iterations. To establish the phylogenetic relationships, the genome of the *Mycobacterium canettii* strain CIPT 140010059 (NC_15848.1) was used as an outgroup (Nguyen et al., 2015). The resulting phylogenetic tree was visualized and annotated using the online phylogenetic tree visualization tool iTOL.[1]

2.5 Genotypic drug resistance prediction

We utilized the web-based tool TBProfiler (version 4.3.0) to analyze *M. tuberculosis* WGS data for drug resistance prediction (Phelan et al., 2019). Drug resistance was predicted using the curated drug-resistance Tuberculosis Database within TBProfiler. This database has undergone extensive testing on over 17,000 samples with genotypic and phenotypic data. The resistance-associated polymorphisms (SNPs and indels) identified by TBProfiler were further evaluated based on the WHO-endorsed catalog of molecular targets for *M. tuberculosis* complex drug-susceptibility testing and resistance interpretation (Walker et al., 2022). This additional assessment ensures reliable and accurate interpretation of drug resistance profiles. For more detailed information on the predicted drug resistance results, please refer to Supplementary Table 3.

2.6 Propagation analysis

To explore the influence of mutations in toxin-antitoxin system genes on the transmission of *M. tuberculosis*, we conducted analyses on transmission clusters and transmission clades (Seto et al., 2017). Building upon prior research (Walker et al., 2013), we defined genome-based transmission clusters as pairs of isolates separated by ≤12 SNPs. Genome-based transmission clades were defined as pairs of isolates separated by ≤25 SNPs. To classify the transmission clades into different categories, we adopted a classification system established by previous scholars. The transmission clades were categorized into three groups based on their size: large (above the 75th percentile), medium (between the 25th and 75th percentiles), and small (below the 25th percentile) (Chiner-Oms et al., 2019). For a comprehensive analysis of global distribution patterns and transmission dynamics among *M. tuberculosis* isolates, we classified them into two main groups: cross-country clades and within-country clades. Cross-country clades consisted of isolates originating from two or more different countries. Additionally, we further classified the *M. tuberculosis* isolates into cross-regional and within-regional clades based on their geographic location, using the United Nations standard regions (UN M.49). Cross-regional clades comprised isolates from two or more different regions.

1 https://itol.embl.de/

2.7 Acquisition of toxin-antitoxin system genes

Initially, our analysis started with the retrieval of all genes correlated with *Mycobacterium tuberculosis* from the NCBI database, which yielded a comprehensive set of 4,015 genes. We concentrated our study on the specific strain, *Mycobacterium tuberculosis H37Rv*, and meticulously filtered that list down to 4,009 genes, guided by their respective organism names. Subsequently, our attention was directed toward refining the gene selection, with a focus on identifying those associated with the toxin-antitoxin system. This involved evaluating their functional descriptions and characteristic annotations, resulting in the successful identification of 78 genes directly implicated in the toxin-antitoxin system. To further our investigation on these genes, we employed Python, a versatile programming language with robust data analysis capabilities, to identify mutations within the set of toxin-antitoxin system genes (Supplementary Table 4).

2.8 Statistical analysis and modeling

Categorical data were presented as frequencies and percentages. In order to improve statistical reliability, Mutations observed fewer than 10 times were discarded prior to continuing analysis. Statistical analyses were performed by generalized linear mixed models (GLMM) in R (version 4.2.3). In addition, Python 3.7.4 with the Scikit-learn library was used to implement random forest and gradient boosting decision tree algorithms for further data analysis. To evaluate the performance of the models, all samples were randomly divided into training and test sets at a ratio of 7:3. Various metrics such as Kappa, sensitivity, specificity, accuracy, positive predictive value (PPV), negative predictive value (NPV), positive likelihood ratio (PLR), negative likelihood ratio (NLR), and area under curve (AUC) were calculated to assess the models' effectiveness (Luo et al., 2022). Importantly, after fitting the models, we assessed the importance of input variables on the model's predictions. By assigning scores to each input feature, we identified the top-performing variables by taking the intersection of both conditions. This approach allowed us to identify the most influential features contributing to the precision of predicting risk factors (Bi et al., 2018; Agarwal et al., 2019). All models included lineage and geographical location as covariates to correct for potential confounding factors. All statistical tests were two-tailed, with *p*-values less than 0.05 considered statistically significant.

3 Results

3.1 Characteristics of study samples

A total of 13,518 isolates were included in this study. We identified a total of 70,346 SNPs related to the toxin-antitoxin system. Out of the included strains, 6,488 (48%) belonged to lineage 4, 5,133 (37.97%) belonged to lineage 2, and only 10 strains (0.07%) belonged to lineage 6, while 29 strains (0.21%) belonged to lineage 7. By dividing the isolates into clusters based on 12 SNPs, a total of 5,717 strains clustered together, resulting in a clustering rate of 0.42. The *M. tuberculosis* isolates were further categorized into 1,955 clusters, with the number of isolates per cluster ranging from 2 to 146. Among the lineage 4 group, 3,245 (50.02%) isolates formed clusters, while within the lineage 2 group, 2,043 (39.80%) isolates formed clusters. Additionally, the majority of the *M. tuberculosis* strains analyzed in this study originated from Eastern Asia ($n = 3,170$, 23.45%) and Northern America ($n = 1,646$, 12.18%). Other regions contributing substantial sample sizes include Eastern Africa ($n = 1731$, 12.81%), Western Europe ($n = 1,578$, 11.67%), Northern Europe ($n = 1,262$, 9.34%), and Eastern Europe ($n = 1,118$, 8.27%), see Figure 1. Applying a threshold of 25 SNPs for clades, a total of 7,808 isolates claded together, resulting in a clading rate of 0.58. The *M. tuberculosis* isolates were further grouped into 2,218 clades, with the number of isolates per clade ranging from 2 to 192. Among these clades, there were 187 cross-country clades, consisting of 2 to 3 countries per clade, and 164 cross-regional clades, consisting of 2 to 3 regions per clade, as shown in Table 1. The phylogenetic tree of *M. tuberculosis* isolates was constructed as described in Figure 2.

3.2 Relationship between toxin-antitoxin system gene mutations and transmission clusters

We conducted a filtering process to exclude sites with less than 10 mutations, resulting in a final selection of 182 SNPs for further analysis. Our investigation aimed to explore the correlation between these 182 SNPs and clustering by comparing isolates within clusters to those outside clusters. The generalized linear mixed model (GLMM) revealed that 27 SNPs were statistically significant for clustering ($p < 0.05$) (Supplementary Table 5). Among these significant SNPs, there were 18 nonsynonymous SNPs, one start lost site, one stop gained site, and seven synonymous SNPs. Notably, these genetic variations showed a positive correlation with transmission clusters in *M. tuberculosis* isolates, see Table 2 for details. Furthermore, we employed random forest and gradient boosting decision tree models to establish prediction models (Table 3; Figure 3; Supplementary Table 14). However, the SNPs *Rv0298* G213A, *Rv1103c* G56A, and *Rv2871* G28C did not contribute significantly to the gradient boosting decision tree model. In summary, our findings suggested that the presence of *Rv0064A* (*vapB1*, G34A), *Rv0239* (*vapB24*, A76C),*Rv0300* (*vapB2*, T171C), *Rv0659c* (*mazF2*, C85T), *Rv0660c* (*mazE2*, G104A), *Rv0748* (*vapB31*, T112C), *Rv1247c* (*relB*, T226A), *Rv1560* (*vapB11*, C54T), *Rv1943c* (*mazE5*, T344C), *Rv1952* (*vapB14*, A29G), *Rv1959c* (*parE1*, C103T, C88T), *Rv1960c* (*parD1*, C134T), *Rv1991A* (*mazE6*, G156A), *Rv2009* (*vapB15*, T6C, G237A), *Rv2142c* (*parE2*, C48G), *Rv2142A* (*parD2*, A196G), *Rv2274c* (*mazF8*, A97G), *Rv2526* (*vapB17*, G213C), *Rv2550c* (*vapB20*, A54C), *Rv2654c* T152C, *Rv2862A* (*vapB23*, T2C), and *Rv3385c* (*vapB46*, G70A) were positively associated with transmission clusters in *M. tuberculosis* isolates.

3.3 Relationship between toxin-antitoxin system gene mutations and transmission clusters of lineages

After excluding sites with less than 10 mutations, a total of 46 SNPs were identified and included for further analysis. Specifically focusing on clustered isolates belonging to lineage 2, we investigated

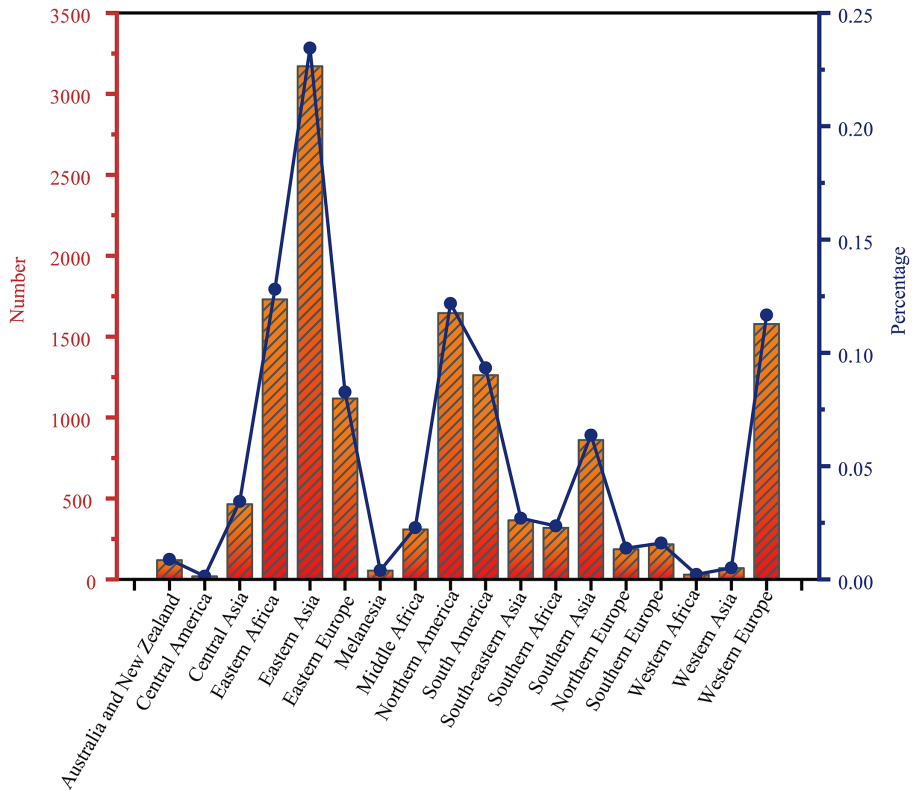

FIGURE 1
Distribution of 13,518 strains of *Mycobacterium tuberculosis* in 18 regions of the world.

the relationship between these 46 SNPs and non-clustered isolates. The GLMM analysis revealed that five SNPs showed statistical significance for clustering ($p < 0.05$) (Supplementary Table 6). Among these significant SNPs, there were three nonsynonymous SNPs, one start lost site, and one synonymous SNP, all of which displayed a positive correlation with clustering. Notably, these significant SNPs included Rv0239 (*vapB24*, A76C), *Rv0659c* (*mazF2*, C85T), *Rv1959c* (*parE1*, C25G), *Rv1991A* (*mazE6*, G156A), and *Rv2862A* (*vapB23*, T2C). Furthermore, prediction models were established using random forest and gradient boosting decision tree algorithms (Supplementary Tables 10, 15; Supplementary Figure 1). The findings demonstrated that *vapB24* A76C, *mazF2* C85T, *parE1* C25G, *mazE6* G156A, and *vapB23* T2C significantly contributed to both the random forest and gradient boosting decision tree models. Overall, our results indicated a positive correlation between the SNPs *vapB24* A76C, *mazF2* C85T, *parE1* C25G, *mazE6* G156A, *vapB23* T2C and transmission clusters within *M. tuberculosis* isolates of lineage 2.

After filtering out sites with less than 10 mutations, we selected a total of 82 SNPs for further analysis. Our focus was specifically on clustered isolates belonging to lineage 4, and we aimed to investigate the relationship between these 82 SNPs and clustered isolates. Using the GLMM analysis, we identified 17 SNPs that showed statistical significance for clustering ($p < 0.05$) (Supplementary Table 7). Among these significant SNPs, 11 were nonsynonymous SNPs, one was a stop gained SNP, and five were synonymous SNPs, all exhibiting a positive correlation with clustering, see Table 4 for details. Furthermore, we established prediction models using random forest and gradient boosting decision tree algorithms (Supplementary Tables 11, 16; Supplementary Figure 2). However, the SNPs *Rv0064A* G34A, *Rv2009* T6C, *Rv2104c* G249T, and *Rv3385c* G70A did not contribute significantly to the gradient boosting decision tree model. In summary, our findings indicated a positive correlation between the SNPs *Rv0300* (*vapB2*, T171C), *Rv0660c* (*mazE2*, G104A), *Rv1560* (*vapB11*, C54T), *Rv1943c* (*mazE5*, T344C), *Rv1952* (*vapB14*, A29G), *Rv1959c* (*parE1*, C88T), *Rv1960c* (*parD1*, C134T), *Rv2009* (*vapB15*, G237A), *Rv2142c* (*parE2*, C48G), *Rv2274c* (*mazF8*, A97G), *Rv2526* (*vapB17*, G213C), *Rv2550c* (*vapB20*, A54C), *Rv2871* (*vapB43*, G28C), and transmission clusters within lineage 4 of *M. tuberculosis* isolates.

3.4 Relationship between toxin-antitoxin system gene mutations and cross-country transmission

After excluding sites with fewer than 10 mutations, a total of 128 SNPs within genes associated with the toxin-antitoxin system were identified and included for analysis. The objective was to investigate the relationship between these SNPs and cross-country transmission clades. The GLMM analysis revealed that seven nonsynonymous SNPs exhibited statistical significance for cross-country transmission clades ($p < 0.05$) (Supplementary Table 8). These significant SNPs included *Rv0657c* (*vapB6*, A29C), *Rv0748* (*vapB31*, T112C), *Rv1960c* (*parD1*, C134T), *Rv2104c* (*vapB37*, G205C), *Rv2547* (*vapB19*, C188T), *Rv2653c* A80C, and *Rv2830c* (*vapB22*, C167T). Additionally, random forest and gradient boosting decision tree models were employed to establish prediction models for these SNPs (Supplementary Tables 11, 17;

TABLE 1 The characteristics of *Mycobacterium tuberculosis* isolates.

Characteristic	Number of isolates (%)	
Lineage		
Lineage 1	851 (6.30)	
Lineage 2	5,133 (37.97)	
Lineage 3	969 (7.17)	
Lineage 4	6,488 (48)	
Lineage 5	38 (0.28)	
Lineage 6	10 (0.07)	
Lineage 7	29 (0.21)	
12 SNPs		
Cluster	5,717 (42.29)	
No-cluster	7,807 (57.71)	
Lineage 2	cluster	2043 (39.80)
	no-cluster	3,090 (60.20)
Lineage 4	cluster	3,245 (50.02)
	no-cluster	3,243 (49.98)
25 SNPs		
Clade	7,808 (57.76)	
No-Clade	5,710 (42.24)	
Cross_country	Yes	704 (9.02)
	No	7,104 (90.98)
Cross_regional	Yes	650 (8.32)
	No	7,158 (91.68)
Clades by size	Small	2,548 (32.63)
	Medium	3,264 (41.80)
	Large	1996 (25.56)

Supplementary Figure 3). The results indicated that *vapB6* A29C, *vapB31* T112C, *parD1* C134T, *vapB37* G205C, *Rv2653c* A80C, and *vapB22* C167T made significant contributions to both the random forest and gradient boosting decision tree models. However, the SNP *vapB19* C188T did not contribute significantly to the gradient boosting decision tree model. Overall, our results showed that *vapB6* A29C, *vapB31* T112C, *parD1* C134T, *vapB37* G205C, *Rv2653c* A80C, and *vapB22* C167T were positively correlated with transmission clades across different countries.

3.5 Relationship between toxin-antitoxin system gene mutations and cross-regional transmission

After excluding sites with less than 10 mutations, we identified and included a total of 128 SNPs of toxin-antitoxin system genes. The GLMM showed that seven nonsynonymous SNPs were found to be statistically significant for transmission clades of cross-country ($p < 0.05$) (Supplementary Table 9), including *Rv0657c* (*vapB6*, A29C), *Rv0748* (*vapB31*, T112C), *Rv1960c* (*parD1*, C134T), *Rv2104c* (*vapB37*, G205C), *Rv2547* (*vapB19*, C188T), *Rv2653c* A80C, *Rv2830c* (*vapB22*, C167T). Two prediction models were established using random forest and gradient boosting decision tree (Supplementary Tables 13, 18; Supplementary Figure 4), we found that *vapB6* A29C, *vapB31* T112C, *parD1* C134T, *vapB37* G205C, *vapB19* C188T and *Rv2653c* A80C also contributed most to the random forest and gradient boosting decision tree. However, the SNP of *vapB22* C167T did not contribute significantly to the gradient boosting decision tree model. Overall, our results showed that *vapB6* A29C, *vapB31* T112C, *parD1* C134T, *vapB37* G205C, *vapB19* C188T, and *Rv2653c* A80C were positively correlated with transmission clades across different regions.

3.6 Relationship between toxin-antitoxin system gene mutations and clade size

After excluding sites with less than 10 mutations, a total of 128 SNPs within the toxin-antitoxin system were identified and included for analysis. The results revealed that 32 SNPs were significantly associated with clade size ($p < 0.05$). Among these significant SNPs, there were 21 nonsynonymous SNPs, two stop gained SNPs, and nine synonymous SNPs, all of which displayed a positive correlation with clade size. Notable examples include *vapB1* G34A, *mazE2* G104A, *vapB11* C54T, *mazE5* T344C, *vapB14* A29G, *parE1* C88T, *parD1* C134T, *vapB15* T6C, *parE2* C48G, *mazF8* A97G, and *vapB46* G70A. For more detailed information, please refer to Supplementary Figure 5.

4 Discussion

Consistent with prior research findings, our study further emphasizes the diverse functionality of TA systems in *M. tuberculosis*. These redundant TA systems serve as a backup mechanism enabling cellular adaptation and survival under adverse conditions (Min et al., 2012). They play a critical role in *M. tuberculosis*'s stress response, including nutrient deprivation, by regulating essential cellular processes like DNA replication, protein translation, and cell division. Moreover, TA systems contribute to the formation of drug resistance and persistence in *M. tuberculosis*. However, it is important to acknowledge that certain studies have reported conflicting results regarding the specific contributions of TA systems to persistence formation and stress conditions (Yu et al., 2020; Sharma et al., 2021). These discrepancies may arise from variations in experimental setups or genetic differences among *M. tuberculosis* strains used in different investigations. Therefore, additional research is needed to precisely determine the roles of TA systems in persistence formation, stress responses, and their impact on *M. tuberculosis* pathogenesis. In our study, we focused on examining the relationship between gene mutations in toxin-antitoxin systems and the transmission dynamics of *M. tuberculosis*. The *M. tuberculosis* genome contains numerous toxin-antitoxin systems, including *VapBC*, *MazEF*, *ParDE*, and *RelBE* (Ramage et al., 2009; Tandon et al., 2019). To gain deeper insights into the significance of these toxin-antitoxin systems in *M. tuberculosis* transmission, we analyzed the prevalence and genetic variation of specific toxin-antitoxin system genes across various clusters and evolutionary branches. Our analysis detected multiple mutations in these genes, suggesting they could be involved in *M. tuberculosis* transmission.

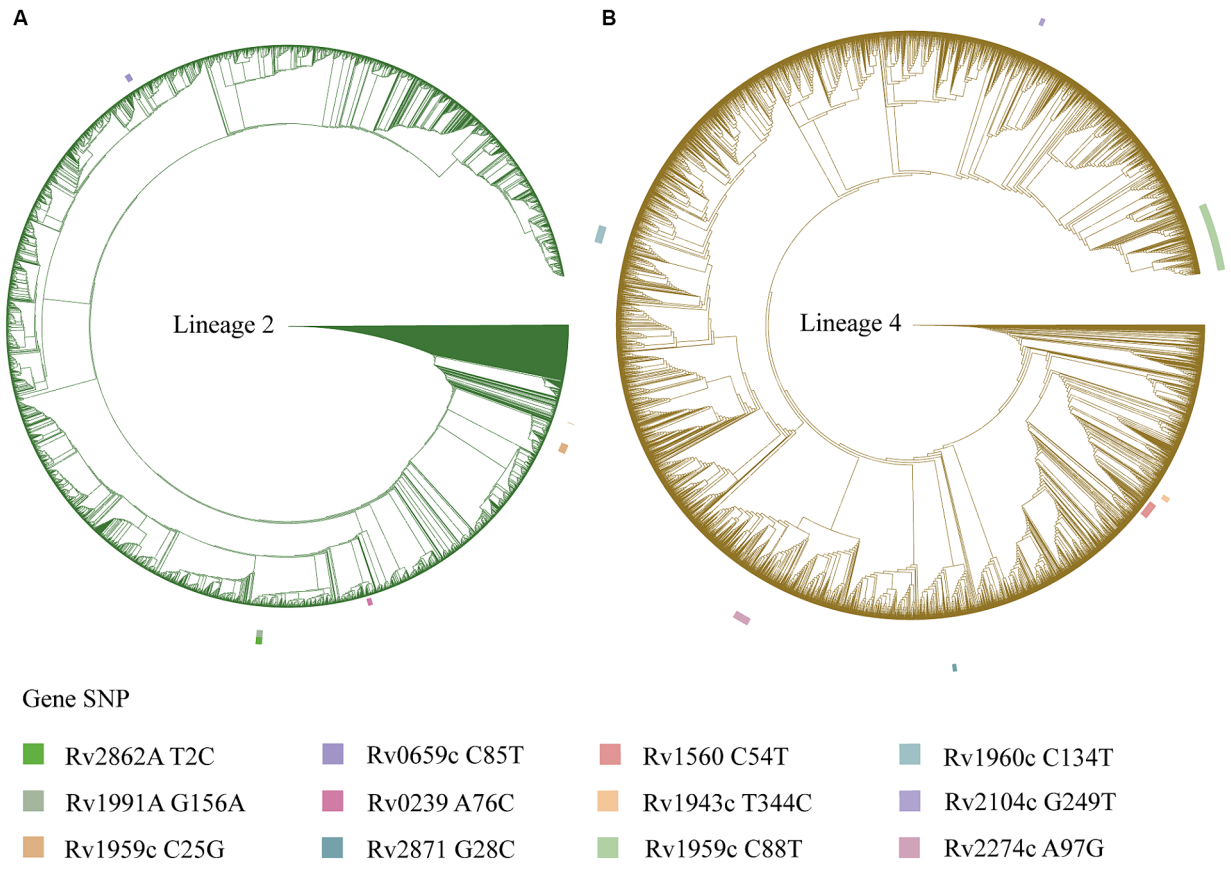

FIGURE 2
A phylogenetic tree is depicted for the *Mycobacterium tuberculosis* isolates, with the outer circle indicating mutation sites of the toxin-antitoxin system genes. **(A)** Phylogenetic tree for the *Mycobacterium tuberculosis* isolates of lineage 2. **(B)** Phylogenetic tree for the *Mycobacterium tuberculosis* isolates of lineage 4.

In our study, we have found a strong association between SNPs in the *VapB* antitoxin-related genes and the transmission of *M. tuberculosis*. Specifically, we identified several significant SNPs that were linked to transmission, including *vapB1* G34A, *vapB24* A76C, *vapB31* T112C, *vapB14* A29G, and *vapB15* (T6C, G237A). We observed that *vapB24* A76C and *vapB23* T2C were particularly associated with transmission, especially in lineage 2. Additionally, *vapB2* T171C, *vapB11* C54T, *vapB14* A29G, *vapB15* G237A, *vapB17* G213C, and *vapB20* A54C were significantly related to transmission, especially in lineage 4. Furthermore, we found that *vapB43* G28C was associated with transmission in lineage 4, while *vapB6* A29C, *vapB31* T112C, and *vapB37* G205C were correlated with cross-country and cross-regional transmission. We also found that *vapB1* G34A, *vapB11* C54T, *vapB14* A29G, *vapB15* T6C, and *vapB46* G70A were related to clade size. The *VapBC* system is crucial for regulating the behavior and adaptation of *M. tuberculosis* under diverse environmental stresses. It comprises stable *VapC* toxins and labile *VapB* antitoxins, whose interplay is essential for bacterial growth, survival, and response to stress conditions (Robson et al., 2009; Winther and Gerdes, 2011). During periods of stress, antitoxin molecules are degraded, leading to the release of toxins, such as *VapC*, through their RNase activity (Min et al., 2012). Consequently, these toxins inhibit or slow down cellular metabolism, providing a survival advantage to the bacterium during adverse conditions. The delicate balance between *VapB* antitoxins and *VapC* toxins is crucial for maintaining bacterial homeostasis and ensuring appropriate responses to external stimuli (McKenzie et al., 2012). Overall, our study provides compelling evidence for the significant association between SNPs in *VapB* antitoxin-related genes and *M. tuberculosis* transmission. These findings shed light on the intricate role of the *VapBC* toxin-antitoxin system in regulating bacterial behavior and underscore the importance of genetic variations within this system in shaping transmission dynamics.

Our study has revealed the association between SNPs in other TA system genes and the transmission of *M. tuberculosis*. Specifically, we focused on the *MazEF* family, which consists of nine TA systems encoded in an operon (Ahmed et al., 2022). We found a close connection between the *mazE6* G156A and *mazF2* C85T gene polymorphisms and the transmission clusters, particularly within lineage 2. These variants exhibited significant correlations with the formation and expansion of transmission clusters. However, *mazE6* G156A is a synonymous mutation (Arg52Arg), which does not directly alter the protein's function but may still affect the protein through other mechanisms. For example, in certain situations, synonymous mutations can lead to changes in transcription regulatory elements, thereby influencing gene expression levels. However, further research is needed to confirm these effects. Similarly, the *mazF2* C85T variant may alter the stability of the *MazF* and modulate the delicate balance between toxin and antitoxin

TABLE 2 Positive correlation between toxin-antitoxin system gene mutations and transmission clusters.

Rv number	Gene	Position	SNP	Amino acid changes	Generalized linear mixed model		Random forest	Gradient boosted classification tree
					p value	OR (95%CI)	Importance score	Importance score
Rv0064A	vapB1	71,622	G34A	Asp12Asn	0.001	3.241 (1.596–6.581)	0.00289	0.00120
Rv0239	vapB24	289,179	A76C	Thr26Pro	0.001	18.331 (3.116–107.848)	0.00364	0.00530
Rv0298	-	363,464	G213A	Arg71Arg	0.041	4.802 (1.068–21.597)	0.00868	0
Rv0300	vapB2	363,996	T171C	Gly57Gly	0.009	3.387 (1.354–8.476)	0.00313	0.00120
Rv0659c	mazF2	754,909	C85T	Arg29Cys	0.015	3.678 (1.283–10.545)	0.00296	0.00040
Rv0660c	mazE2	755,122	G104A	Arg35His	2.82E-04	4.474 (1.993–10.045)	0.01997	0.03120
Rv0748	vapB31	841,058	T112C	Phe38Leu	0.01	19.632 (2.051–187.954)	0.00189	0.00190
Rv1103c	mazE3	1,231,236	G56A	Gly19Asp	0.031	4.242 (1.139–15.798)	0.00030	0
Rv1247c	relB	1,389,019	T226A	Phe76Ile	0.006	8.273 (1.827–37.465)	0.00072	0.00270
Rv1560	vapB11	1,764,808	C54T	Ala18Ala	4.78E-08	15.895 (5.888–42.909)	0.00348	0.00100
Rv1943c	mazE5	2,195,004	T344C	Leu115Pro	0.006	17.911 (2.282–140.553)	0.00319	0.00250
Rv1952	vapB14	2,200,754	A29G	Lys10Arg	0.001	2.262 (1.383–3.7)	0.00959	0.00360
Rv1959c	parE1	2,203,875	C103T	Leu35Leu	0.004	2.254 (1.304–3.895)	0.00730	0.00520
Rv1959c	parE1	2,203,890	C88T	Gln30*	4.27E-12	8.558 (4.662–15.709)	0.01542	0.01690
Rv1960c	parD1	2,204,092	C134T	Thr45Ile	1.08E-04	4.986 (2.211–11.244)	0.00559	0.00600
Rv1991A	mazE6	2,234,736	G156A	Arg52Arg	8.65E-05	9.605 (3.104–29.72)	0.00468	0.00500
Rv2009	vapB15	2,258,035	T6C	Tyr2Tyr	4.42E-05	4.692 (2.235–9.853)	0.00167	0.00340
Rv2009	vapB15	2,258,266	G237A	Glu79Glu	0.014	2.765 (1.231–6.207)	0.00385	0.00170
Rv2142c	parE2	2,402,463	C48G	Phe16Leu	7.44E-06	6.461 (2.857–14.612)	0.00572	0.00910
Rv2142A	parD2	2,402,527	A196G	Ile66Val	0.011	3.531 (1.337–9.327)	0.00143	0.00040
Rv2274c	mazF8	2,546,709	A97G	Ile33Val	4.77E-07	21.31 (6.478–70.103)	0.00772	0.01290
Rv2526	vapB17	2,851,303	G213C	Glu71Asp	0.033	3.93 (1.119–13.795)	0.00187	0.00090
Rv2550c	vapB20	2,870,311	A54C	Glu18Asp	0.044	3.111 (1.033–9.375)	0.00220	0.00270
Rv2654c	-	2,977,083	T152C	Val51Ala	0.049	2.795 (1.002–7.795)	0.00151	0.00030
Rv2862A	vapB23	3,174,748	T2C	Ile1?	0.005	2.271 (1.273–4.05)	0.00280	0.00130
Rv2871	vapB43	3,183,165	G28C	Glu10Gln	0.005	6.967 (1.816–26.73)	0.00277	0
Rv3385c	vapB46	3,799,874	G70A	Ala24Thr	0.002	2.74 (1.427–5.263)	0.00203	0.00140

OR, odds ratio; CI, confidence interval. *Represents a stop SNP.

interactions (Leplae et al., 2011). Furthermore, our study identified a strong correlation between the *mazE2* G104A, *mazE5* T344C, and *mazF8* A97G gene polymorphisms and the transmission clusters, especially within lineage 4 and clade size. While it's plausible that these genetic variations influence the *MazEF* system activity, stability, and domain structure, our ability to fully elucidate these mechanisms is currently limited. Therefore, it's crucial to interpret these functional implications cautiously and consider other potential contributory factors to *M. tuberculosis* transmission. Furthermore, no SNPs in the *MazEF* system were found to be associated with cross-country and cross-regional transmission of *M. tuberculosis* in our study. Future investigations should aim to provide a more comprehensive understanding of these effects, confirm these hypotheses, and uncover the precise impact of these mutations on the dynamics of *M. tuberculosis* transmission.

The *ParDE* toxin-antitoxin system in *M. tuberculosis* plays a crucial role in bacterial transmission dynamics. Our research has identified specific genetic variations in the parE and *parD* genes, such as *parE1* C88T, *parE2* C48G, *parE1* C103T, *parD2* A196G, *parE1* C25G, and *parD1* C134T, that are closely linked to transmission clusters, particularly within lineage 4 and lineage 2. These genetic variants impact cross-country and cross-regional transmissions, highlighting the significance of the *ParD*E system in the spread of *M. tuberculosis*. Variations in the *parD* gene, including those involving *Rv2142A* (*parD2*) and *Rv1960c* (*parD1*), can modify the activity and regulatory mechanisms of the *ParD* antitoxin. Similarly, variations in the *parE* gene, particularly those affecting *Rv1959c* (*parE1*), influence the function and stability of the *ParE* toxin, thus impacting its interaction with the *ParE* antitoxin (Xu et al., 2018). Understanding these genetic interactions is crucial for deciphering *M. tuberculosis*

TABLE 3 The performance of various models for discriminating clustered isolates from non-clustered isolates.

Parameters	Training set (*n* = 9,462, 3,998 clustered isolates, 5,464 non-clustered isolates)		Test set (*n* = 4,056, 1719 clustered isolates, 2,337 non-clustered isolates)	
	Random forest	Gradient boosted classification tree	Random forest	Gradient boosted classification tree
Kappa	0.447	0.43	0.414	0.371
AUC	0.801	0.782	0.777	0.752
(95% CI)	(0.793, 0.809)	(0.774, 0.79)	(0.764, 0.79)	(0.739, 0.765)
Sensitivity	0.625	0.614	0.602	0.586
(95% CI)	(0.615, 0.635)	(0.604, 0.624)	(0.587, 0.617)	(0.571, 0.601)
Specificity	0.815	0.809	0.804	0.779
(95% CI)	(0.807, 0.823)	(0.801, 0.817)	(0.792, 0.816)	(0.766, 0.792)
PPV	0.712	0.701	0.694	0.663
(95% CI)	(0.703, 0.721)	(0.692, 0.71)	(0.68, 0.708)	(0.648, 0.678)
NPV	0.748	0.742	0.733	0.717
(95% CI)	(0.739, 0.757)	(0.733, 0.751)	(0.719, 0.747)	(0.703, 0.731)
PLR	2.826	2.717	2.6	2.346
(95% CI)	(2.811, 2.841)	(2.702, 2.732)	(2.577, 2.623)	(2.322, 2.37)
NIR	0.354	0.368	0.385	0.426
(95% CI)	(0.321, 0.387)	(0.335, 0.401)	(0.336, 0.434)	(0.38, 0.472)
Accuracy	0.735	0.727	0.719	0.697
(95% CI)	(0.726, 0.744)	(0.718, 0.736)	(0.705, 0.733)	(0.683, 0.711)

AUC, area under the curve; PPV, positive predictive value; NPV, negative predictive value; PLR, positive likelihood ratio; NLR, negative likelihood ratio; CI, confidence.

transmission dynamics and developing targeted interventions to effectively combat tuberculosis. Additionally, our research has identified a unique SNP, T226A, in the *relB* gene that is associated with transmission clusters in *M. tuberculosis*. This genetic variation further adds to the complexity of bacterial transmission dynamics, highlighting the intricate interplay between genetic factors and the spread of *M. tuberculosis*.

In terms of drug development and therapeutic interventions, our research findings could potentially have significant implications. The diverse functions of TA systems suggest potential targets for novel therapeutic strategies in *M. tuberculosis*. Understanding the relationship between genetic variations and functional consequences within these TA systems might help us discover new methods to disrupt or modulate their activity, thereby affecting the survival and transmission dynamics of the bacterium. Firstly, interventions targeting specific SNPs in TA systems such as *VapBC*, *MazEF*, *ParD*E, and *RelB*E could possibly directly alter the stability and activity of their toxins or antitoxins, thus impacting the growth, survival, and adaptability of *M. tuberculosis* (Robson et al., 2009; Leplae et al., 2011; Winther and Gerdes, 2011; McKenzie et al., 2012; Ahmed et al., 2022). The SNPs we discovered, including *vapB24* A76C and *vapB23* T2C, have the potential to serve as genetic markers for targeted drug design, allowing for more personalized treatment approaches. Additionally, mutations like *parE1* C88T, *parE2* C48G, and *parE1* C103T show associations with cross-national and cross-regional transmissions of *M. tuberculosis*, which could aid in the development of more effective treatment plans to reduce global transmission. However, it's important to note that while these genetic insights hold potential, they still require experimental validation to confirm their clinical significance and functional implications. Each mutation may lead to different functional impacts, and there might be other complexities involved, such as drug tolerance or adaptability of the bacterium under different environmental conditions. Therefore, further research is needed to delve deeper into the functional impacts of these genetic variations and precisely determine their roles in new drug development and treatment strategies. It is crucial to validate these findings through rigorous experimental studies and clinical trials before implementing them in clinical practice. Future research should aim to elucidate the specific mechanisms underlying these genetic variations and their contributions to drug response and transmission dynamics. By gaining a better understanding of the functional implications, we can more accurately tailor treatment strategies and contribute to the development of more targeted and effective interventions.

Our findings emphasize that both synonymous and non-synonymous mutations can influence the transmission of *M. tuberculosis*, suggesting that synonymous mutations in TA system genes are not universally neutral, in line with prior research by Shen et al. (2022). We believe that synonymous mutations may affect mRNA stability, splicing, or secondary structure formation. Changes in these regulatory elements can influence gene expression patterns and protein folding, thereby impacting bacterial adaptability and transmission capacity. Additionally, synonymous mutations may be part of a compensatory mechanism. While synonymous mutations themselves may not directly provide selective advantages, they may be associated with compensatory changes in other regions of the genome. These compensatory mutations could restore proper

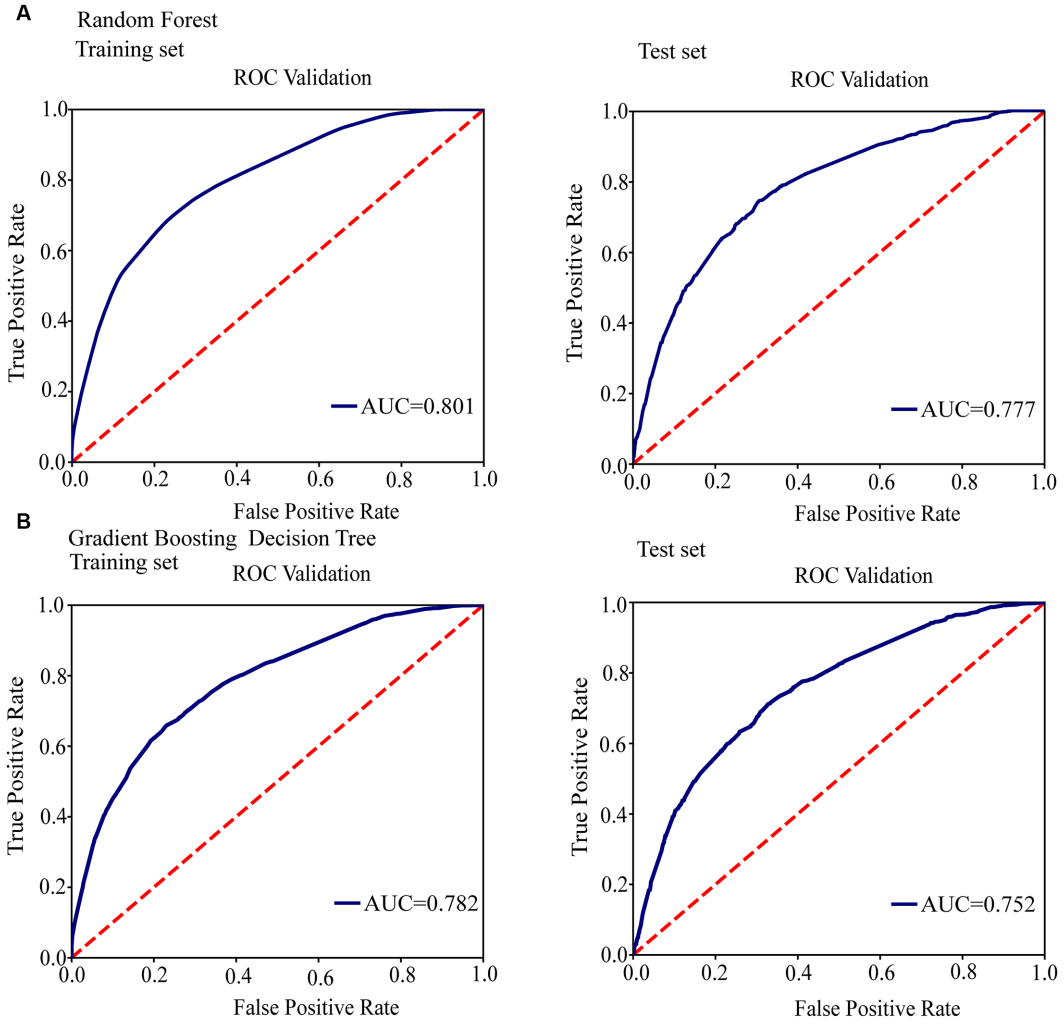

FIGURE 3
Conduct ROC curve analysis to evaluate the performance of models for the relationship between mutations in toxin-antitoxin system genes and transmission clusters. **(A)** ROC analysis showing the performance of the random forest model. **(B)** ROC analysis showing the performance of the gradient boosting decision tree.

interactions between proteins, maintain enzyme activity, or optimize cellular functions affected by primary mutations, ultimately enhancing transmission capacity. Although the specific mechanisms and advantages of synonymous mutations in tuberculosis transmission are not yet fully understood, we cannot overlook their potential significance. Future research should consider the functional consequences of synonymous mutations and explore their interactions with other genetic factors, including non-synonymous mutations, drug resistance mutations, or virulence determinants. In our study, we combined local and global datasets to increase sample size for robust analysis of *M. tuberculosis* genetic variations. This approach helped identify shared and distinct variants across regions, enhancing our understanding of global pathogen diversity. Despite potential limitations such as variability from different protocols and sequencing technologies, stringent quality control measures, including SNP filtering within repetitive regions, were applied to minimize biases. Our novel findings contribute valuable insights into global *M. tuberculosis* genetic characteristics, advancing knowledge on tuberculosis pathogenesis and evolution. In future research, separate and comparative analyses of local and global data can be considered to highlight region-specific variations.

In our study, we investigated the impact of mutations in TA system genes on tuberculosis transmission. However, it is crucial to acknowledge that these correlations alone do not establish a causal relationship and should be interpreted with caution. Our modeling approach has limitations, notably in addressing potential confounding factors, such as population mobility, social networks, and inter-regional interactions. These elements may influence *M. tuberculosis* transmission but were not fully integrated into our models. We recognize that our primary focus on mutations within TA system genes may have led us to overlook other significant genetic influences, including SNPs related to drug resistance mutations or virulence determinants. While our findings contribute to the growing body of knowledge regarding the impact of toxin-antitoxin system gene mutations on tuberculosis transmission, further research is necessary to explore these intersections and understand their functional significance in detail. Limitations also arise from the sheer number of genes and computational resources required, which restricted our

10.3389/fmicb.2024.1398886

TABLE 4 Positive correlation between toxin-antitoxin system gene mutations and transmission clusters of lineage4.

Rv number	Gene	Position	SNP	Amino acid changes	Generalized linear mixed model		Random forest	Gradient boosted classification tree
					p value	OR (95%CI)	Importance score	Importance score
Rv0064A	vapB1	71,622	G34A	Asp12Asn	0.005	2.806 (1.371–5.741)	0.00503	0
Rv0300	vapB2	363,996	T171C	Gly57Gly	0.024	2.818 (1.144–6.94)	0.00791	0.00400
Rv0660c	mazE2	755,122	G104A	Arg35His	0.006	3.115 (1.378–7.038)	0.04155	0.09480
Rv1560	vapB11	1,764,808	C54T	Ala18Ala	6.78E-06	10.003 (3.669–27.271)	0.00691	0.00690
Rv1943c	mazE5	2,195,004	T344C	Leu115Pro	0.005	19.158 (2.435–150.733)	0.00847	0.00890
Rv1952	vapB14	2,200,754	A29G	Lys10Arg	0.002	2.219 (1.357–3.63)	0.02088	0.00870
Rv1959c	parE1	2,203,890	C88T	Gln30*	5.10E-13	10.267 (5.457–19.315)	0.03006	0.05750
Rv1960c	parD1	2,204,092	C134T	Thr45Ile	0.001	4.27 (1.862–9.791)	0.01080	0.00620
Rv2009	vapB15	2,258,035	T6C	Tyr2Tyr	0.04	2.218 (1.036–4.753)	0.00410	0
Rv2009	vapB15	2,258,266	G237A	Glu79Glu	0.008	2.993 (1.333–6.721)	0.00346	0.00770
Rv2104c	vapB37	2,364,533	G249T	Gly83Gly	0.006	8.238 (1.804–37.608)	0.00494	0
Rv2142c	parE2	2,402,463	C48G	Phe16Leu	0.005	3.301 (1.438–7.575)	0.00375	0.00340
Rv2274c	mazF8	2,546,709	A97G	Ile33Val	0.001	29.592 (3.984–219.821)	0.01375	0.02100
Rv2526	vapB17	2,851,303	G213C	Glu71Asp	0.037	3.828 (1.087–13.487)	0.00452	0.00050
Rv2550c	vapB20	2,870,311	A54C	Glu18Asp	0.02	3.792 (1.228–11.705)	0.00432	0.00080
Rv2871	vapB43	3,183,165	G28C	Glu10Gln	0.004	7.272 (1.882–28.103)	0.00923	0.00140
Rv3385c	vapB46	3,799,874	G70A	Ala24Thr	0.041	2.014 (1.03–3.937)	0.00303	0.00000

OR, odds ratio; CI, confidence interval. *Represents a stop SNP.

ability to analyze SNPs beyond the scope of our current investigation. Moreover, we lack a clear understanding of the cross-interactions and mutual regulation among the TA systems of *M. tuberculosis*, adding another layer of complexity to our study. Additionally, uncertainties inherent in the phylogenetic inference method used, such as homoplasy or recombination events, can present challenges when accurately determining evolutionary relationships. Therefore, future research should consider alternative methods to validate these findings and develop a more nuanced understanding of tuberculosis transmission. Further experimental validation is necessary to confirm the specific impact of TA system gene mutations. Future investigations should focus on refining our models to account for potential biases or shortcomings, and expanding research scope to explore the functional significance of these mutations and their direct influence on tuberculosis transmission.

We also discuss the limitations of using H37Rv as a single reference genome for analyzing *M. tuberculosis* WGS data, particularly regarding virulence and transmission. Recent studies suggest that relying solely on H37Rv may not fully capture the virulence characteristics of *M. tuberculosis*. H37Rv, commonly used as a reference genome in molecular epidemiology and drug resistance studies, does not represent the genetic diversity and variations present across all *M. tuberculosis* strains. Polymorphic loci involving genes associated with pathogenicity and host immune response, such as phospholipase C, membrane lipoproteins, adenylate cyclase gene family members, and PE/PPE gene family members, show significant differences between H37Rv and clinical isolates. Several gene families, including PE/PPE, exhibit higher substitution frequencies compared to the entire genome. Widespread genetic variability is observed at these polymorphic loci among *M. tuberculosis* clinical isolates (Fleischmann et al., 2002; O'Toole and Gautam, 2017). Phylogenetic and epidemiological analyses reveal independent occurrences of these polymorphisms, suggesting selective pressures driving these changes. Future research should incorporate genome sequences of additional reference strains, especially those directly obtained from clinical isolates, to comprehensively understand factors related to *M. tuberculosis* virulence and enable further investigations. For drug resistance inference, our analysis primarily utilized the TBProfiler platform. While incorporating additional tools/methods such as PhyResSE or bioinformatic SNP analysis could enhance robustness, resource constraints limited their implementation in this study. Thus, our results should be interpreted within the context of utilizing TBProfiler alongside the WHO-endorsed catalog. Future studies with expanded resources could consider alternative tools/methods for validation and complementation.

5 Conclusion

The results of this study suggest that mutations in toxin-antitoxin genes may increase the risk of *M. tuberculosis* transmission, underscoring the significance of conducting further research to explore the impact of these mutations on *M. tuberculosis* control and transmission. These findings offer new insights into the development of drug treatment strategies against tuberculosis.

Data availability statement

The whole genome sequences have been submitted to the NCBI under the accession number PRJNA1002108.

Author contributions

YH: Conceptualization, Formal analysis, Software, Writing – original draft, Writing – review & editing. YiL: Conceptualization, Formal analysis, Methodology, Writing – review & editing. NT: Conceptualization, Formal analysis, Investigation, Project administration, Software, Validation, Writing – review & editing. XK: Conceptualization, Data curation, Formal analysis, Investigation, Methodology, Software, Validation, Writing – original draft. YamL: Conceptualization, Data curation, Formal analysis, Investigation, Methodology, Project administration, Software, Supervision, Validation, Writing – review & editing. YaoL: Data curation, Formal analysis, Methodology, Project administration, Supervision, Validation, Writing – review & editing. HL: Conceptualization, Data curation, Funding acquisition, Investigation, Resources, Visualization, Writing – original draft, Writing – review & editing. ZW: Conceptualization, Data curation, Formal analysis, Funding acquisition, Investigation, Project administration, Resources, Software, Supervision, Visualization, Writing – original draft.

Funding

The author(s) declare that financial support was received for the research, authorship, and/or publication of this article. This study was supported by grants from the Science & Technology Fundamental Resources Investigation Program (Grant no. 2022FY102001), the Shandong Provincial Natural Science Foundation (No. ZR2020KH013; No. ZR2021MH006), the Department of Science & Technology of Shandong Province (CN) (No. 2007GG30002033; No. 2017GSF218052), and the Jinan Science and Technology Bureau (CN) (No. 201704100).It is important to note that the funding bodies provided financial support for the study but were not involved in the study design, data collection, analysis, interpretation, or manuscript writing process.

Acknowledgments

We thank Shandong Public Health Clinical Research Center and Weifang Respiratory Clinical Hospital for providing us with the clinical sample data. Additionally, we extend our thanks to all the authors who have shared their sequence datasets on NCBI.

Conflict of interest

The authors declare that the research was conducted in the absence of any commercial or financial relationships that could be construed as a potential conflict of interest.

Publisher's note

All claims expressed in this article are solely those of the authors and do not necessarily represent those of their affiliated organizations, or those of the publisher, the editors and the reviewers. Any product that may be evaluated in this article, or claim that may be made by its manufacturer, is not guaranteed or endorsed by the publisher.

Supplementary material

The Supplementary material for this article can be found online at:https://www.frontiersin.org/articles/10.3389/fmicb.2024.1398886/full#supplementary-material

References

Agarwal, G., Saade, S., Shahid, M., Tester, M., and Sun, Y. (2019). Quantile function modeling with application to salinity tolerance analysis of plant data. *BMC Plant Biol.* 19:526. doi: 10.1186/s12870-019-2039-9

Ahmed, S., Chattopadhyay, G., Manjunath, K., Bhasin, M., Singh, N., Rasool, M., et al. (2022). Combining cysteine scanning with chemical labeling to map protein-protein interactions and infer bound structure in an intrinsically disordered region. *Front. Mol. Biosci.* 9:997653. doi: 10.3389/fmolb.2022.997653

Aizenman, E., Engelberg-Kulka, H., and Glaser, G. (1996). An *Escherichia coli* chromosomal "addiction module" regulated by guanosine [corrected] 3′,5′-bispyrophosphate: a model for programmed bacterial cell death. *Proc. Natl. Acad. Sci. USA* 93, 6059–6063. doi: 10.1073/pnas.93.12.6059

Bi, X., Xu, Q., Luo, X., Sun, Q., and Wang, Z. (2018). Weighted random support vector machine clusters analysis of resting-state fMRI in mild cognitive impairment. *Front. Psych.* 9:340. doi: 10.3389/fpsyt.2018.00340

Chen, X., He, G., Wang, S., Lin, S., Chen, J., and Zhang, W. (2019). Evaluation of whole-genome sequence method to diagnose resistance of 13 anti-tuberculosis drugs and characterize resistance genes in clinical multi-drug resistance *Mycobacterium tuberculosis* isolates from China. *Front. Microbiol.* 10:1741. doi: 10.3389/fmicb.2019.01741

Chiner-Oms, Á., Sánchez-Busó, L., Corander, J., Gagneux, S., Harris, S. R., Young, D., et al. (2019). Genomic determinants of speciation and spread of the *Mycobacterium tuberculosis* complex. *Sci. Adv.* 5:eaaw3307. doi: 10.1126/sciadv.aaw3307

Cingolani, P., Platts, A., Wang, L. L., Coon, M., Nguyen, T., Wang, L., et al. (2012). A program for annotating and predicting the effects of single nucleotide polymorphisms, SnpEff: SNPs in the genome of *Drosophila melanogaster* strain w1118; iso-2; iso-3. *Fly* 6, 80–92. doi: 10.4161/fly.19695

Coll, F., McNerney, R., Guerra-Assunção, J. A., Glynn, J. R., Perdigão, J., Viveiros, M., et al. (2014). A robust SNP barcode for typing *Mycobacterium tuberculosis* complex strains. *Nat. Commun.* 5:4812. doi: 10.1038/ncomms5812

Coll, F., Phelan, J., Hill-Cawthorne, G. A., Nair, M. B., Mallard, K., Ali, S., et al. (2018). Genome-wide analysis of multi- and extensively drug-resistant *Mycobacterium tuberculosis*. *Nat. Genet.* 50, 307–316. doi: 10.1038/s41588-017-0029-0

Dai, Z., Wu, T., Xu, S., Zhou, L., Tang, W., Hu, E., et al. (2022). Characterization of toxin-antitoxin systems from public sequencing data: a case study in *Pseudomonas aeruginosa*. *Front. Microbiol.* 13:951774. doi: 10.3389/fmicb.2022.951774

Fineran, P. C., Blower, T. R., Foulds, I. J., Humphreys, D. P., Lilley, K. S., and Salmond, G. P. C. (2009). The phage abortive infection system, ToxIN, functions as a protein–RNA toxin–antitoxin pair. *Proc. Natl. Acad. Sci. USA* 106, 894–899. doi: 10.1073/pnas.0808832106

Fleischmann, R. D., Alland, D., Eisen, J. A., Carpenter, L., White, O., Peterson, J., et al. (2002). Whole-genome comparison of *Mycobacterium tuberculosis* clinical and laboratory strains. *J. Bacteriol.* 184, 5479–5490. doi: 10.1128/JB.184.19.5479-5490.2002

Guo, Y., Yao, J., Sun, C., Wen, Z., and Wang, X. (2016). Characterization of the Deep-Sea Streptomyces sp. SCSIO 02999 derived VapC/VapB toxin-antitoxin system in *Escherichia coli*. *Toxins* 8:195. doi: 10.3390/toxins8070195

Hicks, N. D., Yang, J., Zhang, X., Zhao, B., Grad, Y. H., Liu, L., et al. (2018). Clinically prevalent mutations in *Mycobacterium tuberculosis* alter propionate metabolism and

mediate multidrug tolerance. *Nat. Microbiol.* 3, 1032–1042. doi: 10.1038/s41564-018-0218-3

Huang, H., Ding, N., Yang, T., Li, C., Jia, X., Wang, G., et al. (2019). Cross-sectional whole-genome sequencing and epidemiological study of multidrug-resistant *Mycobacterium tuberculosis* in China. *Clin. Infect. Dis.* 69, 405–413. doi: 10.1093/cid/ciy883

Jajou, R., Kohl, T. A., Walker, T., Norman, A., Cirillo, D. M., Tagliani, E., et al. (2019). Towards standardisation: comparison of five whole genome sequencing (WGS) analysis pipelines for detection of epidemiologically linked tuberculosis cases. *Euro Surveill.* 24:1900130. doi: 10.2807/1560-7917.ES.2019.24.50.1900130

Jiang, Q., Liu, Q., Ji, L., Li, J., Zeng, Y., Meng, L., et al. (2020). Citywide transmission of multidrug-resistant tuberculosis under China's rapid urbanization: a retrospective population-based genomic spatial epidemiological study. *Clin. Infect. Dis.* 71, 142–151. doi: 10.1093/cid/ciz790

Kim, D.-H., Kang, S.-M., Park, S. J., Jin, C., Yoon, H.-J., and Lee, B.-J. (2018). Functional insights into the *Streptococcus pneumoniae* HicBA toxin–antitoxin system based on a structural study. *Nucleic Acids Res.* 46, 6371–6386. doi: 10.1093/nar/gky469

Koster, K. J., Largen, A., Foster, J. T., Drees, K. P., Qian, L., Desmond, E., et al. (2018). Genomic sequencing is required for identification of tuberculosis transmission in Hawaii. *BMC Infect. Dis.* 18:608. doi: 10.1186/s12879-018-3502-1

Leplae, R., Geeraerts, D., Hallez, R., Guglielmini, J., Drèze, P., and Van Melderen, L. (2011). Diversity of bacterial type II toxin–antitoxin systems: a comprehensive search and functional analysis of novel families. *Nucleic Acids Res.* 39, 5513–5525. doi: 10.1093/nar/gkr131

Li, H., Handsaker, B., Wysoker, A., Fennell, T., Ruan, J., Homer, N., et al. (2009). 1000 genome project data processing subgroup. The sequence alignment/map format and SAMtools. *Bioinformatics* 25, 2078–2079. doi: 10.1093/bioinformatics/btp352

Liu, F., Zhang, Y., Zhang, L., Li, Z., Fang, Q., Gao, R., et al. (2019). Systematic comparative analysis of single-nucleotide variant detection methods from single-cell RNA sequencing data. *Genome Biol.* 20:242. doi: 10.1186/s13059-019-1863-4

Liu, Q., Ma, A., Wei, L., Pang, Y., Wu, B., Luo, T., et al. (2018). China's tuberculosis epidemic stems from historical expansion of four strains of *Mycobacterium tuberculosis*. *Nat. Ecol. Evol.* 2, 1982–1992. doi: 10.1038/s41559-018-0680-6

Lobato-Márquez, D., Díaz-Orejas, R., and García-Del, P. F. (2016). Toxin-antitoxins and bacterial virulence. *FEMS Microbiol. Rev.* 40, 592–609. doi: 10.1093/femsre/fuw022

Luo, T., Comas, I., Luo, D., Lu, B., Wu, J., Wei, L., et al. (2015). Southern east Asian origin and coexpansion of *Mycobacterium tuberculosis* Beijing family with Han Chinese. *Proc. Natl. Acad. Sci. USA* 112, 8136–8141. doi: 10.1073/pnas.1424063112

Luo, Y., Xue, Y., Song, H., Tang, G., Liu, W., Bai, H., et al. (2022). Machine learning based on routine laboratory indicators promoting the discrimination between active tuberculosis and latent tuberculosis infection. *J. Infect.* 84, 648–657. doi: 10.1016/j.jinf.2021.12.046

Magnuson, R. D. (2007). Hypothetical functions of toxin-antitoxin systems. *J. Bacteriol.* 189, 6089–6092. doi: 10.1128/JB.00958-07

McKenzie, J. L., Robson, J., Berney, M., Smith, T. C., Ruthe, A., Gardner, P. P., et al. (2012). A VapBC toxin-antitoxin module is a posttranscriptional regulator of metabolic flux in mycobacteria. *J. Bacteriol.* 194, 2189–2204. doi: 10.1128/JB.06790-11

Merfa, M. V., Niza, B., Takita, M. A., and De Souza, A. A. (2016). The MqsRA toxin-antitoxin system from *Xylella fastidiosa* plays a key role in bacterial fitness, pathogenicity, and Persister cell formation. *Front. Microbiol.* 7:904. doi: 10.3389/fmicb.2016.00904

Min, A. B., Miallau, L., Sawaya, M. R., Habel, J., Cascio, D., and Eisenberg, D. (2012). The crystal structure of the Rv0301-Rv0300 VapBC-3 toxin—antitoxin complex from *M. tuberculosis* reveals a mg $^{2+}$ ion in the active site and a putative RNA-binding site. *Protein Sci.* 21, 1754–1767. doi: 10.1002/pro.2161

Nguyen, L.-T., Schmidt, H. A., von Haeseler, A., and Minh, B. Q. (2015). IQ-TREE: a fast and effective stochastic algorithm for estimating maximum-likelihood phylogenies. *Mol. Biol. Evol.* 32, 268–274. doi: 10.1093/molbev/msu300

O'Toole, R. F., and Gautam, S. S. (2017). Limitations of the *Mycobacterium tuberculosis* reference genome H37Rv in the detection of virulence-related loci. *Genomics* 109, 471–474. doi: 10.1016/j.ygeno.2017.07.004

Ogura, T., and Hiraga, S. (1983). Mini-F plasmid genes that couple host cell division to plasmid proliferation. *Proc. Natl. Acad. Sci. USA* 80, 4784–4788. doi: 10.1073/pnas.80.15.4784

Page, R., and Peti, W. (2016). Toxin-antitoxin systems in bacterial growth arrest and persistence. *Nat. Chem. Biol.* 12, 208–214. doi: 10.1038/nchembio.2044

Phelan, J. E., O'Sullivan, D. M., Machado, D., Ramos, J., Oppong, Y. E. A., Campino, S., et al. (2019). Integrating informatics tools and portable sequencing technology for rapid detection of resistance to anti-tuberculous drugs. *Genome Med.* 11:41. doi: 10.1186/s13073-019-0650-x

Ramage, H. R., Connolly, L. E., and Cox, J. S. (2009). Comprehensive functional analysis of *Mycobacterium tuberculosis* toxin-antitoxin systems: implications for pathogenesis, stress responses, and evolution. *PLoS Genet.* 5:e1000767. doi: 10.1371/journal.pgen.1000767

Robson, J., McKenzie, J. L., Cursons, R., Cook, G. M., and Arcus, V. L. (2009). The vapBC operon from *Mycobacterium smegmatis* is an autoregulated toxin–antitoxin module that controls growth via inhibition of translation. *J. Mol. Biol.* 390, 353–367. doi: 10.1016/j.jmb.2009.05.006

Schippers, A., Neretin, L. N., Kallmeyer, J., Ferdelman, T. G., Cragg, B. A., Parkes, R. J., et al. (2005). Prokaryotic cells of the deep sub-seafloor biosphere identified as living bacteria. *Nature* 433, 861–864. doi: 10.1038/nature03302

Schuster, C. F., and Bertram, R. (2013). Toxin-antitoxin systems are ubiquitous and versatile modulators of prokaryotic cell fate. *FEMS Microbiol. Lett.* 340, 73–85. doi: 10.1111/1574-6968.12074

Seto, J., Wada, T., Suzuki, Y., Ikeda, T., Mizuta, K., Yamamoto, T., et al. (2017). *Mycobacterium tuberculosis* transmission among elderly persons, Yamagata prefecture, Japan, 2009–2015. *Emerg. Infect. Dis.* 23, 448–455. doi: 10.3201/eid2303.161571

Sharma, A., Sagar, K., Chauhan, N. K., Venkataraman, B., Gupta, N., Gosain, T. P., et al. (2021). HigB1 toxin in *Mycobacterium tuberculosis* is upregulated during stress and required to establish infection in Guinea pigs. *Front. Microbiol.* 12:748890. doi: 10.3389/fmicb.2021.748890

Shen, X., Song, S., Li, C., and Zhang, J. (2022). Synonymous mutations in representative yeast genes are mostly strongly non-neutral. *Nature* 606, 725–731. doi: 10.1038/s41586-022-04823-w

Tandon, H., Sharma, A., Wadhwa, S., Varadarajan, R., Singh, R., Srinivasan, N., et al. (2019). Bioinformatic and mutational studies of related toxin–antitoxin pairs in *Mycobacterium tuberculosis* predict and identify key functional residues. *J. Biol. Chem.* 294, 9048–9063. doi: 10.1074/jbc.RA118.006814

Walker, T. M., Ip, C. L., Harrell, R. H., Evans, J. T., Kapatai, G., Dedicoat, M. J., et al. (2013). Whole-genome sequencing to delineate *Mycobacterium tuberculosis* outbreaks: a retrospective observational study. *Lancet Infect. Dis.* 13, 137–146. doi: 10.1016/S1473-3099(12)70277-3

Walker, T. M., Miotto, P., Köser, C. U., Fowler, P. W., Knaggs, J., Iqbal, Z., et al. (2022). The 2021 WHO catalogue of *Mycobacterium tuberculosis* complex mutations associated with drug resistance: a genotypic analysis. *Lancet Microbe* 3, e265–e273. doi: 10.1016/S2666-5247(21)00301-3

Wang, X., and Wood, T. K. (2011). Toxin-antitoxin systems influence biofilm and Persister cell formation and the general stress response ▽. *Appl. Environ. Microbiol.* 77, 5577–5583. doi: 10.1128/AEM.05068-11

Winther, K. S., and Gerdes, K. (2011). Enteric virulence associated protein VapC inhibits translation by cleavage of initiator tRNA. *Proc. Natl. Acad. Sci. USA* 108, 7403–7407. doi: 10.1073/pnas.1019587108

World Health Organization (2023). Global tuberculosis report 2023. Geneva: World Health Organization.

Xu, J., Zhang, N., Cao, M., Ren, S., Zeng, T., Qin, M., et al. (2018). Identification of three type II toxin-antitoxin systems in *Streptococcus suis* serotype 2. *Toxins* 10:467. doi: 10.3390/toxins10110467

Yang, C., Luo, T., Shen, X., Wu, J., Gan, M., Xu, P., et al. (2017). Transmission of multidrug-resistant *Mycobacterium tuberculosis* in Shanghai, China: a retrospective observational study using whole-genome sequencing and epidemiological investigation. *Lancet Infect. Dis.* 17, 275–284. doi: 10.1016/S1473-3099(16)30418-2

Yang, T., Wang, Y., Liu, Q., Jiang, Q., Hong, C., Wu, L., et al. (2021). A population-based genomic epidemiological study of the source of tuberculosis infections in an emerging city: Shenzhen, China. *Lancet Reg. Health West Pac.* 8:100106. doi: 10.1016/j.lanwpc.2021.100106

Yu, X., Gao, X., Zhu, K., Yin, H., Mao, X., Wojdyla, J. A., et al. (2020). Characterization of a toxin-antitoxin system in *Mycobacterium tuberculosis* suggests neutralization by phosphorylation as the antitoxicity mechanism. *Commun. Biol.* 3:216. doi: 10.1038/s42003-020-0941-1

frontiers | Frontiers in Microbiology

TYPE Original Research
PUBLISHED 14 November 2024
DOI 10.3389/fmicb.2024.1398999

OPEN ACCESS

EDITED BY
Axel Cloeckaert,
Institut National de Recherche pour L'agriculture, L'alimentation et L'environnement (INRAE), France

REVIEWED BY
Guoliang Zhang,
Shenzhen Third People's Hospital, China
Ikhwan Rinaldi,
RSUPN Dr. Cipto Mangunkusumo, Indonesia
Johid Malik,
University of Nebraska Medical Center, United States
Juraj Ivanyi,
King's College London, United Kingdom
Emmanuel Babafemi,
Liverpool John Moores University, United Kingdom

*CORRESPONDENCE
Jeel Moya-Salazar
✉ jeel.moya@uwiener.edu.pe
Hans Contreras-Pulache
✉ hans.contreras@uwiener.edu.pe

RECEIVED 09 April 2024
ACCEPTED 29 August 2024
PUBLISHED 14 November 2024

CITATION
Moya-Salazar J, Samán J, Pasco IA, Moya-Salazar MM, Rojas-Zumaran V and Contreras-Pulache H (2024) Reduced bacillary load in elderly patients with active extrapulmonary and pulmonary tuberculosis in Peru: analysis of confirmatory culture after acid-fast bacilli test.
Front. Microbiol. 15:1398999.
doi: 10.3389/fmicb.2024.1398999

Reduced bacillary load in elderly patients with active extrapulmonary and pulmonary tuberculosis in Peru: analysis of confirmatory culture after acid-fast bacilli test

Jeel Moya-Salazar[1]*, Jonathan Samán[2], Israel A. Pasco[3], Marcia M. Moya-Salazar[4], Víctor Rojas-Zumaran[5] and Hans Contreras-Pulache[1]*

[1]Vicerrectorado de Investigación, Universidad Norbert Wiener, Lima, Peru, [2]CENEX, Hospital Nacional Hipólito Unanue, Lima, Peru, [3]Department of Laboratory Medicine, Centro de Salud Hermitaño Bajo, Lima, Peru, [4]Infectious Unit, Nesh Hubbs, Lima, Peru, [5]Department of Pathology, Hospital Nacional Docente Madre-Niño San Bartolomé, Lima, Peru

Background: Older adults with tuberculosis (TB) present unusual clinical features and can be challenging to diagnose. Culture after evaluation of sputum smear (AFB) may result in improved diagnosis performance, however it has not yet been evaluated in Peruvian older adults. We aimed to evaluate the diagnostic relation of TB culture after the AFB in patients aged ≥ 65 years derived for the diagnosis of pulmonary (PTB) and extra-pulmonary (EPTB) in Lima, Peru.

Methods: A cross-sectional study was developed in Lima, Peru, in order to evaluate the relationship of TB culture after AFB test in older adults (≥ 65 years) during the PTB and EPTB diagnosis. The frequency of contaminated cultures and the discrepancies between the conventional AFB test and Ogawa-Kudoh culture were analyzed.

Results: Of the 10,461 sputum and 2,536 extrapulmonary samples analyzed during 2015–2017, PTB was diagnosed in 282 (2.7%) and EPTB in 88 (3.5%), respectively. The performance of AFB in the diagnosis of PTB had a sensitivity of 78.2% and specificity of 99.8%. The performance of AFB in EPTB had a sensitivity of 45.5% and specificity of 99.9%. Negative AFB with positive culture was more frequent in ≥ 82 years (p = 0.031). We determined a good agreement in the diagnosis of PTB (κ = 0.84) and moderate for EPTB (κ = 0.55).

Conclusion: Our findings suggest that diagnosis through culture should be performed after the AFB smear evaluation due to the moderate performance of AFB, especially in patients ≥ 82 years old.

KEYWORDS

tuberculosis, aged, Ogawa, smear, extrapulmonary tuberculosis, Peru

1 Introduction

For many centuries, tuberculosis (TB) has caused significant economic and social impacts worldwide, particularly in low-income countries where it remains one of the leading causes of mortality (World Health Organization, 2022). TB is a complex issue that requires the combined efforts of governments, the private sector, and civil society.

Peru is a middle-income country—with more than 33 million inhabitants - that has a TB incidence of 87.6 per 100,000 inhabitants in 2017 (Alarcón et al., 2017). Although the population is constantly exposed to this disease, there are risk groups such as prisoners, healthcare workers, patients with type 2 diabetes, and the elderly where the disease worsens (Rojas-Bolivar et al., 2018; Ugarte-Gil et al., 2021). Pulmonary TB (PTB) accounts for more than 80% of cases, with diagnosis primarily conducted through acid-fast bacilli (AFB) smear analysis and bacteriological culture (Ministerio de Salud, 2006, 2023). Given the high incidence of this disease, it is crucial to prioritize accurate and rapid diagnostic methods that align with the community's reality (Pan-American Health Organization, 2013).

In Peru, it is estimated that there are around 4 million elderly people. The most common diseases in this population include hypertension, diabetes, and cardiovascular diseases (Instituto Nacional de Estadística e Informática, 2020, 2023). TB also affects the elderly, with a rate of approximately 120 cases per 100,000 people, and 11–20% of these cases being new each year (Alarcón et al., 2017; Ministerio de Salud, 2024). Diagnostic complications have been observed in elderly patients with TB that could interfere with the current diagnostic approach in Peru, focused on AFB smear analysis (Ministerio de Salud, 2018). The elderly population presents a different clinical profile with fewer evident symptoms, a distinct immune response to TB, and complex reactions to treatment due to physiological changes associated with aging. These factors pose challenges for diagnostic tests (Teo et al., 2023; Sharma et al., 2022; Yoshikawa and Rajagopalan, 2001), potentially leading to a lack of confirmed diagnoses in these patients.

The absence of culture confirmation in the majority of AFB-based studies hinders the ability to estimate test performance differences, which may affect diagnostic quality. Cross-contamination of cultures is a common error, estimated at 2% of all positive TB cultures, resulting in 9.2% of patients receiving false positive results and inadequate treatment (Barac et al., 2019). Additionally, previous reports have emphasized the importance of laboratory performance for PTB diagnosis (Symes et al., 2020; Silva et al., 2013; Cruz-Hervert et al., 2012; Rivas et al., 2010; Yoshikawa and Rajagopalan, 2001). However, the impact of diagnostic tests on extrapulmonary TB (EPTB) samples has not been thoroughly evaluated.

In the context of global aging, the elderly have a high mortality rate, poor clinical clarity in TB symptoms, and face limitations with current diagnostic methods. Thus, the diagnostic performance of AFB smear and culture should be carefully evaluated (Sood, 2000; Partridge et al., 2018; Teo et al., 2023; Sharma et al., 2022). Improving TB diagnostic programs for the elderly is essential, especially in countries with high TB prevalence and complex social, demographic, health access, and economic conditions (Purohit and Mustafa, 2015; Colegio Médico del Perú, 2021; Huarachi et al., 2024).

We aimed to evaluate the diagnostic relation of TB culture after the evaluation of sputum smear (AFB) in older patients derived for the diagnosis of PTB and EPTB in Lima, Peru. We also determined the frequency of contaminated results by sex, age group, and treatment history.

2 Materials and methods

2.1 Study design and sample

This cross-sectional study was conducted at the Hipólito Unanue National Hospital in Lima, Peru. The hospital is located in the Lima downtown, in the district of El Agustino (12°4′0″S, 77°1′0″W), one of the districts with a high incidence of TB, high poverty rates, and high population density (15,416.19 inhabitants/km^2) (Instituto Nacional de Estadística e Informática, 2015). The patients included in this study were all aged 65 years or older and resided in this district. All patients attending the TB Diagnostic Service had been referred by their treating physician after consultation to be included in the TB Control Program (PCT). This program has nationwide coverage to promote the prevention and control of TB, ensuring consistent diagnosis and treatment for both TB and non-TB patients.

We included patients over 65 years of age from both genders, from the PCT and outpatient clinics of the hospital, regardless of previous TB treatment history. Both pulmonary and extrapulmonary samples (i.e., cerebrospinal fluid) were included. Patients with extremely drug-resistant TB (XDR-TB) or multidrug-resistant TB (MDR-TB) were excluded to avoid bias in the interpretation of AFB smear and culture results. The clinical diagnosis for PTB involved identifying respiratory symptoms (i.e., cough) or a recent positive PPD test, abnormal chest X-ray findings, positive AFB smear, and initiating or controlling treatment according to the Peruvian treatment regimen (Ministerio de Salud, 2023).

2.2 TB diagnostic methods

All sputum and extrapulmonary samples were processed by the Microbiology Area team and the Research Department for TB diagnosis and treatment, following the hospital's bacteriological guidelines (Sequeira de Latini and Barrera, 2008; Barrera, 2008). The conventional AFB sputum test was performed by preparing a slide with the patient's sample and staining it with Ziehl-Neelsen following national guidelines (Ministerio de Salud, 2023). Cultures were performed on Ogawa-Kudoh agar (Merck, Darmstadt, Germany) in accordance with international quality standards (Rivas et al., 2010; Sequeira de Latini and Barrera, 2008; Barrera, 2008; Asencios et al., 2012; Clinical and Laboratory Standards Institute, 2008). Extrapulmonary specimens, such as gastric aspirate, feces, urine, and pleural fluid, were collected by hospital departments teams (i.e., gastroenterology) and promptly sent for laboratory analysis. These samples were also processed using smear microscopy and cultured on Ogawa-Kudoh agar.

As previously reported (Moya-Salazar et al., 2018), the evaluation of samples adheres to national quality regulations (Ministerio de Salud, 2020, 2023). This ensures that processes are continuously monitored under protocols established by the National Institute of Health and the Ministry of Health of Peru (Asencios et al., 2012). By following these diagnostic and result interpretation guidelines, we minimize interpretation bias in AFB smears and acknowledge the limitations of culture results.

2.3 Confirmatory culture evaluation and data analysis

We analyzed all patients with discordant or concordant AFB and culture results (primarily AFB-negative with positive culture) and evaluated the frequency of contaminated results. To establish the relationship between results, they were categorized into the following groups:

1. Sputum smear (AFB): paucibacillary results (AFB per 100x fields), one cross 1 (+), two crosses 2 (++), and three crosses 3 (+++).
2. Culture: number of colonies grown in the medium (No. 1 to 19 colonies), one cross 1 (+), two crosses 2 (++), and three crosses 3 (+++).

All these results (PTB and EPTB) were coded from the hospital's data storage system (MS-Excel 2010, Redmond, US) into the data matrix (EPIDAT v4.1, Xunta de Galicia, Spain). We used descriptive statistics and non-parametric correlation between study variables, considering a 95% confidence interval (CI 95%) and a p-value < 0.05 as statistically significant. To determine the performance of the AFB smear, diagnostic tests (sensitivity, specificity, Positive Predictive Value (PPV), Negative Predictive Value (NPV), accuracy, and Youden's Index) and the Receiver Operating Characteristic (ROC) curve were used. Statistical analysis was performed using the Statistical Package for the Social Sciences (SPSS) v25.0 (IBM, Armonk, US) and EPIDAT v4.1 for Windows.

2.4 Ethical aspects

We follow the Helsinki declaration guidelines (World Medical Association, 2013) and this study was approved by the IRB of the Universidad Norbert Wiener (Exp. N° 103-2017-UNW, March 12, 2017).

3 Results

3.1 Descriptive results

Out of 31,819 patients, we enrolled 12,997 (45%) who were older than 65 years. The distribution by year was as follows: 4,136 (31.8%) patients in 2015, 4,511 (34.7%) in 2016, and 4,350 (33.5%) in 2017. The average age was 75 ± 7.5 years (CI 95%, 75 to 75.3 years). Of these, 6,499 (50.1%) were women, with no significant age difference between genders ($p = 0.101$). Five patients (0.03%) had no recorded sex. We registered 10,357 (79.7%) patients without previous treatment, 1,942 (14.9%) with previous treatment, and 698 (5.4%) without registration (Table 1).

Out of the 10,461 sputum samples analyzed, TB was diagnosed in 282 (2.7%) samples from patients aged ≥ 65 years with and without symptoms. In 2015, 3,311 (31.7%) sputum samples were evaluated, with 109 (1%) positive and 37 (0.4%) showing culture contamination. In 2016, 3,666 (35%) samples were evaluated, with 94 (0.9%) positive and 28 (2.5%) contaminated. In 2017, 3,484 (33.3%) sputum samples were evaluated, with 79 (0.8%) positive and 17 (0.2%) contaminated in the Ogawa culture.

Of the 2 536 extrapulmonary samples that were analyzed, TB was diagnosed in 88 (3.5%) samples from patients ≥ 65 years with and without symptoms. In 2015, 824 (32.5%) sputum samples were evaluated, with 37 (1.5%) testing positive and 40 (1.6%) showing culture contamination. In 2016, 845 (33.3%) samples were evaluated, with 21 (0.8%) testing positive and 39 (1.5%) contaminated. In 2017, 867 (34.2%) sputum samples were evaluated, 30 (1.2%) were positive and 31 (1.22%) were contaminated in the Ogawa culture.

A very good diagnostic agreement between AFB test and culture was determined for the diagnosis of PTB (κ = 0.84, CI 95%, 0.79 to 0.89%) and moderate agreement for EPTB (κ = 0.55, CI 95%, 0.25 to 0.86%).

3.2 Diagnostic performance of PTB

The diagnostic agreement of positive results in pulmonary samples was evidenced in 1.1% of sputum smears (111/10461). The average age of these patients was 70.5 ± 6 (CI 95%, 69.3 to 71.7), where 45 were women and the history of previous treatment was not significant ($p = 0.0334$). We found that 0.05% of samples (5/10,461) presented positive sputum smears and negative culture results; all these samples were from women without prior treatment, with an average age of 72 ± 7.1 years. Additionally, 0.1% (12/10,461) of sputum smears were negative, but culture-positive. Five of these samples were from women (72.2 ± 6.5 years, CI 95%, 68.5 to 75.8), eight samples came from the Emergency Services, and only two had previous treatment.

In the sputum analysis, the proportion of false positives was 0.2% (CI 95%, 0.1 to 0.3), and the proportion of false negatives was 21.8% (CI 95%, 15.8 to 29.3). From the analysis of the AFB tests in PTB diagnosis we obtained a sensitivity of 78.2% (CI 95%, 70.7 to 84.2), a specificity of 99.8% (CI 95%, 99.7 to 99.9), a PPV of 91% (CI 95%, 84.6 to 94.9), to NPV of 99.6% (CI 95%, 99.4 to 99.7), an accuracy of 99.4% (CI 95%, 99.2 to 99.6), and a Youden's Index of 0.8 (Figure 1A).

3.3 Diagnostic performance of EPTB

Concerning extrapulmonary samples, diagnostic agreement of positive results was evidenced in 0.24% of samples (12/2,536). The average age of these patients was 76.2 ± 7 years (CI 95%, 70.1 to 82.3), with none having a history of treatment, and all samples

10.3389/fmicb.2024.1398999

TABLE 1 Baseline characteristics of elderly patients (≥ 65 years) with extra-pulmonary and pulmonary tuberculosis. Data in *n* (%).

Characteristics		Tuberculosis¶						
		Normal		PTB*		EPTB*		Total
		61–82	≥ 82	61–82	≥ 82	61–82	≥ 82	
Study period†								
	2015	3104 (24)	846 (6.5)	76 (0.57)	33 (0.25)	26 (0.2)	11 (0.08)	4096 (31.5)
	2016	3402 (26)	955 (7.3)	84 (0.65)	10 (0.08)	11 (0.08)	10 (0.08)	4472 (34.4)
	2017	3314 (25)	896 (6.9)	64 (0.45)	15 (0.12)	19 (0.15)	11 (0.08)	4319 (33.2)
Gender								
	Women	4897 (37.7)	1472 (11.3)	88 (0.7)	23 (0.18)	18 (0.14)	16 (0.12)	6514 (50.12)
	Men	5014 (38.6)	1243 (9.6)	134 (1.03)	39 (0.3)	23 (0.18)	30 (0.23)	6483 (49.88)
Treatment								
	BT‡	1580 (12.2)	270 (1.6)	65 (0.5)	11 (0.08)	9 (0.07)	1 (0.008)	1936 (14.9)
	NT	7819 (60.2)	2300 (17.7)	149 (1.15)	37 (0.28)	39 (0.3)	29 (0.22)	10373 (79.8)
	NR	503 (3.8)	158 (1.22)	17 (0.13)	0 (0)	8 (0.06)	2 (0.015)	688 (5.3)
Types of samples								
	Sputum	8117 (62.5)	2054 (15.8)	234 (1.8)	48 (0.36)	. . .**	. . .	10453 (80.4)
	Gastric aspirate	457 (3.5)	310 (2.4)	. . .	. . .	16 (0.2)	15 (0.11)	798 (6.14)
	Pleura liquid	300 (2.3)	111 (0.85)	. . .	. . .	3 (0.023)	2 (0.015)	416 (3.2)
	Bronchial aspirate	383 (2.9)	117 (0.9)	. . .	. . .	18 (0.13)	9 (0.06)	527 (4)
	Post. Bronchial aspirate	130 (1)	9 (0.06)	. . .	. . .	5 (0.03)	3 (0.023)	147 (1.13)
	Urine	180 (1.38)	33 (0.25)	. . .	. . .	4 (0.03)	0 (0)	217 (1.7)
	Stool	76 (0.6)	16 (0.12)	. . .	. . .	1 (0.008)	0 (0)	90 (0.7)
	Tracheal aspirate	64 (0.5)	16 (0.12)	. . .	. . .	3 (0.023)	2 (0.015)	85 (0.6)
	Cerebrospinal fluid	52 (0.4)	18 (0.13)	. . .	. . .	0 (0)	0 (0)	70 (0.5)
	Pericardium biopsy	10 (0.08)	0 (0)	. . .	. . .	0 (0)	0 (0)	10 (0.08)
	Cervical abscess	9 (0.06)	1 (0.008)	. . .	. . .	0 (0)	0 (0)	10 (0.08)
	Endotracheal tube	8 (0.06)	0 (0)	. . .	. . .	0 (0)	0 (0)	8 (0.06)
	Pericardial fluid	7 (0.05)	1 (0.008)	. . .	. . .	0 (0)	0 (0)	1 (0.008)
	Others	110 (0.8)	25 (0.2)	. . .	. . .	6 (0.05)	1 (0.008)	32 (0.24)

¶ All patients were subdivided into two age groups: first group of 65–71 years, and second of ≥ 82 years. *Diagnosis with both AFB test and culture test are included. †The total of contaminated cultures pear year were excluded: 2015 (n = 40), 2016 (n = 39), and 2017 (n = 31). **Includes patients with previous diagnosis and treatment control. No samples are recorded. EPTB, Extra-pulmonary tuberculosis; PTB, Pulmonary tuberculosis; NT, Never treated; NR, No report.

being bronchial aspirates. Additionally, 0.07% (2/2,536) of samples had positive AFB but negative culture results. Conversely, 0.25% (6/2,536) of samples showed negative sputum smears but positive culture results. All these samples were bronchial aspirates, and one was from a woman (72 ± 5.7 years, CI 95%, 67 to 77).

The analysis of extrapulmonary samples allowed us to estimate a false positive rate of 0.1% (CI 95%, 0.0% to 0.3%) and a false negative rate of 54.5% (CI 95%, 28% to 78.7%). The analysis of extrapulmonary samples allowed us to estimate a false positive rate of 0.1% (CI 95%, 0.0% to 0.3%) and a false negative rate of 54.5% (CI 95%, 28% to 78.7%). From the analysis of the AFB tests in EPTB diagnosis, we obtained a sensitivity of 45.5% (CI 95%, 21.3 to 72), a specificity of 99.9% (CI 95%, 99.7 to 100), a PPV of 71.4% (CI 95%, 35.9 to 91.8), an NPV of 99.8% (CI 95%, 99.5 to 99.9), an accuracy of 99.7% (CI 95%, 99.4 to 99.8), and a Youden's Index of 0.5 (Figure 1B).

3.4 Contamination frequency

Regarding the results with contaminated culture, 40 (14.2%) sputum samples presented a contaminated result in 2015, one of which had a positive AFB result (2 + +) and a history of previous treatment. In 2016 and 2017 there were 39 (13.8%) and 31 (11%) sputum samples with contaminated culture, respectively. In the diagnosis of EPTB, 82 (29.1%) cases were recorded in total, with

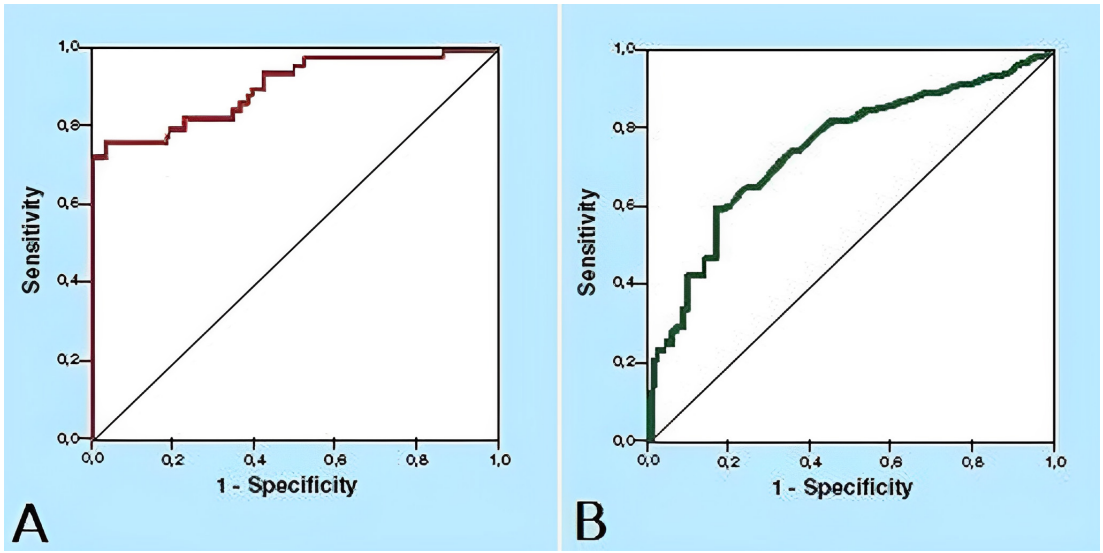

FIGURE 1
Receiver operating characteristic (ROC) curves for AFB test on the diagnosis of pulmonary and extrapulmonary tuberculosis in elderly patients (≥ 65 years) in Lima, Peru. **(A)** ROC curve for AFB test on the diagnosis of pulmonary tuberculosis. **(B)** ROC curve for AFB test on the diagnosis of extrapulmonary tuberculosis.

12 (4.3%) contaminated cultures having positive sputum smears. No correlation was found between the contaminated cultures and the age of the patients (p = 0.573), nor with the history of previous treatment ($p = 0.415$) (Figure 2).

3.4 Performance analysis by age group

The performance analysis of the AFB test was conducted in two age groups (65–81 years and ≥ 82 years) for the diagnosis of PTB and EPTB. In the first group (65–81 years), it was observed that 0.24% (24/10,201) presented AFB-negative results with a positive culture, and 0.1% (10/10,201) presented AFB-positive results with a negative culture. In the second group (≥ 82 years), 0.25% (7/2,796) had AFB-negative results with a positive culture, and 0.07% (2/2,796) had AFB-positive results with a negative culture. Negative sputum smears were more frequent in the ≥ 82 years group ($p = 0.031$), resulting in a false-positive rate of 0.1% (CI 95%, 0.1 to 0.2) and a false-negative rate of 20.3% (CI 95%, 14.1 to 28.5). Additional data is shown in Figure 3.

For the diagnosis of EPTB, the same analysis could not be performed due to the limited number of viable samples. However, AFB-negative with positive culture results were observed only in the first group (6/13). In patients aged ≥ 82 years, only AFB-positive with positive culture results were evident (2/13). Of all AFB-negative with positive culture cases, only two patients had a history of previous treatment (2/167).

4 Discussion

This study evaluated the confirmatory culture of TB following the AFB test, demonstrating moderate performance of the sputum smear in Peruvian patients aged ≥ 65 years. Due to the high false-negative rate and low sensitivity of AFB, particularly in screening for EPTB, performing a culture is crucial to avoid diagnostic errors in elderly patients. Also, the rate of negative sputum smears with positive cultures was slightly higher in patients aged ≥ 82 years.

The performance of the AFB test was assessed based on diagnostic agreement and the rate of contaminated cultures. During PTB diagnosis, a high specificity for the AFB test was observed in sputum samples. Similarly, high specificity was noted in extrapulmonary samples. However, the diagnostic sensitivity was lower than 79% for PTB and less than 50% for EPTB screening, highlighting important limitations of this diagnostic test in primary healthcare settings (Sulis et al., 2016). Previous studies have reported different levels of diagnostic performance for the AFB test (Symes et al., 2020; Park et al., 2014; Cruz-Hervert et al., 2012; Monkongdee et al., 2009; Grupo de trabajo de expertos en tuberculosis, and Grupo de trabajo de Comunidades Autónomas, 2009). Its relevance is particularly evident in the diagnostic assessment of patients with previous treatment, where culture alone should not be the sole useful method for evaluating treatment efficacy (Sharma et al., 2022; Symes et al., 2020; Grupo de trabajo de expertos en tuberculosis, and Grupo de trabajo de Comunidades Autónomas, 2009; Caulfield and Wengenack, 2016).

The diagnostic concordance between AFB and culture was very low, with only 1.1% of sputum smears in pulmonary samples and 0.05% of extrapulmonary samples showed concordance. Despite the limited number of tests with available data, these showed moderate to very good agreement (Figures 2, 3). This evaluation is influenced by multiple factors including specimen collection, the analytical process, the type of diagnostic method used, and the skill and specialization of health workers responsible for laboratory diagnosis (Teo et al., 2020; Ssengooba et al., 2012; Aber et al., 1980). It is important to consider elderly patients with previous treatment as they could skew the performance of

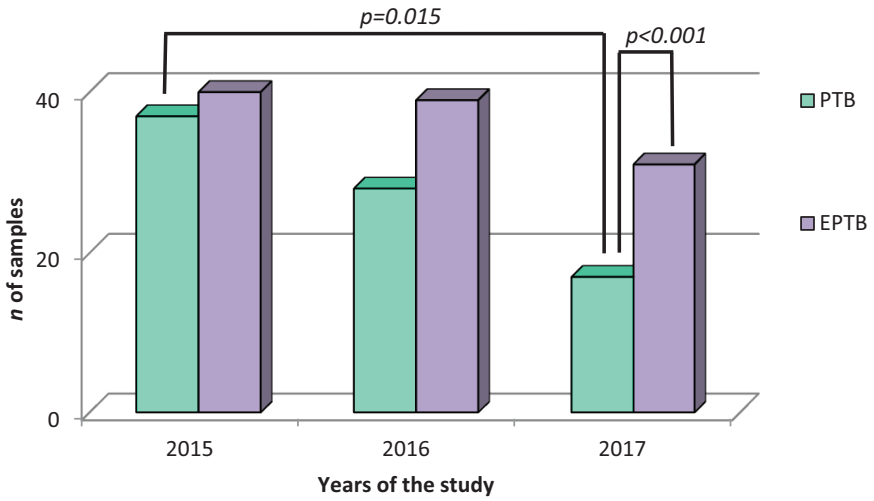

FIGURE 2
Distribution of contaminated cultures of pulmonary and extrapulmonary tuberculosis samples of elderly patients. During the study period shows the significant difference between the samples with contaminated results between 2015 and 2017 and the difference between sputum and extrapulmonary samples of the year 2017 (*n* = 161).

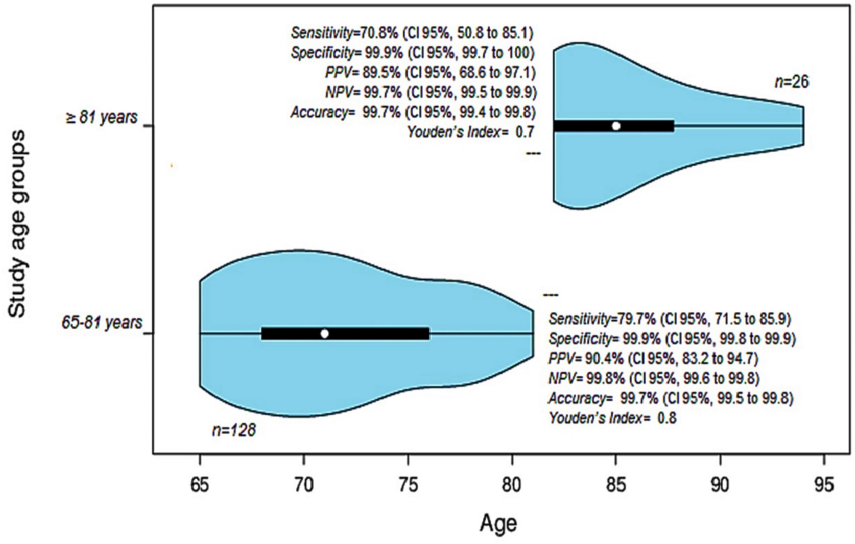

FIGURE 3
Diagnostic tests and analysis of the performance of the AFB test for the diagnosis of PTB in two age groups. The first group of 65–81 years (71 ± 5.2 years, CI95% 71 to 76) is shown in the violin below. The second group ≥ 82 years (85 ± 7.8 years, CI95% 82 to 87.75) is shown in the violin above. PPV, Positive predictive value, NPV, Negative predictive value.

the AFB smear test. However, none of the patients with EPTB analyzed had previous treatment, and for PTB, the two patients with previous treatment were not statistically significant. Therefore, our performance data are robust and free from biases that could hinder their interpretation.

Culturing *Mycobacterium tuberculosis* is essential as it provides a higher diagnostic yield, allows for the identification of the causative agent, and facilitates antimicrobial susceptibility testing. Several studies have demonstrated the high performance of Ogawa-Kudoh agar for isolating TB in sputum samples, significantly contributing to routine diagnostic processes (Rivas et al., 2010; Silva et al., 2013; Agapito et al., 2009; Palaci et al., 2013). However, the performance of this method depends on various factors such as the type of egg used, the type of sample cultivated, and the decontamination time of the samples (Barrera, 2008; Agapito et al., 2009; Rivas et al., 2010; Asencios et al., 2012; Silva et al., 2013; Palaci et al., 2013; Singhal et al., 2014; Noori et al., 2015).

Another factor that may influence performance is the composition of the medium (Rivas et al., 2010; Sequeira de Latini and Barrera, 2008; Barrera, 2008). Ogawa medium uses a base of dried egg and potato starch, whereas Lowenstein-Jensen medium is based on whole egg, glycerol, and mineral salts (Kim and Ryoo, 2011; Lubasi et al., 2004). Ogawa is quicker to prepare and less susceptible to contamination, while Lowenstein-Jensen

provides a richer environment for bacterial growth (Ariami et al., 2018). Large-scale performance comparisons of these media are needed to determine which is better for elderly samples, which may be contaminated by hospital procedures (i.e., endotracheal intubation), have altered sample composition affecting culture outcomes, and may contain contaminants.

Furthermore, we investigated the rate of contaminated cultures in PTB screening and found that 14.2% presented contamination. This contamination rate is more than two times higher reported in previous studies, which range from 5.5% to 7% (Yvette et al., 1995; Rivas et al., 2010). Nonetheless, Ogawa agar has demonstrated a high diagnostic yield with a lower rate of contaminated cultures compared to the Lowenstein-Jensen medium (Ceyhan et al., 2012), using the N-acetyl-L-cysteine-sodium hydroxide decontamination technique (Jobarteh et al., 2017), and with modified Ogawa medium (Lubasi et al., 2004).

Extrapulmonary samples, especially stool samples, typically have higher contamination rates than pulmonary samples. However, in our study, the most frequent contaminated cultures were bronchial aspirate (4.6%), gastric aspirate (3.8%), tracheal aspirate (1.7%), and urine (1.1%). These results differ from previous reports and may explain the low frequency of contaminated cultures in comparison to sputum cultures (Symes et al., 2020; Houston and Macallan, 2014; Banta et al., 2020).

The lack of confirmation of TB cultivation in many studies may account for the differing findings related to the proportion of TB cases in the elderly compared to younger individuals (Sood, 2000; Cruz-Hervert et al., 2012; Shivam et al., 2014; Azadi et al., 2018). Although a lower frequency of positive smears has been reported in patients $\geq$ 65 years, our findings indicate a higher frequency of positive smears in patients aged 65 to 81 years compared to those older than 81 (Table 1).

In the other hand, another critical finding to emphasize is the proportion of false negatives observed in sputum smears (21.8%) and extrapulmonary samples (54.5%). As previously mentioned, the clinical presentation of TB in the elderly is highly heterogeneous. Assuming that over 20% of samples evaluated in these patients contain errors, the results could lead to loss of follow-up and control, and a resurgence of the disease in this population, which already faces high physiological, immunological, nutritional, and social risk factors (Sood, 2000; Yoshikawa and Rajagopalan, 2001; Cruz-Hervert et al., 2012; Zagaria, 2008; Moya-Salazar et al., 2018).

The analysis by age group revealed that the rate of sputum smear-negative with positive culture was significantly higher in patients aged $\geq$ 82 years with PTB. The concerning proportion of false negatives (20.3%) in this age group could lead to diagnostic errors, exposing patients to unnecessary risks, such as invasive investigations or loss of follow-up, thereby compromising prevention programs. This is particularly dangerous given the high comorbidity in the elderly (Schaaf et al., 2010; Salive, 2013). Recently, in Peru, it has been reported that 11–20% of TB cases occur in people $\geq$ 65 years, primarily men (Alarcón et al., 2017; Ministerio de Salud, 2024). For these patients, new diagnostic and therapeutic methods need to be evaluated according to social realities and age groups to ensure efficient management of older adults with TB (Lienhardt et al., 2016; Moya-Salazar et al., 2018).

Additionally, our diagnostic safety analysis revealed that the quality of results was suboptimal. For instance, the diagnosis of EPTB yielded only half the ideal value (Youden's J = 0.5). Due to the poor quality of samples and the challenges in obtaining and analyzing them solely with AFB, culture should be the cornerstone of the TB diagnosis algorithm in older patients. However, expanded testing by smear culture is recommended but challenging to implement in remote and impoverished areas. A more feasible method might be antibody serology, which has shown previous validation (Ivanyi, 2012; Bothamley et al., 1992). Other techniques include liquid culture and fluorescence analysis but are expensive for poor settings (). These need evaluation in a post-pandemic context, as COVID-19 has impacted the development of many diseases and shifted healthcare priorities (Robles et al., 2024; Moya-Salazar et al., 2024; Dutta et al., 2023; Khunti et al., 2022, World Health Organization, 2021). Despite this, governments have continued TB control programs worldwide (Ministerio de Salud, 2024; Williams et al., 2023). It is now crucial to leverage pandemic-era technological advances to enhance TB surveillance and ensure equitable access to care.

This study had limitations. (i) A larger sample size of older patients with EPTB should be evaluated to fully understand their clinical characteristics and their diagnostic patterns. Furthermore, it is crucial to evaluate whether patients over 81 years old are clinically different from those under 81 years old, as well as to compare these results with younger populations to identify differences in the development of AFB and culture for PTB and EPTB. (ii) The impact of the contaminated culture should be estimated due to processing errors. The impact of contaminated cultures should be estimated due to processing errors. In this study, 4.3% of contaminated cultures had positive sputum smears, creating uncertainty about the results and potentially affecting the prevention and treatment of patients with EPTB. (iii) Given Peru's high rates of MDR-TB (World Health Organization, 2022), similar studies should be conducted to assess the efficacy of diagnostic procedures for resistant isolates (MDR- and XDR-TB). In this study, such cases were excluded to avoid bias; however, their influence on performance, as previously reported in the adult population (Tanoue et al., 2002), should not be overlooked. (iv) We found that the older the patient, the higher the proportion of negative AFB smears. Multicenter and multiregional studies should be conducted in populations with similar TB incidence rates to accurately estimate AFB results and determine the need for culture in low-income primary health-care centers (Mamuye, 2012). Finally, (v) Other diagnostic methods, such as molecular tests and the Lowenstein-Jensen culture medium, should be compared to identify the most optimal diagnostic tests for elderly patients with PTB and EPTB (Thomas and Rajagopalan, 2001; Schaaf et al., 2010). Additionally, it is important to report a list of contaminants and disclose any specific microbial associations or mixtures responsible for the contamination of diagnostic samples.

5 Conclusions and future directions

The evaluation of confirmatory TB culture in pulmonary and extrapulmonary samples after AFB smear testing in elderly patients is essential due to the moderate performance of AFB, particularly in patients $\geq$ 82 years and in sputum samples. Diagnosing tuberculosis in the elderly poses a significant challenge for health

systems globally, especially in regions where TB remains almost endemic. Recognizing the limitations of current diagnostic tests is crucial to proposing improvements in diagnostic processes within the framework of the global zero TB plan.

Future studies should investigate how the timing and schedule of TB treatment may influence the results of bacteriological tests. Additionally, analyzing the risk of infection transmission by patients with smear-negative and culture-positive pulmonary TB is imperative. These specific aspects of TB in the elderly may be key pieces in the puzzle of achieving successful diagnosis and effective treatment.

Data availability statement

The original contributions presented in the study are included in the article/supplementary material, further inquiries can be directed to the corresponding author.

Ethics statement

The studies involving humans were approved by the IRB of the Universidad Norbert Wiener (Exp. N° 103-2017-UNW, March 12, 2017). The participants provided written informed consent to participate in this study. The studies were conducted in accordance with the local legislation and institutional requirements. The participants provided their written informed consent to participate in this study.

Author contributions

JM-S: Writing – review and editing, Writing – original draft, Visualization, Software, Methodology, Investigation, Formal analysis, Data curation, Conceptualization. JS: Writing – review and editing, Writing – original draft, Resources, Methodology, Investigation, Data curation, Conceptualization. IP: Writing – review and editing, Writing – original draft, Visualization, Validation, Supervision, Resources, Investigation, Conceptualization. MM-S: Writing – review and editing, Visualization, Validation, Methodology, Investigation, Formal analysis, Data curation. VR-Z: Writing – review and editing, Software, Project administration, Methodology, Investigation, Data curation. HC-P: Writing – review and editing, Visualization, Software, Project administration, Investigation, Formal analysis.

Funding

The author(s) declare that no financial support was received for the research, authorship, and/or publication of this article.

Acknowledgments

We thank to Paola Handal for the critical review of this study. Likewise, we thank the staff of CENEX of the Hipolito Unanue National Hospital for the facilities provided for the development of this study.

Conflict of interest

The authors declare that the research was conducted in the absence of any commercial or financial relationships that could be construed as a potential conflict of interest.

Publisher's note

All claims expressed in this article are solely those of the authors and do not necessarily represent those of their affiliated organizations, or those of the publisher, the editors and the reviewers. Any product that may be evaluated in this article, or claim that may be made by its manufacturer, is not guaranteed or endorsed by the publisher.

References

Aber, V., Allen, B., Mitchison, D., Ayuma, P., Edwards, E., and Keyes, A. (1980). Quality control in tuberculosis bacteriology. 1. Laboratory studies on isolated positive cultures and the efficiency of direct smear examination. *Tubercle* 61, 123–133.

Agapito, J., Cuadros, L., Tarrillo, S., and Soto, A. (2009). Evaluación del medio Middlebrook 7h11 asociado a sangre humana u ovina para la detección de Mycobacterium tuberculosis en muestras de esputo. *Rev. Peru Med. Exp. Salud Publica* 26, 294–298.

Alarcón, V., Alarcón, E., Figueroa, C., and Mendoza-Ticona, A. (2017). Tuberculosis en el Perú: Situación epidemiológica, avances y desafíos para su control. *Rev. Peru Med. Exp. Salud Publica.* 34, 299–310.

Ariami, P., Diarti, M., and Jiwintarum, Y. (2018). Sensitivitas media ogawa dan media lowenstein jensen terhadap hasil pertumbuhan kuman Mycobacterium tuberculosis. *J. Kesehatam Prima.* 8, 1322–1335. doi: 10.32807/jkp.v8i2.54

Asencios, S., Quispe, T., and Vásquez, C. (2012). *Manual para el control de calidad externo de medios de cultivo para el diagnóstico bacteriológico de la tuberculosis*. Lima: Ministerio de Salud, Instituto Nacional de Salud.

Azadi, D., Motallebirad, T., Ghaffari, K., and Shojaei, H. (2018). Mycobacteriosis and Tuberculosis: Laboratory Diagnosis. *Open Microbiol. J.* 12, 41–58. doi: 10.2174/1874285801812010041

Banta, J. E., Ani, C., Bvute, K. M., Lloren, J. I. C., and Darnell, T. A. (2020). Pulmonary vs. extra-pulmonary tuberculosis hospitalizations in the US [1998-2014]. *J. Infect. Public Health* 13, 131–139. doi: 10.1016/j.jiph.2019.07.001

Barac, A., Karimzadeh-Esfahani, H., Pourostadi, M., Rahimi, M. T., Ahmadpour, E., Rashedi, J., et al. (2019). Laboratory Cross-Contamination of Mycobacterium tuberculosis: A Systematic Review and Meta-analysis. *Lung* 197, 651–661. doi: 10.1007/s00408-019-00241-4

Barrera, L. (2008). *Manual Para el Diagnóstico Bacteriológico de la Tuberculosis. Normas y Guía Técnica. Parte II Cultivo*. Washington, D.C: Organización Panamericana de la Salud (OPS/PAHO).

Bothamley, G., Rudd, R., Festenstein, F., and Ivanyi, J. (1992). Clinical value of the measurement of Mycobacterium tuberculosis specific antibody in pulmonary tuberculosis. *Thorax* 47, 270–275. doi: 10.1136/thx.47.4.270

Caulfield, A., and Wengenack, N. (2016). Diagnosis of active tuberculosis disease: From microscopy to molecular techniques. *J. Clin. Tuberc. Other Mycobact. Dis.* 4, 33–43.

Ceyhan, I., Simşek, H., and Tarhan, G. (2012). Comparison and evaluation of Lowenstein-Jensen medium and 2% Ogawa medium for the diagnosis of tuberculosis. *Mikrobiyol. Bul.* 46, 33–38.

Clinical and Laboratory Standards Institute (2008). *Laboratory Detection and Identification of Mycobacteria; Approved Guideline. CLSI supplement M48-A*. Wayne, PA: Clinical and Laboratory Standards Institute.

Colegio Médico del Perú (2021). *Libro del Bicentenario de la Independencia Nacional 1821-2021*. Lima: Fondo Editorial Comunicacional.

Cruz-Hervert, L. P., García-García, L., Ferreyra-Reyes, L., Bobadilla-del-Valle, M., Cano-Arellano, B., Canizales-Quintero, S., et al. (2012). Tuberculosis in ageing: high rates, complex diagnosis and poor clinical outcomes. *Age Ageing* 41, 488–495.

Dutta, D., Liu, J., and Xiong, H. (2023). The Impact of COVID-19 on People Living with HIV-1 and HIV-1-Associated Neurological Complications. *Viruses* 15, 1117. doi: 10.3390/v15051117

Grupo de trabajo de expertos en tuberculosis, and Grupo de trabajo de Comunidades Autónomas (2009). Plan para la prevención y control de la tuberculosis en España. *SEMERGEN* 35, 131–137.

Houston, A., and Macallan, D. (2014). Extrapulmonary tuberculosis. *Medicine* 42, 18–22.

Huarachi, L., Lozano-Zanelly, G., Acosta, J., Huarachi, C., and Moya-Salazar, J. (2024). Inequality in the distribution of resources and health care in the poverty quintiles: Evidence from Peruvian comprehensive health insurance 2018-2019. *Electron. J. Gen. Med.* 21, em568. doi: 10.29333/ejgm/14160

Instituto Nacional de Estadística e Informática (2015). *Estimaciones y Proyecciones de Población*. Lima: INEI.

Instituto Nacional de Estadística e Informática (2023). *Perú: Enfermedades No Transmisibles y Transmisibles 2022*. Lima: INEI.

Intituto Nacional de Estadística e Informática (2020). *Nota de Prensa N° 121. En el Perú existen más de 4 millones de ancianos*. LIMA: INEI.

Ivanyi, J. (2012). Serodiagnosis of tuberculosis: due to shift track. *Tuberculosis* 92, 31–37. doi: 10.1016/j.tube.2011.09.001

Jobarteh, T., Otu, J., Gitteh, E., Mendy, F., Faal-Jawara, T. I., Ofori-Anyinam, B., et al. (2017). Evaluation of the Kudoh Method for Mycobacterial Culture: The Gambia Experience. *Am. J. Respir. Crit. Care Med.* 195, A2081.

Khunti, K., Aroda, V. R., Aschner, P., Chan, J. C., Prato, S. D., Hambling, C. E., et al. (2022). The impact of the COVID-19 pandemic on diabetes services: planning for a global recovery. *Lancet Diabetes Endocrinol.* 10, 890–900. doi: 10.1016/S2213-8587(22)00278-9

Kim, H., and Ryoo, S. (2011). Exploitation of Culture Medium for Mycobacterium tuberculosis. *J Bacteriol. Virol.* 41, 237–244. doi: 10.4167/JBV.2011.41.4.237

Lienhardt, C., Lönnroth, K., Menzies, D., Balasegaram, M., Chakaya, J., Cobelens, F., et al. (2016). Translational Research for Tuberculosis Elimination: Priorities, Challenges, and Actions. *PLoS Med* 13, e1001965. doi: 10.1371/journal.pmed.1001965

Lubasi, D., Habeenzu, C., and Mitarai, S. (2004). Evaluation of an Ogawa Mycobacterium culture method modified for higher sensitivity employing concentration samples. *Trop. Med. Health* 32, 1–4.

Mamuye, Y. (2012). *Comparison of Acidified-Egg Ogawa Medium and L-J Medium for Cultural Isolation of M. tuberculosis*. South Africa: ASLM.

Ministerio de Salud (2006). *Norma Técnica de Salud para el Control de la Tuberculosis*. Lima: MINSA.

Ministerio de Salud (2018). *Compendio normativo sobre prevención y control de la tuberculosis en el Perú*. Lima: Dirección General de Intervenciones Estratégicas en Salud Pública.

Ministerio de Salud (2020). *Resolución Ministerial N.° 920-2020-MINSA. Lima: MINSA*. Available at: https://www.gob.pe/institucion/minsa/normas-legales/1335213-920-2020-minsa

Ministerio de Salud (2023). *Norma Técnica De Salud para El Cuidado Integral de la Persona Afectada por Tuberculosis, Familia y Comunidad. NTS N° 200-MINSA/DGIESP-2023*. Lima: Dirección de Prevención y Control de Tuberculosis.

Ministerio de Salud (2024). *Sala situacional de Tuberculosis 2023*. Lima: Dirección de Prevención y Control de Tuberculosis.

Monkongdee, P., McCarthy, K. D., Cain, K. P., Tasaneeyapan, T., Nguyen, H. D., Nguyen, T. N., et al. (2009). Yield of acid-fast smear and mycobacterial culture for tuberculosis diagnosis in people with human immunodeficiency virus. *Am. J. Respir. Crit. Care Med.* 180, 903–908.

Moya-Salazar, J., Marín, E. A., Palomino-Leyva, C. B., Rivera, J., Torre, R. L., Cañari, B., et al. (2024). Geospatial analysis of cardiovascular mortality before and during the COVID-19 pandemic in Peru: analysis of the national death registry to support emergency management in Peru. *Front. Cardiovasc. Med.* 11:1316192. doi: 10.3389/fcvm.2024.1316192

Moya-Salazar, J., Nemolato, A., Samán, J., Pasco, I., and Olivo-López, J. (2018). Extra-pulmonary and pulmonary Tuberculosis among older Peruvian patients. *J. Immunol. Microbiol.* 2, 5–15.

Noori, M., Ali, Z., Khan, G., Sharafat, S., and Masroor, M. (2015). Differences in cultural yield of Mycobacterium tuberculosis on media prepared using commercial and household eggs. *J. Ayub. Med. Coll. Abottabad* 27, 764–766.

Palaci, M., Peres, R. L., Maia, R., Cunha, E. A., Ribeiro, M. O., Lecco, R., et al. (2013). Contribution of the Ogawa-Kudoh swab culture method to the diagnosis of pulmonary tuberculosis in Brazil. *Int. J. Tuberc. Lung Dis.* 17, 782–786.

Pan-American Health Organization (2013). *Tuberculosis in the Americas: Regional Report 2021. Epidemiology, Control and Financing*. Washington, DC: PAHO/WHO.

Park, S.-H., Kim, C.-K., Jeong, H.-R., Son, H., Kim, S.-H., and Park, M.-S. (2014). Evaluation and comparison of molecular and conventional diagnostic tests for detecting tuberculosis in Korea, 2013. *Osong Public Health Res.* 5, S3eS7.

Partridge, L., Deelen, J., and Slagboom, P. (2018). Facing up to the global challenges of ageing. *Nature* 561, 45–56. doi: 10.1038/s41586-018-0457-8

Purohit, M., and Mustafa, T. (2015). Laboratory Diagnosis of Extra-pulmonary Tuberculosis (EPTB) in Resource-constrained Setting: State of the Art, Challenges and the Need. *J. Clin. Diagn. Res.* 9, EE01–EE6. doi: 10.7860/JCDR/2015/12422.5792

Rivas, C., Coitinho, C., Dafond, V., Corbo, M., and Baldjian, M. (2010). Performance of the Ogawa-Kudoh method for isolation of mycobacteria in a laboratory with large-scale workload. *Rev. Argentina Microbiol.* 42, 87–90.

Robles, C., Monfil, L., Ibáñez, R., Roura, E., Font, R., Peremiquel-Trillas, P., et al. (2024). Impact of the COVID-19 pandemic on cervical cancer screening participation, abnormal cytology prevalence and screening interval in Catalonia. *Front. Oncol.* 14:1338859. doi: 10.3389/fonc.2024.1338859

Rojas-Bolivar, D., Zhu, Z., Hurtado, Y. (2018). Tuberculosis and Diabetes Mellitus Among Prison Inmates in Peru: Results of a National Survey, 2016. *Open Forum Infectious Dis.* 5, S274–S275. doi: 10.1093/ofid/ofy210.772

Salive, M. (2013). Multimorbidity in older adults. *Epidemiol. Rev.* 35, 75–83. doi: 10.1093/epirev/mxs009

Schaaf, S., Collins, A., Bekker, A., and Davies, P. (2010). Tuberculosis at extremes of age. *Respirology* 15, 747–763.

Sequeira de Latini, M., and Barrera, L. (2008). *Manual para el diagnóstico bacteriológico de la tuberculosis: Normas y Guía Técnica. Parte I Baciloscopía*. Washington, D.C: Organización Panamericana de la Salud (OPS/PAHO).

Sharma, M. V., Arora, V. K., and Anupama, N. (2022). Challenges in diagnosis and treatment of tuberculosis in elderly. *Ind. J. Tuberc.* 69, S205–S208. doi: 10.1016/j.ijtb.2022.10.001

Shivam, S., Saha, I., Mondal, T., Dasgupta, S., Bhattacharyya, K., and Roy, R. (2014). Comparative analysis of tuberculosis in geriatric and younger age group: An experience from rural West Bengal, India. *Sahel Med J.* 17, 71–74.

Silva, F., Castilho, A., Maltempe, F., et al. (2013). Use of the Ogawa-Kudoh method to isolate mycobacteria in a tuberculosis reference laboratory in northwestern Paraná, Brazil. *Braz. J. Pharm. Sci.* 49, 567–570.

Singhal, K., Sethi, G., and Hanif, M. (2014). Comparison of yield of acid fast bacilli (AFB) from induced sputum versus gastric lavage for diagnosis of pulmonary tuberculosis in children. *Eur. Respir. J.* 44, 2670.

Sood, R. (2000). The problema of Geriatric Tuberculosis. *J. Indian Acad. Clin. Med.* 5, 156–162.

Ssengooba, W., Kateete, D. P., Wajja, A., Bugumirwa, E., Mboowa, G., Namaganda, C., et al. (2012). An early morning sputum sample is necessary for the diagnosis of pulmonary tuberculosis, even with more sensitive techniques: a prospective cohort study among adolescent TB-suspects in Uganda. *Tuberc. Res. Treat.* 2012:970203.

Sulis, G., Centis, R., Sotgiu, G., D'Ambrosio, L., Pontali, E., Spanevello, A., et al. (2016). Recent developments in the diagnosis and management of tuberculosis. *NPJ Prim. Care Respir. Med.* 26, 16078.

Symes, M. J., Probyn, B., Daneshvar, C., and Telisinghe, L. (2020). Diagnosing pulmonary tuberculosis in the elderly. *Curr. Geriatr. Rep.* 9, 30–39. doi: 10.1007/s13670-020-00319-5

Tanoue, S., Mitarai, S., and Shishido, H. (2002). Comparative study on the use of solid media: Löwenstein-Jensen and Ogawa in the determination of anti-tuberculosis drug susceptibility. *Tuberculosis* 82, 63–67. doi: 10.1054/TUBE.2002.0323

Teo, A. K. J., Ork, C., Eng, S., Sok, N., Tuot, S., Hsu, L. Y., et al. (2020). Determinants of delayed diagnosis and treatment of tuberculosis in Cambodia: A mixed-methods study. *Infect. Dis. Poverty* 9:49. doi: 10.1186/s40249-020-00665-8

Teo, A. K. J., Rahevar, K., Morishita, F., Ang, A., Yoshiyama, T., Ohkado, A., et al. (2023). Tuberculosis in older adults: case studies from four countries with rapidly ageing populations in the western pacific region. *BMC Public Health* 23:370. doi: 10.1186/s12889-023-15197-7

Thomas, T. Y., and Rajagopalan, S. (2001). Tuberculosis and aging: A global health problem. *Clin. Infect. Dis.* 33, 1034–1039. doi: 10.1086/322671

Ugarte-Gil, C., Curisinche, M., Herrera-Flores, E., Hernandez, H., and Rios, J. (2021). Situation of the tuberculosis-diabetes comorbidity in adults in Peru: 2016-2018. *Rev. Per. Med. Exp. Salud Public.* 38, 254–260. doi: 10.17843/rpmesp.2021.382.6764

Williams, V., Vos-Seda, A. G., Calnan, M., Mdluli-Dlamini, L., Haumba, S., Grobbee, D. E., et al. (2023). Tuberculosis services during the COVID-19 pandemic: A qualitative study on the impact of COVID-19 and practices for continued services delivery in Eswatini. *Public Health Pract.* 6, 100405. doi: 10.1016/j.puhip.2023.100405

World Health Organization (2021). *Impact of the COVID-19 Pandemic on TB detection and mortality in 2020*. Geneva: WHO.

World Health Organization (2022). *Global tuberculosis report 2017*. Geneva: World Health Organization.

World Medical Association (2013). World Medical Association Declaration of Helsinki: Ethical principles for medical research involving human subjects. *JAMA* 310, 2191–2194. doi: 10.1001/jama.2013.281053

Yoshikawa, T., and Rajagopalan, S. (2001). Tuberculosis and Aging: A Global Health Problem. *Clin. Infec. Dis.* 7, 1034–1039.

Yvette, M., Barez, C., Mendoza, M., Celada, R., and Santos, H. (1995). Accuracy of AFB in Relation to TB Culture in Detection of Pulmonary Tuberculosis. *Phil. J. Microbiol. Infect. Dis.* 24, 33–36.

Zagaria, M. (2008). Tuberculosis: A Preventable Cause of Death in the Elderly. *US Pharm.* 33, 23–25.

frontiers | Frontiers in Tuberculosis

TYPE Original Research
PUBLISHED 08 January 2025
DOI 10.3389/ftubr.2024.1377540

OPEN ACCESS

EDITED BY
Robert Jansen,
Radboud University, Netherlands

REVIEWED BY
Luis Anibarro,
Complexo Hospitalario Universitario Pontevedra, Spain
Sridhar Rathinam,
Government of Tamil Nadu, India

*CORRESPONDENCE
Mohlopheni J. Marakalala
✉ mohlopheni.marakalala@ahri.org

RECEIVED 27 January 2024
ACCEPTED 06 December 2024
PUBLISHED 08 January 2025

CITATION
Rapulana AM, Mpotje T, Mthiyane N, Smit TK, McHugh TD and Marakalala MJ (2025) Analyses of blood-derived host biomarkers for pulmonary tuberculosis diagnosis in human immunodeficiency virus co-infected individuals in sub-Saharan Africa: a systematic review and meta-analysis.
Front. Tuberc. 2:1377540.
doi: 10.3389/ftubr.2024.1377540

Analyses of blood-derived host biomarkers for pulmonary tuberculosis diagnosis in human immunodeficiency virus co-infected individuals in sub-Saharan Africa: a systematic review and meta-analysis

Antony M. Rapulana[1,2,3], Thabo Mpotje[1,2], Nondumiso Mthiyane[2,4], Theresa K. Smit[1,2], Timothy D. McHugh[3] and Mohlopheni J. Marakalala[1,2,3]*

[1]School of Laboratory Medicine and Medical Science, University of Kwazulu-Natal, Durban, Kwazulu-Natal, South Africa, [2]Basic and Translational Science, Africa Health Research Institute, Durban, Kwazulu-Natal, South Africa, [3]Centre for Clinical for Clinical Microbiology, Division of Infection and Immunity, University College London, London, United Kingdom, [4]Institute for Global Health, University College London, London, United Kingdom

Objective: Our objective was to conduct a review of host blood-derived biomarkers as potential diagnostic targets for pulmonary TB and as alternative tests to identify active tuberculosis in HIV co-infected individuals.

Methods: A systematic review and meta-analysis of host blood-derived biomarkers with potential for diagnosis of active tuberculosis in HIV co-infected individuals was conducted. Cochrane Library, Embase, MEDLINE, PubMed and Web of Science databases were searched up to 7 November 2023. A hierarchical summary receiver operating characteristic (HSROC) model was used to evaluate the pooled sensitivity, specificity, positive likelihood ratio (PLR), negative likelihood ratio (NLR) and diagnostic odds ratio (DOR) of the following potential biomarkers: C-reactive protein (CRP), Interferon gamma induced protein-10 (IP-10), Neopterin, IGRA, Kynurenine to tryptophan (K/T) ratio and use of different panels of combined biomarkers; including 5 biomarker panel (IL-6, INF-y, MIG, CRP, and IL-18), 4 biomarker panel (IL-6, IL-21, INF-y, IL-1a), 6 biomarker panel (APO-ACIII, CXCL1, CXCL9, CCL8, CCL-1, and CD56), and 9 biomarker panel (Alpha-2-macroglobulin, fibrinogen, CRP, MMP-a, transthyretin, complement factor H, INF-y, IP-10, and TNF-α).

Results: Twenty-three studies were included. The pooled sensitivity of CRP, IP-10, Neopterin, combined biomarker signatures, IGRA and K/T ratio were 77% (60–88), 79% (72 - 84), 82% (43–96), 78% (64–88), 71% (65–76), 95% (90–98), respectively and the pooled specificity were 90% (80–96), 82% (59–93), 42% (22–66), 85% (73–92), 33% (18–54), and 95% (82–99), respectively.

Conclusion: CRP, IP-10, K/T ratio and the panels of multiple combined biomarkers that include the following cytokines, chemokines, and acute phase proteins IL-6, INF-y, MIG, CRP, IL-18, IL-21, IL-1a, APO-ACIII, CXCL1, CXCL9,

CCL8, CCL-1, CD56, Alpha-2-macroglobulin, fibrinogen, MMP-a, transthyretin, complement factor H, IP-10, and TNF-α are potential blood biomarkers that can aid TB diagnosis in HIV co-infected individuals.

KEYWORDS

cytokines, chemokine, systematic review, TB diagnosis, biomarkers, HIV-TB co-infection

Introduction

The diagnosis of pulmonary tuberculosis (TB) in resource limited areas is mainly by chest X-ray, Acid Fast Bacilli (AFB) staining and molecular methods such as GeneXpert (1). The use of GeneXpert MTB/RIF as a first-line diagnostic test for TB is recommended by WHO (2); however the test has not been fully implemented across all sub-Saharan African countries (3). These countries carry a severe burden of TB infection which is aggravated by emergence of drug resistant strains, a high prevalence of HIV co-infection, poverty, and people living in remote areas without proper access to health facilities (4). In response to the burden of disease, the "End TB strategy" targets a 90% reduction in patients suffering from TB, and a 95% reduction in deaths from TB by 2035 (5). However, studies have shown that deaths among HIV-infected individuals as a result of co-infection with TB are significantly higher in sub-Saharan African low- and middle-income countries (LMIC) compared to high-income countries (HIC) (6, 7).

During TB infection, *Mycobacterium tuberculosis* (*Mtb*) is engulfed by innate immune cells including macrophages, which recruit other immune cells such as T cells and B cells to form a granuloma that contains *Mtb* (8). Cytokines and chemokines play a role in this recruitment of immune cells to the site of mycobacteria infection (9) and so they have been proposed as blood-derived biomarkers with potential for the diagnosis of TB (10–12). However, the clinical value of blood biomarkers remains to be evaluated in a setting in sub-Saharan Africa with a high prevalence of both tuberculosis and HIV.

Diagnosis of TB in HIV-positive individuals can be complex: (I) HIV infection can modify the clinical presentation of TB, leading to atypical or less specific symptoms, (II) HIV-positive individuals often have coinfections or comorbidities that can complicate the clinical picture and may mimic TB symptoms, (III) HIV-induced immunosuppression can lead to atypical immune responses to TB, affecting the performance of conventional TB diagnostic tests such as tuberculin skin tests and interferon-gamma assays (13–16). Two meta-analyses reported the potential of IP-10 and CRP for diagnosis of TB from predominantly HIV negative studies (17, 18). By comparison, this systematic review and meta-analysis focuses on the evaluation of chemokines, cytokines, and acute phase protein as diagnostic biomarkers of TB in HIV co-infected individuals in a sub-Saharan African setting with a high prevalence of both TB and HIV.

Methods

This review was developed in accordance with the Preferred Reporting for Systematic Review and Meta-Analysis protocols (PRISMA-P) diagnostic test accuracy criteria and was registered by the international database of prospectively registered systematic reviews in health and social care (PROSPERO) (CRD42021277685). Ethical approval was not required for this study.

Literature search

The search strategy was designed by combining the medical (MeSH) terms: "'tuberculosis,' 'latent tuberculosis,' 'LTBI,' 'TB,' 'human Immunodeficiency syndrome,' 'HIV,' 'Sub-Saharan Africa,' 'Biomarkers,' 'assay,' 'assays,' 'bio-signature,' 'bio-signatures,' 'expression,' 'marker,' 'markers,' 'profile,' 'profiling,' 'profiles,' 'signature,' 'signatures,' 'surrogate endpoint,' 'test,' 'tests,' 'tool,' 'tools.'" in the following electronic databases: Embase, PubMed, and Web of Science up to and including 7 November 2023. The MeSH terms were used together using "OR," and the results were further combined using "AND" to obtain the result. The full search strategy is described in the Supplementary data 2.

Literature selection

We included studies that assessed the diagnostic accuracy of blood-based biomarkers for TB in HIV co-infected individuals, TB negative in HIV positive individuals, in sub-Saharan Africa. Only manuscripts written in English were included. Studies focused only on human pulmonary TB. For inclusion, there must have been a confirmed TB disease by either culture (liquid or solid), Acid fast bacilli (AFB) or GeneXpert MIT/RIF, as well as confirmed HIV infection. The studies that met our inclusion criteria were published between 2009 and 2023. We included studies that reported sensitivity, specificity, or sufficient information on any biomarker/s of pulmonary TB diagnosis assessed to construct tables of outcome. We included studies focused on both hospital and community-based participants of all ages. We also included case control, cohort, cross sectional studies and only studies that have clear reference standards for laboratory diagnosis of pulmonary TB. Reviews, letters, case reports, clinical trials, conference abstracts, and animal experiments were excluded.

Data extraction

Two reviewers (AR and NM) independently performed quality assessment on the extracted data and any discrepancies were resolved by discussion and consensus. The following data were extracted: author, year, country where study was conducted, participant information, reference standards, tests index, cut-offs,

true positive (TP), false positive (FP), false negative (FN) and true negative (TN).

Quality assessment

The quality assessment of diagnostic accuracy studies tool-2 (QUADAS-2) was used to evaluate the risk of bias and applicability in each study (19). Each reviewer performed an independent quality assessment of included studies by evaluating four domains (patient selection, index tests, reference standard, and flow and timing) for risk bias and three domains (patient selection, index tests and reference standard) for applicability. The Review Manager software (version 5.4, Cochrane Collaboration) was used to process the quality assessment of the included studies.

The first domain is patient selection i.e., selection of the participants based on a consecutive or at random basis, case-control design was avoided, and verifying whether the study avoided unnecessary exclusions. The participants of articles included in this review were also required to have the test condition. Thus, the risk of bias is high since only participants suspected of TB were selected. The second domain is the index test i.e., index test results interpreted without knowledge of the results of the reference standard and accurate explanation of detection threshold. The third domain is the reference standard 99% accuracy, but interpretation without considering the results of the index test and ensuring that all patients were assessed using the same reference standard. The last or fourth domain is the flow and timing (for risk bias only) describing the patients receiving the index test, the time interval between index tests, and reference standard. After independent evaluations, the reviewers discussed the article. Each domain was discussed to achieve a single view.

Statistical analysis

We used sensitivity and specificity of the biomarker reported in the studies to recalculate the sample numbers in each group. R

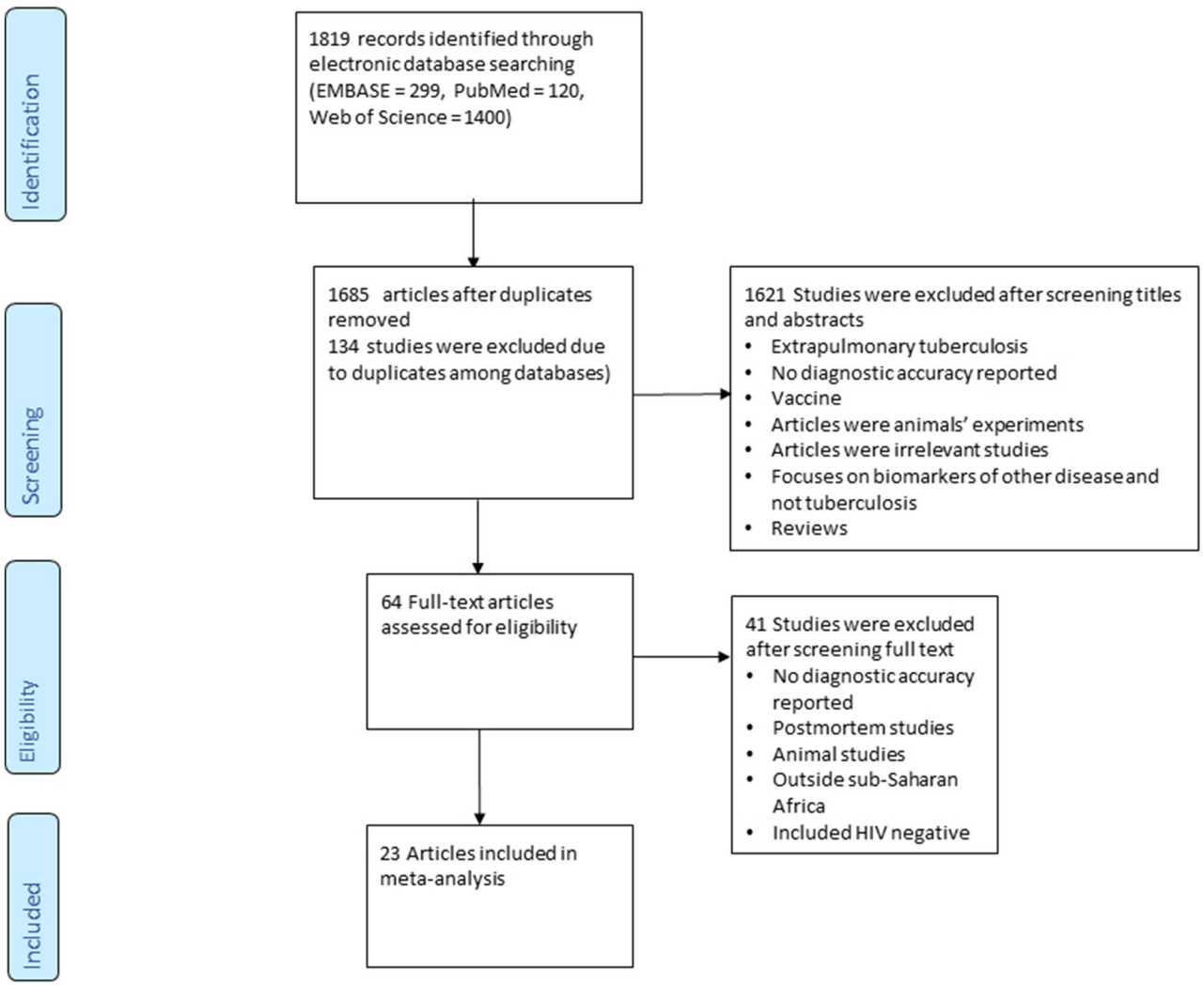

FIGURE 1
PRISMA flow diagram of inclusion and exclusion criteria.

software (version 4.12) was used to perform the statistical analyses. The pooled sensitivity, specificity, diagnostic odd ratios (DOR) were calculated, and summary receiver characteristics curves (SROC) were plotted for diagnostic efficiency of each biomarker of TB in HIV infected individuals from relevant articles relating to each biomarker. Index Q* was calculated from the corresponding value of DOR using Walter's formula (20). The DOR reflects the effectiveness of the index tests: DOR > 1 indicates that positive tests suggest active TB and DOR < 1 indicates that negative tests suggest that disease is absent. I^2 statistic was used to quantify the amount of variation across studies. A *p*-value of <0.05 indicated the presence of heterogeneity among included studies.

Results

Literature search

A total of 1,819 articles were identified from database searches (Embase = 299, PubMed = 120 and Web of Science = 1,400). Sixty-four papers were included and of the 1,755 excluded studies, 134 were duplicates; 1,621 studies were excluded after screening titles and abstracts relating to any of the following: (extrapulmonary tuberculosis, no diagnostic accuracy reported, vaccine studies, animal experiments, focus on biomarkers of other diseases, and reviews), 2 were reviews. Forty-one studies were excluded after full paper screening if they (Included HIV negative only, animal studies/experiments, conducted outside Sub-Saharan Africa, or Postmortem studies). Ultimately 23 studies were eligible for inclusion in this study (Figure 1).

The characteristics of the 23 eligible studies are shown Table 1 (21–45). All eligible studies were published in English between 2009 and 2023. Three (13%) studies included only children (21, 28, 31), seventeen (74%) studies included only adults (23, 26–30, 33, 46), three (13%) studies did not report the ages (24, 25).

The reference standard for pulmonary TB diagnosis includes the use of MTB/RIF GeneXpert, Acid Fast Bacillus (AFB) staining, culture (solid and liquid culture) and fluorescence microscopy. Study design, samples used, method, reference standard, index test, cut-off, true positive, false positive, false negative, and true negative for each study are summarized in Table 1. Five individual biomarkers CRP, IGRA, IP-10, Kynurenines to tryptophan ratio and neopterin were reported frequently. Five studies reported mixed biomarker sets for diagnosis of tuberculosis.

Ten (43%) studies used CRP as the index test (21, 23–27, 30, 34, 44, 45, 47) and a total of 1,882 participants were included. The diagnostic odds ratio (DOR) was 28.349 (8.589–93.571) (Figure 2). The pooled sensitivity was 77% (59.5–88.4) and pooled specificity 90.2% (79.5–95.6) (Figures 3, 4). The heterogeneity for CRP was significant with I^2 of 96% for sensitivity and 96% for specificity with both *p*-value of less than <0.01, respectively.

Three (13%) studies used IGRA (35, 40, 41) as index test, with a total of 398 participants. The pooled sensitivity was 70.9% (64.7–76.4), pooled specificity was 33.1% (17.6–53.5), and DOR was 1.372 (0.394–4.771) (Figures 3, 4). The heterogeneity analysis of IGRA yielded an I^2 of 0% for sensitivity and significant heterogeneity of pooled specificity with I^2 of 90% with *p*- value of less than <0.01.

The three (13%) studies which determined the diagnostic accuracy of IP-10 (22, 30, 31), included a total of 436 participants. The pooled sensitivity was 79% (72–84), pooled specificity was 82% (59–93), and DOR was 13.28 (2.18–80.85) (Figures 3, 4). The heterogeneity analysis of IP-10 yielded an I^2 of 34% for sensitivity and significant heterogeneity of pooled specificity with I^2 of 88% with *p*- value of <0.01.

Two (8.7%) studies used K/T ratio (36, 37) as an index test, with a total of 296 participants. The pooled sensitivity was 95.4% (89.5–98.1), pooled specificity was 95.1% (82.1–98.8), and DOR was 450.675 (30.410–6678.882) (Figures 3, 4). The heterogeneity analysis of K/T ratio yielded an I^2 of 0% for sensitivity and significant heterogeneity of pooled specificity with I^2 of 74% with p- value of <0.05.

Two (8.7%) studies used neopterin (23, 33) as an index test, with a total of 388 participants. The pooled sensitivity 82% (42–96), pooled specificity 42% (22–66), and DOR 3.09 (1.07–8.93) (Figures 3, 4). The heterogeneity analyses of neopterin yielded an I^2 of 93% for sensitivity and 96% for specificity and *p*-value of <0.01 respectively.

One (4.3%) study reported antibodies in lymphocyte supernatant (38) and another study (4.3%) reported at 5-transcript signature (43) for diagnosis of pulmonary TB in HIV co-infected participants. The pooled sensitivity and specificity were not done for ALS and 5-transcript signatures.

Among the included studies, five (21.7%) looked at a combination of biomarkers as signatures to evaluate the diagnostic accuracy of active tuberculosis. The combination of biomarker signatures in the five studies included five biomarkers (IL-6, INF-y, MIG, CRP, and IL-18) (25), four biomarkers (IL-6, IL-21, INF-y, IL-1a) (28), six biomarkers (APO-ACIII, CXCL1, CXCL9, CCL8, CCL-1, and CD56) (29), nine biomarkers (Alpha-2-macroglobulin, fibrinogen, CRP, MMP-a, transthyretin, complement factor H, INF-y, IP-10, and TNF-α) (30), and four biomarkers (INF-y, TNF-a, IL-2, and IL-12) (42). The DOR was 25.267 (15.224–41.937) (Figure 2). The pooled sensitivity and specificity were 78.4% (64.4–87.9) and 84.6% (73.2–91.7) (Figures 3, 4). There was significant heterogeneity in both pooled sensitivity and specificity with I^2 of 79 and 77%, and the *p*-value of <0.01 and <0.01, respectively. We performed SROC analysis to assess the power of CRP, IP-10, Neopterin, selected combined biomarkers, IGRA, and K/T ratio and all had good diagnostic accuracy (Supplementary Figure 1).

Quality assessment

QUADAS-2 was used to assess risk bias and applicability of the study. Two studies (26, 29) showed high risk of bias and 8 (24, 25, 28, 30, 31, 38, 40, 41) had unclear risk for patient selection. Three studies (21, 28, 30) had high risk for index test and two (24, 43) showed an unclear risk of bias for index test. For applicability concerns one study (28) showed high risk of bias and one (29) showed unclear risk of bias (Supplementary Figure 2).

TABLE 1 Main characteristics of included studies.

References	Country study conducted	Samples	Method	Reference standard	Index test (s)	Test and cutoffs	TP	FP	FN	TN
Aabye et al. (35)	Tanzania	Plasma	QFT-IT ELISA	Sputum Culture	QFT-IT	0.35 IU/mL	44	24	NR	NR
Adu-Gyamfi et al. (36)	South Africa	Plasma	LC-MS	Culture, Chest radiography and Clinical signs and syptoms	Kyn to Trp Ratio	0.8	36	1	1	69
Adu-Gyamfi et al. (37)	South Africa	Plasma	ELISA	Liquid culture, flouresence microscopy and Expert MTB/RIF	Kyn to Trp Ratio	0.1	68	4	105	12
Alvarez et al. (21)	South Africa	NR	NR	Culture	CRP	>11 mg/dl	82	6	4	136
Ashenafi et al. (38)	Ethiopia	PBMC	ELISA and Flow cytometry	Culture	ALS	NR	29	47	NR	NR
Bedell et al. (34)	Malawi	blood	CRP latex	Culture and MTB/RIF GeneXpert	CRP	>10 mg/L	45	45	7	151
Cattamanchi et al. (40)	Uganda	Peripheral blood and bronchoalveolar lavage	ELISPOT	Culture	IGRA	NR	26	10	46	12
Cattamanchi et al. (41)	Uganda	Peripheral blood	ELISPOT	Culture	IGRA	NR	93	33	59	51
Chegou et al. (22)	South Africa	Quantiferon Supernatant	Luminex multiplex	MGIT and Chest radiography	IP-10	>6,768 pg/mL	12	25	7	32
Ciccacci et al. (23)	Mozambique	Plasma	ELISA	MTB/RIF	CRP	>10 mg/L 10 nmol/L	16	6	5	116
				GeneXpert	Neopterin		49	143	3	53
Drain et al. (24)	South Africa	Blood	Dimension RXL analyser	AFB and Culture (Solid and Liquid)	CRP	>8 mg/L	43	24	2	24
Farr et al. (25)	Uganda	Plasma	Multiplex	AFB, MGIT and MTB/RIF GeneXpert	Combination of CRP with IL-6, INF-y, MIG	20, 23, 2994, 248, 69 mg/L	44	5	10	15
Gersh et al. (26)	Kenya	Blood and spot	NR	AFB, MGIT and MTB/RIF GeneXpert	CRP	>10 mg/L	1	38	5	340
Lawn et al. (27)	South Africa	Serum	ELISA	Liquid culture, fluorescence microscopy and MTB/RIF GeneXpert	CRP	<10 mg/L	69	179	12	239

(Continued)

10.3389/ftubr.2024.1377540

TABLE 1 (Continued)

References	Country study conducted	Samples	Method	Reference standard	Index test (s)	Test and cutoffs	TP	FP	FN	TN
Kisuya et al. (42)	Kenya	PBMC Supernatant	Flow Cytometry and ELISA	Culture	IFN-y, TNF-a, IL-2, and IL-12	NR	36	4	5	41
Lundtoft et al. (28)	Ghana	Quantiferon Spernatant	Luminex multiplex	Chest radiography and sputum culture	Combination of IL-6, IL-21, TNF-α and IL-1α	NR	18	7	NR	NR
Manngo et al. (29)	South Africa	QuantiFERON Supernatant	Luminex Multiplex	MTB/RIF GeneXpert and MGIT	Combination of Apo-ACIII, CXCL1, CXCL9, CCL8, CCL-1, CD56	<20,360.2, >381.7, >940.3, −0.1554, <124,132 ng/mL	26	9	9	60
Morris et al. (30)	South Africa and Malawi	Serum	Luminex multiplex	Culture	CRP	NR	110	37	12	90
					P-10		99	22	23	105
					Nine Protein signature		112	37	10	90
Petrone et al. (31)	Uganda	Blood	Luminex	TB culture (Liquid and solid)	IP-10	209.1 pg/mL	25	5	7	74
Rajan et al. (43)	Uganda	blood	PCR	Culture	5-transcript signature		38	2	10	30
Ruperez et al. (44)	Zambia and South Africa	blood	Alere Afinion AS100 analyser	Culture and MTB/RIF Expert	CRP	5 mg/L	18	7	133	118
Uwimaana et al. (33)	Uganda	Plasma and serum	ELISA	Sputum culture	Neopterin and HO-1	>10.12 and >8.95 ng/mL	40	28	30	42
Yoon et al. (45)	Uganda	whole blood	POC	Culture and MTB/RIF Expert	CRP	10 mg/L	145	18	283	731

AFB, acid-fast bacillus; CRP, C-reactive protein; ELISA, enzyme-linked immunosorbent assay; IP-10, induced protein 10; MGIT, mycobacteria growth indicator tube; TB, tuberculosis; TP, true positive; FP, false positive; FN, false negative; TN, true negative; Nine protein signature (fibrinogen, alpha-2-macroglobulin, CRP, MMP-9, transthyretin, complement factor H, IFN-gamma, IP-10, and TNF-alpha); NR, not reported.

10.3389/ftubr.2024.1377540

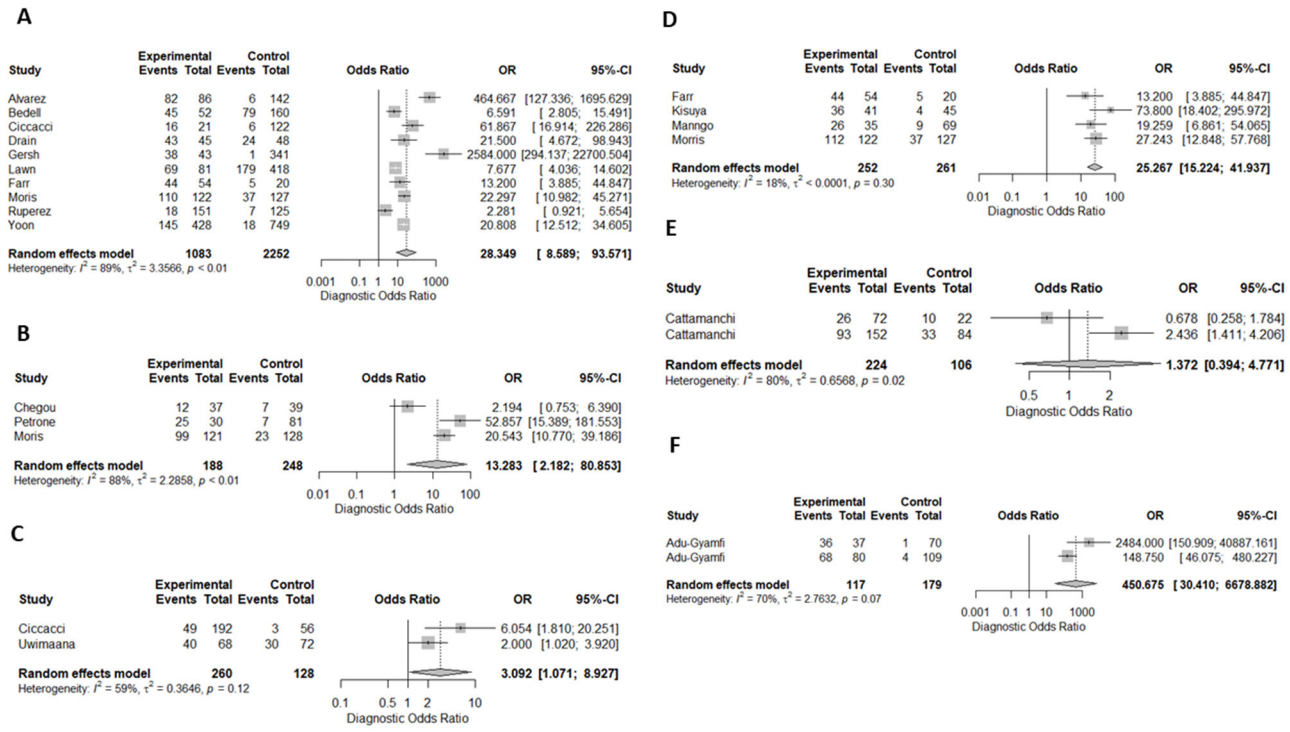

FIGURE 2
Forest plots of diagnostic odds ratio for **(A)** CRP, **(B)** IP-10, **(C)** Neopterin, **(D)** combination of biomarkers, **(E)** IGRA, and Kynurenines to tryptophan ratio in the diagnosis of TB, **(F)** K/T ratio in the dioagnosis of TB. OR, odds ratio; CI, confidence interval.

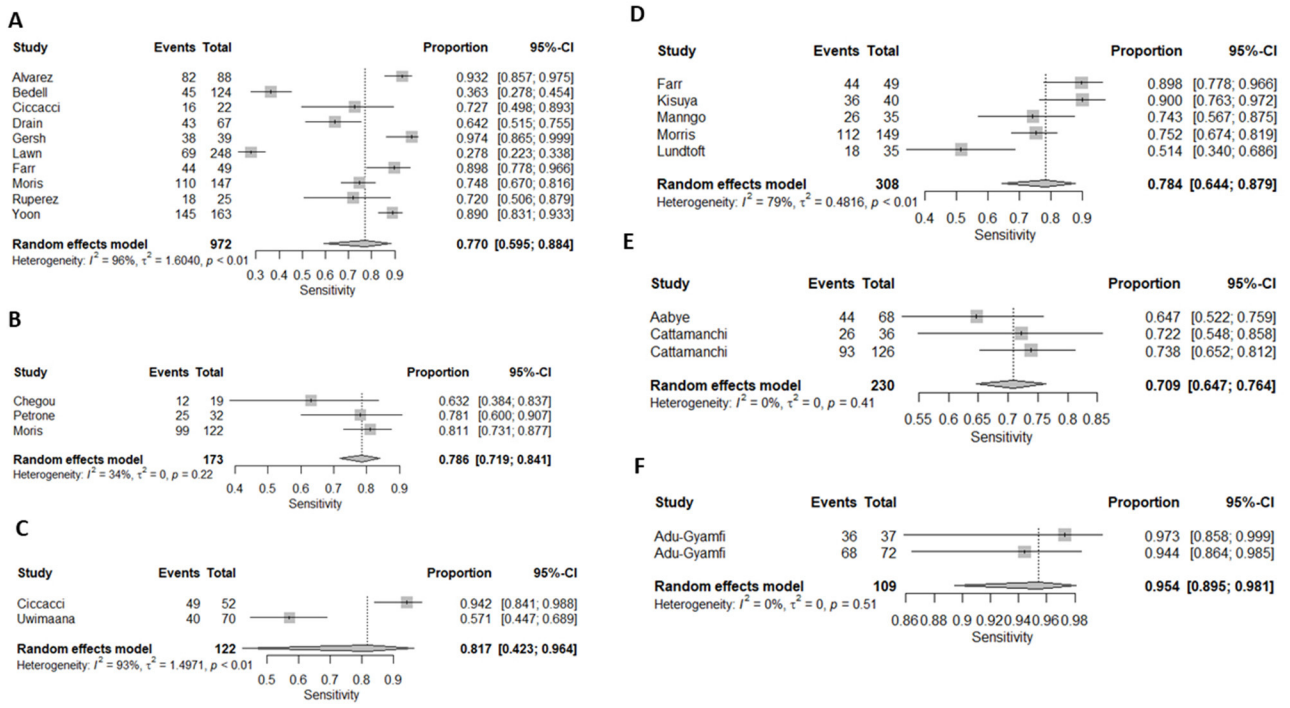

FIGURE 3
Forest plots of **(A)** CRP's, **(B)** IP-10, **(C)** Neopterin, **(D)** combination of biomarkers, **(E)** IGRA, and Kynurenines to tryptophan ratio sensitivity for diagnosis of active tuberculosis, **(F)** K/T ratio sensitivity for diagnosis of active tuberculosis.

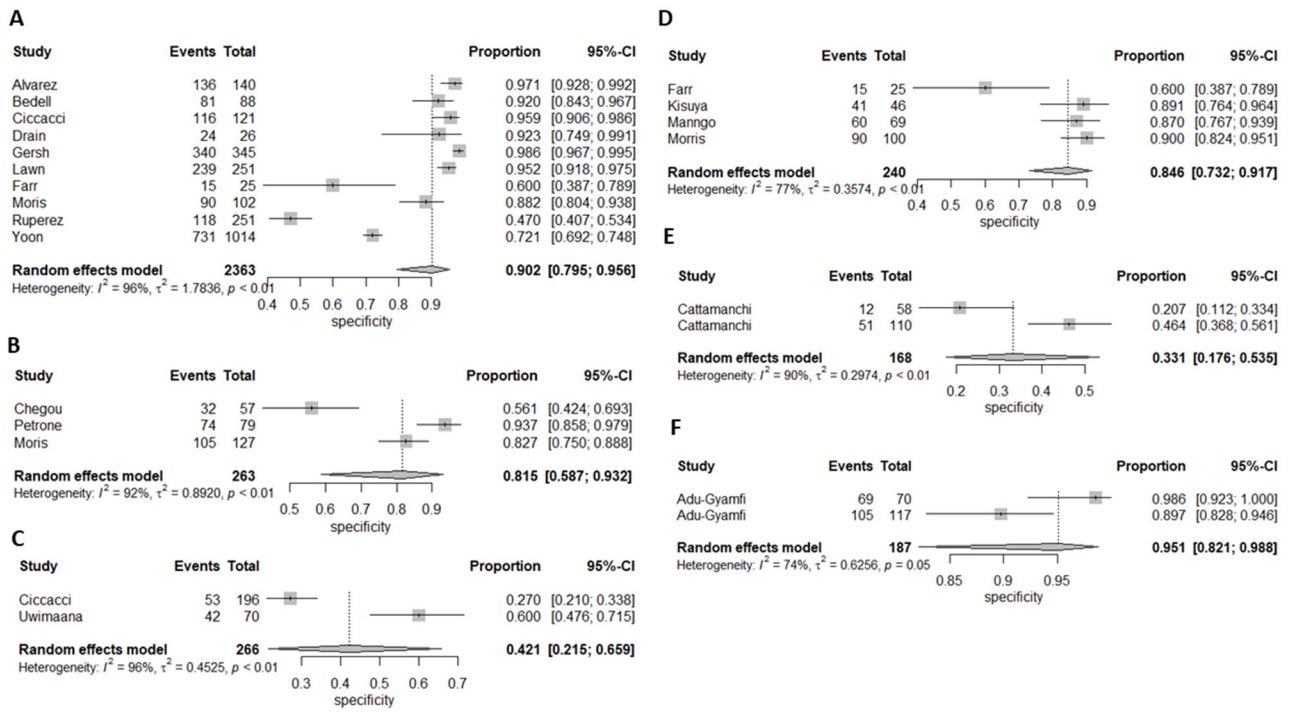

FIGURE 4
Forest plot of **(A)** CRP's, **(B)** IP-10, **(C)** Neopterin, **(D)** combination of biomarkers, **(E)** IGRA, and Kynurenines to tryptophan ratio for specificity for diagnosis of active tuberculosis, **(F)** K/T ratio sensitivity for diagnosis of active tuberculosis.

Discussion

The findings from this systematic review suggest that analyses of CRP (77.0 and 90.0%), IP-10 (78.6 and 81.5%), K/T ratio (95.4 and 95.1%), and a panel of multiple combined cytokines (Table 2), chemokines and acute phase proteins (78.4 and 84.6%) in TB/HIV coinfected individuals are promising potential biomarkers, with pooled sensitivity and specificity of more than 75% in diagnosing TB. With future validation, these blood-based markers may provide alternative ancillary methods for diagnosis of pulmonary TB in HIV co-infected individuals.

Blood-based biomarkers could play a crucial role in improving TB diagnosis in HIV positive individuals by providing a less invasive, more accessible, and faster diagnostic method. It has been shown that individuals with HIV-TB co-infection may have a lower bacterial load in the sputum, therefore making traditional diagnostic tool like sputum microscopy less effective (48, 49). It has been shown that in TB infection, myeloid cells, including macrophages and neutrophils, are essential in the immune response mounted to Mycobacterium tuberculosis acting as the first line of defense by phagocytosing and attempting to kill the bacteria (8, 50). Myeloid-derived suppressor cells (MDSCs) can also amass during TB infection, potentially suppressing immune responses and contributing to disease advancement (51). In HIV infection, myeloid cells such as macrophages and dendritic cells are important targets for and may serve as reservoirs of HIV, enabling the virus to endure even during antiretroviral therapy, as well as facilitate the spread to CD4+T cells (52). In the case of HIV and TB coinfection, HIV infection may impair the function of myeloid cells, reducing their ability to control *M.tb* which may lead to a higher risk of latent TB reactivation and more advanced disease (53). In addition, the dysfunction of macrophages and dendritic cells due to HIV can exacerbate TB outcome. Most of the studied biomarkers with potential to diagnose TB in HIV-co-infected individuals are produced by myeloid cells including macrophages and neutrophils, as well as dendritic cells (54–57). Thus, mechanistically, these myeloid specific responses would be expected to be higher in TB-HIV co-infection compared to HIV infection alone, and could aid in the diagnoses of TB in people living with HIV. However, such proposed mechanism need validation.

The results of this study were consistent with those reported in the systematic review by Santos et al. where both high- and low-income countries were included (18), however our study considered HIV infected individuals only. The meta-analysis by Santos et al. reported higher sensitivity of IP-10, the same sensitivity of CRP and low specificity of both IP-10 and CRP in HIV uninfected participants compared to our study and showed that IP-10 and CRP can also be used to diagnose pulmonary TB in patients with other lung diseases (18). It should be noted that some studies tested different sets of biomarkers, the SROC plots include diagnostic accuracy of combined cytokines, chemokines, and acute phase proteins from those studies.

It has been estimated that the current limitation in TB diagnosis has led to ~3.6 million TB cases never being detected or properly treated (58). There is an urgent need for more sensitive and specific TB diagnostic tests with a short turnaround time. Even

TABLE 2 The role/function of cytokines and chemokines and cells producing them.

Biomarkers	Cells producing	Function/role
CRP	Liver, atherosclerotic plaques by activated vascular cells	Sent into bloodstream in response to inflammation
IP-10	T-cells	It is chemokine secreted from cells stimulated with type I and II IFNs and LPS, is a chemoattractant for activated T cells. It plays important role in recruiting activated T cells into sites of tissue inflammation.
Neopterin	Macrophages, lymphocytes, dendritic cells	It is biomarker for immune system activation. The monocytes and dendritic cells activate gene expression of inducible NOS to increase neopterin levels. It is member of the pteridine family, is derived from guanosine triphosphate via guanosine triphosphate cyclohydrolase and is released from macrophages as a consequence of T cell-dependent interactions involving interferon-y
IL-6	Macrophages	It is a soluble mediator with a pleiotropic effect on inflammation, immune response, and hematopoiesis
INF-y	Lymphocytes	It is effector cytokine with pleiotropic role associated with antiproliferative, pro-apoptotic and antitumor mechanisms
MIG	Endothelial cell, infiltrating neutrophil, and macrophage	It is CXC chemokine active as a chemoattractant for activated T cells.
IL-18	Kupffer cells or macrophage	It is proinflammatory cytokine that has pleiotropic function involved in the regulation of both innate and acquired immune responses, playing a key role in autoimmune, inflammatory, and infectious diseases
IL-1a	macrophage or activated monocytes and senescent cells	pro-inflammatory that stimulates the activity of genes involved in inflammation and immunity
IL-21	T helper cells	It is cytokine that has regulatory effects on cells of the immune system, including natural killer (NK) cells and cytotoxic T cells that can destroy virally infected or cancerous cells
APO-ACIII	Liver	
CXCL1/MGSA	Macrophage, Neutrophil, Epithelial cell and TH17 population	It is chemokine that plays a pivotal role in the host immune response by recruiting and activating neutrophils for microbial killing at the tissue site
CXCL9	Monocytes, Endothelial cells, Fibroblasts and cancer cells	It is chemokine which plays role to induce chemotaxis, promote differentiation and multiplication of leukocytes, and cause tissue extravasation
CCL8/MCP2	T helper type 2 cells	It is belonging to CC chemokine sub family that plays a pivotal role in the control of leukocyte chemotaxis, HIV enry and other inflammatory disease
CCL-1	Activated monocytes, Macrophage, T lymphocytes and Endothelial cells	It is glycoprotein that binds to the chemokine receptor CCR8 and induces Ca2+ influx, chemotaxis and regulate apoptosis
CD56/NCAM	Natural Killer cells	The recognition of target cells and in the induction of cytotoxicity
Alpha-2-macroglobulin	liver, macrophages, fibroblasts and adrenocortical	Binding host or foreign peptides and particles, thereby serving as humoral defense barriers against pathogens in the plasma and tissue
Fibrinogen	liver hepatocyte	Formation of fibrin that binds together platelets and some plasma proteins in a hemostatic plug
Transthyretin	liver, pancreatic cells, retina, epithelial cells of choroid plexus	Is a transport protein in the plasma and cerebrospinal fluid that transports the thyroid hormone thyroxine and retinol to the liver
Complement factor H	Podocytes	It is a soluble complement regulator essential for controlling the alternative pathway in blood and on cell surfaces
TNF-α	Activated macrophages, T lymphocytes, natural killer cells	Inflammatory cytokine that is responsible for a diverse range of signaling events within cells, leading to necrosis or apoptosis

with the extensive rollout by WHO of MTB/RIF GeneXpert, the low sensitivity in sputum samples and challenges of diagnosis in infants and children, who may not be able to provide sputum samples (32), remains a critical limitation on improved diagnostics. The limitation of this study was the lack of data to analyze levels of the biomarkers at different time points of TB disease, from asymptomatic subclinical disease to infection and to severe advanced cavitary diseases. Secondly, we could not analyze the source of significant heterogeneity for CRP, IP-10, and Neopterin studies due to fewer number of studies, However, for CRP, the use of different sample types (blood, plasma, dried blood spots, and serum) may have contributed to the observed heterogeneity. Third limitation of the study is inability to investigate impact of CD4 count on the biomarkers.

In conclusion, the CRP, IP-10, neopterin, K/T ratio and panels of multiple combined biomarkers are promising tests for diagnosis of tuberculosis in HIV co-infected individuals. However, more studies need to be conducted to examine the combination of biomarkers in HIV infected individuals vs. HIV uninfected individuals to support the finding of this systematic review. We recommend future studies are also conducted to determine and evaluate the use of biomarker algorithms to (i) accurately diagnose

active TB in HIV coinfected individuals; (ii) assess the impact of HIV treatment on TB diagnosis; (iii) determine the transition from latent to active TB; and (iv) assess if there is any strain variation in diagnosing TB using host biomarkers.

Data availability statement

The original contributions presented in the study are included in the article/Supplementary material, further inquiries can be directed to the corresponding author.

Author contributions

AR: Conceptualization, Data curation, Formal analysis, Funding acquisition, Investigation, Methodology, Project administration, Writing – original draft, Writing – review & editing. TM: Data curation, Formal analysis, Investigation, Methodology, Validation, Writing – review & editing. NM: Data curation, Formal analysis, Investigation, Methodology, Software, Validation, Writing – review & editing. TS: Conceptualization, Funding acquisition, Resources, Supervision, Validation, Writing – review & editing. TM: Conceptualization, Funding acquisition, Resources, Supervision, Validation, Writing – review & editing, Formal analysis. MM: Conceptualization, Funding acquisition, Resources, Supervision, Validation, Writing – review & editing.

Funding

The author(s) declare financial support was received for the research, authorship, and/or publication of this article. The work reported herein was made possible through funding by DST/NRF (Grant Number: MND200429517780), UKZN College of Health Science, and the South African Medical Research Council through its Division of Research Capacity Development under the Mid-Career Scientist Program (MM) from funding received from the South African National Treasury. The content hereof is the sole responsibility of the authors and does not necessarily represent the official views of the funders. MM was funded by Wellcome Trust (grant# 206751/A/17/Z) and Bill & Melinda Gates Foundation (OPP1210776).

Conflict of interest

The authors declare that the research was conducted in the absence of any commercial or financial relationships that could be construed as a potential conflict of interest.

The author(s) declared that they were an editorial board member of Frontiers, at the time of submission. This had no impact on the peer review process and the final decision.

Publisher's note

Supplementary material

The Supplementary Material for this article can be found online at: https://www.frontiersin.org/articles/10.3389/ftubr.2024.1377540/full#supplementary-material

References

1. Caulfield AJ, Wengenack NL. Diagnosis of active tuberculosis disease: from microscopy to molecular techniques. *J Clin Tuberc Other Mycobact Dis.* (2016) 4:33–43. doi: 10.1016/j.jctube.2016.05.005

2. WHO. *Guidelines Approved by the Guidelines Review Committee. Policy Statement: Automated Real-Time Nucleic Acid Amplification Technology for Rapid and Simultaneous Detection of Tuberculosis and Rifampicin Resistance: Xpert MTB/RIF System*. Geneva: World Health Organization Copyright © World Health Organization (2011).

3. Ford N, Matteelli A, Shubber Z, Hermans S, Meintjes G, Grinsztejn B, et al. TB as a cause of hospitalization and in-hospital mortality among people living with HIV worldwide: a systematic review and meta-analysis. *J Int AIDS Soc.* (2016) 19:20714. doi: 10.7448/IAS.19.1.20714

4. Chakaya J, Khan M, Ntoumi F, Aklillu E, Fatima R, Mwaba P, et al. Global tuberculosis report 2020 - reflections on the global TB burden, treatment and prevention efforts. *Int J Infect Dis.* (2021) 113 Suppl 1:S7–s12. doi: 10.1016/j.ijid.2021.02.107

5. WHO. *The End TB Strategy*. Geneva: World Health Organization (2015).

6. Braitstein P, Brinkhof MW, Dabis F, Schechter M, Boulle A, Miotti P, et al. Mortality of HIV-1-infected patients in the first year of antiretroviral therapy: comparison between low-income and high-income countries. *Lancet.* (2006) 367:817–24. doi: 10.1016/S0140-6736(06)68337-2

7. Farahani M, Vable A, Lebelonyane R, Seipone K, Anderson M, Avalos A, et al. Outcomes of the Botswana national HIV/AIDS treatment programme from 2002 to 2010: a longitudinal analysis. *Lancet Glob Health.* (2014) 2:e44–50. doi: 10.1016/S2214-109X(13)70149-9

8. Ramakrishnan L. Revisiting the role of the granuloma in tuberculosis. *Nat Rev Immunol.* (2012) 12:352–66. doi: 10.1038/nri3211

9. Cambier CJ, Takaki KK, Larson RP, Hernandez RE, Tobin DM, Urdahl KB, et al. Mycobacteria manipulate macrophage recruitment through coordinated use of membrane lipids. *Nature.* (2014) 505:218–22. doi: 10.1038/nature12799

10. Chiappini E, Della Bella C, Bonsignori F, Sollai S, Amedei A, Galli L, et al. Potential role of *M. tuberculosis* specific IFN-γ and IL-2 ELISPOT assays in discriminating children with active or latent tuberculosis. *PLoS ONE.* (2012) 7:e46041. doi: 10.1371/journal.pone.0046041

11. Goletti D, Raja A, Kabeer BSA, Rodrigues C, Sodha A, Carrara S, et al. Is IP-10 an accurate marker for detecting *M. tuberculosis*-specific response in HIV-infected persons? *PLoS ONE.* (2010) 5:e0012577. doi: 10.1371/journal.pone.0012577

12. Walzl G, McNerney R, du Plessis N, Bates M, McHugh TD, Chegou NN, et al. Tuberculosis: advances and challenges in development of new diagnostics and biomarkers. *Lancet Infect Dis.* (2018) 18:e199–210. doi: 10.1016/S1473-3099(18)30111-7

13. Sterling TR, Pham PA, Chaisson RE. HIV infection-related tuberculosis: clinical manifestations and treatment. *Clin Infect Dis.* (2010) 50 Suppl 3:S223–30. doi: 10.1086/651495

14. Mayer KH, Dukes Hamilton C. Synergistic pandemics: confronting the global HIV and tuberculosis epidemics.

Clin Infect Dis. (2010) 50 Suppl 3:S67–70. doi: 10.1086/651475

15. Lawn SD, Wood R. Tuberculosis in antiretroviral treatment services in resource-limited settings: addressing the challenges of screening and diagnosis. *J Infect Dis.* (2011) 204 Suppl 4:S1159–67. doi: 10.1093/infdis/jir411

16. Syed Ahamed Kabeer B, Sikhamani R, Swaminathan S, Perumal V, Paramasivam P, Raja A. Role of interferon gamma release assay in active TB diagnosis among HIV infected individuals. *PLoS ONE.* (2009) 4:e5718. doi: 10.1371/journal.pone.0005718

17. Yoon C, Chaisson LH, Patel SM, Allen IE, Drain PK, Wilson D, et al. Diagnostic accuracy of C-reactive protein for active pulmonary tuberculosis: a meta-analysis. *Int J Tuberc Lung Dis.* (2017) 21:1013–9. doi: 10.5588/ijtld.17.0078

18. Santos VS, Goletti D, Kontogianni K, Adams ER, Molina-Moya B, Dominguez J, et al. Acute phase proteins and IP-10 as triage tests for the diagnosis of tuberculosis: systematic review and meta-analysis. *Clin Microbiol Infect.* (2019) 25:169–77. doi: 10.1016/j.cmi.2018.07.017

19. Whiting PF, Rutjes AW, Westwood ME, Mallett S, Deeks JJ, Reitsma JB, et al. QUADAS-2: a revised tool for the quality assessment of diagnostic accuracy studies. *Ann Intern Med.* (2011) 155:529–36. doi: 10.7326/0003-4819-155-8-201110180-00009

20. Walter SD. Properties of the summary receiver operating characteristic (SROC) curve for diagnostic test data. *Stat Med.* (2002) 21:1237–56. doi: 10.1002/sim.1099

21. Alvarez GG, Sabri E, Ling D, Cameron DW, Maartens G, Wilson D, et al. model to rule out smear-negative tuberculosis among symptomatic HIV patients using C-reactive protein. *Int J Tuberc Lung Dis.* (2012) 16:1247–51. doi: 10.5588/ijtld.11.0743

22. Chegou NN, Detjen AK, Thiart L, Walters E, Mandalakas AM, Hesseling AC, et al. Utility of host markers detected in Quantiferon supernatants for the diagnosis of tuberculosis in children in a high-burden setting. *PLoS ONE.* (2013) 8:e64226. doi: 10.1371/journal.pone.0064226

23. Ciccacci F, Floridia M, Bernardini R, Sidumo Z, Mugunhe RJ, Andreotti M, et al. Plasma levels of CRP, neopterin and IP-10 in HIV-infected individuals with and without pulmonary tuberculosis. *J Clin Tuberc Other Mycobacter Dis.* (2019) 16:100107. doi: 10.1016/j.jctube.2019.100107

24. Drain PK, Mayeza L, Bartman P, Hurtado R, Moodley P, Varghese S, et al. Diagnostic accuracy and clinical role of rapid C-reactive protein testing in HIV-infected individuals with presumed tuberculosis in South Africa. *Int J Tuberc Lung Dis.* (2014) 18:20–6. doi: 10.5588/ijtld.13.0519

25. Farr K, Ravindran R, Strnad L, Chang E, Chaisson LH, Yoon C, et al. Diagnostic performance of blood inflammatory markers for tuberculosis screening in people living with HIV. *PLoS ONE.* (2018) 13:e0206119. doi: 10.1371/journal.pone.0206119

26. Gersh JK, Barnabas RV, Matemo D, Kinuthia J, Feldman Z, Lacourse SM, et al. Pulmonary tuberculosis screening in anti-retroviral treated adults living with HIV in Kenya. *BMC Infect Dis.* (2021) 21:218. doi: 10.1186/s12879-021-05916-z

27. Lawn SD, Kerkhoff AD, Vogt M, Wood R. Diagnostic and prognostic value of serum C-reactive protein for screening for HIV-associated tuberculosis. *Int J Tuberc Lung Dis.* (2013) 17:636–43. doi: 10.5588/ijtld.12.0811

28. Lundtoft C, Awuah AAA, Nausch N, Enimil A, Mayatepek E, Owusu-Dabo E, et al. Alternative quantiferon cytokines for diagnosis of children with active tuberculosis and HIV co-infection in Ghana. *Med Microbiol Immunol.* (2017) 206:259–65. doi: 10.1007/s00430-017-0501-6

29. Manngo PM, Gutschmidt A, Snyders CI, Mutavhatsindi H, Manyelo CM, Makhoba NS, et al. Prospective evaluation of host biomarkers other than interferon gamma in QuantiFERON Plus supernatants as candidates for the diagnosis of tuberculosis in symptomatic individuals. *J Infect.* (2019) 79:228–35. doi: 10.1016/j.jinf.2019.07.007

30. Morris TC, Hoggart CJ, Chegou NN, Kidd M, Oni T, Goliath R, et al. Evaluation of host serum protein biomarkers of tuberculosis in sub-Saharan Africa. *Front Immunol.* (2021) 12:639174. doi: 10.3389/fimmu.2021.639174

31. Petrone L, Cannas A, Aloi F, Nsubuga M, Sserumkuma J, Nazziwa RA, et al. Blood or urine IP-10 cannot discriminate between active tuberculosis and respiratory diseases different from tuberculosis in children. *Biomed Res Int.* (2015) 2015:589471. doi: 10.1155/2015/589471

32. Petrone L, Cannas A, Aloi F, Nsubuga M, Sserumkuma J, Nazziwa RA, et al. Blood and urine IP-10 associate with active TB in HIV-infected patients. *Eur Respir J.* (2016) 48:OA3039. doi: 10.1183/13993003.congress-2016.OA3039

33. Uwimaana E, Bagaya BS, Castelnuovo B, Kateete DP, Godwin A, Kiwanuka N, et al. Heme oxygenase-1 and neopterin plasma/serum levels and their role in diagnosing active and latent TB among HIV/TB co-infected patients: a cross sectional study. *BMC Infect Dis.* (2021) 21:711. doi: 10.1186/s12879-021-06370-7

34. Bedell RA, van Lettow M, Meaney C, Corbett EL, Chan AK, Heyderman RS, et al. Predictive value of C-reactive protein for tuberculosis, bloodstream infection or death among HIV-infected individuals with chronic, non-specific symptoms and negative sputum smear microscopy. *Trop Med Int Health.* (2018) 23:254–62. doi: 10.1111/tmi.13025

35. Aabye MG, Ravn P, PrayGod G, Jeremiah K, Mugomela A, Jepsen M, et al. The impact of HIV infection and CD4 cell count on the performance of an interferon gamma release assay in patients with pulmonary tuberculosis. *PLoS ONE.* (2009) 4:e0004220. doi: 10.1371/journal.pone.0004220

36. Adu-Gyamfi C, Mikhathani L, Snyman T, Hoffmann C, Martinson NA, Chaisson RE, et al. Plasma indoleamine 2,3-dioxygenase, a highly sensitive blood-based screening tool for active tuberculosis disease in HIV-infected pregnant women. *Int J Infect Dis.* (2020) 101:456. doi: 10.1016/j.ijid.2020.09.1194

37. Adu-Gyamfi C, Savulescu D, Mikhathani L, Otwombe K, Salazar-Austin N, Chaisson R, et al. Plasma kynurenine-to-tryptophan ratio, a highly sensitive blood-based diagnostic tool for tuberculosis in pregnant women living with human immunodeficiency virus (HIV). *Clin Infect Dis.* (2021) 73:1027–36. doi: 10.1093/cid/ciab232

38. Ashenafi S, Aderaye G, Zewdie M, Raqib R, Bekele A, Magalhaes I, et al. BCG-specific IgG-secreting peripheral plasmablasts as a potential biomarker of active tuberculosis in HIV negative and HIV positive patients. *Thorax.* (2013) 68:269–76. doi: 10.1136/thoraxjnl-2012-201817

39. Bwanga F, Disque C, Lorenz MG, Allerheiligen V, Worodria W, Luyombya A, et al. Higher blood volumes improve the sensitivity of direct PCR diagnosis of blood stream tuberculosis among HIV-positive patients: an observation study. *BMC Infect Dis.* (2015) 15:48. doi: 10.1186/s12879-015-0785-3

40. Cattamanchi A, Ssewanyana I, Magala R, Miller CR, Den Boon S, Davis JL, et al. Performance of bronchoalveolar lavage enzyme-linked immunospot for diagnosis of smear-negative tuberculosis in HIV-infected patients. *Am J Respir Crit Care Med.* (2011) 183:A1202. doi: 10.1164/ajrccm-conference.2011.183.1_MeetingAbstracts.A1202

41. Cattamanchi A, Ssewenyana I, Davis JL, Huang L, Worodria W, den Boon S, et al. Role of interferon-gamma release assays in the diagnosis of pulmonary tuberculosis in patients with advanced HIV infection. *BMC Infect Dis.* (2010) 10:75. doi: 10.1186/1471-2334-10-75

42. Kisuya J, Chemtai A, Raballah E, Okumu W, Keter A, Ouma C. The role of Mycobacterium tuberculosis antigen specific cytokines in determination of acid fast bacilli culture status in pulmonary tuberculosis patients co-infected with human immunodeficiency virus. *Pan Afr Med J.* (2018) 31:17294. doi: 10.11604/pamj.2018.31.166.17294

43. Rajan JV, Semitala FC, Mehta T, Seielstad M, Montalvo L, Andama A, et al. A novel, 5-transcript, whole-blood gene-expression signature for tuberculosis screening among people living with human immunodeficiency virus. *Clin Infect Dis.* (2019) 69:77–83. doi: 10.1093/cid/ciy835

44. Ruperez M, Shanaube K, Mureithi L, Wapamesa C, Burnett MJ, Kosloff B, et al. Use of point-of-care C-reactive protein testing for screening of tuberculosis in the community in high-burden settings: a prospective, cross-sectional study in Zambia and South Africa. *Lancet Global Health.* (2023) 11:E704–E14. doi: 10.1016/S2214-109X(23)00113-4

45. Yoon C, Semitala FC, Atuhumuza E, Katende J, Mwebe S, Asege L, et al. Point-of-care C-reactive protein-based tuberculosis screening for people living with HIV: a diagnostic accuracy study. *Lancet Infect Dis.* (2017) 17:1285–92. doi: 10.1016/S1473-3099(17)30488-7

46. Petrone L, Cannas A, Vanini V, Cuzzi G, Aloi F, Nsubuga M, et al. Blood and urine inducible protein 10 as potential markers of disease activity. *Int J Tuberc Lung Dis.* (2016) 20:1554–61. doi: 10.5588/ijtld.16.0342

47. Lawn SD, Kerkhoff AD, Vogt M, Wood R. HIV-associated tuberculosis: relationship between disease severity and the sensitivity of new sputum-based and urine-based diagnostic assays. *BMC Med.* (2013) 11:231. doi: 10.1186/1741-7015-11-231

48. Yang Q, Han J, Shen J, Peng X, Zhou L, Yin X. Diagnosis and treatment of tuberculosis in adults with HIV. *Medicine.* (2022) 101:e30405. doi: 10.1097/MD.0000000000030405

49. Hanrahan CF, Theron G, Bassett J, Dheda K, Scott L, Stevens W, et al. Xpert MTB/RIF as a measure of sputum bacillary burden. Variation by HIV status and immunosuppression. *Am J Respir Crit Care Med.* (2014) 189:1426–34. doi: 10.1164/rccm.201312-2140OC

50. Scordo JM, Olmo-Fontánez AM, Kelley HV, Sidiki S, Arcos J, Akhter A, et al. The human lung mucosa drives differential Mycobacterium tuberculosis infection outcome in the alveolar epithelium. *Mucosal Immunol.* (2019) 12:795–804. doi: 10.1038/s41385-019-0156-2

51. Leukes V, Walzl G, du Plessis N. Myeloid-derived suppressor cells as target of phosphodiesterase-5 inhibitors in host-directed therapeutics for tuberculosis. *Front Immunol.* (2020) 11:451. doi: 10.3389/fimmu.2020.00451

52. Herskovitz J, Gendelman HE. HIV and the macrophage: from cell reservoirs to drug delivery to viral eradication. *J Neuroimmune Pharmacol.* (2019) 14:52–67. doi: 10.1007/s11481-018-9785-6

53. Hoerter A, Arnett E, Schlesinger LS, Pienaar E. Systems biology approaches to investigate the role of granulomas in TB-HIV coinfection. *Front Immunol.* (2022) 13:1014515. doi: 10.3389/fimmu.2022.1014515

54. Ganor Y, Real F, Sennepin A, Dutertre CA, Prevedel L, Xu L, et al. HIV-1 reservoirs in urethral macrophages of patients under suppressive antiretroviral therapy. *Nat Microbiol.* (2019) 4:633–44. doi: 10.1038/s41564-018-0335-z

55. Watters SA, Mlcochova P, Gupta RK. Macrophages: the neglected barrier to eradication. *Curr Opin Infect Dis.* (2013) 26:561–6. doi: 10.1097/QCO.0000000000000014

56. Okoye AA, Picker LJ. CD4(+) T-cell depletion in HIV infection: mechanisms of immunological failure. *Immunol Rev.* (2013) 254:54–64. doi: 10.1111/imr.12066

57. Gupta RK, Abdul-Jawad S, McCoy LE, Mok HP, Peppa D, Salgado M, et al. HIV-1 remission following CCR5Δ32/Δ32 haematopoietic stem-cell transplantation. *Nature.* (2019) 568:244–8. doi: 10.1038/s41586-019-1027-4

58. WHO. *Global Tuberculosis Report 2020.* Geneva: World Health Organization (2020).

Frontiers in Microbiology

Explores the habitable world and the potential of microbial life

The largest and most cited microbiology journal which advances our understanding of the role microbes play in addressing global challenges such as healthcare, food security, and climate change.

Discover the latest Research Topics

See more →

Frontiers

Avenue du Tribunal-Fédéral 34
1005 Lausanne, Switzerland
frontiersin.org

Contact us

+41 (0)21 510 17 00
frontiersin.org/about/contact